Development of an Analytical Method to determine Cavity Pressure in Cold-Bent Insulating Glass Units

Thijs Schuiling | November 2022
Delft University of Technology | Faculty of Civil Engineering and Geosciences

TU Delft

octatube

Master Thesis Report

Development of an Analytical Method to determine Cavity Pressure in Cold-Bent Insulating Glass Units

By

T.H. Schuiling

In partial fulfilment of the requirements for the degree of

Master of Science

in Civil Engineering

At the Delft University of Technology,

to be defended publicly on Friday November 11th, 2022, at 16:00.

Supervisor:	Ir. J. (Joey) Janssen,	Octatube Space Structures B.V.
Thesis committee:	Prof.dr.ir. P.C. (Christian) Louter	TU Delft
	Ir. C. (Chris) Noteboom	TU Delft
	Dr.ir. W.H. (Willem) van der Spoel	TU Delft

An electronic version of this thesis is available at http://repository.tudelft.nl/.

Cover image by (Kramer, 2015)

Contact information

Below the details of the student and the graduation committee are given. The thesis is done in collaboration with Octatube Space Structures B.V.

Student

Name	**T.H. (Thijs) Schuiling**
Student Nr.	5158346
Institution	Delft University of Technology
Faculty	Civil Engineering and Geosciences
Track	Building Engineering, Structural Design

Graduation committee

Name	**Prof.dr.ir. P.C. (Christian) Louter**
Organisation	Delft University of Technology
Faculty	Civil Engineering and Geosciences
Section	Applied Mechanics

Name	**Ir. C. (Chris) Noteboom**
Organisation	Delft University of Technology
Faculty	Civil Engineering and Geosciences
Section	Applied Mechanics

Name	**Ir. J.P. (Joey) Janssen**
Organisation	Octatube Space Structures B.V.

Name	**Dr.ir. W.H. (Willem) van der Spoel**
Organisation	Delft University of Technology
Faculty	Architectural Engineering + Technology
Section	Building Physics

Preface

This report is the result of my graduation research on cavity pressures in cold-bent insulating glass units. It also represents the last period of my time as a Building Engineering student, specialised in Structural Design, at the Faculty of Civil Engineering at the Delft University of Technology.

Over the course of my time as a student, I had a special interest in the design of special structures and challenging architecture. Therefore, after my bachelors at the University of Twente in Enschede, I decided to take the leap and move to Delft to start my masters. Despite the many online classes, a lot of courses sparked my interest, of which Structural Glass, lectured by Chris Noteboom, was one of my favourites. After a guest lecture by Joey Janssen from Octatube B.V., I decided to write the company for graduation possibilities.

Now, 10 months later, I'm happy to say that I have (almost) finished my master thesis, which has resulted in the development of a simplified analytical method to determine effective cavity pressures in cold-bent IGU's. I will be grateful if the developed method can contribute to the development of the fascinating applications of cold-bent glass. Feel free to contact me for questions and discussions.

I could not have finished this thesis without help of the graduation committee. Therefore, I want to thank the committee members for their professional guidance throughout my thesis. I want to thank Christian Louter for his input from an academic point of view, which has helped me to write a more concise and professional thesis. I want to thank Willem van der Spoel for being (what he self calls) an 'outsider'. His feedback helped me to broaden my tunnel vision and make the thesis not only more understandable for others, but also for myself. Special thanks goes to Chris Noteboom, his courses on Structural Glass sparked my interest into the topic. His weekly feedback sessions helped me a lot to setup the project, and to focus and set priorities when I was stuck. Last but not least I want to thank Joey Janssen from Octatube for his daily supervision throughout project. His endless enthusiasm and insights helped me gain knowledge in a rather theoretical topic.

Besides the graduation committee, I want to thank everyone at Octatube for the pleasant time I had as a graduate intern. The office days and coffee breaks were a nice variety from the study hours spent at home. Special thanks goes to the structural engineering team, which has provided me with insights in a number of challenging architecture projects. I'm looking forward to work as a structural engineer and I'm happy to say that I will start my career at Octatube.

Last thanks goes to my group of friends, fellow board members, football team, athletics club, study mates from Enschede and Delft, roommates and family, for providing me with distractions when needed and making my time as a student one to not forget!

Thijs (T.H.) Schuiling

Delft, November 2022

Abstract

Cold-bent insulating glass units (IGU) have the potential to be one of the answers to current needs and wishes of modern and sustainable architecture. Curved glass is stiffer against out-of-plane loads and therefore the structural behaviour of cold-bent IGU's is different compared to flat IGU's. Structural behaviour of flat glass in buildings is assessed using standards such as EN 16612 and NEN 2608. Within these norms, isochoric and load sharing cavity pressures are assessed using simplified analytical equations. In case of cold-bent IGU's, the additional assessment of increased stiffness, permanent cold-bending stresses and optical distortions are of importance. Currently, no standards are available for building envelopes containing curved glass elements. Methods from current standards have proved to be sufficient to quantify the complex role of cavity pressure in flat IGU's. The goal of this research is to develop an analytical method to determine the effect of cavity pressure on the structural behaviour of cold-bent insulating glass units.

For the structural assessment of cold-bent IGU's three stages are defined: 'Bending phase', 'Fixation moment' and 'Use phase'. Numerical models are developed to gain insights into the structural behaviour of cold-bent glass plates. Insights are then used to derive and validate simplified analytical methods.

The bending phase is numerically modelled with a geometrically nonlinear analysis in which curvatures are realized by prescribed displacements along two opposite edges of the plate. Results show that maximum cold-bending stresses are independent of plate size. By defining a tensile bending strength, insights are gained into the maximum radius of curvature of a plate with a specified thickness. A closed form equation is derived, which is used to calculate cold-bending stresses considering plate thickness and radius of curvature as input parameters. Resulting principal stresses have an average accuracy of 99.1% compared to numerical outcomes. Validity of the cold-bending stresses is limited to linearly fixed plates, up to a size of 6x3m, with equivalent plate thicknesses ranging from 4-20mm and design radii ranging from 3m to 25m.

Numerical results from the fixation moment show an anticlastic double or triple (w-shape) curvature in single curved plates, that cause optical distortions. The extent and shape of anticlastic bending depend on the Poisson's ratio, plate thickness, radius of curvature and plate size. Based on regression between the parameters of influence, a result-based approach is developed to determine anticlastic bending displacements at the centre of curved plates. The approach is simplified to a curved plate with a sinusoidal anticlastic bending curvature. The displacements are expressed in a parameter for the radius at midspan and are calculated using tabulated coefficients with an average accuracy of 99.3%. Validity of the radius at midspan is limited to the previously mentioned boundary conditions.

For the use phase, the calculation of cavity pressures depends on the volume of deformation per pane of a linearly supported cold-bent IGU. Interaction between the panes is modelled using pressure loads derived from Boyle's law. Using numerical models, volumes of deformation (v) from curved plates subjected to pressure loads (p) are presented in P-V diagrams. These diagrams are used calculate cavity pressures ranging from -1 to 1 kN/m^2, considering plate sizes up to 6x3m, plate thickness of 8, 10 and 12mm and design radii up to 8m. Due to the increased stiffness of curved IGU's, a higher load is shared by the pane onto which an external pressure is applied. Furthermore, as a result of anticlastic bending, a permanent isochoric pressure is present inside cavities of asymmetric IGU's, which increases as curvatures increase.

A simplified analytical method to calculate effective cavity pressures is derived from shell theory. Load sharing pressures of symmetric IGU's are calculated with an average accuracy of 95%, compared to results from the numerical P-V diagrams. Load sharing pressures of asymmetric IGU's (91% accuracy) are summed with isochoric pressures due to cold-bending (92% accuracy) to calculate combined effective pressures with an average accuracy of 87%.

The equations are summarized in a guideline, which is complemented by an interactive calculation tool. The developed analytical method is effective in calculating effective cavity pressures and can be used to quickly explore various design options in a wide range of cold-bent IGU's.

Content

Contact information iii
Student iii
Graduation committee iii
Preface iv
Abstract v
List of figures viii
List of tables xi
List of symbols xii
1. Introduction 1
1.1. Glass as a building material 1
1.2. Research definition 5
1.3. Methodology and report structure 8
1.4. Terms and definitions 10
2. Literature study 12
2.1. Properties of float glass 12
2.2. Cold bending of glass 17
2.3. Cavity pressure 23
2.4. Structural mechanics 30
2.5. Numerical modelling 34
3. Bending phase 39
3.1. Goal 39
3.2. Boundary conditions 39
3.3. Numerical modelling 41
3.4. Analytical modelling 43
4. Fixation moment 49
4.1. Goal 49
4.2. Boundary conditions 49
4.3. Numerical modelling 51
4.4. Analytical modelling 55
4.5. Cavity pressure 62
5. Use phase 67
5.1. Goal 67
5.2. Boundary conditions 67
5.3. Numerical modelling 69
5.4. Analytical modelling 76
5.5. Cavity pressure 82
6. Analytical method 86
6.1. Cold-bending stresses 87

6.2. Load sharing pressures 87
6.3. Isochoric pressures 89
6.4. Excel tool 92
6.5. Case study 96
7. Discussion 100
7.1. Bending phase 100
7.2. Fixation moment 102
7.3. Use phase 106
8. Conclusion 111
9. Recommendations 114
References 115
Appendix A. Principal stresses 118
A.1. Numerical modelling – Fixation moment 119
A.2. Analytical modelling – Arch theory 120
A.3. Analytical modelling – Cold-bending theory 121
A.4. Analytical modelling – Engineering approach 122
Appendix B. Anticlastic bending 123
B.1. Radius at midspan 123
B.2. Volume of deformation 139
Appendix C. Cavity pressure 155
C.1. P-V tables and diagrams 155
C.2. Cavity pressure symmetric IGU's 177
C.3. Cavity pressure asymmetric IGU's 188

List of figures

Figure 1: Fully glazed facades, London (Spatari, 2021) ... 1
Figure 2: Apple Fifth Avenue, New York (Delgado, 2020) ... 1
Figure 3: Steve Jobs Theater, Cupertino (Foster + Partners, 2017) ... 1
Figure 4: Opus, Dubai (Zaha Hadid Architects, 2020) ... 1
Figure 5: Typical intersection of an IGU (Clear Glass Solutions, 2019) ... 3
Figure 6: Radiation, conduction and convection through cavity ... 3
Figure 7: Pillowing effect (Marinov & Griffith, 2012) ... 4
Figure 8: Kissing effect (MORN, 2019) ... 4
Figure 9: Isochoric pressure due to temperature differences ... 4
Figure 10: Distinction of stages of the cold-bending process of IGU’s ... 8
Figure 11: Report structure ... 9
Figure 12: IGU elements, configuration and direction of loads ... 10
Figure 13: Direction of forces and stresses ... 11
Figure 14: Annealed float glass production line (van der Velden & Nijsse, 2019) ... 12
Figure 15: Stress-strain curves of steel and glass (Pölzl, 2017) ... 13
Figure 16: Tempering of glass (van der Velden & Nijsse, 2019) ... 13
Figure 17: Principle of superposition for stresses in heat threated cold-bent glass, redrawn from (Pölzl, 2017) & (van der Velden & Nijsse, 2019) ... 14
Figure 18: Direction of forces and stresses ... 16
Figure 19: Schematic transfer of forces ... 17
Figure 20: Simplified load systems ... 17
Figure 21: Two types of rectangular plate bending, single curved vs. twisted ... 17
Figure 22: Mock-up Spartherm Melle (Octatube, 2021) ... 18
Figure 23: On site bending using a robotic vacuum machine (Bijster, Noteboom, & Eekhout, 2016) ... 18
Figure 24: Differences in boundary conditions and stress distributions, between 'Bending phase' and ‘Fixation moment’ (Bijster, Noteboom, & Eekhout, 2016). ... 20
Figure 25: Glaskap Essent, 's-Hertogenbosch (ABT bv, 2006) ... 20
Figure 26: Floriade Paviljoen, Haarlemmermeer (Octatube, 2002) ... 20
Figure 27: Spartherm, Melle (Octatube, 2021) ... 20
Figure 28: Superposition of permanent and live load stresses in cold-bent glass plates ... 21
Figure 29: Simplified cold-bending stress theory (Janssen, 2017) ... 22
Figure 30: Sum of barometric pressure and cavity pressure changes on the panes of an IGU ... 24
Figure 31: External pressure load shared between glass panes of an IGU ... 24
Figure 32: Anticlastic bending according to Poisson’s ratio ... 30
Figure 33: Visual distortions due to anticlastic bending (Octatube, 2015) ... 30
Figure 34: Simplification of a single curved 2D plate, to a 1D curved beam ... 31
Figure 35: Specified load case ... 32
Figure 36: Tabulated values for the specified load case ... 32
Figure 37: Specified load case and directions of displacements ... 33
Figure 38: Quadrilateral curved shell element (DIANA FEA, 2021) ... 34
Figure 39: Cauchy stresses for curved shell elements (DIANA FEA, 2021) ... 34
Figure 40: Mesh size comparison ... 35
Figure 41: Large deflection of a cantilever under end moment; plot of deformations ... 36
Figure 42: Large deflection of a cantilever under transverse end load; plot of deformations ... 36
Figure 43: Large deflection of a cantilever under end moment; displacement at free end ... 36
Figure 44: Large deflection of a cantilever under transverse end load; displacement at free end ... 37
Figure 45: Shape properties ... 38
Figure 46: Material properties ... 38
Figure 47: Geometry properties ... 38
Figure 48: Nonlinear analysis properties ... 38
Figure 49: Boundary conditions 'Bending phase' ... 40
Figure 50: Nonconservative surface load ... 40
Figure 51: Displacements in x-direction ... 40

Figure 52: Displacements in y-direction......40
Figure 53: Displacements in z-direction......40
Figure 54: Stresses in layer 3 of S1......40
Figure 55: Maximum principal stress compared to design radius (2000x2000mm plate)......41
Figure 56: Comparison of deformation shapes, example of a 2000x2000x10mm plate, R=3000......43
Figure 57: Iterative scheme – step 1......44
Figure 58: Iterative scheme – step 2......44
Figure 59: Iterative scheme – step 3......44
Figure 60: Iterative scheme – step 4......44
Figure 61: Results geometrically nonlinear arch theory, for a 2000x2000mm plate......45
Figure 62: Maximum principal stress compared to plate thickness (2000x2000mm plate)......46
Figure 63: Boundary conditions ‘Fixation moment’......50
Figure 64: Prescribed displacements......50
Figure 65: Displacements in x-direction......50
Figure 66: Displacements in y-direction......50
Figure 67: Displacements in z-direction......50
Figure 68: Stresses in layer 3 of S1......50
Figure 69: Anticlastic bending line for a 2000x2000x20mm, R=25000mm......51
Figure 70: Postprocessing of results in Python, anticlastic bending line plot y-z plane......51
Figure 71: Anticlastic bending line for a 2000x2000x10mm, R=12000mm plate, v=.23......52
Figure 72: Anticlastic bending lines for different Poisson ratios......52
Figure 73: Anticlastic bending line for different plate thicknesses......53
Figure 74: Anticlastic bending line for different design radii......53
Figure 75: Anticlastic bending line for different plate widths......54
Figure 76: Decreased radius at midspan due to anticlastic bending......56
Figure 77: Regression between radius at midspan and plate thickness for a 2000x2000mm plate, R=12000mm......57
Figure 78: Regression between radius at midspan and plate thickness for a 2000x2000mm plate......57
Figure 79: 3rd order polynomial approximation of 'a' coefficients......58
Figure 80: 3rd order polynomial approximation of 'b' coefficients......58
Figure 81: Curvature height differences between edge and centre, as a result of anticlastic bending 62
Figure 82: Anticlastic curved glass panel......63
Figure 83: Isochoric pressure due to cold-bending of asymmetric IGU’s......65
Figure 84: Boundary conditions ‘Use phase’......68
Figure 85: Combined prescribed displacements and pressure load......68
Figure 86: Displacement in x-direction due to pressure load......68
Figure 87: Displacement in y-direction due to pressure load......68
Figure 88: Displacement in z-direction due to pressure load......68
Figure 89: Maximum principal stress in layer 3 of S1, before and after pressure load......68
Figure 90: External load sharing in cold-bent IGU's......69
Figure 91: Deformation of the interior pane in z-direction due to pressure load $p2 = .5$kN/m^2......69
Figure 92: P-V diagram DIANA (2000x2000x10mm, R=12000mm)......71
Figure 93: External load sharing of a symmetric cold-bent IGU, manual computation vs. P-V diagrams......72
Figure 94: P-V diagram DIANA (2000x2000x10mm)......72
Figure 95: Load sharing pressures for different design radii (2000x2000mm)......73
Figure 96: Equilibrium in volume of deformation due to anticlastic bending......74
Figure 97: Overview and direction of cold bending isochoric pressure and load sharing pressure......74
Figure 98: External load sharing of an asymmetric IGU (2000x2000x8-16-10mm)......75
Figure 99: Deflection of a portion of a curved shell (Timoshenko & Woinowsky-Krieger, 1989)......76
Figure 100: Comparison between analytical and numerical results 'Use phase', example 1......78
Figure 101: Comparison between analytical and numerical results 'Use phase', example 2......79
Figure 102: Comparison between analytical and numerical results 'Use phase', example 3......79
Figure 103: P-V diagram, 2000x2000x10mm plate, analytical versus numerical results......80
Figure 104: Overview and direction of cold bending isochoric pressure and load sharing pressure......82
Figure 105: Analytical and numerical load sharing pressures for different design radii......83

Figure 106: Analytical external load sharing of an asymmetric IGU (2000x2000x8-16-10mm) 84
Figure 107: Overview of effective isochoric loads and effective load sharing pressures 86
Figure 108: Load sharing due to an external load 87
Figure 109: Overview of isochoric pressures in cold-bent IGU's 89
Figure 110: Decreased radius at midspan due to anticlastic bending 89
Figure 111: Change in cavity distance in the centre of an asymmetric IGU 89
Figure 112: Overview Excel tool 92
Figure 113: Component 1: Input parameters 92
Figure 114: Component 2: Effective pressures... 93
Figure 115: Component 3: Interactive load sharing diagram 93
Figure 116: Component 4: Comparison flat IGU 94
Figure 117: Component 5: Cold-bending stresses 94
Figure 118: Component 6: Anticlastic bending 94
Figure 119: Component 7: Load sharing pressures 95
Figure 120: Component 8: Isochoric pressures 95
Figure 121: Dimensions example case studies Van Gogh Museum and Innovationszentrum Melle ... 96
Figure 122: Report structure 100
Figure 123: Diverging numerical model 102
Figure 124: Comparison between numerical and analytical anticlastic bending lines 102
Figure 125: Deviations between results from numerical modelling and result based approach 104
Figure 126: Regression between radius at midspan and plate thickness for a 2000x2000mm plate, R=12000mm 104
Figure 127: Decreased radius at midspan due to anticlastic bending 105
Figure 128: Anticlastic bending line 2000x20000x8mm, R = 8000mm 105
Figure 129: Resulting effective pressures asymmetric IGU (2000x2000x10-16-8mm) 109

List of tables

Table 1: List of symbols ... xii
Table 2: Material properties glass (NEN 2608, 2014) ... 14
Table 3: Design values of the tensile bending strength of prestressed glass, including calculation factors (NEN 2608, 2014) ... 15
Table 4: Maximum principal stresses per plate size ... 42
Table 5: Linear regression coefficients (2000x2000mm) ... 46
Table 6: Values of C_B for different plate sizes ... 47
Table 7: Principal stresses per plate width ... 47
Table 8: Average deviations per set B and C_B ... 47
Table 9: Validation Poisson's ratio method ... 55
Table 10: Validation Timoshenko method ... 56
Table 11: Regression coefficients, 2000x2000mm plate ... 58
Table 12: Average deviations in radius at midspan per plate size ... 59
Table 13: Tabulated regression coefficients, per plate size ... 60
Table 14: Guiding table for interpolation ... 61
Table 15: Average deviations in volume below a curved plate, per plate size ... 64
Table 16: External load sharing of cold-bent IGU, manually calculated using DIANA ... 70
Table 17: External load sharing of cold-bent IGU, calculated using P-V diagrams ... 71
Table 18: Deviations between volumes of deformation from numerical and analytical outcomes ... 80
Table 19: Deviations between P-V diagrams from numerical and analytical outcomes ... 81
Table 20: Guiding table for interpolation ... 90
Table 21: Results of Amn until Gmn, for values of m and n of 1 and 3 ... 97
Table 22: Results $K1$and $K2$ ... 97
Table 23: Interpolation step 1 ... 98
Table 24: Regression coefficients, 3000x1000mm plate ... 98
Table 25: Interpolation step 2 ... 98
Table 26: Interpolation step 3 ... 98
Table 27: Deviation in effective pressures, case study Van Gogh ... 99
Table 28: Deviation in effective pressures, case study Spartherm Melle ... 99
Table 29: Average deviations between numerical outcomes and analytical methods 'Bending phase' ... 101
Table 30: Validation of analytical radius at midspan compared to numerical outcomes ... 103
Table 31: Validation of simplified volume of deformation calculation compared to numerical outcomes ... 103
Table 32: Overview deviations of analytical P-V diagrams with numerical outcomes, per design radius ... 106
Table 33: Overview deviations load sharing pressure symmetric IGU's, per design radius ... 107
Table 34: Overview deviations combined pressure asymmetric IGU's, per design radius ... 107

List of symbols

In this thesis the following symbols and units are used. Terms and definitions in line with these symbols are shown in Chapter 1.3.

Table 1: List of symbols

Symbol	Definition	Unit
$A_{B:H}, B_{B:H}$	Linear coefficients per plate height-to-width ratio	-
$a_{A_{B:H}}, \dots, d_{B_{B:H}}$	Polynomial coefficients per plate height-to-width ratio	-
$A_{mn}, \dots, G_{mn}$	Constants for components volume of deformation equation	-
B	Width of the element	mm
C_c	Factor for the increase of isochoric pressure due to temperature differences	kN/m^{2}K
C_H	Factor for the increase of isochoric pressure due to height differences	kN/m^2/m
D	Flexural rigidity of a plate	(N/mm^2)·mm^3
d	Spacer distance of the IGU	mm
Δd	Difference in cavity distance in the centre of glass plate	mm
d_{cav}	Cavity distance in the centre of the IGU	mm
δ_i	Load sharing factor of glass plate i	-
E	Young's modulus, whereby the value for glass is E_g= 70000 N/mm^2	N/mm^2
f	Deformation height or arch height of a curved glass plate	mm
$f_{b;k}$	Characteristic value of the tensile bending strength of prestressed glass	N/mm^2
$f_{g;k}$	Characteristic value of the tensile bending strength of glass, whereby $f_{g;k}$= 45 N/mm^2;	N/mm^2
$f_{mt;u;d}$	Design value of the tensile bending strength	N/mm^2
$\gamma_{m;A}$	Material factor of glass	-
$\gamma_{m;V}$	Material factor for the pretension of prestressed glass	-
γ_u	Desired extent of utilisation of cold-bending stresses	-
H	Height of the element	mm
h	Height compared to NAP (Normaal Amsterdams Peil) after placement of the IGU	m
h_p	Height compared to NAP during production at the time of sealing of the IGU	m
K_i	Constant for calculating volume of deformation due to effective pressure loads, whereby $v_i = K_i * p_i$	-
k_a	Factor for the surface effect of a glass pane	-
k_e	Factor for the edge quality of a glass pane	-
k_{mod}	Modification factor of a glass pane, depending on the load duration and reference period	-
k_{sp}	Factor for the surface structure of a glass pane	-
k_z	Factor for the zone of the plate	-
L	Arch span of the element	mm
M_x, M_y	Bending moments in positive x- and y-direction	Nmm
N_x, N_y	Normal forces in positive x- and y-direction	N

$P_{c;P}$	Barometric pressure during production at the time of sealing	kN/m^2
$P_{c;A}$	Barometric pressure at the location of application of the IGU	kN/m^2
$P_{o;F}$	Final combined isochoric pressure inside the IGU during application	kN/m^2
$P_{o;H}$	Isochoric pressure inside the IGU due to height differences	kN/m^2
$P_{o;c}$	Isochoric pressure inside the IGU due to climatic loads	kN/m^2
$P_{o;CB}$	Isochoric pressure inside the IGU due to change in cavity volume from cold-bending of the IGU	kN/m^2
$P_{o;LS}$	Isochoric pressure inside the IGU due to change load sharing of an external load	kN/m^2
p_{ext}	External pressure load on the exterior pane of the IGU	kN/m^2
$p_{i;F}$	Final combined effective pressure load on pane i of the IGU	kN/m^2
$p_{i;H}$	Effective pressure load on pane i of the IGU, due to height differences	kN/m^2
$p_{i;c}$	Effective pressure load on pane i of the IGU, due to climatic loads	kN/m^2
$p_{i;CB}$	Effective pressure load on pane i of the IGU, due to cold-bending	kN/m^2
$p_{i;LS}$	Effective pressure load on pane i of the IGU, due to load sharing of an external pressure load	kN/m^2
φ	Insulating glass factor for flat, rectangular double glazed IGU's	-
R	Design radius of the element	mm
R_{mid}	Radius at midspan due to anticlastic bending of cold-bent glass plates	mm
ρ	Density, whereby the value for glass at 18 ˚C is ρ_g = 2500 kg/m^3	kg/m^3
s	Arch length of the element	mm
σ	Normal stress	N/mm^2
σ'_{max}	Design value for the maximum principal tensile bending stress in cold-bent glass plates	N/mm^2
T_p	Temperature of the filling gas in IGU's during production	˚C
T_s	Temperature of the filling gas in IGU's during application	˚C
$t_{gg;ser}$	Equivalent thickness of laminated glass in the serviceability limit state	mm
$t_{pl;i}$	Thickness of glass plate i	mm
τ	Shear stress	N/mm^2
U	Thermal transmittance in an IGU	W/(m^{2}K)
V	Reference cavity volume at place of production, whereby $V = d * H * B$	mm^3
V_o	Cavity volume according to Boyle's law due to an isochoric pressure	mm^3
V'_H	Change in cavity volume due to isochoric pressure from height differences	mm^3
V'_c	Change in cavity volume due to isochoric pressure from climatic loads	mm^3
V'_{CB}	Change in cavity volume due to cold-bending	mm^3
V'_{LS}	Change in cavity volume due to load sharing of external load	mm^3
ΔV_i	Volume below cold-bent glass pane i of the IGU	mm^3
V_x, V_y	Shear forces in positive x- and y-direction	N

v_i	Volume of deformation of curved glass plate i, due to an effective pressure load	mm^3
Δv	Reduction in cavity volume inside the IGU	mm^3
ν	Poisson's ratio, whereby the value for glass is $\nu_g = 0.23$	-
$w_i(x, y)$	Deflection of the glass plate i at point x, y	mm

1. Introduction

The role of glass in architecture has evolved over the years. What started as a luxury product in the form of small stained-glass windows in cathedrals and churches, has become a versatile construction material in all types of buildings. The use of glass as a building component was made possible after centuries of glass manufacturing developments. The development of the Pilkington manufacturing process for float glass (US Patent No. 2.911.759, 1959), made it possible to create large flat glass panes with a high and consistent quality. Nowadays, around 80% of the production of flat glass is used for the construction industry (Glass for Europe, 2021).

1.1. Glass as a building material

Due to its combination of qualities, glass has become increasingly popular as a building material, especially over the past 25 years (IStructE, 2015). Glass is transparent, sustainable, strong, easily available and cheap. It is hard to envision the practicality of a dwelling without windows, but glass has also become more important as an architectural feature. Famous skylines around the world are filled with fully glazed skyscrapers (Figure 1) and there are numerous examples of museums (Cover image), train stations, hotels and stores (Figure 2), in which glass plays an important architectural role.

Figure 1: Fully glazed facades, London (Spatari, 2021)

Figure 2: Apple Fifth Avenue, New York (Delgado, 2020)

An increasingly popular style within modern architecture of the 21st century, is curvilinear architecture (Januszkiewicz & Banachowicz, 2016). Rectangular glass is widely used in this style, since it can be bend into the desired shape, is easy to install and provides optical, thermal and aesthetic enhancements. The style is practiced by multiple renowned architecture offices, like Foster + Partners (Figure 3) and Zaha Hadid Architects (Figure 4). Furthermore, by bending the glass, it gains stiffness against out-of-plane loads. This causes the glass to deflect less under lateral loads and therefore larger panels or thinner glass can be realised.

Figure 3: Steve Jobs Theater, Cupertino (Foster + Partners, 2017)

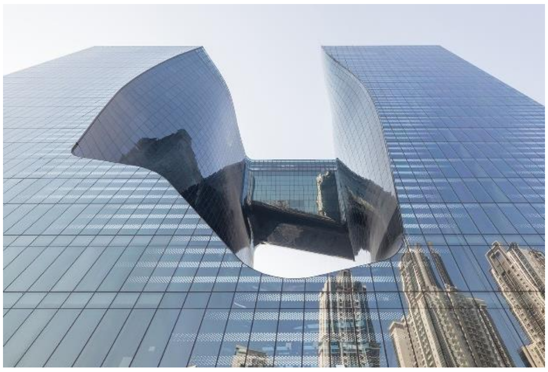

Figure 4: Opus, Dubai (Zaha Hadid Architects, 2020)

1.1.1. Curved glass

The increasing demand of curved glass is currently mostly realised using thermally curved or 'hot-bent' glass (Feldmann, Kasper, Bucak, Illguth, & Bues, 2010). After the production of float glass, the flat panels are heated until they soften and brought into shape using a mould. An alternative to the hot-bending process is cold-bending, in which the flat glass is curved by steadily increasing out of plane forces, without having to heat the material. After the cold-bent glass has reached its desired shape, it has to be fixed onto the substructure to maintain its curvature.

Hot-bending

The transformation of glass during the hot-bending process starts at a temperature of around 550˚C (Neugebauer, 2014). At this temperature, individual particles in the glass 'matrix' start to move, due to the thermal energy that is supplied. Because of these movements, bonds between the particles start to fall apart. At higher temperatures, more bonds fall apart and the glass becomes more viscous, which result in a decrease of the Young's modulus. At 800˚C, the glass is soft and extreme curvatures can be reached, to form for example corrugated glass.

To get glass into its desired shape, different techniques such as 'gravity sag bending' and 'press bending' can be used. The heated glass becomes viscous and using gravitational or compression forces the required shape is realised. For both of these techniques a mould is required, which must be specially designed for each unique shape. After the bending process, the glass is gradually cooled down and bonds between the particles restore. Due to the reheating, shaping and cooling of the glass, residual stresses occur in the curved glass panes (Elstner & Kramer, 2012). These residual stresses decrease the characteristic bending tensile strength of the glass and must be accounted for in the design. After the bending process, the curved glass can be heat- or chemically treated to increase its strength. Furthermore, it is possible to laminate the curved panels to increase safety.

Due to the high temperatures, the bending process has to be conducted in a glass factory, which makes the bending part of the production process. This means the glass panels have to be transported to site after bending. Since architectural designs often consist of multiple unique glass panels, it is a costly procedure to make each unique mould. Furthermore, in order to transport the curved panels, additional formwork is needed to support the shape and the panels require more space. In order to make sure that the panels fit on site, the bending process only allows for small tolerances.

Cold-bending

The cold-bending process uses the limited strain capacity of glass under ambient temperatures, to create curvatures. Since glass is a brittle material, it only has an elastic deformation capacity before stress limits are reached and failure occurs. The maximum curvature is therefore limited by the bending strength of the glass. In contrary to the hot bending process, flat glass panes can first be heat- or chemically treated and laminated, which allows for more tolerances.

After production, the flat glass is transported to site, where it is bent into the desired shape. During transport, the glass can be stacked on top of each other, which is more efficient and safer compared to transport of curved panels. On site, machinery is needed for bending of the glass, which has to be done slowly in order for the stresses to redistribute within the glass. After the glass has reached the desired curvature, it has to be fixed onto the structure. Due to the elastic deformation of glass, the curved panels want to deflect back into its original state. This means that peak stresses will occur around the spots where the glass is fixed into position. These cold-bending stresses are in general much higher than residual stresses due to hot-bending. It is therefore of importance that during the design phase these stresses are taken into consideration.

Benefits of cold-bending
Both bending techniques have their advantages and disadvantages. The main advantage of hot-bending is its freedom of shape to create extreme and complicated curvatures. However, due to reheating of the glass additional energy is needed, which comes with environmental impact and sustainability issues. Furthermore, the hot-bending is part of the production process. The extra measures this comes with such as creating moulds, transportation and installation, also have an impact on the environment.

The main advantage of the cold-bending of glass is that it is not part of the production process. This reduces the environmental impact compared to the extra measures needed for hot-bending. The main disadvantage of cold bending are the curvature limits, which will limit the freedom of shape in the architectural design. In general, it can be concluded that when small curvatures are required, cold bending is more cost effective than hot bending (Quaglini, 2020).

1.1.2. Insulating Glass Units
In order for glazed envelopes to be thermally sufficient, the principle of an Insulating Glass Unit (IGU) is used. An IGU is realized by hermetically sealing a cavity between two or more glass panes (Figure 5), which reduces the total heat transfer through the glass unit. Heat can be transferred by the mechanisms of conduction, convection and radiation (Figure 6). The combination of these three factors, results in the total heat resistance of the IGU. To increase the heat resistance of the IGU, the cavity can be filled with a lower density gas like argon or krypton, which reduces the heat transfer through conduction. Furthermore, by increasing the cavity width, conduction can also be reduced. In terms of the total heat resistance, an increase in cavity width up to 12mm is significant (Stazi, 2019). In cavities larger than 20mm, convection currents can occur, which transfers heat from hot to the cold pane. The optimum cavity distance is therefore between 12 and 20mm. Heat transfer through radiation can be decreased by applying a low emissivity coating onto the glass.

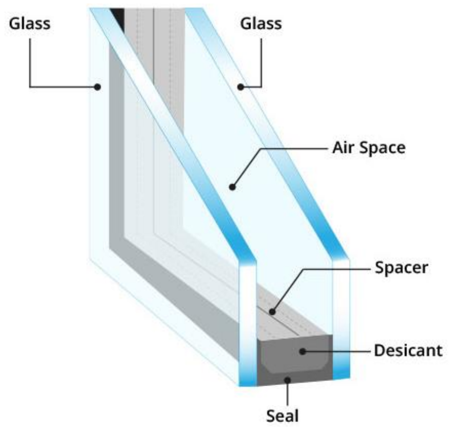

Figure 5: Typical intersection of an IGU (Clear Glass Solutions, 2019)

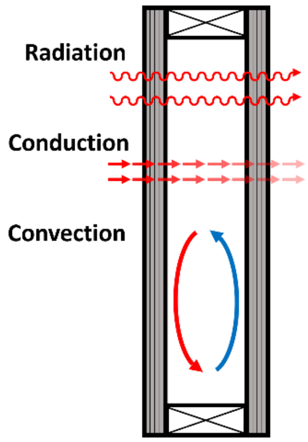

Figure 6: Radiation, conduction and convection through cavity

The total heat transmittance is often expressed in terms of the thermal transmittance U in W/(m^{2}K). The lower the U-value, the better the thermal performance. The U-value of a single glass pane is around 5.8 W/(m^{2}K). For a standard IGU, consisting of uncoated double glass and an air cavity the U-value is already reduced to a value between 2.7 and 3.3 W/(m^{2}K). By applying a low-E coating and filling the cavity with argon, the U-value of a double glazed IGU (HR++) is between 1.1 and 1.2 W/(m^{2}K), which is currently most used for Dutch building envelopes (ACG Nederland, 2022). The requirements of the maximum allowable U-value differ per country. The Dutch building code employs a maximum value of 1.65 W/(m^{2}K) (Bouwbesluit, 2012).

The use of an IGU is essential in creating a thermally sufficient envelope for the transparent part of a building. Especially in current times, the need for sustainable and environmentally friendly solutions is high. At the level of individual buildings, thermal insulation is one of the main answers to lower energy usage and thereby reducing the environmental impact of the build environment (Partridge, 2020).

1.1.3. Cavity pressure

To prevent thermal diminution of an IGU, the cavity must be free of leaks and therefore can be considered as airtight. Because of this consideration, Boyle's gas law can be applied. At the place of production of the IGU, the barometric pressure gets 'trapped' inside the IGU, which is considered as the cavity pressure. At the location of application, a different barometric pressure outside of the IGU, will result in an effective pressure load on the panes of an IGU. Changes in cavity pressure are referred to as isochoric pressures. Besides differences in barometric pressures, isochoric pressures can be caused by height differences between production and application of the IGU, and temperature differences.

Cavity pressure has a structural role since it enables load sharing between the panes of an IGU. Due to for example an external wind load, the exterior plate of an IGU wants to deflect inwards. Due to this deflection, the cavity decreases in volume, resulting in an increased cavity pressure according to Boyle's law. Due to this interaction, the external load is shared by the exterior and interior plate of the IGU, which enhances its structural performance compared to single glazing.

A change in cavity pressure itself can cause deformations of the glass panes of an IGU. An example of this is the 'pillowing effect', which can cause unwanted visual distortions (Figure 7). For example, if the temperature during production is 20˚C, and the temperature during application is 25˚C, the gas inside the cavity will expand, resulting in an isochoric pressure (Figure 9). During winter, the opposite can happen. A decrease of temperate results in a decrease of cavity pressure, which can cause deformations referred to as the 'kissing effect' (Figure 8). From a serviceability point of view, it is desired to prevent such visual distortions.

Figure 7: Pillowing effect (Marinov & Griffith, 2012)

Figure 8: Kissing effect (MORN, 2019)

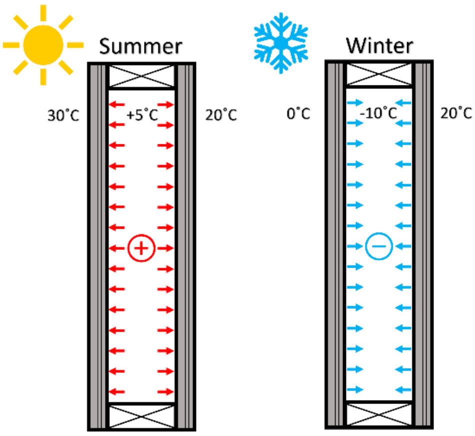

Figure 9: Isochoric pressure due to temperature differences

Besides visual distortions, high isochoric cavity pressures can also cause leakages through the adhesive which seals the glass panes and spacer. In that case, the cavity is not hermetically sealed anymore and thermal diminution will occur. Furthermore, air currents can flow inside the cavity, which can cause condensation on the inside of the IGU. From a serviceability point of view, it is therefore important to gain insights into cavity pressures in IGU's.

1.2. Research definition

Cold-bent insulating glass units have the potential to be one of the answers to the current needs and wishes of modern and sustainable architecture. From a structural point of view, it is required to gain sufficient knowledge on the effect of cavity pressure in cold-bent IGU's, in order to guarantee serviceability, structural safety and provide efficient design options. Ideally, a standardized method, similar to those from European Standards (EN 16612, 2019) or Dutch Standards (NEN 2608, 2014), is desired to determine the structural behaviour of cold-bent IGU's.

1.2.1. State of the art

Current standards and methods for evaluating the effect of cavity pressure on the structural behaviour of insulating glass units are discussed below.

NEN 2608

In the Dutch standard for glass in buildings, two equations are given to determine the cavity pressure of rectangular, flat, double glazed IGU's, under an external load (NEN 2608, 2014). The first equation (Appendix B, equation B.1) is for an equally distributed surface load over the entire exterior glass pane. The equation consists out of two components, a calculation of the change of volume in the cavity and an insulating glass factor. The equation is based on the Combined gas law, a derivation of the formula can be found in (Feldmeier, 2003). In the derivation, the volume per load v in $m^3/(N/m^2)$, is used to calculate the volume of the deformation of a glass pane under a uniform surface load. The value of v is determined with Finite Element Methods, but in some cases, e.g., rectangular panes, it is directly calculable. To calculate the stiffness of the entire IGU, relative stiffnesses are used for the inner and outer pane. The second component, the insulating glass factor, describes the extent of load sharing between the two panes. The factor depends on the IGU dimensions and a characteristic length. This length is calculated using the shape, size, height-width ratio, cavity width and stiffness of both glass panes. In (Feldmeier, 2003), tabulated coefficients, are used to calculate the characteristic length. The table contains coefficients for circular, equilateral triangular, right-angled triangular and rectangular shaped panes. Equation B.1 (NEN 2608, 2014) only considers rectangular IGU's and therefore uses a direct equation.

The second equation (Appendix B, equation B.2) is used for line-, point- and concentrated loads on a flat and rectangular IGU. This equation also consists of an insulation factor and the change of volume in the cavity. The same insulation factor is used as for Equation B.1. The change of volume in the cavity is calculated using geometric linear plate theory for a simply supported rectangular plate (Timoshenko & Woinowsky-Krieger, 1989). The application of this theory is a simplified method, which was proved to be effective compared to geometrical non-linear methods (Wörner, Shen, & Sagmeister, 1993).

The determination of the cavity pressure according to NEN 2608 can be used for double glazed rectangular IGU's, where it is assumed that the glass panes are linearly simply supported on all sides by a spacer which has an infinite stiffness. Furthermore, it is assumed that the deformation of the panes is geometrically linear. Finally, it is assumed that the cavity gas is incompressible. In case of a uniform load, the derivation in (Feldmeier, 2003) can be used to calculate the cavity pressure for other standard shapes using tabulated coefficients.

Betti's analytical method

In addition to current standards, like NEN 2608, an analytical method based on Betti's Reciprocal Work Theorem to evaluate the load sharing in IGU's, is proposed by (Galuppi & Royer-Carfagni, 2019). The method can be applied to rectangular and equilateral triangular shapes, under any load condition, without the use of tables or charts. Also, it considers the compressibility of cavity gas. The method is later on revised with more practical expressions and the addition of right-angled triangles (Galuppi, 2020). There is also a revision for triple glazed IGU's (Galuppi & Royer-Carfagni, 2020). Similar to NEN 2608, the method relies on geometrically linear theory and linearly simply supported conditions.

Curved Insulating Glass Units

The previous methods are all based on flat IGU's. A workflow, which can be used to optimise the thickness of curved IGU's, is presented by (Marinov & Griffith, 2012). The procedure involves a calculation of the cavity pressure due to climatic loads with a parametric finite element routine. With the use of optimisation algorithms, the design tool determines the minimum thickness of glass required to resist the combination of external and climatic loads. The paper claims that the design time of IGU's is 30 times faster with application of the proposed workflow, compared to manual design. The workflow consists of a numerical approach and does require prior knowledge of different software packages to conduct. Furthermore, the workflow is based on single-curved glass panels without additional cold-bending stresses.

1.2.2. Problem definition

Currently, there are no standards available for building envelopes containing curved glass elements. Therefore, assessment criteria like geometrical tolerances, optical distortion, material strength or breakage patterns of flat panels are generally assumed for curved glass, which comes with risks and sometimes failures (Feldmann, Kasper, Bucak, Illguth, & Bues, 2010). Furthermore, with regards to the specific case of the cold-bending of insulating glass units, assessment criteria like permanent cold-bending stresses and cavity pressure become of importance. These criteria further increase the already complex and challenging design of curved glass. Currently the assessment of such criteria is done using finite element software. However, without a standardized method to do so, risks become evident.

Still, considering the increasing demand of curved glass and the benefits of cold-bent insulating glass units as an answer for this demand, there are opportunities to be sought. The Van Gogh Museum in Amsterdam (Bijster, Noteboom, & Eekhout, 2016), is one of the leading examples of such an opportunity. It shows the potential of cold-bent IGU's in the built environment. In order to make a wider application feasible, it is amongst others desired to have a standardized method which can be used to assess the most critical criteria of cold-bent IGU's, during the early stages of the design phase.

1.2.3. Research goal and scope

The goal of this thesis is to develop a method which can be used to assess the most important criteria of cold-bent IGU's. In order for the developed method to be comprehensive, the following assessment criteria are considered:

- Permanent stresses due to cold-bending.
- Increased stiffness due to curved glass.
- Cavity pressure.

In order for the method to be efficient during the early design stage, the goal is to develop an analytical method. In the context of this thesis 'analytical' holds that the method can be conducted using closed form expressions, without having to use numerical models. Simplified analytical methods have proved to be efficient to quantify the complex role of cavity pressure in flat IGU's and therefore are used as a guideline during this thesis. The main goal of the thesis is formulated as follows:

Development of an analytical method to determine the effect of cavity pressure on the structural behaviour of cold-bent insulating glass units.

In order to narrow down the research topic, the scope is defined by stating the following boundary conditions and simplifications. First of all, the structural behaviour of the spacer is left out of consideration for simplification reasons, which means that the spacer is considered as rigid. Furthermore, since most practical applications of cold-bent glass are those of rectangular sheets, this is the only shape taken into consideration. In line with standardized methods to determine cavity pressure, the cavity gas is assumed to be incompressible. Since the cavity pressure is a pressure load, the focus in this thesis is on deformations due to pressure loads. Deformations due to point or line loads are left out of consideration. As of yet, no practical applications of triple glazed cold-bent IGU's are known, therefore the focus will solely be on double glazing. Last, for simplification reasons, only IGU's with a single curvature are considered and all glass panes are considered to be monolithic.

1.2.4. Research questions

In line with the research goal of this thesis, the main research question is as follows:

How can the effect of cavity pressure on the structural behaviour of cold-bent insulating glass units be analytically determined?

To answer the main research question, the goal is divided into four subsequent goals, with each their own objectives. Each subgoal is formulated as a sub-research question (RQ). The research questions are answered throughout this thesis and reflected on in the discussion and conclusions.

The first subgoal is to conduct a literature review, the sub-question and corresponding objectives are defined as follows:

RQ 1. Which information about the effect of cavity pressure on the structural behaviour of IGU's can be found in literature?

1.1. Collect analytical and numerical methods from literature, used to determine cavity pressure in IGU's.
1.2. Identify the unknowns from literature, necessary to determine the cavity pressure in cold-bent IGU's.
1.3. Setup a theoretical framework of processes necessary to determine the effect of cavity pressure in cold-bent IGU's.

The second subgoal is to create a numerical model, which enhances understanding of the behaviour of cold-bent glass panes loaded by pressure loads.

RQ 2. How can the structural behaviour of cold-bent glass panes be modelled numerically and which insights are gained from outcomes?

2.1. Evaluate numerical methods used to model the structural behaviour of cold-bent glass panes.
2.2. Define the model objectives, parameters, boundary conditions and assumptions to be considered for numerical modelling.
2.3. Build a numerical model in which all necessary processes are implemented.
2.4. Validate outcomes of numerical modelling with literature.
2.5. Improve the numerical model for accuracy and computational running time.
2.6. Evaluate outcomes to gain insights into the structural behaviour of cold-bent glass panes.

The third subgoal is to derive analytical methods which can be used to assess the effect of cavity pressure on the structural behaviour of cold-bent IGU's. This done by analysing analytical methods from literature and exploring relations between outcome variables of numerical modelling.

RQ 3. Which analytical derivations can be used to determine the effect of cavity pressure on the structural behaviour of cold-bent insulating glass units?

3.1. Evaluate analytical methods with boundary conditions similar to that of cold-bent glass.
3.2. Identify similarities and differences between boundary conditions from analytical derivations and numerical approaches.
3.3. Use data analysis techniques to identify relations between key parameters from numerical outcomes.
3.4. Validate outcomes from analytical methods with numerical results.
3.5. Evaluate outcomes to gain insights into cavity pressure in cold-bent IGU's.

The fourth and last subgoal is to develop a reliable and efficient analytical method to determine the effect of cavity pressure in cold-bent insulating glass, which can be used during the early design stages.

RQ 4. Which derived equations are suitable for the development of an analytical method which can be used during the early design stages?

4.1. Identify the key parameters for the design of cold-bent IGU's, necessary to setup the developed analytical method.

4.2. Evaluate the analytical expressions necessary, to calculate the key parameters for determining the structural performance of cavity pressure in cold-bent IGU's

4.3. Design and present the workflow of the analytical method.

4.4. Summarize and present the analytical method in a calculation tool, which can be used in the early design stage.

1.3. Methodology and report structure

In line with RQ 1, the first step in understanding the complex behaviour of cold-bent insulated glass units with regards to cavity pressure, is to conduct a literature review. The literature review is discussed in Chapter 2. The cold-bending process itself is divided into three parts, which are the three main parts of methodology in this thesis. The distinction is made due to differences in boundary conditions between the stages. Per stage the boundary conditions are similar for both numerical modelling (RQ 2) and analytical modelling (RQ 3). The three stages are referred to as 'Bending phase', 'Fixation moment' and 'Use phase', as shown in Figure 10. For each stage, the goal of modelling is specified first, after which the boundary conditions are defined. Second, the numerical modelling approach and results are discussed. Last, analytical methods are derived, of which results are validated with numerical outcomes. Each stage is concluded with a component which is used for the final analytical method. As answer to RQ 4, the developed analytical method is presented in Chapter 6, including an example exercise which is based on a case study. Furthermore, an application of the analytical method in the form of an Excel tool is presented.

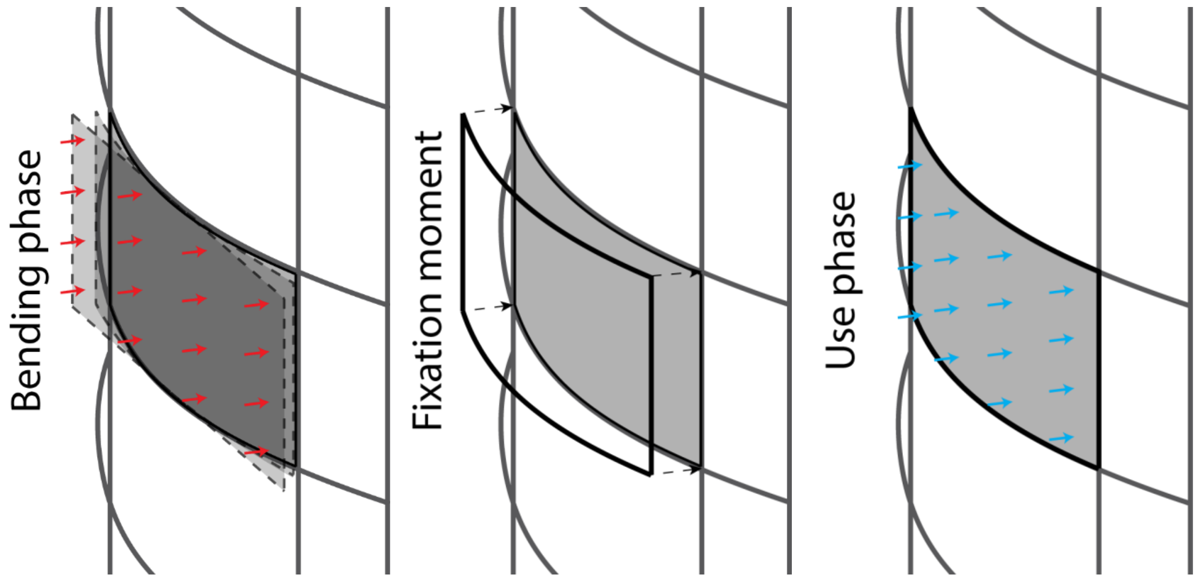

Figure 10: Distinction of stages of the cold-bending process of IGU's

The structure between the research questions and methodology is defined in Figure 11. The stages of the cold-bending process are divided between RQ 2 and RQ 3. RQ 2 focusses on numerical modelling and RQ 3 on analytical modelling. Since the modelling goal and boundary conditions are the same for both numerical and analytical modelling, they are mentioned in both columns. Furthermore, cavity pressures are calculated with the same method for both modelling techniques and therefore also shown in both columns. The research questions and methodology are reflected on with a discussion, in Chapter 7. The final conclusions and recommendations are discussed in Chapter 8 and Chapter 9, respectively.

Chapter	RQ 1	RQ 2	RQ 3	RQ 4
2. Literature study	Chapter 2.1. - 2.5.			
3. Bending phase		3.1. Goal 3.2. Boundary conditions 3.3. Numerical modelling	3.1. Goal 3.2. Boundary conditions 3.4. Analytical modelling	
4. Fixation moment		4.1. Goal 4.2. Boundary conditions 4.3. Numerical modelling 4.5. Cavity pressure	4.1. Goal 4.2. Boundary conditions 4.4. Analytical modelling 4.5. Cavity pressure	
5. Use phase		5.1. Goal 5.2. Boundary conditions 5.3. Numerical modelling 5.5. Cavity pressure	5.1. Goal 5.2. Boundary conditions 5.4. Analytical modelling 5.5. Cavity pressure	
6. Analytical method				Chapter 6.1. - 6.5.

Figure 11: Report structure

1.3.1. Software programs

Throughout this thesis, different software programs have been used. The programme of choice for numerical modelling is the finite element analysis software DIANA (DIANA FEA, 2021). Within the Interactive Environment of DIANA (DianaIE), all operations are logged as Python commands (.py), which made it possible to do pre- and postprocessing of numerical models using .py command lines in the Integrated Development Environment of Spyder (Spyder, 2022). Also, iterative calculations, data analysis and data visualisations are done using Python coding language in Spyder. The derivation and simplification of equations for the development of the analytical method, has been done using Maplesoft (Maplesoft, 2022). By performing sample checks between outcomes from Maplesoft and Spyder, the risk of execution errors minimized.

1.4. Terms and definitions

IGU elements, configuration and direction of loads
In Figure 12 the different elements of a (cold-bent) IGU are shown.

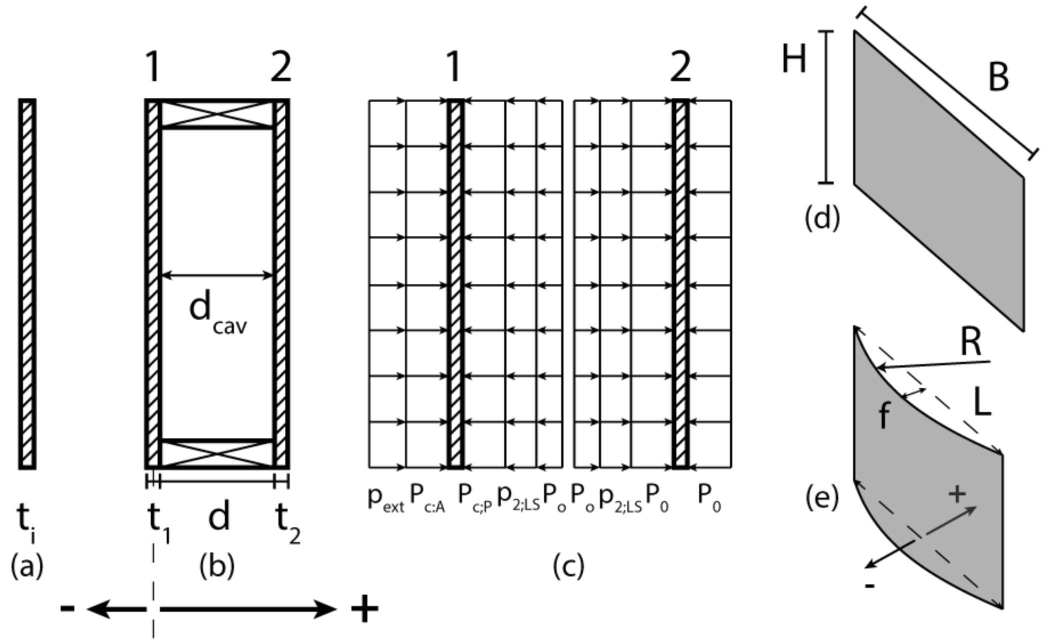

Figure 12: IGU elements, configuration and direction of loads

(1) **Glass plate,** Figure 12 (a), is a single sheet of glass, also referred to as **single glazing.**
- All glass plates are considered as **monolithic.**

(2) **Glass pane** (b) is referred to when a glass plate is part of an IGU.
- All IGU's are considered as **double** glazed IGU's (**DGU**).

(3) **Glass thickness**, referred to as $t_{pl;i}$ in mm (a, b), is the thickness of a monolithic glass plate.

(4) **Spacer distance**, referred to as d in mm (b), is the width of the spacer between two glass panes of an IGU.
- Since the spacer is considered as rigid, spacer distance d is constant.

(5) **Cavity distance**, referred to as d_{cav} in mm (b), is the distance between the two glass panes in the centre $\left(\frac{H}{2}, \frac{B}{2}\right)$ of an IGU.

(6) The **exterior plate** is referred to as plate 1, and is the reference point for directions.

(7) The **interior plate** is referred to as plate 2, and is in the positive direction compared to plate 1.

(8) **Barometric pressures** are referred to as P_c in kN/m^2 (c).

(9) **Effective pressures** are referred to as p in kN/m^2 (c).
- In the overview (a, b, c), the loads going from left to right, are in the **positive direction.**
- The loads going from right to left, are in the **negative** direction.
- All positive loads are illustrated on the left side of the plate, the negative loads are illustrated on the right side of the plate.

(10) The **IGU** (b), is considered to be **hermetically sealed**.

(11) The **IGU** (b), can be simplified to 2 separate plates, which have loads acting on both sides of the plate (c).
- For example, if the barometric pressure $P_{c;P}$ at the time of production is the same as that of the time of application $P_{c;A}$, the pressures cancel each other out.
- In case of a positive external pressure p_{ext} on the exterior of the IGU, the load is shared by the exterior (**windward**) and interior plate (**leeward**). The resulting positive pressure on the exterior plate is $p_1 = p_{ext} - p_2$. The resulting positive pressure on the interior plate is p_2.

(12) **Isochoric pressure** P_o (c), is a pressure inside the IGU, expressed as the difference between the pressure inside the cavity and the pressure outside of the cavity. The difference in pressure depends upon:

- Differences in barometric pressure between hermetically sealing of the cavity ($P_{c;P}$) and application ($P_{c;A}$).
- Height difference between hermetically sealing of the cavity and current state ($P_{o;H}$).
- Temperature differences between the exterior, inside and interior of the IGU ($P_{o;c}$).
- Deformations due to external pressure loads ($P_{o;LS}$).
- Deformations due to cold-bending of the IGU ($P_{o;CB}$).

(13)Isochoric overpressures result in a negative effective pressure on the exterior plate, and a positive effective pressure on the interior plate. The opposite holds for isochoric underpressures.

(14) **Final combined effective pressure** is referred to as $p_{o;F}$ in kN/m^2, which is the sum of effective pressures acting in positive direction of the interior plate of the IGU.

(15) Plate or IGU **height** (d) is referred to as H in mm, and is considered as the **straight** edge of the curved plate or IGU.

(16) Plate or IGU **width** (d) is referred to as B in mm, and is considered at the **curved** edge of the curved plate or IGU.

(17) **Radius** (e) of the plate is referred to as R in mm, which defines the extent of curvature $\left(\kappa = \frac{1}{R}\right)$ of the single curved plate or IGU, i.e., a small value of R results a high curvature. Calculation of R is based on the geometry of a circle.

(18) L is the **span** of a single curved plate or IGU in mm.

(19) f is the **deformation height** of the plate IGU, also referred to as sag, at midspan of the curved edge $\left(\frac{L}{2}\right)$.

(20) All plates are curved towards the **exterior** side of the IGU (e), i.e., in the **negative** direction.

(21) **Volume of curvature** under a curved plate is referred to as ΔV_i, in mm^3, which is the difference in volume between the flat and curved state of the plate.

(22) **Volume of deformation** of a (curved) plate due to external loads is referred to as v_i, in mm^3, which is the difference in volume between the deflected on undeflected state of a (curved) plate.

(23) The **reference cavity volume** is referred to as V in mm^3. Volumes below curved plates ΔV_i, and volumes of deformation v_i can be added or subtracted from the cavity volume (V_o).

- The exterior plate of the IGU is used as reference for summation of the volumes. For example, the cavity volume after due to cold-bending is $V_{o;CB} = V + \Delta V_1 - \Delta V_2$.
- In case of a positive external load on the exterior of a cold-bent IGU, the cavity volume is $V_{o;CB+LS} = V + \Delta V_1 - v_1 - \Delta V_2 + v_2$.

(24) For calculations of single plates only, the radius, sag, volume of curvature and volume of deformation are all considered as positive values.

Direction of forces and stresses

In Figure 13 the direction of forces and stresses are defined in their positive direction. In relation to Figure 12.a, b and c, the positive z-direction is from left to right, the positive x-direction is directing outwards of the screen / paper and the positive y-direction is from top to bottom. In relation to Figure 12.d en e, the positive z-direction is indicated with the positive arrow, the x-direction is along the plate width / span and the y-direction is along the plate height.

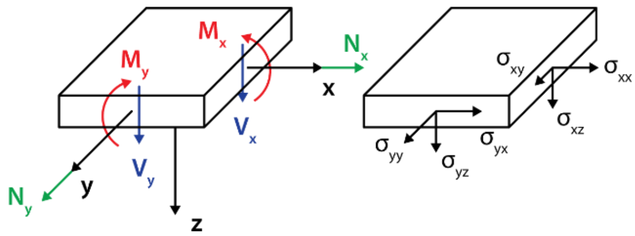

Figure 13: Direction of forces and stresses

2. Literature study

In this chapter, the literature study which is conducted in line with the research goals, questions, objectives and scope, is presented. First, the mechanical properties of float glass are discussed. Second, additional specifications of curved glass compared to flat glass are considered. The focus in this paragraph is on cold-bent glass, including references to practical examples. Furthermore, the distinction of the three phases, as discussed in Chapter 1.3, is elaborated in this paragraph. Third, the physical and structural behaviour of a hermetically sealed cavity is discussed. After that, structural mechanics theories, which are in line with the boundary conditions from the distinct stages, are considered. Last, the setup and validation of the geometrically nonlinear numerical modelling using DIANA FEA, which is used throughout this thesis, is discussed.

2.1. Properties of float glass

In this paragraph, the material, mechanical and design properties of float glass are discussed. Most information in this paragraph is retrieved from the reader of the course on structural glass at the TU Delft, CIE4285 (van der Velden & Nijsse, 2019).

2.1.1. Float glass production

The most used application of glass in the build environment is that of float glass, which is also used for the cold-bending of glass plates. The float line process, in which the production of annealed glass (AN) is realised, is shown in Figure 14. The most common type of glass used for the production of float glass is soda-lime-silica glass ($Na_2O{\cdot}CaO{\cdot}SiO_2$). The raw materials, which include silica sand, soda ash, limestone and salt cake are mixed in with recycled broken glass (or cullet). Burner flames melt the chemical materials at temperatures of approximate 1600˚C or above. A refinement furnace slightly cools the glass to a temperature of around 1100-1300˚C and removes air bubbles. The glass is then poured onto a melted tin bath, which evenly spreads the glass to ensure uniform thickness and width. The glass is then gradually cooled from 500˚C to 100˚C, which is called annealing. After inspection, the glass is cut into the required length. Float lines have a length of up to 600m and produce 24 hours a day, 7 days a week, for periods up to 16 years (Glass for Europe, 2020). It is advised to keep elements within the size the 'Jumbo' plates, which are 3.21x6.0m. Otherwise, significantly higher costs and delivery time should be considered. Furthermore, the most commonly used glass thicknesses are 8, 10 and 12mm. In general glass thicknesses range between 4mm and 25mm, however, similar to case plate sizes, glass thicknesses outside the range of common thicknesses are expensive and can be dangerous to handle.

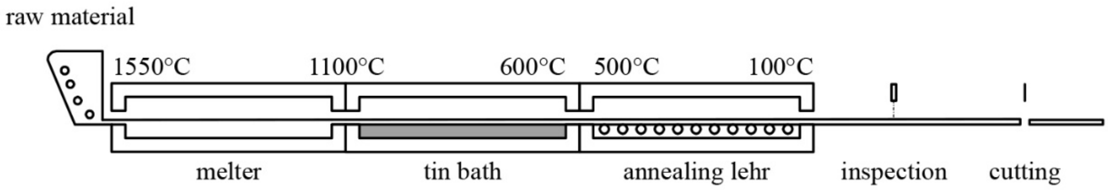

Figure 14: Annealed float glass production line (van der Velden & Nijsse, 2019)

2.1.2. Brittle behaviour

Glass is a brittle material, as it shows little deformation before it fractures very rapidly. Glass has an almost perfect linear elastic isotropic behaviour under loading, as shown in stress-strain diagrams in Figure 15. Brittleness is however not a desirable property of a (structural) building material and in particular not very suited to bend under ambient temperatures.

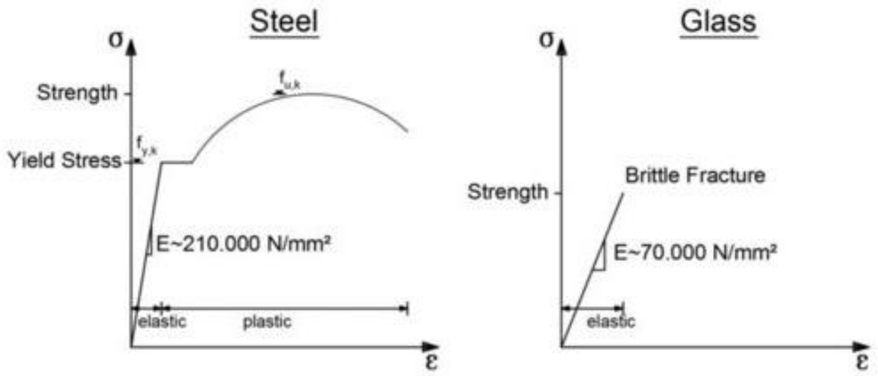

Figure 15: Stress-strain curves of steel and glass (Pölzl, 2017)

2.1.3. Safety strategies

The risk of brittle fracture can be reduced with safety strategies to increase the bending tensile strength of glass, such as thermal and chemical treatment, and with design strategies, such as lamination and use of interlayers. Since chemical treatment is not a frequent practice and the lamination of glass lies outside the scope of this thesis, only the safety strategy of thermal treatment is considered.

Thermal treatment

The tempering of glass is a common practice to increase the tensile bending strength of glass. The practice, as shown in Figure 16, is conducted by first heating the glass to a temperature of around 600˚C. Then, the outer edge of the glass is rapidly cooled while the inside is still hot. As the inside gradually cools, it tries to shrink and pulls the already cold edge inside. Thereby, the outer edge is permanently pulled into compression.

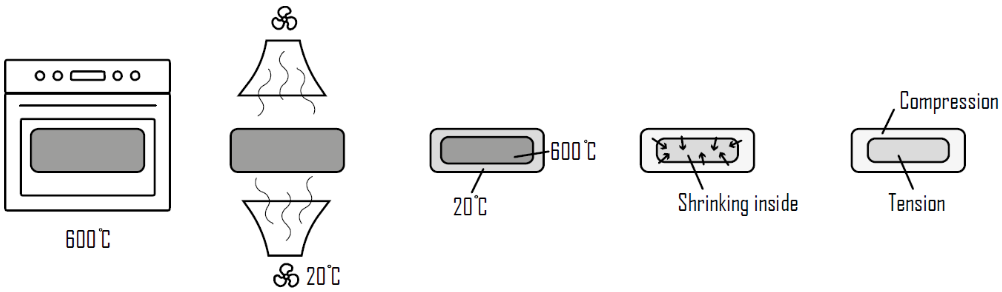

Figure 16: Tempering of glass (van der Velden & Nijsse, 2019)

In terms of thermal treatment, there is the gradation of heat-strengthened glass (HSG) and the gradation of fully tempered glass (FTG). Both glass types are heat treated by using the same process, however for HSG the cooling rate is slower, resulting in a lower tensile strength. According to (NEN 2608, 2014), both HSG and FTG can be considered as prestressed glass. Annealed glass is not considered as a prestressed glass. The prestress in HSG and FTG makes the glass suitable for the application of cold-bending, as is shown in Figure 24. The thermal prestresses (a, d) are added to cold-bending stresses (b, e), based on the principle of superposition, resulting in the combined stresses (c, f).

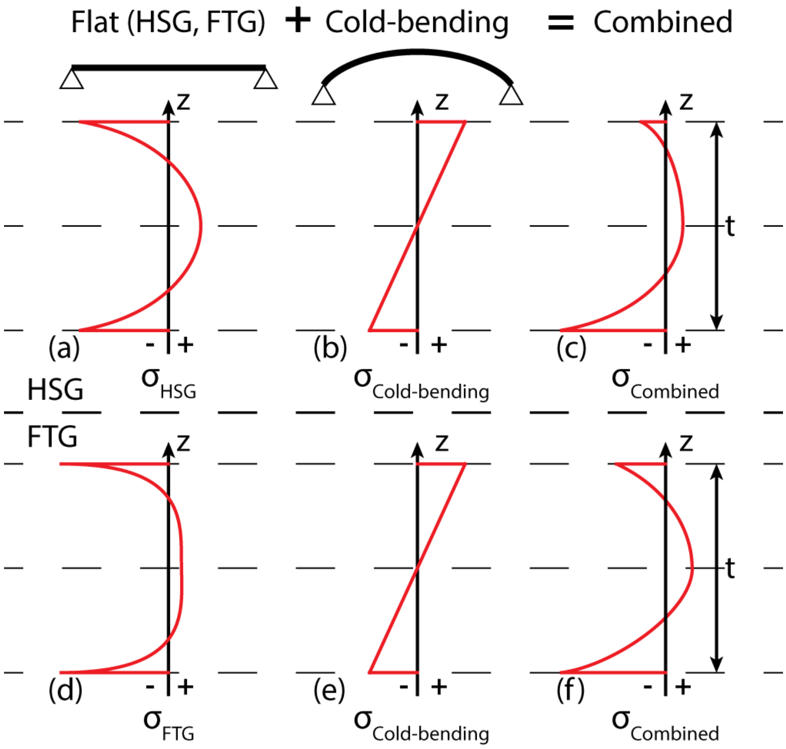

Figure 17: Principle of superposition for stresses in heat threated cold-bent glass, redrawn from (Pölzl, 2017) & (van der Velden & Nijsse, 2019)

2.1.4. Design values

The material properties in Table 2 are considered for soda-lime-silica glass and used throughout this thesis.

Table 2: Material properties glass (NEN 2608, 2014)

Property	***Symbol***	***Soda-lime-silica glass***	***Units***
Density (at 18˚C)	ρ	2500	kg/m^3
Modulus of elasticity	E	70000	N/mm^2
Poisson's ratio	ν	.23	-

The calculation of the design values for the tensile bending strength of HSG and FTG is done according to (NEN 2608, 2014). Cold-bending is considered as a permanent load (P), comparable to that from self-weight. Live loads (L) are simplified to those from wind only, having a load time of 5 seconds. Furthermore, a distinction is made between the edges (E) and middle zone (M) of the plate. This leaves four different design values per glass type. The design values are calculated using equation (1) and presented in Table 3, including the factors per load case.

$$f_{mt;u;d} = \frac{k_e * k_a * k_{mod} * k_{sp} * f_{g;k}}{\gamma_{m;A}} + \frac{k_e * k_z * (f_{b;k} - k_{sp} * f_{g;k})}{\gamma_{m;V}} \qquad (1)$$

In which:

$f_{mt;u;d}$ is the design value of the tensile bending strength of prestressed glass, in N/mm²;

k_e is the factor for the edge quality of the glass pane;

k_a is the factor for the surface effect;

k_{mod} is the modification factor, depending on the load duration and reference period;

k_{sp} is the factor for the surface structure of the glass pane;

$f_{g;k}$ is the characteristic value of the tensile bending strength of glass, in N/mm², whereby $f_{g;k} = 45$ N/mm²;

$\gamma_{m;A}$ is the material factor of glass, whereby:

- $\gamma_{m;A} = 1.6$ for situation in which wind or isochoric pressure is the governing live load.
- $\gamma_{m;A} = 1.8$ for other situations;

k_z is the factor for the zone of the plate;

$f_{b;k}$ is the characteristic value of the tensile bending strength of prestressed glass, in N/mm²;

$\gamma_{m;V}$ is the material factor for the pretension of prestressed glass, whereby $\gamma_{m;V} = 1.2$.

Table 3: Design values of the tensile bending strength of prestressed glass, including calculation factors (NEN 2608, 2014)

Glass type	E/M	L/P	$f_{mt;u;d}$ [N/mm²]	k_e	k_a	k_{mod}	k_{sp}	$f_{g;k}$ [N/mm²]	$\gamma_{m;A}$	k_z	$f_{b;k}$ [N/mm²]	$\gamma_{m;V}$
HSG	M	P	28.08	1	1	.29	1	45	1.8	1	70	1.2
HSG	E	P	28.08	1	1	.29	1	45	1.8	1	70	1.2
HSG	M	L	48.96	1	1	1	1	45	1.6	1	70	1.2
HSG	E	L	48.96	1	1	1	1	45	1.6	1	70	1.2
FTG	M	P	63.50	1	1	.29	1	45	1.8	1	120	1.2
FTG	E	P	63.50	1	1	.29	1	45	1.8	.9	120	1.2
FTG	M	L	90.63	1	1	1	1	45	1.6	1	120	1.2
FTG	E	L	84.38	1	1	1	1	45	1.6	.9	120	1.2

2.1.5. Principal stresses

Since glass is a brittle material, the maximum 2D principal stress theory, based on Mohr's theory (Hartsuijker, 2001), is used to calculate the stresses. The equations to calculate the 2D principal stress in the x-y, y-z and x-z plane are shown below, in equation (2)-(4). The normative stress is the maximum of the 2D principal stresses, equation (5). The normal and shear stress components of the plates, necessary to calculate the principal stresses, are given in equation (6) and (7). The out of plane stresses are considered to be zero. The directions of forces and stresses are shown Figure 13.

$$\sigma_{xy} = \frac{\sigma_{xx} + \sigma_{yy}}{2} + \frac{\sqrt{(\sigma_{xx} - \sigma_{yy})^2 + 4\tau_{xy}^2}}{2} \quad (2)$$

$$\sigma_{yz} = \frac{\sigma_{yy} + \sigma_{zz}}{2} + \frac{\sqrt{(\sigma_{yy} - \sigma_{zz})^2 + 4\tau_{yz}^2}}{2} \quad (3)$$

$$\sigma_{xz} = \frac{\sigma_{xx} + \sigma_{zz}}{2} + \frac{\sqrt{(\sigma_{xx} - \sigma_{zz})^2 + 4\tau_{xz}^2}}{2} \quad (4)$$

$$\sigma'_{max} = \max(\sigma_{xy}, \sigma_{yz}, \sigma_{xz}) \quad (5)$$

Whereby:

$$\sigma_{xx} = -\frac{N_x}{H * t} + \frac{6 * M_x}{H * t^2}, \qquad \sigma_{yy} = -\frac{N_y}{B * t} + \frac{6 * M_y}{B * t^2}, \qquad \sigma_{zz} = 0 \quad (6)$$

$$\tau_{xy} = 0, \qquad \tau_{yz} = \frac{6 * V_y}{B * t}, \qquad \tau_{xz} = \frac{6 * V_x}{L * t} \quad (7)$$

In which:

$\sigma_{xy}, \sigma_{yz}, \sigma_{xz}$	are the 2D principal stresses, in N/mm²;
$\sigma_{xx}, \sigma_{yy}, \sigma_{zz}$	are the normal stresses, in N/mm²;
$\tau_{xy}, \tau_{yz}, \tau_{xz}$	are the shear stresses, in N/mm²;
σ'_{max}	is the maximum 2D principal stress, in N/mm²;
N_x, N_y	are the normal forces, in N;
M_x, M_y	are the bending moments, in Nmm;
V_x, V_y	are the shear forces, in N;
H	is the height of the plate, in mm;
B	is the width of the plate, in mm;
t	is the thickness of the plate, in mm.

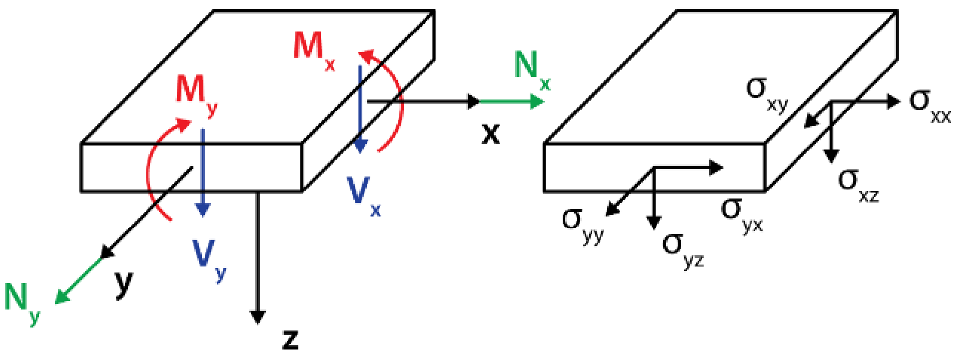

Figure 18: Direction of forces and stresses

2.2. Cold bending of glass

Curved glass has an increased stiffness against out of plane loads, which can be realised by applying a single or double curvature. The process of cold-bending glass plate into a single curvature, can be split into three stages. The first stage is the cold-bending process itself, which is referred to as the 'Bending phase'. The second stage is the fixation of the curved glass onto a substructure, which is referred to as the 'Fixation moment'. Last is the 'Use phase', which considers the in-service time of the curved glass. Below, first the principles of curved glass are considered. Thereafter, the three stages are elaborated on with practical examples.

2.2.1. Curved glass

The increased stiffness of curved structures against out of plane forces is something that has already understood for more than 6000 years. The Romans were the first to use the principle of arches in large monumental structures, of which the Titus Arch in Rome (Figure 19) is the oldest example still existing today (Cartwright, 2013). The principle of curved structures relies on the fact that out of plane forces are transferred not only via bending forces, but also via axial forces (Figure 20). The larger the curvature, the more out of plane forces are transferred axially. In the case of an arch as a perfect inverted catenary, all out of plane forces are transferred axially and no bending moments occur. Building components such as concrete and bricks, but also glass, have a much larger compressive strength than tensile strength, which makes them stiffer with respect to axial forces. Due to the increased stiffness of curved structures, they can be designed thinner and lighter compared to flat alternatives.

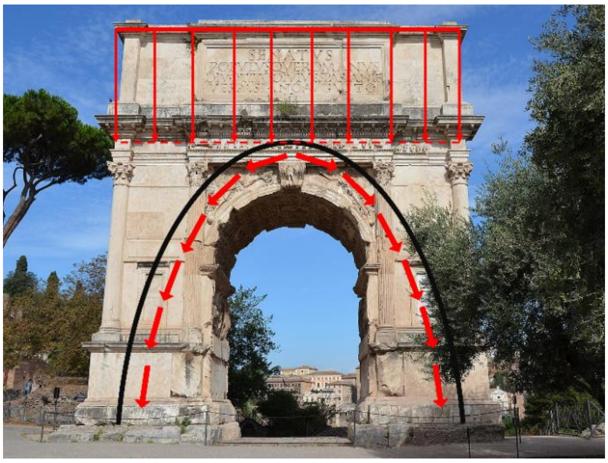

Figure 19: Schematic transfer of forces

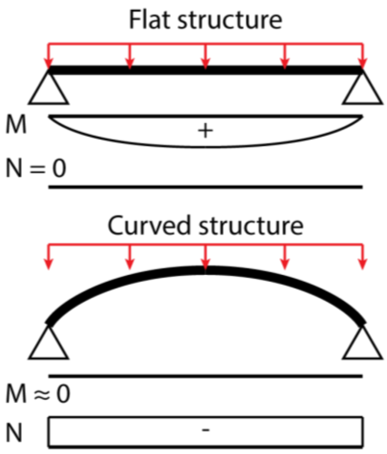

Figure 20: Simplified load systems

The stiffness of flat rectangular plates can be increased by introducing either a single or double curvature, the latter is also known as twisting (Figure 21). In line with the scope of this thesis, the focus will be on single curved plates only. The structural performance of cold-bent twisted plates is researched by (Staaks, 2003) and (Eekhout, Lockefeer, & Staaks, 2012). In Chapter 9 is discussed how the findings of this research and that of the research on cold-twisted glass, can be combined for future research.

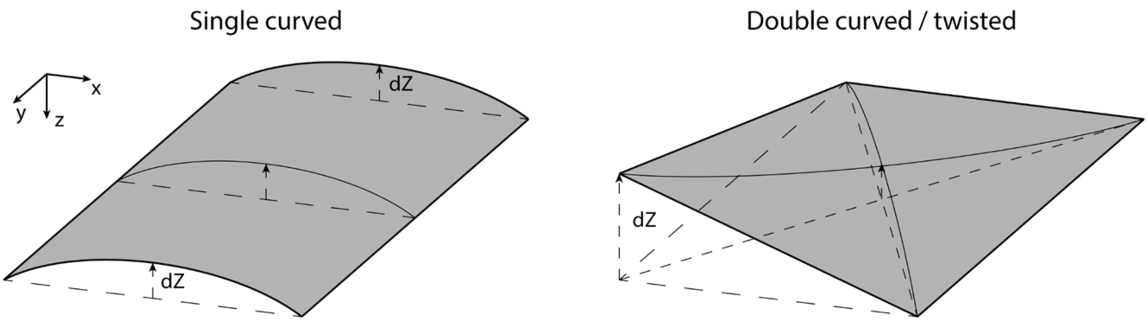

Figure 21: Two types of rectangular plate bending, single curved vs. twisted

2.2.2. Bending phase

During the cold-bent phase, a flat glass plate is curved towards a desired shape under ambient temperatures. Practical applications of cold-bent glass show that this has been done in a variety of ways. One of the most used applications is that of bending glass over a curved substructure. An example of this application are the cold-bent glass panels used for the Spartherm Innovationszentrum in Melle (van de Rotten, 2019), of which the mock-up is shown in Figure 22. The principle of bending over a curvature is also often used in case of twisted glass (van Herwijnen, 2008), (Eekhout, Lockefeer, & Staaks, 2012) and (Staaks, 2003). Considering that most buildings are unique, the application of cold-bending over a substructure is project specific.

Another example of a single curved cold-bending application is used for the Van Gogh Museum in Amsterdam (Bijster, Noteboom, & Eekhout, 2016). For this project, a specially built robotic machine is used (Figure 23), that holds the centre of the glass using a vacuum machine and bends the edges using roller arms. The arms are calibrated for the required radius of curvature the glass has to reach. The technique is also be referred to as 'three-point bending' or 'four-point bending', depending on the horizontal distance between the suction cups of the vacuum machine.

Figure 22: Mock-up Spartherm Melle (Octatube, 2021)

Figure 23: On site bending using a robotic vacuum machine (Bijster, Noteboom, & Eekhout, 2016)

In general, it can be concluded that the execution of the cold-bending process is project specific, and thus boundary and load conditions differ per project. Still, all bending applications have in common that the bending stresses should not exceed strength limits as a result of too large curvatures. The curvature of single curved glass plates can be expressed as $\kappa = \frac{1}{R}$, in which the radius is a common design factor. The equation for curvature shows that larger curvatures are equal to smaller radii.

Based on the curvature, a simplified expression can be derived to examine cold-bending stresses, as presented in (Molter & Wolf, 2011) and derived in (Janssen, 2017). The derivation, which is based on beam theory, is as follows:

Cold-bending stress:	$\sigma = \frac{M}{W}$	$\sigma_{CB} = \frac{M}{W}$	(8)
Euler-Bernoulli beam theory:	$M = E * I * \frac{d^2w}{dx^2}$	$\sigma_{CB} = \left(E * I * \frac{d^2w}{dx^2}\right) * \frac{1}{W}$	(9)
Radius of curvature:	$\frac{d^2w}{dx^2} = \frac{d\theta}{dx} = \kappa = \frac{1}{R}$	$\sigma_{CB} = \left(E * I * \frac{1}{R}\right) * \frac{1}{W}$	(10)
Moment of inertia:	$I = \frac{1}{12} * b * t^3$	$\sigma_{CB} = \left(E * \frac{b * t^3}{12} * \frac{1}{R}\right) * \frac{1}{W}$	(11)
Elastic section modulus:	$W_{el} = \frac{1}{6} * b * t^2$	$\sigma_{CB} = \left(E * \frac{b * t^3}{12} * \frac{1}{R}\right) * \frac{6}{b * t^2}$	(12)
Cold-bending theory:		$\sigma_{CB} = \frac{E * t}{2 * R}$	(13)

In which:

σ_{CB}	is the stress due to cold bending curvature, in N/mm²;
M	is the moment due to curvature of a beam, in Nmm;
W_{el}	is the elastic section modulus of the beam, in mm³;
I	is the moment of inertia of the beam, in mm⁴;
w	is the deflection of a beam, in mm;
θ	is the rotation of deflection of a beam, in radian;
κ	is the curvature, in mm⁻¹;
R	is the radius of curvature, in mm;
b	is the width of the beam, in mm. In the context of this thesis referred as plate height H;
t	is the thickness of the beam, in mm;
E	is the Young's modulus of glass, in N/mm²;

After the design radius of curvature is reached during the cold-bent process, the plate has undergone a large displacement. The definition of large displacements according to (Young & Budynas, 2002), is that of deflections larger than ½ times the thickness of the plate. Looking at for example the deformation height of the largest curvature in the Van Gogh Museum, $R = 11500mm \rightarrow f = 140.6\ mm \gg \frac{1}{2} * t = 5mm$, it can be concluded that the deflections as a result of cold-bending can be considered as large. Due to these large deformations, stresses in the middle plane of a plate must be taken into consideration when deriving differential plate equations (Timoshenko & Woinowsky-Krieger, 1989). By doing so, nonlinear equations are obtained. Furthermore, the edges of a cold-bent glass plate are free to move during the bending process, resulting in a considerable effect upon the magnitude of displacements and stresses of the plate. From these observations can be concluded that for the 'Bending phase', linear theories become irrelevant and geometrically nonlinear theory must be considered. A powerful tool to calculate the geometrically nonlinear behaviour of plate elements, is finite element analysis, which is elaborated in Chapter 2.5.

2.2.3. Fixation moment

When the cold-bent glass plate has reached its design radius of curvature, it has to be fixed onto a substructure in order to maintain its shape. After fixation, the glass wants to 'push back' against the fixed elements due to its restrained elastic deformation energy. The type of fixing therefore plays a crucial role in the way the boundary conditions are considered, and are different from the load conditions under which the curved glass has been bend. The 'Fixation moment' is therefore considered as the second stage in the cold-bending of glass.

Like the different bending techniques, there are also different techniques to fix a cold-bent glass plate into position. For the van Gogh Museum, clamp plates are installed close to the corners of the curved glass. These clamp plates cause a redistribution of stresses compared to the 'Bending phase', as can be seen in Figure 24. The figure also shows the differences in load conditions between the two stages.

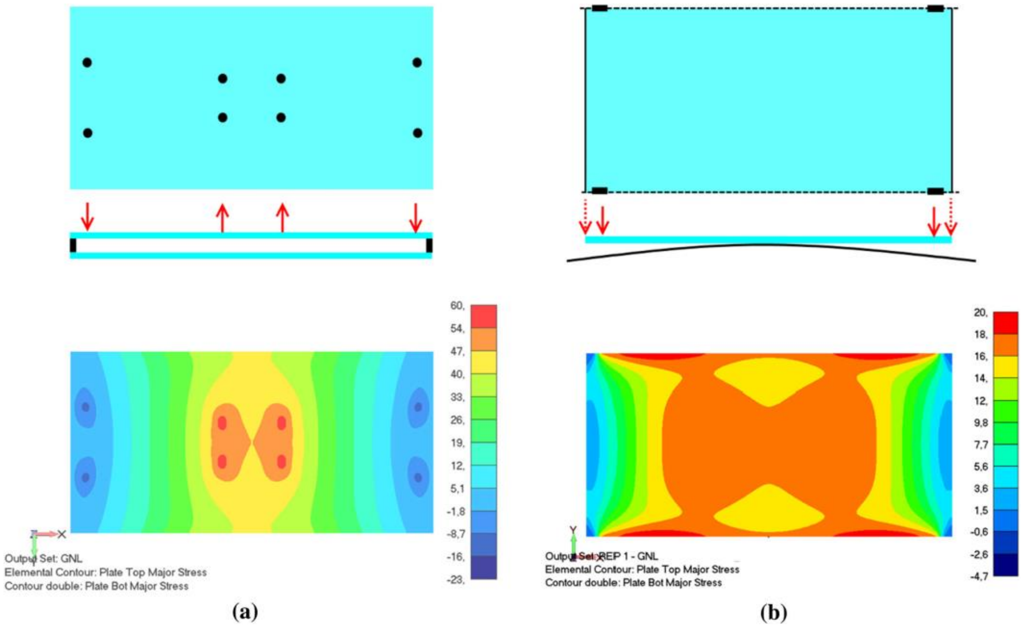

Figure 24: Differences in boundary conditions and stress distributions, between 'Bending phase' and 'Fixation moment' (Bijster, Noteboom, & Eekhout, 2016).

Another method of fixing a curved glass plate is by rosettes, of which an example is shown in Figure 25. Furthermore, glass spider mountings have been used to fix cold-bent glass (Figure 26). The fixings for the cold-bent glass for the project of Spartherm in Melle are similar to line supports, in combination with clamp plates (Figure 27).

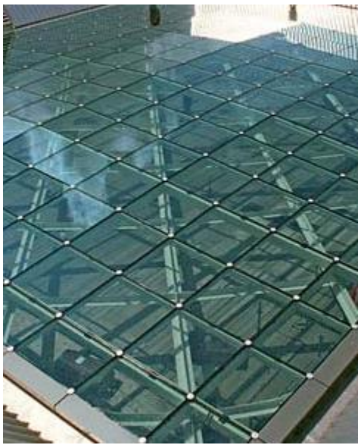

Figure 25: Glaskap Essent, 's-Hertogenbosch (ABT bv, 2006)

Figure 26: Floriade Paviljoen, Haarlemmermeer (Octatube, 2002)

Figure 27: Spartherm, Melle (Octatube, 2021)

2.2.4. Use phase

The ‘Fixation moment’ is followed by the ‘Use phase’, in which the external and internal live loads during the service lifetime of the curved glass are considered. External live loads are for example due to wind, snow or maintenance. Internal loads are only considered for IGU’s and occur due to differences in isochoric pressure. Both internal and external loads can be determined using standardized codes. Depending on building specifications such as height, location and shape, all kinds of live load combinations have to be considered, in order for the element to be conform norms. Since all building projects are unique, there are endless combinations possible. In order to simplify the load conditions for the ‘Use phase’, a unity pressure load of 1 kN/m^2 is used as external live load. Point and line loads are left out of consideration.

As a result of the elastic deformation of the cold-bent plates, part of the stress limit of glass is already utilised by permanent bending stresses. The extent of utilisation of cold-bent stresses depends on the radius of curvature and thickness of the plate. During the ‘Use phase’, deformations due to live loads also cause stresses, which could add to the already permanent cold-bending stresses. Such encounters of ‘unfavourable’ stress combinations must be accounted for in design. Stress combinations due to live loads and cold-bending loads can however also work in ‘favour’ of the curved glass. Due to the increased stiffness of the curved glass, deflections will be less. Furthermore, due to cold-bending the glass is ‘prestressed’, against loads opposite to the direction of curvature. In Figure 28, two examples of permanent and live loads are shown. The shown stress distributions are illustrative. The combination of stresses is based on the principle of superposition and is elaborated on as follows:

Due to the heat treatment of glass (HSG or FTG), a permanent prestress is present in the glass (a). This prestress allows for additional permanent cold-bending stresses (b), up to the point the tension stresses in the upper half of the plate exceed the prestress (c). In the ‘Use phase’, additional stresses occur on top of the combined prestress and cold-bending stresses. In case of a favourable live load (d), the glass is pushed back, and cold-bending stresses and live load stresses partially cancel each other out (e). In case of unfavourable live load conditions (f), the curved glass is pushed into a larger curvature. In that case, cold-bending stresses and live load stresses enhance each other (g), which can lead to failure of the glass. It is crucial to design the curved glass with a sufficiently low utilisation of cold-bending stresses, such that there is enough capacity for live load stresses.

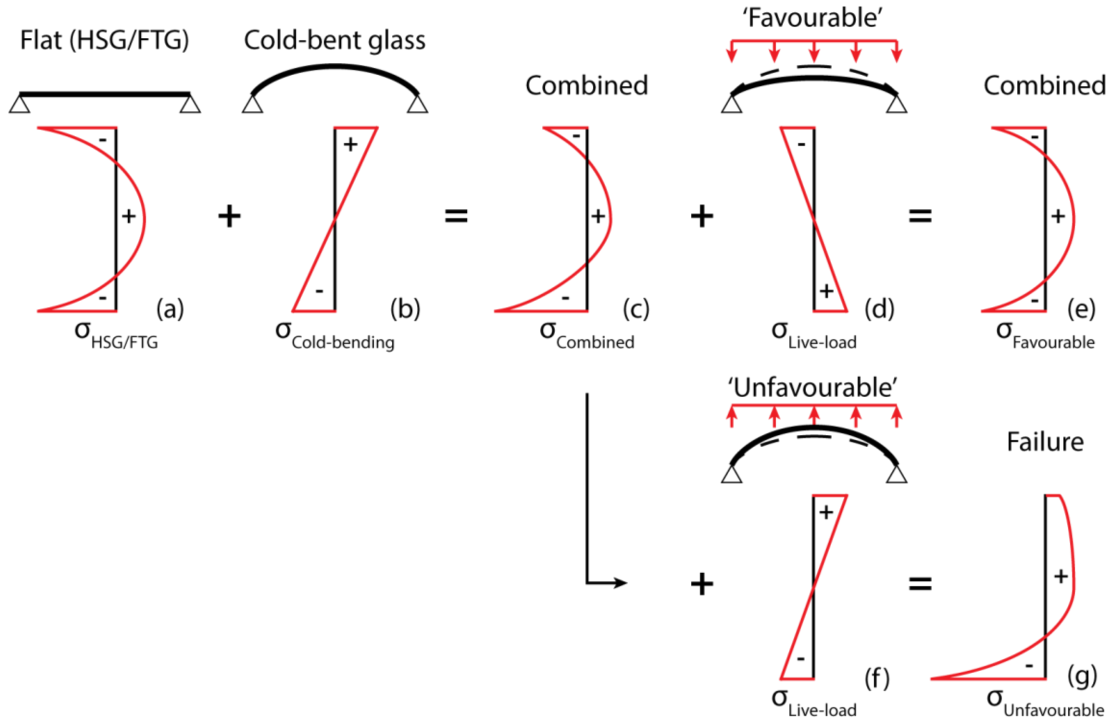

Figure 28: Superposition of permanent and live load stresses in cold-bent glass plates

From the superposition of the stresses, it can be concluded that there is a trade-off in stiffness, between the ‘Bending phase’ and ‘Use phase’. During the ‘Bending phase’, a larger plate thickness, results in higher cold-bending stresses. In the ‘Use phase’ however, a thicker plate means a stiffer structure, which will deflect less and therefore results in lower live-load stresses. The same principle holds for the radius of curvature. During the ‘Bending phase’, the cold-bending stress increases as the curvatures increase, which results in a stiffer structure. In the design of cold-bent glass, the optimum between these two trade-offs must be sought for.

An example of this trade-off is visualised in (Janssen, 2017), for which the cold-bent stress theory as shown in equation (13) is extended with a simplified equation for stresses due to live loads, equation (14). The live load stress component is incorporated into the cold-bending theory is as follows:

Live load bending stress: $\sigma = \frac{M}{W}$ $$\sigma_{LL} = \frac{M}{W} \tag{14}$$

Elastic section modulus: $W_{el} = \frac{1}{6} * b * t^2$ $$\sigma_{LL} = \frac{6 * M}{b * t^2} \tag{15}$$

Total stress: $\sigma_{Ed} = \sigma_{CB} + \sigma_{LL}$ $$\sigma_{Ed} = \frac{E * t}{2 * R} + \frac{6 * M}{b * t^2} \tag{16}$$

In which:

σ_{LL}	is the stress due to live loads, in N/mm²;
M	is the moment due to live loads, in Nmm;
W_{el}	is the elastic section modulus of the beam, in mm³;
R	is the radius of curvature, in mm;
b	is the width of the beam, in mm. In the context of this thesis referred as plate height H;
t	is the thickness of the beam, in mm;
E	is the Young’s modulus of glass, in N/mm²;

In equation (16), the trade-off in terms of thickness is clearly visible. In the ‘Bending phase’ part of the equation, the thickness parameter is above the fraction bar ($\gg t \rightarrow \gg \sigma_{Ed}$), in the ‘Use phase’ part of the equation the quadratic thickness is below the fraction bar ($> t \rightarrow \gg \sigma_{Ed}$). To visualise this trade-off, the following illustrative values are used: $f_{mt;u;d} = 45$ N/mm², $b = 1$ m, $M = 0.3$ kNm, $E = 70000$ N/mm², and $R = 20$ m. Figure 29 shows a clear trade-off in thickness of the glass, with an optimum thickness of t_{opt} =12.7 mm, and a minimum and maximum thickness of t_{min} = 7.5 mm and t_{max} =23.9 mm, respectively. The theory does however not take into account the increased stiffness as a result of the curvature.

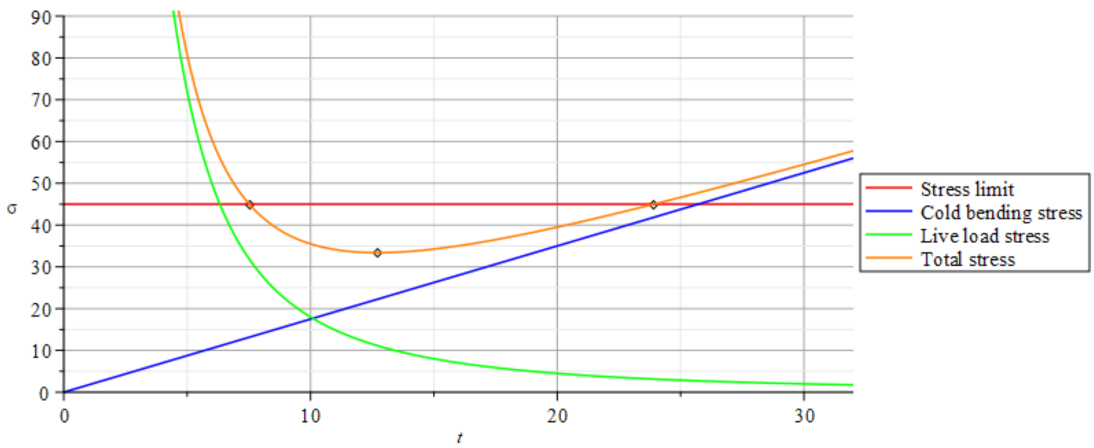

Figure 29: Simplified cold-bending stress theory (Janssen, 2017)

2.3. Cavity pressure

In Chapter 1.2.1, methods are discussed which consider cavity pressure in relation to structural performance of an IGU. In the upcoming paragraphs, the development behind these methods is discussed in further detail.

2.3.1. Combined gas law

In order for a cavity to function as an insulating layer, it must be hermetically sealed. If the cavity is not free of leaks, air currents will flow in freely, which increases heat transfer through convection. Furthermore, air currents can cause condensation inside the cavity of the IGU. Also, argon or krypton can leak if the cavity is not sealed sufficiently. To prevent thermal diminution, the cavity must be free of leaks and therefore will be considered as airtight. Because of this consideration, the 'Ideal gas law', which is a combination of Boyle's, Gay-Lussac's, Avogadro's and Charles' laws (Clapeyron, 1983), can be applied:

$$PV = nRT \tag{17}$$

In which:

P	is pressure in N/mm^2;
V	is volume in mm^3;
T	is temperature in K;
n	is the amount of substance in mol;
R	is the ideal gas constant in (N/mm^2)·mm^2·K^{-1}·mol^{-1}

By assuming than n and R are constant, the ratio of PV to T can be taken as constant and Avogadro's law can be left out of the consideration. This leaves for Boyle's, Gay-Lussac's and Charles' laws, which is the 'Combined gas law' (Raymond, 2009):

$$\frac{PV}{T} = k \tag{18}$$

In which:

k	is a constant.

When comparing the same substance, under two different sets of conditions (1 and 2), the law can be rewritten to equation (19). In terms of a hermetically sealed cavity of an IGU, the sets of conditions are for example those at the location of sealing the cavity (0) compared to the location of application (cav).

$$\frac{P_1V_1}{T_1} = \frac{P_2V_2}{T_2}, \qquad \frac{P_0V_0}{T_0} = \frac{P_{cav}V_{cav}}{T_{cav}} \tag{19}$$

The Combined gas law can be rewritten as a function for the cavity pressure, with symbol indications similar to (NEN 2608, 2014) and Table 1:

$$P_{o;F} = \frac{T_s}{T_p} * \frac{V}{V - V'} * P_{c;P} \tag{20}$$

In which:

$P_{c;P}$	is the barometric pressure during production at the time of sealing, in kN/m^2;
$P_{o;F}$	is the final combined isochoric pressure inside the IGU, in kN/m^2;
T_p	is the temperature of the filling gas in IGU's during production, in ˚C;
T_s	is the temperature of the filling gas in IGU's during application, in ˚C;
V	is the cavity volume, in mm^3;
V'	is the change in cavity volume in mm^3.

According to (Feldmeier, 2003), the current, or final state isochoric pressure $P_{o;F}$ can be considered as the sum of the barometric pressure at the time of sealing $P_{c;P}$, and the isochoric pressure in the cavity P_o (Figure 30). Therefore, changes in cavity pressure can be caused by:

- Differences in barometric pressure between hermetically sealing of the cavity ($P_{c;P}$) and application ($P_{c;A}$).
- Height difference between hermetically sealing of the cavity and current state ($P_{o;H}$).
- Temperature differences between the place of production and installation of the IGU ($P_{o;c}$).
- Deformations due to external pressure loads ($P_{o;LS}$).
- Deformations due to cold-bending of the IGU ($P_{o;CB}$).

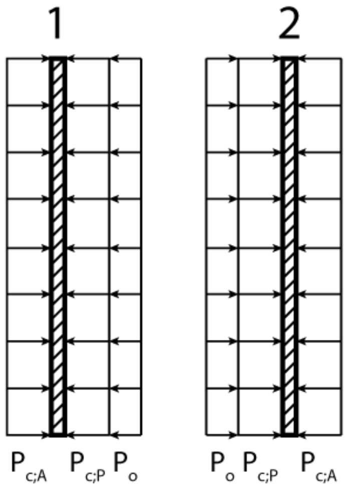

Figure 30: Sum of barometric pressure and cavity pressure changes on the panes of an IGU

Cavity pressure also has a structural role since it enables load sharing between the panes of an IGU. The percentage of load shared by the interior plane is called the Load Sharing Factor (LSF) $\delta_2 = p_2/p_{ext}$, which can be calculated using current standards for a number of boundary conditions (EN 16612, 2019), (NEN 2608, 2014). The amount of external load shared by each pane depends on multiple factors, such as IGU size, cavity width and stiffness of the panes. For symmetric and flat IGU's, larger than 2x2m, the load sharing is around 50% per plate. However, in case of asymmetric IGU's, larger percentages of up to 80% are shared by the stiffer plate. Currently, there are no standards to determine the load sharing of curved IGU's. In the next paragraphs, derivations and simplifications that have led to the development of current standardized methods for calculating load sharing in flat, rectangular IGU's, are shown.

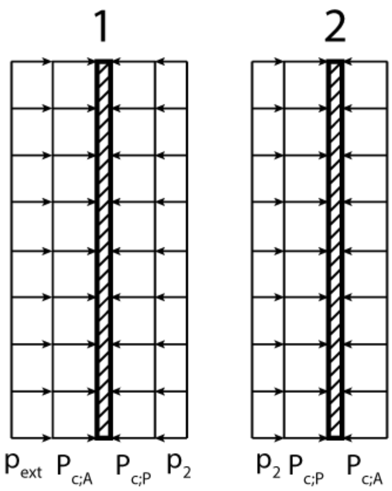

Figure 31: External pressure load shared between glass panes of an IGU

2.3.2. Interactive Nonlinear Analysis of Insulating Glass Units (Vallabhan & Chou, 1986)

An early mention of a theoretical framework to evaluate the load sharing of external pressures in IGU's is that of (Vallabhan & Chou, 1986). In the paper it is concluded that 'compatibility of displacements of the entire unit is achieved when the volume change inside the IGU is exactly equal to the difference in volume between the deformed and undeformed surfaces of each plate'. This means that an equilibrium needs to be found for which holds:

1. The sum of effective pressures shared by the interior and exterior plate is equal to the external pressure.
2. The difference volume of deformation due to these effective pressures, is equal to the volume change inside the cavity.

These requirements translate to equation (21) and (22). The total applied pressure is:

$$p_{ext} = p_1 + p_2 \tag{21}$$

In which:

p_{ext}	is the external pressure load on the exterior plate of the IGU, in kN/m^2;
p_1	is the effective pressure load shared by the exterior plate of the IGU, in kN/m^2;
p_2	is the effective pressure load shared by the interior plate of the IGU, in kN/m^2.

The reduction in cavity volume is:

$$\Delta v = v_1 - v_2 \tag{22}$$

In which:

Δv	is the reduction in cavity volume of the IGU, in mm^3;
v_1	is the volume of deformation due to effective pressure load p_1 in mm^3
v_2	is the volume of deformation due to effective pressure load p_2 in mm^3

Using the Combined gas law, the reduction in cavity volume Δv can be calculated. Since an external pressure is a short-term load, a difference in temperature can be neglected and only Boyle's law remains. Before the external pressure load, the 'state' of the cavity is $P_{c;P}V = k$. During the pressure load, the cavity state is $(P_{c;P} + p_2) * (V - \Delta v) = k$. The combined gas law holds:

$$P_{c;P} * V = (P_{c;P} + p_2) * (V - \Delta v) \tag{23}$$

$$\rightarrow \quad \Delta v = \frac{p_2 V}{P_{c;P} + p_2} \tag{24}$$

In which:

Δv	is the reduction in cavity volume of the IGU, in mm^3;
$P_{c;P}$	is the reference cavity pressure at the time of sealing in N/mm^2;
V	is the reference cavity volume at the time of sealing in mm^3;
p_2	is the effective pressure load shared by the interior plate of the IGU, in N/mm^2.

In equation (24), p_2 is still an unknown, however due to the requirements of equilibrium, a value of p_2 can be found for which both requirements are met. At the time of publication of the paper it was understood that deformation of the plates of an IGU had to be calculated using geometrically non-linear theory with Von Karman plate equations. Due to this nonlinearity an iterative scheme is essential in finding the value of p_2 for which equilibrium is met. In order to simplify the process, the results of the von Karman equations are presented in non-dimensional P-V diagrams. With that, the iterative scheme is as follows:

Step 1: Let $i = 1$ and the pressure on the interior plate be a small increment load p_2.
Step 2: Find the volume of deformation v_2 due to pressure p_2 using the P-V curves.
Step 3: Calculate $\Delta v = p_2 V \; / \; (P_{c;P} + p_2)$.
Step 4: $v_1 = v_2 + \Delta v$.
Step 5: The corresponding pressure p_1 on the exterior plate is determined using the P-V curves. For in-between values, the results are linearly interpolated.
Step 6: Error in total pressure: $\Delta p = p_{ext} - (p_1 + p_2)$.
Step 7: If $\Delta p > 0$, then $p_2^L = p_2$, $i = i + 1$ and p_2 is increased by the load increment. The process is repeated from step 2.
Step 8: If $\Delta p < 0$, then $p_2^U = p_2$ and the iterative process is continued.
Step 9: Average $p_2^a = 1/2 * (p_2^U + p_2^L)$.
Step 10: Calculate Δv due to p_2^a: $\Delta v = p_2^a V \; / \; (P_{c;P} + p_2^a)$.
Step 11: Determine v_2 corresponding to p_2.
Step 12: Calculate $v_1 = v_2 + \Delta v$.
Step 13: Determine p_1 corresponding to v_1.
Step 14: Error in total pressure: $\Delta p = p_{ext} - (p_1 + p_2^a)$. If $|\Delta p / p_{ext}|$ < allowable tolerance ∈, the iteration can be stopped. In the paper the allowable tolerance is kept as 0.001.
Step 15: If $\Delta p < 0$, then $p_2^U = p_2^a$, otherwise $p_2^L = p_2^a$. Steps 9-15 are repeated until the solution converges to the allowable tolerance.

From the iterative scheme can be concluded that by calculating volumes of deformation due to pressure loads, the structural behaviour of the interior and exterior plate is evaluated separately. The Combined gas law functions as a conduit to relate the effective pressures and volumes of deformation between both panes. Although simplified linear methods have proved to be more efficient, the iterative scheme presented in the paper is still relevant as a general framework, for example for the case of geometrically nonlinear deformations.

2.3.3. Determination of Load Sharing in Insulating Glass Units (Wörner, Shen, & Sagmeister, 1993)

In succession to the conclusions and results in the paper by (Vallabhan & Chou, 1986), the determination of load sharing of IGU's due to an external pressure load was further investigated by (Wörner, Shen, & Sagmeister, 1993). In the paper it is concluded that instead of using non-linear deformations, linear deformations suffice in the determination of load sharing. The deflection function of a simply supported rectangular plate under a uniformly distributed pressure load p, is calculated using linear plate theory (Timoshenko & Woinowsky-Krieger, 1989). The equation to calculate the volume between the deformed and undeformed plates is as follows:

$$v_i = \int_0^B \int_0^H w_i \, dxdy = \frac{64B^5Hp_i}{\pi^8 D_i} \sum_{m=1,3,5,..} \sum_{n=1,3,5...} \frac{1}{m^2n^2\left(m^2 + \frac{B^2}{H^2} * n^2\right)^2} \tag{25}$$

Whereby:

$$D_i = \frac{Et_i^3}{12(1-\nu^2)} \tag{26}$$

In which:

v_i	is the volume of deformation of glass plate i due to a pressure load, in mm^3;
B	is the width of the IGU, in mm;
H	is the height of the IGU, in mm;
w_i	is the deflection of the glass plate i at point x, y, in mm;
p_i	is the effective pressure load on glass plate i, N/mm^2;
D_i	is the flexural rigidity of glass plate i in (N/mm^2)·mm^3;
E	is the Young's modulus of glass, whereby $E_g = 70000$ N/mm^2;
t_i	is the thickness of glass pane i, in mm;
ν	is the Poisson's ratio of glass, whereby $\nu_g = .23$;

Due to the linearity of the equation, the load sharing can also be calculated linearly using Boyle's law. To do so, equation (25) is rewritten to: $v_i = A_i p_i$. By substituting equation (25) and (22) into (19), the following equation is derived:

$$(A_1 + A_2)p_2^2 + \left[(A_1 + A_2) * P_{c;P} - p_{ext} * A_1 + V\right]p_2 - P_{c;P} * p_{ext} * A_1 = 0 \tag{27}$$

In case of a symmetric IGU, equation (27) is simplified to:

$$2p_2^2 + \left[2P_{c;P} - p_{ext} + \frac{V}{A}\right]p_2 - P_{c;P} * p_{ext} = 0 \tag{28}$$

2.3.4. Insulating Units Exposed to Wind – Load Sharing and Internal Loads (Feldmeier, 2003)

Further development of the method is conducted in the publication by (Feldmeier, 2003). Using a linear approximation, it is possible to rewrite the quadratic equation (27) to the following expression:

$$p_2 = (1 - \varphi) * (\delta_2 * p_{ext}) \tag{29}$$

Whereby:

$$\varphi = \frac{1}{1 + (v_1 + v_2) * \frac{P_{c;P}}{V}} \tag{30}$$

$$\delta_2 = \frac{v_2}{v_1 + v_2} \tag{31}$$

In which:

p_2	is the effective pressure load on the interior glass plate, in kN/m^2;
φ	is the insulating glass factor, as shown in equation (30);
δ_2	is the relative stiffness of the interior glass plate, as shown equation (31);
p_{ext}	is the external pressure load on the exterior plate of the IGU, in kN/m^2;
v_i	is the volume of deformation of glass plate i due to a pressure load, in mm^3;
$P_{\mathrm{c;P}}$	is the reference cavity pressure at the time of sealing in kN/m^2;
V	is the reference cavity volume at the time of sealing in mm^3.

Instead of calculating the volume of deformation v_i using linear plate theory, the volumes can be calculated using tabulated values, including a factor depending on the shape of the plate. The equation to calculate the volume of deformation is thereby simplified to equation (32), in which B_V is the tabulated value for the glass shape.

$$v_i = A * \frac{a^4}{E * t_i^3} * B_V \tag{32}$$

With equation (32), equation (30) can be simplified to:

$$\varphi = \frac{1}{1 + \left(\frac{a}{a^*}\right)^4} \tag{33}$$

Whereby a^* is the for cavity characteristic length, in mm:

$$a^* = \sqrt[4]{\frac{E}{P_{c;P}} * \frac{d_{cav}}{\frac{1}{t_1^3} + \frac{1}{t_2^3}} * \frac{1}{B_V}} \tag{34}$$

Furthermore, with equation (32), equation (31) can be simplified to:

$$\delta_2 = \frac{t_2^3}{t_1^3 + t_2^3} \tag{35}$$

The findings by (Feldmeier, 2003), have been key in the development of the current standardized methods to determine the load sharing of an IGU exposed to a pressure load.

2.3.5. NEN2608:2014, Appendix B: Load sharing in IGU's (NEN 2608, 2014)

The equation in NEN2608:2014 to calculate 'the resulting pressure in the cavity of a double insulating glass unit p_2, due to an external equally distributed pressure load p_{ext} with load surface B·H on glass pane 1', is as follows:

$$p_2 = (1-\varphi) * \frac{t^3_{blad;2;ser}}{t^3_{blad;1;ser} + t^3_{blad;2;ser}} * p_{ext} \tag{36}$$

In which:

p_2	is the effective pressure load on the interior glass plate, in kN/m²;
φ	is the insulating glass factor, according to equation (33);
p_{ext}	is the external pressure load on the exterior plate of the IGU, in kN/m²;
$t_{blad;i;ser}$	is the equivalent thickness of glass pane i, for serviceability limit state of laminated glass, in mm.

Equation (36) is similar to equation (29) as derived in (Feldmeier, 2003). The insulating glass factor is calculated using equation (33). However, for cavity characteristic length a^*, a slightly different equation is used:

$$a^* = 28.9 * \left(\frac{d_{cav} * t^3_{blad;1;ser} * t^3_{blad;2;ser}}{(t^3_{blad;1;ser} + t^3_{blad;2;ser}) * \chi}\right)^{.25} \tag{37}$$

By considering $E = 70000$ N/mm², $P_{c;P} = 101.325$ kN/m² and $B_V = \chi$, equation (34) and (37) are the same. In the code, the shape factor χ is further elaborated with two more equations, for the specific case of a rectangular IGU. On account of the methods and equations which have led to the currently used standardized methods as discussed above, insights are gained on how to derive and simplify analytical expressions. These insights are used in the development of the analytical method as presented in Chapter 6.

2.3.6. NEN2608:2014, Chapter 6: Isochoric pressures (NEN 2608, 2014)

In NEN2608:2014, equations are given to calculate isochoric pressures inside the cavity of an IGU due to climatic loads and height differences. Equation (38) shows the equation for climatic loads, with a factor for isochoric pressure due to temperature differences.

$$P_{c;o} = C_c * (T_s - T_p) - (P_{c;A} - P_{c;P}) \tag{38}$$

In which:

$P_{c;o}$	is the isochoric pressure due to climatic loads, in kN/m²;
C_c	is the factor for the increase of isochoric pressure due to temperature differences, in kN/m²K, whereby $C_C = 0.340$ kN/m²K;
T_s	is the temperature of the filling gas in IGU's during application, in ˚C;
T_P	is the temperature of the filling gas in IGU's during production, in ˚C;
$P_{c;A}$	is the barometric pressure at the location of application of the IGU, in kN/m²;
$P_{c;P}$	is the barometric pressure during production at the time of sealing, in kN/m².

The equation for an increase in isochoric pressure due to height differences is shown below. The equation only has to be considered in case the height difference is larger than 150 m.

$$P_{H;o} = C_H * (h - h_p) \tag{39}$$

In which:

$P_{H;o}$	is the isochoric pressure due to climatic loads, in kN/m²;
C_H	is the factor for the increase of isochoric pressure due to height differences, in kN/m²/m, whereby $C_C = 0.012$ kN/m²/m;
h	is the height compared to NAP after placement of the IGU, in m;
h_P	is the height compared to NAP during production of the IGU, in m.

2.4. Structural mechanics

In this paragraph, theories of structural mechanics which have similarities to the case of cold-bending of glass into a single curvature, are discussed. First, general principles in relation to the displacements of plates are discussed. Second, the simplification of a 2D plate to a 1D beam is considered. Last, 2D load cases are presented which have similarities to the load-cases from the different stages of cold-bending as discussed in Chapter 2.1.

2.4.1. Plate principles

Rectangular single curved plates are prone to anticlastic bending as a result of the effect of Poisson's ratio (Timoshenko & Woinowsky-Krieger, 1989). This is explained using the following example case in which a simply supported plate is bend out of plane using a moment as shown in Figure 32.a. Due to the deformations, tension will occur in the upper half of the plate, causing lateral elongation (Figure 32.b). Simultaneously compression occurs in the bottom half of the plate, causing lateral contraction (Figure 32.c). As a result of the elongation and contraction, biaxial bending moments occur, resulting in anticlastic bending (Figure 32.d). When considering the cold-bending of glass plates, bending moments occur as a result of large deformations. Depending on size, thickness and curvature, the 2D geometry of a curved glass plate can be heavily influenced by anticlastic bending.

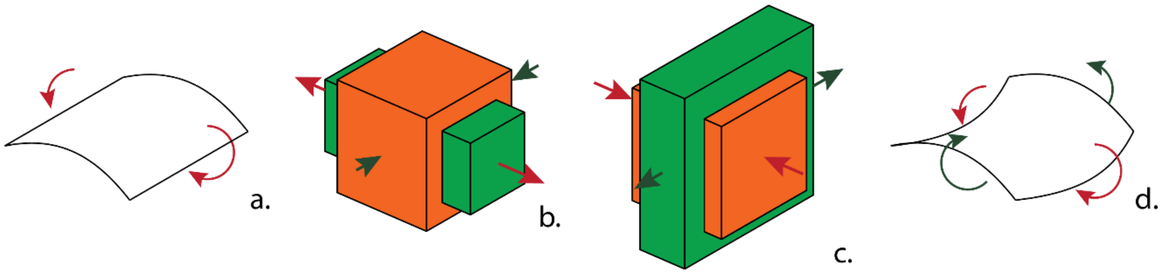

Figure 32: Anticlastic bending according to Poisson's ratio

A practical example of anticlastic bending behaviour was found during the completion of the Van Gogh Museum in Amsterdam. The behaviour was discovered due to visual distortions of the glass. A picture of the visual distortion is shown in Figure 33.

Figure 33: Visual distortions due to anticlastic bending (Octatube, 2015)

Besides anticlastic bending, the principle of stress stiffening occurs when considering large deformations of plates. As discussed in Chapter 2.2.1, curved structures not only transfer forces via bending, but also via axial forces. At larger curvatures, higher percentages of the load are being transferred via axial forces instead of bending forces. Stress stiffening effects needs to be considered for thin structures with bending stiffness insignificant compared to axial stiffness, such as cables, thin beams, and shells, and couples the in-plane and transverse displacements (ANSYS, 2017). Stress stiffening increases until all the forces are distributed axially, resulting in a catenary shape, which will not deflect any further. In terms of geometrically nonlinear analysis, this means that a plate will decrease less per predefined load step, as the curvature increases. The effect of stress stiffening therefore becomes important when determining the amount of load needed to bend a plate into a required curvature.

2.4.2. 1D simplification

Single curved 2D plates show similarities to very wide 1D curved beams (Figure 34). A plate with two opposite sides simply supported and the other two free, can be treated as a very wide -beam, considering the following adjustments (Young & Budynas, 2002). The reduced stiffness of a plate compared to a beam, can be approached by multiplying the Young's Modulus with a factor including Poisson's ratio, equation (40).

$$E_{beam} = E * (1 - v^2) \tag{40}$$

In which:

E_{beam} is the adjusted Young's modulus of glass, in N/mm²;
E is the Young's modulus of glass, whereby $E = 70000$ N/mm²;
v is the Poisson's ratio of glass, whereby $v = .23$.

Furthermore, the bending moment in y-direction, except for close to the free edges, can be calculated using Poisson's' ratio, equation (41).

$$M_y = v * M_x \tag{41}$$

In which:

M_y is the bending moment in y-direction, according to Figure 13, in Nmm;
v is the Poisson's ratio of glass, whereby $v = .23$;
M_x is the bending moment in x-direction, according to Figure 13, in Nmm;

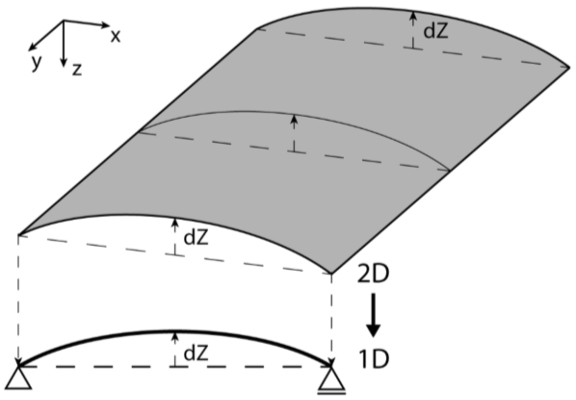

Figure 34: Simplification of a single curved 2D plate, to a 1D curved beam

Theory of arches

In line with the simplification of a flat plate to a beam, a curved plate can be simplified to an arch. The structural assessment of the arch is done according to the theory of arches by (Welleman, 2019). The theory considers a predefined arch shape function. In case of a statically indeterminate arch system, the following ordinary differential equations can be used to calculate the deflection, bending moment, normal and shear forces in an arch.

$$EI * \frac{d^4w}{dx^4} = q_z - H_x * \frac{d^2z}{dx^2} \tag{42}$$

$$M = -EI * \frac{d^2w}{dx^2} \tag{43}$$

$$N = -H_x \cos\alpha + \left(-EI\frac{d^3w}{dx^3} - H\frac{dz}{dx}\right)\sin\alpha\,, \;\text{ with: } \tan\alpha = \frac{dz}{dx} \tag{44}$$

$$V = -H_x \sin\alpha + \left(-EI\frac{d^3w}{dx^3} - H\frac{dz}{dx}\right)\cos\alpha\,, \;\text{ with: } \tan\alpha = \frac{dz}{dx} \tag{45}$$

In which:

- E is the Young's modulus of glass, whereby $E = 70000$ N/mm^2;
- I is the moment of inertia of a beam in mm^4, in context of Figure 34, the moment of inertia is $I = \frac{H*t^3}{12}$
- w is the deflection of the arch at point x, in mm;
- q_z is the vertical distributed load on the arch, in N/mm;
- H_x is the horizontal reaction forces of the support condition, in N;
- z is the shape function for the height of the arch at point x, in mm.

2.4.3. 2D load cases

Regarding the structural behaviour of plates and shells, load cases which show similarities with the different cold-bending stages are found in literature. The first one being 'the deflection of a rectangular plate, with two opposite edges simply supported and the other two free', which shows similarities with the boundary conditions of the 'Bending phase'. The second load case is the 'deflection of portion of a cylindrical shell', which shows similarities to the 'Use phase'.

Rectangular plates with two opposite edges simply supported and the other two free

In (Timoshenko & Woinowsky-Krieger, 1989) the deflections and bending moments due to uniformly distributed loads on the described load case (Figure 35), are calculated using tabulated values (Figure 36). Using the tabulated values, the deflection and bending moments at midspan of the free edge (α_2 and β_2) and centre of the plate (α_1, β_1 and β_1') can be calculated. From the tabulated values can be concluded that the deflection in the centre of the plate is smaller than the deflection along the edge, which is inline with the anticlastic bending behaviour as discussed in Chapter 2.4.1.

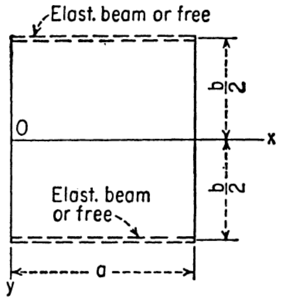

Figure 35: Specified load case

b/a	$x = a/2,\ y = 0$			$x = a/2,\ y = \pm b/2$	
	$w = \alpha \frac{qa^4}{D}$	$M_x = \beta_1 qa^2$	$M_y = \beta_1' qa^2$	$w = \alpha_2 \frac{qa^4}{D}$	$M_x = \beta_2 qa^2$
	α_1	β_1	β_1'	α_2	β_2
0.5	0.01377	0.1235	0.0102	0.01443	0.1259
1.0	0.01309	0.1225	0.0271	0.01509	0.1318
2.0	0.01289	0.1235	0.0364	0.01521	0.1329
∞	0.01302	0.1250	0.0375	0.01522	0.1330

Figure 36: Tabulated values for the specified load case

Deflection of a portion of a cylindrical shell

In (Timoshenko & Woinowsky-Krieger, 1989) the deflection of a portion of a cylindrical shell (Figure 37), which is supported along the edges and submitted to a uniformly distributed pressure load normal to the surface, is calculated using the following series:

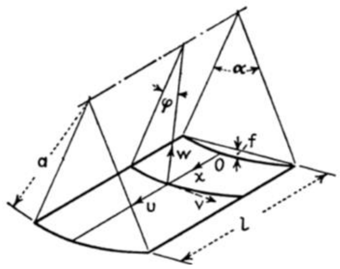

Figure 37: Specified load case and directions of displacements

$$u = \sum\sum A_{mn} \sin\left(\frac{n\pi\varphi}{\alpha}\right)\cos\left(\frac{m\pi x}{L}\right) \quad (46)$$

$$v = \sum\sum B_{mn} \cos\left(\frac{n\pi\varphi}{\alpha}\right)\sin\left(\frac{m\pi x}{L}\right) \quad (47)$$

$$w = \sum\sum C_{mn} \sin\left(\frac{n\pi\varphi}{\alpha}\right)\sin\left(\frac{m\pi x}{L}\right) \quad (48)$$

$$q = \sum\sum D_{mn} \sin\left(\frac{n\pi\varphi}{\alpha}\right)\sin\left(\frac{m\pi x}{L}\right) \quad (49)$$

The general derivation of the system of equations for the case of deformations of thin cylindrical shells, is shown given in equation (50)-(52), (Timoshenko & Woinowsky-Krieger, 1989).

$$\frac{\partial^2 u}{\partial x^2} + \frac{1-\nu}{2a^2}\frac{\partial^2 u}{\partial\varphi^2} + \frac{1+\nu}{2a} * \frac{\partial^2 v}{\partial x\partial\varphi} - \frac{\nu}{a}\frac{\partial w}{\partial x} = 0 \quad (50)$$

$$\frac{1+\nu}{2} * \frac{\partial^2 u}{\partial x\partial\varphi} + a\frac{1-\nu}{2}\frac{\partial^2 v}{\partial x^2} + \frac{1}{a}\frac{\partial^2 v}{\partial\varphi^2} - \frac{1}{a}\frac{\partial w}{\partial\varphi} = 0 \quad (51)$$

$$\nu\frac{\partial u}{\partial x} + \frac{\partial v}{a\partial\varphi} - \frac{w}{a} - \frac{h^2}{12}\left(a\frac{\partial^4 w}{\partial x^4} + \frac{2}{a} * \frac{\partial^4 w}{\partial^2 x\partial\varphi^2} + \frac{\partial^4 w}{a^3 x\partial\varphi^4}\right) = \frac{aq(1-\nu^2)}{Eh} \quad (52)$$

By substituting the series of expressions for $u, v, w,$ and $q,$ into the system of equations, the following system of linear equations is derived, which can be used to solve for the coefficients A_{mn}, B_{mn} and C_{mn}:

$$A_{mn}\pi\left[\left(\frac{am}{L}\right)^2 + \frac{(1-\nu)n^2}{2\alpha^2}\right] + B_{mn}\pi\frac{(1+\nu)amn}{2\alpha L} + C_{mn}\frac{\nu am}{L} = 0 \quad (53)$$

$$A_{mn}\pi\frac{(1+\nu)amn}{2\alpha L} + B_{mn}\pi\left[\frac{(1-\nu)a^2m^2}{2L^2} + \frac{n^2}{\alpha^2}\right] + C_{mn}\frac{n}{\alpha} = 0 \quad (54)$$

$$A_{mn}\nu\pi\frac{am}{L} + B_{mn}\frac{n\pi}{\alpha} + C_{mn}\left[1 + \frac{\pi^4h^2}{12a^2}\left(\frac{a^2m^2}{L^2} + \frac{n^2}{\alpha^2}\right)^2\right] = D_{mn}\frac{a^2(1-\nu^2)}{Eh} \quad (55)$$

Whereby:

$$D_{mn} = \frac{16q}{\pi^2 mn} \quad (56)$$

The solution to the set of equations and further specification of the parameters is given in Chapter 5.4, in which the application of the load case with respect to the ‘Use phase’ is presented.

2.5. Numerical modelling

In addition to analytical modelling, numerical modelling is conducted. Results of numerical modelling are used to gain insights into the behaviour of cold-bent glass plates under a variety of boundary conditions. The boundary conditions are in line with the different stages of the cold-bending process, as discussed in Chapter 2.1. Results from numerical modelling are used to validate the different developed analytical methods. Therefore, it is of importance that the setup of the numerical models is computed correctly. In this chapter, various aspects of the model setup are discussed. Furthermore, in order to verify the model setup, numerical results are validated with results from literature.

The programme of choice for numerical modelling is the finite element analysis software DIANA (DIANA FEA, 2021). This is due to the availability of licenses for TU Delft students and the practical knowledge about the software within the faculty of Civil Engineering. Within the Interactive Environment of DIANA (DianaIE), all operations are logged as Python commands, which made it possible to do the pre- and postprocessing of the numerical models using .py command lines in an Integrated Development Environment (IDE). On account of this possibility, the workflow for the use of DIANA has been highly optimised. Furthermore, within DIANA it is possible to perform a 'Phased Analysis', which allows for in-between changes in boundary conditions and sequential combinations of loads. The possibility of a phased analysis is essential for modelling deformed cold-bent glass plates, subjected to additional live loads.

2.5.1. Geometric nonlinearity

Due to the large deformations of single curved cold-bent glass plates, a geometrically nonlinear analysis is required to model deformations and stresses. In DIANA, the following settings define the setup of the geometrically nonlinear analysis. The step size and convergence tolerance determine the number of iterations necessary per load step. In first instance, the automatic step size option is used as setting, with a predefined convergence tolerance. In case of divergence of the model, the step size and convergence tolerance are adjusted accordingly.

Due to application of the load in steps, geometrically nonlinear phenomena, such as stress stiffening, are taken into account (DIANA FEA, 2021). Because of changes in geometry per load step, the load conditions are heavily influenced by changes in area and load direction. These load changes are considered per step by using the option of nonconservative loading. The analysis is setup with a Total Lagrange description. This description is useful if displacements and rotations are large, and strains small, which is the case for glass materials. Due to the brittle behaviour of glass, strains will only occur elastically. This means they are linearly dependent on the stresses in the glass, and thus can be considered as relatively small.

2.5.2. Plate modelling

Glass plates can be considered as thin plate or shell structures. In finite element modelling, a number of element types can be used to model thin plate and shells structures. According to (Argyris, Haase, Mlejnek, & Schmolz, 1986), '2D curved shell elements are known to be efficient in the study of geometrically nonlinear problems, and can also be categorized in the most reliable and efficient group of elements', which is therefore the choice of element type. Furthermore, since only rectangular plates are considered, a quadrilateral mesh shape is chosen. In Figure 38, a quadrilateral curved shell element with a uniform thickness, as used in DIANA, is shown. The positive directions of the Cauchy stress tensors are shown in Figure 39. In DIANA tensions stresses are positive.

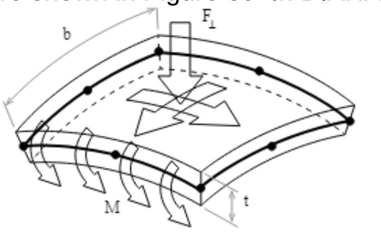

Figure 38: Quadrilateral curved shell element (DIANA FEA, 2021)

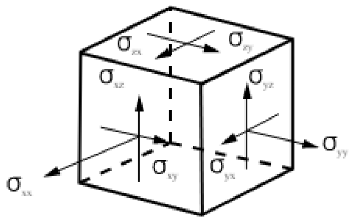

Figure 39: Cauchy stresses for curved shell elements (DIANA FEA, 2021)

2.5.3. Model accuracy

DIANA is a powerful software package which can solve detailed and complex problems accurately. In order to model geometrically nonlinear behaviour, loads are applied in steps and multiple iterations are calculated per step. This means that mesh size and step size will have a considerable influence on the computational running time of the models. Due to the option of 'automatic step size', the step size and number of iterations per step size are already optimised for. In case of divergence of the models, either the maximum automatic step size, or tolerance is decreased. By decreasing maximum step size or convergence tolerance, the computational time is increased. Due to an optimised workflow with automated .py command lines, it was possible to run models in the background or at night, and therefore, if necessary, define small maximum step sizes to reach convergence.

In order to determine the optimal mesh size, a single curved panel of 1000x1000x6mm, simply supported on one side, rolled supported on the opposite side, with the other ends free and loaded by a uniform pressure, is modelled. Since the shape of the mesh is quadrilateral, it means that for a square plate, halving the mesh size results in an increase of the number of elements by a factor of 4. In order to decide on a sufficiently detailed mesh size, but also an efficient computational time, a comparison is made between a mesh size of 5mm, 10mm, 25mm, 50mm and 100mm. The 5mm mesh is assumed to be the most accurate and is used as reference to calculate the differences with the other meshes. The analysis is set-up for 100 load steps, with a load per step of 0.1 kN/m^2. For each load step, the volume of deformation under the plate is calculated and compared to the 5mm mesh. Performance on computational efficiency is based on the size of the output file, the size of the 5mm mesh output file is considered to be 100%. Performance on accuracy is based on the differences in volume of deformation, for which the difference between the volume of the 100mm and 5mm mesh is considered to be 100%. In Figure 40 the comparison between the average deviation in results and size of the output file is shown per mesh size. From the comparison it is decided to select a mesh size of 25x25mm for numerical modelling of 1x1m plates. However, during the course of modelling larger plates, the number of diverging plate models increased. Therefore, it is decided to increase the mesh size to 50x50mm for plates larger than 2x2m, and to 100x100mm, for plates larger than 4x3m.

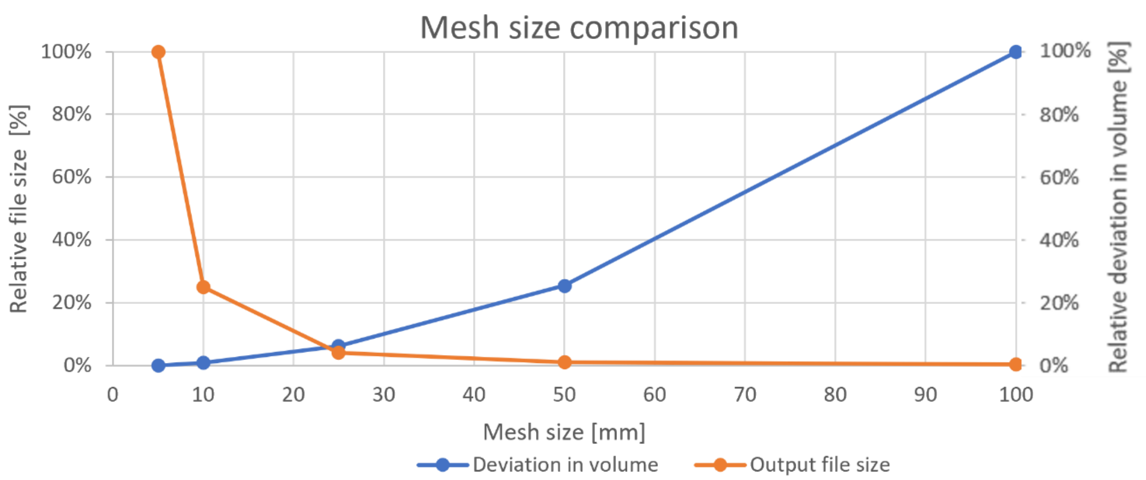

Figure 40: Mesh size comparison

2.5.4. Validation model setup

In order to validate the geometrically nonlinear model setup, two comparisons are made between analytical results from literature and numerical results from DIANA. This is done for the case of large deflections of a cantilever, one with a constant end moment (Figure 41) and one with a non following transverse end load (Figure 42). When an end moment is applied, the bending moment in a cantilever will be constant over the length of the cantilever. Therefore, the deflection of the cantilever will follow a circular bending pattern, which is considered as the analytical solution (Argyris, Haase, Mlejnek, & Schmolz, 1986). In case of an end point load, the moment and curvature are not constant over the length of the beam. In a paper by (Bisshopp & Drucker, 1945), the analytic derivation of a cantilever beam with a transverse point load is given and used as validation.

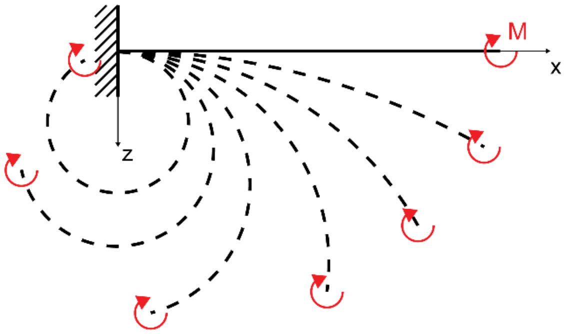

Figure 41: Large deflection of a cantilever under end moment; plot of deformations

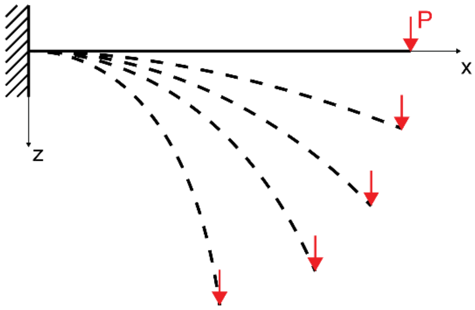

Figure 42: Large deflection of a cantilever under transverse end load; plot of deformations

Large deflection of a cantilever under end moment

In Figure 43, the non dimensional horizontal and vertical displacement of the free end of a cantilever with a circular bending pattern are shown. Also, the displacements of a cantilever beam and plate, modelled in DIANA with geometrically nonlinear settings, are shown. It can be seen that the solution of both the beam and plate are in good agreement with the analytical solution. The difference between the 1D beam model and 2D plate model is due to the anticlastic bending, as discussed in Chapter 2.4.1. In case of a plate with zero Poisson's ratio, anticlastic bending does not occur and beam and plate solution are almost identical.

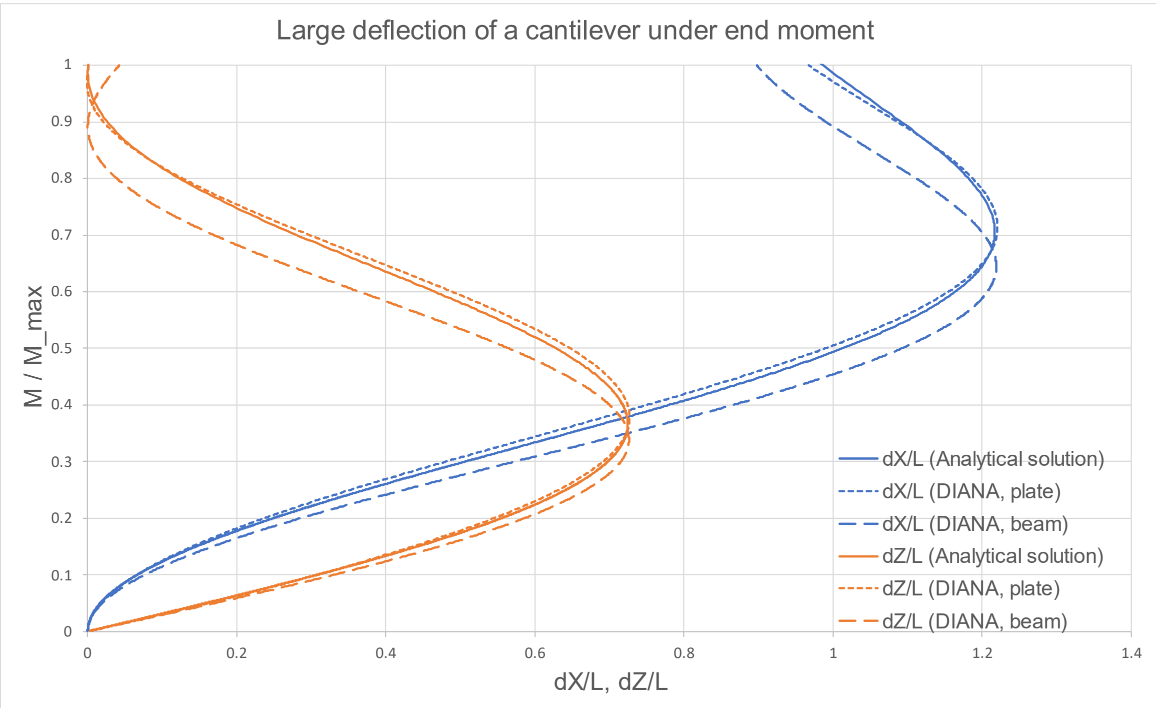

Figure 43: Large deflection of a cantilever under end moment; displacement at free end

Large deflection of a cantilever under (non following) transverse end load
Another comparison between an analytic solution and geometrically nonlinear DIANA model is made for a cantilever under transverse end load. Figure 44 shows the comparison of the analytical solution with the results from DIANA. From the comparisons it is concluded that the geometric nonlinear analysis in DIANA is setup properly.

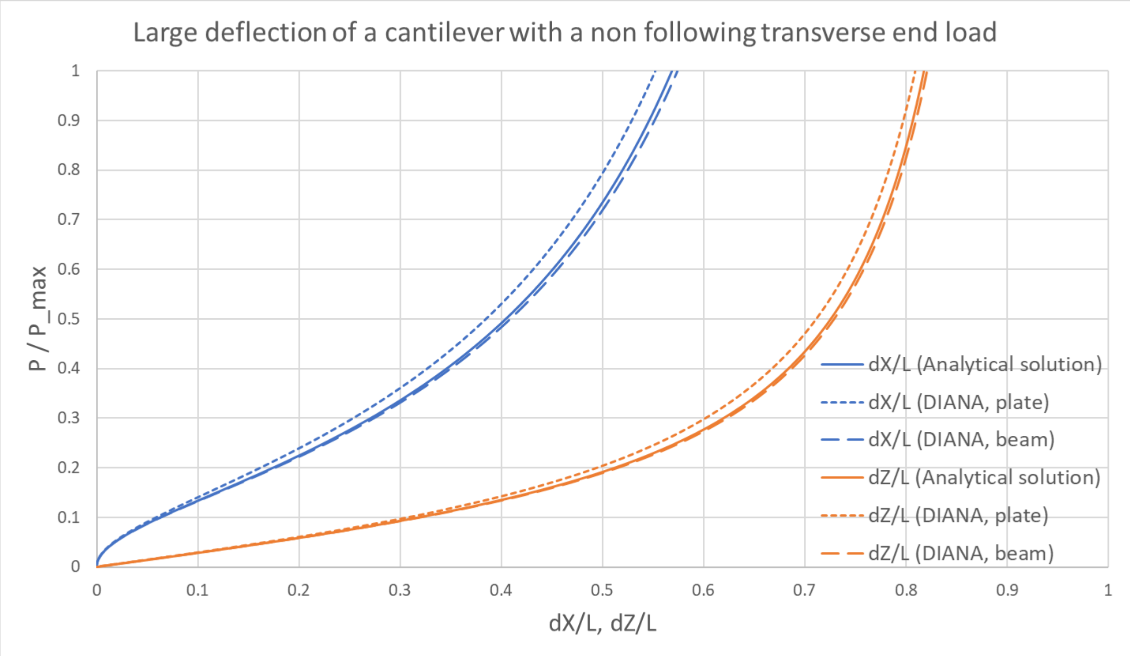

Figure 44: Large deflection of a cantilever under transverse end load; displacement at free end

2.5.5. Final setup

From the evaluation of the different methods to determine the cavity pressure in IGU's in Chapter 2.3, it is concluded that the plates of an IGU can be considered separately, by modelling the load sharing as external pressure loads on the different panes. This conclusion is only justified when considering the boundary conditions of the spacer as rigid and simply supported. Since this simplification is in line with the scope thesis, the numerical modelling for this thesis will be simplified to that of single plates only. Cavity pressure loads are calculated using previously discussed analytical methods. The resulting pressures are then used to model the plate behaviour numerically. The resulting volume of deformation is then used as input value for the analytical cavity pressure calculation. With the application of this workflow, the interaction between two plates of an IGU can be numerically modelled. A similar approach has been proven to be effective in the research conducted by (van Driel, 2021).

The final model setup, which is used for the numerical models for Chapter 3, 4 and 5, is as follows. First a rectangular surface area is defined, using a 'Polygon sheet'. The shape properties of this sheet are shown in Figure 45, of which the material properties are defined in Figure 46 and the geometry properties in Figure 47. As discussed in Chapter 2.5.2, the type of elements are 'Regular Curved Shells'. For the material properties, only linear properties are considered. The underlying geometry is defined as 'flat' and a predefined flatness tolerance of 1e-7 mm is used. Eccentricities are considered to be zero. The structural nonlinear analysis properties are shown in Figure 48, which are in line with the findings from Chapter 2.5. The load steps are defined by automatic step sizes, of which the maximum step size is initially set to a value of 1. Depending on the type of loading, the convergence norm for equilibrium of iterations is set on either 'displacement' or 'force', with an initial convergence tolerance of 0.001 and continuation of the analysis if no tolerance is reached after a maximum number of 25 iterations. Depending on the divergence of models, the automatic step size, convergence tolerance or number of iterations are adjusted when necessary.

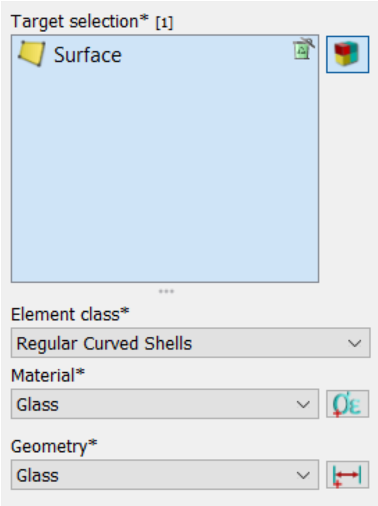

Figure 45: Shape properties

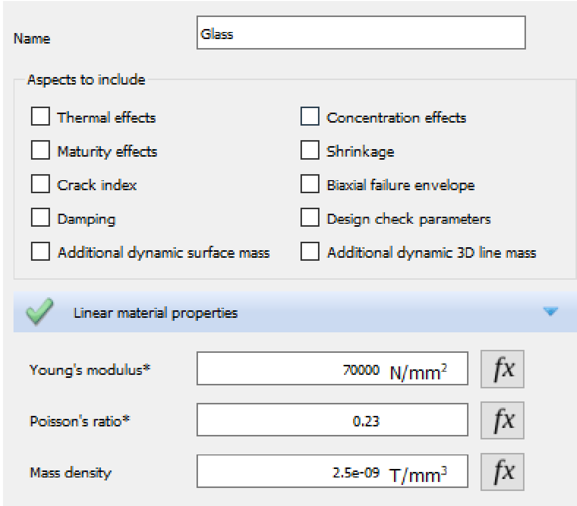

Figure 46: Material properties

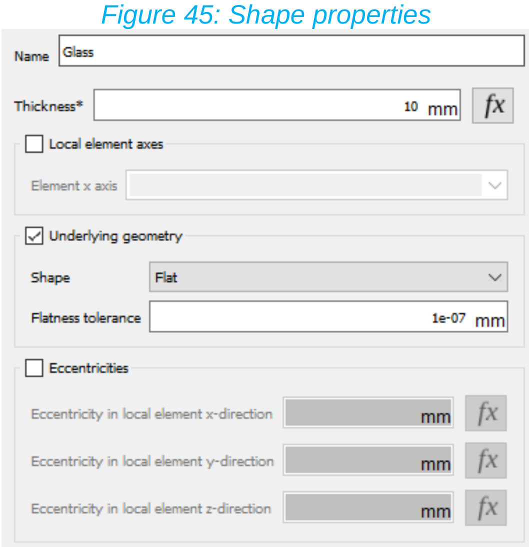

Figure 47: Geometry properties

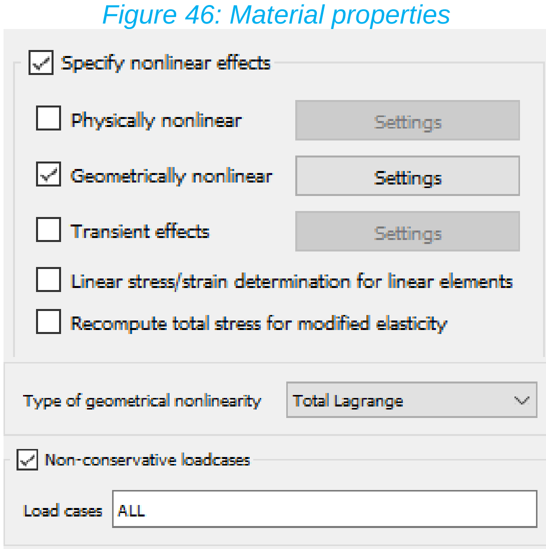

Figure 48: Nonlinear analysis properties

After completion of the nonlinear analysis, deformations and stresses are exported to .csv files using .py command lines. The .csv files are then postprocessed using Python coding in Spyder. Deformations are exported as X, Y and Z coordinates of each node in the mesh. For each load step, a set of coordinates is exported. With the coordinates, the volume of deformation below the plate can be calculated using a Delaunay triangulation of the points (de Berg, van Kreveld, Overmars, & Schwarzkopf, 2000), demonstrated in (van Driel, 2021). For each triangle, the surface area is multiplied with its average height. The sum of volumes of the triangular prisms is then the total volume below the curved plate. By subtracting the volumes below a curved plate between different load conditions, the volume of deformation can be calculated.

Stresses are defined as 'Total Cauchy Principal Stresses', and exported as $\sigma_1, \sigma_2, \sigma_3$, per layer and per element. The stresses are ordered such that $\sigma_1 \geq \sigma_2 \geq \sigma_3$ (DIANA FEA, 2021). Based on geometrically nonlinear deformations of a single curved plate, with its curved edge along the x-axis, it can be expected that based on equation (2), (3) and (4), $\sigma_1 \geq \sigma_2 \geq \sigma_3 = \sigma_{xy} \geq \sigma_{xz} \geq \sigma_{yz}$. The layers 1, 2, and 3, resemble the bottom, middle and top plane of the plate, respectively. For each element four stresses are exported, which resemble the corner points of the respective element. This means that for all nodes, except for side and corner nodes, 3x3x4 = 36 stresses are exported. In line with the equation for maximum principal stress, equation (5), and the consideration of tensile stresses as positive values, the maximum principal stress per node σ', is considered to be the maximum positive value of the 36 stresses.

3. Bending phase

In this chapter, the 'Bending phase', as defined in Chapter 2.1, is modelled numerically and analytically. First, the goal of modelling is set by defining the key parameter to be approached by analytical modelling. Second, the scope of the 'Bending Phase' is defined by considering the boundary conditions which are applicable to the phase. Third, numerical modelling is conducted, of which the results are used to validate the proposed analytical methods. Last, analytical methods are proposed of which the results are compared to numerical outcomes.

3.1. Goal

The execution of the cold-bending of IGU's is project specific, which results in different boundary conditions per application. Furthermore, after fixation of the cold-bent IGU onto the substructure, the boundary conditions change. Which means that the already project specific load conditions of the 'Bending phase', are only applicable during the cold-bending of the IGU itself. In order to still develop a comprehensive analytical method, which can be used to resemble the 'Bending phase' of cold-bent IGU's, a common design parameter must be considered which is applicable under all kinds of boundary conditions.

One performance indicator that all cold-bent IGU applications have in common, is that during cold-bending, stresses should not exceed the design value of the tensile bending strength. Furthermore, it is desired to know the stresses due to cold-bending, in order to design for sufficient capacity of additional live load stresses. Therefore, the goal of the analytical component for the 'Bending phase' is to develop a comprehensive method which can be used to determine cold-bending stresses based on a set of design parameters.

3.2. Boundary conditions

The boundary conditions for the 'Bending phase' are determined using the insights gained in the literature study. First, it is determined to only model the behaviour of a single plate, as discussed in Chapter 2.5.5. Second, based on the large deformations during bending, a geometrically nonlinear analysis is considered. The model setup as discussed in Chapter 2.5 is used for this analysis. Due to the variety of project specific boundary conditions, a simplified set of boundary conditions is considered. In order for the 'Bending phase' to be relevant, insights are gained on how the large deformations affect bending stresses. These cold-bending stresses are then 'preserved' in the glass at the 'Fixation moment'. Due to the change of boundary conditions after bending, cavity pressures will also change, and are therefore assumed to be irrelevant for the 'Bending phase' itself.

The simplified set of boundary conditions which is used to model the relation between geometrically nonlinear deformations and stresses, is shown in Figure 49. The example is shown for a 2000x2000x10mm plate that is close to R=12m. Points E and F are point supports, fixed in x-direction, which makes the EF line the reference point for deformations. Sides AB and CD are linearly supported in y- and z-direction, allowing for a single curved, geometrically nonlinear deformation. A normal surface load is defined to deform the plate, which is a nonconservative load and updates its direction during each load step of the geometrically nonlinear analysis (Figure 50). By doing so, the loads follow the curvature of the plate during bending, which is similar to load conditions from practical applications.

In Figure 51 an example of the resulting displacements in x-direction is shown. It can be seen that sides AB and CD have moved towards reference line EF, which is line with expectations of the geometrically nonlinear deformations. The displacements in y-direction are shown in Figure 52. Although they are minimal, it can be concluded that there is a degree of freedom in this direction, which is important in numerical modelling to prevent peak stresses due to stretching of the glass. The displacements in z-direction are, as expected, maximum at midspan of the plate (Figure 53). In Figure 54 the layer and principal stress component with the largest tensile stresses is shown, i.e., layer 3, S1. In line with Chapter 2.5.5 it can be concluded that this resembles the σ_{xy} principal stress in the top layer, which is the expected result for out of plane cold-bending. Based on these evaluations of results, it is concluded that the boundary conditions are setup correctly.

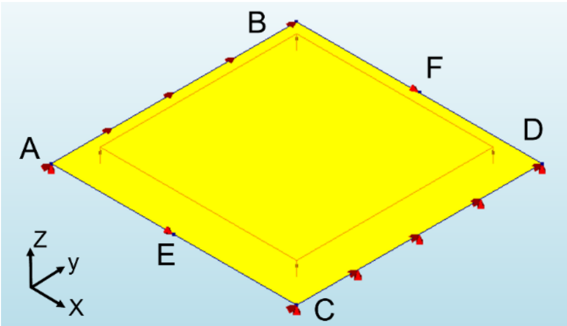

Figure 49: Boundary conditions 'Bending phase'

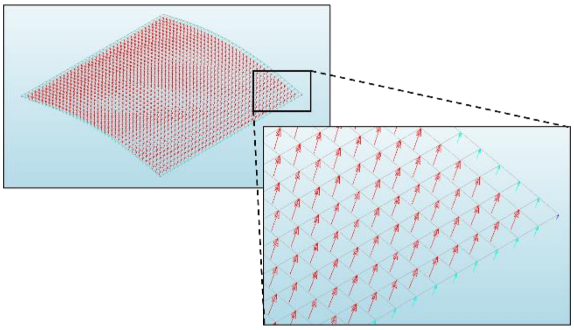
Figure 50: Nonconservative surface load

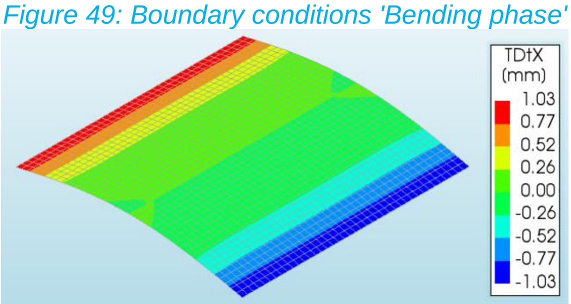

Figure 51: Displacements in x-direction

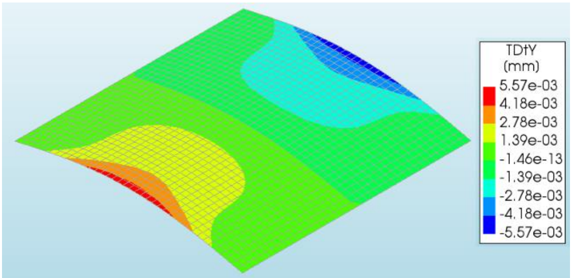

Figure 52: Displacements in y-direction

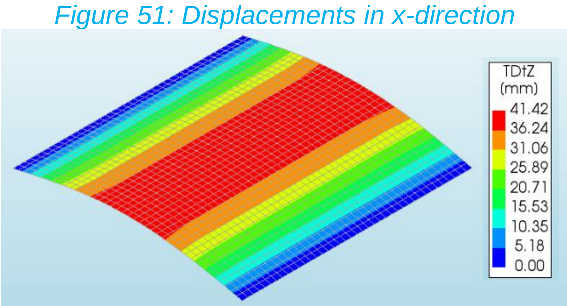

Figure 53: Displacements in z-direction

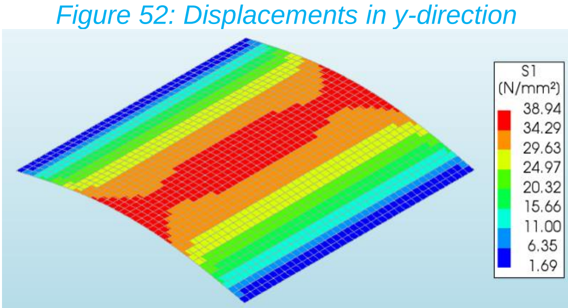

Figure 54: Stresses in layer 3 of S1

3.3. Numerical modelling

In this paragraph, results of numerical modelling of the 'Bending phase' are discussed. In order to gain insights in the bending stresses for a variety of displacements, the load per step and number of steps are defined such that curvature radii of up to 2m are reached. This is done by first determining the deformation height based on the geometry of a circle, using equation (57). Then using the forget-me-not for a simply supported beam under a uniformly distributed load, an estimation is made of the required surface load necessary to reach the deformation height. In order to make sure the required radius is reached the total load is multiplied by 1.5. The load per step is defined by dividing total required load with the number of steps. Based on sufficient accuracy and efficient computational running time, the number of steps is considered as 100. Using a python script, all numerical modelling steps are written as .py command lines, resulting in a highly optimised workflow in which all actions in the Interactive Environment of DIANA are automated.

$$f = R - \sqrt{R^2 - \cos^2\left(\frac{B}{2R}\right)} \tag{57}$$

In which:

f	is the deformation height of the curved glass plate, in mm;
R	is the design radius of the curved glass plate, in mm;
B	is the width of the plate, in mm.

Results show that at a radius of 2m, all glass thicknesses ranging between 4 to 20mm, reach a cold-bending stress of higher than 75.0 N/mm², which is considered as the maximum tensile bending strength due to permanent loads. By doing so, the limits of the radius of curvatures per glass thickness can be explored. In Figure 55, the maximum principal stresses of a 2x2m plate with different thicknesses is compared to design radii ranging between 25m to 3m. The stresses are interpolated between load steps, using equation (58) and the deformation coordinates per load step. By plotting a line for the maximum tensile bending strength, the maximum curvatures per plate thickness can be determined.

$$R = \frac{f}{2} + \frac{L^2}{8f} \tag{58}$$

In which:

R	is the design radius of the curved glass plate, in mm;
f	is the deformation height of the curved glass plate, in mm;
L	is the span of the curved glass plate, in mm.

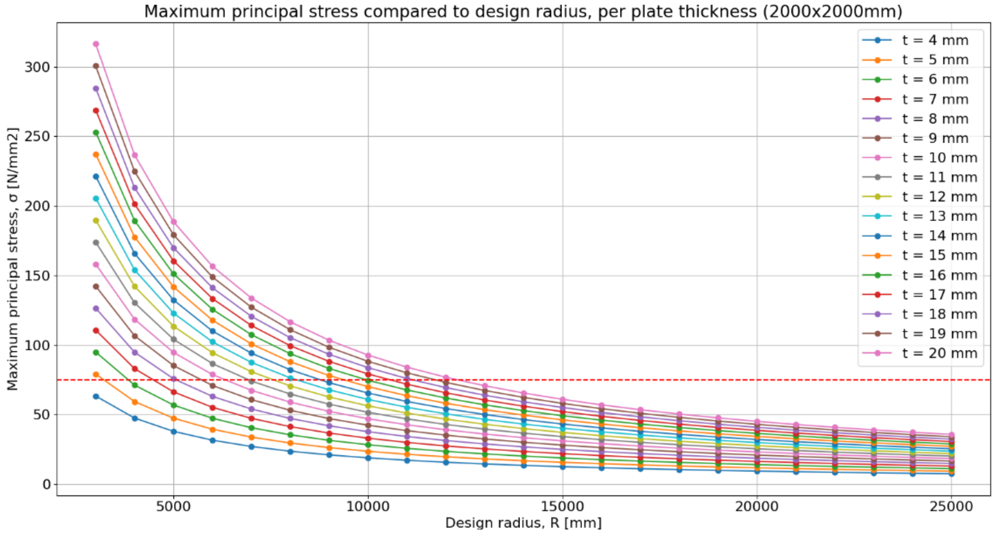

Figure 55: Maximum principal stress compared to design radius (2x2mm plate)

A conclusion which is drawn from numerical results, is that when comparing the cold-bending stresses, differences between plate sizes are small. In Table 4 an example of this conclusion is shown for a plate with a thickness of 10mm and design radius of 12m. It can be seen that for the considered plate dimensions, all maximum principal stresses are within 2.0 N/mm^2 of each other. Comparable results hold for other parameters of design radii and plate thicknesses. Results show that by expressing the principal stresses in terms of thickness and design radius, they are independent on plate dimensions.

Table 4: Maximum principal stresses per plate size

Maximum principal stress [N/mm2] t = 10mm, R = 12000mm			
B \ H	1000	2000	3000
1000	37.26		
2000	39.29	39.08	
3000	39.73	39.44	39.42
4000	39.86	39.58	39.55
5000	39.92	39.66	39.65
6000	39.95	39.70	39.73

The range in height (H) and width (B) used in the table, is based on the maximum size of a standardized jumbo glass plate (3.21x6m, Chapter 2.1.1), for which it is considered cold-bending is only done along the longest edge of a rectangular plate. The numerical modelling of the 'Bending phase' and evaluation of principal stresses has been done for a database of all plate sizes considered in Table 4, with design radii ranging from 3m to 25m and plate thicknesses from 4mm to 20mm. The necessity of this database is explained in Chapter 4. Furthermore, the maximum principal stresses change after fixation onto the substructure. These changes are small and the same relations and conclusions hold as discussed before. Still, since the stresses after fixation are considered as the permanent stresses during the structures' lifetime, it is concluded that these stresses overrule the 'Bending phase' stresses. In Appendix A.1, tables of the minimum, average and maximum principal stress of the 15 evaluated plates as part of the 'Fixation moment', are considered per plate thickness and design radius. The average stresses are used to validate the results from the proposed analytical methods.

3.4. Analytical modelling

The goal of the analytical method for the 'Bending Phase' is to find an efficient and accurate way to determine the permanent cold-bending stresses based on design parameters of curved glass. First, a method which is based on the geometrically non-linear deformations of single curved glass plates simplified to arches, is presented. The method is developed to gain insights in geometrically nonlinear modelling. Second, results of the theory for calculating cold-bending stresses as discussed in Chapter 2.1, are considered. Last, an analytical method based on a result-based engineering approach is considered.

3.4.1. Geometrically non-linear method

The first proposed method is based on the simplification of a single curved plate to a very wide 1D arch, as discussed in Chapter 2.4.2. The method is setup with an iterative geometrically nonlinear approach by calculating the horizontal and vertical displacements of an arch using load steps. The goal of the method is to mimic the geometrically nonlinear approach as considered in DIANA.

In order to apply the arch theory, first a place function must be considered for the arch. In Figure 56 an example of the comparison between the deformed curvature from DIANA and different arch function is shown for a 2000x2000x10mm plate with a design radius R=3m. Similar comparisons have been made for a range of other plate sizes, thickness and radii. From these comparisons it is concluded that the deformed shape along the edge of the curved plates in DIANA, is most similar to that from a sinusoidal function. Therefore, equation (59) is used as place function of the arch.

$$z = f \sin\left(\frac{\pi x}{L}\right) \qquad (59)$$

In which:

z	is the height of arch at point x, in mm;
f	is the height of the arch at midspan, in mm;
L	is the arch span, in m.

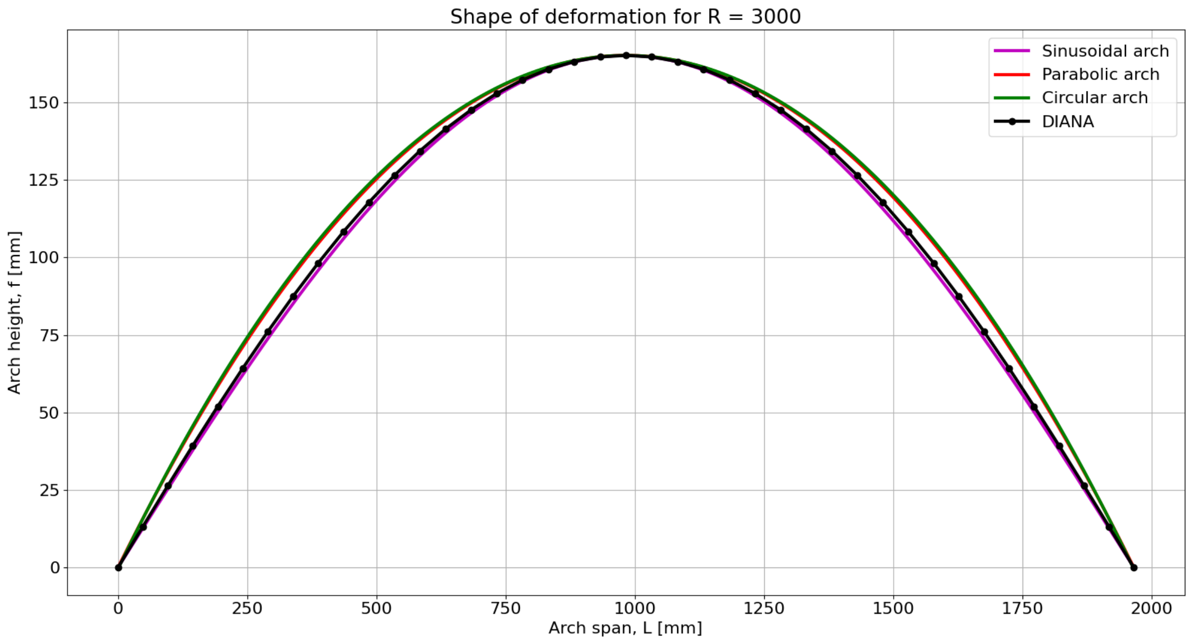

Figure 56: Comparison of deformation shapes, example of a 2000x2000x10mm plate, R=3m

The iterative process to calculate the geometrically nonlinear deformation of the arch is visualised in Figure 57 to Figure 60. First, a statically indeterminate arch is defined, subjected to a pressure load. The pressure load is decomposed in a horizontal distributed load q_x and vertical distributed load q_z. This is done by calculating the curvature of the arch, using the derivative of the arch function with respect to x-axis, as shown in equation (60).

$$q_x = q * \sin(\alpha)\ and\ \ q_z = q * \cos(a)\ with\ \tan(\alpha) = \frac{dz}{dx} \tag{60}$$

Second, the vertical displacement of the arch is calculated, using the ordinary differential equation (ODE) for arches as discussed in Chapter 2.4.2. The ODE is adjusted according to the boundary conditions, in which the horizontal reaction force H_x is now considered as the acting force q_x, equation (61).

$$EI * \frac{d^4w}{dx^4} = q_z - q_x * \frac{d^2z}{dx^2} \tag{61}$$

In the third step, the corresponding horizontal displacement of the arch is calculated. This is done by determining the centre angle of the arch using arch length B and arch height after displacement $f_{new} = f + w$, as shown equation (62).

$$\theta = \frac{B * (1 - \cos(\theta))}{2 * f_{new}} \rightarrow R = \frac{B}{2 * \theta} \rightarrow L = 2 * R * \sin{(\theta)} \tag{62}$$

Using the newly calculated arch span and height, the geometry for the next iteration is defined and the iterative scheme can be repeated until a required design radius is reached.

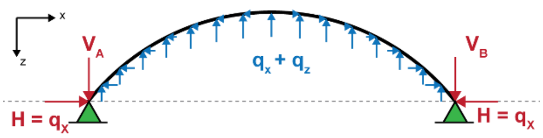

Figure 57: Iterative scheme – step 1

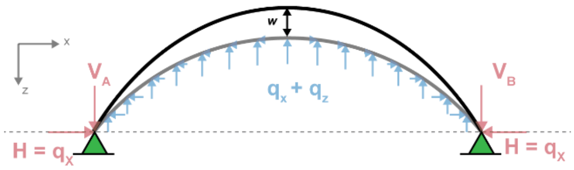

Figure 58: Iterative scheme – step 2

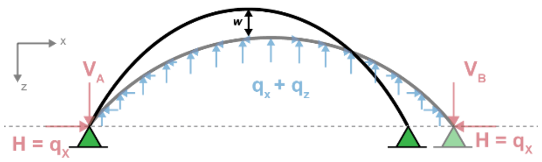

Figure 59: Iterative scheme – step 3

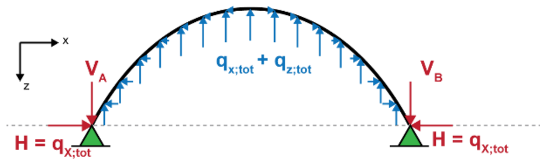

Figure 60: Iterative scheme – step 4

Using the ODE, the moments, shear forces and normal forces in x-direction can be calculated for each iteration. The total moment, shear and normal forces are calculated by summing the forces of each step until the design radius is reached. In order to account for plate behaviour, the forces in y-direction are calculated by multiplying the forces in x-direction with the Poisson's ratio for glass, as discussed in Chapter 2.4.2. Furthermore, the adjusted value for the Young's modulus is used, $E_{beam} = E * (1 - v^2)$. The maximum principal stress is then calculated using the equations discussed in Chapter 2.1.5. Due to the considerable number of iterations and extensive calculations, a Python script is developed for calculating the results.

In Figure 61 the results of the method are shown for the case of the maximum principal stresses of a 2x2m plate. It can be seen that the results show similarities to those from numerical modelling. Furthermore, the results show minor difference between different plate sizes, which is also in line with results from numerical modelling. Compared to numerical modelling, the differences between the plate sizes are smaller. In Appendix A.2., results of the method are presented in tables of the minimum, average and maximum principal stress of the same 15 plates as evaluated for numerical modelling. To quantitatively determine the accuracy of the method, the principal stresses are compared to those from numerical modelling. The comparison is done based on the averaged maximum stresses, resulting in an average deviation of -12%. Interpretation of the results is discussed in Chapter 7.

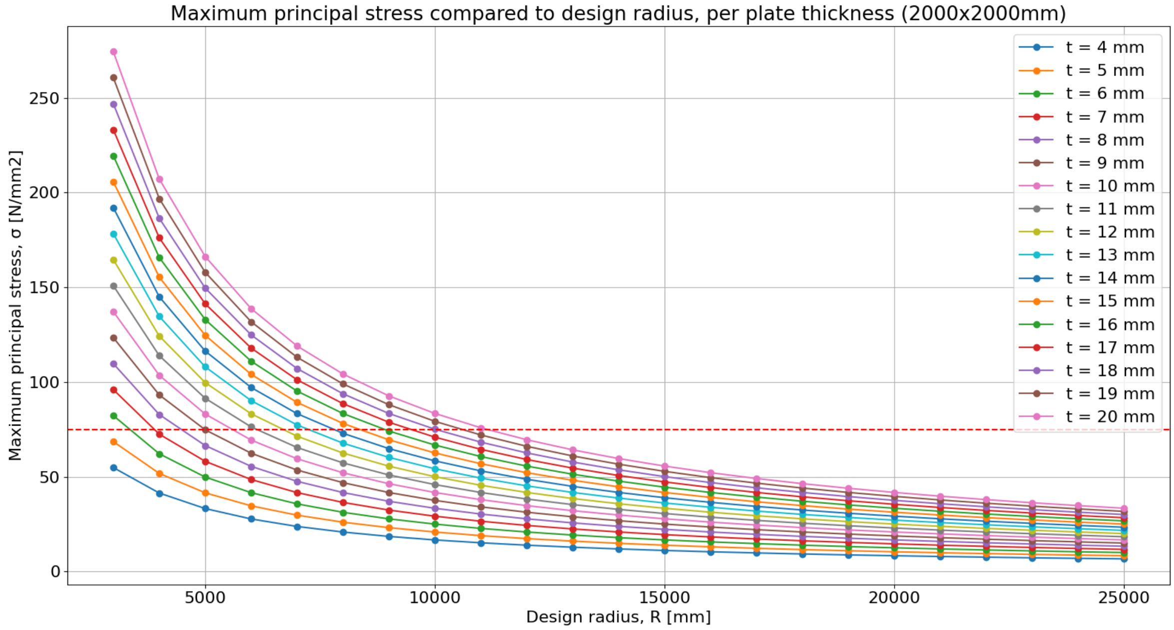

Figure 61: Results geometrically nonlinear arch theory, for a 2x2m plate

3.4.2. Cold-bending stresses theory

The second analytical approach is the cold-bending stress theory, as discussed in Chapter 2.1, of which the equation is repeated below. The equation is independent on the plate dimensions, which is in line with earlier findings. Results from the cold-bending theory are compared to the total average stress from numerical modelling. From the results it is concluded that the average deviation is -26%.

$$\sigma_{CB} = \frac{E * t}{2 * R} \qquad (63)$$

In which:

σ_{CB} is the stress due to cold bending curvature, in N/mm^2;

E is the Young's modulus of glass, in N/mm^2;

t is the thickness of the plate, in mm;

R is the radius of curvature, in mm;

3.4.3. Result based engineering method

Since the deviations of the previous methods are relatively high, a third analytical approach is considered. The method is based on regression that is found during the analysis of numerical results. In Figure 62 the maximum principal stresses are plotted against the thickness of the plate. Each line resembles the stresses of a radius. The stresses show a linear regression and seem to go through $\sigma' = 0$ for $t = 0$ mm. Based on this regression, the lines are approached with a linear function, which in general form can be considered as equation (64). The values of a_R and b_R, for the case of a 2x2m plate are shown in Table 5. The b_R coefficients all have a value of close to zero. By evaluating the a_R coefficients, i.e., the slopes, a noticeable relation was found. When dividing the slopes with the height of deformation of the curved plate f, an almost constant value is found. For the case of a 2x2m plate, as shown in the table, the average value is $f_R/a_R \approx 11$. Based on these findings, equation (68) is derived which can be used to calculate the maximum principal stress. Derivation of the equation is shown on the next page.

$$\sigma' = t * a_R + b_R \tag{64}$$

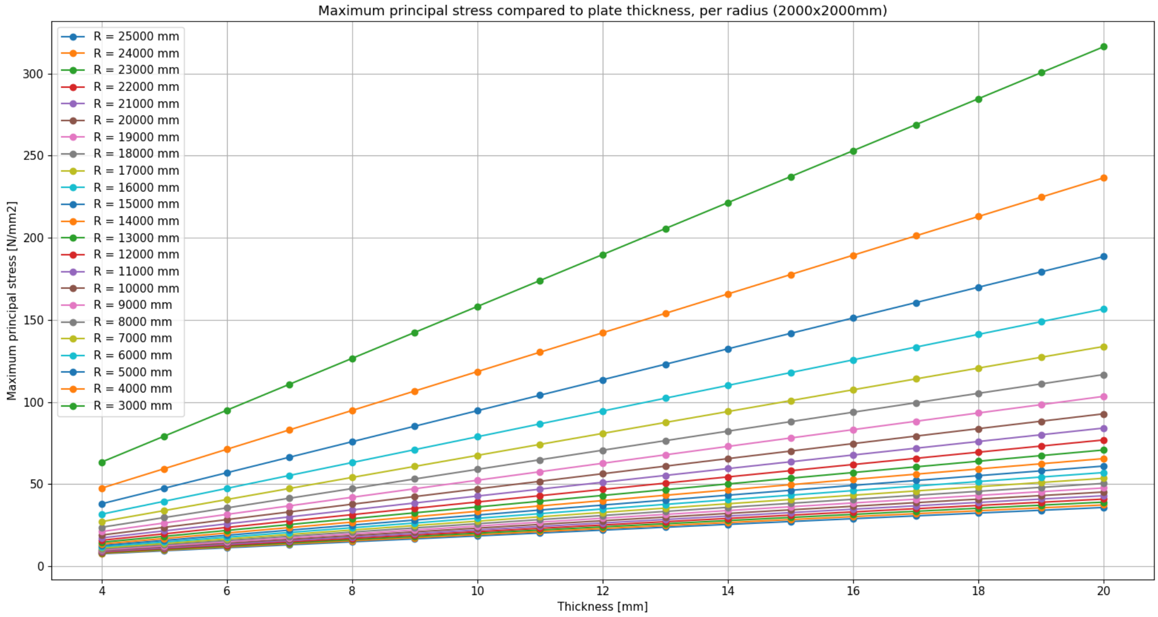

Figure 62: Maximum principal stress compared to plate thickness (2x2m plate)

Table 5: Linear regression coefficients (2x2m)

2000x2000				
R [mm]	**f [mm]**	**a [-]**	**b [-]**	**f / a**
25000	20.00	1.76	0.69	11.35
24000	20.83	1.84	0.70	11.32
23000	21.74	1.92	0.72	11.29
22000	22.72	2.02	0.73	11.26
21000	23.81	2.12	0.74	11.23
20000	24.99	2.23	0.74	11.20
19000	26.31	2.36	0.75	11.16
18000	27.77	2.50	0.76	11.13
17000	29.40	2.65	0.76	11.09
16000	31.24	2.83	0.76	11.06
15000	33.32	3.02	0.77	11.02
14000	35.70	3.25	0.77	10.98

2000x2000				
R [mm]	**f [mm]**	**a [-]**	**b [-]**	**f / a**
13000	38.44	3.51	0.76	10.94
12000	41.64	3.82	0.76	10.90
11000	45.42	4.18	0.75	10.86
10000	49.96	4.62	0.73	10.82
9000	55.50	5.15	0.71	10.78
8000	62.42	5.82	0.68	10.73
7000	71.31	6.67	0.63	10.69
6000	83.14	7.82	0.55	10.64
5000	99.67	9.42	0.45	10.58
4000	124.35	11.82	0.30	10.52
3000	165.13	15.81	0.06	10.44
			Avg:	10.72

The constant factor is considered as C_B and is written to equation form as follows:

$$\frac{\sum_R^n \frac{f_R}{a_R}}{n} = C_B, \qquad with\ R = 3000, 4000, 5000, \ldots, 25000\ and\ n = 23 \tag{65}$$

Next, equation (64) can be simplified to equation (66), since $b_R \approx 0$.

$$\sigma' = t * a_R \tag{66}$$

Deformation height f is calculated using the length of the plate along its curved edge and the design radius, as shown in equation (67).

$$f = R - \sqrt{R^2 * \cos^2\left(\frac{B}{2 * R}\right)} \tag{67}$$

Equations (65), (66) and (67), are combined into equation (68), which can be used to calculate the principal stress.

$$\sigma' = \frac{t * \left(R - \sqrt{R^2 * \cos^2\left(\frac{B}{2 * R}\right)}\right)}{C_B} \tag{68}$$

From the derived equation can be concluded that the value of C_B needs to be computed first, in order to solve the equation. In Table 6 the values of C_B are shown for the different plate sizes. From this table can be concluded that the factor depends on the width of the plate. In line with earlier findings, this should mean that the principal stress for a certain thickness and design radius are approximately the same for different 'sets' of C_B and B. The resulting stresses per set of C_B and B for the example case of a 10mm thick plate with a radius of 12m are shown in Table 7. It can be seen that the results are approximately the same, except for the case of a plate width of 1m.

Table 6: Values of C_B for different plate sizes

Values of C_B [-]				
B \ H	**1000**	**2000**	**3000**	**Round**
1000	2.94			**3.0**
2000	11.09	10.96		**11.0**
3000	24.42	23.92	23.99	**24.0**
4000	43.01	42.06	41.93	**42.0**
5000	66.75	65.19	65.45	**66.0**
6000	95.68	93.43	93.37	**94.0**

Table 7: Principal stresses per plate width

Width [mm]	C_B [-]	Principal stress [N/mm2]
1000	3.0	34.72
2000	11.0	37.86
3000	24.0	39.01
4000	42.0	39.59
5000	66.0	39.31
6000	94.0	39.69

In order to determine the most accurate set of C_B and B, a comparison is made with averaged principal stresses from numerical modelling. The absolute average deviations of the different sets are shown in Table 8. From the table can be concluded that the set of $C_B = 42.0$ and $B = 4000$, results in the lowest deviation. By filling in this set into equation (120), the equation is simplified to be only dependent on thickness and design radius.

Table 8: Average deviations per set B and C_B

Width [mm]	C_B [-]	Absolute average deviation [%]
1000	3.0	11.84%
2000	11.0	3.91%
3000	24.0	1.27%
4000	42.0	0.93%
5000	66.0	1.23%
6000	94.0	1.51%

3.4.4. Method of choice

From the validation and interpretation of results of the proposed analytical methods, it can be concluded that the 'Engineering method' is most accurate. Therefore, equation (69) is used for the first component of the final developed analytical method (Chapter 6). Generalizability and validity of results from numerical modelling and the developed analytical models are discussed Chapter 7.

$$\sigma' = \frac{t * \left(R - \sqrt{R^2 * \cos^2\left(\frac{2000}{R}\right)}\right)}{42} \tag{69}$$

4. Fixation moment

In this chapter, the transition of the cold-bent IGU from 'Bending phase' to 'Fixation moment' is discussed. The same approach is used as in the previous paragraph. First the goal of modelling and corresponding boundary conditions of the 'Fixation moment' are discussed, which are in line with the findings from literature and practice, as discussed in Chapter 2.1. To gain insights in the differences in structural behaviour of the curved plates after the 'Fixation moment', results from numerical modelling are generated. These insights are then used for the development of an analytical method.

4.1. Goal

After fixation of the curved glass onto a substructure, the bending forces are released and the IGU gets subjected to its permanent support conditions. Due to this release of bending forces, the centre of the plate is free to move within its restrained support conditions. Furthermore, this release redistributes the cold bending stresses to a least stressed state. From exploratory numerical modelling and literature study it is concluded that this least stressed state is governed by the anticlastic bending behaviour of the plate. Therefore, the goal of modelling of the 'Fixation moment' is to gain insights in the anticlastic bending behaviour of curved plates. By doing so, parameters which influence the anticlastic behaviour are identified, and if necessary, can be accounted for in the design phase to reduce visual distortions. Furthermore, it is investigated whether the anticlastic deformations have influence on the cavity pressure inside the IGU.

4.2. Boundary conditions

As discussed in Chapter 2.1, the support conditions at the 'Fixation moment' of IGU, are defined by the type of fixing of the glass, which differ per project. Still, all types of fixing have in common that both plates of the IGU have to be hermetically sealed by the spacer. A spacer can be considered as a continuous line support along all edges of the IGU. Since the spacer is simplified to be rigid, the support conditions are simplified to be line supports. Second, the change in boundary conditions from 'Bending phase' to 'Fixation moment' must be accommodated. This is done by using the finite element modelling option of 'prescribed displacements', which is the same approach as used in (Bijster, Noteboom, & Eekhout, 2016). The prescribed displacements are attached to nodes, the nodes therefore have to be modelled as supports. An example of the supported displacement nodes is shown in Figure 63. The nodes are placed at a mesh size distance apart from each other along sides AC and BD. Besides fixing these nodes in z-direction to accommodate the out-of-plane displacements, they are also fixed in x-direction to accommodate the geometrically nonlinear displacement. The nodes are free in y-direction to create a degree of freedom, which is lines with the design tolerances from practice. Sides AB and CD are line supported in y- and z-direction, in which they accommodate model stability for y-displacements and function as base points of the curved edges.

The prescribed displacements in y- and z-direction are derived from the DIANA models for the 'Bending phase' (Figure 64). Based on a design radius, the curvature height and span are interpolated between the x-, y- and z-coordinates from the closest two load steps from the 'Bending phase' models. This is done for each node along AC and BD, with the mesh size distance in between nodes. The reference point of deformation is the midspan of the curved edge, line EF. Therefore, nodes E and F have only a displacement in z-direction, which are relative largest. Nodes A, B, C and D, only have a displacement in x-direction. All other displacements are somewhere in between these limits. The interpolation and calculation of the displacements are done using a python script, in which also the command lines to create these displacements and their respective support conditions are generated. All other actions, such as setting material properties, creating a plate element, setup and execution of the analysis and exportation of nodes and stresses are automated using .py command lines as well. Due to this optimised workflow, multiple DIANA models can be solved after each other, without the involvement of a user. Still, during postprocessing, some diverging models are identified for which the analysis commands have to be manually adjusted.

An example of the results of a 2000x2000x10mm plate, with a radius of 12m and the setup of boundary conditions is shown in Figure 65 to Figure 68. The most noticeable difference in results between the ‘Bending phase’ and ‘Fixation moment’ are displacements in y- and z-directions. As can be seen in Figure 66, due to the release of bending forces, sides AC and BD are pulled towards each other as a result of anticlastic bending. In line with the displacements in y-direction, the height around the midspan of the plate is lowered as a result of anticlastic bending. This can be seen when looking at the colour grading for the displacements in z-direction (Figure 67), in contrary to the bending phase, the lines which distinct the colours are not parallel. There is also a clear reduction of maximum principal tensile stresses around midspan (Figure 68), compared to the bending phase. The peak stresses are however approximately the same, along the supported sides of the curved glass plate.

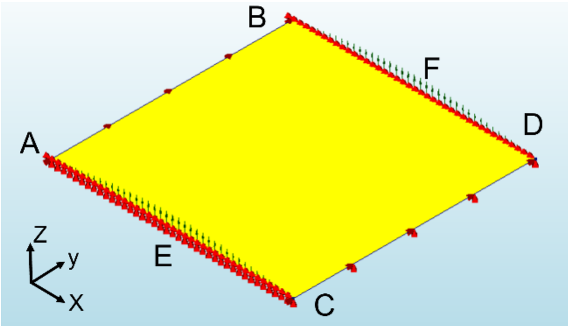

Figure 63: Boundary conditions ‘Fixation moment’

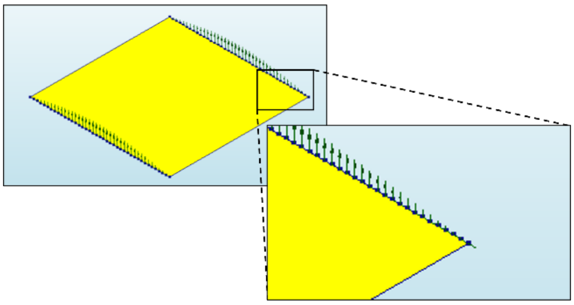

Figure 64: Prescribed displacements

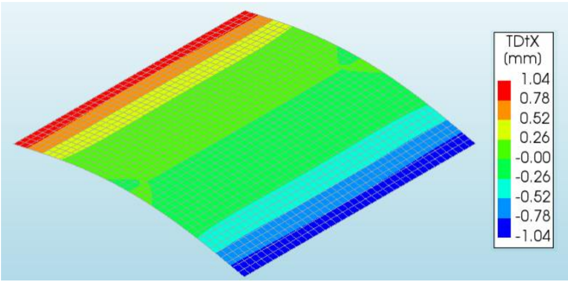

Figure 65: Displacements in x-direction

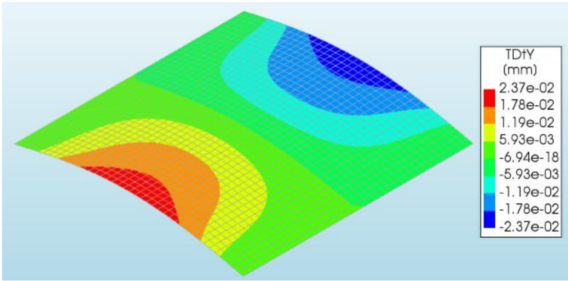

Figure 66: Displacements in y-direction

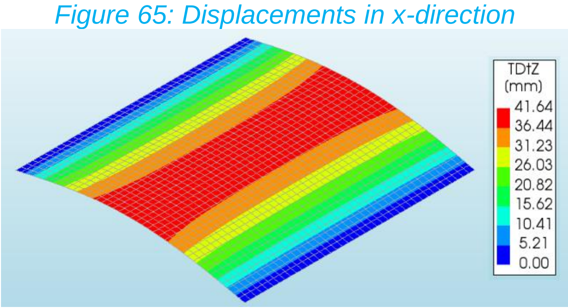

Figure 67: Displacements in z-direction

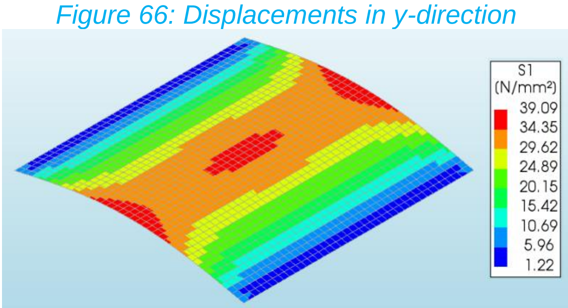

Figure 68: Stresses in layer 3 of S1

4.3. Numerical modelling

In this paragraph, the most noticeable results from the modelling of the 'Fixation moment' are discussed. In line with the goal of this modelling phase, the emphasis is on the anticlastic bending behaviour of plate. This behaviour is clearly observed, when looking at the deformation along midspan EF of the curved plate. In Figure 69, a 2000x2000x20mm plate with a radius of 25m is shown as illustrative example, the plate has a clear anticlastic bending deformation, which is highlighted in red. The results from DIANA are postprocessed using Python, as shown in Figure 70. In order to accentuate anticlastic bending, the deformation in z-direction is not scaled compared to the height and width of the plate. The line highlighted in red is referred to as the anticlastic bending line and is plotted in the y-z plane to clearly show the shape of the line. This particular example shows a saddle like double curvature. Based on an exploratory study, it is concluded that the extent and shape of the anticlastic bending line are dependent on Poisson's ratio, plate thickness, radius of curvature and plate height width ratio. For each of these parameters, examples are given below.

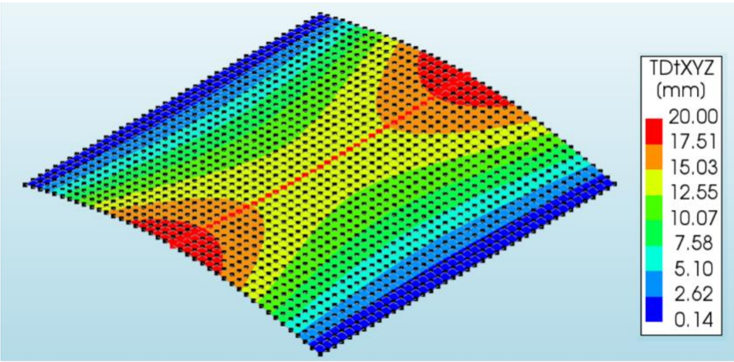

Figure 69: Anticlastic bending line for a 2000x2000x20mm, R=25m

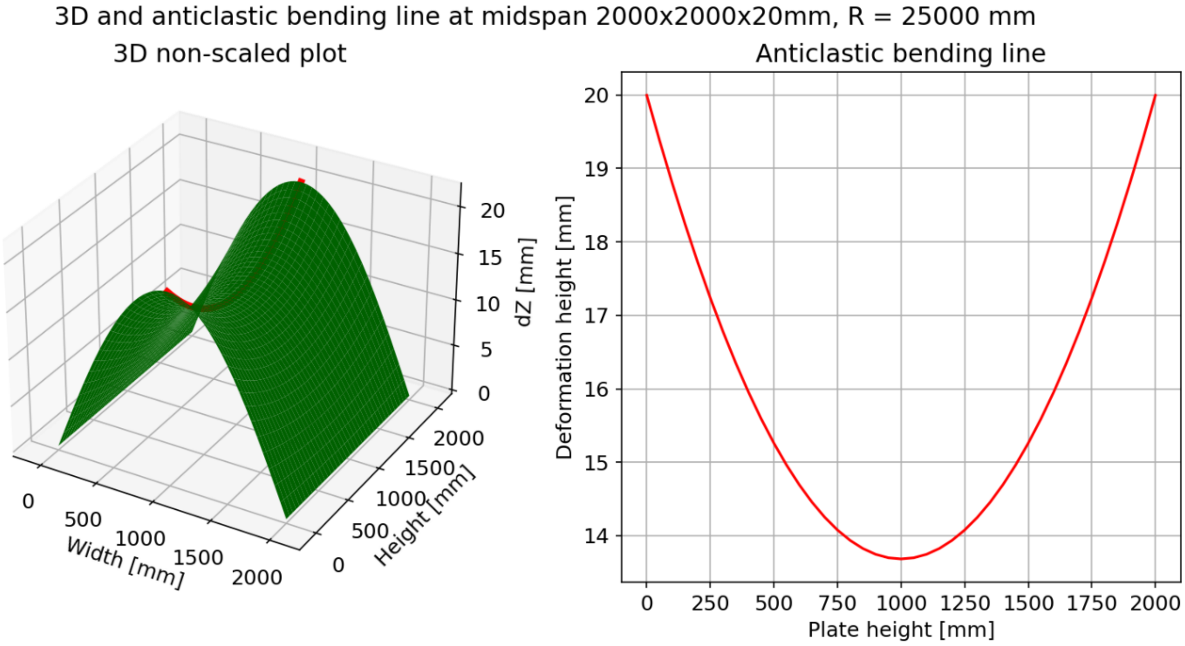

Figure 70: Postprocessing of results in Python, anticlastic bending line plot y-z plane

4.3.1. Poisson's ratio

According to plate theory, anticlastic bending is a result of Poisson's ratio. Therefore, the relations between the anticlastic bending behaviour and Poisson's ratio are investigated. Below an example is shown of the comparison for a 2000x2000x10mm, R=12m plate, with Poisson ratios ranging from $\nu = 0.115$, $\nu = 0.23$, $\nu = 0.345$ to $\nu = 0.46$, which are, respectively 0.5x, 1x, 1.5x and 2x the Poisson's ratio of glass. The first example is that of $\nu = 0.23$, which is shown as reference for comparison in Figure 71. It can be seen that the anticlastic effect is much smaller than that of the example shown in the previous paragraph, furthermore the shape of the line is rounder.

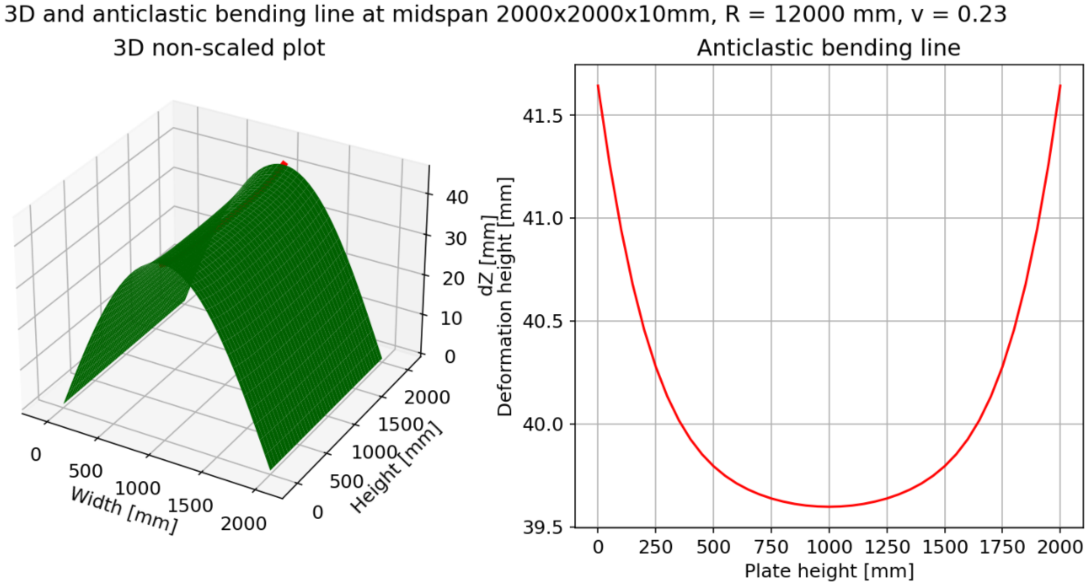

Figure 71: Anticlastic bending line for a 2000x2000x10mm, R=12m plate, v=0.23

Based on the comparison between the different Poisson ratios (Figure 72), it can be concluded that a higher ratio results in a larger anticlastic effect, which is in line with the expectation of the behaviour of Poisson's ratio. From these findings it is concluded that the double curved shape is indeed a result of anticlastic bending behaviour due to Poisson's ratio. Other parameters are also of influence, as is shown in the next paragraphs.

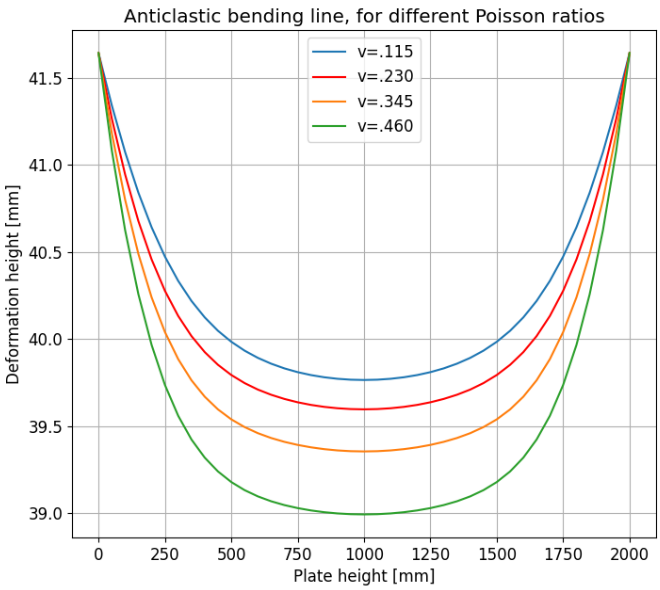

Figure 72: Anticlastic bending lines for different Poisson ratios

4.3.2. Plate thickness

From results it has been concluded that the thickness of the plate is also a parameter of influence on the anticlastic behaviour. An illustrative example is shown below in Figure 73, for a 2x2m plate thicknesses ranging from 4mm to 20mm. The same reference case as shown in the previous paragraph is used, with the red line with markings being the anticlastic bending line for a thickness of 10mm. It can be seen that the anticlastic effect is largest for thicker plates. Furthermore, it can be seen that for small thicknesses, the shape of the anticlastic line changes from a single curved line to a ‘w-shape’.

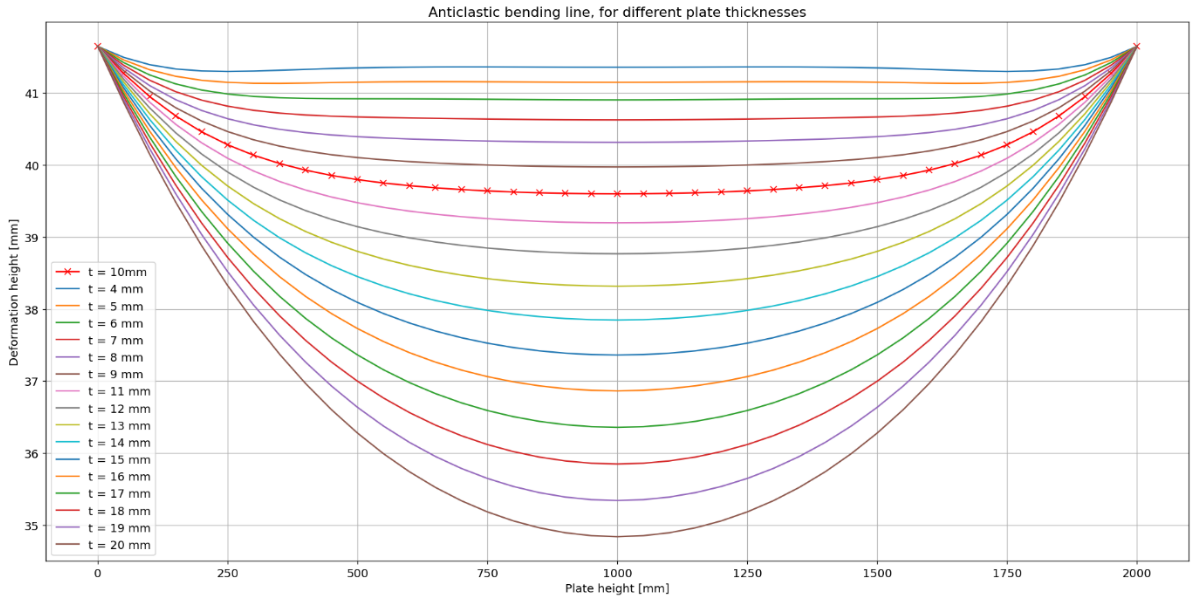

Figure 73: Anticlastic bending line for different plate thicknesses

4.3.3. Radius of curvature

The radius of curvature has also shown to be influencing the anticlastic bending, as shown in Figure 74. In order to compare the lines, the deformation height corresponding to the design radius, is subtracted, such that all lines start at 0. Again, the comparison is based on that of the reference case as showed in Figure 71. The marked red line resembles a radius of 12m. It can be seen that smaller radii have a smaller anticlastic effect. Furthermore, the smallest radii have the most apparent w-shape.

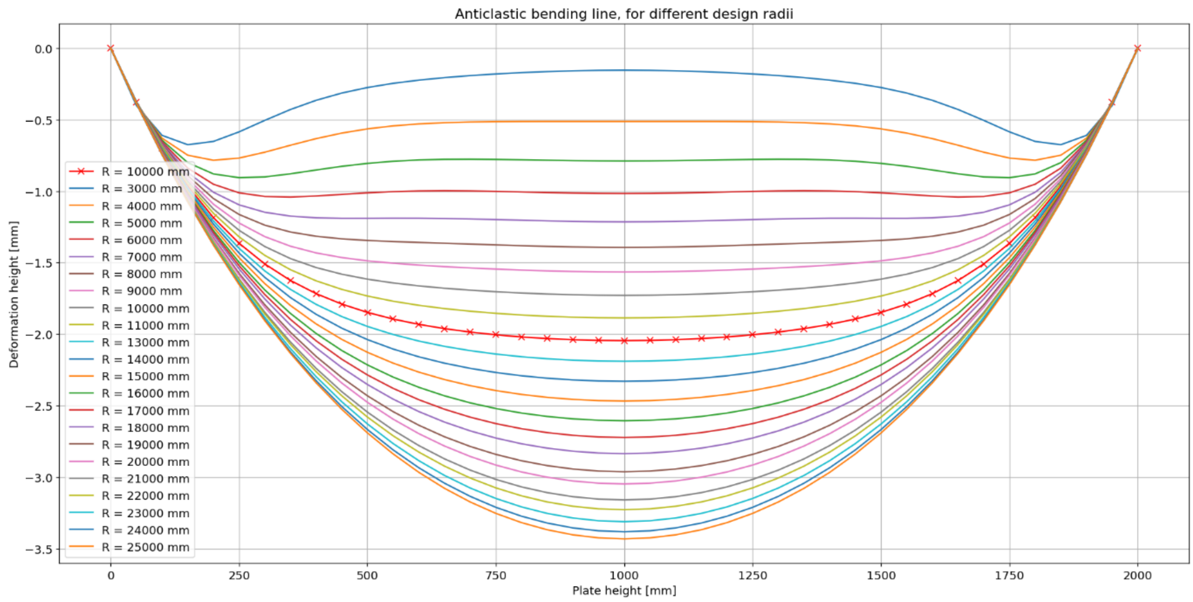

Figure 74: Anticlastic bending line for different design radii

4.3.4. Plate size

The last design parameter that is of influence on the anticlastic bending behaviour is the height-width ratio of the plate. Below four examples are shown of a plate with a height of 3m, a radius of 12m and a thickness of 10mm. The plate widths are ranging from 3m to 6m, the results are shown in Figure 75. Noticeable is the 'non-chronological' order of anticlastic lines. It can be seen that the square plate has the largest anticlastic effect. For the 4:3 ratio, the effect is smallest. The results for the 5:3 and 6:3 ratio are in between. This non-chronological order is in contrast with the other parameters of influence, which all show a gradual course in anticlastic deflection.

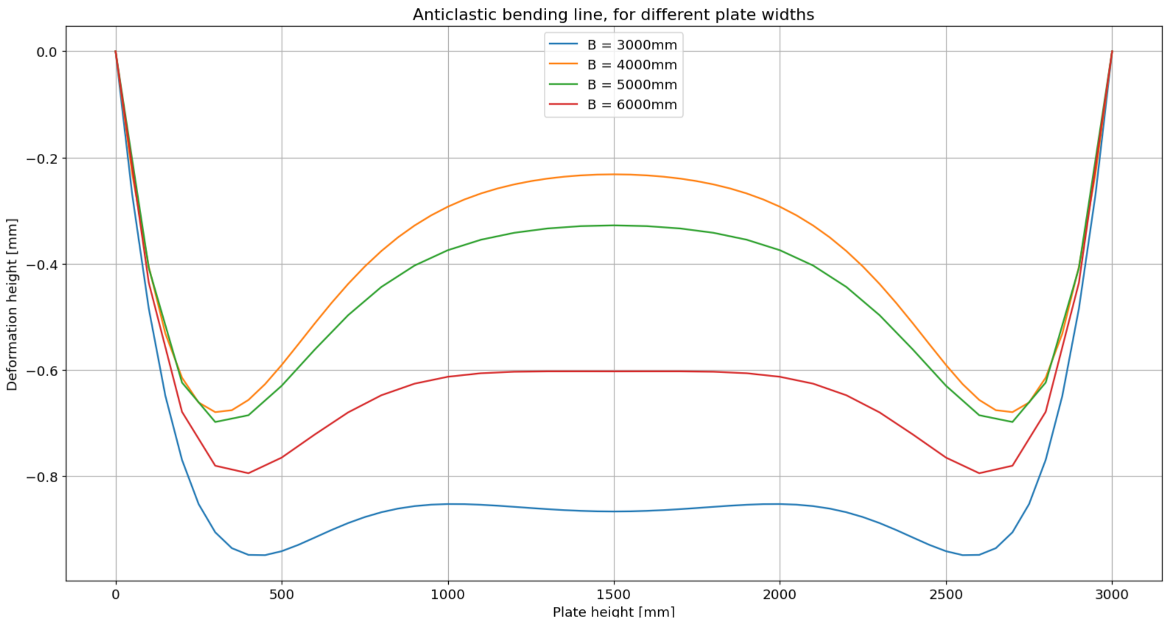

Figure 75: Anticlastic bending line for different plate widths

4.3.5. Conclusion

From the evaluation of results, the following conclusions are drawn. In general holds that anticlastic bending effects are smaller for thinner plates and smaller radii. Furthermore, thinner plates tend to 'buckle' into a w-shape at a certain radius. However, from results it is not clear at which point this shift of single curved to w-shape occurs. Due to the occurrence of diverging models, analysis parameters had to be adjusted, resulting in for example smaller load steps. These adjustments can result in inconsistencies when comparing plates which each other. Furthermore, as can be seen in Figure 75, different mesh sizes have been used per plate size, to decrease the number of diverging models. This also can result in inconsistencies when comparing effects between different plate sizes. These findings and conclusions have been taken into account in the development of the analytical model.

4.4. Analytical modelling

In literature no analytical derivations are found which are exactly in line with the boundary conditions as considered for the 'Fixation moment'. Therefore, based on the knowledge gained with numerical modelling, theories are explored which show similarities with the discussed results.

4.4.1. Poisson's ratio method

The first simplified approach is based on Poisson's ratio, for which it is considered the moment in y-direction at midspan of the plate is $M_y = \nu * M_x$. The equation is the same as that from (Young & Budynas, 2002) in which it is used to simplify a 2D plate to a 1D beam. The theory also states that at the edges $M_y = 0$. Using the Euler Bernoulli beam theory, equation (70) is derived for the anticlastic bending line along the height of the plate at midspan of the width (Figure 76, page 56).

$$w_y = f - \frac{\nu * M_x * y(-y + H)}{2EI} \tag{70}$$

In which:

w_y	is the height function of the anticlastic bending line in y-direction at midspan of the width, in mm;
f	is the curvature height of the arch at midspan, in mm
M_x	is the bending moment in x-direction at midspan of the curved edge, in Nmm;
ν	is the Poisson's ratio of glass, whereby $\nu = 0.23$;
y	is a point on the anticlastic bending line, in mm;
H	is the height of the plate, in mm;
EI	is the stiffness of the plate simplified to a beam, in Nmm^2.

In order to assess the validity of the method, the values of M_x are used from numerical modelling. The results are compared to those from numerical modelling by calculating the difference in height at the centre of the plate. The comparison is made for 102 cases, with different Poisson ratio's, plate thicknesses and height-width ratios. For each case, 6 radii of curvature are considered. From the validation, shown in Table 9, can be concluded that the method is inaccurate, especially when different height-width ratios are considered.

Table 9: Validation Poisson's ratio method

Comparison	Nr of cases [-]	Deviation [%]
Poisson	24	15.08%
Thickness	36	9.61%
Ratio	42	138.30%
Total	**102**	**54.33%**

4.4.2. Timoshenko method

Due to the large differences between the Poisson's ratio method and results from DIANA, another method is considered. This method is based on the Timoshenko plate theory for rectangular plates with two opposite edges simply supported and the other two free, as presented in Chapter 2.4.3. The tabulated values per height-width ratio of the plate are used to determine the anticlastic bending line at midspan, using equation (71). The line is simplified to have a sinusoidal shape function.

$$w_y = f - \frac{f * \alpha_1 * \sin\left(\frac{y * \pi}{H}\right)}{\alpha_2} \tag{71}$$

In which:

w_y	is the height function of the anticlastic bending line in y-direction at midspan, in mm;
f	is the curvature height of the arch at midspan, in mm
y	is a point on the anticlastic bending line, in mm;
H	is the height of the plate, in mm;
α_1, α_2	are tabulated coefficients from Figure 36, Chapter 2.4.3.

The results of this method are calculated for the similar load cases as discussed before and shown in Table 10. It can be seen that the height-width ratio has been accounted for by using the tabulated values. Although the method is more accurate than the Poisson's ratio method, it is still concluded that deviations are too large. Therefore, a third method is considered, which is based on regression between results.

Table 10: Validation Timoshenko method

Comparison	Nr. of cases [-]	Deviation [%]
Poisson	24	5.38%
Thickness	36	6.48%
Ratio	42	12.42%
Total	**102**	**8.62%**

4.4.3. Result based approach

The third method that is considered to analytically model the anticlastic bending behaviour, is based on regression between the results from numerical modelling. The regression is based on the relation between the anticlastic bending line and plate thickness, as shown in Figure 73, Chapter 4.3. In the figure can be seen that the midpoints of the anticlastic bending lines are almost equally spaced apart per plate thickness. The midpoint of the anticlastic bending line can be expressed as a radius of midspan, as shown in Figure 76. Using the radius at midspan and the design radius, a simplified anticlastic bending line is considered, which is based on a sinusoidal shape function. Due to this simplification, all anticlastic bending lines have the same shape, meaning that for example the occurrence of the w-shape is not considered. A benefit of the simplification is that the total geometry of the anticlastic curved plate can now be determined with the parameters of width, height, thickness, design radius and radius at midspan. By defining regression between the radius at midspan and plate thickness, the geometry can be defined by design parameters only.

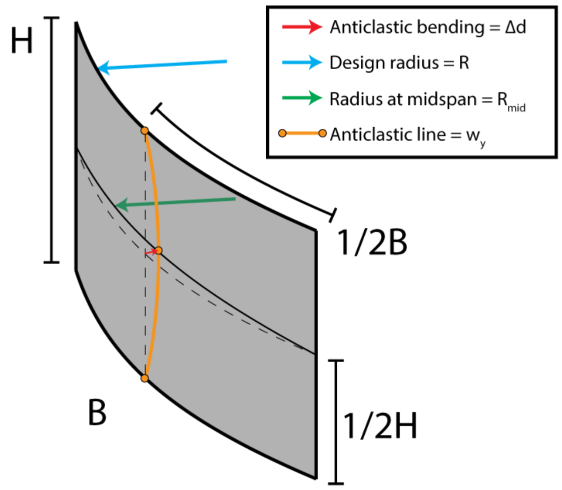

Figure 76: Decreased radius at midspan due to anticlastic bending

In Figure 77 the regression between the radius at midspan and plate thickness is shown for a 2x2m plate with a radius of 12m. The markers resemble that height of the anticlastic bending line at midspan, as shown in Figure 73, Chapter 4.3. The red line shows the linear approximation of the data points per plate thickness. In Figure 78, the linear approximations for radii ranging from 3m (bottom line) to 25m (top line) are shown. The validity and interpretation of results is discussed in Chapter 7.

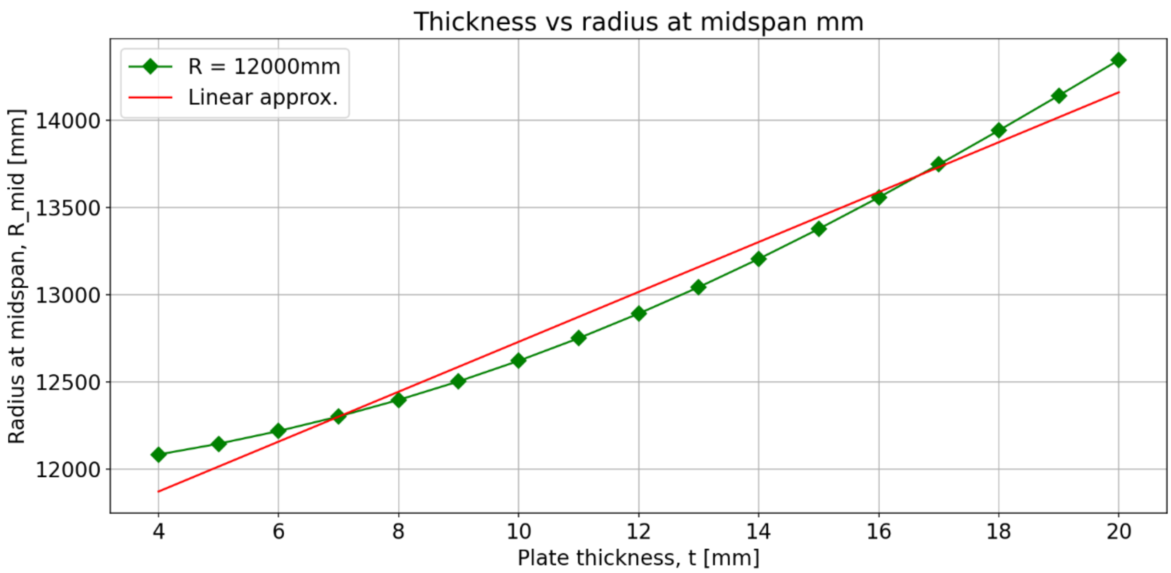

Figure 77: Regression between radius at midspan and plate thickness for a 2x2m plate, R=12m

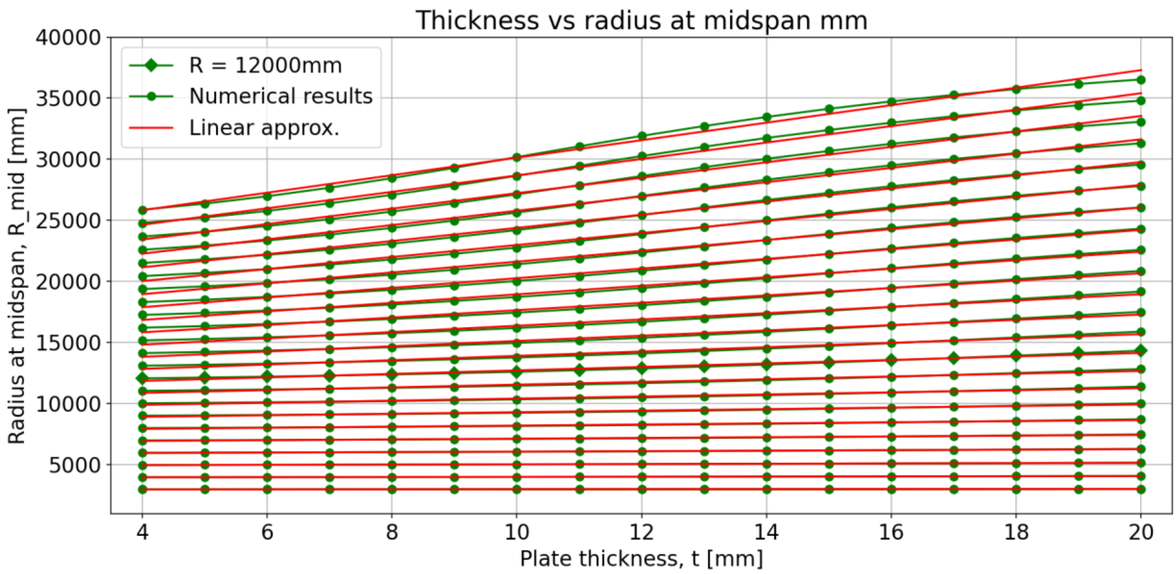

Figure 78: Regression between radius at midspan and plate thickness for a 2x2m plate

With the linear approximations, each design radius has an 'a' and 'b' coefficient for which the radius at midspan can be determined using the thickness. This means that, to determine the radius at midspan of a 2x2m plate, 34 tabulated coefficients are needed. However, by plotting these 'a' and 'b' coefficients against the design radius of the plate, another trend can be seen. In Figure 79 and Figure 80 can be seen that by using a 3rd order polynomial, both the trends of the 'a' and 'b' values can be accurately determined. The 3rd order polynomial consists of 4 coefficients, which means that the number of coefficients can be reduced from 34 to 8 per plate size. The resulting coefficients of a 2x2m plate are shown in Table 11.

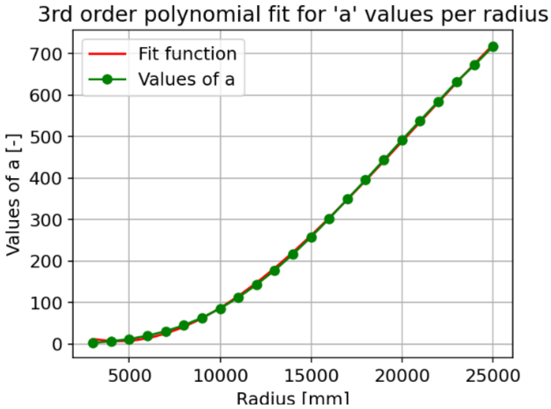

Figure 79: 3rd order polynomial approximation of 'a' coefficients

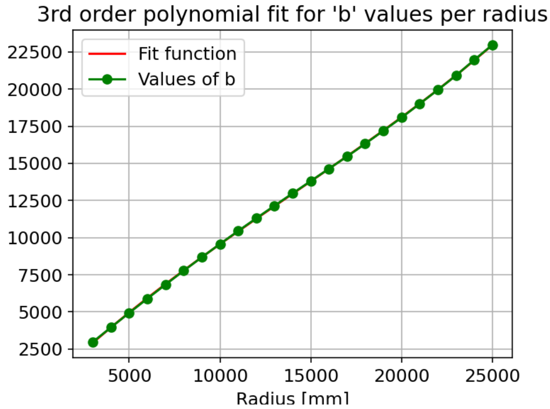

Figure 80: 3rd order polynomial approximation of 'b' coefficients

Table 11: Regression coefficients, 2x2m plate

2000x2000		
	A	***B***
a	-5.862E-11	6.047E-10
b	3.664E-06	-2.548E-05
c	-2.881E-02	1.196E+00
d	6.701E+01	-4.545E+02

Using the eight regression coefficients, the radius at midspan for a certain design radius and plate thickness is calculated as follows:

$$A_{B:H} = a_{A_{B:H}} * R^3 + b_{A_{B:H}} * R^2 + c_{A_{B:H}} * R + d_{A_{B:H}} \tag{72}$$

$$B_{B:H} = a_{B_{B:H}} * R^3 + b_{B_{B:H}} * R^2 + c_{B_{B:H}} * R + d_{B_{B:H}} \tag{73}$$

$$R_{mid} = A_{B:H} * t + B_{B:H} \tag{74}$$

In which:

$a_{A_{B:H}}, \dots, d_{B_{B:H}}$ are the polynomial coefficients per plate height-to-width ratio
$A_{B:H}, B_{B:H}$ are the linear coefficients per plate height-to-width ratio;
R is the design radius of the IGU, in mm;
R_{mid} is the radius at midspan of glass plate as a result of anticlastic bending, in mm;
t is the thickness of glass plate, in mm.

Validity of the method is discussed in Chapter 7. From the validation of the 2x2m plate it is concluded that the method has a great potential to accurately determine the radius at midspan as a result of anticlastic bending. A downside of the method, however, is that the regression coefficients are plate size specific. Furthermore, in order for the method to be comprehensive for a wide range of plate thicknesses and design radii, a lot of numerical models have to be analysed. On account of the optimised workflow, it is decided to generate the regression coefficients for a range of 1x1m up to 6x3m plate, with a 1m interval. This size range is in line with the maximum size of standardized jumbo glass plates. Furthermore, since cold-bending over the short edge of a rectangular plate is not practical, plates with a larger height than width ratio are left out of consideration. These considerations leave for a database of regression coefficients for 15 different height-width ratios, of which all ratios have plate thickness from ranging from 4mm to 20mm and in radius of curvature ranging from 25m to 3m. In total 15 x 23 x 17 = 5865 plates have been modelled and post-processed, to generate the regression coefficients. The results per plate size are shown in Appendix B.1 and discussed in Chapter 7. An overview of the accuracy of the method for the considered plate sizes is shown in Table 12. The regression coefficients for all considered plate sizes are shown in Table 13.

Table 12: Average deviations in radius at midspan per plate size

B:H	1000	2000	3000
1000	2.46%		
2000	0.31%	0.67%	
3000	0.10%	0.15%	0.33%
4000	0.05%	0.08%	0.10%
5000	0.03%	0.04%	0.06%
6000	0.02%	0.02%	0.03%
		Average deviation:	**0.30%**

4.4.4. Tabulated regression coefficients

Table 13: Tabulated regression coefficients, per plate size

1000x1000		
	A	**B**
a	7.689E-11	-1.382E-09
b	-4.668E-06	7.889E-05
c	8.653E-02	2.764E-01
d	-1.931E+02	1.307E+03

2000x1000		
	A	**B**
a	-7.993E-12	1.055E-11
b	2.574E-07	2.382E-06
c	2.835E-03	9.522E-01
d	-1.073E+01	1.331E+02

2000x2000		
	A	**B**
a	-5.862E-11	6.047E-10
b	3.664E-06	-2.548E-05
c	-2.881E-02	1.196E+00
d	6.701E+01	-4.545E+02

3000x1000		
	A	**B**
a	-3.179E-12	1.230E-11
b	1.167E-07	3.846E-07
c	6.110E-04	9.886E-01
d	-2.874E+00	3.600E+01

3000x2000		
	A	**B**
a	-3.164E-13	2.959E-11
b	3.254E-07	-2.264E-06
c	-2.396E-03	1.015E+00
d	4.562E+00	-2.620E+01

3000x3000		
	A	**B**
a	1.521E-11	-7.717E-11
b	2.747E-08	6.874E-08
c	2.619E-04	9.935E-01
d	-1.902E+00	1.903E+01

4000x1000		
	A	**B**
a	-1.464E-12	2.529E-12
b	5.329E-08	3.264E-07
c	3.522E-04	9.934E-01
d	-1.432E+00	1.962E+01

4000x2000		
	A	**B**
a	-8.339E-14	8.344E-12
b	1.338E-07	-9.377E-07
c	-1.289E-03	1.010E+00
d	3.178E+00	-2.136E+01

4000x3000		
	A	**B**
a	2.322E-12	-1.107E-11
b	7.000E-08	-4.085E-07
c	-7.032E-04	1.003E+00
d	1.140E+00	-1.263E-01

5000x1000		
	A	**B**
a	-9.329E-13	7.205E-14
b	3.112E-08	2.892E-07
c	2.645E-04	9.947E-01
d	-1.054E+00	1.649E+01

5000x2000		
	A	**B**
a	2.155E-14	2.448E-12
b	6.132E-08	-3.760E-07
c	-6.106E-04	1.005E+00
d	1.816E+00	-1.330E+01

5000x3000		
	A	**B**
a	1.113E-12	-7.436E-12
b	2.323E-08	-1.356E-07
c	-4.166E-04	1.004E+00
d	1.260E+00	-9.043E+00

6000x1000		
	A	**B**
a	-7.658E-13	1.205E-12
b	2.590E-08	1.466E-07
c	1.218E-04	9.971E-01
d	-4.530E-01	7.556E+00

6000x2000		
	A	**B**
a	-3.932E-13	4.633E-12
b	4.603E-08	-2.625E-07
c	-3.913E-04	1.003E+00
d	1.209E+00	-8.937E+00

6000x3000		
	A	**B**
a	4.670E-13	-5.046E-12
b	3.500E-09	9.762E-08
c	-7.279E-05	1.001E+00
d	4.522E-01	-2.650E+00

4.4.5. Interpolation for in-between plate sizes

In case the dimensions of the plate are in between the given heights and widths in the coefficients table, the radii at midspan must be linearly interpolated for. Since the values of the coefficients are specific and there are no relations between the values of plate sizes, it is not possible to interpolate the coefficients themselves. Therefore, first the radii at midspan of plates which in size are close to the specified case must be calculated. After that, the radii at midspan can be interpolated for. In order to accommodate an organised interpolation scheme, Table 14 can be used. First, the specified plate dimensions are filled in cells H and B. Then, the closest lower and upper dimensions which are included in the coefficient table are filled in, in cells B_L, B_U, H_L and H_U. The radii at midspan of the lower and upper dimensions can then be calculated using the 3rd order polynomials and the linear approximation, equation (72)-(74). After filling in $R_{mid;i;LL}$, $R_{mid;i;LU}$, $R_{mid;i;UL}$ and $R_{mid;i;UU}$ in the table, it is clear which upper and lower boundaries must be interpolated for. The interpolation is done using the standard linear equation for interpolation between two points, as shown in (75). In order to accommodate an organised calculation of the interpolated radii, all equations are written out in the final developed analytical method (Chapter 6.3). The final interpolated radius at midspan $R_{mid;i}$ is calculated using the average of the four interpolated radii.

$$y - y_1 = \frac{(y_2 - y_1)}{x_2 - x_1} * (x - x_1) \tag{75}$$

Table 14: Guiding table for interpolation

	B_L	$\boldsymbol{B}$	B_U
H_L	$R_{mid;i;LL}$	$R_{mid;i;1}$	$R_{mid;i;LU}$
$\boldsymbol{H}$	$R_{mid;i;2}$	$\boldsymbol{R_{mid;i}}$	$R_{mid;i;3}$
H_U	$R_{mid;i;UL}$	$R_{mid;i;4}$	$R_{mid;i;UU}$

4.5. Cavity pressure

From the numerical and analytical results of the radius at midspan can be concluded that anticlastic bending differs per plate thickness. In case of an asymmetric IGU, this difference results in a change in cavity volume, and therefore an isochoric pressure inside the cavity after the 'Fixation moment'. Using Boyle's law, the isochoric pressure can be calculated. To get an idea about the change in cavity volume, first the cavity distance as a result of anticlastic bending is determined. Second, a simplified equation is derived which can be used to determine the volume below the anticlastic curved glass plates. Last, an iterative method to find equilibrium between the differences in volume of deformation due to asymmetric anticlastic bending is considered.

4.5.1. Change in cavity distance as a result of anticlastic bending

By using the result-based approach as discussed in the previous paragraph, the radius at midspan of the plate is calculated. Using this radius, the difference in height between the edge and the centre of the plate can be calculated. In Figure 81, these differences in height are visualised using the red and green arrows. When $t_1 \neq t_2$, there will be a difference in cavity volume, as $\Delta d_1 \neq \Delta d_2$.

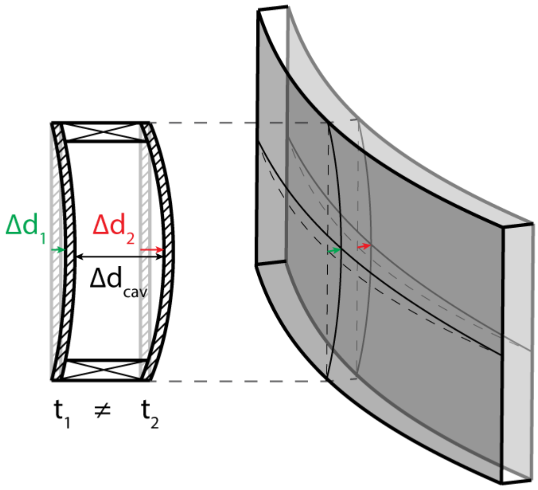

Figure 81: Curvature height differences between edge and centre, as a result of anticlastic bending

The values of Δd_1 and Δd_2 are calculated by subtracting the curvature height at midspan, from the curvature height at the edge, $\Delta d = f_{edge} - f_{mid}$. The curvature height is calculated using the radius of curvature and plate width B, as shown in equation (76). Both equations are then combined into equation (77), which is used to calculate the height difference at the centre of the plate due to anticlastic bending. For asymmetric IGU's holds that if $\Delta d_1 < \Delta d_2$, the cavity volume increases and there will be an isochoric underpressure. If $\Delta d_1 > \Delta d_2$, the cavity volume decreases and there will be an overpressure in the cavity.

$$f = R - \sqrt{R^2 * \cos^2\left(\frac{B}{2R}\right)}, \qquad f_{mid} = R_{mid} - \sqrt{R_{mid}^2 * \cos^2\left(\frac{B}{2R_{mid}}\right)} \tag{76}$$

$$\Delta d = R - \sqrt{R^2 * \cos^2\left(\frac{B}{2R}\right)} - R_{mid} + \sqrt{R_{mid}^2 * \cos^2\left(\frac{B}{2R_{mid}}\right)} \tag{77}$$

In which:

f	is the curvature height at midspan of the curved edge of the plate, in mm;
R	is the design radius of the IGU, in mm;
f_{mid}	is the curvature height at the centre of the plate, in mm;
R_{mid}	is the radius at midspan as a result of anticlastic bending, in mm;
B	is the width of the IGU, in mm;
Δd	is the difference at the centre of the plate due to anticlastic bending, in mm.

4.5.2. Change in cavity volume as a result of anticlastic bending

On account of simplification of the anticlastic bending line to a sinusoidal function, the volume below an anticlastic curved glass plate can be calculated. The calculation is based on simplifying an average curvature height. In Figure 82, the anticlastic bending line is highlighted in orange. The average height of the anticlastic bending line along the height of the plate can be simplified to $\Delta d_{avg} = \frac{1}{2} * \pi * d$. Using this value, the average curvature height of the curved plate is $f_{avg} = f - \Delta d_{avg}$.

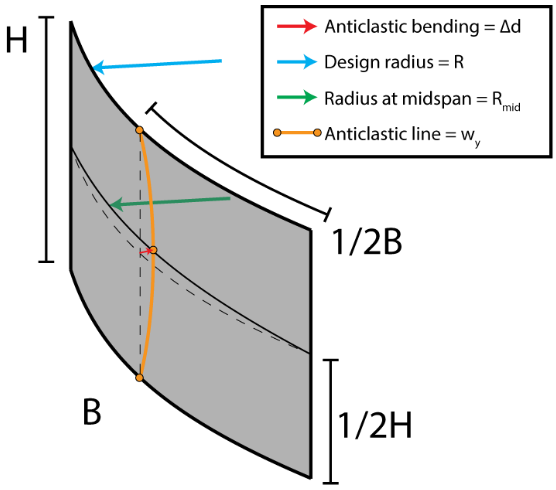

Figure 82: Anticlastic curved glass panel

In Chapter 3.3 it is concluded that the shape of curved edge B, is similar to a sinusoidal function. The area below a sinusoidal function is calculated using equation (79). By multiplying this area with the height of the plate, a simplified volume below the curved glass plate is calculated. The equations, necessary to calculate the simplified volume, are shown below.

$$\Delta V = A * H \tag{78}$$

Whereby:

$$A = 2 * L * f_{avg}/\pi \tag{79}$$

$$L = 2 * R * \sin\left(\frac{B}{2R}\right) \tag{80}$$

$$f_{avg} = f - \frac{1}{2} * \pi * d \tag{81}$$

By substituting equation (76) and (77) into equation (81) and then substituting the above equations (79), (80) and (81) into the equation for the volume, the following equation is derived to calculate the volume below a curved glass pane i in an IGU:

$$\Delta V = \frac{4HR\sin\left(\frac{B}{2R}\right)}{\pi^2} * \left((-\pi + 2) * \sqrt{R^2 * \cos^2\left(\frac{B}{2R}\right)} - 2\sqrt{R_{mid}^2 * \cos^2\left(\frac{B}{2R_{mid}}\right)} + 2R_{mid} - 2R_{mid} + R\pi \right) \tag{82}$$

In which:

ΔV	is the volume below the cold-bent glass plate, in mm³;
R	is the design radius of the IGU, in mm;
R_{mid}	is the radius at midspan of a glass plate as a result of anticlastic bending, in mm;
H	is the height of the IGU, in mm;
B	is the width of the IGU, in mm.

To validate the simplified equation, the results are compared to results from numerical modelling. This is done in the same way as for the validation of the radii at midspan. Results and comparisons of all evaluated plates are shown in Appendix B.2. The total averaged deviations in volume below the anticlastic curved plates, are shown in Table 15. From the results it is concluded that the simplified calculation is sufficient in determining the volume below curved plates.

Table 15: Average deviations in volume below a curved plate, per plate size

B:H	1000	2000	3000
1000	1.76%		
2000	0.20%	0.69%	
3000	0.41%	0.22%	0.47%
4000	0.62%	0.31%	0.27%
5000	0.75%	0.58%	0.42%
6000	0.91%	0.83%	0.72%
		Average deviation:	**0.61%**

4.5.3. Isochoric pressure as a result of anticlastic bending

Now that the change in volume below an anticlastic curved glass plate can be calculated, the change in cavity volume due to asymmetry of an IGU can be determined. The change in cavity volume is calculated as follows:

$$V_{o;CB} = V - \Delta V_1 + \Delta V_2, \qquad V'_{CB} = -\Delta V_1 + \Delta V_2 \tag{83}$$

Whereby:

$$V = d * B * H \tag{84}$$

In which:

$V_{o;CB}$	is the cavity volume due to isochoric pressures from cold-bending, in mm³;
ΔV_i	is the volume below curved glass pane i of the IGU, in mm³;
V'_{CB}	is the change in cavity volume due to anticlastic bending, in mm³;
V	is the cavity volume, in mm³;
d	is the spacer distance, in mm;
B	is the width of the IGU, in mm;
H	is the height of the IGU, in mm.

Using Boyle's law, the isochoric pressure due to cold-bending is calculated with equation (85), in which $P_{c:P}$ is the barometric pressure at time of sealing the cavity.

$$P_{o;CB} = P_{c;P} - \frac{P_{c;P} * V}{V_{CB}} \tag{85}$$

The isochoric pressure due to cold-bending is shared by effective pressures on the interior and exterior pane of the IGU. Therefore, the change in cavity volume V'_{CB} and isochoric pressure $P_{o;CB}$, should be considered as those from before equilibrium. As it is stated in (Vallabhan & Chou, 1986), equilibrium inside the cavity of an IGU is achieved when:

1. The sum of effective pressures shared by the interior and exterior plate is equal to the external pressure load: $p_{ext} = p_1 + p_2$
2. The difference in volume of deformation due to these effective pressures, is equal to the volume change inside the cavity: $\Delta v = v_1 - v_2$, with $v_1 \leftrightarrow p_1$ and $v_2 \leftrightarrow p_2$

In case of isochoric pressures, the requirements for equilibrium are changed. Since there is no external pressure, the first requirement is left out of consideration. An isochoric pressure will cause both panes of the IGU to either deflect outwards, or inwards. In terms of volume of deformation inside the cavity, this holds that a negative pressure load on the exterior pane, t_1, results in a positive cavity volume change, i.e., $-p_1 \leftrightarrow v_1$ and $p_1 \leftrightarrow -v_1$. The volume change for p_2 is in line with its direction of pressure load: $p_2 \leftrightarrow v_2$ and $-p_2 \leftrightarrow -v_2$. Furthermore, since an isochoric pressure is considered, the effective pressures on the interior and exterior pane will be equal in load, e.g., $-p_1 = p_2$ Based on these findings, the second requirement is changed to:

2. The difference volume of deformation due to these effective pressures, is equal to the volume change inside the cavity: $\Delta v = v_1 - v_2, with\ v_1 \leftrightarrow -p_2\ and\ v_2 \leftrightarrow p_2$

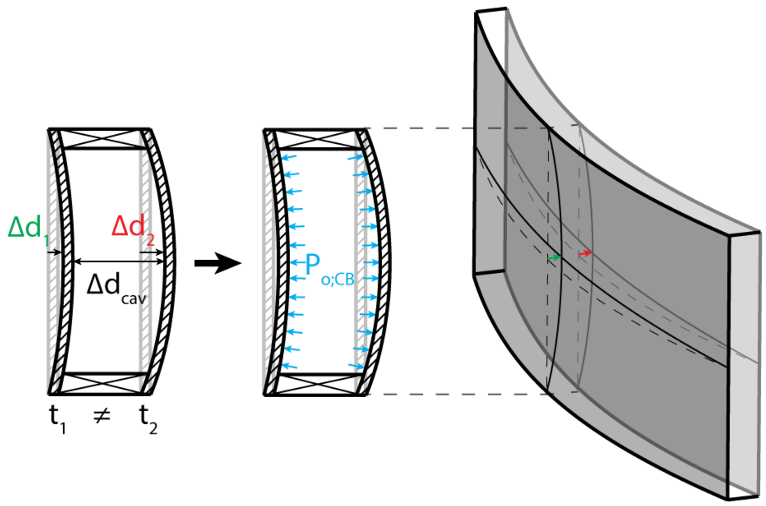

Figure 83: Isochoric pressure due to cold-bending of asymmetric IGU's

By defining the change in volume due to anticlastic bending as V'_{CB}, there is equilibrium in the cavity if $V'_{CB} = v_1 - v_2$. In which v_1 and v_2 are the volume of deformations due to effective pressure load $-p_{2;CB}$ and $p_{2;CB}$. With these findings, the iterative scheme as presented in Chapter 2.3.2, is changed as follows. Instead of finding equilibrium for which holds that $\Delta p = p_{ext} - (p_1 + p_2) \approx 0$, the equilibrium requirement has become $\Delta v = V'_{CB} - (v_1 - v_2) \approx 0$. The isochoric pressure $P_{o;CB}$, is always larger than the resulting pressure $p_{2;CB}$. Therefore, in case of overpressure, $0 < p_{2;CB} < P_{o;CB}$, and in case of underpressure, $P_{o;CB} < p_{2;CB} < 0$. In line with these findings, the first two steps of the iterative scheme are as follows:

Step 1: Let $j = 1$, If $P_{o;CB} < 0$ then $p^L_{2;CB} = P_{o;CB}$ and $p^U_{2;CB} = 0$, otherwise $p^L_{2;CB} = 0$ and $p^U_{2;CB} = P_{o;CB}$.

Step 2: Average $p^a_{2;CB;j} = \frac{1}{2} * (p^L_{2;CB} + p^U_{2;CB})$.

For example, if the isochoric pressure, calculated using equation (85), is $P_{o;CB} = 1$ kN/m², $p^L_{2;CB} = 0$ and $p^U_{2;CB} = P_{o;CB}$. The first estimation of the load shared by the interior pane is then $p^a_{2;CB;1} =$ .5 kN/m². With this effective pressure load, the volume of deformation of the interior and exterior pane can be calculated, which is considered as step 3.

Step 3: Calculate $v_{1;j}$ due to effective pressure load $-p^a_{2;CB;j}$ and $v_{2;j}$ due to $p^a_{2;CB;j}$.

With the requirement of equilibrium for isochoric pressures, step 4 becomes:

Step 4: In order to get equilibrium, the sum of $\left|v_{1;j}\right|$ and $\left|v_{2;j}\right|$ must be equal to $|V'_{CB}|$. Therefore, the error in difference in cavity volume $\Delta v_j = V'_{CB} - \left(v_{1;j} - v_{2;j}\right)$. If $\left|\frac{\Delta v_j}{\Delta V_0}\right| < \epsilon$, the iterative scheme can be stopped.

In which ϵ is a predefined allowable tolerance. The tolerance used in the paper is $\epsilon = .001$, which will therefore also be considered for this iterative scheme (Vallabhan & Chou, 1986). In case the initial estimation for $p^a_{2;CB;j}$ is too high, the sum of $v_{1;j}$ and $v_{2;j}$ will be larger than the change in cavity volume before equilibrium V'_{CB} and $\Delta v_j < 0$. Therefore, second estimation of $p^a_{2;CB;j}$ must be lower, which is done by defining the upper limit $p^U_{2;CB}$ as $p^a_{2;CB;j}$ and keeping the lower limit the same as discussed in step 1. In case the initial estimation is too low, the opposite holds. With this, the final step of the iterative scheme is defined as step 5. Steps 2 until 4 are repeated until the solution converges to a tolerance lower than the predefined tolerance.

Step 5: If $\Delta v_j < 0$, then $p^U_{2;CB} = p^a_{2;CB;j}$, otherwise $p^L_{2;CB} = p^a_{2;CB;j}$. Furthermore, $j = j + 1$, repeat steps 2-4 until the solution converges.

The iterative scheme only needs to be considered in case of a nonlinear relation between effective pressure loads and volumes of deformation (Wörner, Shen, & Sagmeister, 1993). Application of the iterative method is considered in Chapter 5.3.3, where nonlinear P-V diagrams from numerical modelling are used to calculate effective pressure loads to due to asymmetric cold-bending. In case of linear deformations, a direct formula can be derived, which is discussed in Chapter 5.5.2.

5. Use phase

The last distinction made between the different boundary conditions for a cold-bent IGU is the ‘Use phase’. The ‘Use phase’ has the same support conditions as the ‘Fixation moment’, however an additional load condition is considered as an external load due to for example wind, snow or isochoric pressures.

5.1. Goal

As discussed in Chapter 2.3 and 2.5.5, the cavity pressure inside an IGU can be modelled by combining the structural behaviour of two separate plates, with external pressure loads calculated using the principles of Boyle’s law. Therefore, the goal of modelling the ‘Use phase’ is to gain insights in the structural behaviour of single cold-bent glass plates with respect to pressure loads. Furthermore, a framework in which the interaction between two cold-bent glass plates due to cavity pressures can be modelled, is setup.

5.2. Boundary conditions

In continuation with the permanent support conditions as considered for the ‘Fixation moment’, the only change in boundary conditions for the ‘Use phase’, is that of an extra pressure load. In DIANA this is done by means of a ‘Phased analysis’, for which in phase 1 the prescribed deformations are modelled, after which in phase 2 the curved glass plate is subjected to a pressured load (Figure 84 and Figure 85, page 68). The pressure load is defined as a normal load perpendicular the curved surface, in either positive or negative direction.

In Figure 86 to Figure 89 an example of the results of a 2000x2000x10mm plate, with a radius of 12m, subjected to a pressure load 1kN/m^2 in opposite direction of curvature is shown. Figures (a) show the relative displacement due to the pressure load, figure (b) show the displacements after the fixation moment and figure (c) shows the total combined displacement. From the displacements in x-direction (Figure 86) it can be seen that due to tolerances defined for the ‘Fixation moment’, sides AB and CD are free to move. Similarly, sides AC and BD are free to move in y-direction (Figure 87). Due to the increased stiffness of the curved plate, the deformation pattern in z-direction is different from that of a flat plate. In Figure 89 the principal stresses in the top layer of the x-y plane, before and after the pressure load are shown. From the example can be seen that these tensile stresses are reduced due to the pressure load, as the centre of the structure gets pushed backwards into a lesser curvature. The maximum tensile stress along the curved edges remains approximately the same.

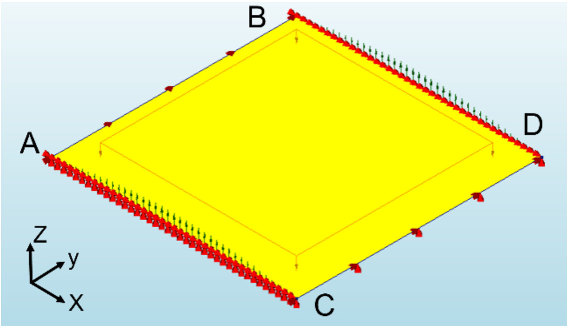

Figure 84: Boundary conditions 'Use phase'

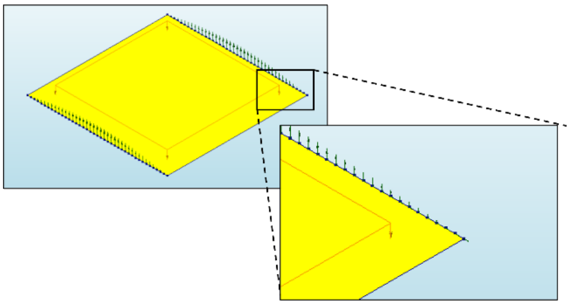

Figure 85: Combined prescribed displacements and pressure load

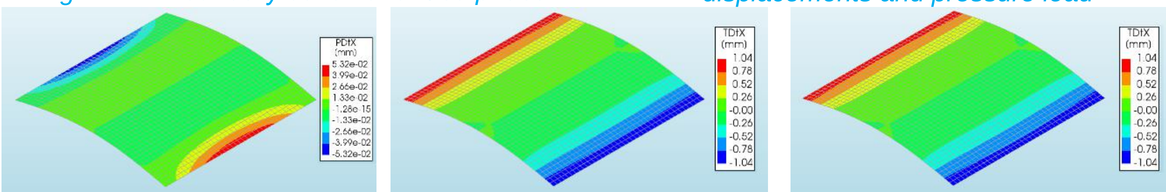

(a) (b) (c)

Figure 86: Displacement in x-direction due to pressure load

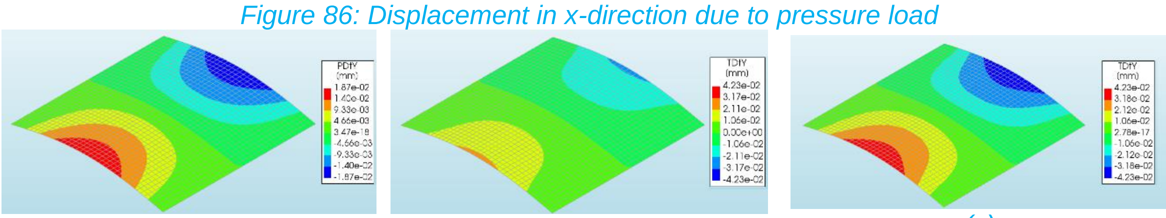

(a) (b) (c)

Figure 87: Displacement in y-direction due to pressure load

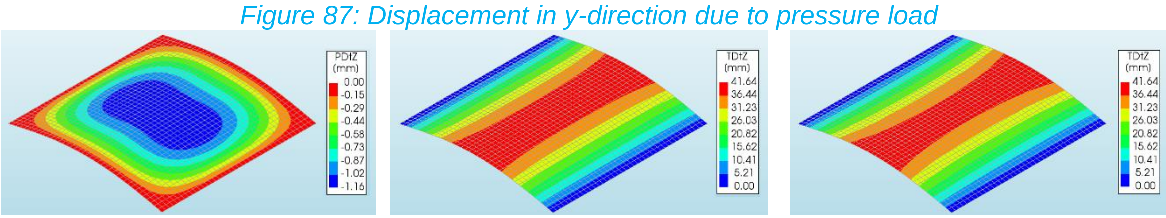

(a) (b) (c)

Figure 88: Displacement in z-direction due to pressure load

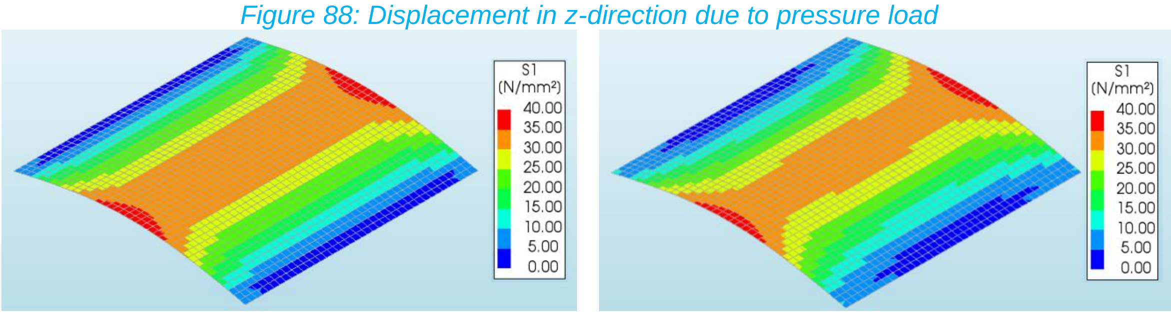

Figure 89: Maximum principal stress in layer 3 of S1, before and after pressure load

5.3. Numerical modelling

The determination of effective pressure loads for numerical modelling is done using the iterative scheme as discussed in Chapter 2.3.2, presented by (Vallabhan & Chou, 1986). In the paper, P-V diagrams of nonlinear deformations due to pressure loads are used to compute the iterative scheme. Similar P-V diagrams are made for the nonlinear deformations calculated in DIANA. In order to check the accuracy of the P-V diagrams, first the load sharing of an IGU is calculated manually by adding pressure loads on the plates as calculated with the scheme. The results of this calculation are then compared to the resulting load sharing pressures computed using linear interpolation of the P-V diagrams.

5.3.1. External load sharing DIANA

First, the manual calculation the cavity pressure due to an external pressure load is done. The example is shown for the case of a 2000x2000x10-16-10mm IGU configuration with a design radius of 12m, subjected to an external pressure load opposite of the curvature of the IGU of $p_{ext} = 1$ kN/m². The direction of the pressure load with respect to the IGU configuration is shown in Figure 90.

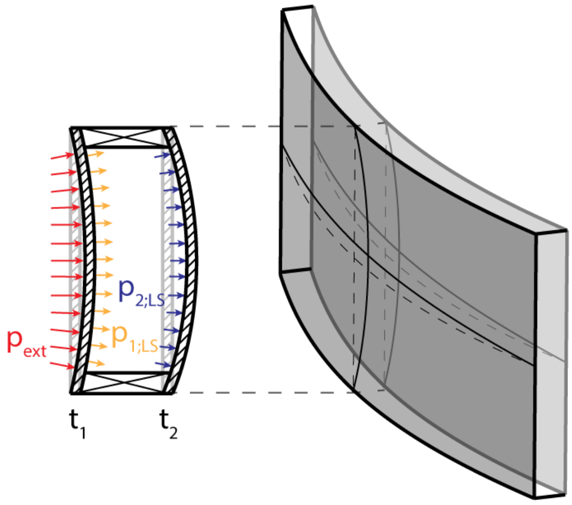

Figure 90: External load sharing in cold-bent IGU's

Step 1: Let $j = 1$ and the pressure on the interior of the plate be a load p_2.

➔ An initial estimation of the load sharing of the IGU is made using the relative stiffness of both panes, $p_{2;LS} = \delta_2 * p_{ext} = t_2^3/(t_1^3 + t_2^3) * p_E = .5 * 1 = 0.5$ kN/m².

Step 2: Calculate the volume of deformation v_2 due to pressure load $p_{2;LS}$.

➔ Using DIANA, the deformation due to the pressure load is modelled, Figure 91. Note difference in positive z-direction as used for the calculation of cavity pressure. This means that p_{ext} is modelled as a negative load and the deformation will lead to an increase in cavity pressure.

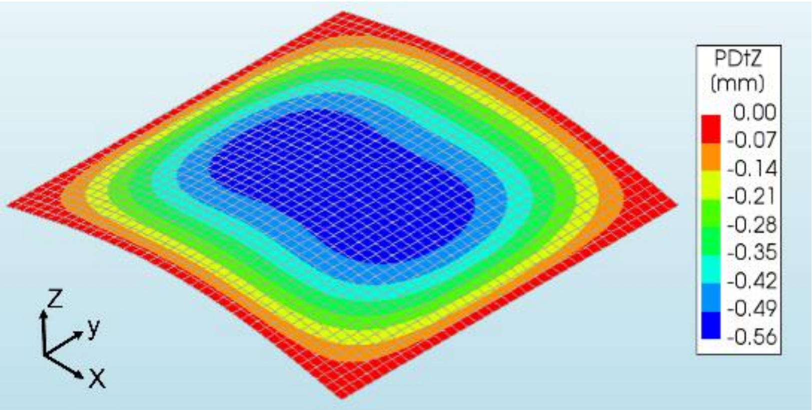

Figure 91: Deformation of the interior pane in z-direction due to pressure load $p_2 = .5kN/m^2$

- ➔ The cavity pressure is calculated using postprocessing in Python, by subtracting the volume below the curved plate after external pressure, with that from before external pressure. $v_2 = \Delta V_{2;0} - \Delta V_{2;1} = 101842766 - 100657040 = 1185726$ mm³. This results in a decrease in volume below the interior plate, and therefore an increase in cavity pressure.

Step 3: Calculate $\Delta v = p_{2;LS}V/(P_{c;P} + p_{2;LS})$.

- ➔ $\Delta v = .5 * (2000 * 2000 * 16)/(101.325 + .5) = 314265$ mm³.

Step 4: $v_1 = v_2 + \Delta v$.

- ➔ $v_1 = 1185726 + 314265 = 1499991$ mm³.

Step 5: The corresponding pressure $p_{1;LS}$ on the exterior plate is determined using the P-V curves. For in-between values, the results are linearly interpolated.

- ➔ Since it is not possible to calculate a pressure load as a result of a nonlinear volume of deformation, an estimation of the pressure load is based on a cross comparison: $p_{1;LS;est} = p_{2;LS} * v_1/v_2 = 0.632$kN/m². The cross comparison is then checked by examining if $|(v_{1;est} - v_1)/v_1| < .1\%$. For the this first step the resulting deviation is .662%, resulting in a second estimation of $p_{1;est} = p_{1;est} * (1 - .00662) = 0.628$kN/m². From this second estimation the deviation is $|-.025\%| < .1\%$.

Step 6: Error in total pressure: $\Delta p = p_{ext} - (p_{1;LS} + p_{2;LS})$.

- ➔ $\Delta p = 1 - (0.628 + .5) = -0.128$ kN/m², i.e., the resulting shared load is 12.83% too high compared to the external load.

Step 7: If $\Delta p > 0$, then $p^L_{2;LS} = p_{2;LS}$, $i = i + 1$ and $p_{2;LS}$ is increased by the load increment. The process is repeated from step 2.

Step 8: If $\Delta p < 0$, then $p^U_{2;LS} = p_{2;LS}$ and the iterative process is continued.

- ➔ Based on the difference in pressure, an estimation of $p_{2;LS}$ is made using a cross reference: $p_{2;2} = p_{2;LS;1} * (1 - .128) = .467$ kN/m².
- ➔ Steps 2 until 8 are repeated until the allowable tolerance is reached. For the example case tolerance is reached after 8 iterations. The results are presented in Table 16.

Table 16: External load sharing of cold-bent IGU, manually calculated using DIANA

Iteration [-]	$p_{1;LS}$ [kN/m²]	$p_{2;LS}$ [kN/m²]	$p_{1;LS} + p_{2;LS}$ [kN/m²]	Δp [%]
1	.628	.500	1.128	12.83%
2	.588	.467	1.055	5.54%
3	.572	.454	1.026	2.68%
4	.564	.448	1.012	1.21%
5	.560	.445	1.005	0.55%
6	.559	.444	1.003	0.33%
7	.558	.443	1.001	0.16%
8	.557	.443	1.000	0.08%

5.3.2. External load sharing using P-V diagrams from DIANA

From the iterative scheme can be concluded that the manual method is tedious and prone to computation errors. Therefore, the accuracy of the method with P-V diagrams is compared to that of the manual method. To do so, a P-V diagram is made with pressures from -1 until 1 kN/m², considering a load-step of 0.1 kN/m². The results of the P-V diagram from DIANA for a single plate, are shown in Figure 92. Although not very explicit, it can be concluded from the diagram that the relation is nonlinear.

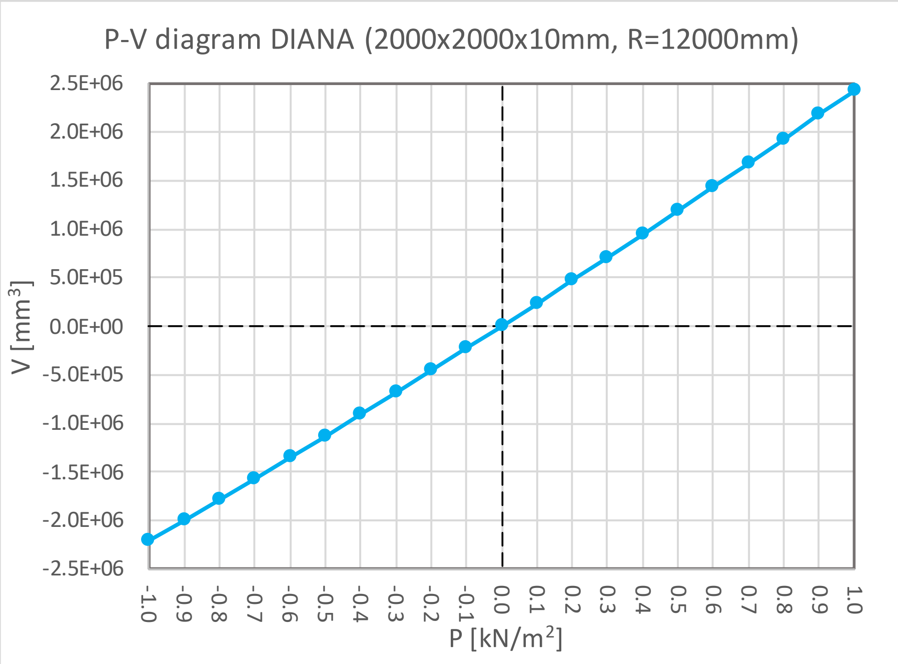

Figure 92: P-V diagram DIANA (2000x2000x10mm, R=12m)

The steps to calculate the external load sharing using a P-V diagram are similar to those in Chapter 2.3.2. In Table 17 the load sharing pressures per iteration are shown. It can be seen that despite the linear interpolation, the results are still in agreement with the manual method. In general, it can be concluded that more iterations are needed, however due to the P-V diagrams, the deformation volumes do not have to be calculated via numerical modelling in DIANA, resulting in faster computation times and less risk of computation errors. In Figure 93 can be seen how the two different approaches compare to each other, it can be seen that the resulting load sharing pressures are almost identical.

Table 17: External load sharing of cold-bent IGU, calculated using P-V diagrams

Iteration [-]	$p_{1;LS}$ [kN/m²]	$p_{2;LS}$ [kN/m²]	$p_{1;LS} + p_{2;LS}$ [kN/m²]	Δp [%]
1	.126	.100	0.226	-77.38%
2	.253	.200	0.453	-54.70%
3	.379	.300	0.679	-32.10%
4	.502	.400	0.902	-9.78%
5	.626	.500	1.126	12.69%
6	.567	.450	1.017	1.71%
7	.535	.425	0.96	-3.94%
8	.551	.437	0.988	-1.11%
9	.559	.443	1.002	0.30%
10	.555	.440	0.995	-0.41%
11	.557	.442	0.999	-0.06%

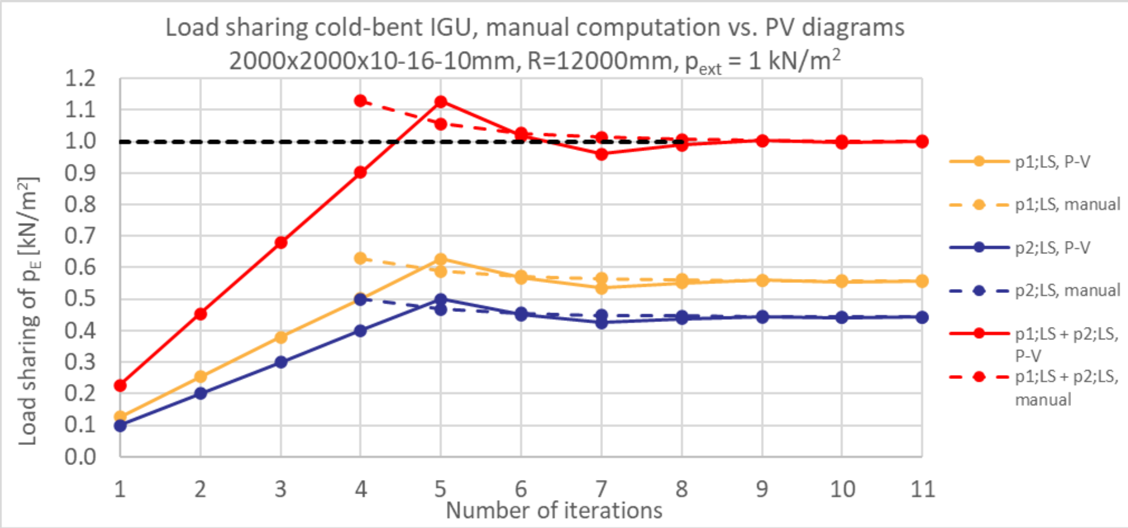

Figure 93: External load sharing of a symmetric cold-bent IGU, manual computation vs. P-V diagrams

Using the P-V diagram method, insights can be gained on how the external load sharing of an IGU relates to its increasing stiffness as a result of larger curvatures. In Figure 94 a P-V diagram is shown for the case of a 2000x2000x10mm with design radii ranging from 20m until 8m. The result of a flat IGU is also included. From the diagram can be concluded that already for small radii, there is a significant increase in stiffness. Furthermore, it can be seen that for stiffer plates, the volumes of deformation are more towards a linear relation. In Appendix C.1, the results are presented for a 1x1m, 2x2m, 3x3m, 4x3m, 5x3m and 6x3m plate, which covers the range of plates up to the size of jumbo glass plates, bent along their longest edge. The thicknesses considered for each plate size are 8mm, 10mm and 12mm. The radius of curvature ranges from flat to 8m, which is within realistic curvatures based on a maximum cold-bending stress along the edge of the plate of $\sigma'_{max} < 63.5$ N/mm². Furthermore, results of two case studies, as discussed in Chapter 6.4, are presented.

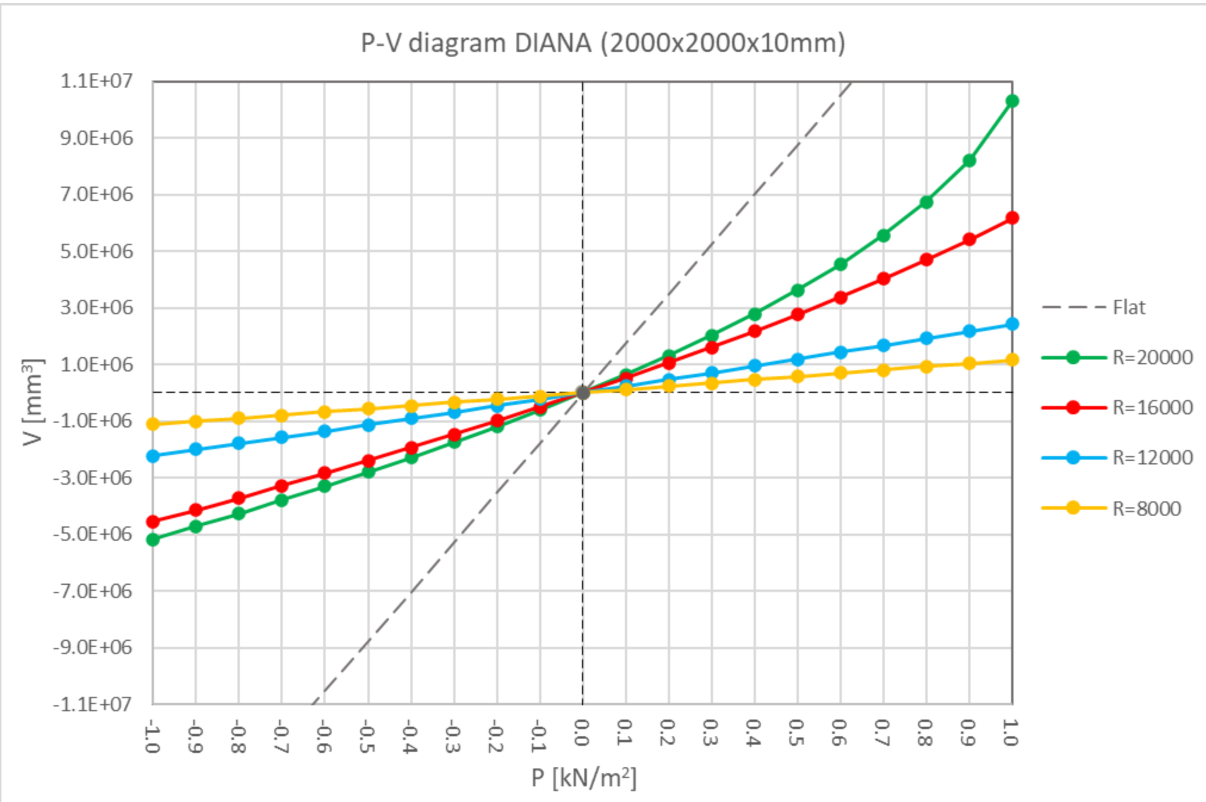

Figure 94: P-V diagram DIANA (2000x2000x10mm)

In Figure 95 the load sharing pressure are shown of a 2x2m symmetric IGU with increasing curvature, subjected to an external unit load of 1 kN/m^2. The starting point is the load sharing of a flat configuration, calculated according to NEN 2608. As the curvature increases, a lower percentage of the load is shared by the interior pane. Furthermore, can be concluded that for thicker configurations, more load is shared by the exterior pane. In Appendix C.2 the load sharing diagrams for symmetric IGU configurations are given. In general, can be concluded that as IGU sizes increase, the difference in load sharing per pane get smaller.

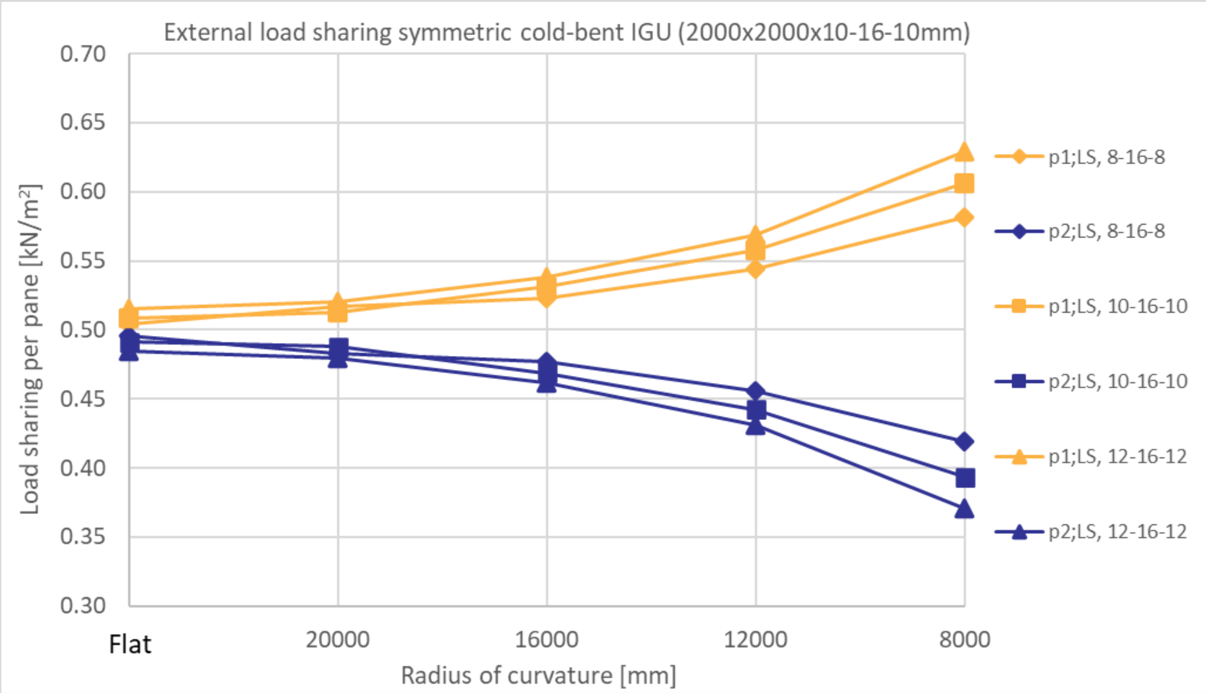

Figure 95: Load sharing pressures for different design radii (2x2m)

5.3.3. Asymmetric IGU's

The P-V diagrams from DIANA can also be used to determine the isochoric pressure due to anticlastic bending in asymmetric IGU's. To do so, first the difference in cavity volume before equilibrium is calculated. Then, using the P-V diagrams, the iterative scheme from Chapter 5.3.3 can be followed until the solution converges towards the allowed tolerance. Below the example configuration of an 2000x2000x8-16-10mm with a design radius of 12m is considered. The difference in volume below the anticlastic curved plates is $V'_{CB} = 1269500$mm³, resulting in a change of isochoric pressure of $P'_{CB} = -2.051$ kN/m². The difference in cavity distance due to anticlastic bending is $\Delta d_{cav} = 16 - 1.33 + 2.05 = 16.71$ mm. In Figure 96 the results of the iterative scheme are shown for which instead of equilibrium in pressures, equilibrium in volumes of deformation is found. From the iterative scheme is calculated that equilibrium is found at the combined volume of deformations of $V'_{CB} = v_1 + v_2 = 717659 + 552554 = 1269213$ mm³, resulting in a negative effective pressure on the inside of the interior pane of $p_{2;CB} = -0.241$ kN/m².

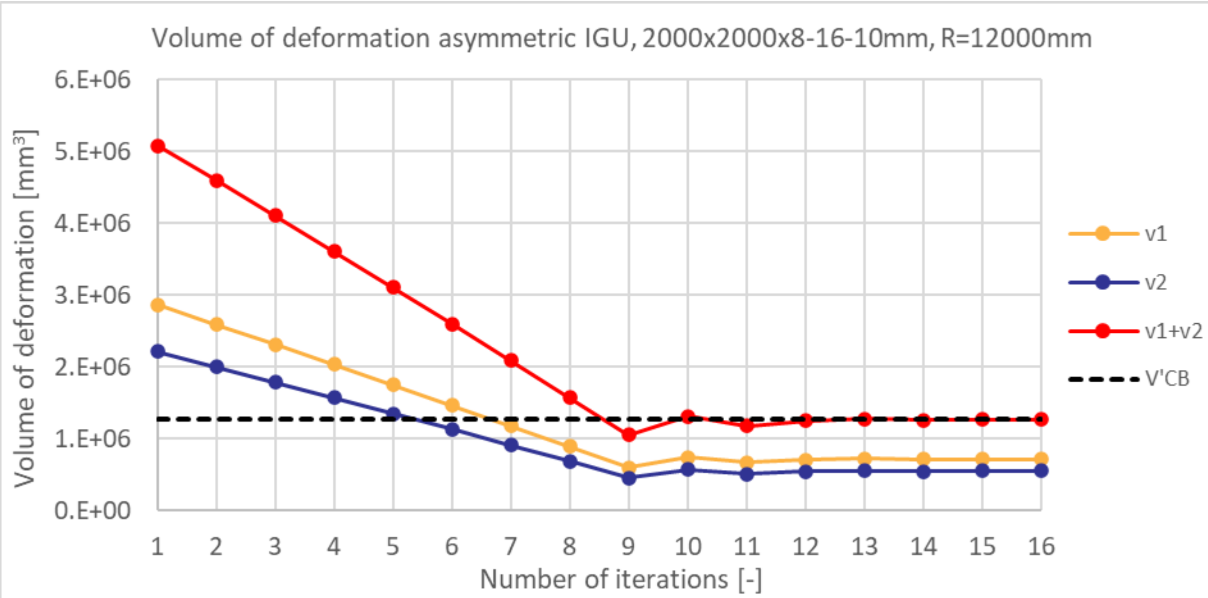

Figure 96: Equilibrium in volume of deformation due to anticlastic bending

To examine combined resulting pressures, the load sharing is first calculated separately. Thereafter, the isochoric pressure and shared external pressure are summed. A schematic overview of the isochoric pressure and load sharing pressure is shown in Figure 97.

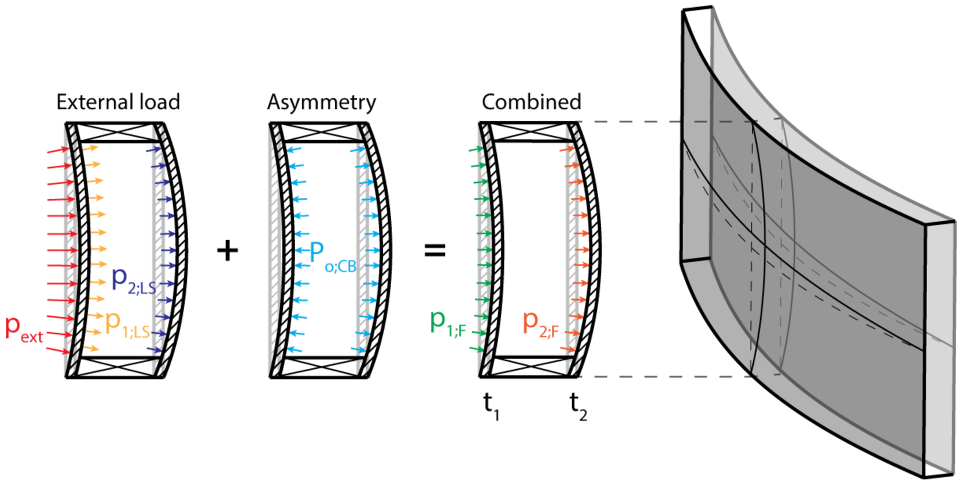

Figure 97: Overview and direction of cold bending isochoric pressure and load sharing pressure

The external load sharing of the IGU due to an external unit load of 1 kN/m² is shown in Figure 98. Although anticlastic bending effects decrease as curvatures increase, the isochoric pressure increases for smaller radii. This can be explained by the increase in stiffness of the panes, resulting in a higher effective pressure relative to the volume of deformation. Furthermore, can be concluded that, as curvatures increase, the isochoric pressure plays an increasingly significant role in the load sharing of the IGU. For the case of a design radius of 8m, the effective load on the interior pane is only 0.098 kN/m² and the load on the exterior pane is almost as large as the pressure load itself, 0.902 kN/m², due to an effective isochoric cold-bending pressure of -0.377 kN/m².

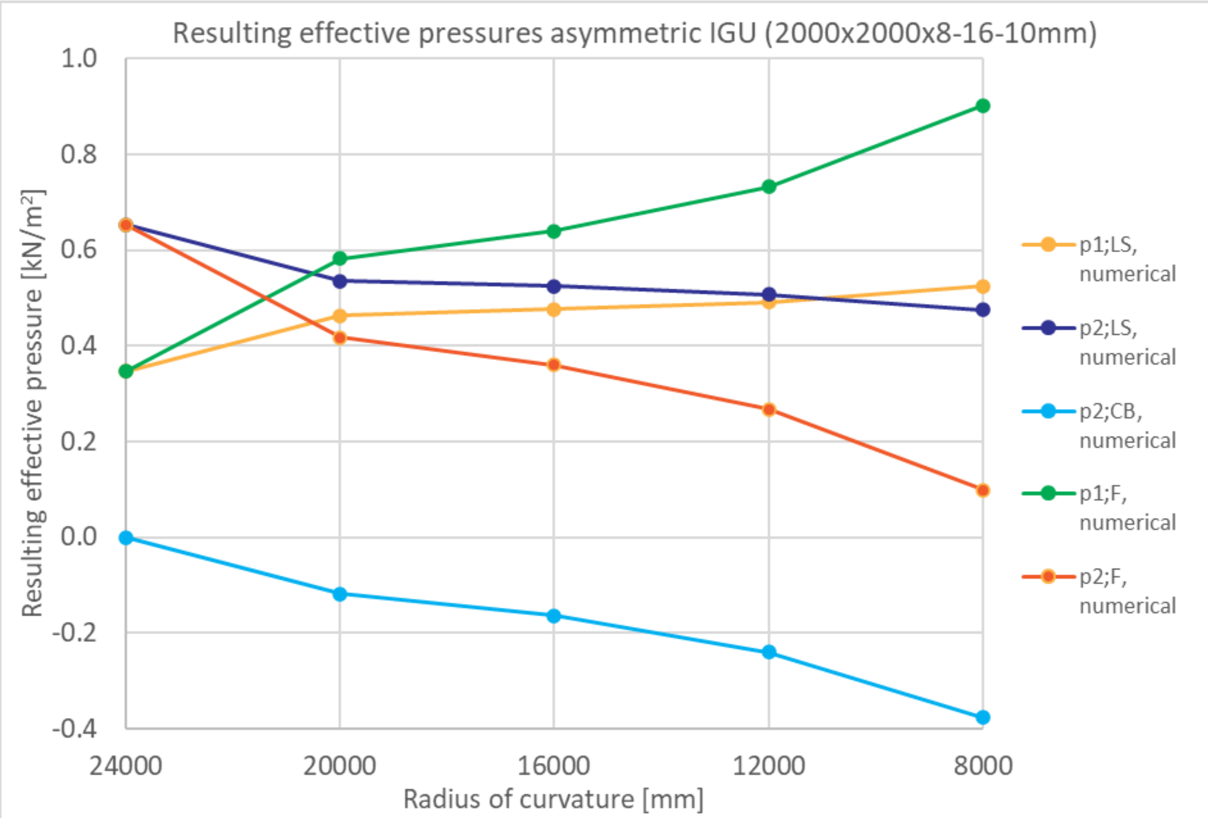

Figure 98: External load sharing of an asymmetric IGU (2000x2000x8-16-10mm)

Resulting effective pressure diagrams of other asymmetric configurations and plate sizes are found in Appendix C.3. In general, it can be concluded that for small IGU's, the differences in isochoric pressures due to anticlastic bending are largest. The configuration of a 1000x1000x8-16-12mm, R=8m IGU, is the utmost example of this conclusion, as it has a resulting pressure of 1.933 kN/m² and -0.933 kN/m² for the exterior and interior pane, respectively. For larger IGU's the differences are less significant. For the case of a 3x3m IGU, the utmost example is that of the 8-16-12mm, R=8m configuration, with a resulting pressure of 1.224 kN/m² and -0.244 kN/m², respectively. Since the P-V diagrams only cover volumes of deformation for effective pressures ranging between -1 until 1 kN/m², pressures outside the range are linearly extrapolated. Therefore, it should be noted that reliability of the calculations decreases, if the resulting pressures are larger than 1 kN/m².

Numerical calculations of resulting effective pressures due to changes in isochoric pressures are limited to those from cold-bending ($P_{o;CB} \leftrightarrow p_{2;CB}$). The same iterative method can however also be applied for changes in isochoric pressure due to climatic loads ($P_{o;c} \leftrightarrow p_{2;c}$) and height differences ($P_{o;H} \leftrightarrow p_{2;H}$). Since it can be expected that conclusions from outcomes of these pressures are similar, only combined loads due to asymmetric cold-bending pressures and load sharing pressures are numerically evaluated. In Chapter 9, a recommendation is given on how all combined loads can be calculated numerically for validation purposes.

5.4. Analytical modelling

In this paragraph a simplified analytical approach of the 'Use phase' is considered. The approach is based on the deflection of a portion of a cylindrical shell, as discussed in (Timoshenko & Woinowsky-Krieger, 1989) and Chapter 2.4.3. The consideration of this method is based on the similarities in boundary conditions to those discussed in Chapter 5.2.

In Figure 99 the considered geometry is shown, which is redrawn to correspond with the parameters used throughout this thesis. The geometry is expressed in terms of design radius and height, which is convenient for the application of the analytical method since these are design parameters. The equally distributed pressure load ($q \rightarrow p_{ext}$), is normal to the surface. The considered boundary conditions differ from those of numerical modelling on the following aspects. First, all sides for the portion of the cylindrical shell are simply supported, meaning that there are no tolerances along the sides. Therefore, it can be expected that deformations from the analytical approach are lower. Furthermore, the shape of shell is cylindrical and no anticlastic bending behaviour in considered. From previous findings it is concluded that the shape of the curved IGU as a result of the boundary conditions of the 'Bending Phase' is close to sinusoidal. Also, it has been concluded that anticlastic bending plays a significant role in the geometry of the curved plate. Last, the calculated deformations are linear, which is likely to show large deviations when compared to nonlinear deformations as considered for the numerical P-V diagrams. However, considering the deflection in the centre of the curved glass plates, it can be concluded that in almost all cases it is smaller than ½ times the thickness of the glass plate. Therefore, the deformation of the 'Bending phase' can be categorised as small deflections, which means linear calculations suffice. The same consideration is justified in the publication by (Wörner, Shen, & Sagmeister, 1993), where it is concluded that external load sharing of flat IGU's can be calculated linearly. Based on these considerations is decided to use the load case geometry for the 'Use phase'. It can however be expected that deviations between analytical and numerical modelling are large considering the difference in boundary conditions.

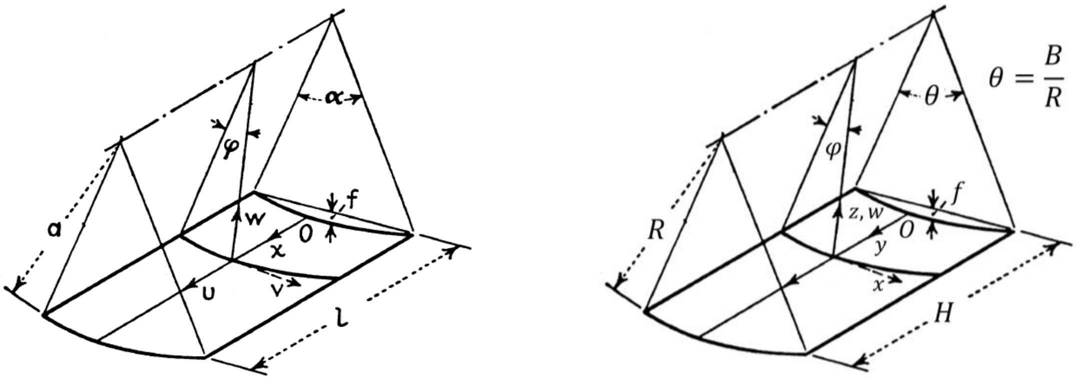

Figure 99: Deflection of a portion of a curved shell (Timoshenko & Woinowsky-Krieger, 1989)

5.4.1. Derivation volume of deformation

The solution of the system of equations (53) - (57), is shown below in equation (86). Due to the simply supported edges, deformations in y- and x-direction are negligible small. Therefore, the system is only solved for deformations in z-directions. In order to make the equation more readable and easier to compute, it is split into components. The parameter for the external pressure load is excluded from the components since it is the most variable parameter. When calculating for example the deformations due to varying pressure loads in the iterative scheme, the components A_{mn} until H_{mn} remain constant, which makes it easier to compute repetitive calculations.

$$w(x,\varphi) = \sum_{m=1,3,\dots} \sum_{n=1,3,\dots} \frac{p_{ext} * B_{mn}}{A_{mn} * H_{mn}(C_{mn} * (D_{mn} + E_{mn}) + F_{mn} + G_{mn})} \tag{86}$$

Whereby:

$$A_{mn} = \frac{E * t * \pi^4 * m^2 * n^2}{192(1+\nu) * (\cos(m\pi) - 1) * (\cos(n\pi) - 1)} \tag{87}$$

$$B_{mn} = R^2 * B^5 * H^5 * (R^4 * m^2 * n^2 * (1+\nu) - 4H^2 * B^2) * (1-\nu) \tag{88}$$

$$C_{mn} = -4H^2 * B^2 * R^2 \tag{89}$$

$$D_{mn} = t^2 * \pi^4 * (H^4 * n^4 + m^4 * B^4) - 12H^4 * n^2 * B^2 \tag{90}$$

$$E_{mn} = 2m^2 * B^2 * H^2 * (\pi^4 * n^2 * t^2 - 6B^2 * \nu^2) \tag{91}$$

$$F_{mn} = R^6 * m^2 * n^2 * t^2 * \pi^4 * (H^2 * n^2 + m^2 * B^2)^2 * (1+\nu) \tag{92}$$

$$G_{mn} = -24H^4 * B^4 * \left(R^4 * m^2 * n^2 * \left(\nu^2 + \frac{3\nu}{2} - \frac{1}{2}\right) + 2H^2 * B^2\right) \tag{93}$$

$$H_{mn} = \frac{B * H * (\cos(m\pi) - 1) * (\cos(n\pi) - 1)}{m * n * \pi^2 * \sin\left(\frac{m\pi x}{H}\right) * \sin\left(\frac{n\pi\varphi R}{B}\right)} \tag{94}$$

In which:

$w(x,\varphi)$	is the deflection in z-direction at point x, φ, in mm;
p_{ext}	is the external pressure load on the cylindrical shell, in kN/m^2;
E	is the Young's modulus of glass, whereby E_g = 70000 N/mm^2;
t	is the thickness of the cylindrical shell, in mm;
ν	is the Poisson's ratio of glass, whereby ν_g = .23;
R	is the design radius of the IGU, in mm;
B	is the width of the IGU, in mm;
H	is the height of the IGU, in mm.

The volume of deformation between the non-deflected and deflected surfaces is then calculated using equation (95). The components are defined in such a way that the H_{mn} component can be left out of consideration after integration. Components A_{mn} until G_{mn} remain the same.

$$v = R * \int_0^H \int_0^\theta w \, dx \, d\varphi = \sum_{m=1,3,\dots} \sum_{n=1,3,\dots} \frac{p_{ext} * B_{mn}}{A_{mn} * (C_{mn} * (D_{mn} + E_{mn}) + F_{mn} + G_{mn})} \tag{95}$$

5.4.2. Comparison with numerical results

In order to see how the deflections and volumes of deformation compare to results from numerical modelling, example cases are considered. First, qualitative comparisons are shown based on the deflection of the plates. These are made to gain insights on how the boundary conditions affect the resulting volume of deformations. The volumes of deformation are then compared quantitatively using P-V diagrams. In the next paragraph, external load sharing and isochoric pressures are compared to results from numerical modelling.

Qualitative comparison deflections

In Figure 100 a comparison is shown of the differences in results between the analytical approach and numerical modelling. The example is shown for the case of a 2000x2000x10mm plate with a design radius of R=12m, subjected to a unit pressure load of 1 kN/m^2. The volumes of deformation are considered as absolute values. Furthermore, the z-axis is not scaled to the height-width ratio, in order to highlight the deformations.

From the comparison can be seen that the analytical deformations (top left) are significantly smaller than the numerical results (bottom left), which is in line with expectations of linear versus nonlinear modelling. Furthermore, can be seen that there is a significant difference in the geometries at the 'Fixation moment' (middle). In the numerical deformation, the anticlastic bending effect is clearly visible, which is however not taken into account for the analytical approach. The combination of deviations amplify each other, which is shown in the deformed geometries after pressure load (right).

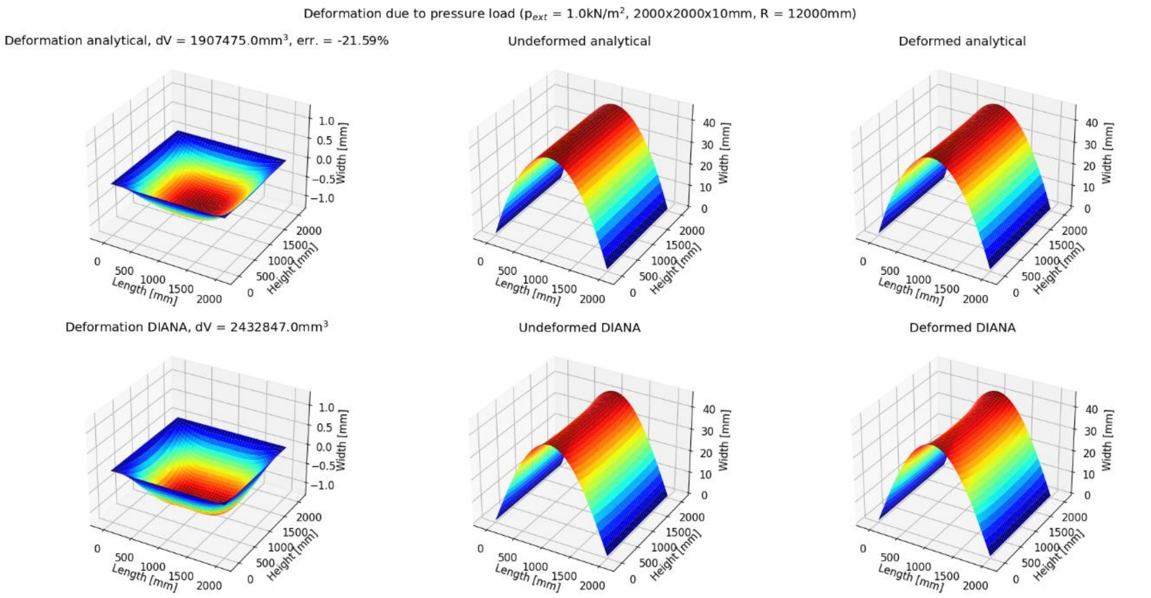

Figure 100: Comparison between analytical and numerical results 'Use phase', example 1

In general, it can be concluded that the deviations increase for larger curvatures, as shown in the example for a 2000x2000x10mm plate with a radius of 8m (Figure 101). The analytical volume of deformation is on average 40% lower. The relative displacements do however show similarities in deformation patterns. Based on this observation it is concluded that the theoretical principles behind the two load cases are similar, however due to the difference between a linear and nonlinear approach, results differ significantly.

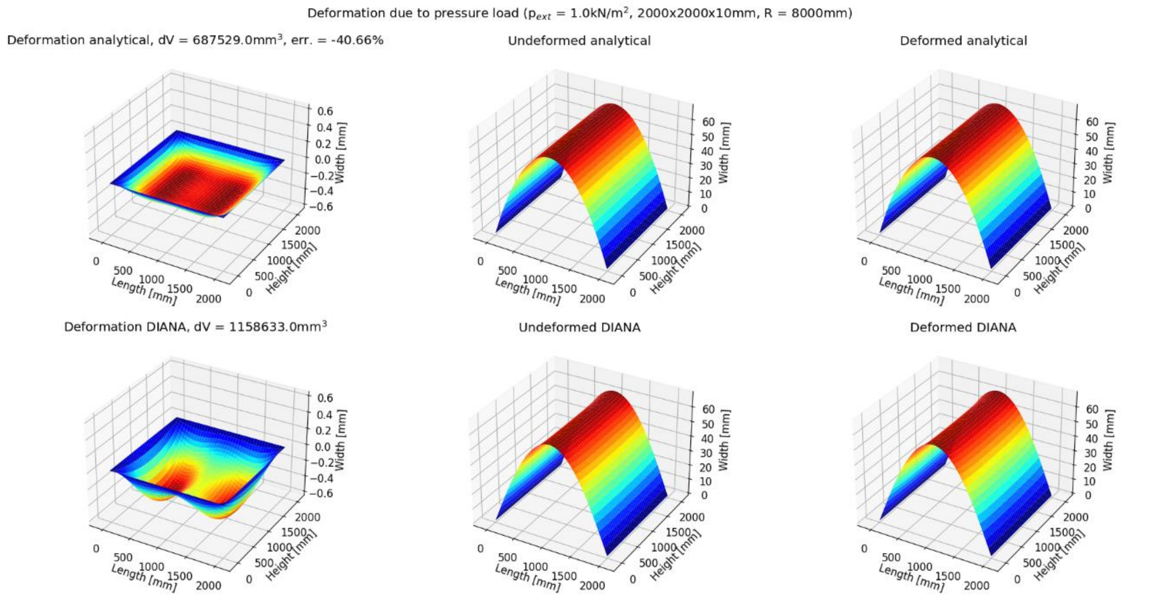

Figure 101: Comparison between analytical and numerical results 'Use phase', example 2

The last general conclusion which is drawn from the qualitative comparison, is that as plate sizes increase, deviations increase. In Figure 102, a 3000x3000x10mm plate with a radius of 12m is shown. Compared to the 2x2m plate shown in Figure 100, it can be seen that the deviation is more than doubled. Again, the explanation for the increase in deviation between the different plate sizes is due to the difference in linear and nonlinear calculations.

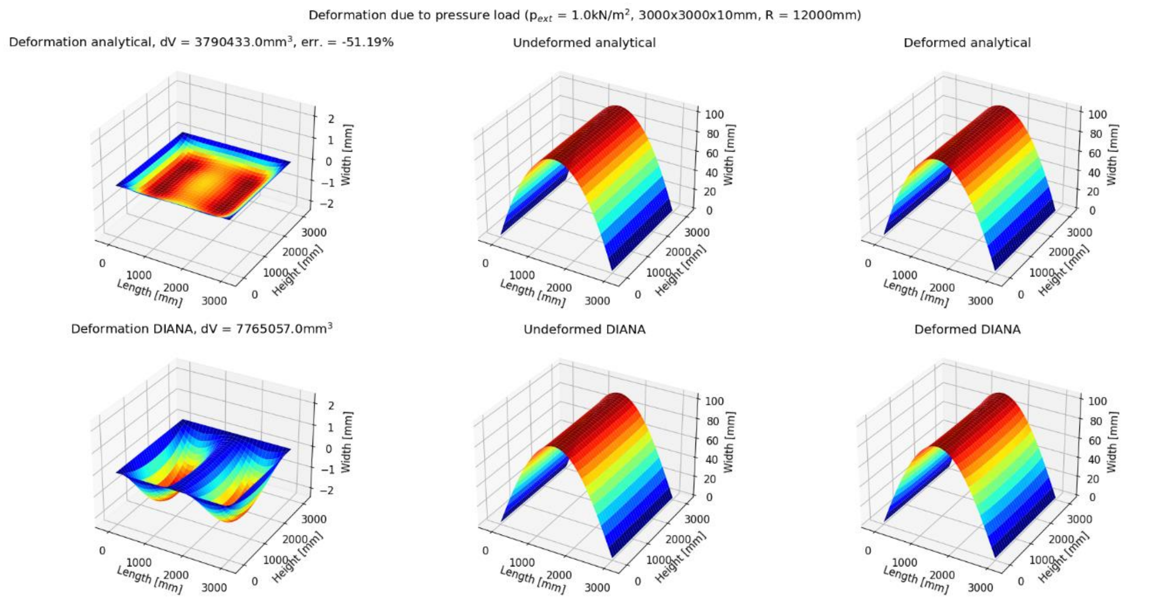

Figure 102: Comparison between analytical and numerical results 'Use phase', example 3

Quantitative comparison volume of deformation

The resulting volumes of deformation from the analytical approach are compared to those from numerical modelling. This is done to gain insights in how these deviations affect cavity pressure calculations. In Figure 103 the P-V diagrams of a 2000x2000x10mm plate are compared. The dotted lines represent the numerical results, as shown in Figure 94. Differences in linearity and nonlinearity of the results are clearly visible in the diagram. It can be seen that analytical outcomes are subsequently lower, i.e., the panes are stiffer against pressure loads. Based on the conclusions drawn from the numerical cavity pressure calculations, it can be expected that the load sharing from analytical calculations is higher for the exterior plate. Furthermore, it can be expected that these effects amplify for smaller plate sizes and smaller design radii. The analytical P-V diagrams and tables for other thicknesses and plate sizes are shown in Appendix C.1. In Table 18 the relative and absolute deviations per considered plate size are shown, from which can be concluded that the analytical results are significantly lower, with an average absolute deviation of 42.55%.

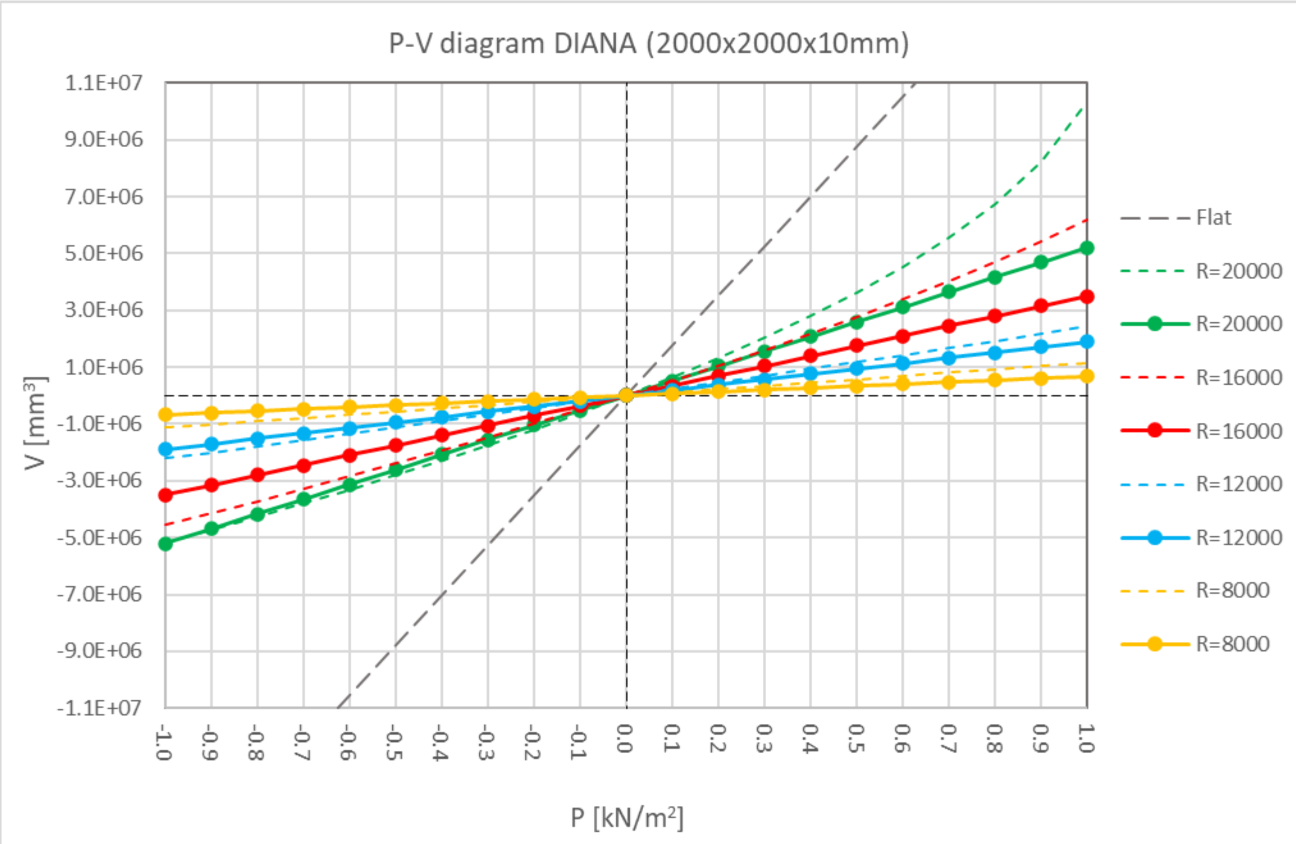

Figure 103: P-V diagram, 2000x2000x10mm plate, analytical versus numerical results

Table 18: Deviations between volumes of deformation from numerical and analytical outcomes

Overview deviations P-V diagrams		
	Relative deviation	**Absolute deviation**
1000x1000	-22.07%	22.07%
2000x2000	-24.27%	24.95%
3000x3000	-42.90%	42.90%
4000x3000	-47.06%	48.29%
5000x3000	-52.10%	52.68%
6000x3000	-63.44%	64.43%
Average	**-41.97%**	**42.55%**

5.4.3. Number of iterations

In equation (95), the calculation of the volume of deformation is based on a double summation, using uneven m and n values. In line with findings from (Timoshenko & Woinowsky-Krieger, 1989), a value of 9 is used for m and n for the previous calculations. This means that per volume calculation, the equation has to be computed 4x4=16 times, after which it is summed. Using a coding language like Python, calculation of such repetitive equations is straightforward. However, for an analytical approach which is designed for the early design phase, such numbers of repetition can become tedious and prone to errors. Therefore, the calculations are considered for m and n of 1 and 3 only, resulting in 4 repetitions per volume calculation. In Table 19 the same comparison is made as in the previous paragraph. The deviations are similar to that from the extensive calculation with 16 repetitions. It is therefore concluded that a double summation of uneven m and n values up to 3 is sufficient for the calculation.

Table 19: Deviations between P-V diagrams from numerical and analytical outcomes

Overview deviations P-V diagrams		
	Relative deviation	**Absolute deviation**
1000x1000	-21.02%	21.02%
2000x2000	-23.56%	24.22%
3000x3000	-42.05%	42.05%
4000x3000	-45.25%	46.44%
5000x3000	-50.58%	51.15%
6000x3000	-62.20%	63.17%
Average	**-40.78%**	**41.34%**

5.5. Cavity pressure

In this chapter the methods to calculate effective pressures using the analytical approach are considered, after which the results are compared to numerical modelling. First, the method is considered for load sharing due to an external pressure load. Thereafter, the method to calculate effective pressures due to changes in isochoric pressures is considered. An overview of the cold-bending isochoric pressure and effective load sharing pressures is shown in Figure 104.

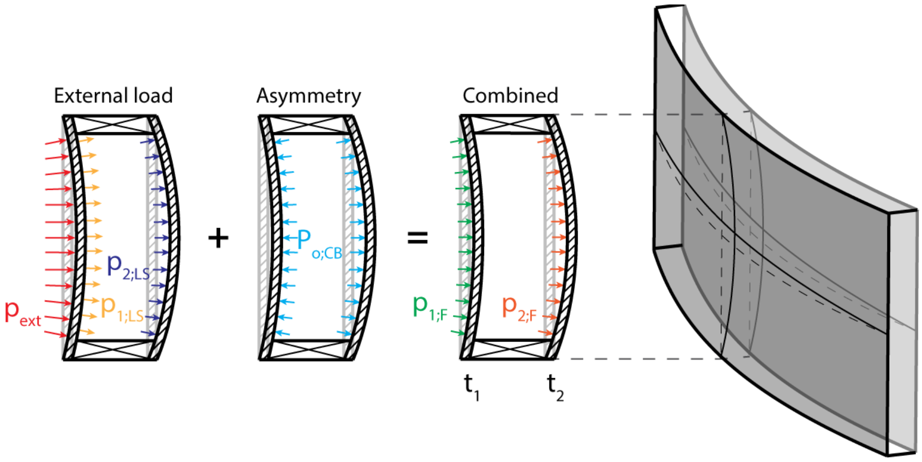

Figure 104: Overview and direction of cold bending isochoric pressure and load sharing pressure

5.5.1. Load sharing pressures

An advantage of the linear volume calculation is that the load sharing of the panes due to an external pressure load can be calculated linearly (Wörner, Shen, & Sagmeister, 1993). The equation to calculate the effective pressure load shared by the interior pane is shown below. The equation is a derivation of equation (27), discussed in Chapter 2.3.3, and is based on the principles of Boyle's law. Component A_{mn} until G_{mn} are the same as considered in equations (87) until (94).

$$p_{2;LS} = \left[\sqrt{(K_1+K_2)^2 * P_{c;P}^2 + 2P_{c;P} * (p_{ext} * K_1 + V) * (K_1+K_2) + (p_{ext} * K_1 - V)^2} - V + K_1 * \left(p_{ext} - P_{c;P}\right) - P_{c;P} * K_2\right] * \frac{1}{2K_1 + 2K_2} \qquad (96)$$

Whereby:

$$K_i = \sum_{m=1,3}\sum_{n=1,3} \frac{B_{mn}}{A_{i;mn} * (C_{mn} * \left(D_{i;mn} + E_{mn}\right) + F_{i;mn} + G_{mn})} \qquad (97)$$

In which:

- $p_{2;LS}$ is the effective pressure load on the inside of the interior pane of the IGU, due to load sharing of an external pressure load, in kN/m²
- K_i is the constant for calculating volume of deformation due to effective pressure loads, whereby $v_i = K_i * p_i$;
- $P_{c;P}$ is the reference pressure inside the cavity at the time of sealing, whereby $P_{c;P} = 101.325$ kN/m²;
- p_{ext} is the external pressure load on the exterior plate of the IGU, in kN/m²;
- V is the reference cavity volume at the time of sealing, in mm³.

In case of a symmetric IGU, equation (96) is simplified to:

$$p_{2;LS} = \frac{\sqrt{4K^2 * \left(P_{c;P} + \frac{p_{ext}}{2}\right)^2 + 4K * V * \left(P_{c;P} - \frac{p_{ext}}{2}\right) + V^2} + K * \left(p_{ext} - 2P_{c;P}\right) - V}{4K} \qquad (98)$$

In Figure 105, the resulting load sharing pressures are shown for symmetric 2x2m configuration, with an increasing radius of curvature up to 8m, subjected to an external load of 1 kN/m². The dotted lines represent the results from numerical modelling, the continuous lines are analytical results. In Appendix C.2 the load sharing diagrams for other plate sizes are shown. From results it can be concluded that in general the analytical load sharing percentages deviate more for increasing curvatures and larger plate sizes. A more in-depth interpretation and validation of the results is discussed in Chapter 7.3.

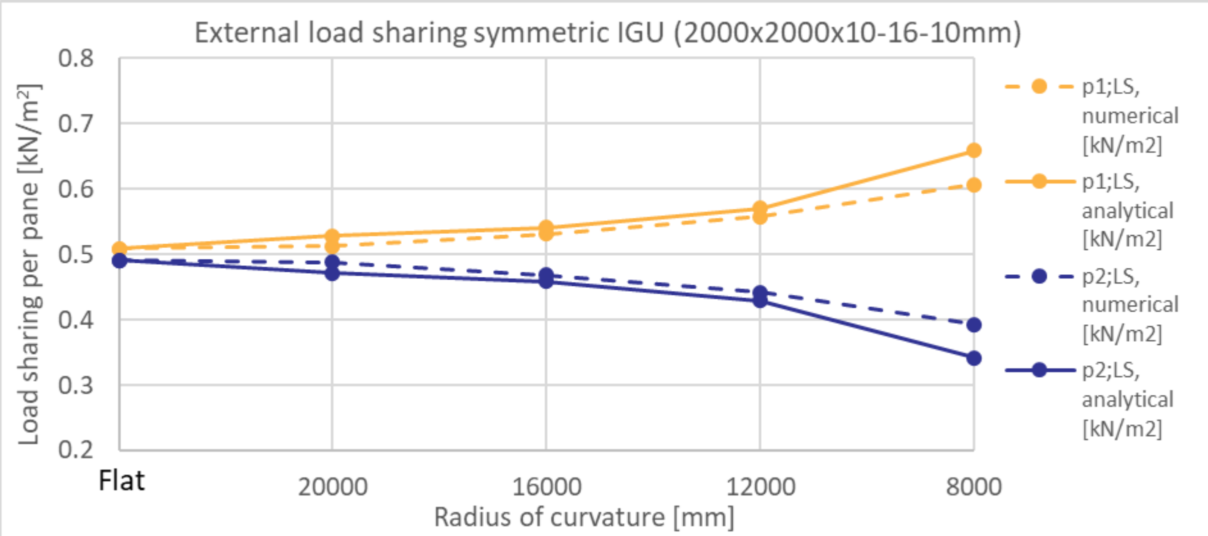

Figure 105: Analytical and numerical load sharing pressures for different design radii

5.5.2. Isochoric pressures

Similar to the equation for load sharing, effective pressure loads due to an isochoric pressure can be calculated linearly. In Chapter 4.5.3 is discussed that in order to get equilibrium inside the cavity, the change in cavity volume must be equal to the change in volumes of deformation of the exterior and interior pane. This means that $V' = v_1 - v_2$, for which holds that $v_1 \leftrightarrow -p_2$ and $v_2 \leftrightarrow p_2$. By using the same component K_i, as discussed in the previous paragraph, $v_1 = -p_2 * K_1$ and $v_2 = p_2 * K_2$. Thereby, the linear equation to calculate the effective pressure load on the inside of the interior pane of the IGU, due to an isochoric pressure, is calculated using equation (99).

$$p_{2;o} = \frac{V'}{K_1 + K_2} \quad (99)$$

Whereby:

$$K_i = \sum_{m=1,3} \sum_{n=1,3} \frac{B_{mn}}{A_{i;mn} * (C_{mn} * (D_{i;mn} + E_{mn}) + F_{i;mn} + G_{mn})} \quad (100)$$

In which:

$p_{2;o}$	is the effective pressure load on the inside of the interior pane of the IGU, due to an isochoric pressure, in kN/m²;
V'	is the change in cavity volume, in mm³
K_i	is the constant for calculating volume of deformation due to effective pressure loads, whereby $v_i = K_i * p_i$;

In case of a symmetric IGU, equation (99) is simplified to:

$$p_{2;o} = \frac{V'}{2K} \quad (101)$$

Effective isochoric pressure load due to cold-bending of asymmetric IGU's

From evaluation of cold-bending of asymmetric IGU's it is concluded there is a change in cavity volume due to anticlastic bending, $V'_{CB} = -\Delta V_1 + \Delta V_2$. Thereby, equation (99) can be rewritten to:

$$p_{2;CB} = \frac{-\Delta V_1 + \Delta V_2}{K_1 + K_2} \quad (102)$$

With the calculation for external load sharing, the combined effective pressures for cold-bent asymmetric IGU's can be calculated analytically. Below an example is shown of the results for a 2000x2000x8-16-10mm IGU configuration with design radii ranging from flat to R=8m (Figure 106). The results from numerical modelling are represented using dotted lines, results from analytical modelling have continuous lines. In line numerical results can be concluded resulting effective pressures increase as the curvature increases. In Appendix C.3 the results of different asymmetric configurations and plate sizes are shown. In general, it can be concluded that deviations between analytical and numerical modelling increase for larger plate sizes and smaller design radii. In Chapter 7 and 8 a more in-depth consideration is given of the discussed results.

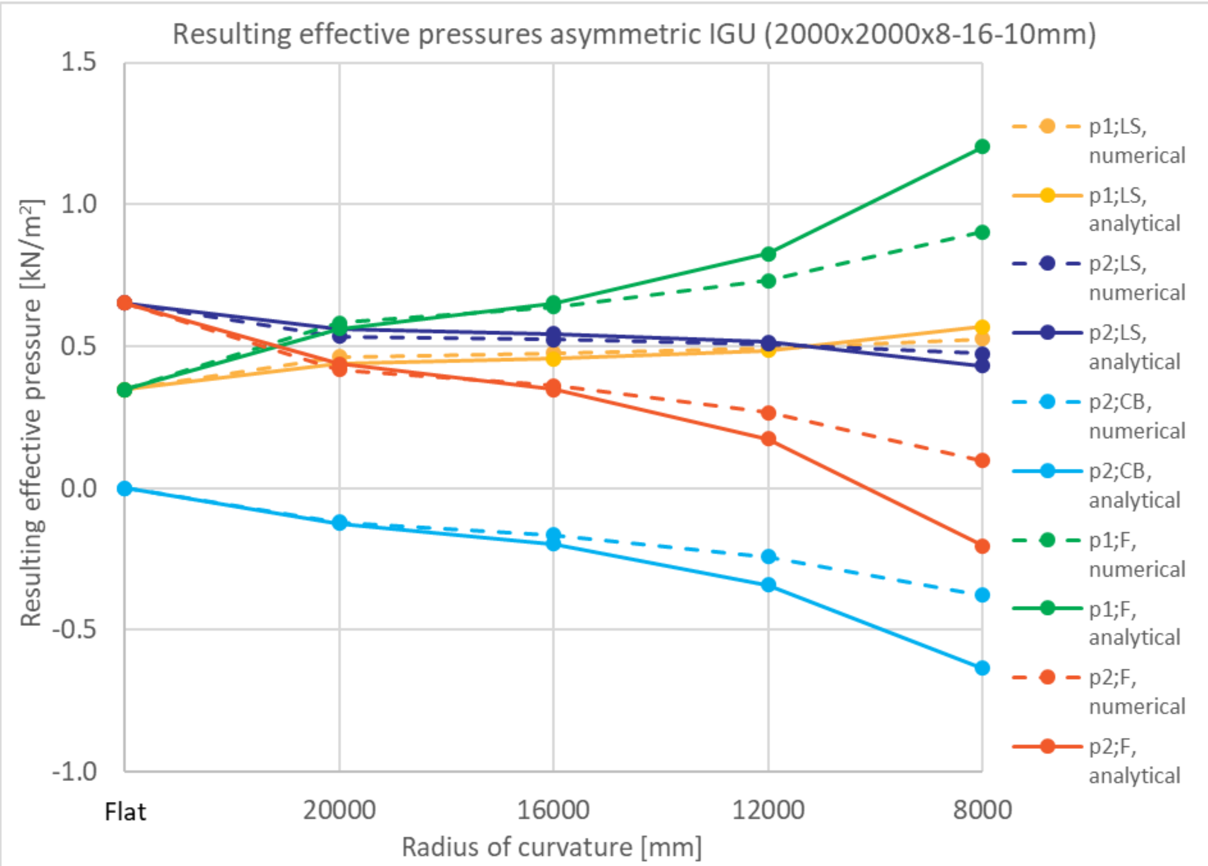

Figure 106: Analytical external load sharing of an asymmetric IGU (2000x2000x8-16-10mm)

Effective isochoric pressure load due to climatic loads and height differences
With equation (99), effective loads due to climate loads and height differences, as discussed in Chapter 4.5.3, can also be calculated. The change in cavity pressure is calculated using Boyle's law, resulting in the following equations:

$$p_{2;c} = \frac{V * P_{o;c}}{(P_{c;p} - P_{o;c}) * (K_1 + K_2)} \tag{103}$$

$$p_{2;H} = \frac{V * P_{o;H}}{(P_{c;p} - P_{o;H}) * (K_1 + K_2)} \tag{104}$$

In which:

$p_{2;c}$	is the effective pressure load on the inside of the interior pane of the IGU, due to climatic loads, in kN/m^2;
$p_{2;H}$	is the effective pressure load on the inside of the interior pane of the IGU, due to height differences, in kN/m^2;
$P_{c;P}$	is the barometric pressure during production at the time of sealing, in kN/m^2;
$P_{o;c}$	is the isochoric pressure due to climatic loads, in kN/m^2, calculated using equation (38);
$P_{o;H}$	is the isochoric pressure due to height differences, in kN/m^2, calculated using equation (39);
V	is the cavity volume, in mm^3;
K_i	is the constant for calculating volume of deformation due to effective pressure loads, whereby $v_i = K_i * p_i$.

Since the equation (103) and (104) are based on the same principles as equation (99), it is assumed that the same findings, conclusions and validity holds for changes in isochoric pressures due to these boundary conditions. Therefore, numerical validation of the effective loads due to climatic loads and height differences is left out of consideration. Validity of the isochoric pressures due to cold-bending is discussed in Chapter 7.3. In Chapter 9, a recommendation is given how combinations of isochoric pressures can be validated with numerical outcomes.

6. Analytical method

In this chapter the developed analytical method, which is divided into three steps, is presented. The equations are presented in a step-by-step guideline, using a similar style as NEN 2608. The first step is the calculation of maximum principal stresses, as a result of the cold-bending phase. The engineering method as discussed in Chapter 3, is used to calculate this stress. The second step is used to calculate the load sharing of the cold-bent IGU due to an external pressure load. The equations used for this component are derived in Chapter 5.5.1. The third step is the calculation of effective loads due to changes isochoric pressures. In case of asymmetric cold-bent IGU's, three different isochoric pressures can be calculated. First is the isochoric pressure due to cold-bending of asymmetric IGU's, as discussed in Chapter 4.5. For the calculation of this effective load, the change in cavity distance and cavity volume are calculated first. Second and third are isochoric pressures as a result of climatic loads and height differences.

The effective isochoric and load sharing pressures can be combined to gain insights into the cavity pressure inside cold-bent IGU's under different load conditions (Figure 107). In order to quickly explore different design options and load combinations, a fully interactive Excel tool is created. An overview of the components of this tool is presented, in which combinations of all effective pressures can be considered.

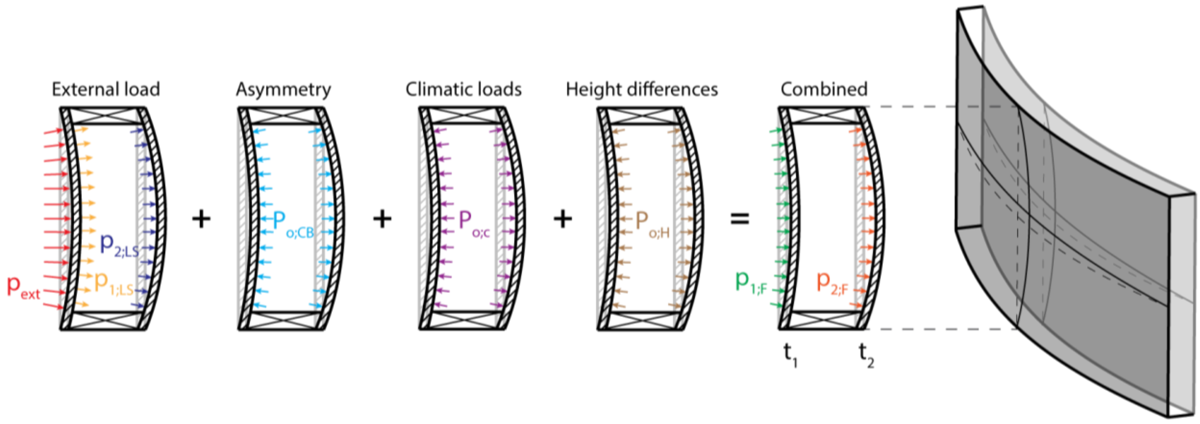

Figure 107: Overview of effective isochoric loads and effective load sharing pressures

Last, an example of the analytical method is shown for a case study of the Van Gogh museum in Amsterdam. For illustrative purposes, an asymmetric configuration is considered, which is subject to an external pressure load. The analytical results are then compared to results from numerical outcomes. Results of a case study based on the Spartherm Innovationszentrum in Melle, are also presented and compared.

6.1. Cold-bending stresses

Equation (105) is used to calculate the maximum principal stress due to cold-bending of an IGU. It can be used to gain insights in the maximum allowable curvature of the IGU or the desired utilisation of cold-bending stresses. The derivation is based linear fixation of the cold-bent IGU, as discussed in Chapter 3. Since the peak stresses are along the edge of the plate, the design value of the bending strength must be considered for edge conditions. The tensile bending strength in glass plate i, must meet the following requirement:

$$\sigma'_{max;i} = \frac{t_i * \left(R - \sqrt{R^2 * \cos^2\left(\frac{2000}{R}\right)}\right)}{42} \leq \gamma_u * f_{mt;u;d} \tag{105}$$

In which:

- σ'_i is the design value for the maximum principal tensile bending stress in glass plate i, in N/mm²;
- R is the design radius of the IGU, in mm;
- t_i is the thickness of glass plate i, in mm;
- γ_u is the desired extent of utilisation of cold-bending stresses;
- $f_{mt;u;d}$ is the design value of the tensile bending strength on the edge of the plate in N/mm² as discussed in Chapter 2.1.4:
  - Heat Strengthened (HSG): $f_{mt;u;d;HSG}$ = 28.08 N/mm².
  - Fully Tempered (FTG): $f_{mt;u;d;FTG}$ = 63.50 N/mm².

6.2. Load sharing pressures

The resulting pressure on the cavity side of the interior plate (Figure 108) is calculated using equation (106), as shown on the next page. Derivation of the equations is discussed in Chapter 5.4.1 and 5.5.1.

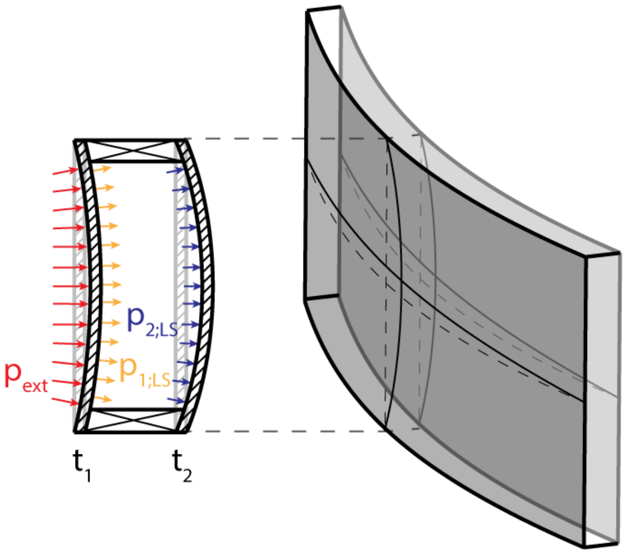

Figure 108: Load sharing due to an external load

$$p_{2;LS} = \left[\sqrt{(K_1+K_2)^2 * P_{c;P}^2 + 2P_{c;P} * (p_{ext} * K_1 + V) * (K_1+K_2) + (p_{ext} * K_1 - V)^2} - V + K_1 * \left(p_{ext} - P_{c;P}\right) - P_{c;P} * K_2\right] * \frac{1}{2K_1 + 2K_2} \quad (106)$$

Whereby:

$$K_i = \sum_{m=1,3}\sum_{n=1,3} \frac{B_{mn}}{A_{i;mn} * (C_{mn} * \left(D_{i;mn} + E_{i;mn}\right) + F_{i;mn} + G_{mn})} \quad (107)$$

$$A_{i;mn} = \frac{E * t_{pl;i} * \pi^4 * m^2 * n^2}{192(1+\nu) * (\cos(m\pi) - 1) * (\cos(n\pi) - 1)} \quad (108)$$

$$B_{mn} = R^2 * B^5 * H^5 * (R^4 * m^2 * n^2 * (1+\nu) - 4H^2 * B^2) * (1-\nu) \quad (109)$$

$$C_{mn} = -4H^2 * B^2 * R^2 \quad (110)$$

$$D_{i;mn} = t_{pl;i}^2 * \pi^4 * (H^4 * n^4 + m^4 * B^4) - 12H^4 * n^2 * B^2 \quad (111)$$

$$E_{mn} = 2m^2 * B^2 * H^2 * (\pi^4 * n^2 * t^2 - 6B^2 * \nu^2) \quad (112)$$

$$F_{i;mn} = R^6 * m^2 * n^2 * t_{pl;i}^2 * \pi^4 * (H^2 * n^2 + m^2 * B^2)^2 * (1+\nu) \quad (113)$$

$$G_{mn} = -24H^4 * B^4 * \left(R^4 * m^2 * n^2 * \left(\nu^2 + \frac{3\nu}{2} - \frac{1}{2}\right) + 2H^2 * B^2\right) \quad (114)$$

In which:

$p_{2;LS}$	is the effective pressure load on the inside of the interior pane of the IGU, due to load sharing of an external pressure load, in kN/m^2
K_i	is the constant for calculating volume of deformation due to effective pressure loads, whereby $v_i = K_i * p_i$;
$P_{c;P}$	is the reference pressure inside the cavity at the time of sealing, whereby $P_{c;P} =$ 101.325 kN/m^2;
p_{ext}	is the external pressure load on the exterior plate of the IGU, in kN/m^2;
V	is the reference cavity volume at the time of sealing, in mm^3.
E	is the Young's modulus of glass, whereby E_g = 70000 N/mm^2;
$t_{pl;i}$	is the thickness of the glass pane i, in mm;
ν	is the Poisson's ratio of glass, whereby ν_g = .23;
R	is the design radius of the IGU, in mm;
B	is the width of the IGU, in mm;
H	is the height of the IGU, in mm.

In case of symmetric IGU's, equation (106) is simplified to:

$$p_{2;LS} = \frac{\sqrt{4K^2 * \left(P_{c;P} + \frac{p_{ext}}{2}\right)^2 + 4K * V * \left(P_{c;P} - \frac{p_{ext}}{2}\right) + V^2} + K * \left(p_{ext} - 2P_{c;P}\right) - V}{4K} \quad (115)$$

After calculating the pressure load on the interior pane $p_{2;LS}$, the load on the windward pane is defined by $p_{1;LS} = p_{ext} - p_{2;LS}$, as shown in Figure 108. The load sharing factors are calculated by dividing the load on the panes by the external load, i.e., $\delta_1 = \frac{p_{1;LS}}{p_{ext}}$ and $\delta_2 = \frac{p_{2;LS}}{p_{ext}}$.

6.3. Isochoric pressures

Derivation of the equations to calculate the effective pressures due to asymmetric cold-bending, climatic loads and height differences (Figure 109), are discussed in Chapter 5.5.2. First, the steps to calculate the isochoric pressure due to cold-bending are considered. Thereafter, the equations for climatic loads and height differences are presented.

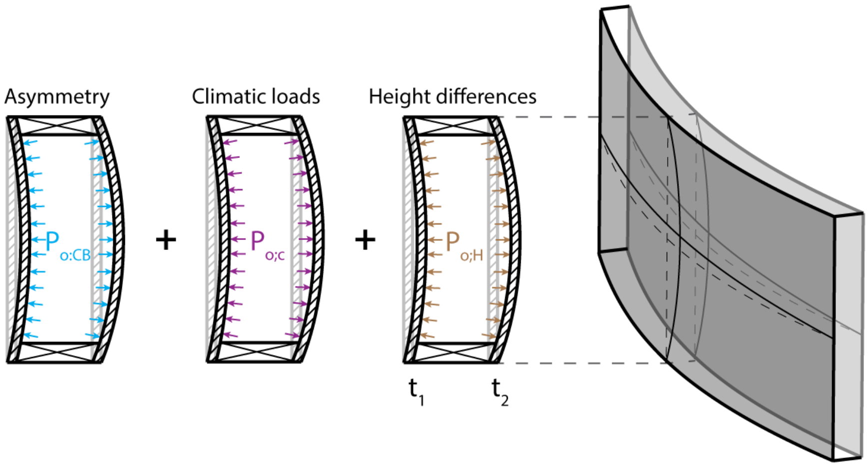

Figure 109: Overview of isochoric pressures in cold-bent IGU's

6.3.1. Effective isochoric pressure load due to cold-bending of asymmetric IGU's

To calculate the effective pressure load due to cold-bending of an asymmetric IGU, first the change in cavity distance (Figure 111) is calculated using the radius at midspan of the curved plates (Figure 110). The radius at midspan is calculated using equation (116).

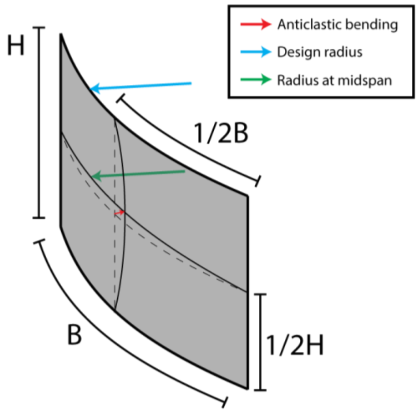

Figure 110: Decreased radius at midspan due to anticlastic bending

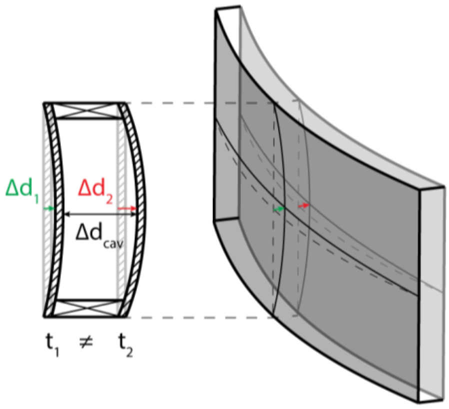

Figure 111: Change in cavity distance in the centre of an asymmetric IGU

$$R_{mid;i} = A_{B:H} * t_{pl;i} + B_{B:H} \tag{116}$$

$$A_{B:H} = a_{A_{B:H}} * R^3 + b_{A_{B:H}} * R^2 + c_{A_{B:H}} * R + d_{A_{B:H}} \tag{117}$$

$$B_{B:H} = a_{B_{B:H}} * R^3 + b_{B_{B:H}} * R^2 + c_{B_{B:H}} * R + d_{B_{B:H}} \tag{118}$$

In which:

$a_{A_{B:H}}, \dots, d_{B_{B:H}}$ are the polynomial coefficients per plate height-to-width ratio, according to Chapter 4.4.3 and Table 13;

$A_{B:H}, B_{B:H}$ are the linear coefficients per plate height-to-width ratio;

R is the design radius of the IGU, in mm;

R_i is the radius at midspan of glass plate i, in mm;

$t_{pl;i}$ is the thickness of glass plate i, in mm.

The cavity distance in the centre of the cold-bent IGU is then calculated using equation (119).

$$\Delta d_{cav} = d - \Delta d_1 + \Delta d_2 \quad (119)$$

Whereby:

$$\Delta d_i = R - \sqrt{R^2 * \cos^2\left(\frac{B}{2R}\right)} - R_{mid;i} + \sqrt{R_{mid;i}^2 * \cos^2\left(\frac{B}{2R_{mid;i}}\right)} \quad (120)$$

In which:

Δd_{cav}	is the cavity distance in the centre of the IGU due to anticlastic bending, in mm;
Δd_i	is the difference in cavity distance at midpoint of glass pane i due to anticlastic bending, in mm;
d	is the design cavity distance, in mm;
R	is the design radius of the IGU, in mm;
$R_{mid;i}$	is the radius at midspan of glass pane i as a result of anticlastic bending, in mm;
B	is the width of the IGU, in mm.

In case the dimensions of the plate are in between the heights and widths in the coefficients table (Table 13), the radii at midspan are linearly interpolated. This can be done using the guiding table below (Table 20). First, the closest lower and upper dimensions are selected from the coefficient table and filled in, in cells B_L, B_U, H_L and H_U. Second, the radii at midspan of the lower and upper dimensions of the plate are calculated using equation (116), and filled in $R_{mid;i;LL}$, $R_{mid;i;LU}$, $R_{mid;i;UL}$ and $R_{mid;i;UU}$. The interpolated radius $R_{mid;i;avg}$ is then calculated using equation (121), after calculating equation (122) until (125).

Table 20: Guiding table for interpolation

	B_L	$\boldsymbol{B}$	B_U
H_L	$R_{mid;i;LL}$	$R_{mid;i;1}$	$R_{mid;i;LU}$
$\boldsymbol{H}$	$R_{mid;i;2}$	$\boldsymbol{R_{mid;i}}$	$R_{mid;i;3}$
H_U	$R_{mid;i;UL}$	$R_{mid;i;4}$	$R_{mid;i;UU}$

$$R_{mid;i} = \frac{R_{mid;i;1} + R_{mid;i;2} + R_{mid;i;3} + R_{mid;i;4}}{4} \quad (121)$$

In which:

$$R_{mid;i;1} = \frac{R_{mid;i;LL}(B_U - B) + R_{mid;i;LU}(B - B_L)}{B_U - B_L} \quad (122)$$

$$R_{mid;i;2} = \frac{R_{mid;i;LL}(H_U - H) + R_{mid;i;UL}(H - H_L)}{H_U - H_L} \quad (123)$$

$$R_{mid;i;3} = \frac{R_{mid;i;LU}(H_U - H) + R_{mid;i;UU}(H - H_L)}{H_U - H_L} \quad (124)$$

$$R_{mid;i;4} = \frac{R_{mid;i;UL}(B_U - B) + R_{mid;i;UU}(B - B_L)}{B_U - B_L} \quad (125)$$

Using the radius at midspan, the volume below curved glass pane i, can be calculated using equation (126). Derivation of the equation is shown in Chapter 4.5.2.

$$\Delta V = \frac{4HR\sin\left(\frac{B}{2R}\right)}{\pi^2} * \left((-\pi + 2) * \sqrt{R^2 * \cos^2\left(\frac{B}{2R}\right)} - 2\sqrt{R_{mid}^2 * \cos^2\left(\frac{B}{2R_{mid}}\right)} + 2R_{mid} - 2R_{mid} + R\pi \right) \tag{126}$$

In which:

ΔV	is the volume below the cold-bent glass plate, in mm³;
R	is the design radius of the IGU, in mm;
R_{mid}	is the radius at midspan of a glass plate as a result of anticlastic bending, in mm;
H	is the height of the IGU, in mm;
B	is the width of the IGU, in mm.

The effective pressure load on the inside of the interior pane of the IGU is calculated using equation (127). Derivation of the equation is shown in Chapter 5.5.2.

$$p_{2;CB} = \frac{-\Delta V_1 + \Delta V_2}{K_1 + K_2} \tag{127}$$

Whereby:

$$K_i = \sum_{m=1,3} \sum_{n=1,3} \frac{B_{mn}}{A_{i;mn} * (C_{mn} * (D_{i;mn} + E_{mn}) + F_{i;mn} + G_{mn})} \tag{128}$$

In which:

$p_{2;CB}$	is the effective pressure load on the inside of the interior pane of the IGU, due to cold-bending of asymmetric IGU's, in kN/m²;
ΔV_i	is the change in cavity volume, in mm³;
K_i	is the constant for calculating volume of deformation due to effective pressure loads, whereby $v_i = K_i * p_i$;
$A_{mn}, \dots, G_{mn}$	are the constants used to calculate the volume of deformation, as shown in equations (108) until (114).

6.3.2. Effective isochoric pressure load due to climatic loads and height differences

Effective pressures due to climate loads and height differences, are calculated using equation (129).

$$p_{2;c} = \frac{V * P_{o;c}}{(P_{c;p} - P_{o;c}) * (K_1 + K_2)}, \qquad p_{2;H} = \frac{V * P_{o;H}}{(P_{c;P} - P_{o;H}) * (K_1 + K_2)} \tag{129}$$

In which:

$p_{2;c}$	is the effective pressure load on the inside of the interior pane of the IGU, due to climatic loads, in kN/m²;
$p_{2;H}$	is the effective pressure load on the inside of the interior pane of the IGU, due to height differences, in kN/m²;
$P_{c;P}$	is the barometric pressure during production at the time of sealing, in kN/m²;
$P_{o;c}$	is the isochoric pressure due to climatic loads, in kN/m², calculated using equation (38);
$P_{o;H}$	is the isochoric pressure due to height differences, in kN/m², calculated using equation (39);
V	is the cavity volume, in mm³;
K_i	is the constant for calculating volume of deformation due to effective pressure loads, whereby $v_i = K_i * p_i$.

6.4. Excel tool

All equations are implemented in an interactive Excel tool which can be used to quickly calculate cavity pressures in cold-bent IGU configurations. The tool considers the symbols, units, colours and direction of pressures, discussed throughout this thesis. An information sheet is included, in which a guideline and the equations corresponding to the calculation cells are presented. Calculation of equations, generation of interactive diagram data and coefficient Table 13, are included in separate sheets. An overview of the tool is shown in Figure 112, below the different components are discussed.

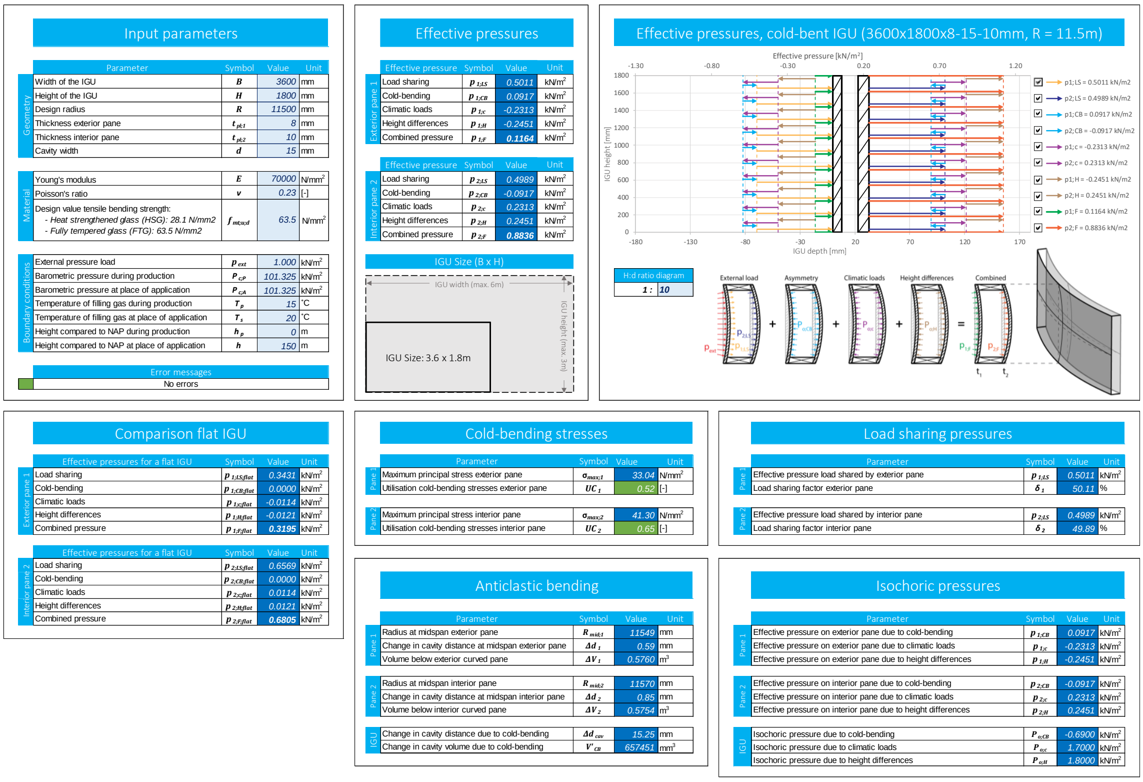

Figure 112: Overview Excel tool

6.4.1. Component 1: Input parameters

Input parameters

	Parameter	Symbol	Value	Unit
Geometry	Width of the IGU	B	3600	mm
	Height of the IGU	H	1800	mm
	Design radius	R	11500	mm
	Thickness exterior pane	$t_{pl;1}$	8	mm
	Thickness interior pane	$t_{pl;2}$	10	mm
	Cavity width	d	15	mm
Material	Young's modulus	E	70000	N/mm²
	Poisson's ratio	v	0.23	[-]
	Design value tensile bending strength: - *Heat strengthened glass (HSG): 28.1 N/mm2* - *Fully tempered glass (FTG): 63.5 N/mm2*	$f_{mt;u;d}$	63.5	N/mm²
Boundary conditions	External pressure load	p_{ext}	1.000	kN/m²
	Barometric pressure during production	$P_{c;P}$	101.325	kN/m²
	Barometric pressure at place of application	$P_{c;A}$	101.325	kN/m²
	Temperature of filling gas during production	T_p	15	°C
	Temperature of filling gas at place of application	T_s	20	°C
	Height compared to NAP during production	h_p	0	m
	Height compared to NAP at place of application	h	150	m

Error messages
No errors

Figure 113: Component 1: Input parameters

In Component 1, the different design parameters of cold-bent IGU's can be filled in. The first block considers the geometry parameters. Second, the material properties are considered. Third, input parameters which influence load sharing and isochoric pressures can be filled in. Effective pressures due external loads, a change in barometric pressure, temperature differences and height differences are included. Furthermore, a message box is included, which indicates if there is a remark in one of the calculations. In case of cold-bending stresses higher than the tensile bending strength, a warning (orange) is given. In case of effective pressures which are higher than the isochoric pressure, a warning is given that results may be inaccurate due to extreme curvatures. In case the input dimensions are outside the range of the coefficient table, an error (red) is given and corresponding results are defined as N/A (Not Available).

6.4.2. Component 2: Effective pressures

Effective pressures

	Effective pressure	Symbol	Value	Unit
Exterior pane 1	Load sharing	$p_{1;LS}$	0.5011	kN/m²
	Cold-bending	$p_{1;CB}$	0.0917	kN/m²
	Climatic loads	$p_{1;c}$	-0.2313	kN/m²
	Height differences	$p_{1;H}$	-0.2451	kN/m²
	Combined pressure	$p_{1;F}$	0.1164	kN/m²

	Effective pressure	Symbol	Value	Unit
Interior pane 2	Load sharing	$p_{2;LS}$	0.4989	kN/m²
	Cold-bending	$p_{2;CB}$	-0.0917	kN/m²
	Climatic loads	$p_{2;c}$	0.2313	kN/m²
	Height differences	$p_{2;H}$	0.2451	kN/m²
	Combined pressure	$p_{2;F}$	0.8836	kN/m²

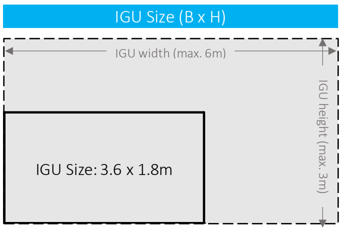

Figure 114: Component 2: Effective pressures

In Component 2, an overview of the resulting effective pressures is given. In the first block the resulting pressures on the exterior pane are considered. The second block shows the results on the interior pane. In both blocks, the effective load sharing pressure is considered first. Thereafter, the effective isochoric pressures due to cold-bending, climatic loads and height differences are shown. The pressures are then summed to calculate the combined final effective pressure.

The component also considers an interactive diagram, which shows the considered IGU size in comparison to the maximum IGU size. In case the input parameters are outside of the limits of the coefficient table (Table 13), the interactive diagram is larger than the diagram limits and an error message occurs.

6.4.3. Component 3: Interactive load sharing diagram

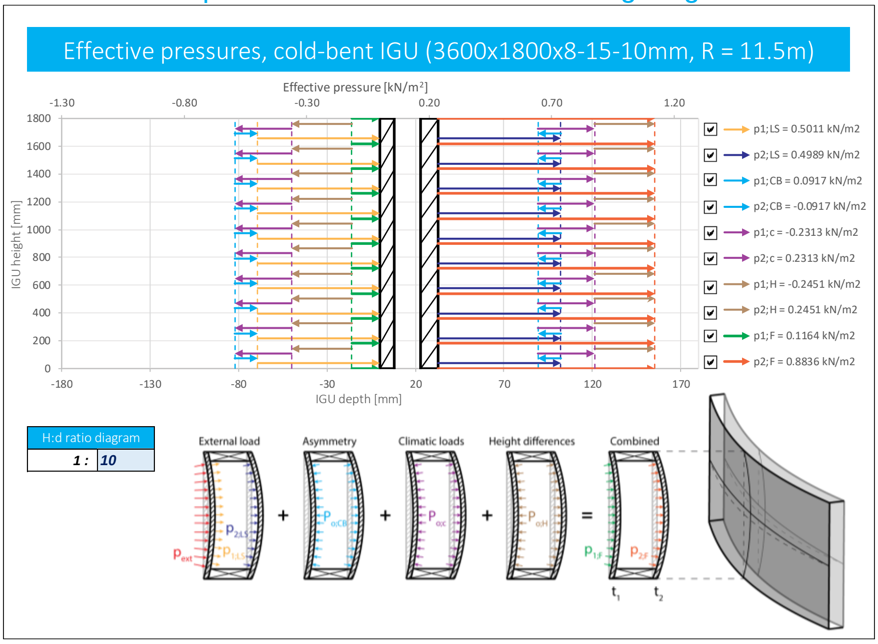

Figure 115: Component 3: Interactive load sharing diagram

In Component 3, a cross section of the IGU is shown, including the direction and extent of the effective pressure loads on both panes. The diagram is fully interactive and scales itself automatically.

On the bottom x-axis, the depth of the IGU in mm is considered. The scale of this x-axis is based on the ratio between the height and depth of the diagram (H:d ratio diagram), which can be adjusted to create a wider or narrower presentation. Thickness of the panes and cavity width changes according to the input parameters. All distances are relative to the outside of the exterior pane.

The top x-axis considers the effective pressure loads in kN/m². Notation, colour and direction of the loads is in line with the overview shown in Figure 107, which is also included in the sheet. The loads on the exterior pane are relative to the outside of the exterior pane (left). The loads on the interior pane are relative to the outside of the interior pane (right), for which a reference value is considered based on a cross calculation with the depth of the IGU. In order to create a clear overview, the different loads are presented on top of each other. To gain insights into specific loads, it is possible to tick-off pressure loads in the legenda.

6.4.4. Component 4: Comparison flat IGU

Comparison flat IGU

	Effective pressures for a flat IGU	Symbol	Value	Unit
Exterior pane 1	Load sharing	$p_{1;LS;flat}$	0.3431	kN/m^2
	Cold-bending	$p_{1;CB;flat}$	0.0000	kN/m^2
	Climatic loads	$p_{1;c;flat}$	-0.0114	kN/m^2
	Height differences	$p_{1;H;flat}$	-0.0121	kN/m^2
	Combined pressure	$p_{1;F;flat}$	**0.3195**	kN/m^2

	Effective pressures for a flat IGU	Symbol	Value	Unit
Interior pane 2	Load sharing	$p_{2;LS;flat}$	0.6569	kN/m^2
	Cold-bending	$p_{2;CB;flat}$	0.0000	kN/m^2
	Climatic loads	$p_{2;c;flat}$	0.0114	kN/m^2
	Height differences	$p_{2;H;flat}$	0.0121	kN/m^2
	Combined pressure	$p_{2;F;flat}$	**0.6805**	kN/m^2

Figure 116: Component 4: Comparison flat IGU

In Component 4, the pressures considered for Component 2, are presented for a flat IGU. Equations from (NEN 2608, 2014) are used to calculate the effective pressures, as discussed in Chapter 2.3.5 and 2.3.6. Using the flat results, insights can be gained on how effective pressures change as curvatures increase.

6.4.5. Component 5: Cold-bending stresses

Cold-bending stresses

	Parameter	Symbol	Value	Unit
Pane 1	Maximum principal stress exterior pane	$\sigma_{max;1}$	33.04	N/mm^2
	Utilisation cold-bending stresses exterior pane	UC_1	0.52	[-]
Pane 2	Maximum principal stress interior pane	$\sigma_{max;2}$	41.30	N/mm^2
	Utilisation cold-bending stresses interior pane	UC_2	0.65	[-]

Figure 117: Component 5: Cold-bending stresses

In Component 5, the cold-bending stresses are calculated. The equation used for this calculation is derived from a result-based engineering method, as discussed in Chapter 3.4.3. Furthermore, a unity check is included, based on the design value for bending strength along the curved edge of the plate. In case of a unity check above 1.0, the filling colour changes to red and a warning is given in the message box in Component 1.

6.4.6. Component 6: Anticlastic bending

Anticlastic bending

	Parameter	Symbol	Value	Unit
Pane 1	Radius at midspan exterior pane	$R_{mid;1}$	11548	mm
	Change in cavity distance at midspan exterior pane	Δd_1	0.58	mm
	Volume below exterior curved pane	ΔV_1	0.6078	m^3
Pane 2	Radius at midspan interior pane	$R_{mid;2}$	11567	mm
	Change in cavity distance at midspan interior pane	Δd_2	0.81	mm
	Volume below interior curved pane	ΔV_2	0.6071	m^3
IGU	Change in cavity distance due to cold-bending	Δd_{cav}	15.24	mm
	Change in cavity volume due to cold-bending	V'_{CB}	659357	mm^3

Figure 118: Component 6: Anticlastic bending

In Component 6, the simplified analytical results of anticlastic behaviour due to cold-bending of the IGU are presented. Per pane, the radius at midspan, change in cavity distance at centre of the pane and the volume below the curved plate are calculated. The results are combined to determine the cavity distance and change in cavity volume after cold-bending. Per plate size, the corresponding tabulated coefficients are derived from a separate sheet, from which the radius at midspan is calculated. In case of in-between plate sizes, the interpolation table is used.

6.4.7. Component 7: Load sharing pressures

Load sharing pressures

	Parameter	Symbol	Value	Unit
Pane 1	Effective pressure load shared by exterior pane	$p_{1;LS}$	0.5026	kN/m^2
	Load sharing factor exterior pane	δ_1	50.26	%
Pane 2	Effective pressure load shared by interior pane	$p_{2;LS}$	0.4974	kN/m^2
	Load sharing factor interior pane	δ_2	49.74	%

Figure 119: Component 7: Load sharing pressures

In Component 7, the load sharing due to an external pressure load is calculated per pane. Furthermore, the load sharing factor per pane is given as a percentage of the external pressure.

6.4.8. Component 8: Isochoric pressures

Isochoric pressures

	Parameter	Symbol	Value	Unit
Pane 1	Effective pressure on exterior pane due to cold-bending	$p_{1;CB}$	0.0886	kN/m^2
	Effective pressure on exterior pane due to climatic loads	$p_{1;c}$	-0.2350	kN/m^2
	Effective pressure on exterior pane due to height differences	$p_{1;H}$	-0.2491	kN/m^2
Pane 2	Effective pressure on interior pane due to cold-bending	$p_{2;CB}$	-0.0886	kN/m^2
	Effective pressure on interior pane due to climatic loads	$p_{2;c}$	0.2350	kN/m^2
	Effective pressure on interior pane due to height differences	$p_{2;H}$	0.2491	kN/m^2
IGU	Isochoric pressure due to cold-bending	$P_{o;CB}$	-0.6557	kN/m^2
	Isochoric pressure due to climatic loads	$P_{o;c}$	1.7000	kN/m^2
	Isochoric pressure due to height differences	$P_{o;H}$	1.8000	kN/m^2

Figure 120: Component 8: Isochoric pressures

In Component 8, the effective isochoric pressures due to cold-bending, climatic loads and height differences are presented. Furthermore, the corresponding all-sided isochoric pressures are given. Cold-bending pressures are only considered in case of asymmetric IGU configurations. Climatic loads are dependent on barometric pressure differences in kN/m^2 and temperature differences in ˚C. Isochoric pressures due to height differences are only considered in case the difference is larger than 150m.

6.5. Case study

Below the application of the developed analytical method is shown using an example case study with specifications from the Van Gogh Museum in Amsterdam (Bijster, Noteboom, & Eekhout, 2016). In the building a symmetric IGU with laminated glass panes is used, however for illustration purposes and completeness, an asymmetric variant with monolithic glass panes is used. Isochoric pressures due to climatic loads and height differences are left out of consideration. Specifications of the IGU are shown Figure 127. Furthermore, specifications of a case study based on the Innovationszentrum of Spartherm in Melle are given (van de Rotten, 2019). Results of both case studies are compared to numerical outcomes to check the validity of the simplified analytical method with examples from practice.

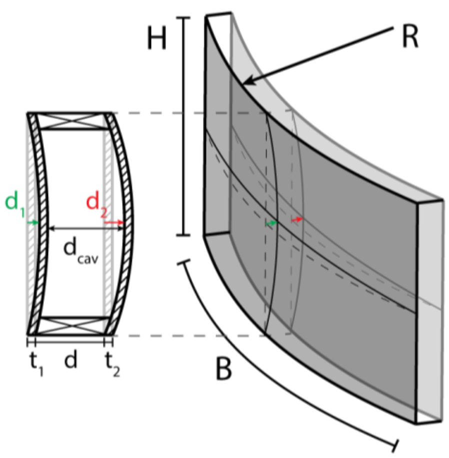

Van Gogh Museum

	Symbol	Value	Unit
Geometry	B	3600	mm
	H	1800	mm
	R	11500	mm
	$t_{pl;1}$	8	mm
	$t_{pl;2}$	10	mm
	d	15	mm
Material	E	70000	N/mm²
	v	0.23	[-]
	$f_{mt;u;d}$	28.1	N/mm²
Boundary conditions	p_{ext}	1.000	kN/m²
	$P_{c;P}$	101.325	kN/m²
	$P_{c;A}$	101.325	kN/m²
	T_p	15	°C
	T_s	15	°C
	h_p	0	m
	h	0	m

Innovationszentrum Spartherm

	Symbol	Value	Unit
Geometry	B	5500	mm
	H	2500	mm
	R	28000	mm
	$t_{pl;1}$	14	mm
	$t_{pl;2}$	16	mm
	d	15	mm
Material	E	70000	N/mm²
	v	0.23	[-]
	$f_{mt;u;d}$	28.1	N/mm²
Boundary conditions	p_{ext}	1.000	kN/m²
	$P_{c;P}$	101.325	kN/m²
	$P_{c;A}$	101.325	kN/m²
	T_p	15	°C
	T_s	15	°C
	h_p	0	m
	h	0	m

Figure 121: Dimensions example case studies Van Gogh Museum and Innovationszentrum Melle

6.5.1. Calculation of cold-bending stresses

The cold-bending stress is calculated using equation (105), which results in σ_1' =33.04 N/mm² for the exterior plate with a thickness of 8mm and σ_2' =41.30 N/mm² for the interior plate with a thickness of 10mm. For the Van Gogh Museum heat-strengthened glass (HSG) is used, which means that in case the two sheets of 5mm glass are considered as monolithic without considering equivalent thicknesses, the utilisation of cold-bending stresses is larger than the allowable strength: $\gamma_u = \frac{\sigma'_{max}}{f_{mt;u;d;HSG}} = \frac{41.30}{28.08}$ =1.47.

Due to the lamination of the two 5mm sheets, the equivalent thickness can be used when calculating stresses due to external loads (Bijster, Noteboom, & Eekhout, 2016). Furthermore, in case of an enforced displacement with no shear interaction, the stresses can be calculated with the thickness of one single sheet. Both considerations are only applicable for long-term loading, which is in the context of this report is in line with the ‘Fixation moment’ and ‘Use phase’. Stresses during the ‘Bending phase’ can be higher due to different load conditions and the shear interaction of the laminated sheets.

The long term cold-bending stresses according equation (105) are $\sigma'_{t;gg,ser,min}$ = 24.99 N/mm² when considering the equivalent thickness of 6.05 mm, and $\sigma'_{t=5}$ =20.65 N/mm² when considering a single sheet only, resulting in an utilisation of γ_u =0.89 and γ_u =0.73 respectively. The stress value of the 5mm is sheet is in compliance with the ‘major principal stresses after geometrical nonlinear of one plate, t = 5mm’, as stated in the paper and shown in Figure 24 (Bijster, Noteboom, & Eekhout, 2016).

6.5.2. External load sharing

Second, the load sharing of the panes of the cold-bent IGU due to an external pressure load is calculated. This is done by first calculating constants A_{mn} until G_{mn} for values of m and n of 1 and 3 (equation (108) until (114)). The results are shown in Table 21.

Table 21: Results of A_{mn} until G_{mn}, for values of m and n of 1 and 3

$m = 1, n = 1$	t_1	t_2
A_{mn}	5.7746E+04	7.2182E+04
B_{mn}	2.4834E+58	2.4834E+58
C_{mn}	-2.2213E+22	-2.2213E+22
D_{mn}	-1.6315E+21	-1.6308E+21
E_{mn}	-3.4493E+20	-3.4464E+20
F_{mn}	4.6548E+42	7.2731E+42
G_{mn}	7.2013E+43	7.2013E+43

$m = 3, n = 1$	t_1	t_2
A_{mn}	5.1971E+05	6.4964E+05
B_{mn}	2.2507E+59	2.2507E+59
C_{mn}	-2.2213E+22	-2.2213E+22
D_{mn}	-1.5477E+21	-1.5000E+21
E_{mn}	-3.1044E+21	-3.1017E+21
F_{mn}	2.2941E+45	3.5845E+45
G_{mn}	6.7654E+44	6.7654E+44

$m = 1, n = 3$	t_1	t_2
A_{mn}	5.1971E+05	6.4964E+05
B_{mn}	2.2507E+59	2.2507E+59
C_{mn}	-2.2213E+22	-2.2213E+22
D_{mn}	-1.4687E+22	-1.4683E+22
E_{mn}	-3.4074E+20	-3.3809E+20
F_{mn}	2.8320E+44	4.4250E+44
G_{mn}	6.7654E+44	6.7654E+44

$m = 3, n = 3$	t_1	t_2
A_{mn}	4.6774E+06	5.8468E+06
B_{mn}	2.0272E+60	2.0272E+60
C_{mn}	-2.2213E+22	-2.2213E+22
D_{mn}	-1.4603E+22	-1.4552E+22
E_{mn}	-3.0667E+21	-3.0428E+21
F_{mn}	3.0540E+46	4.7719E+46
G_{mn}	6.1173E+45	6.1173E+45

Next, the values of K_1 and K_2 are calculated using equation (107), the results are shown in Table 22. First, the values of K are calculated per value of m and n, whereafter the results are summed to calculate the final value.

Table 22: Results K_1 and K_2

	K_1	K_2
$m = 1, n = 1$	3.5669E+09	2.7934E+09
$m = 3, n = 1$	1.4088E+08	7.9403E+07
$m = 1, n = 3$	3.3479E+08	2.3849E+08
$m = 3, n = 3$	1.1698E+07	6.3939E+06
Total	4.0543E+09	3.1177E+09

The values K_1 and K_2 are used to calculated effective load sharing pressures, as well as effective isochoric pressures. The effect load sharing pressures on the cavity side of the interior pane is calculated using equation (106). The IGU configuration of the case study is subjected to an external pressure load of $p_{ext} = 1$ kN/m^2, resulting in an effective pressure of $p_{2;LS} = 0.4989$ kN/m^2. The effective load on the outside of the exterior pane is then $p_{1;LS} = p_{ext} - p_{2;LS} = 0.5011$ kN/m^2. The corresponding load sharing factors are $\delta_1 = 49.89\%$ and $\delta_2 = 50.11\%$. From the comparison with a flat IGU, which has a load sharing of $\delta_1 = 34.31\%$, it can be concluded that due to the increased stiffness of the cold-bent IGU, more load is shared by the thinner exterior pane.

6.5.3. Radius at midspan due to anticlastic bending

The IGU has a size of 3.6x1.8m, which means that the radius at midspan must be interpolated for both plates. The interpolation is done using the table shown in Chapter 6.3.1, Table 20. First the upper and lower boundaries of the IGU are selected:

Table 23: Interpolation step 1

	3000	**3600**	4000
1000	$R_{mid;i;LL}$	$R_{mid;i;1}$	$R_{mid;i;LU}$
1800	$R_{mid;i;2}$	$\boldsymbol{R_{mid;i}}$	$R_{mid;i;3}$
2000	$R_{mid;i;UL}$	$R_{mid;i;4}$	$R_{mid;i;UU}$

Second, the radii at midspan of the four plate sizes are determined using equation (116), (117) and (118), and the coefficient table (Table 13). The coefficients for $R_{i;LL}$ are shown as example in Table 24.

Table 24: Regression coefficients, 3000x1000mm plate

3000x1000		
	A	***B***
a	-3.179E-12	1.230E-11
b	1.167E-07	3.846E-07
c	6.110E-04	9.886E-01
d	-2.874E+00	3.600E+01

The resulting linear coefficients are $A_{B:H}$ =14.75 and $B_{B:H}$ =11474.47, which results in a radius at midspan of $R_{mid;1;LL}$ =11592.48 mm for exterior plate and $R_{mid;2;LL}$ =11621.98 mm for the interior plate. After filling in all the upper and lower radii, the interpolation tables are as follows:

Table 25: Interpolation step 2

t_1	3000	**3600**	4000
1000	11592.48	$R_{mid;1;1}$	11548.38
1800	$R_{mid;1;2}$	$\boldsymbol{R_{mid;1}}$	$R_{mid;1;3}$
2000	11550.25	$R_{mid;1;4}$	11529.70

t_2	3000	**3600**	4000
1000	11621.98	$R_{mid;2;1}$	11587.50
1800	$R_{mid;2;2}$	$\boldsymbol{R_{mid;2}}$	$R_{mid;2;3}$
2000	11565.13	$R_{mid;2;4}$	11541.55

Next, the interpolation is calculated using equation (122) to (125), giving the following results:

Table 26: Interpolation step 3

t_1	3000	**3600**	4000
1000	11592.48	11566.02	11548.38
1800	11558.69	$\boldsymbol{R_{1;mid}}$	11533.44
2000	11550.25	11537.92	11529.70

t_2	3000	**3600**	4000
1000	11621.98	11601.29	11587.50
1800	11576.50	$\boldsymbol{R_{2;mid}}$	11550.74
2000	11565.13	11550.98	11541.55

Last, the average radii at midspan are calculated using the average of the interpolation table, resulting in a radius at midspan $R_{mid;1}$ = 11549 mm for exterior plate and $R_{mid;2}$ = 11570 mm for the interior plate.

6.5.4. Change in cavity distance and volume

The change in cavity distance due to anticlastic bending is calculated using equation (119), resulting in $\Delta d_{cav} = d - \Delta d_1 + \Delta d_2 = 15.00 - 0.59 + 0.85 = 15.25$ mm. The cavity distance increases, meaning the volume of the cavity will get bigger, resulting in an isochoric underpressure. The change in volume is calculated using equation (126), $V'_{CB} = \Delta V_1 - \Delta V_2$ = 5.7602∗10^8^ − 5.7537∗10^8^ = 657451 mm³. The cavity volume due to cold-bending is then $V + V'_{CB}$ = 9.7875∗10^7^ mm³. Using Boyle's law, the isochoric pressure due to cold-bending is calculated, $P_{o;CB}$ = -0.69 kN/m², which is negative and therefore indeed an underpressure.

.

6.5.5. Effective isochoric pressure due to cold-bending

The effective isochoric pressure due to cold-bending is calculated using equation (127). Values of K_1 and K_2 are the same as calculated for the load sharing pressures. The resulting effective isochoric pressure on the inside of the interior pane is $p_{2;CB}$ = -0.0917 kN/m². The same extent of effective pressure is subjected on the inside of the exterior pane of the IGU, but in opposite direction, $p_{1;CB}$ = 0.0917 kN/m².

6.5.6. Combination of effective pressures

Now that the effective pressures are known, they can be combined to evaluate the resulting pressure on the interior and exterior panes, due to a pressure load on the asymmetric cold-bent IGU. The final load shared by exterior pane is $p_{1;F} = p_{1;LS} + p_{1;CB} = 0.5011 + 0.0917 = 0.5928$ kN/m². The final load shared by the interior pane is $p_{2;F} = p_{2;LS} + p_{2;CB} = 0.4989 - 0.0917 = 0.4027$ kN/m². Due to the isochoric pressure, a higher effective load is subjected onto the exterior pane, compared to load sharing only. From the comparison to load sharing of the flat IGU configuration, it can be concluded that effective pressure loads in cold-bent IGU's can result in principally different outcomes.

6.5.7. Comparison of case studies with numerical outcomes

Configurations based on specifications of the case studies discussed in Chapter 6.5.1 are modelled numerically. The resulting effective pressures are calculated using P-V diagrams, shown in Appendix C.1. For the Van Gogh Museum, symmetric cold-bent IGU's with a combined laminated thickness of 10mm per pane are used. To gain insight in effective pressures due to asymmetry, P-V diagrams are made for a thickness of 8mm and 12mm as well. The same is done for the case study of Spartherm in Melle, where a combined laminated thickness of 16mm is used. The other P-V diagrams for this case study are for a 14mm and 18mm plate. From earlier findings it is concluded that deviations between numerical and analytical outcomes increase, as curvatures increase. Therefore, the smallest design radii used in the final design of both case studies are considered. For the Van Gogh museum a radius of 11.5m is considered, for Spartherm a radius of 28m. Deviations in effective pressures of the case studies are shown in Table 27 and Table 28. The deviations from Spartherm Melle are slightly higher than for the Van Gogh Museum, from which it can be concluded that in this case the increase in plate size has a more significant role than the increase in curvature. Furthermore, it can be concluded that the isochoric pressures due to cold-bending deviate more from numerical modelling than the load sharing pressures. The analytical load sharing pressures are consistently higher than numerical outcomes and cold-bending isochoric pressures are consistently lower. In line with this finding, the deviations in combined pressures are lower than the cold-bending pressures.

Table 27: Deviation in effective pressures, case study Van Gogh

Deviation in effective pressures, case study Van Gogh Museum										
t_1-t_2 [mm]	8-8	10-10	12-12	8-10	8-12	10-8	10-12	12-8	12-10	Average
$p_{2;LS}$	0.94%	0.28%	1.45%	3.78%	5.51%	2.97%	1.99%	5.33%	3.27%	**2.84%**
$p_{2;CB}$	-	-	-	3.13%	8.47%	2.53%	6.93%	6.87%	6.23%	**5.69%**
$p_{2;F}$	-	-	-	0.65%	2.95%	0.44%	4.94%	1.53%	2.96%	**2.24%**
Average	**0.94%**	**0.28%**	**1.45%**	**2.52%**	**5.64%**	**1.98%**	**4.62%**	**4.58%**	**4.15%**	**3.59%**

Table 28: Deviation in effective pressures, case study Spartherm Melle

Deviation in effective pressures, case study Spartherm Melle										
t_1-t_2 [mm]	14-14	16-16	18-18	14-16	14-18	16-14	16-18	18-14	18-16	Average
$p_{2;LS}$	0.84%	1.43%	1.92%	0.23%	0.20%	2.53%	1.30%	2.87%	2.28%	**1.51%**
$p_{2;CB}$	-	-	-	4.52%	10.08%	4.52%	5.85%	9.78%	5.85%	**6.77%**
$p_{2;F}$	-	-	-	4.75%	9.88%	2.00%	7.16%	6.91%	3.57%	**5.71%**
Average	**0.84%**	**1.43%**	**1.92%**	**3.17%**	**6.72%**	**3.02%**	**4.77%**	**6.52%**	**3.90%**	**4.67%**

7. Discussion

In this chapter the validity, interpretation and limitations of numerical and analytical results are discussed. In line with the report structure discussed in Chapter 1.3 and shown in Figure 122, the discussion is addressed per cold-bending stage.

Chapter	RQ 1	RQ 2	RQ 3	RQ 4
2. Literature study	Chapter 2.1. - 2.5.			
3. Bending phase		3.1. Goal 3.2. Boundary conditions 3.3. Numerical modelling	3.1. Goal 3.2. Boundary conditions 3.4. Analytical modelling	
4. Fixation moment		4.1. Goal 4.2. Boundary conditions 4.3. Numerical modelling 4.5. Cavity pressure	4.1. Goal 4.2. Boundary conditions 4.4. Analytical modelling 4.5. Cavity pressure	
5. Use phase		5.1. Goal 5.2. Boundary conditions 5.3. Numerical modelling 5.5. Cavity pressure	5.1. Goal 5.2. Boundary conditions 5.4. Analytical modelling 5.5. Cavity pressure	
6. Analytical method				Chapter 6.1. - 6.5.

Figure 122: Report structure

7.1. Bending phase

Goal of modelling the ‘Bending phase’ is to gain insights into the maximum design curvature of a cold-bent IGU. Numerical and analytical models are discussed in Chapter 3 and results are presented in Appendix A.

7.1.1. Validity of results

There are number of different bending techniques, all resulting in different boundary conditions for modelling. Furthermore, due to a change in boundary conditions between stages, cold-bending stresses during the ‘Bending phase’ are different compared to those after ‘Fixation moment’. The stresses after ‘Fixation moment’ are considered as the permanent bending stresses. Therefore, the resulting principal stresses from numerical modelling are simplified to those from after ‘Fixation moment’. These numerical results are then used for comparison with analytical modelling. Therefore, validity of the analytical results is restricted to a cold-bent IGU which is fixed linearly along all edges as discussed in Chapter 4.2.

Due to large deformations of the modelled plates, some numerical models diverge. By adjusting the geometrically nonlinear analysis settings, most of the diverging models are solved. However, a number of models still diverges after considering the smallest workable load step. In order to exclude principal stresses from diverging models during the evaluation of numerical outcomes, outliers are excluded using a 95% confidence interval.

Validation of the analytical results is based on the average deviations in comparison to numerical results. Due to simplification of boundary conditions to linear fixation supports only, generalizability of the permanent cold-bending stresses should be evaluated. Recommendations on how to validate the generalizability of the analytical results are discussed in Chapter 9.

Since only closed form analytical expressions are used, calculation of the equations is done using Python coding. To minimize the risk of execution mistakes, results are randomly sample checked using Maplesoft. Cross validation checks between the calculation programmes are also done for analytical results from the ‘Fixation moment’ and the ‘Bending phase’.

The resulting principal stresses of the three developed analytical methods are shown in Appendix A. An overview of deviations of the results compared to numerical modelling is shown in Table 29. From the deviations it can be concluded that the engineering approach is most accurate in determining cold-bending stresses for the considered boundary conditions. Therefore, equation (105), as derived in Chapter 3.4.3, is used in the developed analytical method (Chapter 6.1).

Table 29: Average deviations between numerical outcomes and analytical methods 'Bending phase'

	Relative deviation	Absolute deviation	Minimum deviation	Maximum deviation	Standard deviation
Arch theory	-11.78%	11.78%	-13.20%	-9.40%	0.81%
Cold-Bent Theory	-25.92%	25.92%	-26.54%	-24.09%	0.57%
Engineering approach	0.28%	0.93%	-2.98%	3.23%	1.22%

7.1.2. Interpretation of results

From results of numerical modelling is shown that, within the considered boundary conditions, differences in permanent cold-bending stresses between different plate sizes are small. This finding is in line with the analytical derivation of the equation for cold-bending theory. The equation is based on Euler-Bernoulli beam theory, in which plate size parameters are not considered. The small differences in principal stresses between the plate sizes from numerical modelling can be explained by the influence of anticlastic bending.

Table 29 shows that the standard deviation of all three analytical approaches is low. From this can be interpreted that the theory behind the different approaches is valid. However, due to simplifications, the results are off by a certain constant. Accuracy of the cold-bent theory can for example be improved by multiplying the results with a constant. Within the boundary conditions of the 'Fixation moment' the constant is $1/(1-0.2592) = 1.35$, resulting in an absolute deviation of 0.63% and a standard deviation of 0.77%, which is slightly more accurate than the engineering approach. The lower average outcomes from the 'Cold-Bent Theory', can be explained by the simplification to a beam, for which the bending moments are considered in only one direction. A benefit of the cold-bent theory is that the Youngs' Modulus is an input parameter, meaning the theory could also be used for other materials such as steel. Further research has to point out the applicability of the methods under different boundary conditions. It is recommended to evaluate whether the aforementioned constant is boundary condition specific. In that case, tabulated values can be developed for different boundary conditions.

Due to differences in boundary conditions of the 'Bending phase' itself, it is possible that actual peak stresses during bending are higher. Also, lamination of the glass plate can affect peak stresses during bending. The method can however be used to gain insights into the long term cold-bending stress of laminated panes by using the equivalent thickness as input parameter. It should be noted that a difference in thickness will affect the stiffness of the IGU, and thereby impacting cavity pressure calculations. Therefore, equivalent thickness should only be considered to gain insights into permanent cold-bending stresses. The total laminated thickness must be considered for the cavity pressure calculations. In case no lamination shear interaction is considered, the single pane thicknesses can be used as input parameter. In case of full shear interaction, the total thickness of the laminated pane can be considered. On account of the wide range of plate thicknesses analysed for numerical modelling, also full laminated thicknesses are likely to be within the evaluated data set.

7.1.3. Limitations

Since boundary conditions of the 'Fixation moment' are simplified to linear supports on all edges, validity of the resulting principal stresses is limited to this type of fixing. Other types of fixing can result in higher permanent bending stresses. In order to ensure peak stresses do not exceed bending strength limits, the final design and bending method of the cold-bent IGU should be double checked with finite element analysis. Application of the analytical method is therefore limited to the early design phase, in which it can be used to explore curvature limits of the cold-bent glass.

7.2. Fixation moment

The goal of modelling of the ‘Fixation moment’ is to gain insight into the anticlastic bending behaviour of single curved glass plates. Numerical and analytical models are discussed in Chapter 4 and results are presented in Appendix B.

7.2.1. Validity of results

In Chapter 4.3, validity of the numerical model setup is discussed. The outcomes from numerical modelling are considered reliable, if results are in line with expectations. Per plate model it is for example checked whether the deformation height at midspan is in line with the design radius used as input parameter. Furthermore, is checked whether there are no peak stresses along the displaced edges of the curved plate. In case the resulting deformation height is not in line with the design radius, it can be seen that within DIANA the analysis has been terminated due to equilibrium tolerances not being met. In such cases the load step is decreased and the plate model is analysed again. As discussed before, the outcomes of some numerical models still diverge after consideration of the smallest workable load step. Based on computational running time, the minimum load step is considered as 0.001 (1000 steps). An example of a diverging model is shown in Figure 123. In case of a diverging model, the radius at midspan and volume of deformation are linearly interpolated with results from adjacent plate sizes, plate thicknesses and curvature radii.

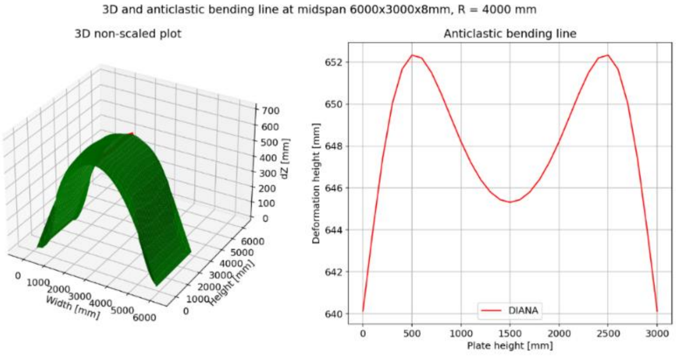

Figure 123: Diverging numerical model

After analysis of anticlastic bending behaviour, it is decided to simplify the result-based approach to a sinusoidal anticlastic bending line. Key parameter of the result-based approach is the height at midspan of the sinusoidal shape, also referred to as radius at midspan. Therefore, validity of the simplified anticlastic bending behaviour is restricted to the deformation height at the centre of the plate. In Figure 124, examples of the resulting simplified anticlastic bending lines are shown.

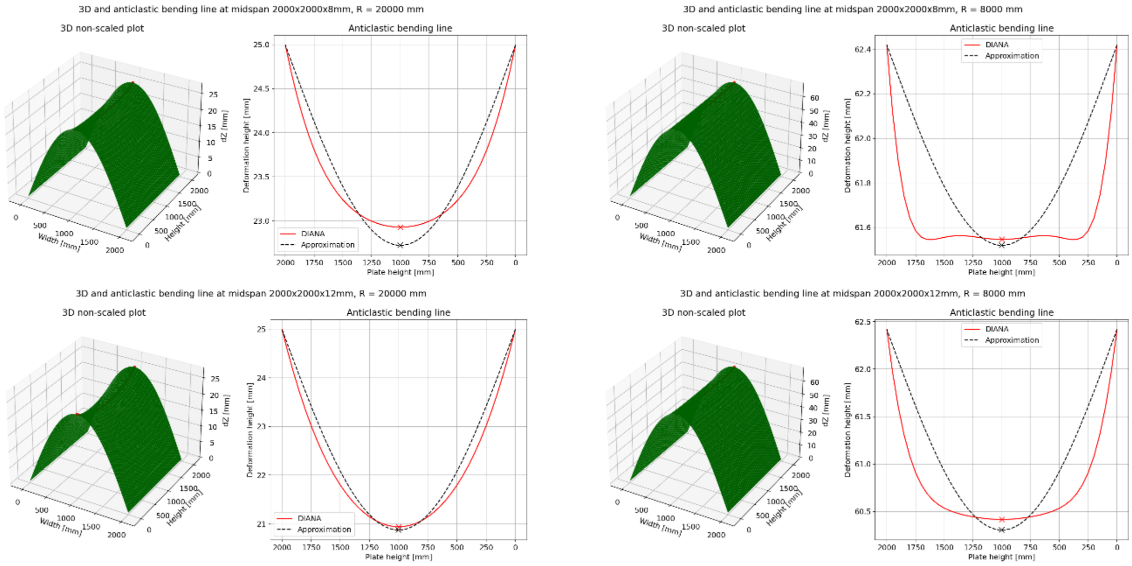

Figure 124: Comparison between numerical and analytical anticlastic bending lines

In Appendix B.1, numerical and analytical results of the radius at midspan of all considered cases are presented. Table 30 shows the validity of the results. Within the specified boundary conditions and simplifications, the absolute and standard deviations are low. However, due to the simplifications and specifications, generalizability of the result-based approach for other boundary conditions should be evaluated. Recommendations on how to validate the applicability of the analytical method for other boundary conditions, are discussed in Chapter 9.

Table 30: Validation of analytical radius at midspan compared to numerical outcomes

	Absolute deviation	Minimum deviation	Maximum deviation	Standard deviation
1000x1000mm	2.46%	0.03%	10.51%	1.98%
2000x1000mm	0.31%	0.00%	1.37%	0.25%
2000x2000mm	0.67%	0.00%	2.34%	0.48%
3000x1000mm	0.10%	0.00%	0.44%	0.08%
3000x2000mm	0.15%	0.00%	0.53%	0.10%
3000x3000mm	0.33%	0.00%	1.56%	0.29%
4000x1000mm	0.05%	0.00%	0.20%	0.04%
4000x2000mm	0.08%	0.00%	0.30%	0.06%
4000x3000mm	0.10%	0.00%	0.41%	0.08%
5000x1000mm	0.03%	0.00%	0.12%	0.03%
5000x2000mm	0.04%	0.00%	0.19%	0.03%
5000x3000mm	0.06%	0.00%	0.28%	0.05%
6000x1000mm	0.02%	0.00%	0.09%	0.02%
6000x2000mm	0.02%	0.00%	0.11%	0.02%
6000x3000mm	0.03%	0.00%	0.20%	0.03%
Average	**0.30%**	**0.00%**	**1.24%**	**0.24%**

Besides defining the double curvature, anticlastic bending also influences the volume below the curved plate. In case of an asymmetric IGU, anticlastic bending behaviour is different for both plates and an isochoric under- or overpressure will occur. Therefore, the volume below the curved plates is validated as well. Derivation of the simplified equation to calculate the volume is discussed in Chapter 4.5.2. The simplification is based on the average height of the sinusoidal anticlastic bending line. In Table 31, the average absolute and standard deviations are shown. All results can be found in Appendix B.2. Similar to the results for the radius at midspan, deviations are low. Again, applicability of the analytical method for other boundary conditions should be further investigated.

Table 31: Validation of simplified volume of deformation calculation compared to numerical outcomes

	Absolute deviation	Minimum deviation	Maximum deviation	Standard deviation
1000x1000mm	1.76%	0.00%	4.68%	1.09%
2000x1000mm	0.20%	0.00%	1.13%	0.16%
2000x2000mm	0.69%	0.02%	1.95%	0.47%
3000x1000mm	0.41%	0.17%	1.94%	0.18%
3000x2000mm	0.22%	0.00%	1.80%	0.19%
3000x3000mm	0.47%	0.00%	4.68%	1.09%
4000x1000mm	0.62%	0.41%	3.06%	0.24%
4000x2000mm	0.31%	0.00%	4.68%	1.09%
4000x3000mm	0.27%	0.00%	3.03%	0.31%
5000x1000mm	0.75%	0.52%	4.61%	0.36%
5000x2000mm	0.58%	0.14%	4.42%	0.41%
5000x3000mm	0.42%	0.00%	4.51%	0.47%
6000x1000mm	0.91%	0.59%	6.09%	0.51%
6000x2000mm	0.83%	0.36%	6.55%	0.55%
6000x3000mm	0.72%	0.00%	6.51%	0.59%
Average	**0.61%**	**0.15%**	**3.98%**	**0.51%**

7.2.2. Interpretation of results

In Chapter 4.4.3, derivation of the simplified analytical method to determine anticlastic bending of cold-bent glass plate is discussed. The approach is based on linear regression between the radius at midspan and plate thickness, of which an example is shown in Figure 78, page 57. An example of the validation of the radii at midspan for a 2x2m plate is shown in Figure 125. The permanent maximum tensile bending strength of fully tempered cold-bent glass is 63.50 N/mm^2, as discussed in Chapter 2.1.4. Plate configurations with a higher bending stress are left out of consideration. In the resulting deviations, linear approximation patterns are clearly visible. When for example looking at a radius of 12m, highlighted with the red box, deviations have a sort of wave pattern. This pattern can be explained by looking at the corresponding linear interpolation, shown in Figure 126. At a thickness of 4mm, deviation between the linear approximation and numerical results is largest. Then, at 7mm, both lines intersect each other, resulting in an exact approximation. Between 16 and 17mm both lines intersect again. Between the intersections, deviations increase. Similar patterns can be found for the other analysed design radii. The resulting volumes of deformation can be interpreted in the same way since they are calculated using the radius at midspan.

	Absolute deviation	Minimum deviation	Maximum deviation	Standard deviation
2000x2000mm	0.67%	0.00%	2.34%	0.48%

Radius at midspan - validation analytical results - 2000x2000mm plate

Thickness [mm] \ Radius [mm]	25000	24000	23000	22000	21000	20000	19000	18000	17000	16000	15000	14000	13000	12000	11000	10000	9000	8000	7000	6000	5000	4000	3000
4	0.12%	0.67%	1.00%	1.38%	1.69%	1.92%	2.12%	2.24%	2.30%	2.34%	2.31%	2.21%	2.07%	1.86%	1.63%	1.35%	1.06%	0.74%	0.45%	0.21%	0.09%	0.24%	0.97%
5	0.71%	0.27%	0.00%	0.33%	0.59%	0.80%	0.99%	1.14%	1.22%	1.30%	1.34%	1.32%	1.25%	1.14%	1.03%	0.86%	0.69%	0.49%	0.29%	0.12%	0.03%	0.10%	
6	1.14%	0.77%	0.63%	0.40%	0.19%	0.04%	0.13%	0.25%	0.34%	0.45%	0.52%	0.54%	0.56%	0.52%	0.49%	0.43%	0.36%	0.27%	0.17%	0.07%	0.00%	0.01%	
7	1.19%	0.97%	0.92%	0.80%	0.66%	0.60%	0.47%	0.41%	0.33%	0.22%	0.16%	0.10%	0.03%	0.00%	0.04%	0.07%	0.09%	0.09%	0.08%	0.05%	0.00%		
8	0.94%	0.86%	0.91%	0.92%	0.86%	0.91%	0.83%	0.85%	0.80%	0.71%	0.67%	0.60%	0.51%	0.42%	0.33%	0.23%	0.13%	0.04%	0.03%	0.06%			
9	0.49%	0.53%	0.67%	0.80%	0.83%	0.98%	0.98%	1.08%	1.08%	1.04%	1.03%	0.97%	0.87%	0.75%	0.62%	0.47%	0.30%	0.14%	0.00%	0.09%			
10	0.05%	0.08%	0.29%	0.52%	0.62%	0.87%	0.94%	1.12%	1.19%	1.21%	1.24%	1.20%	1.11%	0.98%	0.83%	0.63%	0.42%	0.20%	0.01%				
11	0.56%	0.38%	0.14%	0.15%	0.31%	0.63%	0.77%	1.02%	1.15%	1.23%	1.31%	1.31%	1.24%	1.11%	0.96%	0.73%	0.48%	0.21%	0.04%				
12	0.97%	0.78%	0.55%	0.23%	0.03%	0.31%	0.52%	0.81%	0.98%	1.14%	1.26%	1.30%	1.27%	1.15%	1.00%	0.77%	0.49%	0.18%					
13	1.20%	1.05%	0.86%	0.56%	0.36%	0.02%	0.21%	0.53%	0.73%	0.94%	1.11%	1.19%	1.20%	1.10%	0.97%	0.74%	0.45%						
14	1.24%	1.15%	1.04%	0.79%	0.62%	0.32%	0.09%	0.22%	0.43%	0.68%	0.88%	1.00%	1.04%	0.98%	0.87%	0.64%	0.35%						
15	1.07%	1.06%	1.04%	0.87%	0.77%	0.55%	0.35%	0.08%	0.12%	0.38%	0.59%	0.74%	0.82%	0.79%	0.70%	0.49%							
16	0.71%	0.79%	0.88%	0.81%	0.79%	0.66%	0.54%	0.33%	0.18%	0.07%	0.27%	0.43%	0.53%	0.53%	0.47%	0.28%							
17	0.17%	0.35%	0.55%	0.59%	0.67%	0.66%	0.62%	0.51%	0.43%	0.23%	0.05%	0.10%	0.20%	0.23%	0.18%								
18	0.52%	0.24%	0.07%	0.22%	0.41%	0.53%	0.60%	0.60%	0.60%	0.48%	0.36%	0.25%	0.15%	0.12%									
19	1.34%	0.97%	0.56%	0.29%	0.02%	0.27%	0.46%	0.59%	0.70%	0.68%	0.64%	0.58%	0.51%	0.49%									
20	2.28%	1.82%	1.31%	0.92%	0.49%	0.11%	0.21%	0.47%	0.70%	0.80%	0.87%	0.89%	0.87%										

Figure 125: Deviations between results from numerical modelling and result based approach

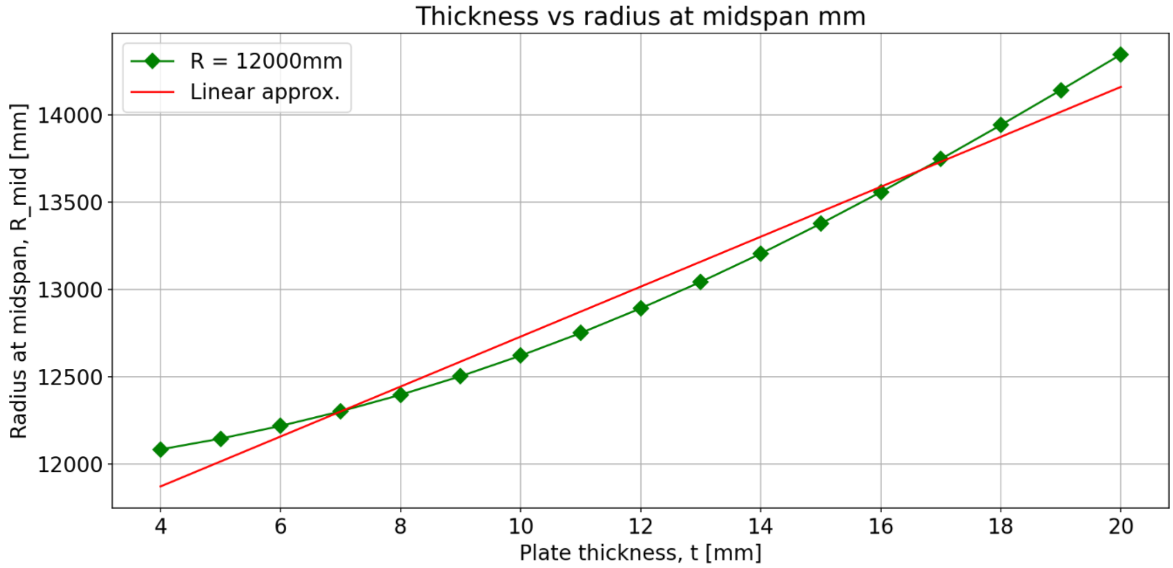

Figure 126: Regression between radius at midspan and plate thickness for a 2x2m plate, R=12m

The radius at midspan has been the key parameter in determining regression for anticlastic bending. Therefore, validation of the analytical approach is based on this parameter. It should however be noted that the radius at midspan, highlighted with the green arrow in Figure 127, is different from the relative anticlastic bending distance in the centre of the plate, shown in red. For example, the resulting deviation of the anticlastic bending line shown in Figure 128 is $\epsilon = |R_{approx.} - R_{numerical}| \,/\, R_{numerical} * 100\% = |22002 - 21805|/21805 \; * 100\% = \; 0.91\%$. However, when looking at the relative anticlastic bending distance, the resulting deviation is $\epsilon = \; |2.27 - 2.07|/2.07 \; * 100\% = \; 9.66\%$. From this finding it can be concluded that the anticlastic bending approximation could be improved by defining the relative anticlastic bending distance as key parameter for regression. By doing so, also the accuracy volume of deformation below the curved plate can be improved. Further research has to point out if regression for this parameter can be found and thereby a more accurate approach can be developed.

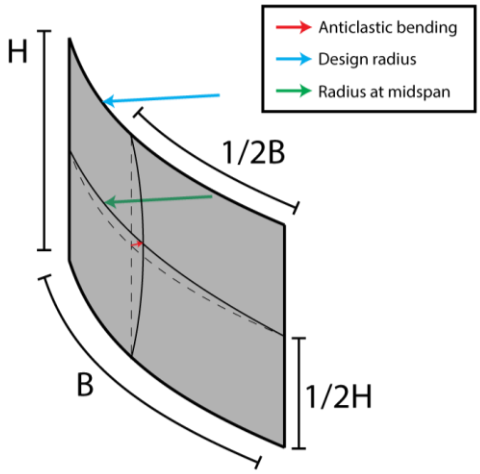

Figure 127: Decreased radius at midspan due to anticlastic bending

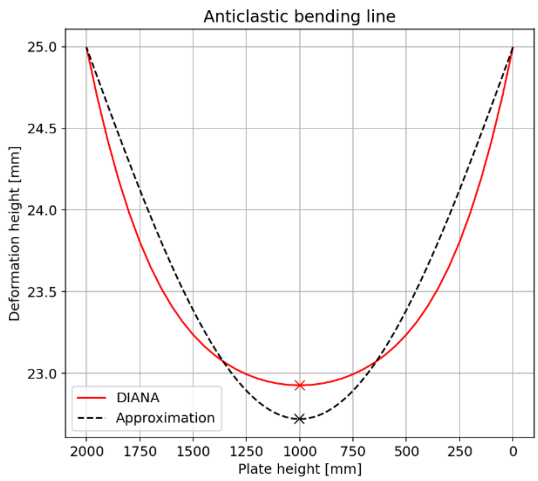

Figure 128: Anticlastic bending line 2000x20000x8mm, R = 8m

7.2.3. Limitations

Validity of the anticlastic bending behaviour is limited to the boundary conditions of a cold-bent single curved plate, fixed with linear supports. In case of other types of fixing, the generalizability of the results must be checked with for example a numerical model. Furthermore, due to simplifications of the anticlastic bending behaviour, calculation of double curvatures from analytical results are limited to sinusoidal shapes. When for example the anticlastic bending behaviour must be analysed for optical distortions in the final design, it is recommended to create a finite element model. Application of the analytical steps from the ‘Fixation moment’ should therefore be limited to the early design phase, in which it can be used to explore isochoric pressures in asymmetric IGU’s. Validation of the isochoric pressures is discussed in Chapter 7.3. The analytical steps can furthermore be used to gain insights in the relative anticlastic bending distance at centre of the plate and thereby give a rough estimation of the expected visual distortions. In case of asymmetric IGU’s the results can be used to estimate the increase or decrease of cavity distance at the centre of the panes.

7.3. Use phase

From analytical and numerical models of the 'Use phase', insights are gained into the structural behaviour of cold-bent single curved glass plates. The results are used to determine effective isochoric pressures and load sharing pressures inside cold-bent IGU's. Methodology of the 'Use phase' is discussed in Chapter 5, overviews of results are shown in Appendix C.

7.3.1. Validity of results

The load sharing pressures for a range of IGU configurations are calculated using linear interpolation of P-V diagrams from numerical modelling. Since the P-V diagrams from numerical modelling are nonlinear, validity of the interpolation of load sharing pressures is compared to step-by-step FEA calculation with DIANA. Based on the comparison, shown in Figure 93 (page 72), it is concluded that the P-V diagrams are reliable in determining load sharing percentages.

The analytical approach of the 'Bending phase' is simplified to the linear deformation of a portion of a cylindrical shell, which is supported on all sides. In Chapter 5.4.2, P-V diagrams from numerical and analytical modelling are compared. From a qualitative comparison it is concluded that there are large deviations in deformations between both modelling approaches, which can be explained by the differences between linear analytical modelling and nonlinear numerical modelling. In Appendix C.1, the results are presented for a 1x1m, 2x2m, 3x3m, 4x3m, 5x3m and 6x3m plate, which covers the range of plates up to the size of jumbo glass plates, bent along their longest edge. The thicknesses considered for each plate size are 8mm, 10mm and 12mm. The radius of curvature ranges from flat to 8m, which is within realistic curvatures based on a maximum cold-bending stress along the edge of the plate of $\sigma'_{max} < 63.5$ N/mm^2. Furthermore, results of two case studies, as discussed in Chapter 6.5, are presented. An overview of the deviations per plate and design radius is shown in Table 32. A more detailed overview is shown in Appendix C.1. From the quantitative comparison of the P-V diagrams the relative average deviation is -41%, which means analytical results are significantly lower. Furthermore, it can be concluded that deviations increase as curvatures and plate sizes increase. Based on the large deviations, reliability of the analytical method should be questioned. In the next paragraph it is interpreted how the deviations impact the calculation of isochoric and load sharing pressures. From these findings conclusions are drawn on reliability and applicability of the analytical method.

Table 32: Overview deviations of analytical P-V diagrams with numerical outcomes, per design radius

Radius [mm]	1000x1000	2000x2000	3000x3000	4000x3000	5000x3000	6000x3000	Average
20000	11.56%	22.58%	14.08%	36.41%	27.57%	55.24%	**27.91%**
16000	16.55%	14.23%	28.17%	29.97%	37.98%	43.38%	**28.38%**
12000	24.04%	18.81%	49.72%	38.95%	59.44%	69.33%	**43.38%**
8000	31.92%	41.27%	76.26%	80.42%	79.60%	84.73%	**65.70%**
Average	**21.02%**	**24.22%**	**42.05%**	**46.44%**	**51.15%**	**63.17%**	**41.34%**

Since the numerical outcomes of P-V diagrams are modelled with one specific set of boundary load conditions, validity of the discussed deviations is restricted to the boundary and load conditions considered for the 'Use phase'. Further research has to point out whether P-V diagrams, retrieved from numerical modelling with other types of boundary support conditions, show similar results. Both numerical and analytical results are not generalizable for other types of loading. Other types of load conditions such as line and point loads, will result in principally different deformation behaviour, as they are dependent on the positioning on the plate. Also, for calculation of flat IGU's in current standards different calculation methods are used for line and point loads.

Due to nonlinearity of the numerical P-V diagrams, load sharing pressures are calculated using the iterative scheme discussed in Chapter 5.3.1. Calculation of analytical load sharing pressures is done linearly, using equations derived from literature, as discussed in Chapter 5.5.1. Results from symmetric IGU's are shown in Appendix C.2. The range of configuration is in line with the plate sizes, thicknesses and radii of curvature, considered for the P-V diagrams. All configurations are subjected to an external pressure load of 1kN/m^2. Both the iterative scheme and linear load sharing equation are based on Boyle's law and therefore only dependent on volumes of deformation due to pressure loads. This means the equations derived from Boyle's law are applicable for any type of support boundary condition as long as it is subjected to a pressure load.

An overview of the deviations per IGU size and design radii is shown in Table 33. In line with findings from validity of the P-V diagrams, deviations in load sharing pressures increase as design radii of the IGU's decrease. It can also be seen that deviations increase, as plate sizes increase. From these findings it can be concluded that the reliability of the analytical approach decreases, as curvatures and plate sizes increase.

Table 33: Overview deviations load sharing pressure symmetric IGU's, per design radius

Radius [mm]	1000x1000	2000x2000	3000x3000	4000x3000	5000x3000	6000x3000	Average
20000	1.20%	1.25%	0.80%	1.18%	0.82%	1.07%	**1.05%**
16000	1.78%	1.08%	1.45%	1.60%	2.15%	2.40%	**1.74%**
12000	2.82%	1.42%	3.95%	5.78%	4.85%	6.57%	**4.23%**
8000	4.53%	5.21%	13.56%	14.39%	14.19%	17.38%	**11.55%**
Average	**2.58%**	**2.24%**	**4.94%**	**5.74%**	**5.50%**	**6.86%**	**4.64%**

Calculation of the load sharing pressures for asymmetric IGU's is done similarly as for the symmetric cases. An overview of the results and deviations of the external load sharing pressures for asymmetric IGU configurations is given in Appendix C.3. The effective isochoric pressure, due to differences in anticlastic bending behaviour of both plates, is calculated numerically using the iterative scheme from Chapter 4.5.3. For the analytical approach, a linear equation is considered, which is derived in Chapter 5.5.2. The resulting pressures of both modelling approaches are found in Appendix C.3. Again, the equations derived from Boyle's law are applicable for all support boundary conditions subjected to pressured loads.

By summing the effective load sharing pressure and isochoric pressure, the cavity pressure of an asymmetric cold-bent IGU subjected to an external load is calculated. The overview of deviations in combined pressures, is shown in Table 34. From the results per effective pressure, shown in Appendix C.3, it can be concluded that the average deviation in load sharing is higher for asymmetric configurations (8.6% compared to 4.6%). The average deviation in isochoric pressures due to cold-bending is 8.0%, which is almost the same as for the asymmetric load sharing pressures. From the increase in average deviation for combined pressures (13.2%), it can be concluded that the external load sharing pressure and isochoric pressure are either both higher or lower than numerical outcomes, and thereby amplify each other.

Table 34: Overview deviations combined pressure asymmetric IGU's, per design radius

Radius [mm]	1000x1000	2000x2000	3000x3000	4000x3000	5000x3000	6000x3000	Average
20000	3.27%	1.66%	2.83%	20.64%	3.77%	16.60%	**8.13%**
16000	5.49%	2.05%	6.88%	5.76%	2.79%	16.05%	**6.50%**
12000	8.87%	11.91%	17.59%	22.42%	4.91%	16.19%	**13.65%**
8000	14.57%	35.46%	50.71%	14.40%	13.98%	17.87%	**24.50%**
Average	**8.05%**	**12.77%**	**19.50%**	**15.81%**	**6.36%**	**16.68%**	**13.20%**

In line with earlier findings for symmetric IGU's, the deviations increase as the stiffness of the IGU increases. The deviations are however independent on plate size, which is in contrast to earlier findings. Noticeable are the low deviations for a plate size of 5x3m. From the effective pressure diagrams presented in Appendix C.3, it can be seen that there are outliers in the numerical outcomes of 4x3m and 6x3 IGU sizes. Due to these outliers, deviations from analytical modelling are high. From this observation it can be concluded that a number of numerical outcomes is not reliable. The relative high deviations for a 1x1m, 2x2m, and 3x3m plate can be explained by looking at the isochoric pressures for this configuration, it can be seen that some numerical results are higher than 1 kN/m^2. This means that instead of linear interpolation, the P-V diagrams are linearly extrapolated up to isochoric pressures of 1.5 kN/m^2, which decreases reliability of the numerical outcomes. In the next paragraph the applicability of the analytical method, under consideration of the reliability, is discussed.

7.3.2. Interpretation of results

From the validation of results, it is concluded that results from analytical P-V diagrams are significantly smaller, with an average relative deviation of -41%. This finding is however in line with expectations of the differences between geometrically nonlinear numerical modelling and linear analytical results, as discussed in Chapter 5.4. Noticeable is the increase of deviations for plates with a larger curvature. As volumes of deformation become smaller for stiffer curvatures, a smaller difference between both methods is expected. The difference can however be explained by the tolerances in x- and y-direction of numerical models. As curvatures increase, a curved plate will transfer a larger amount of load via axial forces. Due to the degrees of freedom, the edges can move outwards. Furthermore, axial deformations are considered for numerical modelling, resulting in an extra degree of deformation.

Boundary conditions of numerical modelling in finite element analysis are setup to represent the structural behaviour of cold-bent glass plates in practice. Considering the large deviations, reliability of the analytical method for application in cavity pressure calculations should be questioned. Based on findings from literature, application of the simplified analytical method can be justified. According to (Timoshenko & Woinowsky-Krieger, 1989), geometrically nonlinear analysis is only necessary when large deformations are considered. Furthermore, according to (Young & Budynas, 2002), deflections can be considered small if they are less than ½ thickness of a plate. From numerical outcomes it is concluded that in almost all cases, deformation at the centre of the plate is smaller than ½ times the thickness of the plate. This also holds for large plate sizes. The P-V diagrams in Appendix C.1 show that already for small curvatures, stiffness properties of large plates increase significantly. Also, similar simplifications have been made in the development of current standardized methods. As discussed in Chapter 2.3.2, nonlinear P-V diagrams are used in the first mentions of calculating cavity pressure in IGU's (Vallabhan & Chou, 1986). Deformations calculated using linear plate theory, are sufficient in determining load sharing pressures of flat IGU's (Wörner, Shen, & Sagmeister, 1993). From these findings it is concluded that linear calculations suffice in calculating the structural behaviour of curved plates.

Anticlastic double curvatures are not considered in the analytical method. Furthermore, the shape is simplified to a cylindrical shell. To check validity of these simplifications, comparisons with linear deformations in finite element analysis should be made.

The justification of simplifications for the analytical method is also validated by the lower deviations in effective pressures, as shown in Table 33 and Table 34. Especially for the smaller considered curvatures up to a radius 12m, analytical effective pressures are in good comparison with numerical outcomes as average accuracy are higher than 90%. Reliability of the method for large curvatures is lower. In practice however, feasibility of cold-bent IGU's with curvature radii up to 8m is limited due to cold-bending stresses. In Chapter 6.5.7, results of IGU configurations based on two case studies from practice with design radii of 11.5m and 28m, are considered. The deviations in external load sharing pressures of the applied symmetric configuration is 0.28% for the case study of the Van Gogh Museum, and 1.43% for Spartherm Melle. For illustration purposes, symmetric and asymmetric configurations with different plate thicknesses are considered, resulting in an average deviation in combined pressures of 3.6% and 4.7%, respectively.

The effective pressure diagrams presented in Appendix C.2, clearly show the relation between increasing curvatures of cold-bent IGU's and load sharing pressures. For all considered symmetric configurations holds that the load shared by the exterior pane increases, as the IGU gets stiffer. Furthermore, as plate thicknesses increase, a higher percentage of the load is shared by the exterior pane. This is due to the fact that as the exterior plate is subjected to an external pressure load, it will deflect less compared to a flat plate. Consequently, differences in cavity volume are less, which results in a lower effective cavity pressure on the inside of the interior pane.

For asymmetric cold-bent IGU's, the resulting effective cavity pressures are less straightforward. The load sharing diagrams in Appendix C.3 show large differences in isochoric and load sharing pressures between different configurations. An example which is contradictory to the evaluation of a flat IGU is shown in Figure 129, for a 2000x2000x10-16-8mm configuration subjected to a pressure load of 1 kN/m². In case of an asymmetric flat IGU, more load is shared by the thicker pane. In this case the exterior pane is thicker (10mm), resulting in load sharing pressure of $p_{1;LS} = 0.66$ kN/m² and $p_{2;LS} = 0.34$ kN/m². In curved asymmetric IGU's however, an isochoric pressure is present as a result of anticlastic bending. Since the anticlastic bending effect of the thicker exterior plate is higher, an overpressure occurs in the cavity as the cavity volume decreases. This overpressure is subtracted from the load sharing of the exterior pane and added to the interior pane. As the curvature increases, the overpressure increases as well. For the example configuration, this results in combined effective pressure of $p_{1;F} = 0.48$ kN/m² on the exterior pane, for a radius of 20m. This means more load is shared by the thinner plate. As the design radii gets smaller, more load is shared by the interior pane. In the graph is shown that for a radius of 8m, the effective load on the exterior pane from external load sharing is $p_{1;LS} = 0.69$ kN/m². However, after combination with an effective isochoric pressure of $p_{CB} = 0.64$ kN/m², the effective load on the exterior pane is $p_{1;F} = 0.05$ kN/m².

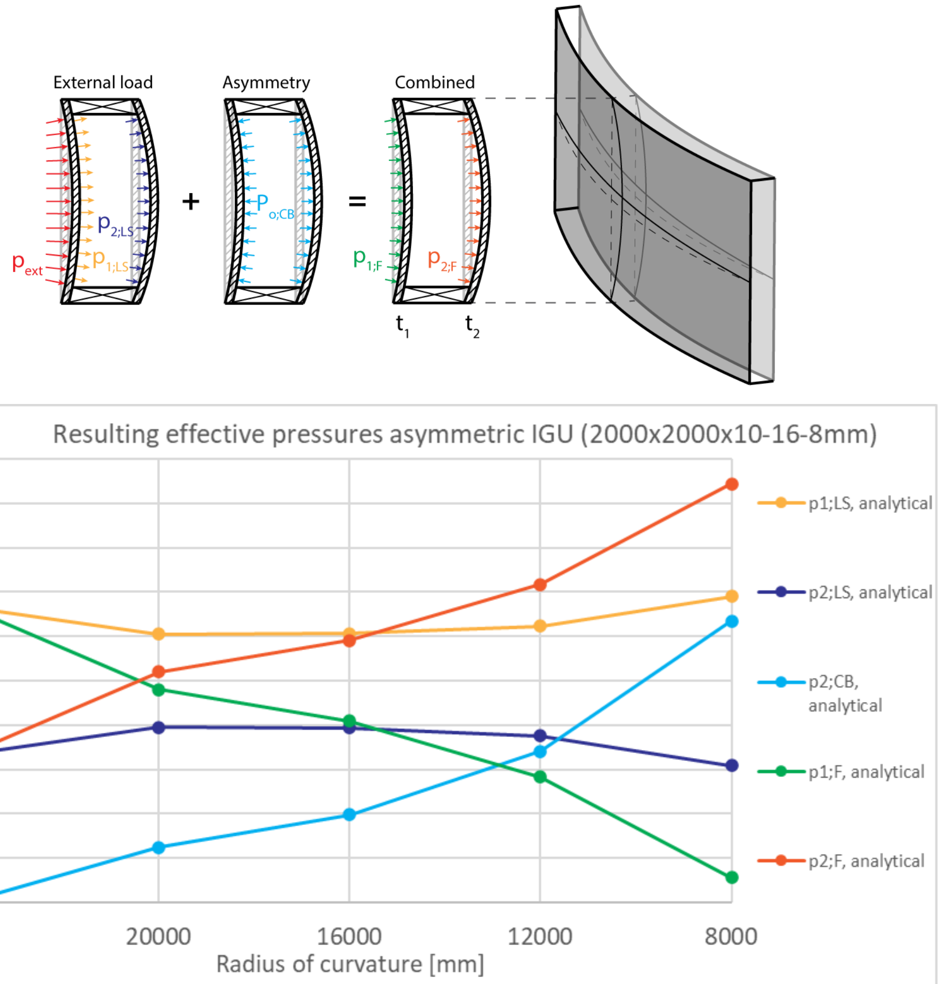

Figure 129: Resulting effective pressures asymmetric IGU (2000x2000x10-16-8mm)

From the load sharing diagrams it can be concluded that the effective isochoric over- or underpressure increases, as curvatures increase. In earlier findings on anticlastic bending behaviour is however shown that effects decrease as curvatures increase. From these two findings it can be concluded that the increasing stiffness of the cold-bent IGU's has a more significant role than the decreasing anticlastic bending effects. The finding implies that isochoric pressures due to for example climatic loads or height differences, also increase as stiffness of the IGU increases. Calculation of these isochoric pressures is done using the equation presented in Chapter 5.5.2. Since validation of numerical outcomes of climatic and height isochoric pressures has been outside the scope of this thesis, a recommendation is given be in Chapter 9 on how this increase of isochoric pressure can be calculated numerically.

Using the developed analytical method, design decisions can be made based on desired isochoric pressures or load sharing percentages. When there is for example a recurring problem of cavity leakages due to high isochoric pressure, the analytical can be used to explore input parameters, favourable for a low effective cavity pressure. By increasing the curvature, more external load is shared by the exterior pane, resulting in lower cavity pressures. However, it should be considered that isochoric pressures increase as curvature increases. Using the Excel tool, these isochoric pressures can be calculated directly, by which an optimum can be found in the design of the cold-bent IGU configuration. Also, an optimum between serviceability and ultimate limit state of the cold-bent IGU can be found. Visual distortions due to anticlastic bending and under-, or overpressures can be decreased by increasing the stiffness of the cold-bent IGU's. However, by doing so, a higher percentage of the strength capacity of the IGU is taken by permanent cold-bending stresses. The analytical method and Excel tool can be used to find an optimum between the two.

7.3.3. Limitations

Similar to the 'Bending phase' and 'Fixation moment', the discussed validity of results is limited to the specified boundary conditions of the 'Use phase'. In case of other types of fixation, the generalizability of results must be checked with for example a linear finite element analysis. Due to the deviations between results from the analytical method and numerical outcomes, application of the analytical method should be limited to explore design options in the early design phase. Furthermore, the method is limited to calculating cavity pressures. Ultimate limit state calculations of for example deformation stresses due to cavity pressures, should be evaluated using finite element software.

The developed analytical method is limited to the calculation of isochoric pressures as a result of differences in pane deformations of asymmetric configurations. Due to simplification of the spacer being rigid, it is assumed that for a symmetric IGU, deformations of both glass panes are exactly the same. This assumption implies that there will be no permanent isochoric pressure in symmetric cold-bent IGU's. In reality however, a spacer will not show a rigid behaviour, as it is subjected to large shear and bending forces. Sequentially, this will result in different deformations per glass pane and therefore resulting in a permanent isochoric pressure in symmetric cold-bent IGU's. In Chapter 9 a suggestion for further research is given on how the isochoric pressure inside a symmetric cold-bent IGU with a non-rigid spacer can be calculated.

8. Conclusion

In this chapter the conclusions which are drawn from the results of this thesis are presented. This is done by first answering the sub-research questions from Chapter 1.2.4 and reflecting on their objectives. The main conclusion is then summarized by answering the main research question: 'How can the effect of cavity pressure on the structural behaviour of cold-bent insulating glass units be analytically determined?'. In Chapter 1.3 the relation between the research questions and methodology is discussed.

RQ 1: Which information about the effect of cavity pressure on the structural behaviour of IGU's can be found in literature?

From findings of the development of current standardized methods, it is concluded that calculation of cavity pressures depends on the volume of deformation per individual pane of an IGU. The interaction between the panes is modelled using Boyle's law. Iterative schemes from literature are used to calculate effective pressures of nonlinear volumes of deformation. Due to simplifications of nonlinear to linear deformations, direct equations are derived to calculate load sharing pressures. Further developments and simplifications of these direct equations have led to the equations in current standards, used to calculate cavity pressures of flat IGU's.

From literature it is concluded that cold-bent IGU's have additional assessment criteria compared to flat IGU's. Since curved structures are stiffer against of out of plane loads, the structural behaviour of a cold-bent IGU is principally different. Furthermore, due to the elastic deformation of a cold-bent IGU into a design radius, permanent cold-bending stresses and anticlastic bending behaviour must be assessed.

Based on the assessment criteria, a theoretical framework of three processes is defined. Distinction between the processes is based on differences in boundary conditions, during and after the installation of cold-bent IGU's. First is the assessment of cold-bending stresses, which is considered as the 'Bending phase' and used to explore curvature limits of cold-bent IGU configurations. Second is the assessment of anticlastic bending, of which the boundary conditions are considered at the 'Fixation moment'. The radius at midspan is used to assess double curvatures as a result of cold-bending, which affect the isochoric pressures in cold-bent IGU's. Third, deformations of curved plates subjected to pressure loads are evaluated for the 'Use phase'. Results are used to calculate load sharing and isochoric cavity pressures. Each stage is modelled numerically, from which results are used to validate simplified analytical methods.

RQ 2: How can the structural behaviour of cold-bent glass panes be modelled numerically and which insights are gained from outcomes?

From literature it is shown that geometrically nonlinear finite analysis is an effective tool to calculate large deformations of glass plate. Therefore, numerical modelling is conducted using DIANA FEA. The glass plates are defined by 2D quadrilateral curved shell elements. Depending on the size of plates, mesh sizes of 50x50mm and 100x100mm are used. With the use of Python command lines, actions within the interactive environment of DIANA are automated. Thereby, a parametric workflow is created in which multiple models can be analysed without user interference. Pre-processing of the command lines is done using Python coding. Within DIANA, the command files are run and results are exported. Post-processing of results is done within the integrated development environment of Spyder. On account of the automated parametric workflow, a large number of numerical models have been analysed.

In line with the definitions of cold-bending stages, numerical modelling is divided into three processes. First, the plates are bent into a single curvature with pressure load steps. Resulting geometries are then converted to prescribed displacements based on a design radius. From results it can be seen that the shape of plates subjected to pressure loads is close to sinusoidal. Furthermore, it is concluded that maximum cold-bending stresses are independent of plate size. By defining a maximum bending strength, insights are gained into the maximum curvatures of cold-bent glass plates with a specified thickness.

Second, the prescribed displacements are modelled. Boundary conditions of the displacements are based on the linear fixation of the cold-bent IGU's. From results it can be seen that the single curved plate has an anticlastic double curvature. It is concluded that the extent and shape of anticlastic bending depend on the Poisson's ratio, plate thickness, radius of curvature and plate size. Double and triple (w-shape) curvatures of the glass plates cause visual distortions. From the insights gained with numerical modelling, design choices can be made to minimize these effects.

Third, the displaced glass plates are subjected to pressure loads. From results it is concluded that due to the increased stiffness of curved IGU's, a higher load is shared by the pane on which an external load is applied. Furthermore, there is a permanent isochoric pressure inside the cavity of asymmetric IGU's due to anticlastic bending. The isochoric pressure depends on the radius of curvature, plate size, cavity width and plate thicknesses. Combinations of effective pressures in cold-bent IGU's result in principally different results compared to the behaviour of flat IGU's.

RQ 3: Which analytical derivations can be used to determine the effect of cavity pressure on the structural behaviour of cold-bent insulating glass units?

Simplified analytical methods have proved to be efficient in determining the complex behaviour of cavity pressure in flat IGU's. Therefore, an analytical method is developed to calculate isochoric and load sharing pressure of curved IGU's. Setup of the method is in line with the three stages of cold-bent IGU's.

First, an analytical method is developed, which calculates the maximum cold-bending principal stresses. The approach is based on results from numerical modelling and considers plate thickness and radius of curvature as input parameters. Resulting principal stresses have an average accuracy of 99.1% compared to numerical outcomes.

Second, a result-based approach is developed to determine anticlastic bending displacements at the centre of curved glass plates. The method is based on regression between different parameters of influence from numerical modelling. Anticlastic effects are expressed in terms of radius at midspan and simplified to a double curvature with sinusoidal shapes. Using the method, the radius at midspan of cold-bent glass plates can be determined using tabulated coefficients (Table 13), with an average accuracy of 99.3%.

Third, an analytical method to calculate volumes of deformation of curved plates subjected to pressure loads is derived. Compared to numerical modelling, the simplified analytical method results in 40% lower outcomes. Based on qualitative observations, quantitative comparisons and findings from literature, it is concluded that application of the analytical method for calculating cavity pressures in cold-bent IGU's is justified.

In case of symmetric IGU's, load sharing pressures are calculated with an average accuracy of 95%, compared to numerical modelling. Load sharing pressures in asymmetric IGU's have an average accuracy of 91%. From results it is concluded that as curvatures increase, a higher percentage of pressure is shared by the pane on which the external load is applied. Effective isochoric pressures due to cold-bending of asymmetric IGU's are calculated with an accuracy of 92%. From results it is concluded that isochoric pressures increase, as curvatures increase. Combinations of isochoric and load sharing pressures are calculated with an average accuracy of 87%. From results it is concluded that as curvatures increase, reliability of the analytical method decreases. From two case studies it is however concluded that feasibility of such curvatures is limited.

RQ 4: Which derived equations are suitable for the development of an analytical method which can be used during the early design stages?

The developed analytical method only consists of closed form equations. The method is presented in Chapter 6, in a similar style as current standards. The equations are complemented by comments and figures to enhance understanding for the user.

The outcome parameters are defined in line with modelling goals of the different stages. For the 'Bending phase', the key parameter is the maximum principal cold-bending stress, of which the equation is shown below. Definition of the input parameters is considered in Chapter 6.1.

$$\sigma'_{max;i} = \frac{t_i * \left(R - \sqrt{R^2 * \cos^2\left(\frac{2000}{R}\right)}\right)}{42}$$

Equation (105)
Page 87

For the 'Fixation moment', the anticlastic bending radius at midspan ($R_{mid;i}$) is calculated. Using this parameter, the relative anticlastic bending distance at the centre of the plate is calculated. In case of asymmetric IGU's, the difference in cavity distance and cavity volume are calculated. Definition of the input parameters and complementary equations is considered in Chapter 6.3.

$$R_{mid;i} = A_{B:H} * t_{pl;i} + B_{B:H}$$

Equation (116)
Page 89

For the 'Use phase', effective pressures on the cavity side of the interior glass pane are calculated. The equation to calculate the effective load sharing pressure due to an external load ($p_{2;LS}$), is shown below. Definition of the input parameters and complementary equations are considered in Chapter 6.2.

$$p_{2;LS} = \left[\sqrt{(K_1 + K_2)^2 * P_{c;P}^2 + 2P_{c;P} * (p_{ext} * K_1 + V) * (K_1 + K_2) + (p_{ext} * K_1 - V)^2} - V + K_1 * (p_{ext} - P_{c;P}) - P_{c;P} * K_2\right] * \frac{1}{2K_1 + 2K_2}$$

Equation (106)
Page 88

Effective isochoric pressures due to asymmetric cold-bending ($p_{2;CB}$), climatic loads ($p_{2;c}$) and height differences ($p_{2;H}$), are calculated using the following general equation. Definition of the input parameters and complementary equations is considered in Chapter 6.3.

$$p_{2;o} = \frac{V * P_o}{(P_{c;p} - P_o) * (K_1 + K_2)}$$

Equation (127) & (129)
Page 91

In addition to the written analytical method, an interactive Excel tool is provided. The tool can be used to directly explore design options in range up to 6x3m cold-bent IGU's. An overview of the tool is shown in Chapter 6.4, Figure 112.

How can the structural performance of cavity pressure in cold-bent insulating glass units be analytically determined?

From this research it is shown that a simplified analytical method is effective in calculating cavity pressures in cold-bent IGU's. Hereby, gas law equations are combined with structural mechanics equations to calculate the volumes of deformation from curved plates subjected to pressure loads. Furthermore, closed form result based equations are derived, to calculate cold-bending stresses and elastic anticlastic bending behaviour. The developed analytical method is presented in a guideline, which is complemented by an interactive calculation tool. The method can be used to quickly explore cavity pressure of various design options in a wide range of cold-bent IGU's.

9. Recommendations

Throughout this thesis, different suggestions for further research are mentioned. In this chapter these suggestions are translated to concrete recommendations, which can be followed to validate generalizability, and widen applicability of the developed analytical method.

Generalizability of validity
Within the scope of this thesis, only linear fixation of cold-bent IGU's is considered for numerical modelling. Since the developed analytical method include derivations based on results from numerical modelling, it is advised to validate generalizability of the methods. For the analysed numerical models, linear supports are considered along all edges of the curved plate. This is done using prescribed nodal displacements along the curved edges of the plate, with a distance between the nodes which is equal to the mesh size. For the case studies of the Van Gogh museum and the Spartherm building in Melle, clamp plates are used for fixation. To validate the applicability of developed analytical methods for such, and other types of fixation, it is recommended to setup a finite element model. Thereby, it is advised to copy the numerical model setup and analysis settings discussed in this thesis. However, instead of applying a prescribed displacement at each mesh node, the nodes should correspond to the position of the clamps. Then, by defining parameter sets based on sample checks, it can be checked whether resulting cold-bending stresses, anticlastic bending behaviour and volumes of deformation correspond to outcomes of the analytically developed method.

Future development
In case of future developments of the analytical method, the following aspects for improvements are suggested. First, considering the insights gained on the anticlastic bending behaviour from numerical modelling, it is recommended to further research structural principles of plate behaviour. In this thesis it is concluded that anticlastic plate effects are dependent on Poisson's ratio, radius of curvature, plate thickness and plate size. A more in-depth research into these parameters and their relation to plate theory, could result in insights to develop a more comprehensible analytical method.

Second, comprehensibility of the analytical method can be improved by consideration of nonrigid spacers. Due to simplification of the spacer as being rigid, deformations of panes of a symmetric cold-bent IGU are considered to be equal. Within the scope of the this, this implies there are no permanent isochoric pressures in symmetric cold-bent IGU's. In reality however, it can be concluded that due to nonrigidity of the spacer, deformations of the panes of a symmetric cold-bent IGU are not equal and therefore permanent isochoric pressures are present in symmetric cold-bent IGU's as well. For future developments, it is therefore recommended to include structural behaviour of spacers, when determining plate deformations of cold-bent glass panes. In (van Driel, 2021), nonrigid behaviour of a spacer is considered for application in a cold-twisted double-glazing unit. Findings and conclusions from this research can enhance understanding of the nonrigid behaviour of spacers, for applications in simplified analytical methods.

Third, application of the analytical method can be widened by consideration of cold-twisted IGU's. In (Staaks, 2003), conclusions are drawn on the deformation patterns of cold-twisted glass plates. From these conclusions, the specific geometry of twisted plates can be predicted. Similar to the calculation of volumes below single curved plates, twisted plate geometries can be translated to volumes below the plates. Within the framework of the developed analytical method, the volumes can then be used to calculate permanent isochoric pressures in asymmetric cold-twisted IGU configurations.

References

ABT bv. (2006). *Glaskap Kantoor Essent, 's-Hertogenbosch.* 's-Hertogenbosch: ABT bv, Delft, Velzen.

ACG Nederland. (2022). *De isolatiewaarde van glas*. Retrieved from AGC Nederland: https://www.agcnederland.nl/architecten/glasadvies-voor-architecten/u-waarde-glas/

ANSYS. (2017). 3.4 Stress Stiffening. *ANSYS User Manual, Release 18.2*.

Argyris, J., Haase, M., Mlejnek, H., & Schmolz, P. (1986). TRUNC for Shells - An Element possibly to the taste of Bruce Irons. *International Journal for numerical Methods in Engineering, Vol. 22*(John Wiley & Sons, Ltd.), 93-115.

Bijster, J., Noteboom, C., & Eekhout, M. (2016). Glass Entrance Van Gogh Museum Amsterdam. *Glass Structural Engineering, 1*, 205-231.

Bisshopp, K., & Drucker, D. (1945). Large Deflection of Cantilever Beams. *Quarterly of Applied Mathematics, III*(3), 272-275.

Bouwbesluit. (2012). *Hoofdstuk 5. Technische bouwvoorschriften uit het oogpunt van energiezuinigheid en milieu.* Rijksoverheid.

Cartwright, M. (2013, June 16). *The Arch of Titus, Rome.* Retrieved from World History Encyclopedia: https://www.worldhistory.org/article/499/the-arch-of-titus-rome/

Clapeyron, E. (1983). Mémoire sur la puissance motrice de la chaleur. *Journal de l'École Polytechnique*, pp. 90-153.

Clear Glass Solutions. (2019). *Insulating Glass Units.* Retrieved from Clearglass.com: https://clearglass.com.au/products/glass-types/insulated-glass-units/

de Berg, M., van Kreveld, M., Overmars, M., & Schwarzkopf, O. (2000). Delaunay Triangulations. In *Computational Geometry* (pp. 183-210). Berlin, Heidelberg: Springer.

Delgado, D. (2020). *Coronavirus Pandemic Causes Climate Of Anxiety And Changing Routines In America.* Retrieved from gettyimages.com: https://www.gettyimages.nl/detail/nieuwsfoto%27s/apples-flagship-5th-avenue-store-is-nearly-empty-on-march-nieuwsfotos/1207148249?adppopup=true

DIANA FEA. (2021). *DIANA Documentation - Release 10.5 - 75.2 Geometric Nonlinearity.* Delft: DIANA FEA.

Eekhout, M., Lockefeer, W., & Staaks, D. (2012, May). Design and Build of a Warped Tram Station Roof in Delft. *Challenging Glass 2*.

Elstner, M., & Kramer, M. (2012). Application of Thermally Curved Glass in the Buidling Industry. *Challenging Glass 3*, pp. 819-828.

EN 16612. (2019). *Glass in building - Determination of the lateral load resistance of glass panes by calculation.* CEN norm committee.

Feldmann, M., Kasper, R., Bucak, O., Illguth, M., & Bues, M. (2010). Curved Glass - Quality and Application. *Challenging Glass 2*, pp. 545-553.

Feldmeier, F. (2003). Insulating Units Exposed to Wind and Wather - Load Sharing and Internal Loads. *Glass Processing Days*, 633-636.

Foster + Partners. (2017). *Steve Jobs Theater.* Retrieved from Foster + Partners: https://www.fosterandpartners.com/projects/steve-jobs-theater/

Galuppi, L. (2020). Practical expressions for the design of DGUs. The BAM approach. *Engineering Structures 221*.

Galuppi, L., & Royer-Carfagni, G. (2019). Betti's Analytical Method for the load sharing in double glazed units. *Composite Structures 235*.

Galuppi, L., & Royer-Carfagni, G. (2020). Green's functions for the load sharing in multiple insulating glazing units. *International Journal of Solids and Structures 206*, 412-425.

Glass for Europe. (2020, April 9). *'Hot hold' operations in the flat glass sector.* Retrieved from Glass for Europe: https://glassforeurope.com/wp-content/uploads/2020/04/Hot-holds-Operations-GfE-paper-April2020.pdf

Glass for Europe. (2021). *Key data*. Retrieved from Glass for Europe: https://glassforeurope.com/the-sector/key-data/

Hartsuijker, C. (2001). *Toegepaste mechanica deel 2 - spanningen, vervormingen en verplaatsingen.* Amsterdam: Boom uitgevers.

IStructE. (2015). *Structural use of glass in buildings.* London, United Kingdom: The Institution of Structural Engineers.

Janssen, J. P. (2017). *Cold bent glass fins in a lattice gridshell.* Eindhoven: TU/e, Eindhoven Uniseristy of Technology.

Januszkiewicz, K., & Banachowicz, M. (2016). Glass as A Component of Curvilinear Architecture in 21st centry . *Procedia Engineering*, 1490-1495.

Kramer, L. (2015). *Van Gogh Museum's New Entrance / Hans van Heeswijk Architects.* Retrieved from ArchDaily: https://www.archdaily.com/772991/van-gogh-museum-hans-van-heeswijk-architects?ad_medium=gallery

Maplesoft. (2022). Retrieved from Maplesoft: https://www.maplesoft.com/

Marinov, V., & Griffith, J. (2012). *Optimisation of Curved Insulated Glass.* London: Ove Arup & Partners Ltd.

Molter, P., & Wolf, T. (2011). Verformen von Gläsern im Bauwesen. *Detail*, pp. 80-86.

MORN. (2019, March 28). *Factors that caused glass curtain wall visual distortion.* Retrieved from mornglass.com: https://www.mornglass.com/factors-that-caused-glass-curtain-wall-visual-distortion.html

NEN 2608. (2014). *Glass in building - Requirements and determination method.* Delft: Nederlands Normalisatie-instituut.

Neugebauer, J. (2014). Applications for curved glass in buildings. *Journal of Facade Design and Engineering*, 67-83.

Octatube. (2002). *Floriade Paviljoen .* Haarlemmermeer: Octatube.

Octatube. (2015). *Van Gogh Museum.* Amsterdam: Octatube.

Octatube. (2021). *Spartherm, Melle.* Melle: Octatube.

Partridge, H. (2020). *Insulation for Sustainability.* Insulation Manufacturers Assocation XC02.

Patenaude, A. (1991). Distortion is Sealed Glazing Units. *Progressive Architecture*.

Pilkington, L., & Bickerstaff, K. (1959). *US Patent No. 2.911.759.*

Pölzl, F. (2017). *Mechanical Behavior of Cold-Bent Insulating Glass Units.* Graz: TU Graz.

Quaglini, V. (2020). Cold bending of vertical glass plates: Wind loads and geometrical instabilities. *Engineering Structures*.

Raymond, K. W. (2009). Gases solutions, colloids and suspensions. In K. W. Raymond, *General Organic and Biological Chemistry* (p. 186). John Wiley & Sons.

Spatari, A. (2021). *Aerial view of skyscrapers in City of London, England, UK.* Retrieved from Gettyimages.com: https://www.gettyimages.nl/detail/foto/aerial-view-of-skyscrapers-in-city-of-london-royalty-free-beeld/1174407001?adppopup=true

Spyder. (2022). Retrieved from Spyder IDE: https://www.spyder-ide.org/

Staaks, D. (2003). *Koud torderen van glaspanelen in blobs.* Delft: TU Delft, faculteit bouwkunde.

Stazi, F. (2019). *Advances BUilding Envelope Components: Comparitive Experiments.* Ancona, Italy: Butterworth-Heinemann, Elsevier.

Timoshenko, S., & Woinowsky-Krieger, S. (1989). *Theory of plates and shells.* New York: McGraw-Hill Book Company.

Vallabhan, G., & Chou, G. (1986). Interactive Nonlinear Analysis of Insulating Glass Units. *Journal of Structural Engineering, 112*(No.6), 1313-1326.

van de Rotten, P. (2019). *Bending vs Twisting of Glass.* Delft: Octatube.

van der Velden, M., & Nijsse, R. (2019). *CIE4285 Structural Glass - Reader.* Delft: TU Delft.

van Driel, T. (2021). *Investigations on the Cold Bending Behaviour of a Cold-Bent Double Glazing Unit with a Rigid Edge-Spacer Frame.* Delft: TU Delft.

van Herwijnen, F. (2008). Warm en koud gebogen glas. *Cement*, pp. 32-37.

Welleman, H. (2019). *Notities over kabels en bogen.* Den Hoorn: Hans Welleman.

Wörner, J.-D., Shen, X., & Sagmeister, B. (1993). Determination of Load Sharing in Insulatede Glass Units. *Journal of Engineering Mechanics*, 386-392.

Young, W. C., & Budynas, R. G. (2002). 11. Flat Plates. In *Roark's Formulas for Stress and Strain* (p. 427). McGraw-Hill.

Zaha Hadid Architects. (2020). *Opus.* Retrieved from zaha-hadid.com: https://www.zaha-hadid.com/architecture/opus/

Appendix A. Principal stresses

In this appendix the resulting principal stresses of numerical and analytical modelling are presented. The results for numerical modelling are considered with boundary conditions from the 'Fixation moment'. Principal stresses in green are lower than 75.00 N/mm^2, stresses in red are higher. Calculation of the deviation is done in comparison to the average results from numerical modelling. For the validation of the arch theory results, also average values are considered. Colour grading of the standard deviations in comparison to the numerical results is done per analytical method, with the respective lowest deviation in green and highest deviation in red. Below, an overview is given of how the results of the analytical methods compare to each other.

Average deviations of principal stresses per analytical method					
	Relative deviation	Absolute deviation	Minimum deviation	Maximum deviation	Standard deviation
Arch theory	-11.78%	11.78%	-13.20%	-9.40%	0.81%
Cold-Bent Theory	-25.92%	25.92%	-26.54%	-24.09%	0.57%
Engineering approach	0.28%	0.93%	-2.98%	3.23%	1.22%

A.1. Numerical modelling – Fixation moment

Average principal stress [N/mm^2]

Average principal stresses [N/mm2]																							
Radius [mm]																							
Thickness [mm]	25000	24000	23000	22000	21000	20000	19000	18000	17000	16000	15000	14000	13000	12000	11000	10000	9000	8000	7000	6000	5000	4000	3000
4	7.61	7.93	8.27	8.65	9.06	9.51	10.01	10.57	11.19	11.89	12.68	13.59	14.63	15.86	17.26	19.02	21.14	23.76	27.13	31.63	37.89	47.23	62.75
5	9.50	9.90	10.33	10.81	11.32	11.89	12.52	13.23	13.99	14.87	15.86	16.99	18.29	19.82	21.62	23.78	26.42	29.72	33.86	39.58	47.45	59.17	78.40
6	11.38	11.86	12.38	12.95	13.57	14.26	15.01	15.85	16.79	17.84	19.06	20.39	21.95	23.79	25.94	28.54	31.63	35.66	40.74	47.45	56.95	70.96	94.20
7	13.25	13.81	14.42	15.09	15.82	16.61	17.50	18.48	19.57	20.80	22.19	23.78	25.61	27.75	30.27	33.30	36.99	41.61	47.55	55.34	66.46	82.82	110.00
8	15.11	15.75	16.45	17.21	18.04	18.96	19.97	21.09	22.35	23.76	25.35	27.17	29.27	31.71	34.60	38.06	42.28	47.56	54.34	63.37	75.96	94.63	125.59
9	16.96	17.68	18.47	19.32	20.26	21.29	22.43	23.70	25.11	26.70	28.49	30.55	32.91	35.67	38.92	42.82	47.57	53.51	61.14	71.29	85.48	106.63	141.25
10	18.80	19.60	20.47	21.43	22.47	23.61	24.88	26.29	27.86	29.63	31.63	33.91	36.54	39.61	43.23	47.57	52.86	59.48	67.94	79.24	94.99	118.48	156.88
11	20.64	21.52	22.47	23.52	24.67	25.93	27.32	28.87	30.60	32.54	34.75	37.27	40.17	43.55	47.53	52.31	58.14	65.41	74.75	87.15	104.28	130.38	173.05
12	22.46	23.42	24.46	25.61	26.86	28.23	29.75	31.44	33.33	35.45	37.86	40.61	43.78	47.47	51.83	57.05	63.42	71.36	81.55	95.10	114.04	142.27	188.43
13	24.28	25.32	26.45	27.68	29.04	30.53	32.17	34.00	36.05	38.35	40.96	43.94	47.38	51.38	56.11	61.77	68.68	77.31	88.36	103.06	123.54	153.81	204.20
14	26.10	27.22	28.43	29.76	31.21	32.82	34.59	36.56	38.76	41.24	44.05	47.26	50.96	55.28	60.38	66.49	73.94	83.24	95.16	111.00	133.10	166.06	219.87
15	27.91	29.10	30.40	31.82	33.38	35.10	36.99	39.10	41.46	44.12	47.13	50.57	54.54	59.17	64.64	71.19	79.19	89.16	101.95	118.94	142.64	177.95	235.67
16	29.71	30.99	32.37	33.88	35.55	37.37	39.39	41.64	44.16	46.99	50.20	53.87	58.11	63.05	68.88	75.88	84.42	95.08	108.74	126.88	152.17	189.88	251.46
17	31.51	32.86	34.33	35.94	37.71	39.64	41.79	44.18	46.85	49.85	53.26	57.16	61.66	66.92	73.12	80.56	89.64	100.98	115.51	134.81	161.72	201.79	267.31
18	33.31	34.74	36.29	37.99	39.86	41.91	44.18	46.71	49.53	52.71	56.32	60.45	65.21	70.77	77.35	85.23	94.86	106.87	122.28	142.76	171.27	213.68	283.47
19	35.10	36.61	38.24	40.04	42.01	44.17	46.56	49.23	52.21	55.56	59.37	63.73	68.75	74.62	81.56	89.89	100.06	112.75	129.03	150.66	180.81	225.69	298.74
20	36.88	38.47	40.19	42.08	44.15	46.43	48.94	51.75	54.88	58.41	62.41	66.99	72.29	78.47	85.77	94.54	105.25	118.62	135.78	158.58	190.35	236.92	315.27

Minimum principal stress [N/mm^2]

Minimum principal stresses [N/mm2]																							
Radius [mm]																							
Thickness [mm]	25000	24000	23000	22000	21000	20000	19000	18000	17000	16000	15000	14000	13000	12000	11000	10000	9000	8000	7000	6000	5000	4000	3000
4	7.52	7.84	8.18	8.56	8.97	9.43	9.93	10.48	11.11	11.80	12.60	13.50	14.55	15.77	16.89	18.94	21.05	23.69	26.77	31.30	37.64	46.80	61.86
5	9.37	9.77	10.20	10.67	11.19	11.75	12.38	13.08	13.85	14.73	15.72	16.85	18.16	19.68	21.48	23.65	26.29	29.59	33.34	39.47	47.20	58.76	77.63
6	11.21	11.68	12.20	12.77	13.38	14.07	14.82	15.65	16.59	17.64	18.83	20.19	21.76	23.59	25.75	28.35	30.79	35.48	40.58	46.66	56.69	70.45	93.32
7	13.03	13.58	14.19	14.85	15.57	16.37	17.24	18.22	19.31	20.54	21.93	23.52	25.35	27.49	30.01	33.04	36.74	41.37	47.31	54.26	66.22	82.07	109.05
8	14.79	15.44	16.14	16.91	17.74	18.65	19.66	20.77	22.02	23.42	25.01	26.83	28.92	31.37	34.25	37.72	41.95	47.24	54.04	63.10	75.70	93.60	124.28
9	16.54	17.26	18.05	18.92	19.86	20.91	22.06	23.31	24.71	26.29	28.08	30.12	32.48	35.23	38.48	42.39	47.15	53.11	60.76	70.96	85.24	105.97	139.15
10	18.27	19.07	19.95	20.91	21.95	23.11	24.39	25.81	27.39	29.15	31.13	33.41	36.03	39.08	42.70	47.04	52.34	58.96	67.47	78.81	94.68	117.68	154.42
11	19.99	20.87	21.82	22.88	24.03	25.30	26.70	28.26	30.01	31.98	34.18	36.68	39.56	42.92	46.90	51.67	57.51	64.80	74.16	86.65	101.62	129.49	171.71
12	21.70	22.65	23.69	24.83	26.08	27.46	28.99	30.69	32.60	34.74	37.18	39.93	43.08	46.75	51.09	56.30	62.66	70.62	80.84	94.47	113.54	141.47	185.39
13	23.40	24.43	25.55	26.78	28.13	29.62	31.27	33.11	35.16	37.48	40.12	43.13	46.59	50.56	55.26	60.91	67.81	76.43	87.51	102.29	122.96	150.46	200.97
14	25.10	26.20	27.40	28.72	30.17	31.76	33.53	35.50	37.71	40.21	43.04	46.28	50.03	54.36	59.43	65.50	72.94	82.23	94.17	110.09	132.37	165.34	216.70
15	26.79	27.97	29.25	30.65	32.19	33.90	35.79	37.89	40.25	42.92	45.94	49.41	53.42	58.10	63.57	70.09	78.05	88.01	100.81	117.88	141.77	176.98	232.42
16	28.48	29.73	31.09	32.58	34.22	36.03	38.03	40.27	42.77	45.61	48.83	52.52	56.79	61.78	67.69	74.66	83.15	93.78	107.44	125.66	151.16	188.98	247.66
17	30.16	31.48	32.92	34.50	36.23	38.15	40.27	42.64	45.29	48.29	51.70	55.62	60.14	65.44	71.72	79.21	88.24	99.53	114.05	133.42	160.53	200.56	262.82
18	31.85	33.24	34.75	36.42	38.25	40.27	42.50	45.00	47.80	50.97	54.57	58.70	63.48	69.08	75.72	83.70	93.31	105.27	120.65	141.17	169.90	212.40	279.98
19	33.53	34.99	36.58	38.34	40.25	42.38	44.73	47.36	50.30	53.63	57.42	61.77	66.80	72.70	79.70	88.11	98.37	111.00	127.24	148.91	179.25	224.46	292.69
20	35.20	36.74	38.41	40.25	42.26	44.49	46.95	49.71	52.79	56.29	60.26	64.83	70.11	76.31	83.66	92.51	103.35	116.71	133.81	156.63	188.58	227.61	311.44

Maximum principal stress [N/mm^2]

Maximum principal stresses [N/mm2]																							
Radius [mm]																							
Thickness [mm]	25000	24000	23000	22000	21000	20000	19000	18000	17000	16000	15000	14000	13000	12000	11000	10000	9000	8000	7000	6000	5000	4000	3000
4	7.66	7.98	8.32	8.70	9.11	9.56	10.06	10.61	11.23	11.93	12.73	13.63	14.67	15.89	17.34	19.08	21.21	23.84	27.23	31.77	38.12	47.61	63.38
5	9.59	9.98	10.42	10.89	11.41	11.97	12.60	13.45	14.06	14.93	15.92	17.05	18.35	19.87	21.67	23.83	26.49	29.81	34.05	39.72	47.65	59.52	79.24
6	11.49	11.98	12.50	13.07	13.70	14.39	15.15	15.98	16.91	17.96	19.45	20.50	22.05	23.87	26.01	28.60	31.76	35.75	40.87	47.66	57.16	71.41	95.10
7	13.37	13.94	14.56	15.23	15.97	16.78	17.67	18.65	19.75	20.98	22.36	23.95	25.77	27.89	30.39	33.39	37.07	41.69	47.67	55.62	66.67	83.35	110.93
8	15.23	15.88	16.59	17.36	18.21	19.14	20.17	21.31	22.56	23.98	25.57	27.40	29.49	31.92	34.79	38.22	42.42	47.67	54.45	63.54	76.25	95.22	126.80
9	17.14	17.85	18.62	19.47	20.43	21.48	22.64	23.92	25.35	26.96	28.76	30.82	33.19	35.94	39.18	43.05	47.78	53.67	61.30	71.48	85.77	107.11	142.70
10	19.05	19.84	20.69	21.64	22.67	23.80	25.09	26.52	28.12	29.91	31.93	34.24	36.88	39.95	43.57	47.89	53.15	59.69	68.13	79.41	95.24	119.02	158.52
11	20.96	21.83	22.77	23.80	24.94	26.18	27.55	29.09	30.86	32.84	35.07	37.62	40.56	43.95	47.95	52.72	58.52	65.74	75.00	87.40	104.80	130.92	174.38
12	22.87	23.82	24.85	25.98	27.21	28.56	30.06	31.73	33.59	35.73	38.19	40.98	44.19	47.92	52.30	57.53	63.89	71.78	81.88	95.41	114.35	142.82	190.28
13	24.79	25.81	26.92	28.15	29.48	30.95	32.57	34.38	36.39	38.67	41.27	44.31	47.81	51.87	56.64	62.33	69.24	77.83	88.79	103.43	123.92	154.73	206.19
14	26.71	27.81	29.01	30.32	31.76	33.34	35.09	37.03	39.20	41.65	44.42	47.62	51.40	55.79	60.95	67.11	74.58	83.86	95.70	111.46	133.53	166.63	221.98
15	28.63	29.81	31.10	32.51	34.05	35.74	37.61	39.69	42.01	44.63	47.60	51.00	54.96	59.68	65.23	71.86	79.90	89.88	102.61	119.50	143.16	178.60	237.88
16	30.54	31.81	33.18	34.69	36.33	38.14	40.13	42.35	44.83	47.62	50.78	54.40	58.58	63.54	69.49	76.58	85.20	95.89	109.51	127.55	152.80	190.61	253.80
17	32.45	33.80	35.26	36.86	38.62	40.54	42.65	45.02	47.65	50.61	53.97	57.82	62.25	67.44	73.72	81.28	90.47	101.87	116.39	135.61	162.50	202.63	269.76
18	34.35	35.79	37.34	39.04	40.90	42.94	45.18	47.69	50.47	53.61	57.17	61.23	65.92	71.41	77.92	85.95	95.72	107.83	123.26	143.66	172.12	214.67	285.74
19	36.25	37.77	39.41	41.22	43.18	45.33	47.70	50.35	53.30	56.61	60.36	64.65	69.60	75.39	82.23	90.59	100.93	113.76	130.11	151.71	181.78	226.73	301.75
20	38.15	39.75	41.48	43.38	45.46	47.73	50.23	53.02	56.12	59.61	63.56	68.08	73.29	79.37	86.58	95.22	106.12	119.67	136.94	159.74	191.44	238.81	317.78

A.2. Analytical modelling – Arch theory

Average principal stress [N/mm^2]

Average principal stresses [N/mm2]																							
Radius [mm]																							
Thickness [mm]	25000	24000	23000	22000	21000	20000	19000	18000	17000	16000	15000	14000	13000	12000	11000	10000	9000	8000	7000	6000	5000	4000	3000
4	6.68	6.96	7.26	7.59	7.96	8.35	8.79	9.28	9.83	10.44	11.13	11.93	12.84	13.91	15.17	16.69	18.53	20.84	23.80	27.74	33.22	41.37	54.73
5	8.35	8.70	9.08	9.49	9.94	10.44	10.99	11.60	12.28	13.05	13.92	14.91	16.06	17.39	18.97	20.86	23.17	26.05	29.75	34.67	41.53	51.71	68.42
6	10.02	10.44	10.90	11.39	11.93	12.53	13.19	13.92	14.74	15.66	16.70	17.89	19.27	20.87	22.76	25.03	27.80	31.26	35.70	41.61	49.83	62.05	82.10
7	11.70	12.18	12.71	13.29	13.92	14.62	15.39	16.24	17.19	18.27	19.49	20.87	22.48	24.35	26.55	29.21	32.44	36.47	41.65	48.54	58.14	72.40	95.78
8	13.37	13.92	14.53	15.19	15.91	16.71	17.58	18.56	19.65	20.88	22.27	23.86	25.69	27.83	30.35	33.38	37.07	41.68	47.60	55.48	66.45	82.74	109.46
9	15.04	15.66	16.34	17.09	17.90	18.79	19.78	20.88	22.11	23.49	25.05	26.84	28.90	31.30	34.14	37.55	41.70	46.89	53.55	62.41	74.75	93.08	123.15
10	16.71	17.40	18.16	18.98	19.89	20.88	21.98	23.20	24.56	26.10	27.84	29.82	32.11	34.78	37.93	41.72	46.34	52.10	59.51	69.35	83.06	103.42	136.83
11	18.38	19.14	19.98	20.88	21.88	22.97	24.18	25.52	27.02	28.70	30.62	32.80	35.32	38.26	41.73	45.90	50.97	57.31	65.46	76.28	91.36	113.76	150.51
12	20.05	20.88	21.79	22.78	23.87	25.06	26.38	27.84	29.48	31.31	33.40	35.78	38.53	41.74	45.52	50.07	55.60	62.52	71.41	83.22	99.67	124.11	164.20
13	21.72	22.62	23.61	24.68	25.86	27.15	28.57	30.16	31.93	33.92	36.19	38.77	41.74	45.22	49.31	54.24	60.24	67.73	77.36	90.15	107.97	134.45	177.88
14	23.39	24.36	25.42	26.58	27.84	29.24	30.77	32.48	34.39	36.53	38.97	41.75	44.95	48.69	53.11	58.41	64.87	72.94	83.31	97.09	116.28	144.79	191.56
15	25.06	26.10	27.24	28.48	29.83	31.32	32.97	34.80	36.84	39.14	41.75	44.73	48.17	52.17	56.90	62.58	69.51	78.15	89.26	104.02	124.59	155.13	205.25
16	26.73	27.84	29.06	30.37	31.82	33.41	35.17	37.12	39.30	41.75	44.54	47.71	51.38	55.65	60.69	66.76	74.14	83.36	95.21	110.96	132.89	165.47	218.93
17	28.40	29.58	30.87	32.27	33.81	35.50	37.37	39.44	41.76	44.36	47.32	50.69	54.59	59.13	64.49	70.93	78.77	88.57	101.16	117.89	141.20	175.82	232.61
18	30.07	31.32	32.69	34.17	35.80	37.59	39.57	41.76	44.21	46.97	50.10	53.67	57.80	62.61	68.28	75.10	83.41	93.78	107.11	124.83	149.50	186.16	246.30
19	31.74	33.06	34.50	36.07	37.79	39.68	41.76	44.08	46.67	49.58	52.89	56.66	61.01	66.08	72.08	79.27	88.04	98.99	113.06	131.76	157.81	196.50	259.98
20	33.42	34.80	36.32	37.97	39.78	41.76	43.96	46.40	49.13	52.19	55.67	59.64	64.22	69.56	75.87	83.45	92.67	104.20	119.01	138.70	166.12	206.84	273.66

Minimum principal stress [N/mm^2]

Minimum principal stresses [N/mm2]																							
Radius [mm]																							
Thickness [mm]	25000	24000	23000	22000	21000	20000	19000	18000	17000	16000	15000	14000	13000	12000	11000	10000	9000	8000	7000	6000	5000	4000	3000
4	6.68	6.96	7.26	7.59	7.95	8.35	8.79	9.28	9.82	10.43	11.13	11.92	12.83	13.90	15.16	16.67	18.51	20.80	23.73	27.63	33.03	40.97	53.80
5	8.35	8.70	9.08	9.49	9.94	10.44	10.99	11.60	12.28	13.04	13.91	14.90	16.04	17.37	18.95	20.83	23.13	26.00	29.67	34.53	41.29	51.21	67.26
6	10.02	10.44	10.89	11.39	11.93	12.52	13.18	13.92	14.73	15.65	16.69	17.88	19.25	20.85	22.73	25.00	27.76	31.19	35.60	41.44	49.55	61.45	80.71
7	11.69	12.18	12.71	13.29	13.92	14.61	15.38	16.24	17.19	18.26	19.47	20.86	22.46	24.32	26.52	29.17	32.38	36.39	41.53	48.35	57.81	71.69	94.16
8	13.36	13.92	14.53	15.18	15.91	16.70	17.58	18.55	19.64	20.86	22.26	23.84	25.67	27.80	30.31	33.33	37.01	41.59	47.47	55.25	66.06	81.93	107.61
9	15.03	15.66	16.34	17.08	17.90	18.79	19.77	20.87	22.10	23.47	25.04	26.82	28.88	31.27	34.10	37.50	41.64	46.79	53.40	62.16	74.32	92.18	121.06
10	16.70	17.40	18.16	18.98	19.88	20.87	21.97	23.19	24.55	26.08	27.82	29.80	32.08	34.75	37.89	41.67	46.26	51.99	59.33	69.07	82.58	102.42	134.51
11	18.37	19.14	19.97	20.88	21.87	22.96	24.17	25.51	27.01	28.69	30.60	32.78	35.29	38.22	41.68	45.83	50.89	57.19	65.27	75.97	90.84	112.66	147.96
12	20.04	20.88	21.79	22.78	23.86	25.05	26.37	27.83	29.47	31.30	33.39	35.76	38.50	41.70	45.47	50.00	55.52	62.39	71.20	82.88	99.10	122.90	161.41
13	21.71	22.62	23.60	24.68	25.85	27.13	28.56	30.15	31.92	33.91	36.17	38.74	41.71	45.17	49.26	54.17	60.14	67.59	77.14	89.79	107.36	133.14	174.86
14	23.39	24.36	25.42	26.57	27.84	29.22	30.76	32.47	34.38	36.51	38.95	41.72	44.92	48.65	53.05	58.33	64.77	72.79	83.07	96.69	115.61	143.38	188.32
15	25.06	26.10	27.24	28.47	29.83	31.31	32.96	34.79	36.83	39.12	41.73	44.70	48.13	52.12	56.84	62.50	69.40	77.99	89.00	103.60	123.87	153.63	201.77
16	26.73	27.84	29.05	30.37	31.81	33.40	35.15	37.11	39.29	41.73	44.51	47.68	51.33	55.60	60.62	66.67	74.02	83.19	94.94	110.51	132.13	163.87	215.22
17	28.40	29.58	30.87	32.27	33.80	35.48	37.35	39.43	41.74	44.34	47.30	50.66	54.54	59.07	64.41	70.83	78.65	88.38	100.87	117.42	140.39	174.11	228.67
18	30.07	31.32	32.68	34.17	35.79	37.57	39.55	41.75	44.20	46.95	50.08	53.64	57.75	62.55	68.20	75.00	83.27	93.58	106.80	124.32	148.65	184.35	242.12
19	31.74	33.06	34.50	36.06	37.78	39.66	41.75	44.07	46.65	49.55	52.86	56.62	60.96	66.02	71.99	79.17	87.90	98.78	112.74	131.23	156.90	194.59	255.57
20	33.41	34.80	36.31	37.96	39.77	41.74	43.94	46.39	49.11	52.16	55.64	59.60	64.17	69.50	75.78	83.33	92.53	103.98	118.67	138.14	165.16	204.83	269.02

Maximum principal stress [N/mm^2]

Maximum principal stresses [N/mm2]																							
Radius [mm]																							
Thickness [mm]	25000	24000	23000	22000	21000	20000	19000	18000	17000	16000	15000	14000	13000	12000	11000	10000	9000	8000	7000	6000	5000	4000	3000
4	6.68	6.96	7.27	7.60	7.96	8.36	8.80	9.28	9.83	10.44	11.14	11.93	12.85	13.92	15.19	16.71	18.56	20.88	23.86	27.83	33.39	41.70	55.52
5	8.35	8.70	9.08	9.49	9.95	10.44	10.99	11.60	12.29	13.05	13.93	14.92	16.07	17.40	18.98	20.89	23.20	26.10	29.83	34.79	41.73	52.12	69.40
6	10.03	10.44	10.90	11.39	11.94	12.53	13.19	13.92	14.74	15.67	16.71	17.90	19.28	20.88	22.78	25.06	27.84	31.32	35.79	41.75	50.08	62.55	83.27
7	11.70	12.18	12.71	13.29	13.93	14.62	15.39	16.24	17.20	18.28	19.50	20.88	22.49	24.36	26.58	29.24	32.48	36.54	41.76	48.71	58.42	72.97	97.15
8	13.37	13.92	14.53	15.19	15.91	16.71	17.59	18.56	19.66	20.89	22.28	23.87	25.71	27.84	30.37	33.42	37.12	41.75	47.72	55.66	66.77	83.40	111.03
9	15.04	15.67	16.35	17.09	17.90	18.80	19.79	20.88	22.11	23.50	25.07	26.85	28.92	31.33	34.17	37.59	41.76	46.97	53.69	62.62	75.12	93.82	124.91
10	16.71	17.41	18.16	18.99	19.89	20.89	21.99	23.21	24.57	26.11	27.85	29.83	32.13	34.81	37.97	41.77	46.40	52.19	59.65	69.58	83.46	104.25	138.79
11	18.38	19.15	19.98	20.89	21.88	22.98	24.19	25.53	27.03	28.72	30.64	32.82	35.35	38.29	41.76	45.95	51.04	57.41	65.62	76.54	91.81	114.67	152.67
12	20.05	20.89	21.80	22.79	23.87	25.07	26.39	27.85	29.49	31.33	33.42	35.80	38.56	41.77	45.56	50.12	55.68	62.63	71.58	83.50	100.16	125.10	166.55
13	21.72	22.63	23.61	24.69	25.86	27.16	28.59	30.17	31.94	33.94	36.21	38.79	41.77	45.25	49.36	54.30	60.32	67.85	77.55	90.45	108.50	135.52	180.43
14	23.39	24.37	25.43	26.58	27.85	29.24	30.78	32.49	34.40	36.55	38.99	41.77	44.99	48.73	53.15	58.48	64.96	73.07	83.51	97.41	116.85	145.94	194.31
15	25.06	26.11	27.24	28.48	29.84	31.33	32.98	34.81	36.86	39.16	41.78	44.75	48.20	52.21	56.95	62.66	69.60	78.29	89.48	104.37	125.19	156.37	208.19
16	26.74	27.85	29.06	30.38	31.83	33.42	35.18	37.13	39.31	41.77	44.56	47.74	51.41	55.69	60.75	66.83	74.24	83.51	95.44	111.33	133.54	166.79	222.07
17	28.41	29.59	30.88	32.28	33.82	35.51	37.38	39.45	41.77	44.38	47.35	50.72	54.63	59.17	64.54	71.01	78.88	88.73	101.41	118.29	141.89	177.22	235.95
18	30.08	31.33	32.69	34.18	35.81	37.60	39.58	41.77	44.23	47.00	50.13	53.70	57.84	62.65	68.34	75.19	83.52	93.95	107.37	125.24	150.23	187.64	249.82
19	31.75	33.07	34.51	36.08	37.80	39.69	41.78	44.09	46.69	49.61	52.92	56.69	61.05	66.13	72.14	79.36	88.16	99.17	113.34	132.20	158.58	198.07	263.70
20	33.42	34.81	36.33	37.98	39.79	41.78	43.98	46.41	49.14	52.22	55.70	59.67	64.27	69.61	75.93	83.54	92.80	104.39	119.30	139.16	166.93	208.49	277.58

Absolute standard deviation [%]

Arch theory - Absolute relative deviation [%]																							
Radius [mm]																							
Thickness [mm]	25000	24000	23000	22000	21000	20000	19000	18000	17000	16000	15000	14000	13000	12000	11000	10000	9000	8000	7000	6000	5000	4000	3000
4	12.17%	12.18%	12.18%	12.20%	12.20%	12.20%	12.21%	12.22%	12.22%	12.23%	12.22%	12.24%	12.24%	12.25%	12.11%	12.26%	12.31%	12.29%	12.26%	12.31%	12.32%	12.41%	12.78%
5	12.09%	12.10%	12.13%	12.15%	12.17%	12.17%	12.19%	12.32%	12.21%	12.23%	12.23%	12.25%	12.24%	12.25%	12.26%	12.27%	12.30%	12.34%	12.14%	12.40%	12.47%	12.60%	12.74%
6	11.94%	11.99%	12.01%	12.05%	12.09%	12.12%	12.16%	12.18%	12.20%	12.22%	12.37%	12.25%	12.25%	12.26%	12.27%	12.28%	12.12%	12.34%	12.35%	12.30%	12.49%	12.55%	12.85%
7	11.76%	11.82%	11.86%	11.92%	11.98%	12.02%	12.06%	12.11%	12.15%	12.18%	12.20%	12.23%	12.24%	12.26%	12.28%	12.29%	12.31%	12.34%	12.39%	12.29%	12.52%	12.59%	12.93%
8	11.55%	11.63%	11.68%	11.76%	11.82%	11.88%	11.95%	12.01%	12.06%	12.12%	12.15%	12.20%	12.23%	12.25%	12.28%	12.29%	12.33%	12.36%	12.39%	12.45%	12.53%	12.57%	12.84%
9	11.35%	11.43%	11.49%	11.58%	11.66%	11.73%	11.81%	11.88%	11.96%	12.02%	12.08%	12.14%	12.20%	12.23%	12.28%	12.30%	12.34%	12.36%	12.40%	12.45%	12.55%	12.71%	12.82%
10	11.14%	11.23%	11.30%	11.39%	11.48%	11.57%	11.66%	11.75%	11.83%	11.92%	11.98%	12.06%	12.13%	12.19%	12.26%	12.29%	12.34%	12.40%	12.41%	12.48%	12.56%	12.71%	12.78%
11	10.94%	11.03%	11.11%	11.21%	11.31%	11.40%	11.50%	11.60%	11.70%	11.80%	11.88%	11.98%	12.06%	12.14%	12.22%	12.27%	12.34%	12.38%	12.44%	12.47%	12.39%	12.75%	13.02%
12	10.74%	10.84%	10.92%	11.03%	11.13%	11.23%	11.34%	11.45%	11.56%	11.67%	11.77%	11.88%	11.98%	12.07%	12.17%	12.24%	12.32%	12.38%	12.44%	12.49%	12.60%	12.77%	12.86%
13	10.55%	10.66%	10.74%	10.85%	10.96%	11.07%	11.18%	11.30%	11.42%	11.54%	11.65%	11.77%	11.89%	12.00%	12.11%	12.20%	12.30%	12.38%	12.45%	12.53%	12.60%	12.59%	12.89%
14	10.37%	10.48%	10.57%	10.68%	10.80%	10.91%	11.03%	11.15%	11.28%	11.41%	11.53%	11.66%	11.79%	11.92%	12.04%	12.15%	12.27%	12.37%	12.45%	12.53%	12.64%	12.81%	12.87%
15	10.20%	10.31%	10.40%	10.52%	10.64%	10.75%	10.87%	11.01%	11.14%	11.27%	11.40%	11.55%	11.69%	11.83%	11.97%	12.09%	12.23%	12.34%	12.45%	12.54%	12.66%	12.82%	12.91%
16	10.03%	10.14%	10.24%	10.36%	10.48%	10.60%	10.73%	10.87%	11.00%	11.14%	11.28%	11.43%	11.58%	11.73%	11.89%	12.03%	12.18%	12.32%	12.44%	12.55%	12.67%	12.85%	12.94%
17	9.86%	9.98%	10.08%	10.20%	10.33%	10.46%	10.58%	10.73%	10.87%	11.02%	11.16%	11.32%	11.48%	11.64%	11.81%	11.96%	12.13%	12.29%	12.42%	12.55%	12.69%	12.87%	12.98%
18	9.70%	9.83%	9.93%	10.05%	10.19%	10.31%	10.44%	10.59%	10.73%	10.89%	11.04%	11.20%	11.37%	11.54%	11.72%	11.88%	12.07%	12.25%	12.40%	12.56%	12.71%	12.88%	13.11%
19	9.55%	9.68%	9.78%	9.91%	10.04%	10.18%	10.31%	10.46%	10.61%	10.77%	10.92%	11.09%	11.26%	11.44%	11.63%	11.81%	12.01%	12.20%	12.38%	12.54%	12.72%	12.93%	12.98%
20	9.40%	9.53%	9.63%	9.77%	9.91%	10.04%	10.18%	10.33%	10.48%	10.64%	10.80%	10.98%	11.16%	11.35%	11.54%	11.73%	11.95%	12.15%	12.35%	12.54%	12.73%	12.69%	13.20%

A.3. Analytical modelling – Cold-bending theory

Principal stresses [N/mm^2]

Principal stresses [N/mm2]																							
Radius [mm]																							
Thickness [mm]	25000	24000	23000	22000	21000	20000	19000	18000	17000	16000	15000	14000	13000	12000	11000	10000	9000	8000	7000	6000	5000	4000	3000
4	5.60	5.83	6.09	6.36	6.67	7.00	7.37	7.78	8.24	8.75	9.33	10.00	10.77	11.67	12.73	14.00	15.56	17.50	20.00	23.33	28.00	35.00	46.67
5	7.00	7.29	7.61	7.95	8.33	8.75	9.21	9.72	10.29	10.94	11.67	12.50	13.46	14.58	15.91	17.50	19.44	21.88	25.00	29.17	35.00	43.75	58.33
6	8.40	8.75	9.13	9.55	10.00	10.50	11.05	11.67	12.35	13.13	14.00	15.00	16.15	17.50	19.09	21.00	23.33	26.25	30.00	35.00	42.00	52.50	70.00
7	9.80	10.21	10.65	11.14	11.67	12.25	12.89	13.61	14.41	15.31	16.33	17.50	18.85	20.42	22.27	24.50	27.22	30.63	35.00	40.83	49.00	61.25	81.67
8	11.20	11.67	12.17	12.73	13.33	14.00	14.74	15.56	16.47	17.50	18.67	20.00	21.54	23.33	25.45	28.00	31.11	35.00	40.00	46.67	56.00	70.00	93.33
9	12.60	13.13	13.70	14.32	15.00	15.75	16.58	17.50	18.53	19.69	21.00	22.50	24.23	26.25	28.64	31.50	35.00	39.38	45.00	52.50	63.00	78.75	105.00
10	14.00	14.58	15.22	15.91	16.67	17.50	18.42	19.44	20.59	21.88	23.33	25.00	26.92	29.17	31.82	35.00	38.89	43.75	50.00	58.33	70.00	87.50	116.67
11	15.40	16.04	16.74	17.50	18.33	19.25	20.26	21.39	22.65	24.06	25.67	27.50	29.62	32.08	35.00	38.50	42.78	48.13	55.00	64.17	77.00	96.25	128.33
12	16.80	17.50	18.26	19.09	20.00	21.00	22.11	23.33	24.71	26.25	28.00	30.00	32.31	35.00	38.18	42.00	46.67	52.50	60.00	70.00	84.00	105.00	140.00
13	18.20	18.96	19.78	20.68	21.67	22.75	23.95	25.28	26.76	28.44	30.33	32.50	35.00	37.92	41.36	45.50	50.56	56.88	65.00	75.83	91.00	113.75	151.67
14	19.60	20.42	21.30	22.27	23.33	24.50	25.79	27.22	28.82	30.63	32.67	35.00	37.69	40.83	44.55	49.00	54.44	61.25	70.00	81.67	98.00	122.50	163.33
15	21.00	21.88	22.83	23.86	25.00	26.25	27.63	29.17	30.88	32.81	35.00	37.50	40.38	43.75	47.73	52.50	58.33	65.63	75.00	87.50	105.00	131.25	175.00
16	22.40	23.33	24.35	25.45	26.67	28.00	29.47	31.11	32.94	35.00	37.33	40.00	43.08	46.67	50.91	56.00	62.22	70.00	80.00	93.33	112.00	140.00	186.67
17	23.80	24.79	25.87	27.05	28.33	29.75	31.32	33.06	35.00	37.19	39.67	42.50	45.77	49.58	54.09	59.50	66.11	74.38	85.00	99.17	119.00	148.75	198.33
18	25.20	26.25	27.39	28.64	30.00	31.50	33.16	35.00	37.06	39.38	42.00	45.00	48.46	52.50	57.27	63.00	70.00	78.75	90.00	105.00	126.00	157.50	210.00
19	26.60	27.71	28.91	30.23	31.67	33.25	35.00	36.94	39.12	41.56	44.33	47.50	51.15	55.42	60.45	66.50	73.89	83.13	95.00	110.83	133.00	166.25	221.67
20	28.00	29.17	30.43	31.82	33.33	35.00	36.84	38.89	41.18	43.75	46.67	50.00	53.85	58.33	63.64	70.00	77.78	87.50	100.00	116.67	140.00	175.00	233.33

Absolute standard deviation [%]

Cold-bending theory - Absolute standard deviation [%]																						
Radius [mm]																						
Thickness [mm]	25000	24000	23000	22000	21000	20000	19000	18000	17000	16000	15000	14000	13000	12000	11000	10000	9000	8000	7000	6000	5000	4000	3000
4	26.40%	26.41%	26.41%	26.42%	26.42%	26.42%	26.43%	26.43%	26.42%	26.42%	26.42%	26.42%	26.41%	26.42%	26.28%	26.40%	26.41%	26.35%	26.27%	26.24%	26.10%	25.89%	25.63%
5	26.34%	26.34%	26.37%	26.38%	26.40%	26.40%	26.41%	26.51%	26.42%	26.42%	26.43%	26.43%	26.42%	26.42%	26.41%	26.41%	26.40%	26.39%	26.18%	26.31%	26.23%	26.06%	25.60%
6	26.21%	26.24%	26.27%	26.30%	26.33%	26.36%	26.38%	26.40%	26.41%	26.42%	26.54%	26.43%	26.42%	26.43%	26.41%	26.41%	26.24%	26.39%	26.35%	26.23%	26.25%	26.01%	25.69%
7	26.06%	26.10%	26.14%	26.19%	26.24%	26.27%	26.31%	26.34%	26.36%	26.39%	26.40%	26.42%	26.42%	26.42%	26.42%	26.42%	26.41%	26.39%	26.39%	26.22%	26.27%	26.04%	25.76%
8	25.88%	25.95%	25.99%	26.05%	26.11%	26.15%	26.21%	26.25%	26.29%	26.33%	26.36%	26.39%	26.41%	26.42%	26.42%	26.42%	26.42%	26.41%	26.39%	26.36%	26.28%	26.03%	25.68%
9	25.72%	25.78%	25.83%	25.90%	25.97%	26.03%	26.09%	26.15%	26.20%	26.25%	26.30%	26.34%	26.38%	26.40%	26.42%	26.43%	26.43%	26.41%	26.40%	26.36%	26.30%	26.15%	25.67%
10	25.54%	25.61%	25.67%	25.75%	25.82%	25.89%	25.96%	26.03%	26.10%	26.16%	26.22%	26.28%	26.33%	26.37%	26.40%	26.42%	26.43%	26.44%	26.40%	26.38%	26.31%	26.15%	25.63%
11	25.37%	25.44%	25.51%	25.59%	25.68%	25.75%	25.83%	25.91%	25.99%	26.06%	26.13%	26.21%	26.27%	26.32%	26.37%	26.40%	26.43%	26.43%	26.42%	26.37%	26.16%	26.18%	25.84%
12	25.21%	25.28%	25.36%	25.44%	25.53%	25.61%	25.70%	25.78%	25.87%	25.96%	26.04%	26.12%	26.20%	26.27%	26.33%	26.38%	26.41%	26.43%	26.43%	26.39%	26.34%	26.20%	25.70%
13	25.05%	25.13%	25.20%	25.29%	25.39%	25.47%	25.56%	25.66%	25.75%	25.85%	25.94%	26.03%	26.12%	26.21%	26.28%	26.35%	26.39%	26.43%	26.44%	26.42%	26.34%	26.05%	25.73%
14	24.89%	24.98%	25.06%	25.15%	25.25%	25.34%	25.44%	25.53%	25.63%	25.74%	25.84%	25.94%	26.04%	26.14%	26.22%	26.30%	26.37%	26.42%	26.44%	26.43%	26.37%	26.23%	25.71%
15	24.75%	24.84%	24.92%	25.01%	25.11%	25.21%	25.30%	25.41%	25.52%	25.62%	25.73%	25.84%	25.95%	26.06%	26.16%	26.26%	26.34%	26.39%	26.43%	26.43%	26.39%	26.24%	25.74%
16	24.61%	24.70%	24.78%	24.88%	24.98%	25.08%	25.18%	25.29%	25.40%	25.51%	25.63%	25.75%	25.86%	25.98%	26.09%	26.20%	26.30%	26.38%	26.43%	26.44%	26.40%	26.27%	25.77%
17	24.47%	24.56%	24.65%	24.75%	24.86%	24.96%	25.06%	25.18%	25.29%	25.41%	25.53%	25.65%	25.78%	25.90%	26.03%	26.14%	26.25%	26.35%	26.41%	26.44%	26.42%	26.28%	25.80%
18	24.34%	24.43%	24.52%	24.62%	24.74%	24.84%	24.95%	25.06%	25.18%	25.30%	25.43%	25.56%	25.69%	25.82%	25.95%	26.08%	26.21%	26.31%	26.40%	26.45%	26.43%	26.29%	25.92%
19	24.21%	24.31%	24.40%	24.50%	24.62%	24.72%	24.83%	24.96%	25.07%	25.20%	25.33%	25.46%	25.60%	25.74%	25.88%	26.02%	26.15%	26.28%	26.37%	26.43%	26.44%	26.34%	25.80%
20	24.09%	24.18%	24.28%	24.38%	24.50%	24.61%	24.72%	24.85%	24.97%	25.10%	25.23%	25.37%	25.51%	25.66%	25.81%	25.95%	26.10%	26.24%	26.35%	26.43%	26.45%	26.13%	25.99%

A.4. Analytical modelling – Engineering approach

Principal stresses [N/mm^2]

Principal stresses [N/mm2]																						
Radius [mm]																						
Thickness [mm]	25000	24000	23000	22000	21000	20000	19000	18000	17000	16000	15000	14000	13000	12000	11000	10000	9000	8000	7000	6000	5000	4000	3000
4	7.61	7.93	8.28	8.65	9.06	9.52	10.02	10.57	11.19	11.89	12.68	13.58	14.62	15.84	17.27	18.98	21.08	23.69	27.03	31.45	37.59	46.64	61.18
5	9.52	9.91	10.35	10.82	11.33	11.89	12.52	13.21	13.99	14.86	15.85	16.98	18.28	19.80	21.59	23.73	26.35	29.61	33.78	39.32	46.99	58.29	76.47
6	11.42	11.90	12.41	12.98	13.60	14.27	15.02	15.86	16.79	17.83	19.02	20.37	21.93	23.75	25.90	28.48	31.62	35.53	40.54	47.18	56.39	69.95	91.76
7	13.33	13.88	14.48	15.14	15.86	16.65	17.53	18.50	19.59	20.81	22.19	23.77	25.59	27.71	30.22	33.22	36.88	41.45	47.30	55.04	65.78	81.61	107.06
8	15.23	15.86	16.55	17.30	18.13	19.03	20.03	21.14	22.38	23.78	25.36	27.16	29.25	31.67	34.54	37.97	42.15	47.37	54.05	62.91	75.18	93.27	122.35
9	17.13	17.85	18.62	19.47	20.39	21.41	22.54	23.79	25.18	26.75	28.53	30.56	32.90	35.63	38.85	42.71	47.42	53.29	60.81	70.77	84.58	104.93	137.64
10	19.04	19.83	20.69	21.63	22.66	23.79	25.04	26.43	27.98	29.72	31.70	33.96	36.56	39.59	43.17	47.46	52.69	59.21	67.57	78.63	93.98	116.59	152.94
11	20.94	21.81	22.76	23.79	24.92	26.17	27.54	29.07	30.78	32.70	34.87	37.35	40.21	43.55	47.49	52.21	57.96	65.14	74.32	86.50	103.37	128.25	168.23
12	22.84	23.80	24.83	25.96	27.19	28.55	30.05	31.71	33.57	35.67	38.04	40.75	43.87	47.51	51.81	56.95	63.23	71.06	81.08	94.36	112.77	139.91	183.53
13	24.75	25.78	26.90	28.12	29.46	30.93	32.55	34.36	36.37	38.64	41.21	44.14	47.53	51.47	56.12	61.70	68.50	76.98	87.84	102.22	122.17	151.56	198.82
14	26.65	27.76	28.97	30.28	31.72	33.31	35.06	37.00	39.17	41.61	44.38	47.54	51.18	55.43	60.44	66.44	73.77	82.90	94.59	110.09	131.57	163.22	214.11
15	28.56	29.74	31.04	32.45	33.99	35.68	37.56	39.64	41.97	44.58	47.55	50.93	54.84	59.39	64.76	71.19	79.04	88.82	101.35	117.95	140.96	174.88	229.41
16	30.46	31.73	33.11	34.61	36.25	38.06	40.06	42.28	44.77	47.56	50.72	54.33	58.49	63.35	69.07	75.94	84.31	94.74	108.11	125.81	150.36	186.54	244.70
17	32.36	33.71	35.17	36.77	38.52	40.44	42.57	44.93	47.56	50.53	53.89	57.72	62.15	67.30	73.39	80.68	89.58	100.66	114.86	133.68	159.76	198.20	259.99
18	34.27	35.69	37.24	38.93	40.79	42.82	45.07	47.57	50.36	53.50	57.06	61.12	65.80	71.26	77.71	85.43	94.85	106.59	121.62	141.54	169.16	209.86	275.29
19	36.17	37.68	39.31	41.10	43.05	45.20	47.58	50.21	53.16	56.47	60.23	64.52	69.46	75.22	82.02	90.18	100.12	112.51	128.37	149.40	178.55	221.52	290.58
20	38.07	39.66	41.38	43.26	45.32	47.58	50.08	52.86	55.96	59.45	63.40	67.91	73.12	79.18	86.34	94.92	105.39	118.43	135.13	157.27	187.95	233.18	305.88

Absolute standard deviation [%]

Engineering approach - Absolute standard deviation [%]																						
Radius [mm]																						
Thickness [mm]	25000	24000	23000	22000	21000	20000	19000	18000	17000	16000	15000	14000	13000	12000	11000	10000	9000	8000	7000	6000	5000	4000	3000
4	0.08%	0.07%	0.06%	0.04%	0.03%	0.03%	0.01%	0.00%	0.01%	0.02%	0.04%	0.07%	0.08%	0.12%	0.02%	0.19%	0.29%	0.32%	0.37%	0.57%	0.79%	1.26%	2.51%
5	0.17%	0.16%	0.12%	0.09%	0.07%	0.05%	0.03%	0.12%	0.00%	0.03%	0.05%	0.07%	0.09%	0.12%	0.15%	0.21%	0.27%	0.37%	0.24%	0.67%	0.97%	1.48%	2.47%
6	0.34%	0.29%	0.26%	0.20%	0.15%	0.11%	0.07%	0.04%	0.01%	0.02%	0.21%	0.07%	0.09%	0.13%	0.15%	0.21%	0.06%	0.37%	0.48%	0.56%	0.99%	1.41%	2.59%
7	0.55%	0.48%	0.42%	0.35%	0.28%	0.23%	0.17%	0.12%	0.07%	0.02%	0.02%	0.06%	0.09%	0.13%	0.17%	0.22%	0.29%	0.38%	0.52%	0.54%	1.02%	1.46%	2.68%
8	0.78%	0.70%	0.63%	0.54%	0.46%	0.39%	0.30%	0.23%	0.17%	0.10%	0.04%	0.02%	0.07%	0.12%	0.17%	0.23%	0.30%	0.40%	0.53%	0.73%	1.03%	1.43%	2.58%
9	1.01%	0.92%	0.85%	0.74%	0.65%	0.56%	0.46%	0.38%	0.29%	0.21%	0.13%	0.05%	0.04%	0.09%	0.17%	0.23%	0.32%	0.40%	0.54%	0.73%	1.06%	1.60%	2.56%
10	1.25%	1.15%	1.06%	0.96%	0.84%	0.75%	0.64%	0.53%	0.43%	0.33%	0.23%	0.13%	0.04%	0.05%	0.14%	0.23%	0.32%	0.44%	0.55%	0.76%	1.07%	1.60%	2.51%
11	1.48%	1.38%	1.28%	1.16%	1.04%	0.94%	0.82%	0.70%	0.58%	0.47%	0.35%	0.23%	0.12%	0.01%	0.10%	0.20%	0.31%	0.42%	0.58%	0.75%	0.87%	1.64%	2.78%
12	1.71%	1.59%	1.49%	1.37%	1.24%	1.13%	1.00%	0.87%	0.74%	0.61%	0.48%	0.34%	0.21%	0.08%	0.04%	0.17%	0.29%	0.42%	0.58%	0.78%	1.11%	1.66%	2.61%
13	1.92%	1.80%	1.70%	1.57%	1.44%	1.31%	1.18%	1.04%	0.90%	0.76%	0.61%	0.47%	0.32%	0.17%	0.02%	0.12%	0.27%	0.43%	0.59%	0.82%	1.11%	1.46%	2.64%
14	2.13%	2.01%	1.90%	1.77%	1.63%	1.49%	1.36%	1.21%	1.06%	0.91%	0.75%	0.60%	0.43%	0.26%	0.10%	0.07%	0.23%	0.41%	0.59%	0.82%	1.15%	1.71%	2.62%
15	2.33%	2.20%	2.09%	1.95%	1.81%	1.67%	1.53%	1.37%	1.22%	1.06%	0.89%	0.72%	0.55%	0.37%	0.18%	0.00%	0.19%	0.37%	0.59%	0.83%	1.18%	1.72%	2.66%
16	2.52%	2.39%	2.27%	2.14%	1.99%	1.85%	1.70%	1.54%	1.38%	1.21%	1.03%	0.85%	0.67%	0.47%	0.27%	0.07%	0.14%	0.35%	0.58%	0.84%	1.19%	1.76%	2.69%
17	2.71%	2.57%	2.45%	2.31%	2.16%	2.01%	1.86%	1.69%	1.53%	1.35%	1.17%	0.98%	0.79%	0.58%	0.37%	0.15%	0.08%	0.31%	0.56%	0.84%	1.21%	1.78%	2.74%
18	2.89%	2.75%	2.62%	2.48%	2.32%	2.17%	2.02%	1.85%	1.68%	1.50%	1.31%	1.11%	0.91%	0.69%	0.47%	0.23%	0.01%	0.27%	0.54%	0.86%	1.24%	1.79%	2.89%
19	3.06%	2.92%	2.79%	2.65%	2.48%	2.33%	2.17%	2.00%	1.82%	1.64%	1.44%	1.24%	1.03%	0.80%	0.57%	0.32%	0.06%	0.22%	0.51%	0.83%	1.25%	1.85%	2.73%
20	3.23%	3.09%	2.96%	2.81%	2.64%	2.49%	2.32%	2.14%	1.97%	1.78%	1.58%	1.37%	1.15%	0.91%	0.67%	0.41%	0.13%	0.16%	0.48%	0.83%	1.26%	1.58%	2.98%

Appendix B. Anticlastic bending

In this appendix results from the simplified analytical methods to calculate the radius at midspan and volume of deformation are compared to outcomes from numerical modelling. The radii at midspan and volumes of deformation are calculated numerically as discussed in Chapter 4.3, and analytically in Chapter 4.4.

B.1. Radius at midspan

	Absolute deviation	Minimum deviation	Maximum deviation	Standard deviation
1000x1000mm	2.46%	0.03%	10.51%	1.98%
2000x1000mm	0.31%	0.00%	1.37%	0.25%
2000x2000mm	0.67%	0.00%	2.34%	0.48%
3000x1000mm	0.10%	0.00%	0.44%	0.08%
3000x2000mm	0.15%	0.00%	0.53%	0.10%
3000x3000mm	0.33%	0.00%	1.56%	0.29%
4000x1000mm	0.05%	0.00%	0.20%	0.04%
4000x2000mm	0.08%	0.00%	0.30%	0.06%
4000x3000mm	0.10%	0.00%	0.41%	0.08%
5000x1000mm	0.03%	0.00%	0.12%	0.03%
5000x2000mm	0.04%	0.00%	0.19%	0.03%
5000x3000mm	0.06%	0.00%	0.28%	0.05%
6000x1000mm	0.02%	0.00%	0.09%	0.02%
6000x2000mm	0.02%	0.00%	0.11%	0.02%
6000x3000mm	0.03%	0.00%	0.20%	0.03%
Average	**0.30%**	**0.00%**	**1.24%**	**0.24%**

Numerical results 1000x1000mm

Radius at midspan - numerical results - 1000x1000mm plate																								
Radius [mm]		25000	24000	23000	22000	21000	20000	19000	18000	17000	16000	15000	14000	13000	12000	11000	10000	9000	8000	7000	6000	5000	4000	3000
Thickness [mm]	4	34738	32997	31240	29515	27778	26070	24372	22713	21067	19468	17914	16406	14949	13548	12201	10907	9663	8466	7313	6197	5113	4056	3020
	5	36514	34789	33035	31296	29547	27797	26050	24310	22573	20860	19171	17513	15896	14332	12833	11397	10027	8726	7489	6308	5178	4090	3036
	6	37603	35904	34176	32455	30727	28988	27250	25502	23751	22006	20265	18533	16822	15143	13516	11947	10451	9035	7700	6443	5257	4132	3054
	7	38299	36618	34915	33215	31510	29792	28073	26342	24604	22864	21117	19366	17621	15885	14178	12512	10907	9379	7942	6601	5350	4180	3075
	8	38766	37098	35414	33731	32044	30345	28646	26933	25214	23490	21754	20010	18262	16510	14767	13044	11362	9741	8208	6778	5456	4235	3099
	9	39094	37437	35767	34096	32423	30739	29055	27358	25657	23949	22228	20498	18760	17013	15262	13515	11788	10101	8485	6970	5574	4297	3126
	10	39335	37685	36025	34364	32701	31029	29357	27673	25985	24292	22585	20870	19146	17411	15664	13913	12166	10440	8763	7172	5702	4366	3156
	11	39517	37873	36220	34567	32912	31248	29585	27912	26236	24553	22860	21158	19447	17725	15989	14244	12492	10746	9029	7378	5838	4441	3189
	12	39661	38020	36373	34725	33076	31420	29764	28099	26431	24758	23075	21385	19685	17976	16251	14516	12769	11017	9277	7580	5979	4521	3224
	13	39776	38139	36496	34852	33208	31557	29906	28247	26587	24921	23246	21566	19876	18178	16464	14740	13000	11251	9500	7774	6123	4607	3263
	14	39871	38237	36597	34957	33316	31669	30022	28369	26713	25053	23386	21713	20032	18342	16640	14925	13195	11451	9699	7955	6265	4696	3304
	15	39952	38319	36682	35044	33406	31762	30119	28469	26818	25163	23502	21835	20161	18479	16785	15080	13359	11624	9873	8121	6403	4787	3348
	16	40022	38390	36755	35119	33483	31842	30201	28555	26907	25256	23599	21937	20269	18594	16907	15210	13499	11771	10027	8272	6535	4879	3394
	17	40083	38453	36819	35184	33550	31910	30272	28628	26983	25335	23682	22024	20361	18691	17011	15322	13618	11898	10160	8408	6659	4971	3442
	18	40138	38508	36876	35242	33609	31971	30334	28692	27050	25404	23754	22100	20440	18775	17101	15417	13720	12009	10278	8529	6774	5062	3492
	19	40188	38559	36927	35294	33661	32025	30389	28749	27108	25465	23817	22165	20509	18848	17178	15500	13809	12105	10381	8637	6881	5150	3543
	20	40234	38605	36974	35342	33709	32074	30439	28800	27161	25519	23873	22224	20570	18912	17246	15572	13887	12189	10472	8734	6979	5235	3595

Analytical results 1000x1000mm

Radius at midspan - analytical results - 1000x1000mm plate																								
Radius [mm]		25000	24000	23000	22000	21000	20000	19000	18000	17000	16000	15000	14000	13000	12000	11000	10000	9000	8000	7000	6000	5000	4000	3000
Thickness [mm]	4	36949	35311	33638	31937	30215	28479	26733	24986	23243	21511	19796	18105	16444	14820	13239	11707	10232	8819	7475	6206	5018	3920	2915
	5	37203	35569	33901	32207	30493	28764	27027	25286	23550	21822	20110	18419	16756	15126	13535	11990	10495	9058	7685	6380	5151	4003	2942
	6	37458	35827	34165	32478	30771	29050	27320	25587	23856	22134	20424	18734	17068	15432	13831	12272	10759	9298	7895	6555	5283	4086	2968
	7	37712	36084	34428	32748	31048	29335	27613	25887	24163	22445	20738	19048	17380	15738	14128	12554	11023	9538	8105	6729	5416	4169	2995
	8	37966	36342	34691	33018	31326	29621	27906	26188	24470	22756	21052	19363	17692	16044	14424	12836	11286	9778	8315	6904	5548	4252	3021
	9	38220	36600	34955	33288	31603	29906	28200	26488	24776	23068	21366	19677	18003	16350	14720	13119	11550	10017	8526	7079	5681	4336	3048
	10	38474	36858	35218	33558	31881	30192	28493	26789	25083	23379	21680	19991	18315	16656	15016	13401	11813	10257	8736	7253	5813	4419	3074
	11	38729	37116	35481	33828	32159	30477	28786	27089	25389	23690	21995	20306	18627	16961	15313	13683	12077	10497	8946	7428	5945	4502	3101
	12	38983	37374	35745	34098	32436	30762	29079	27390	25696	24002	22309	20620	18939	17267	15609	13966	12341	10737	9156	7602	6078	4585	3127
	13	39237	37632	36008	34368	32714	31048	29373	27690	26003	24313	22623	20934	19251	17573	15905	14248	12604	10976	9366	7777	6210	4668	3154
	14	39491	37890	36271	34638	32991	31333	29666	27991	26309	24624	22937	21249	19562	17879	16201	14530	12868	11216	9577	7952	6343	4752	3180
	15	39745	38148	36535	34908	33269	31619	29959	28291	26616	24936	23251	21563	19874	18185	16497	14812	13131	11456	9787	8126	6475	4835	3207
	16	40000	38406	36798	35178	33547	31904	30252	28592	26923	25247	23565	21878	20186	18491	16794	15095	13395	11695	9997	8301	6607	4918	3233
	17	40254	38664	37062	35448	33824	32190	30546	28892	27229	25558	23879	22192	20498	18797	17090	15377	13658	11935	10207	8475	6740	5001	3260
	18	40508	38921	37325	35718	34102	32475	30839	29192	27536	25870	24193	22506	20810	19103	17386	15659	13922	12175	10417	8650	6872	5084	3286
	19	40762	39179	37588	35988	34379	32761	31132	29493	27843	26181	24507	22821	21121	19409	17682	15941	14186	12415	10628	8825	7005	5168	3313
	20	41016	39437	37852	36259	34657	33046	31425	29793	28149	26492	24821	23135	21433	19715	17979	16224	14449	12654	10838	8999	7137	5251	3339

Validation 1000x1000mm

	Absolute deviation	Minimum deviation	Maximum deviation	Standard deviation
1000x1000mm	2.46%	0.03%	10.51%	1.98%

Radius at midspan - validation analytical results - 1000x1000mm plate																								
Radius [mm]		25000	24000	23000	22000	21000	20000	19000	18000	17000	16000	15000	14000	13000	12000	11000	10000	9000	8000	7000	6000	5000	4000	3000
Thickness [mm]	4	6.37%	7.01%	7.68%	8.21%	8.77%	9.24%	9.69%	10.01%	10.33%	10.49%	10.51%	10.36%	10.00%	9.39%	8.51%	7.34%	5.89%	4.16%	2.21%	0.15%	1.84%	3.35%	3.48%
	5	1.89%	2.24%	2.62%	2.91%	3.20%	3.48%	3.75%	4.02%	4.33%	4.61%	4.90%	5.17%	5.41%	5.54%	5.47%	5.20%	4.67%	3.80%	2.62%	1.14%	0.53%	2.14%	
	6	0.39%	0.22%	0.03%	0.07%	0.14%	0.21%	0.26%	0.33%	0.44%	0.58%	0.78%	1.08%	1.46%	1.91%	2.33%	2.72%	2.95%	2.91%	2.53%	1.73%	0.49%	1.11%	
	7	1.53%	1.46%	1.39%	1.41%	1.46%	1.53%	1.64%	1.73%	1.79%	1.83%	1.79%	1.64%	1.37%	0.93%	0.36%	0.34%	1.06%	1.69%	2.05%	1.95%	1.23%		
	8	2.06%	2.04%	2.04%	2.12%	2.24%	2.39%	2.58%	2.77%	2.95%	3.12%	3.22%	3.23%	3.12%	2.82%	2.33%	1.59%	0.67%	0.37%	1.31%	1.86%	1.69%		
	9	2.24%	2.23%	2.27%	2.37%	2.53%	2.71%	2.94%	3.18%	3.43%	3.68%	3.88%	4.01%	4.03%	3.90%	3.55%	2.93%	2.02%	0.83%	0.47%	1.56%			
	10	2.19%	2.19%	2.24%	2.35%	2.51%	2.70%	2.94%	3.20%	3.47%	3.76%	4.01%	4.21%	4.34%	4.34%	4.14%	3.68%	2.90%	1.75%	0.31%				
	11	2.00%	2.00%	2.04%	2.14%	2.29%	2.47%	2.70%	2.95%	3.23%	3.52%	3.78%	4.03%	4.22%	4.31%	4.23%	3.94%	3.33%	2.32%	0.92%				
	12	1.71%	1.70%	1.73%	1.81%	1.94%	2.09%	2.30%	2.52%	2.78%	3.05%	3.32%	3.57%	3.79%	3.94%	3.95%	3.79%	3.35%	2.54%					
	13	1.35%	1.33%	1.34%	1.39%	1.49%	1.61%	1.78%	1.97%	2.20%	2.44%	2.68%	2.93%	3.15%	3.32%	3.40%	3.34%	3.05%	2.44%					
	14	0.95%	0.91%	0.89%	0.91%	0.97%	1.06%	1.19%	1.33%	1.51%	1.71%	1.92%	2.14%	2.34%	2.53%	2.64%	2.65%	2.48%						
	15	0.52%	0.45%	0.40%	0.39%	0.41%	0.45%	0.53%	0.63%	0.75%	0.90%	1.07%	1.24%	1.42%	1.59%	1.71%	1.77%	1.71%						
	16	0.06%	0.04%	0.12%	0.17%	0.19%	0.20%	0.17%	0.13%	0.06%	0.04%	0.14%	0.27%	0.41%	0.55%	0.67%	0.76%							
	17	0.43%	0.55%	0.66%	0.75%	0.82%	0.88%	0.90%	0.92%	0.91%	0.88%	0.83%	0.76%	0.67%	0.57%	0.46%	0.36%							
	18	0.92%	1.07%	1.22%	1.35%	1.47%	1.58%	1.66%	1.74%	1.80%	1.83%	1.85%	1.84%	1.81%	1.75%	1.67%								
	19	1.43%	1.61%	1.79%	1.97%	2.13%	2.30%	2.44%	2.59%	2.71%	2.81%	2.90%	2.96%	2.98%	2.98%									
	20	1.94%	2.16%	2.37%	2.59%	2.81%	3.03%	3.24%	3.45%	3.64%	3.82%	3.97%	4.10%	4.19%	4.24%									

Numerical results 2000x1000mm

Radius at midspan - numerical results - 2000x1000mm plate																								
	Radius [mm]	25000	24000	23000	22000	21000	20000	19000	18000	17000	16000	15000	14000	13000	12000	11000	10000	9000	8000	7000	6000	5000	4000	3000
Thickness [mm]	4	25623	24580	23505	22450	21403	20347	19308	18261	17222	16190	15157	14128	13103	12081	11062	10047	9035	8026	7018	6013	5009	4006	3004
	5	25866	24806	23713	22642	21577	20506	19448	18387	17332	16285	15240	14197	13160	12126	11097	10073	9054	8038	7026	6017	5011	4007	3005
	6	26087	25011	23911	22824	21750	20661	19593	18514	17447	16388	15326	14271	13223	12178	11138	10105	9077	8054	7037	6024	5015	4009	3005
	7	26283	25195	24091	22991	21910	20808	19731	18638	17561	16489	15415	14348	13288	12234	11183	10140	9104	8074	7050	6032	5019	4010	3005
	8	26453	25355	24250	23140	22052	20942	19855	18754	17669	16585	15501	14425	13355	12292	11231	10179	9133	8096	7065	6041	5024	4013	3006
	9	26599	25495	24387	23272	22177	21063	19968	18861	17769	16676	15584	14500	13421	12349	11279	10218	9165	8119	7082	6052	5030	4016	3007
	10	26722	25615	24505	23387	22286	21170	20069	18958	17861	16760	15662	14571	13484	12404	11327	10258	9197	8144	7099	6064	5037	4019	3009
	11	26827	25717	24607	23487	22382	21264	20159	19046	17944	16838	15735	14637	13544	12458	11374	10298	9229	8169	7118	6076	5045	4023	3010
	12	26916	25805	24694	23573	22465	21347	20238	19123	18019	16908	15801	14699	13601	12509	11419	10337	9261	8195	7137	6090	5053	4028	3012
	13	26992	25880	24769	23647	22538	21420	20309	19193	18086	16972	15862	14757	13654	12557	11462	10375	9293	8221	7157	6104	5062	4032	3014
	14	27057	25944	24834	23712	22601	21483	20371	19254	18146	17029	15918	14809	13704	12602	11503	10411	9324	8246	7176	6118	5071	4038	3016
	15	27112	25999	24889	23768	22657	21539	20426	19309	18199	17082	15968	14858	13749	12644	11542	10446	9354	8271	7196	6132	5081	4043	3018
	16	27160	26047	24938	23817	22706	21588	20474	19358	18247	17128	16014	14902	13791	12683	11579	10479	9383	8295	7215	6147	5091	4049	3021
	17	27202	26089	24980	23860	22748	21632	20517	19401	18289	17171	16056	14942	13830	12720	11613	10510	9410	8318	7234	6161	5101	4055	3024
	18	27238	26126	25017	23898	22786	21670	20556	19440	18327	17209	16093	14979	13866	12754	11645	10539	9437	8341	7253	6176	5111	4061	3026
	19	27270	26158	25049	23931	22819	21704	20590	19474	18361	17243	16128	15013	13898	12785	11675	10566	9462	8363	7271	6190	5121	4067	3029
	20	27298	26186	25078	23960	22849	21734	20620	19505	18392	17274	16159	15043	13928	12814	11703	10592	9486	8384	7289	6204	5131	4073	3033

Analytical results 2000x1000mm

Radius at midspan - analytical results - 2000x1000mm plate																								
	Radius [mm]	25000	24000	23000	22000	21000	20000	19000	18000	17000	16000	15000	14000	13000	12000	11000	10000	9000	8000	7000	6000	5000	4000	3000
Thickness [mm]	4	25975	24883	23795	22711	21630	20554	19481	18414	17350	16292	15238	14189	13145	12106	11073	10045	9022	8006	6995	5989	4990	3997	3011
	5	26072	24978	23888	22802	21718	20639	19563	18491	17423	16360	15301	14247	13197	12153	11114	10080	9052	8030	7013	6003	4999	4002	3011
	6	26168	25074	23982	22893	21807	20724	19644	18568	17496	16427	15364	14304	13249	12200	11155	10116	9082	8054	7032	6017	5008	4006	3011
	7	26264	25169	24075	22984	21895	20809	19725	18645	17568	16495	15426	14362	13301	12246	11196	10151	9112	8079	7051	6031	5017	4010	3010
	8	26360	25264	24169	23075	21983	20894	19806	18722	17641	16563	15489	14419	13353	12293	11237	10186	9142	8103	7070	6045	5026	4014	3010
	9	26456	25359	24262	23166	22072	20979	19888	18799	17713	16631	15552	14477	13406	12339	11278	10222	9171	8127	7089	6058	5035	4018	3010
	10	26552	25454	24355	23257	22160	21064	19969	18876	17786	16699	15614	14534	13458	12386	11319	10257	9201	8152	7108	6072	5044	4023	3010
	11	26649	25549	24449	23348	22248	21149	20050	18953	17859	16766	15677	14591	13510	12432	11360	10293	9231	8176	7127	6086	5052	4027	3010
	12	26745	25644	24542	23439	22336	21234	20131	19030	17931	16834	15740	14649	13562	12479	11401	10328	9261	8200	7146	6100	5061	4031	3010
	13	26841	25739	24636	23531	22425	21319	20213	19108	18004	16902	15803	14706	13614	12525	11442	10363	9291	8225	7165	6114	5070	4035	3010
	14	26937	25834	24729	23622	22513	21404	20294	19185	18076	16970	15865	14764	13666	12572	11483	10399	9320	8249	7184	6128	5079	4040	3010
	15	27033	25929	24822	23713	22601	21489	20375	19262	18149	17038	15928	14821	13718	12618	11524	10434	9350	8273	7203	6141	5088	4044	3009
	16	27129	26024	24916	23804	22690	21574	20456	19339	18222	17105	15991	14879	13770	12665	11565	10469	9380	8298	7222	6155	5097	4048	3009
	17	27225	26120	25009	23895	22778	21659	20538	19416	18294	17173	16054	14936	13822	12712	11605	10505	9410	8322	7241	6169	5106	4052	3009
	18	27322	26215	25103	23986	22866	21744	20619	19493	18367	17241	16116	14994	13874	12758	11646	10540	9440	8346	7260	6183	5115	4056	3009
	19	27418	26310	25196	24077	22955	21829	20700	19570	18439	17309	16179	15051	13926	12805	11687	10575	9470	8371	7279	6197	5123	4061	3009
	20	27514	26405	25289	24168	23043	21914	20781	19647	18512	17377	16242	15109	13978	12851	11728	10611	9499	8395	7298	6210	5132	4065	3009

Validation 2000x1000mm

	Absolute deviation	Minimum deviation	Maximum deviation	Standard deviation
2000x1000mm	0.31%	0.00%	1.37%	0.25%

Radius at midspan - validation analytical results - 2000x1000mm plate																								
	Radius [mm]	25000	24000	23000	22000	21000	20000	19000	18000	17000	16000	15000	14000	13000	12000	11000	10000	9000	8000	7000	6000	5000	4000	3000
Thickness [mm]	4	1.37%	1.24%	1.23%	1.16%	1.06%	1.01%	0.90%	0.84%	0.75%	0.63%	0.53%	0.43%	0.32%	0.21%	0.10%	0.02%	0.14%	0.25%	0.34%	0.39%	0.38%	0.22%	0.23%
	5	0.79%	0.69%	0.74%	0.70%	0.65%	0.65%	0.59%	0.56%	0.53%	0.46%	0.40%	0.35%	0.28%	0.23%	0.15%	0.07%	0.02%	0.10%	0.18%	0.24%	0.24%	0.14%	
	6	0.31%	0.25%	0.29%	0.30%	0.26%	0.30%	0.26%	0.29%	0.28%	0.24%	0.24%	0.23%	0.20%	0.18%	0.15%	0.11%	0.05%	0.00%	0.06%	0.11%	0.13%	0.07%	
	7	0.07%	0.10%	0.07%	0.03%	0.07%	0.00%	0.03%	0.04%	0.04%	0.04%	0.08%	0.09%	0.10%	0.10%	0.11%	0.10%	0.09%	0.06%	0.02%	0.01%	0.04%		
	8	0.35%	0.36%	0.34%	0.28%	0.31%	0.23%	0.25%	0.17%	0.16%	0.13%	0.08%	0.04%	0.01%	0.01%	0.06%	0.08%	0.09%	0.09%	0.08%	0.06%			
	9	0.54%	0.53%	0.51%	0.46%	0.47%	0.40%	0.40%	0.33%	0.31%	0.27%	0.21%	0.16%	0.11%	0.08%	0.01%	0.03%	0.07%	0.10%	0.11%	0.11%			
	10	0.64%	0.63%	0.61%	0.56%	0.57%	0.50%	0.50%	0.43%	0.42%	0.37%	0.31%	0.25%	0.20%	0.15%	0.07%	0.01%	0.05%	0.10%	0.13%				
	11	0.67%	0.65%	0.64%	0.59%	0.60%	0.54%	0.54%	0.48%	0.48%	0.42%	0.37%	0.31%	0.26%	0.20%	0.12%	0.05%	0.02%	0.08%	0.13%				
	12	0.64%	0.62%	0.62%	0.57%	0.57%	0.53%	0.53%	0.49%	0.49%	0.44%	0.39%	0.34%	0.29%	0.24%	0.16%	0.09%	0.01%	0.07%					
	13	0.56%	0.54%	0.54%	0.49%	0.50%	0.47%	0.47%	0.44%	0.45%	0.41%	0.38%	0.34%	0.30%	0.25%	0.18%	0.11%	0.03%						
	14	0.44%	0.42%	0.42%	0.38%	0.39%	0.37%	0.38%	0.36%	0.38%	0.35%	0.33%	0.31%	0.27%	0.24%	0.18%	0.12%	0.04%						
	15	0.29%	0.27%	0.27%	0.23%	0.25%	0.24%	0.25%	0.25%	0.28%	0.26%	0.25%	0.25%	0.23%	0.20%	0.16%	0.11%							
	16	0.11%	0.09%	0.09%	0.06%	0.07%	0.07%	0.09%	0.10%	0.14%	0.13%	0.15%	0.16%	0.15%	0.14%	0.12%	0.09%							
	17	0.09%	0.12%	0.12%	0.15%	0.13%	0.12%	0.10%	0.08%	0.03%	0.01%	0.01%	0.04%	0.06%	0.07%	0.06%								
	18	0.31%	0.34%	0.34%	0.37%	0.35%	0.34%	0.31%	0.27%	0.22%	0.19%	0.14%	0.10%	0.06%	0.03%									
	19	0.54%	0.58%	0.59%	0.61%	0.59%	0.57%	0.54%	0.49%	0.43%	0.38%	0.32%	0.26%	0.20%	0.15%									
	20	0.79%	0.83%	0.84%	0.87%	0.85%	0.82%	0.78%	0.73%	0.65%	0.59%	0.52%	0.43%	0.36%										

Numerical results 2000x2000mm

Radius at midspan - numerical results - 2000x2000mm plate																							
Radius [mm]		25000	24000	23000	22000	21000	20000	19000	18000	17000	16000	15000	14000	13000	12000	11000	10000	9000	8000	7000	6000	5000	4000	3000
Thickness [mm]	4	25874	24791	23678	22598	21520	20445	19383	18324	17268	16225	15185	14146	13114	12084	11061	10041	9026	8013	7004	5999	4995	3995	2996
	5	26376	25234	24070	22944	21820	20707	19607	18517	17432	16362	15299	14242	13191	12146	11110	10079	9054	8033	7018	6007	5000	3996	2996
	6	26977	25777	24544	23357	22185	21020	19880	18747	17627	16527	15436	14353	13282	12218	11167	10122	9087	8057	7034	6017	5005	3999	2996
	7	27676	26397	25098	23840	22612	21386	20198	19016	17856	16719	15593	14481	13386	12302	11231	10172	9124	8084	7053	6029	5013	4002	2997
	8	28459	27094	25724	24389	23098	21805	20563	19323	18118	16940	15773	14628	13505	12397	11304	10228	9165	8114	7074	6043	5021	4006	2999
	9	29304	27855	26409	24995	23635	22271	20969	19669	18412	17186	15976	14794	13638	12503	11386	10290	9211	8147	7097	6058	5030	4011	3001
	10	30182	28655	27136	25645	24215	22779	21412	20049	18736	17457	16201	14978	13786	12621	11477	10359	9262	8183	7122	6075	5040	4017	3003
	11	31062	29467	27885	26321	24823	23318	21884	20458	19088	17753	16447	15180	13949	12750	11577	10435	9317	8223	7149	6092	5051	4023	3005
	12	31916	30266	28632	27006	25443	23878	22378	20892	19464	18070	16713	15399	14126	12891	11686	10517	9378	8266	7178	6111	5062	4029	3008
	13	32721	31030	29357	27681	26063	24445	22885	21342	19857	18406	16996	15634	14316	13043	11804	10607	9443	8312	7210	6131	5075	4036	3011
	14	33463	31745	30044	28330	26669	25007	23395	21801	20263	18756	17294	15883	14519	13205	11931	10703	9514	8362	7244	6153	5088	4043	3015
	15	34135	32400	30682	28942	27248	25553	23898	22260	20675	19115	17603	16143	14733	13376	12065	10805	9589	8416	7280	6176	5101	4050	3018
	16	34737	32994	31266	29510	27793	26073	24385	22711	21085	19478	17920	16412	14957	13557	12208	10914	9669	8473	7318	6201	5116	4058	3022
	17	35272	33526	31795	30030	28299	26563	24849	23147	21487	19840	18240	16688	15188	13746	12358	11029	9754	8533	7359	6227	5132	4066	3026
	18	35747	34001	32271	30503	28762	27017	25286	23564	21875	20195	18559	16967	15425	13941	12514	11150	9844	8597	7402	6255	5148	4075	3030
	19	36167	34425	32697	30929	29185	27435	25692	23957	22246	20541	18874	17246	15665	14141	12676	11276	9938	8664	7448	6284	5165	4084	3034
	20	36539	34801	33076	31314	29569	27818	26069	24324	22597	20873	19181	17522	15907	14345	12842	11407	10036	8735	7495	6314	5183	4094	3038

Analytical results 2000x2000mm

Radius at midspan - analytical results - 2000x2000mm plate																							
Radius [mm]		25000	24000	23000	22000	21000	20000	19000	18000	17000	16000	15000	14000	13000	12000	11000	10000	9000	8000	7000	6000	5000	4000	3000
Thickness [mm]	4	25843	24626	23441	22285	21157	20053	18973	17913	16871	15845	14833	13833	12843	11859	10881	9905	8930	7953	6973	5986	4991	3986	2967
	5	26564	25302	24070	22867	21692	20541	19413	18306	17219	16149	15095	14054	13025	12007	10996	9992	8992	7994	6997	5999	4998	3992	2979
	6	27284	25977	24699	23450	22226	21028	19853	18700	17567	16453	15356	14275	13208	12154	11111	10078	9053	8035	7022	6013	5005	3999	2991
	7	28005	26652	25329	24032	22761	21515	20293	19093	17915	16756	15617	14496	13391	12302	11227	10165	9115	8076	7047	6026	5013	4005	3003
	8	28725	27328	25958	24614	23296	22002	20733	19487	18263	17060	15879	14717	13574	12449	11342	10252	9177	8117	7072	6040	5020	4012	3015
	9	29446	28003	26587	25196	23831	22490	21173	19880	18611	17364	16140	14937	13757	12597	11457	10338	9239	8158	7096	6053	5027	4019	3027
	10	30167	28679	27216	25778	24365	22977	21613	20274	18959	17668	16401	15158	13939	12744	11573	10425	9300	8199	7121	6066	5034	4025	3039
	11	30887	29354	27845	26361	24900	23464	22053	20667	19307	17972	16662	15379	14122	12892	11688	10511	9362	8240	7146	6080	5042	4032	3051
	12	31608	30030	28475	26943	25435	23952	22493	21061	19655	18276	16924	15600	14305	13039	11803	10598	9424	8281	7171	6093	5049	4039	3063
	13	32328	30705	29104	27525	25970	24439	22934	21454	20003	18579	17185	15821	14488	13187	11919	10685	9485	8322	7195	6106	5056	4045	3075
	14	33049	31381	29733	28107	26504	24926	23374	21848	20351	18883	17446	16042	14671	13334	12034	10771	9547	8363	7220	6120	5063	4052	3087
	15	33769	32056	30362	28689	27039	25413	23814	22242	20699	19187	17708	16263	14854	13482	12150	10858	9609	8404	7245	6133	5070	4058	3099
	16	34490	32732	30991	29272	27574	25901	24254	22635	21047	19491	17969	16483	15036	13629	12265	10945	9671	8445	7269	6146	5078	4065	3111
	17	35211	33407	31621	29854	28109	26388	24694	23029	21395	19795	18230	16704	15219	13777	12380	11031	9732	8486	7294	6160	5085	4072	3123
	18	35931	34083	32250	30436	28644	26875	25134	23422	21743	20098	18492	16925	15402	13925	12496	11118	9794	8527	7319	6173	5092	4078	3135
	19	36652	34758	32879	31018	29178	27363	25574	23816	22091	20402	18753	17146	15585	14072	12611	11204	9856	8568	7344	6186	5099	4085	3147
	20	37372	35433	33508	31600	29713	27850	26014	24209	22439	20706	19014	17367	15768	14220	12726	11291	9917	8609	7368	6200	5106	4091	3159

Validation 2000x2000mm

	Absolute deviation	Minimum deviation	Maximum deviation	Standard deviation
2000x2000mm	0.67%	0.00%	2.34%	0.48%

Radius at midspan - validation analytical results - 2000x2000mm plate																							
Radius [mm]		25000	24000	23000	22000	21000	20000	19000	18000	17000	16000	15000	14000	13000	12000	11000	10000	9000	8000	7000	6000	5000	4000	3000
Thickness [mm]	4	0.12%	0.67%	1.00%	1.38%	1.69%	1.92%	2.12%	2.24%	2.30%	2.34%	2.31%	2.21%	2.07%	1.86%	1.63%	1.35%	1.06%	0.74%	0.45%	0.21%	0.09%	0.24%	0.97%
	5	0.71%	0.27%	0.00%	0.33%	0.59%	0.80%	0.99%	1.14%	1.22%	1.30%	1.34%	1.32%	1.25%	1.14%	1.03%	0.86%	0.69%	0.49%	0.29%	0.12%	0.03%	0.10%	
	6	1.14%	0.77%	0.63%	0.40%	0.19%	0.04%	0.13%	0.25%	0.34%	0.45%	0.52%	0.54%	0.56%	0.52%	0.49%	0.43%	0.36%	0.27%	0.17%	0.07%	0.00%	0.01%	
	7	1.19%	0.97%	0.92%	0.80%	0.66%	0.60%	0.47%	0.41%	0.33%	0.22%	0.16%	0.10%	0.03%	0.00%	0.04%	0.07%	0.09%	0.09%	0.08%	0.05%	0.00%		
	8	0.94%	0.86%	0.91%	0.92%	0.86%	0.91%	0.83%	0.85%	0.80%	0.71%	0.67%	0.60%	0.51%	0.42%	0.33%	0.23%	0.13%	0.04%	0.03%	0.06%			
	9	0.49%	0.53%	0.67%	0.80%	0.83%	0.98%	0.98%	1.08%	1.08%	1.04%	1.03%	0.97%	0.87%	0.75%	0.62%	0.47%	0.30%	0.14%	0.00%	0.09%			
	10	0.05%	0.08%	0.29%	0.52%	0.62%	0.87%	0.94%	1.12%	1.19%	1.21%	1.24%	1.20%	1.11%	0.98%	0.83%	0.63%	0.42%	0.20%	0.01%				
	11	0.56%	0.38%	0.14%	0.15%	0.31%	0.63%	0.77%	1.02%	1.15%	1.23%	1.31%	1.31%	1.24%	1.11%	0.96%	0.73%	0.48%	0.21%	0.04%				
	12	0.97%	0.78%	0.55%	0.23%	0.03%	0.31%	0.52%	0.81%	0.98%	1.14%	1.26%	1.30%	1.27%	1.15%	1.00%	0.77%	0.49%	0.18%					
	13	1.20%	1.05%	0.86%	0.56%	0.36%	0.02%	0.21%	0.53%	0.73%	0.94%	1.11%	1.19%	1.20%	1.10%	0.97%	0.74%	0.45%						
	14	1.24%	1.15%	1.04%	0.79%	0.62%	0.32%	0.09%	0.22%	0.43%	0.68%	0.88%	1.00%	1.04%	0.98%	0.87%	0.64%	0.35%						
	15	1.07%	1.06%	1.04%	0.87%	0.77%	0.55%	0.35%	0.08%	0.12%	0.38%	0.59%	0.74%	0.82%	0.79%	0.70%	0.49%							
	16	0.71%	0.79%	0.88%	0.81%	0.79%	0.66%	0.54%	0.33%	0.18%	0.07%	0.27%	0.43%	0.53%	0.53%	0.47%	0.28%							
	17	0.17%	0.35%	0.55%	0.59%	0.67%	0.66%	0.62%	0.51%	0.43%	0.23%	0.05%	0.10%	0.20%	0.23%	0.18%								
	18	0.52%	0.24%	0.07%	0.22%	0.41%	0.53%	0.60%	0.60%	0.60%	0.48%	0.36%	0.25%	0.15%	0.12%									
	19	1.34%	0.97%	0.56%	0.29%	0.02%	0.27%	0.46%	0.59%	0.70%	0.68%	0.64%	0.58%	0.51%	0.49%									
	20	2.28%	1.82%	1.31%	0.92%	0.49%	0.11%	0.21%	0.47%	0.70%	0.80%	0.87%	0.89%	0.87%										

Numerical results 3000x1000mm

Radius at midspan - numerical results - 3000x1000mm plate																							
Radius [mm]		25000	24000	23000	22000	21000	20000	19000	18000	17000	16000	15000	14000	13000	12000	11000	10000	9000	8000	7000	6000	5000	4000	3000
Thickness [mm]	4	25214	24190	23174	22157	21138	20125	19108	18096	17082	16071	15061	14051	13043	12036	11030	10024	9019	8015	7011	6008	5006	4004	3002
	5	25296	24261	23239	22220	21190	20174	19151	18135	17115	16099	15085	14071	13059	12049	11039	10032	9024	8019	7012	6011	5007	4005	3003
	6	25376	24332	23304	22284	21247	20225	19197	18174	17150	16131	15113	14094	13077	12064	11051	10040	9031	8024	7018	6013	5009	4006	3003
	7	25447	24398	23364	22344	21301	20274	19243	18217	17188	16165	15140	14118	13099	12081	11065	10051	9039	8029	7021	6015	5010	4007	3004
	8	25508	24456	23419	22396	21350	20320	19286	18256	17224	16198	15170	14144	13119	12099	11079	10062	9048	8035	7026	6018	5012	4007	3004
	9	25559	24507	23468	22442	21395	20362	19326	18293	17258	16230	15198	14169	13142	12118	11094	10076	9057	8042	7030	6021	5014	4008	3005
	10	25604	24552	23511	22483	21435	20400	19363	18327	17290	16260	15225	14193	13164	12137	11111	10088	9068	8050	7035	6024	5015	4009	3005
	11	25641	24591	23548	22518	21471	20433	19396	18358	17320	16288	15250	14216	13184	12155	11127	10101	9078	8058	7041	6028	5017	4011	3006
	12	25674	24625	23581	22549	21503	20463	19425	18385	17347	16314	15274	14238	13204	12173	11142	10114	9089	8066	7047	6032	5020	4012	3006
	13	25702	24655	23610	22576	21531	20490	19452	18411	17371	16336	15295	14258	13223	12189	11157	10127	9100	8074	7053	6036	5022	4013	3007
	14	25727	24680	23635	22601	21555	20514	19476	18433	17393	16357	15315	14277	13240	12205	11171	10140	9110	8083	7060	6040	5025	4014	3007
	15	25749	24703	23658	22622	21577	20535	19497	18453	17414	16376	15333	14294	13256	12220	11185	10151	9120	8091	7066	6045	5028	4016	3008
	16	25768	24723	23677	22641	21597	20554	19516	18472	17432	16393	15350	14310	13271	12234	11198	10163	9130	8099	7073	6049	5031	4017	3009
	17	25785	24740	23695	22658	21614	20571	19533	18488	17448	16408	15365	14325	13286	12247	11210	10174	9140	8108	7079	6054	5034	4019	3009
	18	25799	24756	23710	22673	21630	20587	19548	18503	17463	16423	15379	14339	13299	12259	11222	10184	9149	8116	7086	6059	5037	4021	3010
	19	25813	24769	23724	22686	21643	20600	19562	18517	17476	16436	15392	14351	13311	12271	11233	10194	9158	8123	7092	6064	5041	4023	3011
	20	25824	24781	23737	22698	21656	20613	19574	18529	17489	16447	15404	14363	13322	12281	11243	10203	9166	8131	7098	6069	5044	4025	3012

Analytical results 3000x1000mm

Radius at midspan - analytical results - 3000x1000mm plate																							
Radius [mm]		25000	24000	23000	22000	21000	20000	19000	18000	17000	16000	15000	14000	13000	12000	11000	10000	9000	8000	7000	6000	5000	4000	3000
Thickness [mm]	4	25326	24294	23264	22235	21208	20182	19159	18137	17116	16097	15080	14065	13051	12039	11028	10020	9012	8007	7003	6001	5001	4002	3005
	5	25362	24329	23298	22268	21240	20213	19188	18164	17142	16121	15102	14085	13069	12055	11042	10031	9022	8015	7009	6006	5004	4003	3005
	6	25397	24364	23332	22301	21272	20244	19217	18191	17167	16145	15124	14104	13087	12070	11056	10043	9032	8023	7015	6010	5006	4005	3005
	7	25433	24399	23366	22334	21304	20274	19246	18219	17193	16169	15146	14124	13104	12086	11070	10055	9042	8031	7021	6014	5009	4006	3005
	8	25469	24434	23401	22368	21336	20305	19275	18246	17219	16192	15167	14144	13122	12102	11083	10066	9052	8038	7027	6018	5012	4007	3005
	9	25504	24469	23435	22401	21368	20335	19304	18274	17244	16216	15189	14164	13140	12118	11097	10078	9061	8046	7033	6023	5014	4008	3005
	10	25540	24504	23469	22434	21400	20366	19333	18301	17270	16240	15211	14184	13158	12133	11111	10090	9071	8054	7040	6027	5017	4010	3005
	11	25576	24539	23503	22467	21432	20397	19362	18328	17295	16264	15233	14204	13176	12149	11125	10102	9081	8062	7046	6031	5020	4011	3005
	12	25611	24574	23537	22501	21464	20427	19391	18356	17321	16287	15255	14223	13193	12165	11138	10113	9091	8070	7052	6036	5023	4012	3005
	13	25647	24610	23572	22534	21496	20458	19420	18383	17347	16311	15277	14243	13211	12181	11152	10125	9100	8078	7058	6040	5025	4013	3005
	14	25683	24645	23606	22567	21528	20488	19449	18411	17372	16335	15298	14263	13229	12197	11166	10137	9110	8086	7064	6044	5028	4015	3005
	15	25718	24680	23640	22600	21560	20519	19478	18438	17398	16359	15320	14283	13247	12212	11179	10149	9120	8093	7070	6049	5031	4016	3004
	16	25754	24715	23674	22633	21592	20550	19507	18465	17424	16382	15342	14303	13265	12228	11193	10160	9130	8101	7076	6053	5033	4017	3004
	17	25790	24750	23709	22667	21624	20580	19536	18493	17449	16406	15364	14323	13282	12244	11207	10172	9139	8109	7082	6057	5036	4018	3004
	18	25825	24785	23743	22700	21656	20611	19566	18520	17475	16430	15386	14342	13300	12260	11221	10184	9149	8117	7088	6062	5039	4020	3004
	19	25861	24820	23777	22733	21688	20641	19595	18547	17500	16454	15407	14362	13318	12275	11234	10195	9159	8125	7094	6066	5041	4021	3004
	20	25897	24855	23811	22766	21720	20672	19624	18575	17526	16477	15429	14382	13336	12291	11248	10207	9169	8133	7100	6070	5044	4022	3004

Validation 3000x1000mm

	Absolute deviation	Minimum deviation	Maximum deviation	Standard deviation
3000x1000mm	0.10%	0.00%	0.44%	0.08%

Radius at midspan - validation analytical results - 2000x1000mm plate																							
Radius [mm]		25000	24000	23000	22000	21000	20000	19000	18000	17000	16000	15000	14000	13000	12000	11000	10000	9000	8000	7000	6000	5000	4000	3000
Thickness [mm]	4	0.44%	0.43%	0.39%	0.35%	0.33%	0.28%	0.26%	0.22%	0.20%	0.16%	0.13%	0.10%	0.06%	0.02%	0.01%	0.04%	0.08%	0.10%	0.11%	0.12%	0.10%	0.04%	0.11%
	5	0.26%	0.28%	0.25%	0.22%	0.23%	0.19%	0.19%	0.16%	0.16%	0.14%	0.11%	0.10%	0.07%	0.05%	0.02%	0.00%	0.02%	0.05%	0.04%	0.08%	0.07%	0.04%	
	6	0.08%	0.13%	0.12%	0.08%	0.12%	0.09%	0.10%	0.10%	0.10%	0.08%	0.07%	0.07%	0.07%	0.05%	0.04%	0.03%	0.01%	0.01%	0.03%	0.04%	0.05%	0.03%	
	7	0.06%	0.01%	0.01%	0.04%	0.01%	0.00%	0.02%	0.01%	0.03%	0.02%	0.04%	0.04%	0.04%	0.04%	0.04%	0.04%	0.03%	0.02%	0.00%	0.01%	0.02%		
	8	0.15%	0.09%	0.08%	0.12%	0.07%	0.08%	0.06%	0.06%	0.03%	0.04%	0.02%	0.00%	0.02%	0.02%	0.04%	0.04%	0.04%	0.04%	0.03%	0.01%			
	9	0.21%	0.16%	0.14%	0.18%	0.13%	0.13%	0.12%	0.11%	0.08%	0.09%	0.06%	0.04%	0.02%	0.00%	0.02%	0.03%	0.04%	0.05%	0.05%	0.03%			
	10	0.25%	0.19%	0.18%	0.22%	0.17%	0.17%	0.15%	0.14%	0.12%	0.12%	0.09%	0.07%	0.05%	0.03%	0.00%	0.02%	0.04%	0.05%	0.06%				
	11	0.25%	0.21%	0.19%	0.22%	0.18%	0.18%	0.17%	0.16%	0.14%	0.15%	0.11%	0.09%	0.07%	0.05%	0.02%	0.00%	0.03%	0.05%	0.06%				
	12	0.24%	0.21%	0.18%	0.21%	0.18%	0.18%	0.18%	0.16%	0.15%	0.16%	0.12%	0.10%	0.08%	0.06%	0.03%	0.01%	0.02%	0.05%					
	13	0.21%	0.18%	0.16%	0.19%	0.16%	0.16%	0.16%	0.15%	0.14%	0.16%	0.12%	0.10%	0.09%	0.07%	0.05%	0.02%	0.01%						
	14	0.17%	0.15%	0.12%	0.15%	0.13%	0.13%	0.14%	0.12%	0.12%	0.14%	0.11%	0.10%	0.08%	0.07%	0.05%	0.03%	0.00%						
	15	0.12%	0.09%	0.07%	0.10%	0.08%	0.08%	0.10%	0.08%	0.09%	0.10%	0.09%	0.08%	0.07%	0.06%	0.05%	0.03%							
	16	0.05%	0.03%	0.01%	0.03%	0.02%	0.02%	0.04%	0.04%	0.05%	0.06%	0.05%	0.05%	0.05%	0.05%	0.04%								
	17	0.02%	0.04%	0.06%	0.04%	0.04%	0.04%	0.02%	0.02%	0.01%	0.01%	0.01%	0.02%	0.02%	0.03%	0.03%								
	18	0.10%	0.12%	0.14%	0.12%	0.12%	0.12%	0.09%	0.09%	0.07%	0.04%	0.04%	0.03%	0.01%	0.00%									
	19	0.19%	0.21%	0.22%	0.20%	0.20%	0.20%	0.17%	0.17%	0.14%	0.11%	0.10%	0.08%	0.06%	0.04%									
	20	0.28%	0.30%	0.32%	0.30%	0.29%	0.29%	0.25%	0.25%	0.21%	0.18%	0.16%	0.13%	0.11%										

Numerical results 3000x2000mm

Radius at midspan - numerical results - 3000x2000mm plate																							
	Radius [mm]	25000	24000	23000	22000	21000	20000	19000	18000	17000	16000	15000	14000	13000	12000	11000	10000	9000	8000	7000	6000	5000	4000	3000
Thickness [mm]	4	25103	24085	23082	22068	21055	20055	19039	18039	17028	16024	15021	14019	13014	12011	11010	10009	9008	8007	7006	6005	5004	4003	3002
	5	25181	24150	23139	22120	21098	20094	19071	18066	17049	16041	15035	14028	13022	12016	11012	10009	9008	8007	7004	6004	5003	4003	3002
	6	25277	24232	23210	22186	21152	20142	19111	18101	17077	16064	15055	14043	13033	12026	11018	10013	9009	8007	7006	6005	5002	4003	3002
	7	25388	24328	23293	22263	21218	20198	19159	18142	17112	16094	15079	14061	13048	12036	11026	10019	9013	8011	7006	6005	5002	4001	3002
	8	25511	24436	23388	22350	21292	20262	19215	18191	17152	16128	15107	14083	13065	12050	11036	10026	9017	8013	7009	6004	5004	4003	3002
	9	25643	24554	23493	22444	21374	20334	19277	18243	17197	16167	15139	14109	13086	12067	11048	10035	9024	8016	7009	6005	5002	4001	3002
	10	25783	24680	23607	22545	21463	20413	19346	18302	17247	16208	15174	14138	13109	12085	11062	10045	9031	8020	7012	6006	5002	4003	3001
	11	25933	24813	23725	22654	21558	20495	19419	18364	17301	16255	15211	14169	13135	12105	11077	10057	9039	8026	7015	6008	5003	4004	3001
	12	26087	24951	23848	22768	21658	20582	19497	18431	17359	16304	15252	14203	13162	12129	11094	10070	9049	8032	7019	6010	5004	4000	3002
	13	26243	25093	23976	22885	21761	20673	19578	18501	17420	16356	15296	14239	13191	12151	11114	10084	9059	8039	7027	6013	5008	4001	2998
	14	26401	25237	24106	23005	21868	20768	19662	18574	17484	16412	15342	14277	13222	12176	11132	10099	9070	8047	7029	6016	5010	4005	3002
	15	26558	25382	24237	23124	21977	20864	19749	18649	17550	16469	15389	14317	13255	12202	11153	10115	9082	8055	7034	6019	5008	4001	3001
	16	26712	25526	24369	23244	22087	20962	19838	18727	17618	16528	15439	14359	13290	12230	11176	10132	9096	8064	7040	6023	5010	4002	2998
	17	26863	25670	24501	23363	22198	21061	19928	18806	17688	16589	15491	14402	13326	12259	11199	10150	9108	8073	7047	6027	5012	4003	2998
	18	27012	25812	24632	23483	22309	21161	20018	18886	17759	16652	15543	14447	13363	12290	11223	10169	9122	8085	7054	6031	5015	4004	2998
	19	27157	25950	24760	23601	22419	21261	20109	18966	17831	16715	15597	14493	13401	12321	11248	10188	9136	8094	7061	6036	5017	4005	2998
	20	27298	26086	24886	23717	22528	21360	20200	19047	17904	16779	15652	14540	13440	12353	11274	10209	9152	8105	7068	6040	5020	4006	2998

Analytical results 3000x2000mm

Radius at midspan - analytical results - 3000x2000mm plate																							
	Radius [mm]	25000	24000	23000	22000	21000	20000	19000	18000	17000	16000	15000	14000	13000	12000	11000	10000	9000	8000	7000	6000	5000	4000	3000
Thickness [mm]	4	24977	23968	22960	21955	20951	19949	18949	17949	16951	15954	14958	13962	12967	11972	10977	9982	8987	7991	6995	5998	5000	4002	3001
	5	25120	24098	23078	22061	21046	20033	19023	18014	17008	16002	14998	13996	12994	11994	10994	9995	8996	7997	6999	6000	5001	4002	3002
	6	25264	24228	23196	22167	21141	20118	19097	18079	17064	16051	15039	14030	13022	12016	11011	10008	9005	8003	7002	6002	5002	4002	3002
	7	25407	24358	23313	22273	21236	20202	19172	18144	17120	16099	15080	14064	13050	12038	11028	10020	9014	8009	7006	6004	5002	4002	3002
	8	25550	24488	23431	22379	21330	20286	19246	18209	17176	16147	15121	14098	13078	12060	11045	10033	9023	8015	7010	6006	5003	4002	3003
	9	25693	24618	23549	22485	21425	20370	19320	18274	17233	16195	15161	14132	13105	12082	11063	10046	9032	8021	7013	6007	5004	4002	3003
	10	25836	24748	23667	22591	21520	20455	19394	18339	17289	16243	15202	14165	13133	12104	11080	10059	9041	8027	7017	6009	5004	4003	3003
	11	25979	24878	23784	22696	21615	20539	19469	18404	17345	16292	15243	14199	13161	12126	11097	10072	9051	8034	7020	6011	5005	4003	3004
	12	26122	25008	23902	22802	21710	20623	19543	18469	17402	16340	15284	14233	13188	12149	11114	10084	9060	8040	7024	6013	5006	4003	3004
	13	26265	25139	24020	22908	21804	20707	19617	18534	17458	16388	15325	14267	13216	12171	11131	10097	9069	8046	7028	6015	5006	4003	3004
	14	26408	25269	24137	23014	21899	20792	19692	18599	17514	16436	15365	14301	13244	12193	11148	10110	9078	8052	7031	6016	5007	4003	3004
	15	26551	25399	24255	23120	21994	20876	19766	18664	17571	16484	15406	14335	13271	12215	11165	10123	9087	8058	7035	6018	5008	4003	3005
	16	26694	25529	24373	23226	22089	20960	19840	18729	17627	16533	15447	14369	13299	12237	11183	10136	9096	8064	7039	6020	5009	4004	3005
	17	26837	25659	24491	23332	22183	21044	19915	18794	17683	16581	15488	14403	13327	12259	11200	10149	9105	8070	7042	6022	5009	4004	3005
	18	26980	25789	24608	23438	22278	21129	19989	18859	17739	16629	15528	14437	13355	12281	11217	10161	9114	8076	7046	6024	5010	4004	3006
	19	27123	25919	24726	23544	22373	21213	20063	18924	17796	16677	15569	14471	13382	12303	11234	10174	9124	8082	7049	6026	5011	4004	3006
	20	27266	26049	24844	23650	22468	21297	20138	18989	17852	16726	15610	14505	13410	12325	11251	10187	9133	8088	7053	6027	5011	4004	3006

Validation 3000x2000mm

	Absolute deviation	Minimum deviation	Maximum deviation	Standard deviation
3000x2000mm	0.15%	0.00%	0.53%	0.10%

Radius at midspan - validation analytical results - 2000x2000mm plate																							
	Radius [mm]	25000	24000	23000	22000	21000	20000	19000	18000	17000	16000	15000	14000	13000	12000	11000	10000	9000	8000	7000	6000	5000	4000	3000
Thickness [mm]	4	0.50%	0.49%	0.53%	0.51%	0.49%	0.53%	0.48%	0.50%	0.45%	0.43%	0.42%	0.41%	0.36%	0.33%	0.30%	0.27%	0.23%	0.20%	0.15%	0.11%	0.08%	0.05%	0.03%
	5	0.24%	0.21%	0.26%	0.27%	0.25%	0.30%	0.25%	0.28%	0.25%	0.24%	0.24%	0.23%	0.21%	0.19%	0.16%	0.15%	0.13%	0.12%	0.08%	0.06%	0.04%	0.04%	
	6	0.06%	0.02%	0.06%	0.09%	0.05%	0.12%	0.07%	0.12%	0.08%	0.09%	0.10%	0.09%	0.08%	0.08%	0.06%	0.06%	0.05%	0.04%	0.05%	0.05%	0.01%	0.03%	
	7	0.07%	0.12%	0.09%	0.04%	0.08%	0.02%	0.06%	0.01%	0.05%	0.03%	0.01%	0.02%	0.02%	0.01%	0.02%	0.02%	0.01%	0.01%	0.00%	0.02%	0.01%		
	8	0.15%	0.21%	0.18%	0.13%	0.18%	0.12%	0.16%	0.10%	0.14%	0.12%	0.09%	0.10%	0.09%	0.08%	0.09%	0.07%	0.07%	0.03%	0.01%	0.03%			
	9	0.19%	0.26%	0.24%	0.18%	0.24%	0.18%	0.22%	0.17%	0.21%	0.18%	0.15%	0.16%	0.15%	0.13%	0.13%	0.11%	0.09%	0.07%	0.06%	0.04%			
	10	0.20%	0.28%	0.25%	0.20%	0.27%	0.21%	0.25%	0.20%	0.25%	0.22%	0.19%	0.19%	0.18%	0.16%	0.16%	0.13%	0.12%	0.09%	0.07%				
	11	0.18%	0.26%	0.25%	0.19%	0.26%	0.22%	0.26%	0.22%	0.26%	0.23%	0.21%	0.21%	0.19%	0.18%	0.18%	0.15%	0.12%	0.09%	0.07%				
	12	0.14%	0.23%	0.23%	0.15%	0.24%	0.20%	0.24%	0.21%	0.25%	0.22%	0.21%	0.21%	0.20%	0.16%	0.18%	0.14%	0.12%	0.09%					
	13	0.08%	0.18%	0.18%	0.10%	0.20%	0.16%	0.20%	0.18%	0.22%	0.19%	0.19%	0.20%	0.19%	0.17%	0.15%	0.13%	0.11%						
	14	0.03%	0.13%	0.13%	0.04%	0.14%	0.12%	0.15%	0.14%	0.17%	0.15%	0.15%	0.17%	0.16%	0.14%	0.14%	0.11%	0.09%						
	15	0.03%	0.07%	0.07%	0.02%	0.08%	0.06%	0.09%	0.08%	0.12%	0.09%	0.11%	0.13%	0.12%	0.10%	0.11%	0.08%							
	16	0.07%	0.01%	0.01%	0.08%	0.01%	0.01%	0.01%	0.01%	0.05%	0.03%	0.05%	0.07%	0.07%	0.05%	0.06%								
	17	0.10%	0.04%	0.04%	0.13%	0.06%	0.08%	0.06%	0.06%	0.03%	0.05%	0.02%	0.00%	0.01%	0.00%	0.01%								
	18	0.12%	0.09%	0.09%	0.19%	0.14%	0.15%	0.15%	0.14%	0.11%	0.14%	0.10%	0.07%	0.06%	0.07%									
	19	0.12%	0.12%	0.14%	0.24%	0.20%	0.22%	0.23%	0.22%	0.20%	0.23%	0.18%	0.15%	0.14%	0.14%									
	20	0.12%	0.14%	0.17%	0.28%	0.27%	0.29%	0.31%	0.30%	0.29%	0.32%	0.27%	0.24%	0.22%										

Numerical results 3000x3000mm

Radius at midspan - numerical results - 3000x3000mm plate																								
	Radius [mm]	25000	24000	23000	22000	21000	20000	19000	18000	17000	16000	15000	14000	13000	12000	11000	10000	9000	8000	7000	6000	5000	4000	3000
Thickness [mm]	4	25125	24100	23095	22073	21056	20052	19030	18029	17015	16007	15002	14000	12996	11991	10989	9988	8989	7991	6992	5995	4996	3998	3000
	5	25240	24200	23184	22153	21123	20114	19084	18074	17053	16037	15028	14022	13010	12001	10997	9992	8991	7991	6989	5992	4995	3996	2998
	6	25373	24316	23284	22247	21204	20189	19145	18129	17097	16077	15062	14046	13031	12020	11010	10000	8997	7995	6992	5992	4993	3996	2998
	7	25525	24449	23401	22354	21295	20266	19214	18189	17148	16121	15099	14075	13055	12038	11022	10014	9005	7999	6996	5993	4989	3994	2997
	8	25696	24600	23533	22472	21398	20356	19292	18256	17204	16169	15142	14108	13084	12061	11039	10025	9015	8003	6998	5992	4993	3993	2996
	9	25886	24768	23682	22604	21513	20455	19378	18330	17267	16222	15185	14145	13115	12084	11060	10041	9025	8014	7003	5998	4994	3993	2995
	10	26096	24954	23846	22748	21639	20565	19473	18411	17337	16281	15233	14186	13146	12112	11079	10058	9035	8020	7009	5998	4997	3993	2988
	11	26330	25159	24025	22909	21778	20684	19577	18499	17412	16345	15286	14228	13181	12139	11104	10075	9050	8029	7013	6006	4999	3989	2987
	12	26584	25382	24221	23083	21928	20814	19689	18594	17493	16413	15343	14275	13219	12170	11126	10093	9064	8042	7020	6010	4996	3990	2987
	13	26858	25623	24433	23272	22091	20954	19811	18697	17581	16488	15404	14325	13259	12203	11151	10111	9079	8049	7027	6011	5004	3997	2996
	14	27151	25882	24661	23474	22266	21105	19942	18809	17675	16567	15469	14379	13303	12238	11179	10132	9092	8063	7035	6016	5002	3999	2987
	15	27465	26159	24904	23691	22454	21267	20082	18927	17776	16652	15539	14436	13349	12275	11208	10154	9109	8076	7043	6021	5005	3994	2987
	16	27795	26452	25163	23921	22653	21439	20231	19054	17884	16742	15613	14497	13398	12314	11238	10178	9127	8085	7055	6031	5009	4001	2988
	17	28142	26760	25435	24162	22864	21622	20389	19188	17998	16839	15692	14561	13450	12355	11270	10203	9145	8099	7065	6037	5016	3998	2988
	18	28499	27082	25721	24414	23086	21814	20556	19330	18118	16940	15775	14629	13504	12399	11304	10229	9164	8112	7071	6040	5016	4000	2989
	19	28868	27417	26018	24677	23319	22016	20732	19479	18245	17047	15863	14701	13562	12444	11340	10256	9185	8127	7081	6051	5025	4002	2999
	20	29247	27762	26326	24950	23561	22227	20915	19636	18379	17159	15955	14776	13623	12492	11378	10285	9206	8142	7092	6056	5024	4004	2991

Analytical results 3000x3000mm

Radius at midspan - analytical results - 3000x3000mm plate																								
	Radius [mm]	25000	24000	23000	22000	21000	20000	19000	18000	17000	16000	15000	14000	13000	12000	11000	10000	9000	8000	7000	6000	5000	4000	3000
Thickness [mm]	4	24733	23759	22783	21805	20825	19844	18861	17877	16891	15904	14915	13926	12935	11944	10952	9959	8965	7971	6977	5982	4987	3992	2996
	5	24992	23989	22987	21984	20982	19980	18979	17977	16976	15975	14975	13975	12975	11976	10976	9978	8979	7981	6983	5986	4989	3992	2996
	6	25252	24220	23190	22163	21139	20116	19096	18078	17061	16047	15035	14024	13015	12007	11001	9996	8993	7991	6990	5990	4991	3993	2995
	7	25511	24450	23394	22342	21295	20252	19213	18178	17147	16119	15094	14073	13054	12039	11025	10015	9007	8000	6996	5994	4993	3993	2995
	8	25771	24681	23598	22522	21452	20388	19330	18278	17232	16190	15154	14121	13094	12070	11050	10034	9020	8010	7003	5998	4995	3994	2995
	9	26030	24911	23801	22701	21608	20524	19448	18379	17317	16262	15213	14170	13133	12101	11075	10052	9034	8020	7009	6002	4997	3994	2994
	10	26290	25142	24005	22880	21765	20660	19565	18479	17402	16334	15273	14219	13173	12133	11099	10071	9048	8030	7016	6006	4999	3995	2994
	11	26549	25372	24209	23059	21921	20796	19682	18580	17487	16405	15332	14268	13212	12164	11124	10090	9062	8039	7022	6010	5001	3996	2993
	12	26809	25603	24413	23238	22078	20932	19800	18680	17573	16477	15392	14317	13252	12196	11148	10108	9075	8049	7029	6013	5003	3996	2993
	13	27068	25833	24616	23417	22235	21068	19917	18781	17658	16548	15451	14366	13292	12227	11173	10127	9089	8059	7035	6017	5005	3997	2992
	14	27327	26064	24820	23596	22391	21204	20034	18881	17743	16620	15511	14415	13331	12259	11197	10146	9103	8069	7042	6021	5007	3997	2992
	15	27587	26294	25024	23775	22548	21340	20152	18981	17828	16692	15570	14464	13371	12290	11222	10164	9117	8078	7048	6025	5009	3998	2991
	16	27846	26524	25227	23954	22704	21476	20269	19082	17914	16763	15630	14513	13410	12322	11246	10183	9131	8088	7055	6029	5011	3998	2991
	17	28106	26755	25431	24133	22861	21612	20386	19182	17999	16835	15689	14561	13450	12353	11271	10202	9144	8098	7061	6033	5013	3999	2990
	18	28365	26985	25635	24313	23017	21748	20504	19283	18084	16906	15749	14610	13489	12385	11296	10220	9158	8108	7068	6037	5015	3999	2990
	19	28625	27216	25839	24492	23174	21884	20621	19383	18169	16978	15809	14659	13529	12416	11320	10239	9172	8117	7074	6041	5017	4000	2990
	20	28884	27446	26042	24671	23331	22020	20738	19483	18254	17050	15868	14708	13568	12448	11345	10258	9186	8127	7081	6045	5019	4001	2989

Validation 3000x3000mm

	Absolute deviation	Minimum deviation	Maximum deviation	Standard deviation
3000x3000mm	0.33%	0.00%	1.56%	0.29%

Radius at midspan - validation analytical results - 3000x3000mm plate																								
	Radius [mm]	25000	24000	23000	22000	21000	20000	19000	18000	17000	16000	15000	14000	13000	12000	11000	10000	9000	8000	7000	6000	5000	4000	3000
Thickness [mm]	4	1.56%	1.42%	1.35%	1.21%	1.09%	1.04%	0.89%	0.84%	0.73%	0.65%	0.58%	0.53%	0.46%	0.39%	0.34%	0.29%	0.26%	0.24%	0.21%	0.21%	0.19%	0.17%	0.11%
	5	0.98%	0.87%	0.85%	0.76%	0.67%	0.67%	0.55%	0.53%	0.45%	0.39%	0.36%	0.34%	0.27%	0.21%	0.19%	0.14%	0.14%	0.12%	0.08%	0.10%	0.12%	0.10%	
	6	0.48%	0.39%	0.40%	0.38%	0.31%	0.36%	0.26%	0.28%	0.21%	0.19%	0.18%	0.16%	0.13%	0.11%	0.08%	0.04%	0.05%	0.06%	0.03%	0.04%	0.05%	0.08%	
	7	0.06%	0.00%	0.03%	0.05%	0.00%	0.07%	0.00%	0.06%	0.01%	0.02%	0.03%	0.01%	0.01%	0.01%	0.03%	0.01%	0.02%	0.02%	0.01%	0.01%	0.07%		
	8	0.29%	0.33%	0.27%	0.22%	0.25%	0.16%	0.20%	0.12%	0.16%	0.13%	0.08%	0.10%	0.08%	0.07%	0.10%	0.09%	0.06%	0.09%	0.06%	0.10%			
	9	0.56%	0.58%	0.51%	0.43%	0.44%	0.34%	0.36%	0.27%	0.29%	0.24%	0.19%	0.18%	0.14%	0.14%	0.13%	0.11%	0.10%	0.07%	0.08%	0.07%			
	10	0.74%	0.75%	0.67%	0.58%	0.58%	0.46%	0.47%	0.37%	0.38%	0.33%	0.26%	0.24%	0.21%	0.17%	0.18%	0.13%	0.15%	0.12%	0.10%				
	11	0.83%	0.85%	0.76%	0.65%	0.66%	0.54%	0.54%	0.44%	0.44%	0.37%	0.30%	0.28%	0.24%	0.21%	0.18%	0.14%	0.13%	0.13%	0.14%				
	12	0.85%	0.87%	0.79%	0.67%	0.68%	0.57%	0.56%	0.46%	0.46%	0.39%	0.32%	0.29%	0.25%	0.21%	0.20%	0.15%	0.13%	0.09%					
	13	0.78%	0.82%	0.75%	0.62%	0.65%	0.54%	0.54%	0.44%	0.44%	0.37%	0.31%	0.28%	0.24%	0.20%	0.19%	0.16%	0.11%						
	14	0.65%	0.70%	0.64%	0.52%	0.56%	0.47%	0.46%	0.39%	0.38%	0.32%	0.27%	0.25%	0.21%	0.17%	0.17%	0.13%	0.12%						
	15	0.44%	0.52%	0.48%	0.36%	0.42%	0.34%	0.35%	0.29%	0.29%	0.24%	0.20%	0.19%	0.16%	0.12%	0.13%	0.10%							
	16	0.18%	0.28%	0.26%	0.14%	0.23%	0.17%	0.19%	0.15%	0.17%	0.12%	0.11%	0.11%	0.09%	0.06%	0.07%								
	17	0.13%	0.02%	0.02%	0.12%	0.02%	0.04%	0.01%	0.03%	0.01%	0.02%	0.02%	0.00%	0.00%	0.02%	0.00%								
	18	0.47%	0.36%	0.33%	0.41%	0.30%	0.30%	0.26%	0.24%	0.19%	0.20%	0.17%	0.13%	0.11%	0.11%									
	19	0.84%	0.73%	0.69%	0.75%	0.62%	0.60%	0.53%	0.49%	0.42%	0.40%	0.34%	0.28%	0.25%	0.23%									
	20	1.24%	1.14%	1.08%	1.12%	0.98%	0.93%	0.85%	0.77%	0.68%	0.64%	0.54%	0.46%	0.40%										

Numerical results 4000x1000mm

Radius at midspan - numerical results - 4000x1000mm plate																								
Radius [mm]		25000	24000	23000	22000	21000	20000	19000	18000	17000	16000	15000	14000	13000	12000	11000	10000	9000	8000	7000	6000	5000	4000	3000
Thickness [mm]	4	25120	24109	23100	22090	21080	20071	19062	18056	17049	16042	15036	14031	13025	12021	11018	10014	9011	8009	7007	6005	5003	4002	3001
	5	25156	24144	23133	22119	21105	20096	19085	18075	17066	16057	15048	14041	13035	12029	11023	10019	9015	8012	7009	6006	5004	4003	3002
	6	25191	24176	23165	22148	21133	20122	19108	18096	17083	16073	15063	14053	13045	12037	11030	10024	9019	8014	7011	6008	5005	4003	3002
	7	25224	24207	23194	22175	21159	20147	19129	18116	17102	16089	15075	14065	13056	12045	11037	10030	9023	8018	7013	6009	5006	4004	3002
	8	25255	24234	23220	22204	21183	20169	19150	18135	17119	16106	15091	14078	13064	12055	11044	10035	9028	8021	7015	6011	5007	4005	3003
	9	25280	24259	23245	22227	21204	20190	19170	18154	17135	16121	15105	14090	13077	12064	11052	10042	9031	8025	7017	6013	5008	4005	3003
	10	25304	24280	23265	22248	21224	20209	19188	18170	17152	16136	15118	14102	13087	12073	11059	10048	9037	8028	7021	6014	5010	4006	3003
	11	25323	24300	23284	22267	21241	20226	19204	18186	17167	16150	15131	14112	13098	12082	11068	10055	9043	8032	7024	6016	5011	4007	3004
	12	25341	24316	23300	22284	21257	20240	19219	18199	17180	16162	15142	14125	13108	12091	11075	10061	9048	8037	7027	6018	5012	4008	3004
	13	25356	24331	23314	22298	21271	20254	19232	18212	17192	16174	15153	14135	13117	12100	11083	10068	9054	8041	7030	6021	5013	4008	3005
	14	25370	24344	23327	22311	21283	20265	19244	18223	17204	16184	15163	14144	13126	12107	11090	10074	9059	8044	7033	6023	5015	4009	3005
	15	25381	24356	23338	22322	21294	20276	19255	18233	17214	16194	15172	14153	13134	12115	11097	10080	9064	8049	7036	6025	5016	4010	3006
	16	25391	24366	23347	22332	21304	20285	19265	18243	17223	16202	15181	14161	13142	12122	11103	10086	9069	8053	7039	6027	5018	4011	3006
	17	25400	24375	23356	22341	21313	20294	19273	18251	17231	16210	15188	14169	13149	12129	11109	10091	9073	8057	7043	6030	5019	4011	3006
	18	25408	24383	23364	22348	21321	20302	19281	18258	17239	16217	15196	14176	13156	12135	11115	10097	9078	8061	7046	6032	5021	4013	3007
	19	25415	24390	23371	22355	21328	20308	19288	18265	17246	16224	15202	14182	13162	12141	11120	10102	9083	8064	7049	6035	5023	4013	3007
	20	25421	24397	23377	22362	21334	20315	19294	18271	17252	16230	15208	14188	13168	12146	11126	10107	9087	8069	7052	6037	5024	4014	3008

Analytical results 4000x1000mm

Radius at midspan - analytical results - 4000x1000mm plate																								
Radius [mm]		25000	24000	23000	22000	21000	20000	19000	18000	17000	16000	15000	14000	13000	12000	11000	10000	9000	8000	7000	6000	5000	4000	3000
Thickness [mm]	4	25170	24155	23140	22126	21113	20100	19088	18076	17066	16056	15047	14038	13031	12024	11018	10013	9009	8005	7003	6002	5001	4002	3003
	5	25188	24172	23157	22142	21128	20115	19102	18090	17078	16068	15057	14048	13040	12032	11025	10019	9014	8009	7006	6004	5003	4002	3003
	6	25206	24190	23174	22159	21144	20130	19117	18104	17091	16079	15068	14058	13048	12040	11032	10025	9019	8013	7009	6006	5004	4003	3003
	7	25223	24207	23191	22176	21160	20145	19131	18117	17104	16091	15079	14068	13057	12048	11039	10031	9024	8018	7012	6008	5006	4004	3003
	8	25241	24225	23208	22192	21176	20161	19146	18131	17117	16103	15090	14078	13066	12056	11046	10037	9029	8022	7016	6011	5007	4005	3003
	9	25259	24242	23225	22209	21192	20176	19160	18144	17129	16115	15101	14088	13075	12064	11053	10043	9034	8026	7019	6013	5009	4005	3003
	10	25277	24260	23242	22225	21208	20191	19174	18158	17142	16127	15112	14098	13084	12071	11060	10049	9039	8030	7022	6015	5010	4006	3004
	11	25295	24277	23259	22242	21224	20206	19189	18172	17155	16139	15123	14108	13093	12079	11067	10055	9044	8034	7025	6018	5011	4007	3004
	12	25312	24295	23276	22258	21240	20221	19203	18185	17168	16151	15134	14118	13102	12087	11073	10060	9049	8038	7028	6020	5013	4008	3004
	13	25330	24312	23293	22275	21256	20237	19218	18199	17181	16162	15145	14128	13111	12095	11080	10066	9054	8042	7031	6022	5014	4008	3004
	14	25348	24329	23310	22291	21272	20252	19232	18213	17193	16174	15156	14137	13120	12103	11087	10072	9059	8046	7034	6024	5016	4009	3004
	15	25366	24347	23328	22308	21288	20267	19247	18226	17206	16186	15166	14147	13129	12111	11094	10078	9064	8050	7038	6027	5017	4010	3004
	16	25384	24364	23345	22324	21303	20282	19261	18240	17219	16198	15177	14157	13138	12119	11101	10084	9069	8054	7041	6029	5019	4010	3004
	17	25401	24382	23362	22341	21319	20298	19276	18254	17232	16210	15188	14167	13147	12127	11108	10090	9074	8058	7044	6031	5020	4011	3004
	18	25419	24399	23379	22357	21335	20313	19290	18267	17244	16222	15199	14177	13156	12135	11115	10096	9078	8062	7047	6034	5022	4012	3004
	19	25437	24417	23396	22374	21351	20328	19305	18281	17257	16233	15210	14187	13165	12143	11122	10102	9083	8066	7050	6036	5023	4013	3004
	20	25455	24434	23413	22390	21367	20343	19319	18294	17270	16245	15221	14197	13174	12151	11129	10108	9088	8070	7053	6038	5025	4013	3004

Validation 4000x1000mm

	Absolute deviation	Minimum deviation	Maximum deviation	Standard deviation
4000x1000mm	0.05%	0.00%	0.20%	0.04%

Radius at midspan - validation analytical results - 4000x1000mm plate																								
Radius [mm]		25000	24000	23000	22000	21000	20000	19000	18000	17000	16000	15000	14000	13000	12000	11000	10000	9000	8000	7000	6000	5000	4000	3000
Thickness [mm]	4	0.20%	0.19%	0.17%	0.16%	0.15%	0.14%	0.14%	0.11%	0.10%	0.09%	0.07%	0.05%	0.04%	0.03%	0.00%	0.01%	0.03%	0.04%	0.05%	0.05%	0.04%	0.01%	0.07%
	5	0.13%	0.12%	0.10%	0.11%	0.11%	0.10%	0.09%	0.08%	0.07%	0.07%	0.07%	0.05%	0.04%	0.03%	0.01%	0.00%	0.01%	0.03%	0.03%	0.04%	0.03%	0.01%	
	6	0.06%	0.06%	0.04%	0.05%	0.05%	0.04%	0.04%	0.04%	0.05%	0.04%	0.03%	0.04%	0.03%	0.02%	0.02%	0.01%	0.00%	0.01%	0.02%	0.02%	0.03%	0.00%	
	7	0.00%	0.00%	0.01%	0.00%	0.01%	0.01%	0.01%	0.01%	0.01%	0.01%	0.03%	0.02%	0.01%	0.02%	0.02%	0.01%	0.01%	0.00%	0.01%	0.01%	0.01%		
	8	0.05%	0.04%	0.05%	0.05%	0.03%	0.04%	0.02%	0.02%	0.02%	0.02%	0.01%	0.00%	0.01%	0.01%	0.01%	0.01%	0.01%	0.01%	0.00%	0.00%			
	9	0.08%	0.07%	0.08%	0.08%	0.06%	0.07%	0.05%	0.05%	0.03%	0.04%	0.02%	0.02%	0.01%	0.00%	0.00%	0.01%	0.03%	0.01%	0.02%	0.01%			
	10	0.11%	0.09%	0.10%	0.10%	0.07%	0.09%	0.07%	0.07%	0.06%	0.06%	0.04%	0.03%	0.02%	0.01%	0.00%	0.01%	0.01%	0.02%	0.02%				
	11	0.11%	0.09%	0.11%	0.11%	0.08%	0.10%	0.08%	0.08%	0.07%	0.07%	0.05%	0.03%	0.03%	0.02%	0.01%	0.00%	0.01%	0.02%					
	12	0.11%	0.09%	0.10%	0.11%	0.08%	0.09%	0.08%	0.08%	0.07%	0.07%	0.06%	0.05%	0.04%	0.03%	0.02%	0.01%	0.01%	0.01%					
	13	0.10%	0.08%	0.09%	0.10%	0.07%	0.08%	0.08%	0.07%	0.07%	0.07%	0.06%	0.05%	0.04%	0.04%	0.02%	0.01%	0.00%						
	14	0.08%	0.06%	0.07%	0.09%	0.05%	0.07%	0.06%	0.06%	0.06%	0.06%	0.05%	0.05%	0.04%	0.03%	0.02%	0.01%	0.00%						
	15	0.06%	0.04%	0.04%	0.06%	0.03%	0.04%	0.04%	0.04%	0.05%	0.05%	0.04%	0.04%	0.04%	0.03%	0.02%	0.01%							
	16	0.03%	0.01%	0.01%	0.03%	0.00%	0.02%	0.02%	0.01%	0.02%	0.03%	0.02%	0.03%	0.03%	0.03%	0.02%								
	17	0.00%	0.03%	0.02%	0.00%	0.03%	0.02%	0.01%	0.01%	0.00%	0.00%	0.00%	0.01%	0.02%	0.01%	0.01%								
	18	0.04%	0.07%	0.06%	0.04%	0.07%	0.06%	0.05%	0.05%	0.03%	0.03%	0.02%	0.01%	0.00%	0.00%									
	19	0.09%	0.11%	0.11%	0.08%	0.11%	0.10%	0.08%	0.09%	0.07%	0.06%	0.05%	0.04%	0.02%	0.02%									
	20	0.13%	0.15%	0.15%	0.13%	0.15%	0.14%	0.13%	0.13%	0.10%	0.09%	0.08%	0.06%	0.05%										

Numerical results 4000x2000mm

Radius at midspan - numerical results - 4000x2000mm plate																								
Radius [mm]		25000	24000	23000	22000	21000	20000	19000	18000	17000	16000	15000	14000	13000	12000	11000	10000	9000	8000	7000	6000	5000	4000	3000
Thickness [mm]	4	25055	24054	23050	22047	21045	20040	19038	18034	17032	16028	15027	14024	13020	12018	11016	10013	9011	8009	7007	6006	5004	4002	3001
	5	25069	24069	23063	22055	21051	20047	19043	18039	17035	16031	15027	14026	13023	12020	11017	10015	9013	8011	7009	6006	5005	4004	3001
	6	25094	24086	23087	22070	21063	20061	19050	18046	17040	16036	15032	14029	13025	12022	11018	10016	9015	8012	7009	6007	5005	4004	3002
	7	25124	24113	23112	22090	21080	20076	19062	18057	17048	16043	15037	14032	13027	12025	11020	10018	9015	8013	7010	6008	5006	4004	3002
	8	25164	24147	23142	22118	21101	20097	19077	18070	17058	16052	15044	14037	13031	12027	11022	10019	9016	8013	7011	6009	5006	4005	3003
	9	25210	24187	23180	22149	21128	20122	19096	18088	17071	16063	15052	14043	13036	12030	11025	10020	9017	8014	7011	6009	5006	4005	3003
	10	25260	24232	23220	22185	21158	20149	19119	18107	17087	16077	15062	14051	13042	12035	11028	10022	9018	8016	7011	6009	5007	4006	3004
	11	25315	24280	23265	22224	21192	20180	19144	18129	17105	16092	15074	14060	13049	12040	11032	10025	9020	8015	7012	6010	5007	4006	3003
	12	25373	24331	23309	22266	21228	20211	19172	18152	17125	16110	15087	14071	13057	12046	11036	10029	9022	8017	7013	6009	5007	4005	3004
	13	25432	24385	23359	22309	21267	20246	19202	18178	17146	16128	15102	14083	13067	12053	11042	10032	9024	8020	7013	6010	5007	4005	3003
	14	25494	24440	23408	22356	21307	20282	19233	18205	17170	16149	15119	14096	13077	12061	11048	10037	9027	8020	7014	6010	5007	4005	3003
	15	25556	24497	23459	22404	21349	20318	19266	18234	17194	16170	15136	14110	13089	12070	11055	10041	9031	8022	7015	6012	5008	4006	3004
	16	25619	24553	23511	22452	21391	20356	19300	18263	17220	16192	15154	14126	13101	12080	11061	10046	9034	8024	7018	6012	5007	4005	3003
	17	25681	24610	23562	22500	21435	20395	19335	18293	17247	16215	15173	14142	13114	12090	11070	10052	9038	8027	7019	6012	5008	4006	3003
	18	25742	24667	23614	22549	21478	20434	19370	18324	17274	16239	15195	14158	13128	12101	11078	10059	9043	8030	7020	6013	5010	4005	3003
	19	25803	24723	23665	22598	21522	20473	19406	18356	17302	16263	15214	14176	13142	12112	11087	10065	9048	8033	7022	6014	5008	4005	3004
	20	25863	24778	23716	22646	21566	20512	19442	18388	17331	16287	15235	14194	13157	12124	11096	10073	9053	8036	7024	6015	5009	4007	3003

Analytical results 4000x2000mm

Radius at midspan - analytical results - 4000x2000mm plate																								
Radius [mm]		25000	24000	23000	22000	21000	20000	19000	18000	17000	16000	15000	14000	13000	12000	11000	10000	9000	8000	7000	6000	5000	4000	3000
Thickness [mm]	4	24980	23981	22982	21983	20985	19987	18989	17991	16993	15995	14997	13999	13001	12003	11004	10005	9006	8007	7007	6006	5005	4004	3002
	5	25034	24029	23025	22022	21019	20017	19015	18014	17012	16011	15011	14010	13010	12009	11009	10009	9008	8008	7007	6007	5005	4004	3002
	6	25087	24077	23069	22061	21054	20047	19041	18036	17032	16028	15024	14021	13019	12016	11014	10012	9011	8009	7008	6007	5005	4004	3003
	7	25140	24125	23112	22099	21088	20077	19068	18059	17051	16044	15038	14032	13027	12023	11019	10016	9013	8011	7009	6007	5006	4004	3003
	8	25193	24174	23155	22138	21122	20108	19094	18082	17071	16061	15052	14044	13036	12030	11024	10020	9016	8012	7009	6007	5006	4005	3004
	9	25247	24222	23198	22177	21157	20138	19121	18105	17090	16077	15065	14055	13045	12037	11029	10023	9018	8014	7010	6007	5006	4005	3004
	10	25300	24270	23242	22215	21191	20168	19147	18128	17110	16094	15079	14066	13054	12044	11035	10027	9020	8015	7011	6008	5006	4005	3005
	11	25353	24318	23285	22254	21225	20198	19174	18151	17129	16110	15093	14077	13063	12050	11040	10030	9023	8016	7011	6008	5006	4005	3005
	12	25406	24366	23328	22293	21260	20229	19200	18173	17149	16127	15106	14088	13072	12057	11045	10034	9025	8018	7012	6008	5006	4005	3006
	13	25460	24414	23372	22332	21294	20259	19226	18196	17169	16143	15120	14099	13081	12064	11050	10037	9027	8019	7013	6008	5006	4005	3006
	14	25513	24463	23415	22370	21328	20289	19253	18219	17188	16160	15134	14110	13089	12071	11055	10041	9030	8020	7013	6009	5006	4005	3007
	15	25566	24511	23458	22409	21363	20319	19279	18242	17208	16176	15147	14121	13098	12078	11060	10045	9032	8022	7014	6009	5006	4006	3007
	16	25620	24559	23502	22448	21397	20350	19306	18265	17227	16193	15161	14133	13107	12085	11065	10048	9034	8023	7015	6009	5006	4006	3008
	17	25673	24607	23545	22486	21431	20380	19332	18288	17247	16209	15175	14144	13116	12091	11070	10052	9037	8025	7016	6009	5006	4006	3008
	18	25726	24655	23588	22525	21466	20410	19358	18310	17266	16225	15188	14155	13125	12098	11075	10055	9039	8026	7016	6010	5006	4006	3009
	19	25779	24703	23631	22564	21500	20440	19385	18333	17286	16242	15202	14166	13134	12105	11080	10059	9041	8027	7017	6010	5006	4006	3009
	20	25833	24751	23675	22602	21534	20471	19411	18356	17305	16258	15216	14177	13142	12112	11085	10063	9044	8029	7018	6010	5006	4006	3010

Validation 4000x2000mm

	Absolute deviation	Minimum deviation	Maximum deviation	Standard deviation
4000x2000mm	0.08%	0.00%	0.30%	0.06%

Radius at midspan - validation analytical results - 4000x2000mm plate																								
Radius [mm]		25000	24000	23000	22000	21000	20000	19000	18000	17000	16000	15000	14000	13000	12000	11000	10000	9000	8000	7000	6000	5000	4000	3000
Thickness [mm]	4	0.30%	0.30%	0.30%	0.29%	0.29%	0.26%	0.26%	0.24%	0.23%	0.21%	0.20%	0.18%	0.15%	0.13%	0.11%	0.08%	0.06%	0.03%	0.01%	0.01%	0.03%	0.04%	0.03%
	5	0.14%	0.17%	0.17%	0.15%	0.15%	0.15%	0.15%	0.14%	0.13%	0.12%	0.11%	0.11%	0.10%	0.09%	0.07%	0.06%	0.05%	0.03%	0.02%	0.00%	0.01%	0.01%	
	6	0.03%	0.04%	0.08%	0.04%	0.04%	0.07%	0.05%	0.06%	0.05%	0.05%	0.05%	0.06%	0.05%	0.05%	0.04%	0.04%	0.04%	0.03%	0.02%	0.01%	0.00%	0.01%	
	7	0.07%	0.05%	0.00%	0.04%	0.04%	0.01%	0.03%	0.01%	0.02%	0.01%	0.01%	0.01%	0.00%	0.01%	0.00%	0.02%	0.02%	0.02%	0.02%	0.01%	0.01%		
	8	0.11%	0.11%	0.06%	0.09%	0.10%	0.05%	0.09%	0.06%	0.08%	0.06%	0.05%	0.05%	0.04%	0.03%	0.02%	0.01%	0.00%	0.01%	0.02%	0.02%			
	9	0.15%	0.14%	0.08%	0.13%	0.14%	0.08%	0.13%	0.10%	0.12%	0.09%	0.09%	0.08%	0.07%	0.06%	0.04%	0.03%	0.00%	0.00%	0.01%	0.02%			
	10	0.16%	0.16%	0.09%	0.14%	0.16%	0.09%	0.15%	0.12%	0.14%	0.10%	0.11%	0.10%	0.09%	0.07%	0.06%	0.04%	0.02%	0.01%	0.01%				
	11	0.15%	0.16%	0.09%	0.14%	0.16%	0.09%	0.15%	0.12%	0.15%	0.11%	0.12%	0.12%	0.11%	0.09%	0.07%	0.05%	0.03%	0.01%	0.00%				
	12	0.13%	0.14%	0.08%	0.12%	0.15%	0.09%	0.15%	0.12%	0.14%	0.10%	0.13%	0.12%	0.11%	0.09%	0.07%	0.05%	0.03%	0.01%					
	13	0.11%	0.12%	0.05%	0.10%	0.13%	0.06%	0.13%	0.10%	0.13%	0.09%	0.12%	0.12%	0.10%	0.09%	0.07%	0.06%	0.03%						
	14	0.07%	0.09%	0.03%	0.06%	0.10%	0.04%	0.10%	0.08%	0.11%	0.06%	0.10%	0.10%	0.09%	0.08%	0.06%	0.04%	0.03%						
	15	0.04%	0.06%	0.00%	0.02%	0.07%	0.01%	0.07%	0.05%	0.08%	0.03%	0.08%	0.08%	0.07%	0.06%	0.05%	0.04%							
	16	0.00%	0.02%	0.04%	0.02%	0.03%	0.03%	0.03%	0.01%	0.04%	0.00%	0.04%	0.05%	0.05%	0.04%	0.03%								
	17	0.03%	0.01%	0.07%	0.06%	0.02%	0.07%	0.01%	0.03%	0.00%	0.04%	0.01%	0.01%	0.01%	0.01%	0.00%								
	18	0.06%	0.05%	0.11%	0.11%	0.06%	0.12%	0.06%	0.08%	0.05%	0.08%	0.04%	0.03%	0.02%	0.02%									
	19	0.09%	0.08%	0.14%	0.15%	0.10%	0.16%	0.11%	0.12%	0.09%	0.13%	0.08%	0.07%	0.07%										
	20	0.12%	0.11%	0.17%	0.19%	0.14%	0.20%	0.16%	0.17%	0.15%	0.17%	0.13%	0.12%	0.11%										

Numerical results 4000x3000mm

Radius at midspan - numerical results - 4000x3000mm plate																								
	Radius [mm]	25000	24000	23000	22000	21000	20000	19000	18000	17000	16000	15000	14000	13000	12000	11000	10000	9000	8000	7000	6000	5000	4000	3000
Thickness [mm]	4	25002	24000	23005	22005	20999	20004	19001	18003	17002	16003	15003	14004	13004	12004	11004	10004	9004	8004	7004	6004	5003	4002	3001
	5	25020	24027	23025	22012	21014	20010	19007	18007	17006	16004	15006	14004	13001	12004	11003	10004	9004	8004	7003	6004	5003	4002	3000
	6	25046	24045	23053	22030	21025	20028	19015	18021	17009	16008	15007	14003	13003	12004	11002	10003	9003	8002	7001	6003	5003	4001	3002
	7	25083	24075	23084	22053	21045	20045	19030	18032	17019	16016	15012	14008	13004	12004	11002	10002	9001	8002	7002	6002	5003	4002	3002
	8	25124	24110	23113	22083	21068	20071	19046	18045	17029	16027	15021	14014	13008	12005	11003	10001	9003	8000	7000	6001	5000	4002	3001
	9	25171	24152	23153	22115	21097	20094	19066	18064	17044	16039	15030	14019	13013	12011	11006	10002	9001	8002	6999	6001	4999	4002	3001
	10	25226	24200	23193	22152	21128	20123	19090	18083	17060	16054	15039	14028	13020	12017	11009	10005	9001	8002	6999	5998	5002	3999	3002
	11	25283	24251	23241	22193	21163	20154	19116	18106	17079	16069	15052	14039	13028	12023	11014	10008	9003	8001	6999	6000	4999	3998	3001
	12	25347	24306	23288	22238	21202	20191	19145	18129	17100	16088	15066	14050	13038	12027	11022	10011	9008	8005	6999	6001	4996	4000	2998
	13	25415	24367	23342	22285	21242	20225	19178	18157	17122	16106	15082	14063	13048	12035	11025	10015	9008	8004	7000	5997	4996	3998	3000
	14	25487	24430	23398	22336	21286	20263	19209	18187	17147	16127	15098	14076	13058	12043	11031	10020	9012	8005	7001	5997	4996	3995	3000
	15	25564	24498	23458	22390	21333	20304	19245	18215	17174	16149	15116	14091	13070	12052	11038	10025	9015	8012	7007	5998	4996	4000	2999
	16	25645	24570	23521	22448	21382	20347	19282	18247	17200	16173	15135	14106	13083	12062	11046	10031	9019	8010	7004	5998	4999	3994	2999
	17	25730	24645	23588	22507	21435	20392	19322	18280	17228	16198	15155	14123	13096	12075	11054	10037	9024	8013	7011	6005	5002	4000	2998
	18	25818	24724	23658	22570	21489	20440	19364	18316	17259	16224	15176	14143	13110	12084	11063	10044	9029	8016	7007	6003	4996	4000	2998
	19	25909	24805	23730	22636	21546	20489	19407	18353	17291	16251	15199	14159	13127	12096	11072	10051	9038	8020	7013	6002	4996	3993	2998
	20	26004	24889	23805	22703	21605	20541	19452	18392	17324	16279	15222	14178	13140	12108	11081	10058	9039	8024	7011	6003	4997	3993	2999

Analytical results 4000x3000mm

Radius at midspan - analytical results - 4000x3000mm plate																								
	Radius [mm]	25000	24000	23000	22000	21000	20000	19000	18000	17000	16000	15000	14000	13000	12000	11000	10000	9000	8000	7000	6000	5000	4000	3000
Thickness [mm]	4	24900	23909	22918	21926	20934	19941	18948	17955	16961	15966	14972	13976	12981	11984	10988	9991	8994	7996	6998	6000	5002	4003	3004
	5	24963	23966	22968	21971	20973	19975	18977	17980	16982	15984	14986	13988	12990	11991	10993	9995	8996	7998	6999	6000	5001	4002	3003
	6	25027	24022	23018	22015	21012	20009	19006	18004	17003	16001	15000	13999	12998	11998	10998	9998	8998	7999	6999	6000	5001	4002	3003
	7	25090	24079	23069	22059	21050	20042	19035	18029	17023	16018	15014	14010	13007	12005	11003	10001	9000	8000	7000	6000	5001	4002	3003
	8	25154	24136	23119	22103	21089	20076	19064	18054	17044	16036	15028	14022	13016	12012	11008	10005	9003	8001	7000	6000	5000	4001	3003
	9	25218	24192	23169	22148	21128	20110	19093	18078	17065	16053	15042	14033	13025	12018	11013	10008	9005	8002	7001	6000	5000	4001	3002
	10	25281	24249	23219	22192	21167	20143	19122	18103	17086	16070	15057	14045	13034	12025	11018	10012	9007	8003	7001	6000	5000	4000	3002
	11	25345	24306	23270	22236	21205	20177	19151	18128	17107	16088	15071	14056	13043	12032	11023	10015	9009	8005	7002	6000	4999	4000	3002
	12	25408	24363	23320	22280	21244	20211	19180	18153	17127	16105	15085	14067	13052	12039	11028	10019	9011	8006	7002	6000	4999	4000	3001
	13	25472	24419	23370	22325	21283	20244	19209	18177	17148	16122	15099	14079	13061	12046	11033	10022	9014	8007	7002	6000	4999	3999	3001
	14	25536	24476	23420	22369	21322	20278	19238	18202	17169	16140	15113	14090	13070	12052	11038	10025	9016	8008	7003	6000	4998	3999	3001
	15	25599	24533	23471	22413	21360	20312	19267	18227	17190	16157	15128	14102	13079	12059	11043	10029	9018	8009	7003	6000	4998	3998	3001
	16	25663	24589	23521	22458	21399	20345	19296	18251	17211	16174	15142	14113	13088	12066	11048	10032	9020	8011	7004	6000	4998	3998	3000
	17	25726	24646	23571	22502	21438	20379	19325	18276	17232	16192	15156	14124	13097	12073	11053	10036	9022	8012	7004	5999	4997	3998	3000
	18	25790	24703	23621	22546	21477	20413	19354	18301	17252	16209	15170	14136	13106	12080	11058	10039	9024	8013	7005	5999	4997	3997	3000
	19	25854	24759	23672	22590	21515	20446	19383	18325	17273	16226	15184	14147	13115	12086	11063	10043	9027	8014	7005	5999	4997	3997	2999
	20	25917	24816	23722	22635	21554	20480	19412	18350	17294	16244	15198	14158	13123	12093	11067	10046	9029	8015	7006	5999	4996	3996	2999

Validation 4000x3000mm

	Absolute deviation	Minimum deviation	Maximum deviation	Standard deviation
4000x3000mm	0.10%	0.00%	0.41%	0.08%

Radius at midspan - validation analytical results - 4000x3000mm plate																								
	Radius [mm]	25000	24000	23000	22000	21000	20000	19000	18000	17000	16000	15000	14000	13000	12000	11000	10000	9000	8000	7000	6000	5000	4000	3000
Thickness [mm]	4	0.41%	0.38%	0.38%	0.36%	0.31%	0.31%	0.28%	0.27%	0.24%	0.23%	0.21%	0.20%	0.18%	0.16%	0.14%	0.13%	0.11%	0.10%	0.08%	0.06%	0.02%	0.02%	0.07%
	5	0.23%	0.26%	0.25%	0.19%	0.20%	0.18%	0.15%	0.15%	0.14%	0.12%	0.13%	0.12%	0.09%	0.11%	0.09%	0.10%	0.09%	0.08%	0.05%	0.06%	0.04%	0.02%	
	6	0.08%	0.09%	0.15%	0.07%	0.07%	0.10%	0.04%	0.09%	0.04%	0.05%	0.04%	0.03%	0.03%	0.05%	0.04%	0.05%	0.05%	0.04%	0.03%	0.04%	0.04%		
	7	0.03%	0.02%	0.07%	0.03%	0.03%	0.01%	0.03%	0.01%	0.02%	0.01%	0.02%	0.02%	0.02%	0.00%	0.01%	0.01%	0.01%	0.03%	0.04%	0.03%	0.04%		
	8	0.12%	0.11%	0.02%	0.09%	0.10%	0.02%	0.10%	0.05%	0.09%	0.05%	0.05%	0.06%	0.06%	0.06%	0.04%	0.04%	0.00%	0.02%	0.01%	0.01%			
	9	0.18%	0.17%	0.07%	0.15%	0.15%	0.08%	0.14%	0.08%	0.12%	0.09%	0.08%	0.10%	0.09%	0.06%	0.06%	0.06%	0.05%	0.00%	0.03%	0.02%			
	10	0.22%	0.20%	0.11%	0.18%	0.18%	0.10%	0.17%	0.11%	0.15%	0.10%	0.12%	0.12%	0.11%	0.07%	0.08%	0.07%	0.07%	0.02%	0.04%				
	11	0.24%	0.23%	0.12%	0.20%	0.20%	0.11%	0.18%	0.12%	0.16%	0.11%	0.12%	0.12%	0.11%	0.08%	0.08%	0.08%	0.06%	0.05%	0.04%				
	12	0.24%	0.23%	0.14%	0.19%	0.20%	0.10%	0.18%	0.13%	0.16%	0.11%	0.12%	0.12%	0.11%	0.10%	0.05%	0.08%	0.03%	0.01%					
	13	0.23%	0.22%	0.12%	0.18%	0.19%	0.09%	0.16%	0.11%	0.15%	0.10%	0.11%	0.11%	0.10%	0.09%	0.07%	0.07%	0.06%						
	14	0.19%	0.19%	0.09%	0.15%	0.17%	0.07%	0.15%	0.08%	0.13%	0.08%	0.10%	0.10%	0.09%	0.08%	0.06%	0.05%	0.04%						
	15	0.14%	0.14%	0.05%	0.10%	0.13%	0.04%	0.12%	0.06%	0.09%	0.05%	0.08%	0.08%	0.07%	0.06%	0.04%	0.04%							
	16	0.07%	0.08%	0.00%	0.04%	0.08%	0.01%	0.07%	0.02%	0.06%	0.01%	0.04%	0.05%	0.04%	0.03%	0.01%								
	17	0.01%	0.00%	0.07%	0.02%	0.01%	0.07%	0.02%	0.02%	0.02%	0.04%	0.00%	0.01%	0.00%	0.02%	0.02%								
	18	0.11%	0.08%	0.15%	0.11%	0.06%	0.13%	0.05%	0.08%	0.04%	0.09%	0.04%	0.05%	0.04%	0.04%									
	19	0.22%	0.18%	0.25%	0.20%	0.14%	0.21%	0.12%	0.15%	0.10%	0.15%	0.10%	0.08%	0.10%	0.08%									
	20	0.33%	0.29%	0.35%	0.30%	0.24%	0.30%	0.21%	0.23%	0.17%	0.22%	0.15%	0.14%	0.13%										

Numerical results 5000x1000mm

Radius at midspan - numerical results - 5000x1000mm plate																								
	Radius [mm]	25000	24000	23000	22000	21000	20000	19000	18000	17000	16000	15000	14000	13000	12000	11000	10000	9000	8000	7000	6000	5000	4000	3000
Thickness [mm]	4	25077	24069	23060	22056	21050	20044	19039	18034	17029	16025	15021	14018	13014	12008	11010	10008	9007	8005	7004	6001	5002	4003	3001
	5	25099	24091	23083	22075	21068	20060	19053	18047	17041	16035	15030	14025	13021	12017	11014	10012	9009	8006	7005	6003	5002	4002	3001
	6	25121	24112	23103	22094	21084	20076	19068	18060	17052	16045	15039	14033	13028	12023	11018	10014	9011	8009	7006	6004	5003	4000	3001
	7	25140	24130	23123	22111	21100	20091	19082	18071	17064	16056	15048	14042	13034	12028	11023	10018	9014	8011	7007	6005	5003	4002	3001
	8	25157	24146	23139	22126	21115	20105	19095	18085	17075	16063	15057	14049	13041	12034	11028	10022	9016	8013	7010	6007	5004	4002	3021
	9	25171	24160	23153	22141	21127	20118	19107	18096	17086	16075	15066	14057	13048	12040	11033	10026	9020	8015	7011	6008	5005	4003	3002
	10	25184	24173	23165	22153	21139	20129	19118	18106	17096	16084	15074	14064	13055	12046	11038	10030	9023	8018	7013	6009	5006	4004	3002
	11	25196	24184	23176	22164	21149	20139	19128	18115	17105	16092	15082	14072	13061	12052	11043	10034	9027	8020	7015	6010	5007	4004	3002
	12	25206	24194	23186	22174	21158	20148	19137	18123	17114	16100	15089	14078	13067	12057	11047	10038	9030	8023	7017	6012	5008	4004	3002
	13	25215	24202	23194	22183	21166	20156	19145	18130	17122	16107	15096	14084	13073	12062	11052	10042	9034	8026	7019	6013	5008	4005	3003
	14	25223	24210	23202	22191	21174	20163	19152	18137	17128	16113	15102	14090	13078	12067	11056	10046	9037	8028	7021	6014	5009	4006	3003
	15	25229	24216	23208	22197	21180	20169	19159	18143	17134	16119	15108	14095	13083	12072	11061	10050	9040	8031	7023	6016	5010	4006	3004
	16	25235	24222	23214	22203	21186	20175	19165	18149	17140	16124	15113	14100	13088	12076	11065	10054	9043	8034	7025	6017	5011	4007	3004
	17	25241	24228	23219	22209	21191	20180	19170	18154	17144	16129	15118	14105	13092	12080	11068	10057	9046	8036	7027	6019	5012	4007	3004
	18	25246	24233	23223	22213	21196	20184	19174	18158	17149	16133	15123	14109	13096	12084	11072	10060	9049	8039	7029	6020	5013	4008	3005
	19	25250	24237	23227	22218	21200	20188	19179	18162	17153	16137	15127	14112	13100	12087	11075	10064	9052	8041	7031	6022	5015	4009	3005
	20	25254	24241	23231	22221	21204	20192	19182	18166	17156	16141	15130	14116	13103	12090	11078	10066	9054	8043	7033	6023	5016	4009	3005

Analytical results 5000x1000mm

Radius at midspan - analytical results - 5000x1000mm plate																								
	Radius [mm]	25000	24000	23000	22000	21000	20000	19000	18000	17000	16000	15000	14000	13000	12000	11000	10000	9000	8000	7000	6000	5000	4000	3000
Thickness [mm]	4	25107	24098	23089	22080	21071	20063	19056	18048	17041	16035	15029	14024	13019	12014	11011	10007	9005	8003	7001	6001	5001	4002	3003
	5	25118	24108	23099	22090	21081	20073	19064	18057	17049	16042	15036	14030	13024	12019	11015	10011	9008	8005	7003	6002	5002	4002	3003
	6	25128	24118	23109	22100	21091	20082	19073	18065	17057	16050	15043	14036	13030	12024	11019	10015	9011	8008	7005	6004	5003	4003	3003
	7	25138	24129	23119	22110	21100	20091	19082	18073	17065	16057	15049	14042	13036	12029	11024	10019	9014	8011	7007	6005	5004	4003	3003
	8	25149	24139	23129	22119	21110	20100	19091	18082	17073	16064	15056	14048	13041	12034	11028	10022	9017	8013	7009	6007	5005	4003	3003
	9	25159	24149	23139	22129	21119	20109	19100	18090	17081	16072	15063	14055	13047	12039	11033	10026	9021	8016	7011	6008	5006	4004	3003
	10	25170	24160	23149	22139	21129	20119	19108	18098	17089	16079	15070	14061	13052	12044	11037	10030	9024	8018	7013	6010	5006	4004	3003
	11	25180	24170	23160	22149	21138	20128	19117	18107	17096	16086	15076	14067	13058	12049	11041	10034	9027	8021	7015	6011	5007	4005	3003
	12	25191	24180	23170	22159	21148	20137	19126	18115	17104	16094	15083	14073	13064	12054	11046	10038	9030	8023	7017	6012	5008	4005	3003
	13	25201	24191	23180	22169	21158	20146	19135	18123	17112	16101	15090	14079	13069	12059	11050	10041	9033	8026	7019	6014	5009	4006	3003
	14	25211	24201	23190	22179	21167	20155	19144	18132	17120	16108	15097	14086	13075	12064	11054	10045	9036	8029	7021	6015	5010	4006	3003
	15	25222	24211	23200	22189	21177	20165	19152	18140	17128	16116	15104	14092	13080	12069	11059	10049	9040	8031	7024	6017	5011	4006	3003
	16	25232	24222	23210	22199	21186	20174	19161	18148	17136	16123	15110	14098	13086	12074	11063	10053	9043	8034	7026	6018	5012	4007	3003
	17	25243	24232	23220	22208	21196	20183	19170	18157	17144	16130	15117	14104	13091	12079	11068	10056	9046	8036	7028	6020	5013	4007	3003
	18	25253	24242	23231	22218	21206	20192	19179	18165	17151	16138	15124	14110	13097	12084	11072	10060	9049	8039	7030	6021	5014	4008	3003
	19	25264	24253	23241	22228	21215	20202	19188	18174	17159	16145	15131	14117	13103	12089	11076	10064	9052	8041	7032	6023	5015	4008	3003
	20	25274	24263	23251	22238	21225	20211	19196	18182	17167	16152	15137	14123	13108	12094	11081	10068	9055	8044	7034	6024	5016	4009	3003

Validation 5000x1000mm

	Absolute deviation	Minimum deviation	Maximum deviation	Standard deviation
5000x1000mm	0.03%	0.00%	0.12%	0.03%

Radius at midspan - validation analytical results - 5000x1000mm plate																								
	Radius [mm]	25000	24000	23000	22000	21000	20000	19000	18000	17000	16000	15000	14000	13000	12000	11000	10000	9000	8000	7000	6000	5000	4000	3000
Thickness [mm]	4	0.12%	0.12%	0.12%	0.11%	0.10%	0.09%	0.09%	0.08%	0.07%	0.06%	0.05%	0.04%	0.04%	0.05%	0.00%	0.01%	0.03%	0.02%	0.03%	0.00%	0.02%	0.04%	0.08%
	5	0.07%	0.07%	0.07%	0.07%	0.06%	0.06%	0.06%	0.06%	0.05%	0.04%	0.04%	0.03%	0.03%	0.02%	0.01%	0.00%	0.01%	0.01%	0.02%	0.02%	0.01%	0.01%	
	6	0.03%	0.03%	0.02%	0.03%	0.03%	0.03%	0.03%	0.03%	0.03%	0.03%	0.03%	0.02%	0.02%	0.01%	0.01%	0.01%	0.00%	0.01%	0.01%	0.01%	0.00%	0.07%	
	7	0.01%	0.01%	0.02%	0.01%	0.00%	0.00%	0.00%	0.01%	0.01%	0.01%	0.01%	0.00%	0.01%	0.01%	0.01%	0.01%	0.00%	0.00%	0.01%	0.00%	0.01%		
	8	0.03%	0.03%	0.04%	0.03%	0.02%	0.03%	0.02%	0.02%	0.02%	0.01%	0.01%	0.00%	0.00%	0.00%	0.00%	0.00%	0.02%	0.00%	0.00%	0.00%			
	9	0.05%	0.05%	0.06%	0.05%	0.04%	0.04%	0.04%	0.03%	0.03%	0.02%	0.02%	0.02%	0.01%	0.01%	0.01%	0.00%	0.00%	0.01%	0.01%	0.01%			
	10	0.06%	0.05%	0.07%	0.06%	0.05%	0.05%	0.05%	0.04%	0.04%	0.03%	0.03%	0.03%	0.02%	0.01%	0.01%	0.00%	0.00%	0.01%	0.01%				
	11	0.06%	0.06%	0.07%	0.07%	0.05%	0.06%	0.06%	0.04%	0.05%	0.04%	0.04%	0.03%	0.02%	0.02%	0.01%	0.01%	0.00%	0.01%	0.01%				
	12	0.06%	0.06%	0.07%	0.07%	0.05%	0.05%	0.06%	0.04%	0.06%	0.04%	0.04%	0.04%	0.03%	0.02%	0.02%	0.01%	0.00%	0.01%					
	13	0.05%	0.05%	0.06%	0.06%	0.04%	0.05%	0.05%	0.04%	0.06%	0.04%	0.04%	0.04%	0.03%	0.02%	0.02%	0.01%	0.00%						
	14	0.04%	0.04%	0.05%	0.05%	0.03%	0.04%	0.05%	0.03%	0.05%	0.03%	0.04%	0.03%	0.03%	0.02%	0.02%	0.01%	0.01%						
	15	0.03%	0.02%	0.03%	0.04%	0.02%	0.02%	0.03%	0.02%	0.04%	0.02%	0.03%	0.03%	0.02%	0.02%	0.02%	0.01%							
	16	0.01%	0.00%	0.02%	0.02%	0.00%	0.00%	0.02%	0.00%	0.02%	0.01%	0.02%	0.02%	0.01%	0.01%	0.01%								
	17	0.01%	0.02%	0.01%	0.00%	0.02%	0.02%	0.00%	0.02%	0.00%	0.01%	0.01%	0.00%	0.00%	0.01%	0.01%								
	18	0.03%	0.04%	0.03%	0.02%	0.05%	0.04%	0.02%	0.04%	0.02%	0.03%	0.01%	0.01%	0.01%	0.00%									
	19	0.05%	0.07%	0.06%	0.05%	0.07%	0.07%	0.05%	0.06%	0.04%	0.05%	0.03%	0.03%	0.02%	0.02%									
	20	0.08%	0.09%	0.09%	0.08%	0.10%	0.09%	0.07%	0.09%	0.06%	0.07%	0.05%	0.05%	0.04%										

Numerical results 5000x2000mm

Radius at midspan - numerical results - 5000x2000mm plate																							
Radius [mm]	25000	24000	23000	22000	21000	20000	19000	18000	17000	16000	15000	14000	13000	12000	11000	10000	9000	8000	7000	6000	5000	4000	3000
Thickness [mm] 4	25061	24054	23042	22045	21044	20035	19034	18024	17026	16024	15021	14017	13015	12013	11011	10009	9007	8007	7004	6003	5002	4002	3002
5	25067	24058	23054	22053	21048	20039	19040	18037	17032	16027	15026	14021	13018	12015	11013	10011	9009	8007	7005	6004	5002	4002	3002
6	25075	24069	23060	22059	21055	20047	19045	18041	17035	16033	15031	14024	13021	12019	11016	10013	9011	8009	7007	6005	5003	4002	3002
7	25086	24080	23072	22067	21061	20054	19051	18045	17040	16036	15032	14027	13024	12021	11017	10015	9012	8010	7009	6006	5004	4003	3001
8	25100	24091	23086	22077	21070	20062	19056	18051	17044	16040	15035	14029	13026	12023	11020	10016	9013	8011	7009	6006	5005	4003	3002
9	25117	24109	23104	22089	21079	20072	19064	18057	17050	16045	15039	14033	13028	12025	11021	10018	9016	8012	7009	6007	5005	4003	3002
10	25138	24128	23124	22104	21092	20085	19072	18065	17057	16049	15043	14037	13032	12027	11023	10019	9016	8013	7010	6008	5006	4002	3004
11	25162	24150	23145	22121	21106	20098	19084	18074	17064	16056	15048	14041	13035	12030	11025	10021	9017	8014	7011	6008	5007	4005	3006
12	25188	24174	23169	22140	21122	20113	19096	18084	17074	16062	15054	14046	13039	12032	11027	10022	9018	8015	7012	6009	5007	4005	3004
13	25216	24199	23193	22161	21140	20129	19110	18095	17084	16071	15060	14051	13043	12036	11029	10024	9020	8015	7012	6010	5007	4004	3003
14	25245	24226	23218	22184	21159	20147	19125	18108	17095	16080	15068	14058	13047	12039	11033	10026	9020	8016	7013	6010	5008	4005	3003
15	25277	24254	23245	22207	21179	20165	19141	18121	17107	16089	15076	14064	13052	12043	11035	10027	9022	8017	7013	6010	5007	4005	3003
16	25308	24283	23272	22231	21200	20184	19158	18135	17120	16099	15084	14072	13058	12047	11038	10030	9024	8018	7014	6011	5008	4006	3004
17	25340	24312	23299	22257	21222	20204	19175	18150	17133	16110	15094	14079	13064	12052	11041	10033	9025	8020	7015	6012	5008	4006	3004
18	25372	24342	23326	22282	21244	20224	19193	18166	17147	16122	15103	14087	13070	12057	11045	10035	9027	8021	7016	6011	5008	4006	3005
19	25404	24371	23353	22307	21266	20245	19212	18182	17161	16134	15114	14096	13077	12062	11049	10038	9029	8022	7016	6012	5008	4006	3004
20	25436	24400	23380	22333	21289	20265	19231	18198	17176	16146	15124	14105	13084	12068	11054	10042	9032	8023	7016	6012	5008	4007	3005

Analytical results 5000x2000mm

Radius at midspan - analytical results - 5000x2000mm plate																							
Radius [mm]	25000	24000	23000	22000	21000	20000	19000	18000	17000	16000	15000	14000	13000	12000	11000	10000	9000	8000	7000	6000	5000	4000	3000
Thickness [mm] 4	25014	24013	23013	22012	21012	20012	19011	18011	17011	16011	15010	14010	13010	12009	11009	10008	9008	8007	7006	6005	5003	4002	3000
5	25039	24036	23033	22031	21028	20026	19024	18022	17020	16018	15017	14015	13014	12013	11011	10010	9009	8008	7006	6005	5004	4002	3001
6	25064	24059	23054	22049	21044	20040	19036	18033	17029	16026	15023	14021	13018	12016	11014	10012	9010	8008	7007	6005	5004	4003	3001
7	25090	24082	23074	22067	21061	20054	19049	18043	17039	16034	15030	14026	13023	12019	11016	10014	9011	8009	7007	6006	5004	4003	3002
8	25115	24104	23095	22085	21077	20069	19061	18054	17048	16042	15036	14031	13027	12023	11019	10016	9013	8010	7008	6006	5005	4003	3002
9	25140	24127	23115	22104	21093	20083	19074	18065	17057	16050	15043	14037	13031	12026	11022	10018	9014	8011	7009	6007	5005	4004	3003
10	25165	24150	23136	22122	21109	20097	19086	18076	17066	16058	15049	14042	13035	12029	11024	10019	9015	8012	7009	6007	5005	4004	3004
11	25190	24173	23156	22140	21126	20112	19099	18087	17076	16065	15056	14047	13040	12033	11027	10021	9017	8013	7010	6007	5006	4004	3004
12	25216	24195	23176	22159	21142	20126	19111	18098	17085	16073	15063	14053	13044	12036	11029	10023	9018	8014	7010	6008	5006	4005	3005
13	25241	24218	23197	22177	21158	20140	19124	18108	17094	16081	15069	14058	13048	12039	11032	10025	9019	8015	7011	6008	5006	4005	3005
14	25266	24241	23217	22195	21174	20155	19136	18119	17103	16089	15076	14063	13053	12043	11034	10027	9021	8015	7011	6008	5006	4006	3006
15	25291	24264	23238	22213	21190	20169	19149	18130	17113	16097	15082	14069	13057	12046	11037	10029	9022	8016	7012	6009	5007	4006	3006
16	25316	24287	23258	22232	21207	20183	19161	18141	17122	16105	15089	14074	13061	12050	11039	10031	9023	8017	7012	6009	5007	4006	3007
17	25342	24309	23279	22250	21223	20198	19174	18152	17131	16112	15095	14080	13065	12053	11042	10032	9024	8018	7013	6009	5007	4007	3007
18	25367	24332	23299	22268	21239	20212	19186	18163	17141	16120	15102	14085	13070	12056	11044	10034	9026	8019	7014	6010	5008	4007	3008
19	25392	24355	23320	22287	21255	20226	19199	18173	17150	16128	15108	14090	13074	12060	11047	10036	9027	8020	7014	6010	5008	4007	3008
20	25417	24378	23340	22305	21272	20240	19211	18184	17159	16136	15115	14096	13078	12063	11050	10038	9028	8021	7015	6011	5008	4008	3009

Validation 5000x2000mm

	Absolute deviation	Minimum deviation	Maximum deviation	Standard deviation
5000x2000mm	0.04%	0.00%	0.19%	0.03%

Radius at midspan - validation analytical results - 5000x2000mm plate																							
Radius [mm]	25000	24000	23000	22000	21000	20000	19000	18000	17000	16000	15000	14000	13000	12000	11000	10000	9000	8000	7000	6000	5000	4000	3000
Thickness [mm] 4	0.19%	0.17%	0.13%	0.15%	0.15%	0.12%	0.12%	0.07%	0.09%	0.09%	0.07%	0.05%	0.04%	0.03%	0.02%	0.00%	0.01%	0.00%	0.03%	0.03%	0.03%	0.01%	0.05%
5	0.11%	0.09%	0.09%	0.10%	0.09%	0.06%	0.09%	0.08%	0.07%	0.06%	0.06%	0.04%	0.03%	0.02%	0.02%	0.01%	0.00%	0.01%	0.02%	0.03%	0.03%	0.01%	
6	0.04%	0.04%	0.03%	0.04%	0.05%	0.03%	0.05%	0.05%	0.03%	0.04%	0.05%	0.02%	0.02%	0.03%	0.02%	0.01%	0.00%	0.00%	0.00%	0.01%	0.01%	0.02%	
7	0.01%	0.01%	0.01%	0.00%	0.00%	0.00%	0.01%	0.01%	0.01%	0.01%	0.01%	0.00%	0.01%	0.01%	0.01%	0.01%	0.01%	0.01%	0.02%	0.00%	0.01%		
8	0.06%	0.05%	0.04%	0.04%	0.03%	0.03%	0.03%	0.02%	0.02%	0.01%	0.01%	0.02%	0.00%	0.00%	0.00%	0.01%	0.00%	0.01%	0.01%	0.01%			
9	0.09%	0.08%	0.05%	0.07%	0.07%	0.05%	0.05%	0.05%	0.04%	0.03%	0.03%	0.03%	0.02%	0.01%	0.01%	0.00%	0.02%	0.01%	0.01%	0.01%			
10	0.11%	0.09%	0.05%	0.08%	0.08%	0.06%	0.07%	0.06%	0.06%	0.05%	0.04%	0.04%	0.03%	0.02%	0.01%	0.00%	0.01%	0.02%	0.01%				
11	0.11%	0.09%	0.05%	0.09%	0.09%	0.07%	0.08%	0.07%	0.07%	0.06%	0.06%	0.05%	0.04%	0.02%	0.02%	0.00%	0.00%	0.01%	0.02%				
12	0.11%	0.09%	0.03%	0.08%	0.09%	0.06%	0.08%	0.08%	0.07%	0.07%	0.06%	0.05%	0.04%	0.03%	0.02%	0.01%	0.00%	0.02%					
13	0.10%	0.08%	0.02%	0.07%	0.09%	0.05%	0.07%	0.07%	0.06%	0.06%	0.06%	0.05%	0.04%	0.03%	0.02%	0.01%	0.01%						
14	0.08%	0.06%	0.00%	0.05%	0.07%	0.04%	0.06%	0.06%	0.05%	0.06%	0.05%	0.04%	0.04%	0.03%	0.02%	0.01%	0.00%						
15	0.06%	0.04%	0.03%	0.03%	0.06%	0.02%	0.04%	0.05%	0.03%	0.05%	0.04%	0.03%	0.03%	0.03%	0.02%	0.01%							
16	0.03%	0.01%	0.06%	0.00%	0.03%	0.01%	0.02%	0.03%	0.01%	0.03%	0.03%	0.02%	0.02%	0.02%	0.01%								
17	0.01%	0.01%	0.09%	0.03%	0.01%	0.03%	0.01%	0.01%	0.01%	0.01%	0.01%	0.00%	0.01%	0.01%	0.01%								
18	0.02%	0.04%	0.11%	0.06%	0.02%	0.06%	0.04%	0.02%	0.04%	0.01%	0.01%	0.02%	0.00%	0.00%									
19	0.05%	0.07%	0.14%	0.09%	0.05%	0.09%	0.07%	0.05%	0.07%	0.03%	0.04%	0.04%	0.02%										
20	0.07%	0.09%	0.17%	0.13%	0.08%	0.12%	0.10%	0.08%	0.10%	0.06%	0.06%	0.07%	0.04%										

Numerical results 5000x3000mm

Radius at midspan - numerical results - 5000x3000mm plate																							
	Radius [mm]	25000	24000	23000	22000	21000	20000	19000	18000	17000	16000	15000	14000	13000	12000	11000	10000	9000	8000	7000	6000	5000	4000	3000
Thickness [mm]	4	25037	24034	23027	22031	21031	20025	19026	18025	17021	16021	15018	14015	13015	12013	11011	10009	9007	8008	7005	6003	5005	4001	2999
	5	25031	24032	23030	22029	21027	20024	19025	18022	17022	16019	15019	14017	13013	12012	11011	10011	9009	8007	7006	6004	5003	4002	3000
	6	25029	24031	23033	22028	21026	20026	19024	18023	17021	16020	15018	14015	13016	12014	11011	10010	9009	8008	7007	6005	5003	4003	3001
	7	25035	24036	23038	22029	21027	20030	19024	18022	17023	16019	15018	14016	13014	12013	11011	10011	9009	8008	7007	6005	5004	4004	3002
	8	25040	24042	23048	22035	21030	20033	19026	18024	17022	16020	15020	14016	13015	12013	11013	10011	9009	8008	7006	6006	5004	4002	3003
	9	25052	24053	23061	22043	21035	20039	19030	18027	17024	16021	15019	14017	13017	12013	11012	10010	9010	8009	7007	6005	5005	4003	3003
	10	25067	24069	23076	22051	21044	20046	19035	18031	17028	16024	15020	14019	13014	12015	11013	10011	9008	8008	7007	6006	5004	4004	3003
	11	25087	24085	23093	22066	21053	20056	19042	18039	17033	16027	15023	14021	13019	12014	11014	10012	9008	8009	7006	6005	5005	4003	3003
	12	25109	24105	23112	22079	21066	20070	19051	18044	17038	16032	15026	14024	13019	12015	11013	10013	9009	8007	7006	6005	5004	4004	3003
	13	25135	24127	23133	22097	21080	20081	19062	18052	17046	16037	15030	14028	13021	12017	11014	10009	9011	8007	7006	6004	5003	4003	3002
	14	25163	24152	23156	22116	21096	20095	19073	18062	17054	16043	15036	14034	13024	12019	11015	10014	9009	8007	7007	6004	5004	4004	3002
	15	25194	24179	23180	22138	21114	20111	19086	18073	17063	16053	15041	14037	13027	12021	11017	10012	9009	8010	7005	6004	5003	4002	3003
	16	25227	24208	23208	22160	21134	20128	19101	18085	17074	16058	15051	14042	13031	12024	11018	10013	9010	8007	7005	6004	5004	4002	3003
	17	25261	24239	23235	22185	21155	20146	19117	18098	17085	16067	15055	14048	13035	12027	11021	10015	9011	8007	7005	6003	5002	4005	3003
	18	25298	24271	23264	22211	21177	20165	19134	18112	17097	16077	15063	14054	13040	12030	11023	10017	9012	8008	7005	6003	5002	4003	3002
	19	25336	24305	23294	22239	21200	20186	19151	18127	17110	16087	15071	14061	13045	12034	11026	10019	9013	8008	7005	6003	5001	4001	3003
	20	25376	24341	23326	22267	21227	20208	19170	18142	17124	16098	15080	14068	13051	12043	11029	10020	9015	8009	7006	6008	5001	4000	3003

Analytical results 5000x3000mm

Radius at midspan - analytical results - 5000x3000mm plate																							
	Radius [mm]	25000	24000	23000	22000	21000	20000	19000	18000	17000	16000	15000	14000	13000	12000	11000	10000	9000	8000	7000	6000	5000	4000	3000
Thickness [mm]	4	24971	23976	22981	21986	20990	19993	18997	17999	17002	16004	15005	14006	13007	12008	11008	10008	9008	8007	7006	6005	5004	4003	3001
	5	24993	23996	22999	22001	21003	20005	19006	18007	17008	16009	15009	14009	13009	12009	11009	10008	9008	8007	7006	6005	5004	4003	3002
	6	25016	24016	23016	22016	21016	20016	19015	18015	17014	16014	15013	14012	13012	12011	11010	10009	9008	8007	7006	6005	5004	4003	3002
	7	25039	24036	23034	22031	21029	20027	19025	18023	17021	16019	15017	14015	13014	12012	11011	10010	9008	8007	7006	6005	5004	4003	3002
	8	25062	24056	23051	22046	21042	20038	19034	18030	17027	16024	15021	14018	13016	12014	11012	10010	9008	8007	7006	6005	5004	4003	3002
	9	25084	24076	23069	22062	21055	20049	19043	18038	17033	16029	15025	14021	13018	12015	11013	10011	9009	8007	7006	6005	5004	4003	3003
	10	25107	24096	23086	22077	21068	20060	19053	18046	17040	16034	15029	14024	13020	12017	11014	10011	9009	8007	7005	6004	5004	4003	3003
	11	25130	24116	23104	22092	21081	20071	19062	18054	17046	16039	15033	14028	13023	12018	11015	10012	9009	8007	7005	6004	5003	4003	3003
	12	25153	24136	23121	22107	21094	20082	19071	18061	17052	16044	15037	14031	13025	12020	11016	10012	9009	8007	7005	6004	5003	4003	3003
	13	25175	24156	23139	22122	21107	20093	19081	18069	17059	16049	15041	14034	13027	12021	11017	10013	9009	8007	7005	6004	5003	4003	3004
	14	25198	24176	23156	22138	21120	20105	19090	18077	17065	16055	15045	14037	13029	12023	11018	10013	9010	8007	7005	6004	5003	4003	3004
	15	25221	24196	23174	22153	21133	20116	19100	18085	17072	16060	15049	14040	13032	12025	11019	10014	9010	8007	7005	6004	5003	4003	3004
	16	25244	24216	23191	22168	21147	20127	19109	18093	17078	16065	15053	14043	13034	12026	11020	10014	9010	8007	7005	6003	5003	4003	3004
	17	25266	24236	23209	22183	21160	20138	19118	18100	17084	16070	15057	14046	13036	12028	11021	10015	9010	8007	7005	6003	5003	4003	3005
	18	25289	24257	23226	22198	21173	20149	19128	18108	17091	16075	15061	14049	13038	12029	11022	10015	9010	8007	7004	6003	5003	4003	3005
	19	25312	24277	23244	22214	21186	20160	19137	18116	17097	16080	15065	14052	13040	12031	11022	10016	9011	8007	7004	6003	5003	4003	3005
	20	25335	24297	23261	22229	21199	20171	19146	18124	17103	16085	15069	14055	13043	12032	11023	10016	9011	8007	7004	6003	5002	4003	3005

Validation 5000x3000mm

	Absolute deviation	Minimum deviation	Maximum deviation	Standard deviation
5000x3000mm	0.06%	0.00%	0.28%	0.05%

Radius at midspan - validation analytical results - 5000x3000mm plate																							
	Radius [mm]	25000	24000	23000	22000	21000	20000	19000	18000	17000	16000	15000	14000	13000	12000	11000	10000	9000	8000	7000	6000	5000	4000	3000
Thickness [mm]	4	0.26%	0.24%	0.20%	0.21%	0.19%	0.16%	0.15%	0.14%	0.11%	0.11%	0.09%	0.06%	0.06%	0.04%	0.02%	0.01%	0.00%	0.01%	0.02%	0.03%	0.01%	0.03%	0.08%
	5	0.15%	0.15%	0.13%	0.13%	0.12%	0.10%	0.10%	0.08%	0.08%	0.07%	0.07%	0.05%	0.03%	0.03%	0.02%	0.02%	0.01%	0.00%	0.01%	0.02%	0.02%	0.02%	
	6	0.05%	0.06%	0.07%	0.05%	0.05%	0.05%	0.05%	0.05%	0.04%	0.04%	0.03%	0.02%	0.03%	0.02%	0.01%	0.01%	0.01%	0.01%	0.01%	0.00%	0.02%	0.00%	
	7	0.02%	0.00%	0.02%	0.01%	0.01%	0.02%	0.00%	0.00%	0.01%	0.00%	0.01%	0.00%	0.00%	0.01%	0.00%	0.01%	0.01%	0.01%	0.02%	0.01%	0.01%		
	8	0.09%	0.06%	0.01%	0.05%	0.06%	0.03%	0.04%	0.04%	0.03%	0.03%	0.01%	0.02%	0.01%	0.00%	0.01%	0.01%	0.00%	0.01%	0.00%	0.02%			
	9	0.13%	0.10%	0.03%	0.09%	0.09%	0.05%	0.07%	0.06%	0.05%	0.05%	0.04%	0.03%	0.01%	0.02%	0.01%	0.00%	0.01%	0.02%	0.02%	0.02%			
	10	0.16%	0.11%	0.04%	0.11%	0.12%	0.07%	0.09%	0.08%	0.07%	0.07%	0.06%	0.04%	0.05%	0.01%	0.01%	0.00%	0.00%	0.02%	0.02%				
	11	0.17%	0.13%	0.05%	0.12%	0.13%	0.07%	0.11%	0.08%	0.08%	0.08%	0.07%	0.05%	0.03%	0.03%	0.01%	0.00%	0.01%	0.02%	0.01%				
	12	0.17%	0.13%	0.04%	0.13%	0.13%	0.06%	0.11%	0.10%	0.08%	0.08%	0.07%	0.05%	0.04%	0.04%	0.03%	0.00%	0.01%	0.00%					
	13	0.16%	0.12%	0.02%	0.12%	0.13%	0.06%	0.10%	0.09%	0.08%	0.08%	0.07%	0.04%	0.05%	0.03%	0.03%	0.03%	0.02%						
	14	0.14%	0.10%	0.00%	0.10%	0.11%	0.05%	0.09%	0.08%	0.06%	0.07%	0.06%	0.02%	0.04%	0.04%	0.02%	0.00%	0.01%						
	15	0.11%	0.07%	0.03%	0.07%	0.09%	0.02%	0.07%	0.07%	0.05%	0.04%	0.05%	0.02%	0.03%	0.03%	0.02%	0.02%							
	16	0.07%	0.03%	0.07%	0.03%	0.06%	0.01%	0.04%	0.04%	0.03%	0.04%	0.01%	0.01%	0.02%	0.02%	0.01%								
	17	0.02%	0.01%	0.11%	0.01%	0.02%	0.04%	0.01%	0.02%	0.00%	0.02%	0.02%	0.01%	0.01%	0.01%	0.01%								
	18	0.03%	0.06%	0.16%	0.06%	0.02%	0.08%	0.03%	0.02%	0.04%	0.01%	0.01%	0.04%	0.01%	0.01%									
	19	0.10%	0.12%	0.22%	0.11%	0.07%	0.13%	0.08%	0.06%	0.08%	0.04%	0.04%	0.06%	0.04%										
	20	0.16%	0.18%	0.28%	0.17%	0.13%	0.18%	0.13%	0.10%	0.12%	0.08%	0.08%	0.09%	0.07%										

Numerical results 6000x1000mm

Radius at midspan - numerical results - 5000x1000mm plate																							
Radius [mm]		25000	24000	23000	22000	21000	20000	19000	18000	17000	16000	15000	14000	13000	12000	11000	10000	9000	8000	7000	6000	5000	4000	3000
Thickness [mm]	4	25050	24046	23044	22037	21033	20030	19027	18023	17020	16017	15015	14012	13011	12009	11007	10005	9004	8003	7001	6004	5001	4001	3000
	5	25067	24062	23058	22051	21046	20041	19036	18030	17027	16024	15020	14017	13014	12012	11010	10008	9007	8005	7001	6002	5002	4001	3000
	6	25083	24076	23071	22065	21058	20052	19047	18041	17036	16031	15025	14022	13019	12015	11012	10010	9008	8006	7007	6000	5002	4001	3000
	7	25096	24090	23084	22077	21069	20063	19057	18050	17044	16038	15033	14028	13024	12019	11016	10012	9010	8007	7005	6003	5001	4002	3000
	8	25107	24100	23095	22087	21079	20072	19066	18057	17052	16045	15039	14033	13028	12023	11019	10015	9012	8009	7006	6003	5003	4002	3001
	9	25116	24110	23105	22097	21088	20080	19074	18066	17059	16052	15045	14039	13033	12028	11023	10018	9014	8011	7008	6005	5003	4002	3001
	10	25124	24118	23113	22106	21095	20088	19082	18073	17065	16058	15051	14044	13038	12032	11026	10021	9016	8012	7009	6006	5004	4003	3002
	11	25131	24125	23120	22113	21102	20094	19089	18079	17071	16064	15056	14049	13042	12036	11029	10024	9019	8014	7010	6007	5005	4003	3002
	12	25138	24131	23127	22119	21108	20100	19095	18085	17077	16069	15061	14054	13047	12039	11033	10027	9021	8016	7012	6008	5005	4003	3002
	13	25143	24136	23132	22125	21113	20105	19100	18090	17081	16074	15066	14058	13050	12043	11036	10029	9023	8018	7013	6009	5006	4004	3002
	14	25148	24141	23137	22130	21118	20110	19104	18094	17086	16079	15070	14062	13054	12046	11039	10032	9026	8020	7014	6010	5007	4004	3002
	15	25152	24145	23141	22135	21122	20114	19108	18098	17090	16083	15073	14066	13058	12049	11042	10035	9028	8021	7016	6011	5007	4005	3003
	16	25156	24149	23145	22139	21126	20117	19112	18102	17093	16086	15077	14069	13061	12052	11045	10037	9030	8023	7017	6012	5008	4005	3003
	17	25160	24152	23148	22143	21130	20120	19115	18106	17096	16090	15080	14072	13064	12055	11047	10039	9032	8025	7019	6013	5009	4005	3003
	18	25163	24156	23151	22146	21133	20124	19118	18108	17099	16093	15082	14075	13066	12058	11049	10042	9034	8027	7020	6014	5010	4006	3003
	19	25166	24158	23153	22149	21135	20126	19121	18111	17102	16096	15085	14078	13069	12060	11052	10044	9036	8028	7022	6015	5010	4006	3004
	20	25169	24161	23156	22151	21138	20129	19123	18114	17104	16098	15087	14080	13071	12062	11054	10046	9038	8030	7023	6017	5011	4007	3004

Analytical results 6000x1000mm

Radius at midspan - analytical results - 6000x1000mm plate																							
Radius [mm]		25000	24000	23000	22000	21000	20000	19000	18000	17000	16000	15000	14000	13000	12000	11000	10000	9000	8000	7000	6000	5000	4000	3000
Thickness [mm]	4	25074	24067	23061	22055	21049	20044	19038	18033	17029	16024	15020	14017	13013	12010	11008	10005	9003	8002	7001	6000	5000	4000	3001
	5	25081	24074	23068	22062	21056	20050	19044	18039	17034	16029	15025	14021	13017	12014	11011	10008	9006	8004	7002	6001	5001	4001	3001
	6	25088	24081	23075	22068	21062	20056	19050	18045	17039	16034	15029	14025	13021	12017	11014	10010	9008	8005	7004	6002	5001	4001	3001
	7	25094	24088	23081	22075	21068	20062	19056	18050	17045	16039	15034	14029	13025	12020	11017	10013	9010	8007	7005	6003	5002	4001	3001
	8	25101	24095	23088	22081	21075	20068	19062	18056	17050	16044	15039	14033	13028	12024	11020	10016	9012	8009	7006	6004	5003	4002	3001
	9	25108	24101	23095	22088	21081	20075	19068	18062	17055	16049	15043	14038	13032	12027	11023	10018	9014	8011	7008	6005	5003	4002	3001
	10	25115	24108	23101	22095	21088	20081	19074	18067	17061	16054	15048	14042	13036	12031	11026	10021	9016	8013	7009	6006	5004	4003	3002
	11	25122	24115	23108	22101	21094	20087	19080	18073	17066	16059	15053	14046	13040	12034	11029	10023	9019	8014	7011	6007	5005	4003	3002
	12	25128	24122	23115	22108	21101	20093	19086	18079	17071	16064	15057	14050	13044	12037	11032	10026	9021	8016	7012	6009	5006	4003	3002
	13	25135	24129	23122	22114	21107	20100	19092	18084	17077	16069	15062	14055	13048	12041	11035	10029	9023	8018	7013	6010	5006	4004	3002
	14	25142	24135	23128	22121	21113	20106	19098	18090	17082	16074	15066	14059	13051	12044	11038	10031	9025	8020	7015	6011	5007	4004	3002
	15	25149	24142	23135	22128	21120	20112	19104	18096	17087	16079	15071	14063	13055	12048	11041	10034	9027	8022	7016	6012	5008	4005	3002
	16	25156	24149	23142	22134	21126	20118	19110	18101	17093	16084	15076	14067	13059	12051	11044	10036	9030	8023	7018	6013	5008	4005	3002
	17	25162	24156	23149	22141	21133	20124	19116	18107	17098	16089	15080	14071	13063	12055	11047	10039	9032	8025	7019	6014	5009	4005	3002
	18	25169	24163	23155	22147	21139	20131	19122	18113	17103	16094	15085	14076	13067	12058	11050	10041	9034	8027	7020	6015	5010	4006	3003
	19	25176	24169	23162	22154	21146	20137	19128	18118	17109	16099	15089	14080	13071	12061	11053	10044	9036	8029	7022	6016	5011	4006	3003
	20	25183	24176	23169	22161	21152	20143	19134	18124	17114	16104	15094	14084	13074	12065	11056	10047	9038	8030	7023	6017	5011	4007	3003

Validation 6000x1000mm

	Absolute deviation	Minimum deviation	Maximum deviation	Standard deviation
6000x1000mm	0.02%	0.00%	0.09%	0.02%

Radius at midspan - validation analytical results - 6000x1000mm plate																							
Radius [mm]		25000	24000	23000	22000	21000	20000	19000	18000	17000	16000	15000	14000	13000	12000	11000	10000	9000	8000	7000	6000	5000	4000	3000
Thickness [mm]	4	0.09%	0.09%	0.07%	0.08%	0.08%	0.07%	0.06%	0.06%	0.05%	0.05%	0.03%	0.03%	0.02%	0.01%	0.00%	0.00%	0.01%	0.02%	0.00%	0.07%	0.03%	0.02%	0.04%
	5	0.05%	0.05%	0.04%	0.05%	0.05%	0.05%	0.04%	0.05%	0.04%	0.03%	0.03%	0.03%	0.02%	0.01%	0.01%	0.00%	0.02%	0.01%	0.02%	0.02%	0.02%	0.00%	
	6	0.02%	0.02%	0.02%	0.02%	0.02%	0.02%	0.02%	0.02%	0.02%	0.02%	0.03%	0.02%	0.01%	0.01%	0.01%	0.00%	0.00%	0.00%	0.05%	0.03%	0.02%	0.01%	
	7	0.01%	0.01%	0.01%	0.01%	0.00%	0.00%	0.00%	0.00%	0.00%	0.01%	0.01%	0.01%	0.00%	0.01%	0.01%	0.01%	0.00%	0.00%	0.00%	0.00%	0.03%		
	8	0.02%	0.02%	0.03%	0.03%	0.02%	0.02%	0.02%	0.00%	0.01%	0.01%	0.00%	0.00%	0.00%	0.00%	0.01%	0.00%	0.00%	0.00%	0.00%	0.03%			
	9	0.03%	0.03%	0.04%	0.04%	0.03%	0.03%	0.03%	0.02%	0.02%	0.02%	0.01%	0.01%	0.01%	0.00%	0.00%	0.00%	0.00%	0.00%	0.00%	0.00%			
	10	0.04%	0.04%	0.05%	0.05%	0.04%	0.03%	0.04%	0.03%	0.03%	0.03%	0.02%	0.02%	0.01%	0.01%	0.00%	0.00%	0.00%	0.00%	0.00%				
	11	0.04%	0.04%	0.05%	0.05%	0.04%	0.04%	0.04%	0.03%	0.03%	0.03%	0.02%	0.02%	0.01%	0.01%	0.01%	0.00%	0.00%	0.00%	0.01%				
	12	0.04%	0.04%	0.05%	0.05%	0.03%	0.03%	0.05%	0.03%	0.03%	0.03%	0.03%	0.02%	0.02%	0.02%	0.01%	0.01%	0.00%	0.00%					
	13	0.03%	0.03%	0.05%	0.05%	0.03%	0.03%	0.04%	0.03%	0.03%	0.03%	0.03%	0.02%	0.02%	0.02%	0.01%	0.01%	0.00%						
	14	0.02%	0.02%	0.04%	0.04%	0.02%	0.02%	0.03%	0.02%	0.02%	0.03%	0.02%	0.02%	0.02%	0.02%	0.01%	0.01%	0.00%						
	15	0.01%	0.01%	0.03%	0.03%	0.01%	0.01%	0.02%	0.02%	0.01%	0.02%	0.01%	0.02%	0.02%	0.01%	0.01%	0.01%							
	16	0.00%	0.00%	0.01%	0.02%	0.00%	0.00%	0.01%	0.00%	0.00%	0.01%	0.01%	0.01%	0.01%	0.01%	0.01%								
	17	0.01%	0.01%	0.00%	0.01%	0.02%	0.02%	0.00%	0.01%	0.01%	0.00%	0.00%	0.00%	0.01%	0.00%	0.01%								
	18	0.02%	0.03%	0.02%	0.01%	0.03%	0.04%	0.02%	0.02%	0.03%	0.01%	0.02%	0.01%	0.00%	0.00%									
	19	0.04%	0.04%	0.04%	0.02%	0.05%	0.05%	0.04%	0.04%	0.04%	0.02%	0.03%	0.02%	0.01%	0.01%									
	20	0.06%	0.06%	0.06%	0.04%	0.07%	0.07%	0.05%	0.06%	0.06%	0.04%	0.04%	0.03%	0.03%										

Numerical results 6000x2000mm

Radius at midspan - numerical results - 6000x2000mm plate																							
Radius [mm]	25000	24000	23000	22000	21000	20000	19000	18000	17000	16000	15000	14000	13000	12000	11000	10000	9000	8000	7000	6000	5000	4000	3000
Thickness [mm] 4	25047	24039	23034	22034	21032	20025	19024	18020	17018	16016	15013	14010	13009	12008	11007	10005	9003	8003	7002	6003	5001	4001	3000
5	25060	24052	23042	22041	21038	20034	19027	18027	17023	16020	15019	14015	13014	12011	11009	10007	9006	8006	7004	6003	5002	4001	3000
6	25070	24062	23049	22049	21047	20041	19034	18035	17028	16025	15022	14019	13015	12013	11011	10009	9007	8006	7005	6004	5002	4001	3001
7	25079	24070	23056	22057	21052	20047	19039	18039	17032	16029	15025	14022	13017	12015	11013	10010	9009	8007	7005	6003	5003	4002	3001
8	25087	24076	23064	22064	21060	20053	19044	18044	17036	16034	15029	14025	13020	12017	11011	10012	9010	8008	7006	6007	5003	4002	3001
9	25096	24087	23076	22073	21068	20059	19050	18048	17041	16037	15032	14028	13020	12020	11015	10013	9010	8009	7007	6005	5004	4002	3001
10	25107	24098	23088	22081	21074	20066	19055	18054	17046	16040	15036	14031	13025	12022	11016	10015	9012	8010	7008	6006	5004	4003	3002
11	25118	24109	23101	22091	21082	20073	19065	18059	17050	16045	15038	14034	13027	12024	11020	10016	9014	8011	7008	6006	5005	4003	3002
12	25131	24122	23114	22101	21091	20081	19072	18065	17056	16049	15043	14037	13030	12027	11022	10018	9015	8012	7009	6007	5006	4003	3002
13	25144	24135	23128	22112	21100	20090	19080	18071	17062	16055	15047	14040	13033	12029	11024	10019	9016	8013	7008	6007	5005	4004	3003
14	25159	24150	23143	22125	21110	20099	19089	18078	17068	16058	15051	14044	13036	12031	11026	10021	9017	8014	7010	6008	5006	4004	3002
15	25176	24165	23159	22138	21120	20109	19099	18085	17075	16065	15055	14048	13039	12034	11028	10021	9019	8015	7011	6008	5006	4004	3003
16	25192	24181	23175	22152	21132	20119	19110	18093	17081	16071	15061	14052	13043	12036	11030	10024	9019	8015	7012	6009	5004	4005	3003
17	25208	24196	23190	22167	21144	20130	19120	18101	17089	16077	15066	14056	13046	12039	11032	10025	9021	8017	7012	6010	5009	4005	3004
18	25227	24211	23206	22181	21156	20141	19132	18109	17097	16084	15071	14060	13050	12042	11035	10028	9022	8017	7013	6010	5008	4005	3004
19	25245	24231	23224	22195	21168	20153	19144	18119	17104	16091	15077	14065	13055	12045	11037	10029	9023	8018	7014	6010	5008	4005	3004
20	25263	24247	23240	22212	21180	20164	19155	18128	17113	16098	15083	14070	13059	12048	11039	10031	9025	8019	7014	6011	5009	4005	3004

Analytical results 6000x2000mm

Radius at midspan - analytical results - 6000x2000mm plate																							
Radius [mm]	25000	24000	23000	22000	21000	20000	19000	18000	17000	16000	15000	14000	13000	12000	11000	10000	9000	8000	7000	6000	5000	4000	3000
Thickness [mm] 4	25032	24028	23026	22023	21021	20019	19017	18015	17013	16012	15011	14010	13009	12008	11007	10006	9005	8004	7003	6003	5002	4001	3000
5	25046	24041	23037	22034	21030	20027	19024	18022	17019	16017	15015	14013	13012	12010	11009	10007	9006	8005	7004	6003	5002	4001	3000
6	25060	24054	23049	22044	21040	20036	19032	18028	17025	16022	15019	14017	13015	12013	11011	10009	9007	8006	7005	6003	5002	4001	3001
7	25074	24067	23061	22055	21050	20044	19040	18035	17031	16027	15024	14021	13018	12015	11013	10010	9008	8007	7005	6004	5003	4002	3001
8	25088	24080	23073	22066	21059	20053	19047	18042	17037	16032	15028	14024	13021	12017	11014	10012	9010	8008	7006	6004	5003	4002	3001
9	25102	24093	23084	22076	21069	20062	19055	18049	17043	16038	15033	14028	13024	12020	11016	10013	9011	8008	7006	6005	5003	4003	3002
10	25116	24106	23096	22087	21079	20070	19063	18056	17049	16043	15037	14032	13027	12022	11018	10015	9012	8009	7007	6005	5004	4003	3002
11	25130	24119	23108	22098	21088	20079	19070	18062	17055	16048	15041	14035	13030	12025	11020	10016	9013	8010	7008	6006	5004	4003	3003
12	25144	24132	23120	22109	21098	20088	19078	18069	17061	16053	15046	14039	13033	12027	11022	10018	9014	8011	7008	6006	5005	4004	3003
13	25158	24144	23132	22119	21107	20096	19086	18076	17067	16058	15050	14043	13036	12030	11024	10019	9015	8012	7009	6006	5005	4004	3004
14	25172	24157	23143	22130	21117	20105	19094	18083	17073	16063	15054	14046	13039	12032	11026	10021	9016	8012	7009	6007	5005	4004	3004
15	25186	24170	23155	22141	21127	20114	19101	18090	17079	16068	15059	14050	13042	12035	11028	10022	9017	8013	7010	6007	5006	4005	3005
16	25200	24183	23167	22151	21136	20122	19109	18096	17084	16073	15063	14054	13045	12037	11030	10024	9019	8014	7010	6008	5006	4005	3005
17	25214	24196	23179	22162	21146	20131	19117	18103	17090	16079	15067	14057	13048	12040	11032	10025	9020	8015	7011	6008	5006	4005	3005
18	25228	24209	23190	22173	21156	20140	19124	18110	17096	16084	15072	14061	13051	12042	11034	10027	9021	8016	7012	6009	5007	4006	3006
19	25242	24222	23202	22183	21165	20148	19132	18117	17102	16089	15076	14065	13054	12045	11036	10028	9022	8017	7012	6009	5007	4006	3006
20	25256	24235	23214	22194	21175	20157	19140	18123	17108	16094	15081	14068	13057	12047	11038	10030	9023	8017	7013	6010	5007	4006	3007

Validation 6000x2000mm

	Absolute deviation	Minimum deviation	Maximum deviation	Standard deviation
6000x2000mm	0.02%	0.00%	0.11%	0.02%

Radius at midspan - validation analytical results - 6000x2000mm plate																							
Radius [mm]	25000	24000	23000	22000	21000	20000	19000	18000	17000	16000	15000	14000	13000	12000	11000	10000	9000	8000	7000	6000	5000	4000	3000
Thickness [mm] 4	0.06%	0.05%	0.03%	0.05%	0.05%	0.03%	0.04%	0.03%	0.03%	0.02%	0.02%	0.00%	0.01%	0.00%	0.00%	0.00%	0.02%	0.01%	0.01%	0.01%	0.00%	0.00%	0.02%
5	0.06%	0.04%	0.02%	0.03%	0.04%	0.04%	0.02%	0.03%	0.02%	0.02%	0.02%	0.01%	0.02%	0.01%	0.00%	0.00%	0.00%	0.02%	0.00%	0.01%	0.00%	0.00%	
6	0.04%	0.03%	0.00%	0.02%	0.03%	0.02%	0.01%	0.04%	0.02%	0.02%	0.02%	0.01%	0.00%	0.01%	0.00%	0.00%	0.01%	0.00%	0.00%	0.00%	0.00%	0.00%	
7	0.02%	0.01%	0.02%	0.01%	0.01%	0.01%	0.00%	0.02%	0.01%	0.01%	0.01%	0.01%	0.00%	0.00%	0.00%	0.00%	0.00%	0.00%	0.00%	0.01%	0.00%		
8	0.00%	0.02%	0.04%	0.01%	0.01%	0.00%	0.02%	0.01%	0.00%	0.01%	0.00%	0.01%	0.00%	0.00%	0.03%	0.00%	0.00%	0.00%	0.00%	0.04%			
9	0.02%	0.02%	0.04%	0.02%	0.01%	0.01%	0.03%	0.00%	0.01%	0.00%	0.00%	0.00%	0.03%	0.00%	0.01%	0.00%	0.00%	0.01%	0.01%	0.00%			
10	0.04%	0.03%	0.04%	0.03%	0.02%	0.02%	0.04%	0.01%	0.02%	0.02%	0.01%	0.01%	0.01%	0.00%	0.02%	0.00%	0.00%	0.01%	0.01%				
11	0.05%	0.04%	0.03%	0.03%	0.03%	0.03%	0.03%	0.02%	0.03%	0.02%	0.02%	0.01%	0.02%	0.00%	0.00%	0.00%	0.01%	0.01%	0.01%				
12	0.05%	0.04%	0.03%	0.03%	0.03%	0.03%	0.03%	0.02%	0.03%	0.02%	0.02%	0.01%	0.02%	0.01%	0.00%	0.00%	0.01%	0.01%					
13	0.05%	0.04%	0.01%	0.03%	0.04%	0.03%	0.03%	0.03%	0.03%	0.02%	0.02%	0.02%	0.02%	0.01%	0.00%	0.00%	0.01%						
14	0.05%	0.03%	0.00%	0.02%	0.03%	0.03%	0.02%	0.03%	0.03%	0.03%	0.02%	0.02%	0.02%	0.01%	0.00%	0.00%	0.01%						
15	0.04%	0.02%	0.02%	0.01%	0.03%	0.02%	0.01%	0.03%	0.02%	0.02%	0.02%	0.01%	0.02%	0.01%	0.00%	0.01%							
16	0.03%	0.01%	0.04%	0.00%	0.02%	0.02%	0.00%	0.02%	0.02%	0.02%	0.02%	0.01%	0.02%	0.01%	0.00%								
17	0.03%	0.00%	0.05%	0.02%	0.01%	0.01%	0.02%	0.01%	0.01%	0.01%	0.01%	0.01%	0.01%	0.00%	0.00%								
18	0.00%	0.01%	0.07%	0.04%	0.00%	0.01%	0.04%	0.00%	0.00%	0.00%	0.00%	0.00%	0.00%	0.00%									
19	0.01%	0.04%	0.09%	0.05%	0.01%	0.02%	0.06%	0.01%	0.01%	0.01%	0.01%	0.00%	0.00%										
20	0.03%	0.05%	0.11%	0.08%	0.02%	0.03%	0.08%	0.03%	0.03%	0.03%	0.02%	0.01%	0.01%										

Numerical results 6000x3000mm

Radius at midspan - numerical results - 6000x3000mm plate																								
Radius [mm]		25000	24000	23000	22000	21000	20000	19000	18000	17000	16000	15000	14000	13000	12000	11000	10000	9000	8000	7000	6000	5000	4000	3000
Thickness [mm]	4	25054	24042	23035	22041	21040	20028	19027	18029	17023	16020	15014	14015	13012	12009	11008	10006	9005	8004	7006	6004	5003	4003	3000
	5	25059	24051	23037	22041	21043	20036	19027	18032	17026	16023	15020	14018	13012	12012	11011	10008	9007	8006	7006	6004	5004	4002	3000
	6	25058	24051	23039	22043	21043	20037	19031	18034	17028	16025	15023	14021	13015	12014	11012	10010	9009	8007	7005	6003	5004	4004	3000
	7	25053	24050	23044	22046	21045	20039	19033	18035	17029	16028	15024	14022	13017	12015	11014	10011	9009	8007	7006	6005	5004	4004	3000
	8	25055	24050	23045	22047	21045	20040	19035	18036	17030	16029	15025	14023	13019	12017	11014	10012	9010	8009	7007	6004	5004	4004	3001
	9	25055	24052	23050	22046	21045	20040	19036	18038	17031	16030	15026	14024	13020	12018	11015	10013	9010	8009	7007	6005	5004	4004	3001
	10	25056	24055	23054	22048	21046	20042	19038	18036	17032	16031	15028	14025	13020	12020	11017	10013	9012	8010	7008	6006	5004	4004	3001
	11	25060	24060	23061	22051	21048	20044	19041	18037	17034	16031	15028	14025	13021	12020	11018	10014	9013	8010	7008	6006	5006	4003	3001
	12	25064	24065	23069	22057	21049	20047	19044	18039	17035	16032	15029	14026	13022	12020	11018	10014	9014	8011	7009	6008	5005	4003	3002
	13	25073	24074	23079	22060	21053	20051	19048	18041	17037	16034	15030	14027	13022	12020	11018	10015	9013	8012	7009	6007	5006	4006	3002
	14	25082	24083	23090	22069	21057	20054	19055	18043	17040	16035	15032	14029	13024	12021	11018	10015	9014	8011	7009	6007	5006	4004	3003
	15	25093	24093	23100	22077	21064	20060	19057	18046	17043	16037	15032	14030	13025	12022	11019	10017	9014	8011	7009	6008	5006	4005	3002
	16	25107	24106	23112	22087	21071	20066	19065	18050	17046	16040	15035	14030	13027	12024	11020	10018	9014	8013	7009	6008	5006	4005	3002
	17	25122	24119	23125	22097	21079	20074	19072	18055	17050	16043	15038	14032	13028	12023	11020	10016	9014	8012	7009	6008	5006	4003	3003
	18	25138	24134	23140	22110	21088	20082	19080	18061	17055	16047	15039	14034	13030	12024	11021	10017	9014	8011	7009	6008	5006	4004	3003
	19	25156	24150	23156	22123	21099	20091	19089	18067	17060	16051	15042	14038	13032	12026	11023	10017	9015	8012	7009	6007	5007	4005	3004
	20	25176	24168	23172	22137	21110	20101	19098	18074	17066	16056	15047	14039	13035	12027	11023	10018	9015	8012	7009	6007	5006	4005	3004

Analytical results 6000x3000mm

Radius at midspan - analytical results - 6000x3000mm plate																								
Radius [mm]		25000	24000	23000	22000	21000	20000	19000	18000	17000	16000	15000	14000	13000	12000	11000	10000	9000	8000	7000	6000	5000	4000	3000
Thickness [mm]	4	25025	24025	23025	22025	21024	20023	19022	18021	17020	16018	15017	14016	13014	12013	11011	10009	9008	8007	7005	6004	5003	4002	3001
	5	25033	24032	23031	22030	21029	20027	19026	18024	17022	16021	15019	14017	13015	12013	11012	10010	9008	8007	7005	6004	5003	4002	3001
	6	25041	24040	23038	22036	21033	20031	19029	18027	17025	16023	15021	14018	13016	12014	11012	10011	9009	8007	7006	6004	5003	4002	3001
	7	25049	24047	23044	22041	21038	20035	19033	18030	17027	16025	15022	14020	13017	12015	11013	10011	9009	8008	7006	6005	5003	4002	3002
	8	25058	24054	23050	22047	21043	20040	19036	18033	17030	16027	15024	14021	13019	12016	11014	10012	9010	8008	7006	6005	5004	4003	3002
	9	25066	24061	23057	22052	21048	20044	19040	18036	17032	16029	15026	14023	13020	12017	11015	10012	9010	8008	7007	6005	5004	4003	3002
	10	25074	24068	23063	22058	21053	20048	19043	18039	17035	16031	15027	14024	13021	12018	11015	10013	9011	8009	7007	6005	5004	4003	3002
	11	25082	24075	23069	22063	21057	20052	19047	18042	17037	16033	15029	14025	13022	12019	11016	10013	9011	8009	7007	6006	5004	4003	3003
	12	25090	24083	23075	22069	21062	20056	19050	18045	17040	16035	15031	14027	13023	12020	11017	10014	9011	8009	7007	6006	5005	4004	3003
	13	25098	24090	23082	22074	21067	20060	19054	18048	17042	16037	15033	14028	13024	12021	11017	10014	9012	8010	7008	6006	5005	4004	3003
	14	25106	24097	23088	22080	21072	20064	19057	18051	17045	16039	15034	14030	13025	12021	11018	10015	9012	8010	7008	6006	5005	4004	3004
	15	25114	24104	23094	22085	21077	20069	19061	18054	17048	16042	15036	14031	13026	12022	11019	10015	9013	8010	7008	6007	5005	4004	3004
	16	25123	24111	23101	22091	21081	20073	19065	18057	17050	16044	15038	14032	13028	12023	11019	10016	9013	8011	7008	6007	5006	4005	3004
	17	25131	24118	23107	22096	21086	20077	19068	18060	17053	16046	15039	14034	13029	12024	11020	10017	9013	8011	7009	6007	5006	4005	3004
	18	25139	24126	23113	22102	21091	20081	19072	18063	17055	16048	15041	14035	13030	12025	11021	10017	9014	8011	7009	6007	5006	4005	3005
	19	25147	24133	23120	22107	21096	20085	19075	18066	17058	16050	15043	14037	13031	12026	11021	10018	9014	8012	7009	6008	5006	4005	3005
	20	25155	24140	23126	22113	21101	20089	19079	18069	17060	16052	15045	14038	13032	12027	11022	10018	9015	8012	7010	6008	5006	4006	3005

Validation 6000x3000mm

	Absolute deviation	Minimum deviation	Maximum deviation	Standard deviation
6000x3000mm	0.03%	0.00%	0.20%	0.03%

Radius at midspan - validation analytical results - 6000x3000mm plate																								
Radius [mm]		25000	24000	23000	22000	21000	20000	19000	18000	17000	16000	15000	14000	13000	12000	11000	10000	9000	8000	7000	6000	5000	4000	3000
Thickness [mm]	4	0.12%	0.07%	0.05%	0.08%	0.08%	0.03%	0.03%	0.04%	0.02%	0.01%	0.02%	0.00%	0.02%	0.03%	0.03%	0.03%	0.03%	0.03%	0.01%	0.00%	0.02%	0.03%	0.04%
	5	0.10%	0.08%	0.02%	0.05%	0.07%	0.05%	0.01%	0.04%	0.02%	0.01%	0.01%	0.01%	0.02%	0.01%	0.01%	0.02%	0.02%	0.02%	0.01%	0.00%	0.01%	0.01%	
	6	0.07%	0.05%	0.00%	0.03%	0.05%	0.03%	0.01%	0.04%	0.02%	0.02%	0.01%	0.02%	0.01%	0.00%	0.00%	0.01%	0.00%	0.00%	0.02%	0.02%	0.01%	0.04%	
	7	0.01%	0.01%	0.00%	0.02%	0.03%	0.02%	0.00%	0.03%	0.01%	0.02%	0.01%	0.02%	0.00%	0.00%	0.01%	0.00%	0.00%	0.01%	0.00%	0.01%	0.01%		
	8	0.01%	0.01%	0.02%	0.00%	0.01%	0.00%	0.01%	0.02%	0.00%	0.01%	0.01%	0.02%	0.00%	0.01%	0.01%	0.00%	0.01%	0.01%	0.01%	0.01%			
	9	0.04%	0.04%	0.03%	0.03%	0.01%	0.02%	0.02%	0.01%	0.01%	0.01%	0.00%	0.01%	0.00%	0.01%	0.01%	0.01%	0.01%	0.01%	0.00%	0.00%			
	10	0.07%	0.06%	0.04%	0.04%	0.03%	0.03%	0.03%	0.01%	0.02%	0.00%	0.01%	0.00%	0.01%	0.01%	0.01%	0.00%	0.02%	0.01%	0.01%				
	11	0.09%	0.06%	0.04%	0.05%	0.05%	0.04%	0.03%	0.03%	0.02%	0.02%	0.01%	0.00%	0.01%	0.01%	0.02%	0.01%	0.03%	0.02%	0.01%				
	12	0.10%	0.07%	0.03%	0.05%	0.06%	0.05%	0.03%	0.04%	0.03%	0.02%	0.02%	0.01%	0.01%	0.00%	0.01%	0.00%	0.02%	0.02%					
	13	0.10%	0.07%	0.01%	0.06%	0.07%	0.05%	0.03%	0.04%	0.03%	0.02%	0.02%	0.01%	0.02%	0.00%	0.01%	0.00%	0.02%						
	14	0.10%	0.06%	0.01%	0.05%	0.07%	0.05%	0.01%	0.04%	0.03%	0.03%	0.02%	0.01%	0.01%	0.01%	0.00%	0.01%	0.02%						
	15	0.08%	0.04%	0.02%	0.04%	0.06%	0.04%	0.02%	0.04%	0.03%	0.03%	0.02%	0.01%	0.01%	0.01%	0.00%	0.01%							
	16	0.06%	0.02%	0.05%	0.02%	0.05%	0.03%	0.00%	0.04%	0.02%	0.02%	0.02%	0.02%	0.00%	0.01%	0.01%								
	17	0.04%	0.00%	0.08%	0.01%	0.04%	0.02%	0.02%	0.03%	0.01%	0.02%	0.01%	0.01%	0.01%	0.01%	0.00%								
	18	0.00%	0.03%	0.12%	0.04%	0.01%	0.00%	0.04%	0.01%	0.00%	0.01%	0.01%	0.01%	0.00%	0.00%									
	19	0.04%	0.07%	0.16%	0.07%	0.01%	0.03%	0.07%	0.00%	0.02%	0.01%	0.01%	0.01%	0.01%										
	20	0.08%	0.11%	0.20%	0.11%	0.05%	0.06%	0.10%	0.03%	0.03%	0.03%	0.01%	0.01%	0.02%										

B.2. Volume of deformation

	Absolute deviation	Minimum deviation	Maximum deviation	Standard deviation
1000x1000mm	1.76%	0.00%	4.68%	1.09%
2000x1000mm	0.20%	0.00%	1.13%	0.16%
2000x2000mm	0.69%	0.02%	1.95%	0.47%
3000x1000mm	0.41%	0.17%	1.94%	0.18%
3000x2000mm	0.22%	0.00%	1.80%	0.19%
3000x3000mm	0.47%	0.00%	4.68%	1.09%
4000x1000mm	0.62%	0.41%	3.06%	0.24%
4000x2000mm	0.31%	0.00%	4.68%	1.09%
4000x3000mm	0.27%	0.00%	3.03%	0.31%
5000x1000mm	0.75%	0.52%	4.61%	0.36%
5000x2000mm	0.58%	0.14%	4.42%	0.41%
5000x3000mm	0.42%	0.00%	4.51%	0.47%
6000x1000mm	0.91%	0.59%	6.09%	0.51%
6000x2000mm	0.83%	0.36%	6.55%	0.55%
6000x3000mm	0.72%	0.00%	6.51%	0.59%
Average	**0.61%**	**0.15%**	**3.98%**	**0.51%**

Numerical results 1000x1000mm

Volume of deformation - numerical results - 1000x1000mm plate																								
	Radius [mm]	25000	24000	23000	22000	21000	20000	19000	18000	17000	16000	15000	14000	13000	12000	11000	10000	9000	8000	7000	6000	5000	4000	3000
Thickness [mm]	4	0.0026	0.0027	0.0028	0.0030	0.0032	0.0034	0.0036	0.0038	0.0041	0.0044	0.0047	0.0051	0.0056	0.0061	0.0067	0.0075	0.0084	0.0095	0.0110	0.0129	0.0156	0.0195	0.0261
	5	0.0025	0.0026	0.0028	0.0029	0.0031	0.0032	0.0034	0.0037	0.0039	0.0042	0.0045	0.0049	0.0054	0.0059	0.0065	0.0073	0.0082	0.0093	0.0108	0.0127	0.0154	0.0194	0.0260
	6	0.0025	0.0026	0.0027	0.0028	0.0030	0.0032	0.0033	0.0036	0.0038	0.0041	0.0044	0.0047	0.0052	0.0057	0.0063	0.0071	0.0080	0.0091	0.0106	0.0125	0.0152	0.0193	0.0259
	7	0.0025	0.0026	0.0027	0.0028	0.0030	0.0031	0.0033	0.0035	0.0037	0.0040	0.0043	0.0046	0.0050	0.0055	0.0061	0.0069	0.0078	0.0089	0.0104	0.0123	0.0151	0.0191	0.0258
	8	0.0024	0.0025	0.0027	0.0028	0.0029	0.0031	0.0033	0.0034	0.0037	0.0039	0.0042	0.0045	0.0049	0.0054	0.0060	0.0067	0.0076	0.0087	0.0102	0.0122	0.0149	0.0190	0.0256
	9	0.0024	0.0025	0.0026	0.0028	0.0029	0.0031	0.0032	0.0034	0.0036	0.0039	0.0042	0.0045	0.0049	0.0053	0.0059	0.0066	0.0074	0.0085	0.0100	0.0119	0.0147	0.0188	0.0255
	10	0.0024	0.0025	0.0026	0.0028	0.0029	0.0030	0.0032	0.0034	0.0036	0.0038	0.0041	0.0044	0.0048	0.0053	0.0058	0.0065	0.0073	0.0084	0.0098	0.0117	0.0145	0.0186	0.0253
	11	0.0024	0.0025	0.0026	0.0027	0.0029	0.0030	0.0032	0.0034	0.0036	0.0038	0.0041	0.0044	0.0048	0.0052	0.0057	0.0064	0.0072	0.0082	0.0096	0.0116	0.0143	0.0184	0.0251
	12	0.0024	0.0025	0.0026	0.0027	0.0029	0.0030	0.0032	0.0034	0.0036	0.0038	0.0041	0.0044	0.0047	0.0052	0.0057	0.0063	0.0071	0.0081	0.0095	0.0114	0.0141	0.0182	0.0250
	13	0.0024	0.0025	0.0026	0.0027	0.0029	0.0030	0.0032	0.0034	0.0036	0.0038	0.0041	0.0044	0.0047	0.0051	0.0056	0.0063	0.0070	0.0080	0.0094	0.0112	0.0139	0.0180	0.0248
	14	0.0024	0.0025	0.0026	0.0027	0.0029	0.0030	0.0032	0.0034	0.0036	0.0038	0.0040	0.0043	0.0047	0.0051	0.0056	0.0062	0.0070	0.0079	0.0093	0.0111	0.0137	0.0178	0.0246
	15	0.0024	0.0025	0.0026	0.0027	0.0029	0.0030	0.0032	0.0033	0.0035	0.0038	0.0040	0.0043	0.0047	0.0051	0.0056	0.0062	0.0069	0.0079	0.0092	0.0109	0.0135	0.0176	0.0244
	16	0.0024	0.0025	0.0026	0.0027	0.0029	0.0030	0.0032	0.0033	0.0035	0.0038	0.0040	0.0043	0.0047	0.0051	0.0056	0.0062	0.0069	0.0078	0.0091	0.0108	0.0134	0.0174	0.0242
	17	0.0024	0.0025	0.0026	0.0027	0.0029	0.0030	0.0032	0.0033	0.0035	0.0038	0.0040	0.0043	0.0047	0.0051	0.0055	0.0061	0.0069	0.0078	0.0090	0.0107	0.0132	0.0172	0.0240
	18	0.0024	0.0025	0.0026	0.0027	0.0028	0.0030	0.0032	0.0033	0.0035	0.0038	0.0040	0.0043	0.0046	0.0050	0.0055	0.0061	0.0068	0.0077	0.0090	0.0106	0.0131	0.0170	0.0238
	19	0.0024	0.0025	0.0026	0.0027	0.0028	0.0030	0.0031	0.0033	0.0035	0.0037	0.0040	0.0043	0.0046	0.0050	0.0055	0.0061	0.0068	0.0077	0.0089	0.0106	0.0130	0.0168	0.0236
	20	0.0024	0.0025	0.0026	0.0027	0.0028	0.0030	0.0031	0.0033	0.0035	0.0037	0.0040	0.0043	0.0046	0.0050	0.0055	0.0061	0.0068	0.0077	0.0089	0.0105	0.0129	0.0167	0.0234

Analytical results 1000x1000mm

Volume of deformation - analytical results - 1000x1000mm plate																								
	Radius [mm]	25000	24000	23000	22000	21000	20000	19000	18000	17000	16000	15000	14000	13000	12000	11000	10000	9000	8000	7000	6000	5000	4000	3000
Thickness [mm]	4	0.0025	0.0026	0.0028	0.0029	0.0031	0.0032	0.0034	0.0036	0.0039	0.0042	0.0045	0.0049	0.0053	0.0058	0.0065	0.0072	0.0082	0.0093	0.0109	0.0130	0.0158	0.0201	0.0268
	5	0.0025	0.0026	0.0028	0.0029	0.0030	0.0032	0.0034	0.0036	0.0039	0.0041	0.0044	0.0048	0.0052	0.0058	0.0064	0.0071	0.0080	0.0092	0.0107	0.0127	0.0156	0.0198	0.0267
	6	0.0025	0.0026	0.0027	0.0029	0.0030	0.0032	0.0034	0.0036	0.0038	0.0041	0.0044	0.0048	0.0052	0.0057	0.0063	0.0070	0.0079	0.0091	0.0105	0.0125	0.0153	0.0195	0.0265
	7	0.0025	0.0026	0.0027	0.0029	0.0030	0.0032	0.0034	0.0036	0.0038	0.0041	0.0044	0.0047	0.0051	0.0056	0.0062	0.0069	0.0078	0.0089	0.0104	0.0123	0.0151	0.0193	0.0264
	8	0.0025	0.0026	0.0027	0.0028	0.0030	0.0032	0.0033	0.0035	0.0038	0.0040	0.0043	0.0047	0.0051	0.0056	0.0061	0.0068	0.0077	0.0088	0.0102	0.0121	0.0149	0.0191	0.0262
	9	0.0025	0.0026	0.0027	0.0028	0.0030	0.0031	0.0033	0.0035	0.0037	0.0040	0.0043	0.0046	0.0050	0.0055	0.0061	0.0067	0.0076	0.0087	0.0101	0.0120	0.0147	0.0188	0.0261
	10	0.0025	0.0026	0.0027	0.0028	0.0030	0.0031	0.0033	0.0035	0.0037	0.0040	0.0043	0.0046	0.0050	0.0054	0.0060	0.0067	0.0075	0.0085	0.0099	0.0118	0.0145	0.0186	0.0259
	11	0.0025	0.0026	0.0027	0.0028	0.0030	0.0031	0.0033	0.0035	0.0037	0.0039	0.0042	0.0046	0.0049	0.0054	0.0059	0.0066	0.0074	0.0084	0.0098	0.0116	0.0143	0.0184	0.0258
	12	0.0025	0.0026	0.0027	0.0028	0.0029	0.0031	0.0033	0.0035	0.0037	0.0039	0.0042	0.0045	0.0049	0.0053	0.0059	0.0065	0.0073	0.0083	0.0096	0.0115	0.0141	0.0182	0.0257
	13	0.0024	0.0026	0.0027	0.0028	0.0029	0.0031	0.0032	0.0034	0.0036	0.0039	0.0042	0.0045	0.0049	0.0053	0.0058	0.0064	0.0072	0.0082	0.0095	0.0113	0.0139	0.0180	0.0255
	14	0.0024	0.0025	0.0027	0.0028	0.0029	0.0031	0.0032	0.0034	0.0036	0.0039	0.0041	0.0044	0.0048	0.0052	0.0058	0.0064	0.0071	0.0081	0.0094	0.0112	0.0137	0.0178	0.0254
	15	0.0024	0.0025	0.0026	0.0028	0.0029	0.0030	0.0032	0.0034	0.0036	0.0038	0.0041	0.0044	0.0048	0.0052	0.0057	0.0063	0.0071	0.0080	0.0093	0.0110	0.0136	0.0176	0.0252
	16	0.0024	0.0025	0.0026	0.0028	0.0029	0.0030	0.0032	0.0034	0.0036	0.0038	0.0041	0.0044	0.0047	0.0051	0.0056	0.0062	0.0070	0.0079	0.0092	0.0109	0.0134	0.0174	0.0251
	17	0.0024	0.0025	0.0026	0.0027	0.0029	0.0030	0.0032	0.0034	0.0036	0.0038	0.0040	0.0043	0.0047	0.0051	0.0056	0.0062	0.0069	0.0078	0.0091	0.0108	0.0133	0.0173	0.0250
	18	0.0024	0.0025	0.0026	0.0027	0.0029	0.0030	0.0032	0.0033	0.0035	0.0038	0.0040	0.0043	0.0047	0.0051	0.0055	0.0061	0.0068	0.0078	0.0090	0.0107	0.0131	0.0171	0.0249
	19	0.0024	0.0025	0.0026	0.0027	0.0029	0.0030	0.0031	0.0033	0.0035	0.0037	0.0040	0.0043	0.0046	0.0050	0.0055	0.0061	0.0068	0.0077	0.0089	0.0105	0.0130	0.0170	0.0247
	20	0.0024	0.0025	0.0026	0.0027	0.0028	0.0030	0.0031	0.0033	0.0035	0.0037	0.0040	0.0043	0.0046	0.0050	0.0054	0.0060	0.0067	0.0076	0.0088	0.0104	0.0128	0.0168	0.0246

Validation 1000x1000mm

	Absolute deviation	Minimum deviation	Maximum deviation	Standard deviation
1000x1000mm	1.76%	0.00%	4.68%	1.09%

Volume of deformation - validation analytical results - 1000x1000mm plate																								
	Radius [mm]	25000	24000	23000	22000	21000	20000	19000	18000	17000	16000	15000	14000	13000	12000	11000	10000	9000	8000	7000	6000	5000	4000	3000
Thickness [mm]	4	2.36%	2.70%	3.05%	3.33%	3.64%	3.89%	4.14%	4.33%	4.53%	4.64%	4.68%	4.65%	4.51%	4.24%	3.83%	3.25%	2.51%	1.59%	0.51%	0.67%	1.84%	2.73%	2.65%
	5	0.03%	0.16%	0.38%	0.55%	0.72%	0.88%	1.04%	1.20%	1.38%	1.55%	1.72%	1.89%	2.04%	2.13%	2.12%	2.00%	1.74%	1.29%	0.65%	0.16%	1.10%	2.01%	
	6	1.31%	1.20%	1.09%	1.03%	0.98%	0.93%	0.89%	0.84%	0.77%	0.68%	0.56%	0.38%	0.16%	0.10%	0.35%	0.58%	0.72%	0.72%	0.54%	0.12%	0.54%	1.42%	
	7	1.97%	1.92%	1.87%	1.87%	1.90%	1.93%	1.98%	2.02%	2.05%	2.07%	2.04%	1.95%	1.79%	1.53%	1.20%	0.79%	0.38%	0.00%	0.23%	0.21%	0.15%		
	8	2.28%	2.26%	2.26%	2.29%	2.36%	2.43%	2.54%	2.63%	2.74%	2.83%	2.88%	2.88%	2.82%	2.64%	2.35%	1.92%	1.38%	0.77%	0.21%	0.14%	0.09%		
	9	2.39%	2.38%	2.40%	2.45%	2.53%	2.63%	2.76%	2.89%	3.03%	3.17%	3.27%	3.35%	3.36%	3.28%	3.07%	2.70%	2.16%	1.46%	0.70%	0.05%			
	10	2.37%	2.37%	2.39%	2.45%	2.53%	2.64%	2.77%	2.91%	3.06%	3.22%	3.36%	3.47%	3.54%	3.54%	3.42%	3.14%	2.68%	1.99%	1.15%				
	11	2.28%	2.27%	2.29%	2.34%	2.42%	2.52%	2.64%	2.78%	2.93%	3.09%	3.24%	3.37%	3.48%	3.52%	3.47%	3.29%	2.92%	2.32%	1.50%				
	12	2.13%	2.12%	2.13%	2.17%	2.24%	2.32%	2.43%	2.55%	2.68%	2.83%	2.98%	3.12%	3.23%	3.31%	3.31%	3.20%	2.93%	2.44%					
	13	1.94%	1.92%	1.92%	1.95%	2.00%	2.06%	2.15%	2.25%	2.36%	2.49%	2.62%	2.75%	2.87%	2.96%	2.99%	2.94%	2.75%	2.38%					
	14	1.73%	1.70%	1.69%	1.70%	1.73%	1.77%	1.83%	1.90%	2.00%	2.10%	2.20%	2.31%	2.42%	2.51%	2.56%	2.54%	2.43%						
	15	1.50%	1.46%	1.43%	1.42%	1.43%	1.45%	1.49%	1.53%	1.59%	1.67%	1.74%	1.83%	1.91%	1.99%	2.05%	2.06%	2.00%						
	16	1.26%	1.21%	1.17%	1.13%	1.12%	1.11%	1.12%	1.14%	1.17%	1.21%	1.26%	1.31%	1.37%	1.43%	1.48%	1.51%							
	17	1.01%	0.95%	0.89%	0.84%	0.80%	0.76%	0.74%	0.73%	0.73%	0.73%	0.75%	0.78%	0.81%	0.85%	0.88%	0.91%							
	18	0.76%	0.68%	0.60%	0.53%	0.47%	0.41%	0.36%	0.31%	0.28%	0.25%	0.23%	0.23%	0.23%	0.24%	0.26%								
	19	0.51%	0.41%	0.32%	0.22%	0.14%	0.05%	0.03%	0.11%	0.18%	0.24%	0.29%	0.33%	0.36%	0.37%									
	20	0.25%	0.14%	0.03%	0.09%	0.20%	0.31%	0.42%	0.53%	0.63%	0.73%	0.81%	0.89%	0.95%	0.99%									

Numerical results 2000x1000mm

Volume of deformation - numerical results - 2000x1000mm plate																								
Radius [mm]		25000	24000	23000	22000	21000	20000	19000	18000	17000	16000	15000	14000	13000	12000	11000	10000	9000	8000	7000	6000	5000	4000	3000
Thickness [mm]	4	0.0251	0.0261	0.0273	0.0285	0.0299	0.0315	0.0331	0.0350	0.0371	0.0395	0.0421	0.0452	0.0487	0.0528	0.0576	0.0634	0.0705	0.0793	0.0906	0.1056	0.1265	0.1576	0.2082
	5	0.0249	0.0260	0.0271	0.0284	0.0298	0.0313	0.0330	0.0349	0.0370	0.0393	0.0420	0.0450	0.0485	0.0526	0.0575	0.0633	0.0703	0.0791	0.0905	0.1055	0.1264	0.1574	0.2081
	6	0.0248	0.0258	0.0270	0.0283	0.0296	0.0312	0.0328	0.0347	0.0368	0.0391	0.0418	0.0449	0.0484	0.0525	0.0573	0.0631	0.0702	0.0790	0.0903	0.1054	0.1263	0.1573	0.2080
	7	0.0247	0.0257	0.0269	0.0281	0.0295	0.0310	0.0327	0.0346	0.0367	0.0390	0.0417	0.0447	0.0482	0.0523	0.0572	0.0630	0.0700	0.0789	0.0902	0.1052	0.1261	0.1572	0.2079
	8	0.0246	0.0256	0.0268	0.0280	0.0294	0.0309	0.0326	0.0344	0.0365	0.0389	0.0415	0.0446	0.0481	0.0522	0.0570	0.0628	0.0699	0.0787	0.0900	0.1051	0.1260	0.1571	0.2078
	9	0.0245	0.0255	0.0267	0.0279	0.0293	0.0308	0.0325	0.0343	0.0364	0.0387	0.0414	0.0444	0.0479	0.0520	0.0569	0.0626	0.0697	0.0786	0.0899	0.1049	0.1259	0.1569	0.2076
	10	0.0244	0.0255	0.0266	0.0278	0.0292	0.0307	0.0324	0.0342	0.0363	0.0386	0.0413	0.0443	0.0478	0.0519	0.0567	0.0625	0.0696	0.0784	0.0897	0.1048	0.1257	0.1568	0.2075
	11	0.0244	0.0254	0.0265	0.0278	0.0291	0.0306	0.0323	0.0341	0.0362	0.0385	0.0411	0.0442	0.0477	0.0517	0.0566	0.0623	0.0694	0.0783	0.0896	0.1046	0.1256	0.1567	0.2074
	12	0.0243	0.0253	0.0265	0.0277	0.0291	0.0305	0.0322	0.0340	0.0361	0.0384	0.0410	0.0441	0.0475	0.0516	0.0564	0.0622	0.0693	0.0781	0.0894	0.1045	0.1255	0.1565	0.2073
	13	0.0243	0.0253	0.0264	0.0277	0.0290	0.0305	0.0321	0.0340	0.0360	0.0383	0.0409	0.0439	0.0474	0.0515	0.0563	0.0621	0.0691	0.0780	0.0893	0.1043	0.1253	0.1564	0.2071
	14	0.0242	0.0253	0.0264	0.0276	0.0289	0.0304	0.0321	0.0339	0.0359	0.0382	0.0409	0.0439	0.0473	0.0514	0.0562	0.0619	0.0690	0.0778	0.0891	0.1042	0.1252	0.1563	0.2070
	15	0.0242	0.0252	0.0263	0.0276	0.0289	0.0304	0.0320	0.0338	0.0359	0.0382	0.0408	0.0438	0.0472	0.0513	0.0561	0.0618	0.0689	0.0777	0.0890	0.1040	0.1250	0.1561	0.2069
	16	0.0242	0.0252	0.0263	0.0275	0.0289	0.0303	0.0320	0.0338	0.0358	0.0381	0.0407	0.0437	0.0471	0.0512	0.0559	0.0617	0.0687	0.0775	0.0888	0.1039	0.1248	0.1560	0.2067
	17	0.0242	0.0252	0.0263	0.0275	0.0288	0.0303	0.0319	0.0337	0.0358	0.0380	0.0406	0.0436	0.0471	0.0511	0.0558	0.0616	0.0686	0.0774	0.0887	0.1037	0.1247	0.1558	0.2066
	18	0.0241	0.0252	0.0263	0.0275	0.0288	0.0303	0.0319	0.0337	0.0357	0.0380	0.0406	0.0436	0.0470	0.0510	0.0558	0.0615	0.0685	0.0773	0.0886	0.1036	0.1245	0.1557	0.2065
	19	0.0241	0.0251	0.0262	0.0275	0.0288	0.0302	0.0319	0.0337	0.0357	0.0379	0.0405	0.0435	0.0469	0.0509	0.0557	0.0614	0.0684	0.0771	0.0884	0.1034	0.1244	0.1555	0.2063
	20	0.0241	0.0251	0.0262	0.0274	0.0288	0.0302	0.0318	0.0336	0.0356	0.0379	0.0405	0.0434	0.0469	0.0509	0.0556	0.0613	0.0683	0.0770	0.0883	0.1033	0.1242	0.1554	0.2062

Analytical results 2000x1000mm

Volume of deformation - analytical results - 2000x1000mm plate																								
Radius [mm]		25000	24000	23000	22000	21000	20000	19000	18000	17000	16000	15000	14000	13000	12000	11000	10000	9000	8000	7000	6000	5000	4000	3000
Thickness [mm]	4	0.0248	0.0259	0.0271	0.0283	0.0297	0.0313	0.0330	0.0348	0.0369	0.0393	0.0420	0.0450	0.0486	0.0527	0.0575	0.0633	0.0704	0.0792	0.0905	0.1055	0.1262	0.1568	0.2059
	5	0.0248	0.0259	0.0270	0.0283	0.0297	0.0312	0.0329	0.0347	0.0368	0.0392	0.0419	0.0449	0.0484	0.0525	0.0574	0.0632	0.0703	0.0791	0.0904	0.1053	0.1261	0.1566	0.2059
	6	0.0247	0.0258	0.0269	0.0282	0.0296	0.0311	0.0328	0.0347	0.0367	0.0391	0.0418	0.0448	0.0483	0.0524	0.0572	0.0630	0.0701	0.0789	0.0902	0.1052	0.1259	0.1565	0.2059
	7	0.0247	0.0257	0.0269	0.0281	0.0295	0.0310	0.0327	0.0346	0.0366	0.0390	0.0416	0.0447	0.0482	0.0523	0.0571	0.0629	0.0700	0.0788	0.0901	0.1050	0.1258	0.1564	0.2059
	8	0.0246	0.0257	0.0268	0.0281	0.0294	0.0309	0.0326	0.0345	0.0365	0.0389	0.0415	0.0446	0.0481	0.0522	0.0570	0.0628	0.0698	0.0786	0.0899	0.1049	0.1256	0.1563	0.2059
	9	0.0246	0.0256	0.0267	0.0280	0.0294	0.0309	0.0325	0.0344	0.0365	0.0388	0.0414	0.0445	0.0480	0.0520	0.0568	0.0626	0.0697	0.0785	0.0897	0.1047	0.1255	0.1562	0.2059
	10	0.0245	0.0255	0.0267	0.0279	0.0293	0.0308	0.0324	0.0343	0.0364	0.0387	0.0413	0.0444	0.0478	0.0519	0.0567	0.0625	0.0695	0.0783	0.0896	0.1046	0.1253	0.1561	0.2059
	11	0.0245	0.0255	0.0266	0.0279	0.0292	0.0307	0.0324	0.0342	0.0363	0.0386	0.0412	0.0442	0.0477	0.0518	0.0566	0.0623	0.0694	0.0782	0.0894	0.1044	0.1252	0.1560	0.2059
	12	0.0244	0.0254	0.0266	0.0278	0.0291	0.0306	0.0323	0.0341	0.0362	0.0385	0.0411	0.0441	0.0476	0.0517	0.0565	0.0622	0.0692	0.0780	0.0893	0.1043	0.1251	0.1559	0.2059
	13	0.0243	0.0254	0.0265	0.0277	0.0291	0.0306	0.0322	0.0340	0.0361	0.0384	0.0410	0.0440	0.0475	0.0515	0.0563	0.0621	0.0691	0.0779	0.0891	0.1041	0.1249	0.1558	0.2059
	14	0.0243	0.0253	0.0264	0.0277	0.0290	0.0305	0.0321	0.0339	0.0360	0.0383	0.0409	0.0439	0.0474	0.0514	0.0562	0.0619	0.0690	0.0777	0.0890	0.1040	0.1248	0.1557	0.2059
	15	0.0242	0.0253	0.0264	0.0276	0.0289	0.0304	0.0320	0.0339	0.0359	0.0382	0.0408	0.0438	0.0473	0.0513	0.0561	0.0618	0.0688	0.0776	0.0888	0.1038	0.1246	0.1556	0.2059
	16	0.0242	0.0252	0.0263	0.0275	0.0289	0.0303	0.0320	0.0338	0.0358	0.0381	0.0407	0.0437	0.0472	0.0512	0.0560	0.0617	0.0687	0.0774	0.0887	0.1037	0.1245	0.1555	0.2059
	17	0.0241	0.0251	0.0262	0.0275	0.0288	0.0303	0.0319	0.0337	0.0357	0.0380	0.0406	0.0436	0.0470	0.0511	0.0558	0.0616	0.0686	0.0773	0.0885	0.1035	0.1244	0.1554	0.2060
	18	0.0241	0.0251	0.0262	0.0274	0.0287	0.0302	0.0318	0.0336	0.0356	0.0379	0.0405	0.0435	0.0469	0.0509	0.0557	0.0614	0.0684	0.0772	0.0884	0.1034	0.1242	0.1553	0.2060
	19	0.0240	0.0250	0.0261	0.0273	0.0287	0.0301	0.0317	0.0335	0.0356	0.0378	0.0404	0.0434	0.0468	0.0508	0.0556	0.0613	0.0683	0.0770	0.0883	0.1032	0.1241	0.1551	0.2060
	20	0.0240	0.0250	0.0261	0.0273	0.0286	0.0300	0.0317	0.0335	0.0355	0.0377	0.0403	0.0433	0.0467	0.0507	0.0555	0.0612	0.0681	0.0769	0.0881	0.1031	0.1239	0.1550	0.2060

Validation 2000x1000mm

	Absolute deviation	Minimum deviation	Maximum deviation	Standard deviation
2000x1000mm	0.20%	0.00%	1.13%	0.16%

Volume of deformation - validation analytical results - 2000x1000mm plate																								
Radius [mm]		25000	24000	23000	22000	21000	20000	19000	18000	17000	16000	15000	14000	13000	12000	11000	10000	9000	8000	7000	6000	5000	4000	3000
Thickness [mm]	4	0.84%	0.74%	0.75%	0.71%	0.64%	0.62%	0.55%	0.52%	0.47%	0.39%	0.35%	0.30%	0.24%	0.20%	0.15%	0.11%	0.07%	0.06%	0.06%	0.11%	0.24%	0.51%	1.13%
	5	0.49%	0.42%	0.45%	0.43%	0.39%	0.39%	0.35%	0.34%	0.32%	0.27%	0.24%	0.22%	0.18%	0.17%	0.14%	0.12%	0.09%	0.08%	0.10%	0.14%	0.26%	0.51%	
	6	0.20%	0.16%	0.18%	0.19%	0.16%	0.18%	0.15%	0.17%	0.17%	0.14%	0.14%	0.14%	0.13%	0.12%	0.12%	0.11%	0.10%	0.11%	0.12%	0.17%	0.27%	0.50%	
	7	0.03%	0.05%	0.03%	0.01%	0.04%	0.01%	0.02%	0.02%	0.03%	0.02%	0.04%	0.06%	0.06%	0.07%	0.08%	0.09%	0.10%	0.12%	0.14%	0.19%	0.29%		
	8	0.19%	0.20%	0.19%	0.16%	0.18%	0.13%	0.14%	0.10%	0.09%	0.08%	0.05%	0.02%	0.00%	0.01%	0.05%	0.07%	0.10%	0.12%	0.15%	0.21%			
	9	0.30%	0.30%	0.29%	0.26%	0.27%	0.22%	0.23%	0.19%	0.18%	0.15%	0.12%	0.09%	0.06%	0.04%	0.01%	0.04%	0.08%	0.12%	0.16%	0.22%			
	10	0.35%	0.35%	0.34%	0.31%	0.32%	0.28%	0.28%	0.24%	0.24%	0.21%	0.17%	0.14%	0.10%	0.07%	0.02%	0.02%	0.07%	0.12%	0.17%				
	11	0.37%	0.36%	0.36%	0.32%	0.33%	0.30%	0.30%	0.27%	0.26%	0.23%	0.20%	0.17%	0.13%	0.10%	0.05%	0.00%	0.05%	0.11%	0.17%				
	12	0.35%	0.34%	0.33%	0.30%	0.31%	0.29%	0.28%	0.26%	0.26%	0.23%	0.21%	0.18%	0.15%	0.11%	0.06%	0.02%	0.04%	0.10%					
	13	0.29%	0.28%	0.28%	0.25%	0.26%	0.24%	0.24%	0.23%	0.24%	0.21%	0.19%	0.17%	0.14%	0.11%	0.07%	0.02%	0.04%						
	14	0.22%	0.20%	0.20%	0.18%	0.19%	0.18%	0.18%	0.17%	0.19%	0.17%	0.15%	0.14%	0.12%	0.10%	0.06%	0.02%	0.04%						
	15	0.12%	0.11%	0.11%	0.09%	0.09%	0.09%	0.10%	0.09%	0.11%	0.10%	0.10%	0.10%	0.09%	0.07%	0.04%	0.01%							
	16	0.01%	0.01%	0.01%	0.03%	0.02%	0.02%	0.01%	0.00%	0.02%	0.02%	0.03%	0.04%	0.03%	0.03%	0.01%	0.01%							
	17	0.12%	0.13%	0.14%	0.15%	0.14%	0.14%	0.13%	0.11%	0.08%	0.07%	0.06%	0.04%	0.03%	0.03%	0.03%								
	18	0.25%	0.27%	0.28%	0.29%	0.28%	0.27%	0.26%	0.24%	0.20%	0.18%	0.16%	0.13%	0.11%	0.09%									
	19	0.40%	0.42%	0.43%	0.44%	0.43%	0.42%	0.40%	0.37%	0.33%	0.31%	0.27%	0.23%	0.20%	0.17%									
	20	0.55%	0.58%	0.58%	0.60%	0.59%	0.57%	0.55%	0.52%	0.47%	0.44%	0.39%	0.34%	0.30%										

Numerical results 2000x2000mm

Volume of deformation - numerical results - 2000x2000mm plate																								
Radius [mm]		25000	24000	23000	22000	21000	20000	19000	18000	17000	16000	15000	14000	13000	12000	11000	10000	9000	8000	7000	6000	5000	4000	3000
Thickness [mm]	4	0.0495	0.0516	0.0540	0.0565	0.0593	0.0624	0.0658	0.0695	0.0738	0.0785	0.0838	0.0899	0.0969	0.1051	0.1148	0.1264	0.1405	0.1582	0.1808	0.2108	0.2526	0.3147	0.4160
	5	0.0488	0.0510	0.0534	0.0559	0.0587	0.0618	0.0652	0.0690	0.0732	0.0780	0.0833	0.0894	0.0965	0.1047	0.1144	0.1260	0.1402	0.1578	0.1805	0.2105	0.2523	0.3144	0.4156
	6	0.0481	0.0503	0.0527	0.0553	0.0581	0.0612	0.0646	0.0684	0.0726	0.0774	0.0828	0.0889	0.0960	0.1042	0.1139	0.1256	0.1397	0.1574	0.1801	0.2102	0.2520	0.3141	0.4153
	7	0.0474	0.0495	0.0519	0.0545	0.0574	0.0605	0.0639	0.0677	0.0720	0.0768	0.0822	0.0883	0.0954	0.1037	0.1134	0.1251	0.1393	0.1570	0.1797	0.2098	0.2516	0.3137	0.4151
	8	0.0466	0.0487	0.0511	0.0538	0.0566	0.0598	0.0632	0.0670	0.0713	0.0761	0.0815	0.0877	0.0948	0.1031	0.1129	0.1246	0.1388	0.1565	0.1793	0.2094	0.2513	0.3134	0.4147
	9	0.0457	0.0479	0.0503	0.0530	0.0558	0.0590	0.0624	0.0663	0.0706	0.0754	0.0808	0.0871	0.0942	0.1025	0.1123	0.1240	0.1383	0.1561	0.1788	0.2090	0.2509	0.3131	0.4144
	10	0.0449	0.0471	0.0495	0.0521	0.0550	0.0582	0.0616	0.0655	0.0698	0.0746	0.0801	0.0863	0.0935	0.1018	0.1117	0.1234	0.1377	0.1555	0.1783	0.2085	0.2505	0.3127	0.4141
	11	0.0442	0.0464	0.0487	0.0513	0.0542	0.0573	0.0608	0.0647	0.0690	0.0738	0.0793	0.0856	0.0928	0.1012	0.1110	0.1228	0.1371	0.1550	0.1778	0.2080	0.2501	0.3123	0.4138
	12	0.0435	0.0456	0.0480	0.0506	0.0534	0.0565	0.0600	0.0639	0.0682	0.0730	0.0786	0.0848	0.0921	0.1004	0.1103	0.1221	0.1365	0.1544	0.1772	0.2075	0.2496	0.3119	0.4134
	13	0.0429	0.0450	0.0473	0.0498	0.0526	0.0558	0.0592	0.0631	0.0674	0.0722	0.0778	0.0840	0.0913	0.0997	0.1096	0.1215	0.1359	0.1538	0.1767	0.2070	0.2491	0.3115	0.4130
	14	0.0423	0.0444	0.0467	0.0492	0.0519	0.0550	0.0584	0.0623	0.0666	0.0714	0.0769	0.0832	0.0905	0.0989	0.1089	0.1207	0.1352	0.1532	0.1761	0.2065	0.2486	0.3111	0.4127
	15	0.0419	0.0439	0.0461	0.0486	0.0513	0.0543	0.0577	0.0615	0.0658	0.0706	0.0761	0.0824	0.0897	0.0981	0.1081	0.1200	0.1345	0.1525	0.1755	0.2059	0.2481	0.3106	0.4123
	16	0.0415	0.0434	0.0456	0.0481	0.0507	0.0537	0.0571	0.0608	0.0650	0.0698	0.0753	0.0816	0.0889	0.0973	0.1073	0.1192	0.1338	0.1518	0.1749	0.2053	0.2476	0.3101	0.4119
	17	0.0411	0.0430	0.0452	0.0476	0.0502	0.0531	0.0564	0.0602	0.0643	0.0691	0.0745	0.0808	0.0881	0.0965	0.1065	0.1185	0.1330	0.1511	0.1742	0.2047	0.2471	0.3096	0.4115
	18	0.0408	0.0427	0.0448	0.0472	0.0497	0.0526	0.0559	0.0595	0.0637	0.0684	0.0738	0.0800	0.0872	0.0957	0.1057	0.1177	0.1323	0.1504	0.1735	0.2041	0.2465	0.3091	0.4110
	19	0.0405	0.0424	0.0445	0.0468	0.0493	0.0522	0.0554	0.0590	0.0630	0.0677	0.0731	0.0793	0.0865	0.0949	0.1049	0.1169	0.1315	0.1496	0.1728	0.2035	0.2459	0.3086	0.4106
	20	0.0403	0.0422	0.0442	0.0465	0.0490	0.0518	0.0549	0.0585	0.0625	0.0671	0.0724	0.0785	0.0857	0.0941	0.1041	0.1160	0.1307	0.1489	0.1721	0.2028	0.2453	0.3081	0.4101

Analytical results 2000x2000mm

Volume of deformation - analytical results - 2000x2000mm plate																								
Radius [mm]		25000	24000	23000	22000	21000	20000	19000	18000	17000	16000	15000	14000	13000	12000	11000	10000	9000	8000	7000	6000	5000	4000	3000
Thickness [mm]	4	0.0499	0.0522	0.0547	0.0574	0.0603	0.0635	0.0670	0.0709	0.0752	0.0800	0.0854	0.0915	0.0986	0.1067	0.1163	0.1278	0.1417	0.1591	0.1814	0.2111	0.2524	0.3141	0.4158
	5	0.0490	0.0513	0.0538	0.0564	0.0594	0.0626	0.0661	0.0699	0.0742	0.0790	0.0844	0.0906	0.0977	0.1059	0.1155	0.1271	0.1411	0.1586	0.1810	0.2107	0.2522	0.3138	0.4147
	6	0.0482	0.0505	0.0529	0.0556	0.0585	0.0616	0.0651	0.0690	0.0733	0.0781	0.0835	0.0897	0.0968	0.1051	0.1148	0.1264	0.1405	0.1581	0.1806	0.2104	0.2519	0.3134	0.4136
	7	0.0474	0.0497	0.0521	0.0547	0.0576	0.0608	0.0642	0.0681	0.0724	0.0772	0.0827	0.0888	0.0960	0.1043	0.1140	0.1257	0.1399	0.1576	0.1802	0.2101	0.2517	0.3131	0.4125
	8	0.0467	0.0489	0.0513	0.0539	0.0568	0.0599	0.0634	0.0672	0.0715	0.0763	0.0818	0.0880	0.0952	0.1035	0.1133	0.1250	0.1393	0.1571	0.1798	0.2098	0.2515	0.3127	0.4114
	9	0.0460	0.0482	0.0506	0.0532	0.0560	0.0591	0.0626	0.0664	0.0707	0.0755	0.0810	0.0872	0.0944	0.1027	0.1126	0.1243	0.1387	0.1566	0.1794	0.2095	0.2512	0.3124	0.4103
	10	0.0454	0.0475	0.0499	0.0524	0.0553	0.0584	0.0618	0.0656	0.0699	0.0747	0.0802	0.0864	0.0936	0.1020	0.1119	0.1237	0.1381	0.1561	0.1790	0.2093	0.2510	0.3121	0.4092
	11	0.0447	0.0469	0.0492	0.0517	0.0545	0.0576	0.0611	0.0649	0.0691	0.0739	0.0794	0.0856	0.0928	0.1012	0.1112	0.1231	0.1375	0.1556	0.1786	0.2090	0.2508	0.3117	0.4081
	12	0.0441	0.0462	0.0486	0.0511	0.0539	0.0569	0.0603	0.0641	0.0684	0.0732	0.0786	0.0849	0.0921	0.1005	0.1105	0.1224	0.1370	0.1551	0.1782	0.2087	0.2505	0.3114	0.4071
	13	0.0436	0.0457	0.0479	0.0504	0.0532	0.0563	0.0596	0.0634	0.0677	0.0725	0.0779	0.0842	0.0914	0.0998	0.1098	0.1218	0.1364	0.1546	0.1778	0.2084	0.2503	0.3111	0.4060
	14	0.0430	0.0451	0.0474	0.0498	0.0526	0.0556	0.0590	0.0627	0.0670	0.0718	0.0772	0.0835	0.0907	0.0992	0.1092	0.1212	0.1359	0.1541	0.1774	0.2081	0.2501	0.3107	0.4050
	15	0.0425	0.0445	0.0468	0.0493	0.0520	0.0550	0.0583	0.0621	0.0663	0.0711	0.0765	0.0828	0.0900	0.0985	0.1085	0.1206	0.1353	0.1536	0.1770	0.2078	0.2498	0.3104	0.4039
	16	0.0420	0.0440	0.0462	0.0487	0.0514	0.0544	0.0577	0.0615	0.0657	0.0704	0.0759	0.0821	0.0893	0.0978	0.1079	0.1200	0.1348	0.1532	0.1767	0.2075	0.2496	0.3101	0.4029
	17	0.0415	0.0435	0.0457	0.0482	0.0508	0.0538	0.0571	0.0608	0.0650	0.0698	0.0752	0.0814	0.0887	0.0972	0.1073	0.1194	0.1342	0.1527	0.1763	0.2072	0.2494	0.3097	0.4019
	18	0.0410	0.0430	0.0452	0.0476	0.0503	0.0533	0.0566	0.0603	0.0644	0.0692	0.0746	0.0808	0.0881	0.0966	0.1067	0.1188	0.1337	0.1523	0.1759	0.2069	0.2492	0.3094	0.4009
	19	0.0406	0.0426	0.0447	0.0471	0.0498	0.0527	0.0560	0.0597	0.0638	0.0686	0.0740	0.0802	0.0874	0.0960	0.1061	0.1183	0.1332	0.1518	0.1755	0.2066	0.2489	0.3091	0.3999
	20	0.0402	0.0421	0.0443	0.0467	0.0493	0.0522	0.0555	0.0591	0.0633	0.0680	0.0734	0.0796	0.0868	0.0954	0.1055	0.1177	0.1327	0.1513	0.1752	0.2064	0.2487	0.3088	0.3989

Validation 2000x2000mm

	Absolute deviation	Minimum deviation	Maximum deviation	Standard deviation
2000x2000mm	0.69%	0.02%	1.95%	0.47%

Volume of deformation - validation analytical results - 2000x2000mm plate																								
Radius [mm]		25000	24000	23000	22000	21000	20000	19000	18000	17000	16000	15000	14000	13000	12000	11000	10000	9000	8000	7000	6000	5000	4000	3000
Thickness [mm]	4	0.74%	1.08%	1.25%	1.48%	1.66%	1.78%	1.89%	1.94%	1.95%	1.95%	1.91%	1.80%	1.68%	1.50%	1.31%	1.09%	0.85%	0.60%	0.34%	0.11%	0.08%	0.18%	0.03%
	5	0.33%	0.60%	0.73%	0.93%	1.06%	1.17%	1.27%	1.34%	1.35%	1.37%	1.37%	1.32%	1.23%	1.12%	1.00%	0.84%	0.68%	0.50%	0.30%	0.11%	0.06%	0.19%	
	6	0.15%	0.36%	0.42%	0.55%	0.66%	0.73%	0.82%	0.86%	0.89%	0.92%	0.93%	0.90%	0.87%	0.80%	0.73%	0.64%	0.54%	0.42%	0.28%	0.14%	0.02%	0.20%	
	7	0.16%	0.29%	0.30%	0.36%	0.43%	0.45%	0.51%	0.52%	0.54%	0.58%	0.58%	0.58%	0.58%	0.55%	0.52%	0.48%	0.43%	0.36%	0.28%	0.17%	0.02%		
	8	0.33%	0.37%	0.34%	0.32%	0.35%	0.30%	0.34%	0.30%	0.31%	0.34%	0.33%	0.33%	0.34%	0.35%	0.35%	0.35%	0.35%	0.33%	0.30%	0.22%			
	9	0.60%	0.58%	0.49%	0.41%	0.39%	0.28%	0.28%	0.20%	0.18%	0.18%	0.16%	0.16%	0.18%	0.21%	0.23%	0.27%	0.30%	0.33%	0.33%	0.28%			
	10	0.91%	0.84%	0.72%	0.58%	0.52%	0.36%	0.32%	0.19%	0.14%	0.11%	0.07%	0.06%	0.08%	0.12%	0.16%	0.22%	0.29%	0.34%	0.38%				
	11	1.21%	1.11%	0.97%	0.79%	0.70%	0.51%	0.42%	0.27%	0.19%	0.12%	0.05%	0.03%	0.04%	0.08%	0.12%	0.20%	0.30%	0.38%	0.45%				
	12	1.44%	1.33%	1.20%	1.01%	0.90%	0.70%	0.58%	0.40%	0.29%	0.19%	0.10%	0.06%	0.05%	0.09%	0.13%	0.23%	0.33%	0.44%					
	13	1.57%	1.48%	1.38%	1.20%	1.09%	0.89%	0.75%	0.56%	0.44%	0.31%	0.20%	0.14%	0.11%	0.14%	0.18%	0.28%	0.40%						
	14	1.59%	1.53%	1.47%	1.32%	1.23%	1.06%	0.92%	0.74%	0.62%	0.47%	0.34%	0.26%	0.22%	0.24%	0.27%	0.37%	0.49%						
	15	1.49%	1.48%	1.47%	1.37%	1.31%	1.18%	1.07%	0.91%	0.80%	0.64%	0.51%	0.42%	0.36%	0.37%	0.39%	0.49%							
	16	1.29%	1.33%	1.38%	1.33%	1.32%	1.24%	1.17%	1.05%	0.97%	0.82%	0.70%	0.60%	0.54%	0.53%	0.55%	0.63%							
	17	1.00%	1.09%	1.19%	1.21%	1.25%	1.24%	1.22%	1.15%	1.11%	0.99%	0.89%	0.80%	0.73%	0.71%	0.73%								
	18	0.62%	0.77%	0.93%	1.00%	1.11%	1.16%	1.20%	1.20%	1.20%	1.13%	1.06%	1.00%	0.94%	0.92%									
	19	0.19%	0.38%	0.59%	0.73%	0.89%	1.02%	1.13%	1.19%	1.26%	1.24%	1.22%	1.19%	1.15%	1.14%									
	20	0.29%	0.06%	0.20%	0.40%	0.62%	0.81%	0.99%	1.13%	1.26%	1.31%	1.35%	1.36%	1.36%										

Numerical results 3000x1000mm

Volume of deformation - numerical results - 3000x1000mm plate																								
Radius [mm]		25000	24000	23000	22000	21000	20000	19000	18000	17000	16000	15000	14000	13000	12000	11000	10000	9000	8000	7000	6000	5000	4000	3000
Thickness [mm]	4	0.0857	0.0894	0.0932	0.0975	0.1022	0.1072	0.1130	0.1192	0.1263	0.1342	0.1431	0.1533	0.1651	0.1789	0.1951	0.2145	0.2381	0.2675	0.3052	0.3550	0.4238	0.5247	0.6849
	5	0.0855	0.0892	0.0930	0.0973	0.1020	0.1071	0.1128	0.1190	0.1261	0.1340	0.1429	0.1532	0.1650	0.1787	0.1949	0.2143	0.2380	0.2674	0.3051	0.3548	0.4237	0.5245	0.6848
	6	0.0853	0.0890	0.0929	0.0971	0.1018	0.1069	0.1126	0.1189	0.1259	0.1338	0.1427	0.1530	0.1648	0.1785	0.1947	0.2141	0.2378	0.2672	0.3049	0.3547	0.4235	0.5244	0.6846
	7	0.0852	0.0888	0.0927	0.0969	0.1016	0.1067	0.1124	0.1187	0.1257	0.1336	0.1426	0.1528	0.1646	0.1783	0.1946	0.2139	0.2376	0.2671	0.3047	0.3545	0.4234	0.5242	0.6845
	8	0.0851	0.0887	0.0926	0.0968	0.1015	0.1066	0.1122	0.1185	0.1256	0.1334	0.1424	0.1526	0.1644	0.1781	0.1944	0.2137	0.2374	0.2669	0.3046	0.3544	0.4232	0.5241	0.6843
	9	0.0849	0.0886	0.0924	0.0966	0.1013	0.1064	0.1121	0.1184	0.1254	0.1333	0.1422	0.1524	0.1642	0.1779	0.1942	0.2136	0.2372	0.2667	0.3044	0.3542	0.4230	0.5239	0.6841
	10	0.0849	0.0885	0.0923	0.0965	0.1012	0.1063	0.1119	0.1182	0.1252	0.1331	0.1420	0.1523	0.1641	0.1778	0.1940	0.2134	0.2371	0.2665	0.3042	0.3540	0.4229	0.5238	0.6840
	11	0.0848	0.0884	0.0922	0.0964	0.1011	0.1062	0.1118	0.1181	0.1251	0.1329	0.1419	0.1521	0.1639	0.1776	0.1938	0.2132	0.2369	0.2663	0.3040	0.3539	0.4227	0.5236	0.6838
	12	0.0847	0.0883	0.0922	0.0964	0.1010	0.1061	0.1117	0.1180	0.1250	0.1328	0.1418	0.1520	0.1637	0.1774	0.1936	0.2130	0.2367	0.2662	0.3038	0.3537	0.4225	0.5234	0.6837
	13	0.0846	0.0882	0.0921	0.0963	0.1009	0.1060	0.1116	0.1179	0.1249	0.1327	0.1416	0.1518	0.1636	0.1773	0.1935	0.2128	0.2365	0.2660	0.3037	0.3535	0.4224	0.5233	0.6835
	14	0.0846	0.0882	0.0920	0.0962	0.1008	0.1059	0.1115	0.1178	0.1248	0.1326	0.1415	0.1517	0.1634	0.1771	0.1933	0.2127	0.2363	0.2658	0.3035	0.3533	0.4222	0.5231	0.6834
	15	0.0846	0.0881	0.0920	0.0962	0.1008	0.1059	0.1115	0.1177	0.1247	0.1325	0.1414	0.1516	0.1633	0.1770	0.1931	0.2125	0.2361	0.2656	0.3033	0.3531	0.4220	0.5229	0.6832
	16	0.0845	0.0881	0.0919	0.0961	0.1007	0.1058	0.1114	0.1176	0.1246	0.1324	0.1413	0.1515	0.1632	0.1769	0.1930	0.2124	0.2360	0.2654	0.3031	0.3530	0.4218	0.5227	0.6830
	17	0.0845	0.0880	0.0919	0.0961	0.1007	0.1057	0.1113	0.1176	0.1245	0.1323	0.1412	0.1514	0.1631	0.1767	0.1929	0.2122	0.2358	0.2653	0.3029	0.3528	0.4216	0.5226	0.6829
	18	0.0844	0.0880	0.0918	0.0960	0.1006	0.1057	0.1113	0.1175	0.1244	0.1323	0.1411	0.1513	0.1630	0.1766	0.1927	0.2121	0.2357	0.2651	0.3027	0.3526	0.4215	0.5224	0.6827
	19	0.0844	0.0880	0.0918	0.0960	0.1006	0.1056	0.1112	0.1174	0.1244	0.1322	0.1411	0.1512	0.1629	0.1765	0.1926	0.2120	0.2355	0.2649	0.3026	0.3524	0.4213	0.5222	0.6825
	20	0.0844	0.0879	0.0918	0.0960	0.1005	0.1056	0.1112	0.1174	0.1243	0.1321	0.1410	0.1511	0.1628	0.1764	0.1925	0.2118	0.2354	0.2648	0.3024	0.3522	0.4211	0.5220	0.6823

Analytical results 3000x1000mm

Volume of deformation - analytical results - 3000x1000mm plate																								
Radius [mm]		25000	24000	23000	22000	21000	20000	19000	18000	17000	16000	15000	14000	13000	12000	11000	10000	9000	8000	7000	6000	5000	4000	3000
Thickness [mm]	4	0.0852	0.0887	0.0926	0.0969	0.1015	0.1067	0.1123	0.1186	0.1256	0.1335	0.1424	0.1526	0.1643	0.1780	0.1941	0.2134	0.2369	0.2661	0.3033	0.3525	0.4201	0.5183	0.6717
	5	0.0851	0.0887	0.0926	0.0968	0.1014	0.1066	0.1122	0.1185	0.1255	0.1333	0.1423	0.1524	0.1642	0.1778	0.1939	0.2132	0.2367	0.2659	0.3032	0.3523	0.4199	0.5182	0.6717
	6	0.0850	0.0886	0.0925	0.0967	0.1014	0.1065	0.1121	0.1184	0.1254	0.1332	0.1421	0.1523	0.1640	0.1777	0.1938	0.2131	0.2365	0.2657	0.3030	0.3522	0.4198	0.5181	0.6717
	7	0.0849	0.0885	0.0924	0.0966	0.1013	0.1064	0.1120	0.1182	0.1252	0.1331	0.1420	0.1522	0.1639	0.1775	0.1936	0.2129	0.2364	0.2656	0.3028	0.3520	0.4196	0.5180	0.6717
	8	0.0849	0.0884	0.0923	0.0965	0.1012	0.1063	0.1119	0.1181	0.1251	0.1330	0.1419	0.1520	0.1637	0.1774	0.1935	0.2127	0.2362	0.2654	0.3027	0.3518	0.4195	0.5179	0.6717
	9	0.0848	0.0883	0.0922	0.0964	0.1011	0.1061	0.1118	0.1180	0.1250	0.1329	0.1417	0.1519	0.1636	0.1772	0.1933	0.2126	0.2360	0.2652	0.3025	0.3517	0.4193	0.5178	0.6717
	10	0.0847	0.0883	0.0921	0.0963	0.1010	0.1060	0.1117	0.1179	0.1249	0.1327	0.1416	0.1518	0.1635	0.1771	0.1932	0.2124	0.2359	0.2651	0.3023	0.3515	0.4192	0.5177	0.6718
	11	0.0846	0.0882	0.0920	0.0963	0.1009	0.1059	0.1116	0.1178	0.1248	0.1326	0.1415	0.1516	0.1633	0.1769	0.1930	0.2123	0.2357	0.2649	0.3022	0.3513	0.4190	0.5176	0.6718
	12	0.0846	0.0881	0.0920	0.0962	0.1008	0.1058	0.1115	0.1177	0.1246	0.1325	0.1414	0.1515	0.1632	0.1768	0.1929	0.2121	0.2356	0.2647	0.3020	0.3512	0.4189	0.5175	0.6718
	13	0.0845	0.0880	0.0919	0.0961	0.1007	0.1057	0.1113	0.1176	0.1245	0.1324	0.1412	0.1514	0.1630	0.1767	0.1927	0.2120	0.2354	0.2646	0.3018	0.3510	0.4187	0.5173	0.6718
	14	0.0844	0.0879	0.0918	0.0960	0.1006	0.1056	0.1112	0.1175	0.1244	0.1322	0.1411	0.1512	0.1629	0.1765	0.1926	0.2118	0.2352	0.2644	0.3017	0.3508	0.4186	0.5172	0.6718
	15	0.0843	0.0879	0.0917	0.0959	0.1005	0.1055	0.1111	0.1174	0.1243	0.1321	0.1410	0.1511	0.1628	0.1764	0.1924	0.2116	0.2351	0.2642	0.3015	0.3507	0.4184	0.5171	0.6718
	16	0.0843	0.0878	0.0916	0.0958	0.1004	0.1054	0.1110	0.1172	0.1242	0.1320	0.1408	0.1510	0.1626	0.1762	0.1923	0.2115	0.2349	0.2641	0.3013	0.3505	0.4183	0.5170	0.6718
	17	0.0842	0.0877	0.0915	0.0957	0.1003	0.1053	0.1109	0.1171	0.1241	0.1319	0.1407	0.1508	0.1625	0.1761	0.1921	0.2113	0.2347	0.2639	0.3012	0.3503	0.4181	0.5169	0.6718
	18	0.0841	0.0876	0.0915	0.0956	0.1002	0.1052	0.1108	0.1170	0.1240	0.1318	0.1406	0.1507	0.1623	0.1759	0.1920	0.2112	0.2346	0.2637	0.3010	0.3502	0.4180	0.5168	0.6719
	19	0.0840	0.0876	0.0914	0.0955	0.1001	0.1052	0.1107	0.1169	0.1238	0.1316	0.1405	0.1506	0.1622	0.1758	0.1918	0.2110	0.2344	0.2636	0.3008	0.3500	0.4178	0.5167	0.6719
	20	0.0840	0.0875	0.0913	0.0955	0.1000	0.1051	0.1106	0.1168	0.1237	0.1315	0.1403	0.1504	0.1621	0.1756	0.1917	0.2109	0.2343	0.2634	0.3007	0.3499	0.4177	0.5166	0.6719

Validation 3000x1000mm

	Absolute deviation	Minimum deviation	Maximum deviation	Standard deviation
3000x1000mm	0.41%	0.17%	1.94%	0.18%

Volume of deformation - validation analytical results - 2000x1000mm plate																								
Radius [mm]		25000	24000	23000	22000	21000	20000	19000	18000	17000	16000	15000	14000	13000	12000	11000	10000	9000	8000	7000	6000	5000	4000	3000
Thickness [mm]	4	0.65%	0.68%	0.64%	0.60%	0.63%	0.54%	0.59%	0.51%	0.56%	0.54%	0.49%	0.49%	0.48%	0.49%	0.51%	0.51%	0.53%	0.54%	0.62%	0.71%	0.88%	1.20%	1.94%
	5	0.51%	0.55%	0.53%	0.49%	0.53%	0.47%	0.52%	0.47%	0.51%	0.49%	0.46%	0.47%	0.47%	0.47%	0.50%	0.50%	0.53%	0.55%	0.62%	0.71%	0.88%	1.20%	
	6	0.38%	0.44%	0.44%	0.39%	0.44%	0.41%	0.44%	0.42%	0.45%	0.43%	0.43%	0.45%	0.46%	0.45%	0.49%	0.49%	0.52%	0.56%	0.62%	0.71%	0.88%	1.19%	
	7	0.29%	0.35%	0.36%	0.30%	0.37%	0.35%	0.37%	0.36%	0.40%	0.38%	0.39%	0.42%	0.43%	0.44%	0.47%	0.48%	0.52%	0.56%	0.62%	0.72%	0.88%		
	8	0.23%	0.29%	0.30%	0.25%	0.31%	0.30%	0.32%	0.32%	0.35%	0.34%	0.36%	0.39%	0.41%	0.42%	0.46%	0.47%	0.51%	0.56%	0.62%	0.72%			
	9	0.19%	0.24%	0.25%	0.22%	0.27%	0.26%	0.28%	0.28%	0.31%	0.30%	0.33%	0.36%	0.38%	0.40%	0.44%	0.46%	0.50%	0.56%	0.62%	0.72%			
	10	0.17%	0.21%	0.23%	0.20%	0.24%	0.24%	0.25%	0.26%	0.28%	0.28%	0.31%	0.34%	0.36%	0.38%	0.42%	0.45%	0.49%	0.55%	0.62%				
	11	0.17%	0.20%	0.22%	0.19%	0.23%	0.23%	0.24%	0.25%	0.27%	0.26%	0.29%	0.32%	0.35%	0.37%	0.40%	0.43%	0.48%	0.55%	0.61%				
	12	0.17%	0.20%	0.22%	0.20%	0.23%	0.23%	0.23%	0.25%	0.26%	0.25%	0.29%	0.31%	0.33%	0.36%	0.39%	0.43%	0.47%	0.54%					
	13	0.19%	0.22%	0.23%	0.21%	0.24%	0.24%	0.24%	0.26%	0.26%	0.26%	0.29%	0.31%	0.33%	0.35%	0.38%	0.42%	0.46%						
	14	0.22%	0.24%	0.26%	0.24%	0.26%	0.26%	0.26%	0.27%	0.28%	0.27%	0.30%	0.31%	0.33%	0.35%	0.38%	0.42%	0.46%						
	15	0.25%	0.27%	0.29%	0.27%	0.29%	0.29%	0.28%	0.30%	0.30%	0.29%	0.31%	0.32%	0.34%	0.36%	0.38%	0.42%							
	16	0.29%	0.31%	0.33%	0.31%	0.32%	0.33%	0.32%	0.33%	0.32%	0.32%	0.33%	0.34%	0.35%	0.37%	0.38%								
	17	0.34%	0.35%	0.37%	0.36%	0.37%	0.37%	0.36%	0.36%	0.36%	0.35%	0.36%	0.36%	0.37%	0.38%	0.39%								
	18	0.39%	0.40%	0.42%	0.41%	0.41%	0.41%	0.40%	0.41%	0.40%	0.39%	0.39%	0.39%	0.39%	0.40%									
	19	0.45%	0.46%	0.47%	0.46%	0.47%	0.47%	0.45%	0.45%	0.44%	0.43%	0.43%	0.42%	0.42%	0.42%									
	20	0.50%	0.52%	0.53%	0.52%	0.52%	0.52%	0.50%	0.50%	0.49%	0.47%	0.47%	0.46%	0.45%										

Numerical results 3000x2000mm

Volume of deformation - numerical results - 3000x2000mm plate																							
Thickness [mm] / Radius [mm]	25000	24000	23000	22000	21000	20000	19000	18000	17000	16000	15000	14000	13000	12000	11000	10000	9000	8000	7000	6000	5000	4000	3000
4	0.1712	0.1784	0.1861	0.1947	0.2041	0.2142	0.2257	0.2381	0.2523	0.2681	0.2859	0.3063	0.3298	0.3574	0.3898	0.4286	0.4759	0.5348	0.6101	0.7097	0.8473	1.0490	1.3692
5	0.1707	0.1780	0.1857	0.1942	0.2036	0.2137	0.2252	0.2377	0.2518	0.2676	0.2855	0.3059	0.3295	0.3570	0.3894	0.4282	0.4755	0.5343	0.6096	0.7092	0.8468	1.0485	1.3686
6	0.1702	0.1775	0.1852	0.1937	0.2031	0.2133	0.2247	0.2372	0.2514	0.2672	0.2850	0.3055	0.3291	0.3565	0.3890	0.4278	0.4751	0.5339	0.6093	0.7089	0.8463	1.0481	1.3687
7	0.1696	0.1769	0.1847	0.1932	0.2026	0.2128	0.2243	0.2368	0.2509	0.2667	0.2846	0.3051	0.3286	0.3561	0.3886	0.4273	0.4746	0.5335	0.6088	0.7084	0.8459	1.0476	1.3682
8	0.1691	0.1764	0.1842	0.1927	0.2021	0.2123	0.2237	0.2363	0.2504	0.2662	0.2841	0.3046	0.3282	0.3556	0.3881	0.4269	0.4742	0.5331	0.6085	0.7079	0.8457	1.0475	1.3678
9	0.1685	0.1758	0.1836	0.1921	0.2016	0.2118	0.2232	0.2358	0.2499	0.2657	0.2836	0.3041	0.3277	0.3552	0.3877	0.4265	0.4738	0.5326	0.6080	0.7075	0.8451	1.0467	1.3676
10	0.1679	0.1752	0.1831	0.1915	0.2010	0.2112	0.2227	0.2352	0.2494	0.2652	0.2831	0.3036	0.3272	0.3547	0.3872	0.4260	0.4734	0.5322	0.6076	0.7071	0.8447	1.0466	1.3670
11	0.1673	0.1746	0.1825	0.1909	0.2004	0.2107	0.2221	0.2347	0.2489	0.2647	0.2826	0.3031	0.3268	0.3542	0.3867	0.4256	0.4729	0.5318	0.6071	0.7067	0.8443	1.0463	1.3666
12	0.1667	0.1740	0.1819	0.1903	0.1998	0.2101	0.2215	0.2341	0.2483	0.2641	0.2821	0.3026	0.3263	0.3537	0.3863	0.4251	0.4724	0.5314	0.6067	0.7063	0.8439	1.0455	1.3665
13	0.1661	0.1734	0.1813	0.1897	0.1992	0.2095	0.2209	0.2335	0.2477	0.2636	0.2815	0.3021	0.3257	0.3532	0.3858	0.4246	0.4720	0.5309	0.6064	0.7059	0.8437	1.0450	1.3651
14	0.1654	0.1728	0.1807	0.1891	0.1986	0.2089	0.2203	0.2330	0.2471	0.2630	0.2810	0.3015	0.3252	0.3527	0.3853	0.4241	0.4715	0.5304	0.6058	0.7054	0.8433	1.0451	1.3657
15	0.1648	0.1722	0.1801	0.1885	0.1980	0.2083	0.2197	0.2324	0.2466	0.2624	0.2804	0.3010	0.3246	0.3522	0.3847	0.4236	0.4710	0.5300	0.6054	0.7050	0.8426	1.0442	1.3649
16	0.1643	0.1716	0.1795	0.1879	0.1974	0.2077	0.2191	0.2318	0.2460	0.2618	0.2798	0.3004	0.3241	0.3516	0.3842	0.4231	0.4705	0.5295	0.6049	0.7045	0.8422	1.0437	1.3637
17	0.1637	0.1710	0.1789	0.1873	0.1968	0.2071	0.2185	0.2312	0.2453	0.2612	0.2792	0.2998	0.3235	0.3511	0.3836	0.4225	0.4700	0.5290	0.6044	0.7041	0.8417	1.0433	1.3633
18	0.1632	0.1704	0.1783	0.1867	0.1962	0.2065	0.2179	0.2306	0.2447	0.2606	0.2786	0.2992	0.3229	0.3505	0.3831	0.4220	0.4695	0.5286	0.6039	0.7036	0.8413	1.0428	1.3628
19	0.1626	0.1699	0.1777	0.1862	0.1956	0.2059	0.2173	0.2300	0.2441	0.2600	0.2780	0.2986	0.3223	0.3499	0.3825	0.4214	0.4689	0.5280	0.6035	0.7032	0.8409	1.0424	1.3624
20	0.1621	0.1693	0.1772	0.1856	0.1950	0.2053	0.2167	0.2294	0.2435	0.2593	0.2774	0.2980	0.3217	0.3493	0.3819	0.4209	0.4684	0.5275	0.6030	0.7027	0.8404	1.0420	1.3619

Analytical results 3000x2000mm

Volume of deformation - analytical results - 3000x2000mm plate																							
Thickness [mm] / Radius [mm]	25000	24000	23000	22000	21000	20000	19000	18000	17000	16000	15000	14000	13000	12000	11000	10000	9000	8000	7000	6000	5000	4000	3000
4	0.1718	0.1790	0.1868	0.1954	0.2047	0.2149	0.2262	0.2387	0.2527	0.2685	0.2863	0.3066	0.3300	0.3572	0.3894	0.4278	0.4746	0.5328	0.6071	0.7052	0.8402	1.0368	1.3446
5	0.1712	0.1784	0.1862	0.1948	0.2041	0.2143	0.2256	0.2382	0.2522	0.2680	0.2858	0.3061	0.3295	0.3568	0.3890	0.4275	0.4743	0.5326	0.6069	0.7051	0.8401	1.0367	1.3445
6	0.1706	0.1778	0.1856	0.1942	0.2035	0.2138	0.2251	0.2377	0.2517	0.2674	0.2853	0.3056	0.3291	0.3564	0.3886	0.4271	0.4740	0.5323	0.6067	0.7049	0.8401	1.0367	1.3444
7	0.1700	0.1772	0.1850	0.1936	0.2029	0.2132	0.2245	0.2371	0.2512	0.2669	0.2848	0.3052	0.3286	0.3560	0.3882	0.4267	0.4737	0.5320	0.6065	0.7048	0.8400	1.0367	1.3443
8	0.1694	0.1766	0.1844	0.1930	0.2023	0.2126	0.2240	0.2366	0.2506	0.2664	0.2843	0.3047	0.3282	0.3556	0.3878	0.4264	0.4734	0.5318	0.6063	0.7047	0.8399	1.0367	1.3442
9	0.1688	0.1760	0.1839	0.1924	0.2018	0.2121	0.2234	0.2360	0.2501	0.2659	0.2838	0.3042	0.3278	0.3551	0.3874	0.4260	0.4731	0.5315	0.6061	0.7045	0.8398	1.0366	1.3441
10	0.1682	0.1754	0.1833	0.1918	0.2012	0.2115	0.2229	0.2355	0.2496	0.2654	0.2833	0.3038	0.3273	0.3547	0.3870	0.4257	0.4728	0.5313	0.6059	0.7044	0.8398	1.0366	1.3440
11	0.1676	0.1748	0.1827	0.1913	0.2007	0.2110	0.2223	0.2350	0.2491	0.2649	0.2828	0.3033	0.3269	0.3543	0.3867	0.4254	0.4724	0.5310	0.6057	0.7042	0.8397	1.0366	1.3439
12	0.1670	0.1743	0.1821	0.1907	0.2001	0.2104	0.2218	0.2344	0.2486	0.2644	0.2824	0.3028	0.3264	0.3539	0.3863	0.4250	0.4721	0.5307	0.6055	0.7041	0.8396	1.0365	1.3438
13	0.1665	0.1737	0.1816	0.1902	0.1996	0.2099	0.2213	0.2339	0.2481	0.2639	0.2819	0.3024	0.3260	0.3535	0.3859	0.4247	0.4718	0.5305	0.6053	0.7039	0.8395	1.0365	1.3437
14	0.1659	0.1731	0.1810	0.1896	0.1990	0.2093	0.2208	0.2334	0.2476	0.2634	0.2814	0.3019	0.3256	0.3531	0.3855	0.4243	0.4715	0.5302	0.6051	0.7038	0.8395	1.0365	1.3436
15	0.1653	0.1726	0.1805	0.1891	0.1985	0.2088	0.2202	0.2329	0.2470	0.2629	0.2809	0.3015	0.3251	0.3527	0.3851	0.4240	0.4712	0.5300	0.6049	0.7037	0.8394	1.0365	1.3435
16	0.1648	0.1720	0.1799	0.1885	0.1979	0.2083	0.2197	0.2324	0.2466	0.2625	0.2805	0.3010	0.3247	0.3523	0.3848	0.4236	0.4709	0.5297	0.6047	0.7035	0.8393	1.0364	1.3435
17	0.1642	0.1715	0.1794	0.1880	0.1974	0.2078	0.2192	0.2319	0.2461	0.2620	0.2800	0.3006	0.3243	0.3519	0.3844	0.4233	0.4706	0.5295	0.6045	0.7034	0.8392	1.0364	1.3434
18	0.1637	0.1710	0.1789	0.1875	0.1969	0.2072	0.2187	0.2314	0.2456	0.2615	0.2795	0.3001	0.3239	0.3515	0.3840	0.4229	0.4703	0.5292	0.6043	0.7032	0.8392	1.0364	1.3433
19	0.1632	0.1704	0.1783	0.1869	0.1964	0.2067	0.2182	0.2309	0.2451	0.2610	0.2791	0.2997	0.3234	0.3511	0.3836	0.4226	0.4700	0.5289	0.6041	0.7031	0.8391	1.0363	1.3432
20	0.1626	0.1699	0.1778	0.1864	0.1958	0.2062	0.2177	0.2304	0.2446	0.2606	0.2786	0.2992	0.3230	0.3507	0.3833	0.4223	0.4697	0.5287	0.6039	0.7030	0.8390	1.0363	1.3431

Validation 3000x2000mm

	Absolute deviation	Minimum deviation	Maximum deviation	Standard deviation
3000x2000mm	0.22%	0.00%	1.80%	0.19%

Volume of deformation - validation analytical results - 2000x2000mm plate																							
Thickness [mm] / Radius [mm]	25000	24000	23000	22000	21000	20000	19000	18000	17000	16000	15000	14000	13000	12000	11000	10000	9000	8000	7000	6000	5000	4000	3000
4	0.38%	0.34%	0.37%	0.34%	0.30%	0.33%	0.24%	0.26%	0.19%	0.15%	0.13%	0.09%	0.05%	0.04%	0.12%	0.19%	0.27%	0.36%	0.48%	0.63%	0.83%	1.16%	1.80%
5	0.30%	0.26%	0.29%	0.28%	0.23%	0.28%	0.19%	0.22%	0.14%	0.12%	0.11%	0.07%	0.03%	0.04%	0.11%	0.17%	0.25%	0.33%	0.44%	0.58%	0.78%	1.12%	
6	0.25%	0.19%	0.22%	0.23%	0.18%	0.22%	0.15%	0.19%	0.11%	0.10%	0.09%	0.05%	0.01%	0.04%	0.10%	0.15%	0.22%	0.29%	0.42%	0.56%	0.74%	1.09%	
7	0.21%	0.15%	0.17%	0.19%	0.14%	0.18%	0.12%	0.15%	0.09%	0.08%	0.08%	0.04%	0.00%	0.03%	0.09%	0.14%	0.20%	0.28%	0.38%	0.52%	0.70%		
8	0.18%	0.12%	0.14%	0.17%	0.11%	0.15%	0.10%	0.13%	0.07%	0.07%	0.07%	0.03%	0.00%	0.02%	0.08%	0.12%	0.18%	0.25%	0.36%	0.47%			
9	0.17%	0.11%	0.12%	0.16%	0.10%	0.14%	0.09%	0.12%	0.07%	0.06%	0.07%	0.03%	0.01%	0.01%	0.07%	0.10%	0.15%	0.21%	0.31%	0.43%			
10	0.17%	0.11%	0.12%	0.16%	0.10%	0.14%	0.09%	0.12%	0.07%	0.07%	0.08%	0.04%	0.02%	0.00%	0.05%	0.08%	0.13%	0.18%	0.27%				
11	0.19%	0.13%	0.13%	0.18%	0.11%	0.14%	0.11%	0.12%	0.08%	0.09%	0.09%	0.05%	0.03%	0.02%	0.02%	0.05%	0.10%	0.15%	0.24%				
12	0.21%	0.15%	0.15%	0.20%	0.14%	0.16%	0.13%	0.14%	0.10%	0.11%	0.10%	0.08%	0.06%	0.04%	0.00%	0.02%	0.06%	0.12%					
13	0.24%	0.18%	0.17%	0.23%	0.16%	0.18%	0.15%	0.16%	0.13%	0.14%	0.13%	0.10%	0.08%	0.08%	0.03%	0.01%	0.03%						
14	0.27%	0.21%	0.20%	0.26%	0.20%	0.21%	0.19%	0.20%	0.16%	0.17%	0.16%	0.13%	0.12%	0.11%	0.07%	0.05%	0.01%						
15	0.30%	0.24%	0.23%	0.29%	0.23%	0.25%	0.23%	0.23%	0.20%	0.21%	0.19%	0.17%	0.15%	0.14%	0.11%	0.09%							
16	0.31%	0.27%	0.27%	0.33%	0.27%	0.29%	0.27%	0.27%	0.24%	0.26%	0.23%	0.21%	0.19%	0.18%	0.15%								
17	0.32%	0.29%	0.29%	0.36%	0.31%	0.33%	0.32%	0.31%	0.29%	0.30%	0.28%	0.25%	0.24%	0.23%	0.19%								
18	0.33%	0.31%	0.32%	0.38%	0.35%	0.36%	0.36%	0.36%	0.34%	0.36%	0.33%	0.30%	0.28%	0.27%									
19	0.32%	0.32%	0.34%	0.41%	0.39%	0.40%	0.41%	0.41%	0.39%	0.41%	0.38%	0.35%	0.34%	0.32%									
20	0.31%	0.33%	0.35%	0.43%	0.42%	0.44%	0.45%	0.45%	0.44%	0.47%	0.43%	0.41%	0.39%										

Numerical results 3000x3000mm

Volume of deformation - numerical results - 3000x3000mm plate																								
Radius [mm]		25000	24000	23000	22000	21000	20000	19000	18000	17000	16000	15000	14000	13000	12000	11000	10000	9000	8000	7000	6000	5000	4000	3000
Thickness [mm]	4	0.2562	0.2671	0.2786	0.2915	0.3055	0.3207	0.3379	0.3567	0.3778	0.4016	0.4283	0.4589	0.4943	0.5355	0.5841	0.6422	0.7131	0.8014	0.9143	1.0637	1.2701	1.5726	2.0531
	5	0.2552	0.2661	0.2777	0.2906	0.3046	0.3199	0.3371	0.3558	0.3771	0.4008	0.4275	0.4582	0.4935	0.5347	0.5834	0.6415	0.7124	0.8006	0.9135	1.0629	1.2693	1.5716	2.0525
	6	0.2541	0.2651	0.2768	0.2896	0.3037	0.3189	0.3362	0.3549	0.3762	0.3999	0.4267	0.4574	0.4927	0.5340	0.5827	0.6408	0.7117	0.8000	0.9129	1.0622	1.2685	1.5711	2.0515
	7	0.2530	0.2640	0.2757	0.2885	0.3026	0.3179	0.3352	0.3539	0.3753	0.3990	0.4258	0.4565	0.4919	0.5332	0.5818	0.6401	0.7110	0.7992	0.9123	1.0615	1.2673	1.5702	2.0508
	8	0.2517	0.2627	0.2745	0.2873	0.3015	0.3168	0.3341	0.3529	0.3742	0.3980	0.4249	0.4556	0.4911	0.5323	0.5810	0.6392	0.7103	0.7984	0.9115	1.0605	1.2670	1.5694	2.0502
	9	0.2504	0.2614	0.2732	0.2861	0.3003	0.3157	0.3329	0.3518	0.3732	0.3970	0.4238	0.4547	0.4901	0.5314	0.5802	0.6385	0.7095	0.7978	0.9108	1.0601	1.2663	1.5686	2.0493
	10	0.2490	0.2601	0.2719	0.2847	0.2990	0.3144	0.3317	0.3506	0.3720	0.3958	0.4228	0.4536	0.4891	0.5305	0.5793	0.6376	0.7086	0.7969	0.9101	1.0591	1.2659	1.5679	2.0464
	11	0.2475	0.2586	0.2705	0.2833	0.2977	0.3131	0.3304	0.3494	0.3708	0.3947	0.4216	0.4526	0.4881	0.5294	0.5783	0.6367	0.7078	0.7960	0.9091	1.0587	1.2652	1.5664	2.0456
	12	0.2459	0.2571	0.2690	0.2819	0.2963	0.3117	0.3291	0.3481	0.3696	0.3934	0.4205	0.4514	0.4870	0.5284	0.5773	0.6357	0.7069	0.7954	0.9083	1.0580	1.2638	1.5657	2.0447
	13	0.2443	0.2555	0.2674	0.2803	0.2948	0.3103	0.3277	0.3467	0.3682	0.3922	0.4192	0.4502	0.4859	0.5273	0.5762	0.6346	0.7059	0.7943	0.9074	1.0568	1.2637	1.5661	2.0467
	14	0.2426	0.2538	0.2658	0.2787	0.2932	0.3088	0.3262	0.3453	0.3668	0.3908	0.4179	0.4490	0.4847	0.5261	0.5751	0.6336	0.7048	0.7935	0.9066	1.0560	1.2623	1.5655	2.0432
	15	0.2408	0.2521	0.2642	0.2771	0.2916	0.3073	0.3247	0.3439	0.3654	0.3894	0.4166	0.4477	0.4834	0.5249	0.5740	0.6325	0.7038	0.7926	0.9057	1.0552	1.2615	1.5635	2.0424
	16	0.2390	0.2504	0.2624	0.2754	0.2900	0.3056	0.3231	0.3423	0.3639	0.3880	0.4152	0.4464	0.4821	0.5237	0.5728	0.6314	0.7028	0.7914	0.9049	1.0547	1.2607	1.5638	2.0417
	17	0.2372	0.2486	0.2607	0.2736	0.2882	0.3040	0.3215	0.3407	0.3624	0.3865	0.4138	0.4450	0.4808	0.5224	0.5716	0.6302	0.7017	0.7904	0.9040	1.0537	1.2604	1.5620	2.0409
	18	0.2354	0.2467	0.2589	0.2719	0.2865	0.3023	0.3198	0.3391	0.3608	0.3849	0.4123	0.4436	0.4794	0.5211	0.5703	0.6290	0.7005	0.7894	0.9028	1.0525	1.2591	1.5612	2.0402
	19	0.2336	0.2449	0.2571	0.2701	0.2847	0.3005	0.3181	0.3375	0.3591	0.3833	0.4108	0.4421	0.4780	0.5198	0.5691	0.6278	0.6994	0.7883	0.9018	1.0520	1.2589	1.5605	2.0426
	20	0.2318	0.2431	0.2552	0.2683	0.2829	0.2988	0.3163	0.3357	0.3575	0.3817	0.4092	0.4406	0.4766	0.5184	0.5677	0.6265	0.6982	0.7871	0.9007	1.0509	1.2573	1.5597	2.0387

Analytical results 3000x3000mm

Volume of deformation - analytical results - 3000x3000mm plate																								
Radius [mm]		25000	24000	23000	22000	21000	20000	19000	18000	17000	16000	15000	14000	13000	12000	11000	10000	9000	8000	7000	6000	5000	4000	3000
Thickness [mm]	4	0.2594	0.2700	0.2817	0.2943	0.3082	0.3234	0.3403	0.3591	0.3800	0.4035	0.4302	0.4607	0.4958	0.5367	0.5849	0.6427	0.7130	0.8005	0.9123	1.0597	1.2626	1.5578	2.0194
	5	0.2576	0.2684	0.2801	0.2928	0.3067	0.3220	0.3390	0.3578	0.3788	0.4024	0.4291	0.4596	0.4948	0.5358	0.5841	0.6419	0.7123	0.7999	0.9117	1.0593	1.2623	1.5577	2.0196
	6	0.2560	0.2668	0.2785	0.2913	0.3053	0.3206	0.3376	0.3565	0.3776	0.4012	0.4280	0.4586	0.4938	0.5349	0.5832	0.6411	0.7116	0.7993	0.9112	1.0588	1.2620	1.5575	2.0198
	7	0.2543	0.2652	0.2769	0.2898	0.3038	0.3193	0.3363	0.3552	0.3764	0.4001	0.4269	0.4576	0.4929	0.5340	0.5824	0.6403	0.7109	0.7986	0.9106	1.0583	1.2616	1.5574	2.0201
	8	0.2527	0.2636	0.2754	0.2883	0.3024	0.3179	0.3350	0.3540	0.3752	0.3990	0.4259	0.4566	0.4919	0.5331	0.5816	0.6396	0.7102	0.7980	0.9101	1.0579	1.2613	1.5572	2.0203
	9	0.2511	0.2621	0.2739	0.2869	0.3010	0.3166	0.3337	0.3528	0.3740	0.3978	0.4248	0.4556	0.4910	0.5322	0.5807	0.6388	0.7095	0.7974	0.9095	1.0574	1.2609	1.5571	2.0205
	10	0.2495	0.2605	0.2725	0.2855	0.2997	0.3153	0.3325	0.3516	0.3728	0.3967	0.4237	0.4546	0.4900	0.5313	0.5799	0.6381	0.7088	0.7968	0.9090	1.0570	1.2606	1.5569	2.0207
	11	0.2480	0.2591	0.2710	0.2841	0.2983	0.3140	0.3312	0.3504	0.3717	0.3956	0.4227	0.4536	0.4891	0.5304	0.5791	0.6373	0.7081	0.7961	0.9084	1.0565	1.2603	1.5568	2.0210
	12	0.2465	0.2576	0.2696	0.2827	0.2970	0.3127	0.3300	0.3492	0.3705	0.3945	0.4217	0.4526	0.4882	0.5295	0.5783	0.6365	0.7074	0.7955	0.9079	1.0561	1.2599	1.5566	2.0212
	13	0.2451	0.2562	0.2682	0.2814	0.2957	0.3114	0.3288	0.3480	0.3694	0.3935	0.4206	0.4516	0.4872	0.5287	0.5775	0.6358	0.7067	0.7949	0.9073	1.0556	1.2596	1.5565	2.0214
	14	0.2436	0.2548	0.2669	0.2800	0.2944	0.3102	0.3276	0.3468	0.3683	0.3924	0.4196	0.4506	0.4863	0.5278	0.5767	0.6350	0.7060	0.7943	0.9068	1.0552	1.2593	1.5563	2.0216
	15	0.2422	0.2534	0.2655	0.2787	0.2931	0.3089	0.3264	0.3457	0.3672	0.3913	0.4186	0.4497	0.4854	0.5269	0.5759	0.6343	0.7054	0.7936	0.9062	1.0547	1.2589	1.5562	2.0219
	16	0.2408	0.2520	0.2642	0.2774	0.2919	0.3077	0.3252	0.3445	0.3661	0.3903	0.4176	0.4487	0.4845	0.5261	0.5751	0.6335	0.7047	0.7930	0.9057	1.0542	1.2586	1.5560	2.0221
	17	0.2394	0.2507	0.2629	0.2761	0.2906	0.3065	0.3240	0.3434	0.3650	0.3892	0.4166	0.4478	0.4836	0.5252	0.5743	0.6328	0.7040	0.7924	0.9052	1.0538	1.2583	1.5559	2.0223
	18	0.2381	0.2494	0.2616	0.2749	0.2894	0.3053	0.3229	0.3423	0.3639	0.3882	0.4156	0.4468	0.4827	0.5244	0.5735	0.6321	0.7033	0.7918	0.9046	1.0533	1.2579	1.5557	2.0225
	19	0.2368	0.2481	0.2603	0.2737	0.2882	0.3042	0.3217	0.3412	0.3629	0.3872	0.4146	0.4459	0.4818	0.5235	0.5727	0.6313	0.7026	0.7912	0.9041	1.0529	1.2576	1.5556	2.0228
	20	0.2355	0.2468	0.2591	0.2724	0.2870	0.3030	0.3206	0.3401	0.3618	0.3862	0.4136	0.4449	0.4809	0.5227	0.5719	0.6306	0.7020	0.7906	0.9035	1.0524	1.2573	1.5554	2.0230

Validation 3000x3000mm

	Absolute deviation	Minimum deviation	Maximum deviation	Standard deviation
3000x3000mm	0.47%	0.00%	4.68%	1.09%

Volume of deformation - validation analytical results - 3000x3000mm plate																								
Radius [mm]		25000	24000	23000	22000	21000	20000	19000	18000	17000	16000	15000	14000	13000	12000	11000	10000	9000	8000	7000	6000	5000	4000	3000
Thickness [mm]	4	1.24%	1.12%	1.09%	0.97%	0.87%	0.84%	0.71%	0.67%	0.57%	0.49%	0.44%	0.38%	0.30%	0.21%	0.14%	0.07%	0.02%	0.11%	0.22%	0.38%	0.59%	0.94%	1.64%
	5	0.95%	0.85%	0.84%	0.76%	0.68%	0.68%	0.56%	0.55%	0.45%	0.40%	0.37%	0.32%	0.27%	0.19%	0.12%	0.06%	0.02%	0.09%	0.19%	0.34%	0.56%	0.89%	
	6	0.72%	0.63%	0.63%	0.59%	0.52%	0.55%	0.44%	0.45%	0.36%	0.33%	0.31%	0.26%	0.22%	0.16%	0.09%	0.06%	0.02%	0.09%	0.19%	0.32%	0.52%	0.86%	
	7	0.53%	0.46%	0.46%	0.46%	0.39%	0.43%	0.35%	0.37%	0.29%	0.27%	0.27%	0.23%	0.19%	0.15%	0.09%	0.04%	0.02%	0.07%	0.18%	0.30%	0.45%		
	8	0.38%	0.32%	0.34%	0.36%	0.30%	0.35%	0.28%	0.31%	0.25%	0.24%	0.24%	0.21%	0.17%	0.14%	0.09%	0.06%	0.01%	0.05%	0.16%	0.25%			
	9	0.28%	0.23%	0.26%	0.29%	0.24%	0.30%	0.24%	0.28%	0.22%	0.22%	0.23%	0.20%	0.17%	0.15%	0.09%	0.06%	0.00%	0.05%	0.14%	0.25%			
	10	0.22%	0.18%	0.22%	0.25%	0.22%	0.27%	0.22%	0.27%	0.22%	0.22%	0.24%	0.21%	0.19%	0.15%	0.11%	0.07%	0.03%	0.02%	0.12%				
	11	0.22%	0.18%	0.21%	0.26%	0.22%	0.27%	0.23%	0.28%	0.23%	0.24%	0.26%	0.23%	0.21%	0.18%	0.13%	0.10%	0.05%	0.01%	0.07%				
	12	0.25%	0.20%	0.23%	0.29%	0.25%	0.30%	0.27%	0.31%	0.27%	0.28%	0.29%	0.26%	0.24%	0.22%	0.17%	0.13%	0.08%	0.02%					
	13	0.32%	0.27%	0.30%	0.36%	0.31%	0.36%	0.33%	0.36%	0.32%	0.33%	0.34%	0.31%	0.28%	0.26%	0.21%	0.18%	0.11%						
	14	0.43%	0.37%	0.39%	0.46%	0.40%	0.44%	0.41%	0.44%	0.40%	0.41%	0.40%	0.37%	0.34%	0.32%	0.26%	0.23%	0.17%						
	15	0.57%	0.51%	0.51%	0.59%	0.52%	0.55%	0.52%	0.53%	0.49%	0.49%	0.48%	0.44%	0.41%	0.39%	0.32%	0.28%							
	16	0.74%	0.67%	0.67%	0.74%	0.66%	0.68%	0.64%	0.65%	0.60%	0.60%	0.57%	0.52%	0.49%	0.46%	0.39%								
	17	0.94%	0.86%	0.85%	0.91%	0.83%	0.83%	0.79%	0.78%	0.73%	0.72%	0.68%	0.62%	0.58%	0.54%	0.46%								
	18	1.15%	1.07%	1.05%	1.10%	1.02%	1.01%	0.96%	0.94%	0.87%	0.85%	0.80%	0.73%	0.68%	0.63%									
	19	1.38%	1.31%	1.28%	1.32%	1.23%	1.20%	1.15%	1.11%	1.04%	1.01%	0.93%	0.86%	0.79%	0.73%									
	20	1.62%	1.55%	1.52%	1.55%	1.45%	1.42%	1.36%	1.30%	1.21%	1.17%	1.08%	0.99%	0.91%										

Numerical results 4000x1000mm

Volume of deformation - numerical results - 4000x1000mm plate																								
Radius [mm]		25000	24000	23000	22000	21000	20000	19000	18000	17000	16000	15000	14000	13000	12000	11000	10000	9000	8000	7000	6000	5000	4000	3000
Thickness [mm]	4	0.2040	0.2126	0.2218	0.2317	0.2429	0.2550	0.2683	0.2833	0.2998	0.3185	0.3397	0.3637	0.3914	0.4237	0.4619	0.5073	0.5628	0.6315	0.7192	0.8343	0.9916	1.2180	1.5638
	5	0.2038	0.2123	0.2213	0.2316	0.2426	0.2546	0.2682	0.2828	0.2996	0.3182	0.3393	0.3635	0.3913	0.4236	0.4615	0.5072	0.5626	0.6313	0.7190	0.8340	0.9915	1.2178	1.5637
	6	0.2036	0.2121	0.2212	0.2313	0.2424	0.2543	0.2679	0.2827	0.2994	0.3179	0.3391	0.3633	0.3911	0.4234	0.4614	0.5070	0.5624	0.6312	0.7187	0.8339	0.9913	1.2177	1.5635
	7	0.2033	0.2119	0.2210	0.2311	0.2422	0.2541	0.2677	0.2825	0.2992	0.3176	0.3389	0.3631	0.3908	0.4232	0.4612	0.5068	0.5622	0.6310	0.7185	0.8337	0.9911	1.2175	1.5634
	8	0.2031	0.2117	0.2208	0.2309	0.2420	0.2540	0.2674	0.2823	0.2989	0.3175	0.3387	0.3628	0.3906	0.4229	0.4610	0.5066	0.5619	0.6308	0.7184	0.8335	0.9909	1.2173	1.5631
	9	0.2030	0.2115	0.2207	0.2307	0.2418	0.2538	0.2672	0.2821	0.2987	0.3173	0.3385	0.3626	0.3904	0.4227	0.4608	0.5063	0.5617	0.6306	0.7181	0.8333	0.9907	1.2172	1.5623
	10	0.2028	0.2114	0.2205	0.2305	0.2416	0.2536	0.2671	0.2819	0.2985	0.3171	0.3383	0.3624	0.3901	0.4225	0.4606	0.5061	0.5615	0.6304	0.7180	0.8331	0.9905	1.2169	1.5628
	11	0.2027	0.2112	0.2204	0.2304	0.2415	0.2535	0.2669	0.2817	0.2983	0.3169	0.3381	0.3622	0.3899	0.4223	0.4604	0.5059	0.5613	0.6302	0.7177	0.8329	0.9903	1.2167	1.5626
	12	0.2026	0.2111	0.2203	0.2303	0.2413	0.2534	0.2667	0.2816	0.2981	0.3167	0.3379	0.3620	0.3897	0.4220	0.4601	0.5057	0.5611	0.6299	0.7175	0.8327	0.9901	1.2165	1.5624
	13	0.2025	0.2110	0.2202	0.2302	0.2412	0.2532	0.2666	0.2814	0.2980	0.3166	0.3377	0.3618	0.3895	0.4218	0.4599	0.5054	0.5608	0.6297	0.7173	0.8325	0.9899	1.2163	1.5622
	14	0.2025	0.2109	0.2201	0.2301	0.2411	0.2531	0.2665	0.2813	0.2979	0.3164	0.3376	0.3616	0.3893	0.4216	0.4597	0.5052	0.5606	0.6295	0.7171	0.8323	0.9897	1.2162	1.5620
	15	0.2024	0.2109	0.2200	0.2300	0.2410	0.2531	0.2664	0.2812	0.2977	0.3163	0.3374	0.3615	0.3892	0.4215	0.4595	0.5050	0.5604	0.6293	0.7169	0.8320	0.9895	1.2160	1.5611
	16	0.2023	0.2108	0.2200	0.2299	0.2409	0.2530	0.2663	0.2811	0.2976	0.3162	0.3373	0.3613	0.3890	0.4213	0.4594	0.5048	0.5602	0.6291	0.7167	0.8318	0.9893	1.2158	1.5616
	17	0.2023	0.2108	0.2199	0.2298	0.2409	0.2529	0.2662	0.2810	0.2975	0.3161	0.3372	0.3612	0.3889	0.4211	0.4592	0.5046	0.5600	0.6289	0.7165	0.8316	0.9891	1.2156	1.5614
	18	0.2022	0.2107	0.2199	0.2298	0.2408	0.2528	0.2661	0.2809	0.2974	0.3160	0.3371	0.3611	0.3887	0.4210	0.4590	0.5044	0.5598	0.6286	0.7163	0.8314	0.9889	1.2154	1.5612
	19	0.2022	0.2107	0.2198	0.2297	0.2408	0.2528	0.2661	0.2809	0.2973	0.3159	0.3370	0.3609	0.3886	0.4208	0.4589	0.5043	0.5596	0.6284	0.7160	0.8312	0.9887	1.2152	1.5611
	20	0.2022	0.2106	0.2198	0.2297	0.2407	0.2527	0.2660	0.2808	0.2973	0.3158	0.3369	0.3608	0.3885	0.4207	0.4587	0.5041	0.5595	0.6283	0.7158	0.8309	0.9885	1.2150	1.5608

Analytical results 4000x1000mm

Volume of deformation - analytical results - 4000x1000mm plate																								
Radius [mm]		25000	24000	23000	22000	21000	20000	19000	18000	17000	16000	15000	14000	13000	12000	11000	10000	9000	8000	7000	6000	5000	4000	3000
Thickness [mm]	4	0.2025	0.2110	0.2202	0.2302	0.2411	0.2532	0.2665	0.2813	0.2978	0.3164	0.3374	0.3613	0.3889	0.4209	0.4587	0.5038	0.5586	0.6265	0.7126	0.8254	0.9783	1.1953	1.5159
	5	0.2024	0.2109	0.2201	0.2301	0.2410	0.2531	0.2664	0.2812	0.2977	0.3162	0.3372	0.3611	0.3887	0.4208	0.4585	0.5036	0.5584	0.6262	0.7124	0.8251	0.9781	1.1951	1.5159
	6	0.2023	0.2108	0.2200	0.2300	0.2409	0.2530	0.2663	0.2810	0.2975	0.3161	0.3370	0.3610	0.3885	0.4206	0.4583	0.5034	0.5582	0.6260	0.7122	0.8249	0.9779	1.1949	1.5159
	7	0.2022	0.2107	0.2199	0.2299	0.2408	0.2528	0.2661	0.2809	0.2974	0.3159	0.3369	0.3608	0.3884	0.4204	0.4581	0.5032	0.5580	0.6258	0.7120	0.8247	0.9777	1.1948	1.5158
	8	0.2022	0.2106	0.2197	0.2297	0.2407	0.2527	0.2660	0.2808	0.2972	0.3158	0.3367	0.3606	0.3882	0.4202	0.4580	0.5030	0.5578	0.6256	0.7118	0.8245	0.9775	1.1946	1.5158
	9	0.2021	0.2105	0.2196	0.2296	0.2406	0.2526	0.2659	0.2806	0.2971	0.3156	0.3366	0.3605	0.3880	0.4200	0.4578	0.5028	0.5576	0.6254	0.7116	0.8243	0.9773	1.1945	1.5158
	10	0.2020	0.2104	0.2195	0.2295	0.2405	0.2525	0.2658	0.2805	0.2970	0.3155	0.3364	0.3603	0.3878	0.4199	0.4576	0.5026	0.5574	0.6252	0.7114	0.8241	0.9771	1.1943	1.5158
	11	0.2019	0.2103	0.2194	0.2294	0.2403	0.2524	0.2656	0.2804	0.2968	0.3153	0.3363	0.3602	0.3877	0.4197	0.4574	0.5024	0.5572	0.6250	0.7112	0.8239	0.9769	1.1942	1.5157
	12	0.2018	0.2102	0.2193	0.2293	0.2402	0.2522	0.2655	0.2802	0.2967	0.3152	0.3361	0.3600	0.3875	0.4195	0.4572	0.5023	0.5570	0.6248	0.7109	0.8237	0.9767	1.1940	1.5157
	13	0.2017	0.2101	0.2192	0.2292	0.2401	0.2521	0.2654	0.2801	0.2965	0.3150	0.3360	0.3598	0.3873	0.4193	0.4570	0.5021	0.5568	0.6246	0.7107	0.8235	0.9765	1.1938	1.5157
	14	0.2016	0.2100	0.2191	0.2291	0.2400	0.2520	0.2652	0.2800	0.2964	0.3149	0.3358	0.3597	0.3872	0.4192	0.4568	0.5019	0.5566	0.6244	0.7105	0.8233	0.9763	1.1937	1.5156
	15	0.2015	0.2099	0.2190	0.2290	0.2399	0.2519	0.2651	0.2798	0.2963	0.3147	0.3356	0.3595	0.3870	0.4190	0.4567	0.5017	0.5564	0.6242	0.7103	0.8230	0.9762	1.1935	1.5156
	16	0.2014	0.2098	0.2189	0.2289	0.2398	0.2517	0.2650	0.2797	0.2961	0.3146	0.3355	0.3593	0.3868	0.4188	0.4565	0.5015	0.5562	0.6240	0.7101	0.8228	0.9760	1.1934	1.5156
	17	0.2013	0.2097	0.2188	0.2288	0.2397	0.2516	0.2649	0.2796	0.2960	0.3144	0.3353	0.3592	0.3867	0.4186	0.4563	0.5013	0.5560	0.6238	0.7099	0.8226	0.9758	1.1932	1.5156
	18	0.2013	0.2096	0.2187	0.2287	0.2395	0.2515	0.2647	0.2794	0.2958	0.3143	0.3352	0.3590	0.3865	0.4184	0.4561	0.5011	0.5558	0.6236	0.7097	0.8224	0.9756	1.1930	1.5155
	19	0.2012	0.2095	0.2186	0.2286	0.2394	0.2514	0.2646	0.2793	0.2957	0.3141	0.3350	0.3589	0.3863	0.4183	0.4559	0.5009	0.5556	0.6234	0.7095	0.8222	0.9754	1.1929	1.5155
	20	0.2011	0.2094	0.2185	0.2284	0.2393	0.2513	0.2645	0.2792	0.2956	0.3140	0.3349	0.3587	0.3861	0.4181	0.4557	0.5007	0.5554	0.6232	0.7093	0.8220	0.9752	1.1927	1.5155

Validation 4000x1000mm

	Absolute deviation	Minimum deviation	Maximum deviation	Standard deviation
4000x1000mm	0.62%	0.41%	3.06%	0.24%

Volume of deformation - validation analytical results - 4000x1000mm plate																								
Radius [mm]		25000	24000	23000	22000	21000	20000	19000	18000	17000	16000	15000	14000	13000	12000	11000	10000	9000	8000	7000	6000	5000	4000	3000
Thickness [mm]	4	0.72%	0.77%	0.73%	0.64%	0.73%	0.69%	0.67%	0.69%	0.66%	0.66%	0.68%	0.65%	0.64%	0.66%	0.69%	0.69%	0.75%	0.80%	0.91%	1.07%	1.34%	1.86%	3.06%
	5	0.69%	0.66%	0.57%	0.67%	0.65%	0.61%	0.66%	0.59%	0.65%	0.63%	0.62%	0.65%	0.66%	0.66%	0.65%	0.71%	0.75%	0.80%	0.91%	1.06%	1.34%	1.86%	
	6	0.61%	0.61%	0.54%	0.59%	0.62%	0.53%	0.62%	0.57%	0.62%	0.58%	0.62%	0.64%	0.65%	0.66%	0.67%	0.71%	0.75%	0.81%	0.90%	1.07%	1.35%	1.87%	
	7	0.54%	0.56%	0.51%	0.54%	0.57%	0.51%	0.58%	0.55%	0.59%	0.54%	0.60%	0.62%	0.64%	0.65%	0.67%	0.70%	0.75%	0.82%	0.91%	1.08%	1.35%		
	8	0.49%	0.52%	0.49%	0.48%	0.53%	0.50%	0.54%	0.54%	0.56%	0.54%	0.59%	0.60%	0.62%	0.64%	0.67%	0.70%	0.74%	0.82%	0.92%	1.07%			
	9	0.46%	0.48%	0.46%	0.46%	0.50%	0.47%	0.51%	0.51%	0.54%	0.52%	0.57%	0.59%	0.60%	0.63%	0.66%	0.69%	0.74%	0.82%	0.91%	1.08%			
	10	0.43%	0.46%	0.44%	0.43%	0.48%	0.46%	0.49%	0.50%	0.51%	0.51%	0.55%	0.57%	0.59%	0.62%	0.65%	0.69%	0.74%	0.82%	0.92%				
	11	0.42%	0.45%	0.43%	0.42%	0.47%	0.45%	0.48%	0.48%	0.50%	0.50%	0.54%	0.56%	0.58%	0.61%	0.64%	0.68%	0.73%	0.82%					
	12	0.41%	0.44%	0.43%	0.41%	0.46%	0.45%	0.47%	0.48%	0.49%	0.49%	0.53%	0.55%	0.57%	0.60%	0.64%	0.67%	0.73%	0.82%					
	13	0.41%	0.44%	0.43%	0.42%	0.46%	0.45%	0.46%	0.48%	0.49%	0.49%	0.53%	0.54%	0.56%	0.60%	0.63%	0.67%	0.73%						
	14	0.42%	0.45%	0.44%	0.42%	0.46%	0.46%	0.47%	0.48%	0.49%	0.50%	0.53%	0.54%	0.56%	0.59%	0.63%	0.66%	0.72%						
	15	0.43%	0.46%	0.45%	0.43%	0.47%	0.47%	0.48%	0.49%	0.49%	0.50%	0.53%	0.54%	0.56%	0.59%	0.63%	0.66%							
	16	0.45%	0.47%	0.47%	0.45%	0.49%	0.48%	0.49%	0.50%	0.50%	0.51%	0.54%	0.54%	0.56%	0.59%	0.63%								
	17	0.47%	0.49%	0.49%	0.47%	0.51%	0.50%	0.50%	0.52%	0.52%	0.53%	0.55%	0.55%	0.57%	0.59%	0.63%								
	18	0.49%	0.51%	0.51%	0.49%	0.53%	0.52%	0.52%	0.54%	0.53%	0.54%	0.56%	0.56%	0.57%	0.60%									
	19	0.51%	0.54%	0.54%	0.52%	0.55%	0.55%	0.55%	0.56%	0.55%	0.56%	0.57%	0.58%	0.59%	0.61%									
	20	0.54%	0.56%	0.56%	0.55%	0.58%	0.57%	0.57%	0.58%	0.57%	0.58%	0.59%	0.59%	0.60%										

Numerical results 4000x2000mm

Volume of deformation - numerical results - 4000x2000mm plate																							
Thickness [mm] \ Radius [mm]	25000	24000	23000	22000	21000	20000	19000	18000	17000	16000	15000	14000	13000	12000	11000	10000	9000	8000	7000	6000	5000	4000	3000
4	0.4079	0.4251	0.4432	0.4632	0.4857	0.5096	0.5365	0.5662	0.5994	0.6365	0.6790	0.7271	0.7825	0.8472	0.9235	1.0142	1.1251	1.2628	1.4380	1.6681	1.9828	2.4357	3.1281
5	0.4074	0.4242	0.4425	0.4630	0.4849	0.5091	0.5360	0.5655	0.5989	0.6362	0.6780	0.7265	0.7821	0.8466	0.9228	1.0140	1.1248	1.2622	1.4375	1.6675	1.9824	2.4347	3.1271
6	0.4069	0.4238	0.4417	0.4624	0.4845	0.5084	0.5355	0.5648	0.5985	0.6355	0.6778	0.7262	0.7817	0.8463	0.9222	1.0136	1.1244	1.2617	1.4369	1.6672	1.9819	2.4348	3.1262
7	0.4063	0.4232	0.4413	0.4618	0.4839	0.5078	0.5350	0.5643	0.5979	0.6350	0.6773	0.7257	0.7812	0.8458	0.9218	1.0131	1.1238	1.2614	1.4364	1.6667	1.9815	2.4345	3.1259
8	0.4057	0.4227	0.4408	0.4612	0.4834	0.5072	0.5344	0.5639	0.5974	0.6344	0.6769	0.7252	0.7807	0.8454	0.9214	1.0126	1.1233	1.2609	1.4360	1.6663	1.9810	2.4338	3.1257
9	0.4051	0.4221	0.4402	0.4607	0.4828	0.5066	0.5339	0.5633	0.5968	0.6339	0.6763	0.7246	0.7802	0.8448	0.9209	1.0121	1.1229	1.2604	1.4354	1.6657	1.9804	2.4331	3.1253
10	0.4045	0.4215	0.4397	0.4601	0.4822	0.5061	0.5333	0.5628	0.5963	0.6333	0.6758	0.7241	0.7797	0.8443	0.9204	1.0116	1.1223	1.2600	1.4349	1.6653	1.9801	2.4332	3.1236
11	0.4038	0.4209	0.4391	0.4595	0.4816	0.5055	0.5327	0.5622	0.5957	0.6328	0.6753	0.7236	0.7791	0.8438	0.9199	1.0111	1.1218	1.2594	1.4344	1.6650	1.9794	2.4319	3.1244
12	0.4032	0.4203	0.4385	0.4588	0.4810	0.5050	0.5321	0.5617	0.5951	0.6322	0.6747	0.7230	0.7786	0.8433	0.9194	1.0106	1.1213	1.2589	1.4340	1.6643	1.9789	2.4316	3.1231
13	0.4026	0.4196	0.4379	0.4582	0.4804	0.5044	0.5315	0.5611	0.5946	0.6316	0.6742	0.7225	0.7780	0.8427	0.9188	1.0100	1.1208	1.2586	1.4335	1.6638	1.9785	2.4311	3.1223
14	0.4019	0.4190	0.4373	0.4576	0.4798	0.5038	0.5309	0.5605	0.5940	0.6310	0.6736	0.7219	0.7775	0.8422	0.9183	1.0095	1.1203	1.2579	1.4330	1.6633	1.9780	2.4306	3.1218
15	0.4013	0.4184	0.4367	0.4569	0.4792	0.5032	0.5303	0.5599	0.5933	0.6304	0.6730	0.7213	0.7769	0.8416	0.9178	1.0090	1.1198	1.2574	1.4325	1.6630	1.9775	2.4302	3.1217
16	0.4007	0.4178	0.4361	0.4563	0.4786	0.5026	0.5297	0.5593	0.5927	0.6298	0.6724	0.7207	0.7763	0.8411	0.9172	1.0084	1.1192	1.2569	1.4320	1.6623	1.9769	2.4296	3.1205
17	0.4001	0.4172	0.4355	0.4557	0.4779	0.5020	0.5290	0.5587	0.5921	0.6293	0.6718	0.7201	0.7757	0.8405	0.9167	1.0079	1.1187	1.2564	1.4315	1.6618	1.9764	2.4297	3.1201
18	0.3995	0.4166	0.4349	0.4551	0.4773	0.5014	0.5284	0.5581	0.5915	0.6287	0.6712	0.7195	0.7751	0.8399	0.9161	1.0073	1.1182	1.2558	1.4310	1.6613	1.9764	2.4286	3.1196
19	0.3989	0.4160	0.4343	0.4545	0.4767	0.5008	0.5278	0.5575	0.5909	0.6281	0.6706	0.7189	0.7746	0.8393	0.9156	1.0068	1.1176	1.2553	1.4305	1.6608	1.9754	2.4280	3.1201
20	0.3983	0.4154	0.4337	0.4539	0.4761	0.5002	0.5272	0.5569	0.5902	0.6275	0.6700	0.7183	0.7739	0.8387	0.9150	1.0062	1.1170	1.2548	1.4299	1.6602	1.9749	2.4283	3.1185

Analytical results 4000x2000mm

Volume of deformation - analytical results - 4000x2000mm plate																							
Thickness [mm] \ Radius [mm]	25000	24000	23000	22000	21000	20000	19000	18000	17000	16000	15000	14000	13000	12000	11000	10000	9000	8000	7000	6000	5000	4000	3000
4	0.4070	0.4239	0.4423	0.4623	0.4842	0.5082	0.5348	0.5643	0.5973	0.6343	0.6761	0.7239	0.7789	0.8428	0.9181	1.0081	1.1174	1.2528	1.4248	1.6499	1.9555	2.3896	3.0329
5	0.4064	0.4233	0.4417	0.4617	0.4837	0.5077	0.5343	0.5639	0.5968	0.6338	0.6757	0.7235	0.7785	0.8425	0.9179	1.0079	1.1172	1.2526	1.4247	1.6498	1.9555	2.3895	3.0325
6	0.4059	0.4228	0.4412	0.4612	0.4832	0.5073	0.5339	0.5634	0.5964	0.6334	0.6753	0.7232	0.7782	0.8422	0.9176	1.0076	1.1170	1.2525	1.4246	1.6498	1.9555	2.3894	3.0321
7	0.4053	0.4223	0.4407	0.4607	0.4827	0.5068	0.5334	0.5630	0.5959	0.6330	0.6750	0.7228	0.7778	0.8419	0.9173	1.0074	1.1168	1.2524	1.4245	1.6497	1.9555	2.3894	3.0317
8	0.4048	0.4217	0.4401	0.4602	0.4822	0.5063	0.5329	0.5625	0.5955	0.6326	0.6746	0.7224	0.7775	0.8416	0.9171	1.0072	1.1166	1.2522	1.4244	1.6497	1.9555	2.3893	3.0313
9	0.4042	0.4212	0.4396	0.4597	0.4817	0.5058	0.5325	0.5620	0.5951	0.6322	0.6742	0.7221	0.7772	0.8413	0.9168	1.0069	1.1164	1.2521	1.4243	1.6496	1.9555	2.3892	3.0309
10	0.4037	0.4207	0.4391	0.4592	0.4812	0.5053	0.5320	0.5616	0.5946	0.6318	0.6738	0.7217	0.7768	0.8410	0.9165	1.0067	1.1162	1.2519	1.4242	1.6496	1.9554	2.3892	3.0304
11	0.4032	0.4201	0.4386	0.4587	0.4807	0.5048	0.5315	0.5611	0.5942	0.6314	0.6734	0.7213	0.7765	0.8407	0.9162	1.0065	1.1160	1.2518	1.4241	1.6495	1.9554	2.3891	3.0300
12	0.4026	0.4196	0.4381	0.4582	0.4802	0.5043	0.5311	0.5607	0.5938	0.6309	0.6730	0.7210	0.7762	0.8404	0.9160	1.0062	1.1158	1.2517	1.4240	1.6495	1.9554	2.3890	3.0296
13	0.4021	0.4191	0.4375	0.4577	0.4797	0.5039	0.5306	0.5602	0.5933	0.6305	0.6726	0.7206	0.7758	0.8401	0.9157	1.0060	1.1157	1.2515	1.4239	1.6495	1.9554	2.3890	3.0292
14	0.4016	0.4186	0.4370	0.4572	0.4792	0.5034	0.5301	0.5598	0.5929	0.6301	0.6722	0.7202	0.7755	0.8398	0.9154	1.0058	1.1155	1.2514	1.4239	1.6494	1.9554	2.3889	3.0288
15	0.4010	0.4180	0.4365	0.4567	0.4787	0.5029	0.5297	0.5593	0.5925	0.6297	0.6718	0.7199	0.7751	0.8394	0.9151	1.0055	1.1153	1.2512	1.4238	1.6494	1.9553	2.3888	3.0283
16	0.4005	0.4175	0.4360	0.4562	0.4782	0.5024	0.5292	0.5589	0.5921	0.6293	0.6714	0.7195	0.7748	0.8391	0.9149	1.0053	1.1151	1.2511	1.4237	1.6493	1.9553	2.3888	3.0279
17	0.4000	0.4170	0.4355	0.4557	0.4777	0.5020	0.5287	0.5585	0.5916	0.6289	0.6711	0.7191	0.7745	0.8388	0.9146	1.0051	1.1149	1.2509	1.4236	1.6493	1.9553	2.3887	3.0275
18	0.3995	0.4165	0.4350	0.4552	0.4772	0.5015	0.5283	0.5580	0.5912	0.6285	0.6707	0.7188	0.7741	0.8385	0.9143	1.0048	1.1147	1.2508	1.4235	1.6492	1.9553	2.3886	3.0271
19	0.3989	0.4160	0.4345	0.4547	0.4767	0.5010	0.5278	0.5576	0.5908	0.6281	0.6703	0.7184	0.7738	0.8382	0.9141	1.0046	1.1145	1.2507	1.4234	1.6492	1.9553	2.3886	3.0267
20	0.3984	0.4155	0.4340	0.4542	0.4763	0.5006	0.5274	0.5571	0.5904	0.6277	0.6699	0.7180	0.7735	0.8379	0.9138	1.0044	1.1143	1.2505	1.4233	1.6491	1.9553	2.3885	3.0263

Validation 4000x2000mm

	Absolute deviation	Minimum deviation	Maximum deviation	Standard deviation
4000x2000mm	0.31%	0.00%	4.68%	1.09%

Volume of deformation - validation analytical results - 4000x2000mm plate																							
Thickness [mm] \ Radius [mm]	25000	24000	23000	22000	21000	20000	19000	18000	17000	16000	15000	14000	13000	12000	11000	10000	9000	8000	7000	6000	5000	4000	3000
4	0.22%	0.27%	0.22%	0.20%	0.31%	0.26%	0.31%	0.33%	0.35%	0.36%	0.43%	0.45%	0.47%	0.52%	0.58%	0.60%	0.69%	0.79%	0.92%	1.09%	1.38%	1.89%	3.04%
5	0.25%	0.20%	0.17%	0.27%	0.25%	0.26%	0.31%	0.28%	0.35%	0.37%	0.34%	0.41%	0.46%	0.49%	0.53%	0.60%	0.67%	0.76%	0.89%	1.06%	1.36%	1.86%	
6	0.24%	0.23%	0.12%	0.26%	0.27%	0.22%	0.31%	0.24%	0.35%	0.33%	0.36%	0.42%	0.45%	0.48%	0.50%	0.59%	0.66%	0.73%	0.86%	1.05%	1.33%	1.87%	
7	0.23%	0.23%	0.14%	0.24%	0.26%	0.20%	0.30%	0.24%	0.33%	0.31%	0.35%	0.40%	0.43%	0.47%	0.49%	0.56%	0.63%	0.71%	0.83%	1.02%	1.31%		
8	0.22%	0.23%	0.15%	0.22%	0.26%	0.18%	0.28%	0.25%	0.31%	0.28%	0.34%	0.38%	0.41%	0.44%	0.47%	0.53%	0.60%	0.69%	0.81%	1.00%			
9	0.21%	0.21%	0.14%	0.21%	0.24%	0.17%	0.27%	0.23%	0.30%	0.27%	0.32%	0.36%	0.39%	0.42%	0.44%	0.51%	0.58%	0.66%	0.77%	0.97%			
10	0.19%	0.20%	0.13%	0.19%	0.22%	0.15%	0.25%	0.22%	0.28%	0.24%	0.30%	0.34%	0.36%	0.40%	0.42%	0.48%	0.54%	0.64%	0.74%				
11	0.17%	0.18%	0.12%	0.17%	0.20%	0.14%	0.23%	0.20%	0.25%	0.22%	0.28%	0.31%	0.34%	0.37%	0.40%	0.46%	0.52%	0.60%	0.72%				
12	0.14%	0.16%	0.10%	0.14%	0.18%	0.12%	0.20%	0.18%	0.23%	0.19%	0.26%	0.29%	0.31%	0.34%	0.37%	0.43%	0.49%	0.58%					
13	0.12%	0.13%	0.08%	0.12%	0.16%	0.10%	0.18%	0.15%	0.20%	0.17%	0.23%	0.26%	0.28%	0.32%	0.34%	0.40%	0.46%						
14	0.10%	0.11%	0.06%	0.09%	0.13%	0.08%	0.15%	0.13%	0.17%	0.14%	0.20%	0.23%	0.26%	0.29%	0.32%	0.37%	0.43%						
15	0.07%	0.09%	0.04%	0.06%	0.10%	0.06%	0.12%	0.10%	0.15%	0.11%	0.18%	0.20%	0.23%	0.26%	0.29%	0.34%							
16	0.05%	0.06%	0.02%	0.04%	0.08%	0.03%	0.09%	0.08%	0.11%	0.09%	0.15%	0.17%	0.20%	0.23%	0.26%								
17	0.03%	0.04%	0.00%	0.01%	0.05%	0.00%	0.06%	0.05%	0.08%	0.06%	0.11%	0.14%	0.16%	0.20%	0.23%								
18	0.01%	0.02%	0.02%	0.02%	0.02%	0.02%	0.03%	0.02%	0.05%	0.03%	0.09%	0.11%	0.13%	0.16%									
19	0.01%	0.00%	0.04%	0.04%	0.01%	0.05%	0.01%	0.01%	0.02%	0.00%	0.05%	0.07%	0.10%										
20	0.02%	0.01%	0.06%	0.07%	0.03%	0.07%	0.04%	0.04%	0.02%	0.03%	0.02%	0.04%	0.06%										

Numerical results 4000x3000mm

Volume of deformation - numerical results - 4000x3000mm plate																								
Radius [mm]		25000	24000	23000	22000	21000	20000	19000	18000	17000	16000	15000	14000	13000	12000	11000	10000	9000	8000	7000	6000	5000	4000	3000
Thickness [mm]	4	0.6111	0.6368	0.6639	0.6941	0.7276	0.7634	0.8039	0.8484	0.8982	0.9538	1.0176	1.0898	1.1729	1.2698	1.3842	1.5202	1.6863	1.8930	2.1557	2.5014	2.9728	3.6526	4.6894
	5	0.6104	0.6355	0.6631	0.6938	0.7265	0.7629	0.8032	0.8475	0.8976	0.9535	1.0163	1.0890	1.1719	1.2692	1.3831	1.5202	1.6864	1.8926	2.1548	2.5005	2.9728	3.6517	4.6874
	6	0.6095	0.6348	0.6619	0.6928	0.7258	0.7618	0.8024	0.8464	0.8968	0.9524	1.0157	1.0883	1.1713	1.2686	1.3819	1.5195	1.6856	1.8914	2.1536	2.4996	2.9719	3.6507	4.6882
	7	0.6085	0.6339	0.6609	0.6918	0.7249	0.7608	0.8016	0.8454	0.8959	0.9515	1.0149	1.0875	1.1707	1.2677	1.3815	1.5186	1.6845	1.8908	2.1536	2.4987	2.9713	3.6505	4.6876
	8	0.6075	0.6329	0.6601	0.6908	0.7240	0.7598	0.8006	0.8447	0.8950	0.9505	1.0142	1.0867	1.1699	1.2668	1.3808	1.5175	1.6839	1.8898	2.1523	2.4976	2.9696	3.6487	4.6871
	9	0.6064	0.6319	0.6590	0.6898	0.7230	0.7589	0.7996	0.8437	0.8941	0.9497	1.0133	1.0857	1.1690	1.2660	1.3799	1.5167	1.6828	1.8892	2.1513	2.4972	2.9686	3.6488	4.6838
	10	0.6054	0.6309	0.6581	0.6888	0.7220	0.7578	0.7986	0.8428	0.8931	0.9487	1.0123	1.0848	1.1681	1.2652	1.3790	1.5158	1.6818	1.8884	2.1505	2.4958	2.9687	3.6462	4.6848
	11	0.6042	0.6298	0.6570	0.6877	0.7209	0.7568	0.7976	0.8418	0.8921	0.9478	1.0114	1.0839	1.1672	1.2643	1.3782	1.5150	1.6811	1.8872	2.1497	2.4951	2.9675	3.6451	4.6841
	12	0.6031	0.6286	0.6560	0.6866	0.7199	0.7558	0.7966	0.8408	0.8911	0.9467	1.0104	1.0829	1.1663	1.2632	1.3775	1.5141	1.6804	1.8867	2.1488	2.4949	2.9657	3.6457	4.6799
	13	0.6019	0.6275	0.6548	0.6855	0.7188	0.7547	0.7955	0.8398	0.8901	0.9458	1.0094	1.0819	1.1653	1.2623	1.3764	1.5132	1.6793	1.8855	2.1480	2.4932	2.9648	3.6438	4.6826
	14	0.6007	0.6263	0.6537	0.6843	0.7176	0.7536	0.7944	0.8388	0.8890	0.9447	1.0085	1.0810	1.1643	1.2614	1.3755	1.5123	1.6784	1.8846	2.1471	2.4923	2.9639	3.6421	4.6806
	15	0.5994	0.6251	0.6525	0.6831	0.7165	0.7525	0.7933	0.8377	0.8880	0.9436	1.0074	1.0800	1.1633	1.2604	1.3746	1.5114	1.6775	1.8843	2.1469	2.4914	2.9629	3.6437	4.6795
	16	0.5981	0.6238	0.6513	0.6819	0.7153	0.7513	0.7921	0.8366	0.8868	0.9425	1.0064	1.0789	1.1623	1.2594	1.3736	1.5104	1.6766	1.8829	2.1453	2.4905	2.9622	3.6401	4.6786
	17	0.5968	0.6225	0.6500	0.6806	0.7141	0.7501	0.7909	0.8354	0.8857	0.9414	1.0053	1.0779	1.1613	1.2585	1.3727	1.5095	1.6757	1.8820	2.1452	2.4908	2.9629	3.6420	4.6777
	18	0.5955	0.6212	0.6488	0.6793	0.7128	0.7489	0.7897	0.8343	0.8845	0.9403	1.0042	1.0769	1.1603	1.2574	1.3717	1.5085	1.6748	1.8811	2.1436	2.4892	2.9603	3.6410	4.6768
	19	0.5941	0.6199	0.6475	0.6780	0.7115	0.7477	0.7885	0.8331	0.8834	0.9391	1.0031	1.0757	1.1593	1.2564	1.3707	1.5075	1.6742	1.8802	2.1433	2.4879	2.9593	3.6372	4.6759
	20	0.5927	0.6185	0.6461	0.6767	0.7102	0.7464	0.7872	0.8319	0.8822	0.9379	1.0020	1.0746	1.1581	1.2553	1.3697	1.5065	1.6728	1.8793	2.1418	2.4870	2.9584	3.6379	4.6765

Analytical results 4000x3000mm

Volume of deformation - analytical results - 4000x3000mm plate																								
Radius [mm]		25000	24000	23000	22000	21000	20000	19000	18000	17000	16000	15000	14000	13000	12000	11000	10000	9000	8000	7000	6000	5000	4000	3000
Thickness [mm]	4	0.6117	0.6371	0.6646	0.6946	0.7274	0.7635	0.8033	0.8476	0.8970	0.9525	1.0153	1.0870	1.1695	1.2655	1.3785	1.5135	1.6775	1.8808	2.1388	2.4765	2.9348	3.5850	4.5471
	5	0.6108	0.6361	0.6636	0.6937	0.7265	0.7626	0.8025	0.8468	0.8963	0.9518	1.0147	1.0864	1.1690	1.2650	1.3781	1.5132	1.6773	1.8806	2.1387	2.4765	2.9349	3.5853	4.5475
	6	0.6098	0.6351	0.6627	0.6928	0.7257	0.7618	0.8018	0.8461	0.8956	0.9512	1.0141	1.0858	1.1685	1.2646	1.3777	1.5129	1.6770	1.8804	2.1386	2.4765	2.9351	3.5856	4.5478
	7	0.6088	0.6342	0.6618	0.6919	0.7248	0.7610	0.8010	0.8453	0.8949	0.9505	1.0135	1.0853	1.1679	1.2641	1.3773	1.5125	1.6767	1.8802	2.1386	2.4765	2.9352	3.5858	4.5482
	8	0.6078	0.6332	0.6609	0.6910	0.7240	0.7602	0.8002	0.8446	0.8942	0.9498	1.0128	1.0847	1.1674	1.2636	1.3769	1.5122	1.6765	1.8800	2.1385	2.4765	2.9353	3.5861	4.5485
	9	0.6068	0.6323	0.6600	0.6901	0.7231	0.7594	0.7994	0.8439	0.8935	0.9492	1.0122	1.0841	1.1669	1.2632	1.3765	1.5119	1.6762	1.8798	2.1384	2.4765	2.9355	3.5864	4.5488
	10	0.6058	0.6313	0.6590	0.6892	0.7223	0.7586	0.7986	0.8431	0.8928	0.9485	1.0116	1.0836	1.1664	1.2627	1.3761	1.5115	1.6759	1.8797	2.1383	2.4766	2.9356	3.5866	4.5492
	11	0.6049	0.6304	0.6581	0.6884	0.7214	0.7578	0.7979	0.8424	0.8921	0.9479	1.0110	1.0830	1.1659	1.2622	1.3757	1.5112	1.6757	1.8795	2.1382	2.4766	2.9358	3.5869	4.5495
	12	0.6039	0.6295	0.6572	0.6875	0.7206	0.7570	0.7971	0.8417	0.8914	0.9472	1.0104	1.0824	1.1654	1.2618	1.3753	1.5108	1.6754	1.8793	2.1381	2.4766	2.9359	3.5871	4.5499
	13	0.6030	0.6285	0.6563	0.6866	0.7197	0.7562	0.7963	0.8409	0.8907	0.9466	1.0098	1.0819	1.1648	1.2613	1.3749	1.5105	1.6752	1.8791	2.1380	2.4766	2.9360	3.5874	4.5502
	14	0.6020	0.6276	0.6554	0.6858	0.7189	0.7554	0.7956	0.8402	0.8900	0.9459	1.0092	1.0813	1.1643	1.2609	1.3745	1.5102	1.6749	1.8789	2.1379	2.4766	2.9362	3.5877	4.5505
	15	0.6011	0.6267	0.6545	0.6849	0.7181	0.7546	0.7948	0.8395	0.8893	0.9453	1.0086	1.0808	1.1638	1.2604	1.3741	1.5098	1.6746	1.8788	2.1378	2.4766	2.9363	3.5879	4.5509
	16	0.6001	0.6258	0.6537	0.6840	0.7173	0.7538	0.7940	0.8387	0.8886	0.9446	1.0080	1.0802	1.1633	1.2600	1.3737	1.5095	1.6744	1.8786	2.1377	2.4766	2.9364	3.5882	4.5512
	17	0.5992	0.6249	0.6528	0.6832	0.7164	0.7530	0.7933	0.8380	0.8879	0.9440	1.0074	1.0796	1.1628	1.2595	1.3733	1.5092	1.6741	1.8784	2.1377	2.4767	2.9366	3.5885	4.5516
	18	0.5982	0.6240	0.6519	0.6823	0.7156	0.7522	0.7925	0.8373	0.8873	0.9433	1.0068	1.0791	1.1623	1.2590	1.3729	1.5088	1.6738	1.8782	2.1376	2.4767	2.9367	3.5887	4.5519
	19	0.5973	0.6231	0.6510	0.6815	0.7148	0.7514	0.7918	0.8366	0.8866	0.9427	1.0062	1.0785	1.1618	1.2586	1.3725	1.5085	1.6736	1.8780	2.1375	2.4767	2.9368	3.5890	4.5522
	20	0.5964	0.6222	0.6502	0.6806	0.7140	0.7506	0.7910	0.8359	0.8859	0.9421	1.0056	1.0780	1.1613	1.2581	1.3721	1.5082	1.6733	1.8778	2.1374	2.4767	2.9370	3.5893	4.5526

Validation 4000x3000mm

	Absolute deviation	Minimum deviation	Maximum deviation	Standard deviation
4000x3000mm	0.27%	0.00%	3.03%	0.31%

Volume of deformation - validation analytical results - 4000x3000mm plate																								
Radius [mm]		25000	24000	23000	22000	21000	20000	19000	18000	17000	16000	15000	14000	13000	12000	11000	10000	9000	8000	7000	6000	5000	4000	3000
Thickness [mm]	4	0.11%	0.05%	0.09%	0.07%	0.03%	0.01%	0.07%	0.09%	0.14%	0.14%	0.23%	0.26%	0.29%	0.34%	0.41%	0.44%	0.52%	0.64%	0.78%	1.00%	1.28%	1.85%	3.03%
	5	0.06%	0.09%	0.08%	0.02%	0.00%	0.03%	0.09%	0.08%	0.15%	0.18%	0.16%	0.24%	0.25%	0.33%	0.36%	0.46%	0.54%	0.64%	0.74%	0.96%	1.27%	1.82%	
	6	0.04%	0.05%	0.12%	0.01%	0.02%	0.00%	0.08%	0.03%	0.13%	0.13%	0.16%	0.22%	0.24%	0.32%	0.31%	0.43%	0.51%	0.58%	0.69%	0.92%	1.24%		
	7	0.04%	0.05%	0.13%	0.01%	0.01%	0.02%	0.07%	0.01%	0.12%	0.11%	0.14%	0.20%	0.24%	0.28%	0.31%	0.40%	0.46%	0.56%	0.70%	0.89%	1.21%		
	8	0.05%	0.05%	0.12%	0.02%	0.01%	0.05%	0.05%	0.01%	0.09%	0.07%	0.14%	0.18%	0.21%	0.25%	0.28%	0.35%	0.44%	0.52%	0.64%	0.84%			
	9	0.06%	0.06%	0.14%	0.04%	0.01%	0.07%	0.03%	0.02%	0.07%	0.05%	0.10%	0.14%	0.18%	0.22%	0.24%	0.32%	0.39%	0.50%	0.60%	0.83%			
	10	0.08%	0.07%	0.15%	0.06%	0.04%	0.10%	0.00%	0.04%	0.04%	0.02%	0.07%	0.11%	0.15%	0.19%	0.21%	0.29%	0.35%	0.46%	0.57%				
	11	0.11%	0.10%	0.17%	0.09%	0.07%	0.12%	0.03%	0.07%	0.01%	0.01%	0.04%	0.08%	0.11%	0.16%	0.18%	0.25%	0.32%	0.41%	0.54%				
	12	0.14%	0.13%	0.19%	0.13%	0.09%	0.16%	0.07%	0.10%	0.03%	0.05%	0.00%	0.04%	0.08%	0.11%	0.16%	0.21%	0.30%	0.39%					
	13	0.18%	0.17%	0.23%	0.17%	0.14%	0.20%	0.10%	0.13%	0.07%	0.09%	0.04%	0.01%	0.04%	0.08%	0.11%	0.18%	0.25%						
	14	0.22%	0.21%	0.27%	0.21%	0.18%	0.24%	0.15%	0.17%	0.11%	0.13%	0.07%	0.03%	0.00%	0.04%	0.07%	0.14%	0.21%						
	15	0.27%	0.26%	0.31%	0.26%	0.22%	0.28%	0.19%	0.21%	0.15%	0.17%	0.11%	0.07%	0.04%	0.00%	0.04%	0.10%							
	16	0.33%	0.31%	0.37%	0.32%	0.28%	0.33%	0.24%	0.26%	0.20%	0.22%	0.16%	0.12%	0.08%	0.04%	0.00%								
	17	0.40%	0.38%	0.42%	0.38%	0.33%	0.38%	0.30%	0.31%	0.25%	0.27%	0.21%	0.16%	0.13%	0.08%	0.05%								
	18	0.47%	0.44%	0.49%	0.44%	0.39%	0.44%	0.36%	0.36%	0.31%	0.32%	0.25%	0.21%	0.18%	0.13%									
	19	0.54%	0.51%	0.55%	0.51%	0.46%	0.50%	0.42%	0.42%	0.36%	0.38%	0.31%	0.26%	0.22%	0.18%									
	20	0.62%	0.59%	0.62%	0.58%	0.53%	0.56%	0.48%	0.48%	0.42%	0.44%	0.36%	0.32%	0.28%										

Numerical results 5000x1000mm

Volume of deformation - numerical results - 5000x1000mm plate																								
Radius [mm]		25000	24000	23000	22000	21000	20000	19000	18000	17000	16000	15000	14000	13000	12000	11000	10000	9000	8000	7000	6000	5000	4000	3000
Thickness [mm]	4	0.3992	0.4157	0.4331	0.4530	0.4748	0.4980	0.5241	0.5533	0.5850	0.6217	0.6625	0.7091	0.7632	0.8258	0.8993	0.9869	1.0937	1.2252	1.3923	1.6096	1.9032	2.3147	2.9098
	5	0.3988	0.4151	0.4327	0.4529	0.4744	0.4974	0.5240	0.5528	0.5850	0.6213	0.6624	0.7088	0.7627	0.8253	0.8987	0.9870	1.0933	1.2252	1.3921	1.6096	1.9029	2.3148	2.9099
	6	0.3985	0.4150	0.4326	0.4524	0.4741	0.4975	0.5235	0.5527	0.5845	0.6212	0.6620	0.7087	0.7627	0.8253	0.8988	0.9864	1.0931	1.2248	1.3917	1.6093	1.9028	2.3142	2.9097
	7	0.3982	0.4147	0.4322	0.4522	0.4738	0.4971	0.5233	0.5523	0.5843	0.6208	0.6618	0.7082	0.7623	0.8249	0.8984	0.9864	1.0927	1.2247	1.3916	1.6092	1.9025	2.3141	2.9099
	8	0.3979	0.4144	0.4321	0.4518	0.4735	0.4969	0.5230	0.5520	0.5840	0.6206	0.6615	0.7081	0.7621	0.8247	0.8983	0.9861	1.0926	1.2244	1.3913	1.6090	1.9023	2.3138	2.9082
	9	0.3977	0.4142	0.4319	0.4516	0.4733	0.4967	0.5227	0.5518	0.5837	0.6203	0.6612	0.7079	0.7619	0.8245	0.8980	0.9858	1.0924	1.2241	1.3910	1.6087	1.9021	2.3136	2.9090
	10	0.3975	0.4140	0.4317	0.4513	0.4730	0.4965	0.5224	0.5515	0.5834	0.6200	0.6609	0.7076	0.7616	0.8242	0.8978	0.9855	1.0921	1.2239	1.3908	1.6084	1.9019	2.3134	2.9087
	11	0.3973	0.4138	0.4316	0.4512	0.4728	0.4963	0.5222	0.5513	0.5832	0.6198	0.6606	0.7074	0.7613	0.8239	0.8975	0.9853	1.0919	1.2236	1.3906	1.6082	1.9016	2.3131	2.9086
	12	0.3971	0.4137	0.4314	0.4510	0.4726	0.4961	0.5220	0.5511	0.5830	0.6196	0.6604	0.7071	0.7611	0.8237	0.8973	0.9850	1.0916	1.2234	1.3903	1.6080	1.9014	2.3130	2.9085
	13	0.3970	0.4135	0.4313	0.4508	0.4725	0.4959	0.5218	0.5509	0.5828	0.6193	0.6602	0.7070	0.7609	0.8234	0.8970	0.9847	1.0914	1.2231	1.3901	1.6077	1.9012	2.3127	2.9082
	14	0.3969	0.4134	0.4312	0.4507	0.4723	0.4958	0.5217	0.5507	0.5826	0.6192	0.6599	0.7068	0.7606	0.8232	0.8968	0.9845	1.0912	1.2229	1.3899	1.6075	1.9010	2.3125	2.9079
	15	0.3968	0.4133	0.4311	0.4506	0.4722	0.4957	0.5215	0.5506	0.5825	0.6190	0.6597	0.7066	0.7604	0.8230	0.8966	0.9842	1.0909	1.2227	1.3897	1.6073	1.9008	2.3123	2.9078
	16	0.3967	0.4132	0.4310	0.4505	0.4721	0.4955	0.5214	0.5504	0.5824	0.6188	0.6596	0.7064	0.7602	0.8228	0.8963	0.9840	1.0907	1.2224	1.3894	1.6070	1.9005	2.3121	2.9076
	17	0.3966	0.4131	0.4309	0.4504	0.4720	0.4954	0.5213	0.5503	0.5823	0.6187	0.6594	0.7062	0.7600	0.8226	0.8961	0.9838	1.0905	1.2222	1.3892	1.6068	1.9003	2.3119	2.9073
	18	0.3965	0.4130	0.4309	0.4503	0.4719	0.4953	0.5212	0.5502	0.5822	0.6185	0.6593	0.7061	0.7599	0.8224	0.8959	0.9836	1.0903	1.2220	1.3890	1.6065	1.9001	2.3117	2.9071
	19	0.3965	0.4130	0.4308	0.4503	0.4718	0.4953	0.5211	0.5501	0.5821	0.6184	0.6591	0.7059	0.7597	0.8222	0.8957	0.9834	1.0900	1.2218	1.3887	1.6063	1.8998	2.3114	2.9069
	20	0.3964	0.4129	0.4308	0.4502	0.4717	0.4952	0.5210	0.5500	0.5820	0.6183	0.6590	0.7058	0.7596	0.8220	0.8956	0.9832	1.0898	1.2216	1.3885	1.6060	1.8996	2.3112	2.9066

Analytical results 5000x1000mm

Volume of deformation - analytical results - 5000x1000mm plate																								
Radius [mm]		25000	24000	23000	22000	21000	20000	19000	18000	17000	16000	15000	14000	13000	12000	11000	10000	9000	8000	7000	6000	5000	4000	3000
Thickness [mm]	4	0.3958	0.4123	0.4302	0.4496	0.4710	0.4944	0.5203	0.5490	0.5811	0.6170	0.6577	0.7041	0.7574	0.8193	0.8921	0.9788	1.0837	1.2131	1.3761	1.5870	1.8679	2.2525	2.7758
	5	0.3957	0.4122	0.4300	0.4495	0.4708	0.4943	0.5201	0.5489	0.5809	0.6169	0.6575	0.7039	0.7572	0.8191	0.8919	0.9786	1.0835	1.2128	1.3758	1.5867	1.8677	2.2523	2.7758
	6	0.3956	0.4120	0.4299	0.4494	0.4707	0.4941	0.5200	0.5487	0.5807	0.6167	0.6573	0.7037	0.7570	0.8189	0.8916	0.9783	1.0832	1.2125	1.3756	1.5865	1.8674	2.2521	2.7758
	7	0.3955	0.4119	0.4298	0.4493	0.4706	0.4940	0.5198	0.5485	0.5805	0.6165	0.6572	0.7035	0.7568	0.8187	0.8914	0.9781	1.0829	1.2123	1.3753	1.5862	1.8672	2.2519	2.7758
	8	0.3954	0.4118	0.4297	0.4491	0.4704	0.4938	0.5197	0.5484	0.5804	0.6163	0.6570	0.7033	0.7566	0.8185	0.8912	0.9778	1.0827	1.2120	1.3750	1.5859	1.8669	2.2517	2.7758
	9	0.3953	0.4117	0.4295	0.4490	0.4703	0.4937	0.5195	0.5482	0.5802	0.6161	0.6568	0.7031	0.7564	0.8182	0.8910	0.9776	1.0824	1.2117	1.3748	1.5857	1.8667	2.2515	2.7758
	10	0.3952	0.4116	0.4294	0.4489	0.4702	0.4935	0.5194	0.5480	0.5800	0.6160	0.6566	0.7029	0.7561	0.8180	0.8907	0.9773	1.0822	1.2115	1.3745	1.5854	1.8664	2.2513	2.7758
	11	0.3951	0.4115	0.4293	0.4487	0.4700	0.4934	0.5192	0.5479	0.5799	0.6158	0.6564	0.7027	0.7559	0.8178	0.8905	0.9771	1.0819	1.2112	1.3742	1.5851	1.8662	2.2511	2.7758
	12	0.3950	0.4114	0.4292	0.4486	0.4699	0.4933	0.5191	0.5477	0.5797	0.6156	0.6562	0.7025	0.7557	0.8176	0.8903	0.9769	1.0817	1.2110	1.3740	1.5849	1.8659	2.2509	2.7758
	13	0.3949	0.4113	0.4291	0.4485	0.4697	0.4931	0.5189	0.5476	0.5795	0.6154	0.6560	0.7023	0.7555	0.8174	0.8900	0.9766	1.0814	1.2107	1.3737	1.5846	1.8657	2.2508	2.7758
	14	0.3948	0.4111	0.4289	0.4484	0.4696	0.4930	0.5188	0.5474	0.5793	0.6152	0.6558	0.7021	0.7553	0.8171	0.8898	0.9764	1.0812	1.2104	1.3734	1.5843	1.8654	2.2506	2.7759
	15	0.3947	0.4110	0.4288	0.4482	0.4695	0.4928	0.5186	0.5472	0.5792	0.6151	0.6556	0.7019	0.7551	0.8169	0.8896	0.9761	1.0809	1.2102	1.3732	1.5841	1.8652	2.2504	2.7759
	16	0.3946	0.4109	0.4287	0.4481	0.4693	0.4927	0.5185	0.5471	0.5790	0.6149	0.6554	0.7017	0.7549	0.8167	0.8893	0.9759	1.0807	1.2099	1.3729	1.5838	1.8649	2.2502	2.7759
	17	0.3945	0.4108	0.4286	0.4480	0.4692	0.4925	0.5183	0.5469	0.5788	0.6147	0.6553	0.7015	0.7547	0.8165	0.8891	0.9757	1.0804	1.2097	1.3726	1.5835	1.8647	2.2500	2.7759
	18	0.3943	0.4107	0.4285	0.4478	0.4691	0.4924	0.5182	0.5467	0.5787	0.6145	0.6551	0.7013	0.7545	0.8163	0.8889	0.9754	1.0802	1.2094	1.3724	1.5833	1.8644	2.2498	2.7759
	19	0.3942	0.4106	0.4284	0.4477	0.4689	0.4922	0.5180	0.5466	0.5785	0.6143	0.6549	0.7011	0.7543	0.8160	0.8887	0.9752	1.0799	1.2092	1.3721	1.5830	1.8642	2.2496	2.7759
	20	0.3941	0.4105	0.4282	0.4476	0.4688	0.4921	0.5178	0.5464	0.5783	0.6142	0.6547	0.7009	0.7541	0.8158	0.8884	0.9749	1.0797	1.2089	1.3718	1.5827	1.8639	2.2494	2.7759

Validation 5000x1000mm

	Absolute deviation	Minimum deviation	Maximum deviation	Standard deviation
5000x1000mm	0.75%	0.52%	4.61%	0.36%

Volume of deformation - validation analytical results - 5000x1000mm plate																								
Radius [mm]		25000	24000	23000	22000	21000	20000	19000	18000	17000	16000	15000	14000	13000	12000	11000	10000	9000	8000	7000	6000	5000	4000	3000
Thickness [mm]	4	0.86%	0.82%	0.67%	0.75%	0.81%	0.72%	0.73%	0.77%	0.67%	0.76%	0.72%	0.71%	0.76%	0.78%	0.80%	0.82%	0.91%	0.99%	1.16%	1.41%	1.86%	2.69%	4.61%
	5	0.79%	0.72%	0.62%	0.74%	0.75%	0.62%	0.73%	0.71%	0.71%	0.71%	0.74%	0.69%	0.72%	0.75%	0.76%	0.85%	0.90%	1.02%	1.17%	1.42%	1.85%	2.70%	
	6	0.73%	0.72%	0.62%	0.66%	0.73%	0.67%	0.67%	0.72%	0.64%	0.72%	0.70%	0.70%	0.75%	0.77%	0.80%	0.82%	0.91%	1.00%	1.16%	1.42%	1.86%	2.68%	
	7	0.68%	0.66%	0.56%	0.64%	0.68%	0.62%	0.66%	0.68%	0.65%	0.70%	0.70%	0.67%	0.73%	0.76%	0.78%	0.84%	0.89%	1.01%	1.17%	1.43%	1.86%		
	8	0.64%	0.63%	0.56%	0.60%	0.66%	0.61%	0.63%	0.67%	0.62%	0.69%	0.68%	0.68%	0.73%	0.76%	0.79%	0.83%	0.90%	1.01%	1.17%	1.43%			
	9	0.60%	0.61%	0.55%	0.57%	0.63%	0.60%	0.60%	0.65%	0.60%	0.67%	0.66%	0.67%	0.72%	0.76%	0.79%	0.83%	0.91%	1.01%	1.17%	1.43%			
	10	0.58%	0.58%	0.54%	0.55%	0.61%	0.59%	0.58%	0.63%	0.58%	0.66%	0.65%	0.67%	0.72%	0.75%	0.78%	0.83%	0.91%	1.01%	1.17%				
	11	0.56%	0.57%	0.53%	0.54%	0.59%	0.58%	0.57%	0.62%	0.57%	0.65%	0.64%	0.66%	0.71%	0.75%	0.78%	0.83%	0.91%	1.01%	1.17%				
	12	0.54%	0.55%	0.52%	0.53%	0.58%	0.57%	0.56%	0.61%	0.57%	0.64%	0.63%	0.66%	0.70%	0.74%	0.78%	0.83%	0.91%	1.02%					
	13	0.54%	0.55%	0.52%	0.52%	0.57%	0.57%	0.56%	0.61%	0.56%	0.63%	0.63%	0.66%	0.70%	0.74%	0.78%	0.83%	0.91%						
	14	0.53%	0.55%	0.52%	0.52%	0.57%	0.57%	0.55%	0.60%	0.57%	0.63%	0.62%	0.66%	0.70%	0.74%	0.78%	0.82%	0.92%						
	15	0.53%	0.55%	0.53%	0.52%	0.57%	0.57%	0.56%	0.60%	0.57%	0.63%	0.62%	0.66%	0.70%	0.74%	0.78%	0.82%							
	16	0.54%	0.55%	0.54%	0.53%	0.58%	0.58%	0.56%	0.61%	0.58%	0.63%	0.62%	0.66%	0.70%	0.74%	0.78%								
	17	0.54%	0.56%	0.55%	0.54%	0.58%	0.59%	0.57%	0.61%	0.59%	0.64%	0.63%	0.67%	0.70%	0.74%	0.78%								
	18	0.55%	0.57%	0.56%	0.55%	0.59%	0.60%	0.58%	0.62%	0.60%	0.65%	0.63%	0.68%	0.71%	0.74%									
	19	0.56%	0.58%	0.57%	0.56%	0.60%	0.61%	0.59%	0.63%	0.61%	0.66%	0.64%	0.68%	0.72%	0.75%									
	20	0.58%	0.59%	0.59%	0.58%	0.62%	0.62%	0.60%	0.64%	0.63%	0.67%	0.65%	0.69%	0.72%										

Numerical results 5000x2000mm

Volume of deformation - numerical results - 5000x2000mm plate																								
	Radius [mm]	25000	24000	23000	22000	21000	20000	19000	18000	17000	16000	15000	14000	13000	12000	11000	10000	9000	8000	7000	6000	5000	4000	3000
Thickness [mm]	4	0.7986	0.8312	0.8655	0.9062	0.9496	0.9954	1.0483	1.1063	1.1700	1.2432	1.3249	1.4176	1.5260	1.6512	1.7981	1.9736	2.1866	2.4505	2.7837	3.2179	3.8059	4.6290	5.8134
	5	0.7978	0.8299	0.8655	0.9059	0.9486	0.9944	1.0480	1.1050	1.1700	1.2420	1.3246	1.4174	1.5246	1.6499	1.7971	1.9735	2.1862	2.4501	2.7838	3.2186	3.8054	4.6284	5.8131
	6	0.7972	0.8299	0.8645	0.9049	0.9483	0.9943	1.0470	1.1050	1.1688	1.2420	1.3238	1.4165	1.5249	1.6500	1.7970	1.9726	2.1855	2.4490	2.7826	3.2179	3.8047	4.6278	5.8128
	7	0.7964	0.8290	0.8639	0.9044	0.9474	0.9933	1.0466	1.1041	1.1686	1.2411	1.3234	1.4160	1.5239	1.6492	1.7960	1.9723	2.1849	2.4488	2.7826	3.2168	3.8042	4.6272	5.8170
	8	0.7957	0.8284	0.8631	0.9037	0.9469	0.9930	1.0459	1.1037	1.1678	1.2407	1.3227	1.4152	1.5236	1.6488	1.7957	1.9716	2.1841	2.4482	2.7819	3.2170	3.8032	4.6267	5.8152
	9	0.7950	0.8278	0.8626	0.9029	0.9462	0.9924	1.0452	1.1031	1.1672	1.2401	1.3221	1.4147	1.5230	1.6482	1.7952	1.9711	2.1836	2.4477	2.7813	3.2164	3.8030	4.6261	5.8167
	10	0.7943	0.8271	0.8620	0.9023	0.9455	0.9918	1.0445	1.1025	1.1666	1.2395	1.3214	1.4142	1.5224	1.6476	1.7946	1.9705	2.1831	2.4470	2.7808	3.2157	3.8026	4.6254	5.8119
	11	0.7935	0.8264	0.8613	0.9016	0.9448	0.9912	1.0439	1.1018	1.1659	1.2389	1.3208	1.4136	1.5218	1.6471	1.7940	1.9699	2.1825	2.4465	2.7802	3.2153	3.8019	4.6248	5.7925
	12	0.7928	0.8257	0.8607	0.9009	0.9441	0.9905	1.0432	1.1011	1.1653	1.2382	1.3202	1.4130	1.5212	1.6465	1.7934	1.9694	2.1819	2.4460	2.7797	3.2150	3.8013	4.6242	5.8062
	13	0.7921	0.8250	0.8601	0.9001	0.9434	0.9899	1.0425	1.1005	1.1646	1.2376	1.3195	1.4124	1.5207	1.6459	1.7929	1.9688	2.1817	2.4454	2.7793	3.2142	3.8013	4.6245	5.8137
	14	0.7914	0.8243	0.8595	0.8994	0.9427	0.9893	1.0418	1.0998	1.1639	1.2369	1.3189	1.4119	1.5201	1.6453	1.7924	1.9682	2.1810	2.4448	2.7786	3.2137	3.8004	4.6230	5.8149
	15	0.7906	0.8236	0.8588	0.8987	0.9420	0.9886	1.0411	1.0991	1.1633	1.2363	1.3182	1.4113	1.5194	1.6447	1.7918	1.9676	2.1804	2.4442	2.7780	3.2131	3.7997	4.6227	5.8136
	16	0.7899	0.8229	0.8581	0.8980	0.9413	0.9879	1.0404	1.0984	1.1626	1.2356	1.3176	1.4106	1.5188	1.6441	1.7912	1.9670	2.1799	2.4437	2.7774	3.2126	3.7991	4.6223	5.8091
	17	0.7892	0.8222	0.8575	0.8972	0.9406	0.9872	1.0396	1.0977	1.1619	1.2349	1.3169	1.4100	1.5182	1.6435	1.7906	1.9664	2.1793	2.4431	2.7768	3.2120	3.7986	4.6213	5.8111
	18	0.7885	0.8215	0.8568	0.8965	0.9399	0.9866	1.0389	1.0970	1.1612	1.2342	1.3162	1.4094	1.5175	1.6428	1.7900	1.9657	2.1787	2.4425	2.7763	3.2115	3.7980	4.6211	5.8087
	19	0.7878	0.8208	0.8562	0.8958	0.9392	0.9859	1.0382	1.0963	1.1605	1.2336	1.3155	1.4088	1.5169	1.6422	1.7893	1.9651	2.1781	2.4419	2.7757	3.2109	3.7975	4.6202	5.8100
	20	0.7872	0.8202	0.8556	0.8951	0.9385	0.9852	1.0375	1.0957	1.1598	1.2329	1.3148	1.4081	1.5162	1.6415	1.7887	1.9645	2.1776	2.4413	2.7751	3.2103	3.7969	4.6196	5.8092

Analytical results 5000x2000mm

Volume of deformation - analytical results - 5000x2000mm plate																								
	Radius [mm]	25000	24000	23000	22000	21000	20000	19000	18000	17000	16000	15000	14000	13000	12000	11000	10000	9000	8000	7000	6000	5000	4000	3000
Thickness [mm]	4	0.7935	0.8264	0.8621	0.9011	0.9437	0.9905	1.0422	1.0995	1.1635	1.2353	1.3165	1.4091	1.5155	1.6391	1.7844	1.9575	2.1670	2.4253	2.7510	3.1726	3.7345	4.5047	5.5565
	5	0.7930	0.8259	0.8616	0.9006	0.9432	0.9900	1.0417	1.0991	1.1631	1.2349	1.3162	1.4087	1.5152	1.6388	1.7841	1.9572	2.1668	2.4251	2.7509	3.1724	3.7343	4.5044	5.5556
	6	0.7925	0.8254	0.8611	0.9001	0.9427	0.9896	1.0413	1.0986	1.1627	1.2345	1.3158	1.4084	1.5149	1.6385	1.7839	1.9570	2.1666	2.4250	2.7507	3.1723	3.7342	4.5041	5.5547
	7	0.7920	0.8249	0.8606	0.8996	0.9423	0.9891	1.0408	1.0982	1.1622	1.2341	1.3154	1.4080	1.5145	1.6382	1.7836	1.9568	2.1663	2.4248	2.7506	3.1722	3.7340	4.5038	5.5537
	8	0.7915	0.8244	0.8602	0.8991	0.9418	0.9887	1.0404	1.0978	1.1618	1.2337	1.3150	1.4077	1.5142	1.6379	1.7833	1.9565	2.1661	2.4246	2.7504	3.1720	3.7338	4.5035	5.5528
	9	0.7910	0.8239	0.8597	0.8987	0.9413	0.9882	1.0400	1.0974	1.1614	1.2334	1.3147	1.4073	1.5139	1.6376	1.7831	1.9563	2.1659	2.4244	2.7503	3.1719	3.7337	4.5032	5.5519
	10	0.7905	0.8234	0.8592	0.8982	0.9409	0.9878	1.0395	1.0970	1.1610	1.2330	1.3143	1.4070	1.5136	1.6373	1.7828	1.9561	2.1657	2.4243	2.7501	3.1718	3.7335	4.5028	5.5509
	11	0.7899	0.8229	0.8587	0.8977	0.9404	0.9873	1.0391	1.0965	1.1606	1.2326	1.3139	1.4067	1.5132	1.6370	1.7825	1.9558	2.1655	2.4241	2.7500	3.1716	3.7333	4.5025	5.5500
	12	0.7894	0.8224	0.8582	0.8972	0.9399	0.9869	1.0386	1.0961	1.1602	1.2322	1.3136	1.4063	1.5129	1.6367	1.7823	1.9556	2.1653	2.4239	2.7498	3.1715	3.7332	4.5022	5.5490
	13	0.7889	0.8219	0.8577	0.8968	0.9395	0.9864	1.0382	1.0957	1.1598	1.2318	1.3132	1.4060	1.5126	1.6365	1.7820	1.9553	2.1651	2.4237	2.7497	3.1714	3.7330	4.5019	5.5481
	14	0.7884	0.8214	0.8572	0.8963	0.9390	0.9860	1.0378	1.0953	1.1594	1.2314	1.3128	1.4056	1.5123	1.6362	1.7817	1.9551	2.1649	2.4236	2.7496	3.1712	3.7329	4.5016	5.5472
	15	0.7879	0.8209	0.8568	0.8958	0.9386	0.9855	1.0373	1.0949	1.1590	1.2310	1.3125	1.4053	1.5120	1.6359	1.7815	1.9549	2.1647	2.4234	2.7494	3.1711	3.7327	4.5013	5.5462
	16	0.7874	0.8204	0.8563	0.8954	0.9381	0.9851	1.0369	1.0944	1.1586	1.2307	1.3121	1.4049	1.5116	1.6356	1.7812	1.9546	2.1645	2.4232	2.7493	3.1710	3.7325	4.5010	5.5453
	17	0.7869	0.8200	0.8558	0.8949	0.9376	0.9846	1.0365	1.0940	1.1582	1.2303	1.3117	1.4046	1.5113	1.6353	1.7809	1.9544	2.1643	2.4230	2.7491	3.1708	3.7324	4.5006	5.5444
	18	0.7864	0.8195	0.8553	0.8944	0.9372	0.9842	1.0360	1.0936	1.1578	1.2299	1.3114	1.4042	1.5110	1.6350	1.7806	1.9541	2.1641	2.4229	2.7490	3.1707	3.7322	4.5003	5.5434
	19	0.7859	0.8190	0.8548	0.8939	0.9367	0.9837	1.0356	1.0932	1.1574	1.2295	1.3110	1.4039	1.5107	1.6347	1.7804	1.9539	2.1639	2.4227	2.7488	3.1706	3.7321	4.5000	5.5425
	20	0.7854	0.8185	0.8544	0.8935	0.9363	0.9833	1.0352	1.0928	1.1570	1.2291	1.3107	1.4036	1.5104	1.6344	1.7801	1.9537	2.1637	2.4225	2.7487	3.1704	3.7319	4.4997	5.5416

Validation 5000x2000mm

	Absolute deviation	Minimum deviation	Maximum deviation	Standard deviation
5000x1000mm	0.75%	0.52%	4.61%	0.36%

Volume of deformation - validation analytical results - 5000x2000mm plate																								
	Radius [mm]	25000	24000	23000	22000	21000	20000	19000	18000	17000	16000	15000	14000	13000	12000	11000	10000	9000	8000	7000	6000	5000	4000	3000
Thickness [mm]	4	0.64%	0.58%	0.39%	0.57%	0.62%	0.50%	0.58%	0.61%	0.56%	0.63%	0.63%	0.60%	0.69%	0.73%	0.76%	0.82%	0.90%	1.03%	1.17%	1.41%	1.88%	2.68%	4.42%
	5	0.60%	0.49%	0.44%	0.58%	0.57%	0.44%	0.60%	0.54%	0.59%	0.57%	0.64%	0.61%	0.62%	0.67%	0.72%	0.82%	0.89%	1.02%	1.18%	1.44%	1.87%	2.68%	
	6	0.59%	0.54%	0.39%	0.53%	0.58%	0.48%	0.55%	0.58%	0.53%	0.60%	0.60%	0.58%	0.66%	0.70%	0.73%	0.79%	0.87%	0.98%	1.15%	1.42%	1.86%	2.67%	
	7	0.56%	0.49%	0.38%	0.53%	0.54%	0.42%	0.55%	0.54%	0.54%	0.56%	0.60%	0.56%	0.61%	0.66%	0.69%	0.79%	0.85%	0.98%	1.15%	1.39%	1.85%		
	8	0.54%	0.49%	0.34%	0.50%	0.54%	0.43%	0.52%	0.53%	0.51%	0.56%	0.58%	0.53%	0.61%	0.66%	0.69%	0.77%	0.82%	0.96%	1.13%	1.40%			
	9	0.51%	0.47%	0.34%	0.47%	0.52%	0.43%	0.50%	0.52%	0.49%	0.55%	0.56%	0.52%	0.60%	0.64%	0.67%	0.75%	0.81%	0.95%	1.11%	1.38%			
	10	0.48%	0.45%	0.32%	0.45%	0.49%	0.41%	0.48%	0.50%	0.47%	0.53%	0.54%	0.51%	0.58%	0.63%	0.66%	0.73%	0.80%	0.93%	1.10%				
	11	0.45%	0.42%	0.31%	0.43%	0.47%	0.39%	0.46%	0.48%	0.46%	0.51%	0.52%	0.49%	0.56%	0.61%	0.64%	0.72%	0.78%	0.92%	1.09%				
	12	0.42%	0.39%	0.29%	0.40%	0.44%	0.37%	0.44%	0.46%	0.44%	0.48%	0.50%	0.47%	0.54%	0.59%	0.62%	0.70%	0.76%	0.90%					
	13	0.40%	0.37%	0.27%	0.37%	0.42%	0.35%	0.41%	0.43%	0.41%	0.47%	0.48%	0.46%	0.53%	0.57%	0.61%	0.68%	0.76%						
	14	0.37%	0.35%	0.26%	0.34%	0.39%	0.33%	0.38%	0.41%	0.39%	0.44%	0.46%	0.44%	0.51%	0.56%	0.60%	0.66%	0.74%						
	15	0.34%	0.32%	0.23%	0.32%	0.36%	0.31%	0.36%	0.39%	0.36%	0.42%	0.44%	0.42%	0.49%	0.54%	0.58%	0.65%							
	16	0.31%	0.30%	0.21%	0.29%	0.34%	0.29%	0.33%	0.36%	0.34%	0.40%	0.41%	0.41%	0.47%	0.52%	0.56%								
	17	0.29%	0.27%	0.19%	0.26%	0.31%	0.27%	0.30%	0.34%	0.32%	0.38%	0.39%	0.39%	0.45%	0.50%	0.54%								
	18	0.26%	0.25%	0.17%	0.23%	0.28%	0.24%	0.28%	0.31%	0.29%	0.35%	0.36%	0.37%	0.43%	0.48%									
	19	0.24%	0.23%	0.16%	0.21%	0.26%	0.22%	0.25%	0.29%	0.26%	0.33%	0.34%	0.35%	0.41%										
	20	0.22%	0.21%	0.14%	0.18%	0.23%	0.20%	0.22%	0.26%	0.24%	0.30%	0.31%	0.32%	0.39%										

Numerical results 5000x3000mm

Volume of deformation - numerical results - 5000x3000mm plate

	Radius [mm]	25000	24000	23000	22000	21000	20000	19000	18000	17000	16000	15000	14000	13000	12000	11000	10000	9000	8000	7000	6000	5000	4000	3000
Thickness [mm]	4	1.1974	1.2461	1.2975	1.3588	1.4238	1.4925	1.5719	1.6588	1.7546	1.8641	1.9869	2.1256	2.2883	2.4762	2.6965	2.9600	3.2793	3.6753	4.1751	4.8280	5.7087	6.9423	8.7260
	5	1.1958	1.2441	1.2977	1.3581	1.4221	1.4911	1.5713	1.6567	1.7544	1.8622	1.9863	2.1257	2.2860	2.4739	2.6951	2.9596	3.2788	3.6744	4.1749	4.8271	5.7073	6.9415	8.7252
	6	1.1950	1.2439	1.2957	1.3566	1.4215	1.4905	1.5698	1.6567	1.7526	1.8621	1.9849	2.1238	2.2864	2.4741	2.6944	2.9580	3.2774	3.6729	4.1730	4.8263	5.7063	6.9399	8.7245
	7	1.1937	1.2423	1.2952	1.3558	1.4202	1.4888	1.5690	1.6551	1.7522	1.8606	1.9841	2.1232	2.2847	2.4726	2.6927	2.9574	3.2764	3.6721	4.1731	4.8254	5.7053	6.9368	8.7238
	8	1.1926	1.2415	1.2938	1.3546	1.4192	1.4882	1.5678	1.6543	1.7508	1.8598	1.9831	2.1218	2.2840	2.4719	2.6923	2.9565	3.2751	3.6710	4.1715	4.8247	5.7044	6.9388	8.7230
	9	1.1914	1.2404	1.2927	1.3534	1.4181	1.4873	1.5667	1.6533	1.7497	1.8588	1.9820	2.1208	2.2833	2.4709	2.6912	2.9553	3.2743	3.6703	4.1704	4.8237	5.7037	6.9380	8.7223
	10	1.1903	1.2394	1.2916	1.3523	1.4170	1.4863	1.5656	1.6523	1.7487	1.8578	1.9809	2.1198	2.2821	2.4701	2.6904	2.9543	3.2731	3.6694	4.1701	4.8229	5.7024	6.9352	8.7216
	11	1.1891	1.2382	1.2906	1.3512	1.4159	1.4852	1.5645	1.6513	1.7477	1.8567	1.9798	2.1189	2.2812	2.4689	2.6894	2.9536	3.2721	3.6685	4.1685	4.8209	5.7011	6.9344	8.7176
	12	1.1879	1.2371	1.2895	1.3500	1.4147	1.4842	1.5634	1.6501	1.7466	1.8556	1.9788	2.1179	2.2800	2.4678	2.6882	2.9527	3.2712	3.6671	4.1676	4.8199	5.6993	6.9359	8.7220
	13	1.1868	1.2360	1.2884	1.3489	1.4136	1.4832	1.5623	1.6490	1.7455	1.8546	1.9777	2.1168	2.2791	2.4669	2.6873	2.9513	3.2706	3.6660	4.1665	4.8189	5.6983	6.9320	8.7185
	14	1.1856	1.2348	1.2874	1.3477	1.4125	1.4821	1.5612	1.6479	1.7444	1.8536	1.9767	2.1159	2.2781	2.4659	2.6863	2.9506	3.2691	3.6650	4.1662	4.8179	5.6988	6.9342	8.7187
	15	1.1844	1.2337	1.2863	1.3465	1.4113	1.4810	1.5600	1.6469	1.7433	1.8527	1.9756	2.1148	2.2770	2.4649	2.6853	2.9493	3.2681	3.6647	4.1645	4.8168	5.6963	6.9300	8.7196
	16	1.1831	1.2324	1.2851	1.3453	1.4102	1.4799	1.5589	1.6457	1.7422	1.8514	1.9747	2.1137	2.2760	2.4638	2.6843	2.9482	3.2671	3.6630	4.1632	4.8158	5.6966	6.9285	8.7187
	17	1.1819	1.2313	1.2840	1.3441	1.4090	1.4788	1.5577	1.6446	1.7410	1.8503	1.9734	2.1127	2.2750	2.4628	2.6834	2.9472	3.2662	3.6619	4.1624	4.8148	5.6940	6.9316	8.7178
	18	1.1806	1.2300	1.2828	1.3429	1.4078	1.4777	1.5566	1.6435	1.7399	1.8492	1.9723	2.1117	2.2740	2.4618	2.6824	2.9462	3.2652	3.6609	4.1614	4.8137	5.6930	6.9288	8.7151
	19	1.1793	1.2288	1.2816	1.3417	1.4066	1.4765	1.5554	1.6424	1.7388	1.8481	1.9712	2.1107	2.2729	2.4608	2.6813	2.9452	3.2642	3.6599	4.1604	4.8127	5.6919	6.9251	8.7165
	20	1.1780	1.2275	1.2804	1.3404	1.4054	1.4754	1.5542	1.6412	1.7376	1.8470	1.9700	2.1096	2.2719	2.4601	2.6803	2.9441	3.2632	3.6589	4.1594	4.8138	5.6909	6.9239	8.7107

Analytical results 5000x3000mm

Volume of deformation - analytical results - 5000x3000mm plate

	Radius [mm]	25000	24000	23000	22000	21000	20000	19000	18000	17000	16000	15000	14000	13000	12000	11000	10000	9000	8000	7000	6000	5000	4000	3000
Thickness [mm]	4	1.1916	1.2408	1.2943	1.3526	1.4164	1.4866	1.5640	1.6499	1.7458	1.8535	1.9752	2.1140	2.2735	2.4589	2.6768	2.9363	3.2504	3.6379	4.1263	4.7585	5.6011	6.7560	8.3322
	5	1.1909	1.2402	1.2937	1.3520	1.4159	1.4860	1.5635	1.6495	1.7454	1.8531	1.9749	2.1137	2.2733	2.4587	2.6766	2.9362	3.2504	3.6379	4.1264	4.7586	5.6012	6.7559	8.3316
	6	1.1902	1.2395	1.2930	1.3514	1.4153	1.4855	1.5630	1.6490	1.7450	1.8527	1.9746	2.1134	2.2730	2.4585	2.6764	2.9361	3.2503	3.6379	4.1264	4.7587	5.6013	6.7559	8.3309
	7	1.1895	1.2388	1.2924	1.3508	1.4147	1.4850	1.5625	1.6486	1.7446	1.8523	1.9742	2.1131	2.2728	2.4583	2.6763	2.9360	3.2503	3.6379	4.1265	4.7588	5.6014	6.7558	8.3303
	8	1.1888	1.2382	1.2918	1.3502	1.4142	1.4845	1.5620	1.6481	1.7441	1.8520	1.9739	2.1128	2.2725	2.4581	2.6761	2.9359	3.2502	3.6379	4.1266	4.7589	5.6015	6.7558	8.3296
	9	1.1881	1.2375	1.2912	1.3496	1.4136	1.4839	1.5615	1.6476	1.7437	1.8516	1.9735	2.1125	2.2723	2.4579	2.6760	2.9358	3.2502	3.6379	4.1266	4.7590	5.6015	6.7557	8.3290
	10	1.1874	1.2369	1.2905	1.3490	1.4131	1.4834	1.5610	1.6472	1.7433	1.8512	1.9732	2.1122	2.2720	2.4577	2.6758	2.9357	3.2501	3.6379	4.1267	4.7590	5.6016	6.7557	8.3283
	11	1.1867	1.2362	1.2899	1.3485	1.4125	1.4829	1.5606	1.6467	1.7429	1.8508	1.9729	2.1119	2.2718	2.4575	2.6757	2.9356	3.2501	3.6379	4.1267	4.7591	5.6017	6.7556	8.3276
	12	1.1861	1.2355	1.2893	1.3479	1.4119	1.4823	1.5601	1.6463	1.7425	1.8504	1.9725	2.1116	2.2715	2.4573	2.6755	2.9355	3.2500	3.6379	4.1268	4.7592	5.6018	6.7556	8.3270
	13	1.1854	1.2349	1.2887	1.3473	1.4114	1.4818	1.5596	1.6458	1.7420	1.8501	1.9722	2.1113	2.2713	2.4571	2.6754	2.9354	3.2500	3.6379	4.1268	4.7593	5.6019	6.7555	8.3263
	14	1.1847	1.2342	1.2880	1.3467	1.4108	1.4813	1.5591	1.6454	1.7416	1.8497	1.9718	2.1110	2.2710	2.4569	2.6752	2.9353	3.2500	3.6379	4.1269	4.7594	5.6020	6.7555	8.3257
	15	1.1840	1.2336	1.2874	1.3461	1.4103	1.4808	1.5586	1.6449	1.7412	1.8493	1.9715	2.1107	2.2708	2.4567	2.6751	2.9352	3.2499	3.6379	4.1269	4.7595	5.6020	6.7554	8.3250
	16	1.1833	1.2329	1.2868	1.3455	1.4097	1.4802	1.5581	1.6445	1.7408	1.8489	1.9712	2.1104	2.2705	2.4565	2.6749	2.9351	3.2499	3.6379	4.1270	4.7596	5.6021	6.7554	8.3244
	17	1.1826	1.2323	1.2862	1.3449	1.4092	1.4797	1.5576	1.6440	1.7404	1.8486	1.9708	2.1101	2.2703	2.4563	2.6748	2.9350	3.2498	3.6379	4.1270	4.7597	5.6022	6.7553	8.3237
	18	1.1820	1.2316	1.2856	1.3443	1.4086	1.4792	1.5571	1.6436	1.7400	1.8482	1.9705	2.1099	2.2700	2.4561	2.6746	2.9349	3.2498	3.6379	4.1271	4.7598	5.6023	6.7553	8.3231
	19	1.1813	1.2310	1.2849	1.3437	1.4080	1.4787	1.5566	1.6431	1.7395	1.8478	1.9702	2.1096	2.2698	2.4559	2.6744	2.9348	3.2497	3.6379	4.1272	4.7598	5.6024	6.7552	8.3224
	20	1.1806	1.2303	1.2843	1.3431	1.4075	1.4782	1.5561	1.6426	1.7391	1.8474	1.9698	2.1093	2.2695	2.4557	2.6743	2.9347	3.2497	3.6379	4.1272	4.7599	5.6025	6.7552	8.3218

Validation 5000x3000mm

	Absolute deviation	Minimum deviation	Maximum deviation	Standard deviation
5000x3000mm	0.42%	0.00%	4.51%	0.47%

Volume of deformation - validation analytical results - 5000x3000mm plate

	Radius [mm]	25000	24000	23000	22000	21000	20000	19000	18000	17000	16000	15000	14000	13000	12000	11000	10000	9000	8000	7000	6000	5000	4000	3000
Thickness [mm]	4	0.48%	0.43%	0.24%	0.46%	0.51%	0.39%	0.50%	0.53%	0.50%	0.57%	0.59%	0.55%	0.65%	0.70%	0.73%	0.80%	0.88%	1.02%	1.17%	1.44%	1.88%	2.68%	4.51%
	5	0.41%	0.31%	0.31%	0.45%	0.44%	0.34%	0.49%	0.44%	0.51%	0.49%	0.57%	0.56%	0.55%	0.62%	0.69%	0.79%	0.87%	0.99%	1.16%	1.42%	1.86%	2.67%	
	6	0.40%	0.36%	0.20%	0.38%	0.44%	0.34%	0.43%	0.46%	0.44%	0.50%	0.52%	0.49%	0.58%	0.63%	0.66%	0.74%	0.83%	0.95%	1.12%	1.40%	1.84%	2.65%	
	7	0.35%	0.28%	0.21%	0.36%	0.38%	0.26%	0.41%	0.40%	0.43%	0.44%	0.50%	0.47%	0.52%	0.58%	0.61%	0.73%	0.80%	0.93%	1.12%	1.38%	1.82%		
	8	0.32%	0.27%	0.16%	0.32%	0.35%	0.25%	0.37%	0.38%	0.38%	0.42%	0.47%	0.43%	0.50%	0.56%	0.60%	0.70%	0.76%	0.90%	1.08%	1.36%			
	9	0.28%	0.24%	0.12%	0.28%	0.31%	0.22%	0.33%	0.34%	0.34%	0.39%	0.43%	0.39%	0.48%	0.53%	0.57%	0.66%	0.74%	0.88%	1.05%	1.34%			
	10	0.24%	0.21%	0.08%	0.24%	0.28%	0.19%	0.29%	0.31%	0.31%	0.35%	0.39%	0.36%	0.44%	0.50%	0.54%	0.63%	0.70%	0.86%	1.04%				
	11	0.20%	0.16%	0.05%	0.20%	0.24%	0.16%	0.25%	0.28%	0.27%	0.32%	0.35%	0.33%	0.41%	0.46%	0.51%	0.61%	0.67%	0.83%	1.00%				
	12	0.16%	0.12%	0.02%	0.16%	0.20%	0.12%	0.22%	0.23%	0.24%	0.28%	0.32%	0.30%	0.37%	0.43%	0.47%	0.58%	0.65%	0.80%					
	13	0.12%	0.09%	0.02%	0.12%	0.16%	0.09%	0.17%	0.19%	0.20%	0.25%	0.28%	0.26%	0.34%	0.40%	0.44%	0.54%	0.63%						
	14	0.07%	0.05%	0.05%	0.07%	0.12%	0.06%	0.13%	0.16%	0.16%	0.21%	0.24%	0.23%	0.31%	0.37%	0.41%	0.52%	0.59%						
	15	0.03%	0.01%	0.09%	0.03%	0.07%	0.02%	0.09%	0.12%	0.12%	0.18%	0.21%	0.19%	0.27%	0.33%	0.38%	0.48%							
	16	0.02%	0.04%	0.13%	0.01%	0.03%	0.02%	0.05%	0.08%	0.08%	0.13%	0.18%	0.16%	0.24%	0.30%	0.35%								
	17	0.07%	0.08%	0.17%	0.06%	0.01%	0.06%	0.01%	0.04%	0.04%	0.10%	0.13%	0.12%	0.21%	0.27%	0.32%								
	18	0.12%	0.13%	0.21%	0.11%	0.06%	0.10%	0.04%	0.00%	0.00%	0.06%	0.09%	0.09%	0.17%	0.23%									
	19	0.17%	0.18%	0.26%	0.15%	0.10%	0.15%	0.08%	0.04%	0.05%	0.02%	0.05%	0.05%	0.14%										
	20	0.22%	0.23%	0.30%	0.21%	0.15%	0.19%	0.13%	0.09%	0.09%	0.02%	0.01%	0.02%	0.10%										

Numerical results 6000x1000mm

Volume of deformation - numerical results - 5000x1000mm plate																							
Radius [mm]	25000	24000	23000	22000	21000	20000	19000	18000	17000	16000	15000	14000	13000	12000	11000	10000	9000	8000	7000	6000	5000	4000	3000
Thickness [mm] 4	0.6908	0.7183	0.7481	0.7834	0.8209	0.8605	0.9050	0.9558	1.0101	1.0728	1.1421	1.2237	1.3150	1.4211	1.5469	1.6967	1.8781	2.1005	2.3804	2.7411	3.2196	3.8684	4.7185
5	0.6904	0.7185	0.7484	0.7823	0.8203	0.8607	0.9039	0.9552	1.0106	1.0720	1.1428	1.2230	1.3142	1.4219	1.5477	1.6967	1.8779	2.1001	2.3798	2.7408	3.2188	3.8688	4.7202
6	0.6898	0.7180	0.7480	0.7818	0.8196	0.8600	0.9035	0.9548	1.0099	1.0719	1.1426	1.2227	1.3140	1.4217	1.5473	1.6964	1.8776	2.0999	2.3796	2.7406	3.2188	3.8685	4.7219
7	0.6893	0.7175	0.7476	0.7815	0.8192	0.8596	0.9032	0.9543	1.0095	1.0716	1.1422	1.2224	1.3137	1.4213	1.5470	1.6961	1.8773	2.0997	2.3791	2.7407	3.2187	3.8684	4.7237
8	0.6888	0.7171	0.7473	0.7812	0.8188	0.8593	0.9029	0.9539	1.0092	1.0712	1.1419	1.2220	1.3134	1.4210	1.5468	1.6958	1.8771	2.0994	2.3788	2.7401	3.2183	3.8680	4.7254
9	0.6884	0.7168	0.7471	0.7808	0.8184	0.8590	0.9027	0.9535	1.0089	1.0708	1.1416	1.2216	1.3133	1.4208	1.5465	1.6956	1.8767	2.0992	2.3786	2.7398	3.2180	3.8678	4.6967
10	0.6880	0.7164	0.7468	0.7805	0.8181	0.8587	0.9026	0.9531	1.0086	1.0704	1.1413	1.2212	1.3131	1.4206	1.5462	1.6954	1.8764	2.0988	2.3785	2.7395	3.2178	3.8675	4.7353
11	0.6877	0.7161	0.7466	0.7802	0.8178	0.8584	0.9024	0.9528	1.0083	1.0701	1.1410	1.2209	1.3129	1.4203	1.5459	1.6951	1.8762	2.0986	2.3782	2.7393	3.2176	3.8674	4.7419
12	0.6875	0.7159	0.7464	0.7800	0.8175	0.8581	0.9022	0.9525	1.0080	1.0698	1.1407	1.2206	1.3126	1.4199	1.5456	1.6948	1.8759	2.0983	2.3779	2.7390	3.2173	3.8672	4.7419
13	0.6872	0.7157	0.7462	0.7798	0.8173	0.8579	0.9020	0.9522	1.0078	1.0695	1.1404	1.2203	1.3123	1.4196	1.5453	1.6946	1.8756	2.0980	2.3777	2.7388	3.2174	3.8671	4.7413
14	0.6870	0.7155	0.7461	0.7796	0.8170	0.8577	0.9019	0.9520	1.0075	1.0693	1.1402	1.2200	1.3121	1.4194	1.5450	1.6943	1.8753	2.0978	2.3775	2.7385	3.2172	3.8666	4.7409
15	0.6869	0.7153	0.7460	0.7794	0.8168	0.8575	0.9017	0.9517	1.0073	1.0690	1.1399	1.2197	1.3118	1.4191	1.5447	1.6941	1.8750	2.0975	2.3772	2.7383	3.2168	3.8664	4.7407
16	0.6867	0.7152	0.7458	0.7793	0.8166	0.8573	0.9016	0.9515	1.0071	1.0688	1.1397	1.2195	1.3116	1.4188	1.5445	1.6938	1.8747	2.0972	2.3770	2.7381	3.2165	3.8662	4.7407
17	0.6866	0.7151	0.7457	0.7792	0.8165	0.8571	0.9015	0.9513	1.0069	1.0686	1.1394	1.2192	1.3114	1.4186	1.5442	1.6936	1.8744	2.0969	2.3768	2.7378	3.2162	3.8661	4.7404
18	0.6865	0.7149	0.7456	0.7791	0.8163	0.8570	0.9014	0.9512	1.0067	1.0684	1.1392	1.2190	1.3112	1.4183	1.5440	1.6933	1.8741	2.0966	2.3765	2.7376	3.2160	3.8657	4.7410
19	0.6864	0.7148	0.7455	0.7790	0.8162	0.8568	0.9012	0.9510	1.0066	1.0683	1.1390	1.2188	1.3110	1.4181	1.5437	1.6931	1.8738	2.0963	2.3763	2.7373	3.2157	3.8655	4.7395
20	0.6863	0.7147	0.7455	0.7789	0.8161	0.8567	0.9011	0.9509	1.0064	1.0681	1.1389	1.2186	1.3108	1.4179	1.5435	1.6929	1.8735	2.0960	2.3760	2.7371	3.2155	3.8653	4.7397

Analytical results 6000x1000mm

Volume of deformation - analytical results - 6000x1000mm plate																							
Radius [mm]	25000	24000	23000	22000	21000	20000	19000	18000	17000	16000	15000	14000	13000	12000	11000	10000	9000	8000	7000	6000	5000	4000	3000
Thickness [mm] 4	0.6838	0.7121	0.7429	0.7764	0.8131	0.8534	0.8979	0.9472	1.0022	1.0638	1.1335	1.2128	1.3038	1.4094	1.5331	1.6800	1.8569	2.0738	2.3446	2.6901	3.1393	3.7257	4.4312
5	0.6837	0.7120	0.7428	0.7763	0.8130	0.8532	0.8977	0.9470	1.0020	1.0636	1.1333	1.2126	1.3036	1.4091	1.5328	1.6797	1.8566	2.0735	2.3443	2.6898	3.1390	3.7254	4.4310
6	0.6835	0.7119	0.7426	0.7761	0.8128	0.8531	0.8975	0.9468	1.0018	1.0634	1.1331	1.2123	1.3033	1.4088	1.5325	1.6794	1.8563	2.0731	2.3440	2.6894	3.1386	3.7251	4.4308
7	0.6834	0.7117	0.7425	0.7760	0.8126	0.8529	0.8973	0.9466	1.0016	1.0632	1.1328	1.2121	1.3031	1.4086	1.5323	1.6791	1.8560	2.0728	2.3437	2.6891	3.1383	3.7247	4.4305
8	0.6833	0.7116	0.7423	0.7758	0.8125	0.8527	0.8972	0.9464	1.0014	1.0630	1.1326	1.2119	1.3028	1.4083	1.5320	1.6788	1.8557	2.0725	2.3433	2.6887	3.1379	3.7244	4.4303
9	0.6832	0.7115	0.7422	0.7757	0.8123	0.8526	0.8970	0.9462	1.0011	1.0628	1.1324	1.2116	1.3026	1.4081	1.5317	1.6785	1.8554	2.0722	2.3430	2.6884	3.1376	3.7241	4.4301
10	0.6831	0.7114	0.7421	0.7755	0.8122	0.8524	0.8968	0.9460	1.0009	1.0626	1.1322	1.2114	1.3023	1.4078	1.5314	1.6782	1.8551	2.0719	2.3427	2.6881	3.1372	3.7238	4.4299
11	0.6830	0.7112	0.7419	0.7754	0.8120	0.8522	0.8966	0.9458	1.0007	1.0623	1.1319	1.2111	1.3021	1.4075	1.5311	1.6779	1.8548	2.0716	2.3423	2.6877	3.1369	3.7234	4.4297
12	0.6828	0.7111	0.7418	0.7752	0.8118	0.8521	0.8964	0.9457	1.0005	1.0621	1.1317	1.2109	1.3018	1.4073	1.5309	1.6776	1.8545	2.0712	2.3420	2.6874	3.1366	3.7231	4.4295
13	0.6827	0.7110	0.7417	0.7751	0.8117	0.8519	0.8963	0.9455	1.0003	1.0619	1.1315	1.2107	1.3016	1.4070	1.5306	1.6774	1.8542	2.0709	2.3417	2.6871	3.1362	3.7228	4.4292
14	0.6826	0.7108	0.7415	0.7749	0.8115	0.8517	0.8961	0.9453	1.0001	1.0617	1.1313	1.2104	1.3013	1.4067	1.5303	1.6771	1.8539	2.0706	2.3414	2.6867	3.1359	3.7225	4.4290
15	0.6825	0.7107	0.7414	0.7748	0.8114	0.8516	0.8959	0.9451	0.9999	1.0615	1.1310	1.2102	1.3011	1.4065	1.5301	1.6768	1.8536	2.0703	2.3410	2.6864	3.1355	3.7221	4.4288
16	0.6824	0.7106	0.7412	0.7747	0.8112	0.8514	0.8957	0.9449	0.9997	1.0613	1.1308	1.2100	1.3008	1.4062	1.5298	1.6765	1.8533	2.0700	2.3407	2.6860	3.1352	3.7218	4.4286
17	0.6822	0.7105	0.7411	0.7745	0.8111	0.8512	0.8955	0.9447	0.9995	1.0611	1.1306	1.2097	1.3006	1.4060	1.5295	1.6762	1.8530	2.0697	2.3404	2.6857	3.1349	3.7215	4.4284
18	0.6821	0.7103	0.7410	0.7744	0.8109	0.8510	0.8954	0.9445	0.9993	1.0609	1.1304	1.2095	1.3003	1.4057	1.5292	1.6759	1.8527	2.0694	2.3400	2.6854	3.1345	3.7212	4.4282
19	0.6820	0.7102	0.7408	0.7742	0.8107	0.8509	0.8952	0.9443	0.9991	1.0606	1.1301	1.2092	1.3001	1.4054	1.5290	1.6756	1.8524	2.0690	2.3397	2.6850	3.1342	3.7209	4.4279
20	0.6819	0.7101	0.7407	0.7741	0.8106	0.8507	0.8950	0.9441	0.9989	1.0604	1.1299	1.2090	1.2998	1.4052	1.5287	1.6753	1.8521	2.0687	2.3394	2.6847	3.1338	3.7205	4.4277

Validation 6000x1000mm

	Absolute deviation	Minimum deviation	Maximum deviation	Standard deviation
6000x1000mm	0.91%	0.59%	6.09%	0.51%

Volume of deformation - validation analytical results - 6000x1000mm plate																							
Radius [mm]	25000	24000	23000	22000	21000	20000	19000	18000	17000	16000	15000	14000	13000	12000	11000	10000	9000	8000	7000	6000	5000	4000	3000
Thickness [mm] 4	1.01%	0.86%	0.69%	0.89%	0.94%	0.82%	0.79%	0.91%	0.78%	0.84%	0.75%	0.89%	0.85%	0.83%	0.89%	0.99%	1.13%	1.27%	1.50%	1.86%	2.49%	3.69%	6.09%
5	0.97%	0.91%	0.75%	0.77%	0.89%	0.87%	0.68%	0.86%	0.85%	0.78%	0.83%	0.85%	0.81%	0.90%	0.96%	1.00%	1.13%	1.27%	1.49%	1.86%	2.48%	3.71%	
6	0.90%	0.86%	0.72%	0.73%	0.83%	0.80%	0.66%	0.83%	0.81%	0.79%	0.84%	0.85%	0.81%	0.90%	0.96%	1.00%	1.13%	1.27%	1.50%	1.87%	2.49%	3.71%	
7	0.85%	0.80%	0.69%	0.71%	0.80%	0.78%	0.65%	0.81%	0.79%	0.78%	0.82%	0.84%	0.80%	0.90%	0.95%	1.00%	1.13%	1.28%	1.49%	1.88%	2.50%		
8	0.80%	0.77%	0.67%	0.68%	0.77%	0.76%	0.64%	0.79%	0.78%	0.77%	0.81%	0.83%	0.81%	0.90%	0.96%	1.00%	1.14%	1.28%	1.49%	1.87%			
9	0.76%	0.74%	0.66%	0.65%	0.75%	0.74%	0.64%	0.76%	0.77%	0.75%	0.81%	0.82%	0.81%	0.90%	0.96%	1.01%	1.14%	1.28%	1.50%	1.88%			
10	0.72%	0.70%	0.63%	0.63%	0.72%	0.73%	0.65%	0.74%	0.76%	0.73%	0.81%	0.81%	0.82%	0.90%	0.96%	1.01%	1.14%	1.28%	1.50%				
11	0.69%	0.68%	0.62%	0.62%	0.71%	0.72%	0.64%	0.73%	0.75%	0.73%	0.80%	0.80%	0.82%	0.90%	0.95%	1.01%	1.14%	1.29%	1.51%				
12	0.67%	0.67%	0.61%	0.61%	0.69%	0.71%	0.64%	0.72%	0.74%	0.72%	0.79%	0.80%	0.82%	0.89%	0.95%	1.01%	1.14%	1.29%					
13	0.66%	0.66%	0.61%	0.60%	0.68%	0.70%	0.64%	0.71%	0.74%	0.71%	0.78%	0.79%	0.82%	0.89%	0.95%	1.02%	1.14%						
14	0.65%	0.65%	0.61%	0.60%	0.67%	0.69%	0.65%	0.70%	0.73%	0.71%	0.78%	0.78%	0.82%	0.89%	0.95%	1.02%	1.14%						
15	0.64%	0.64%	0.61%	0.59%	0.67%	0.69%	0.65%	0.70%	0.73%	0.70%	0.78%	0.78%	0.82%	0.89%	0.95%	1.02%							
16	0.64%	0.64%	0.62%	0.59%	0.67%	0.69%	0.65%	0.70%	0.73%	0.70%	0.78%	0.78%	0.82%	0.89%	0.95%								
17	0.63%	0.64%	0.62%	0.60%	0.67%	0.69%	0.66%	0.70%	0.73%	0.70%	0.78%	0.78%	0.83%	0.89%	0.95%								
18	0.63%	0.64%	0.63%	0.60%	0.67%	0.69%	0.67%	0.70%	0.73%	0.71%	0.78%	0.78%	0.83%	0.89%									
19	0.64%	0.65%	0.63%	0.61%	0.67%	0.70%	0.67%	0.70%	0.74%	0.71%	0.78%	0.78%	0.83%	0.89%									
20	0.64%	0.65%	0.64%	0.62%	0.68%	0.70%	0.68%	0.71%	0.74%	0.72%	0.79%	0.79%	0.84%										

Numerical results 6000x2000mm

Volume of deformation - numerical results - 6000x2000mm plate

Thickness [mm] \ Radius [mm]	25000	24000	23000	22000	21000	20000	19000	18000	17000	16000	15000	14000	13000	12000	11000	10000	9000	8000	7000	6000	5000	4000	3000
4	1.3817	1.4359	1.4968	1.5677	1.6421	1.7206	1.8100	1.9106	2.0177	2.1466	2.2837	2.4468	2.6304	2.8424	3.0936	3.3941	3.7553	4.2003	4.7602	5.4810	6.4376	7.7397	9.4882
5	1.3817	1.4373	1.4958	1.5653	1.6412	1.7214	1.8074	1.9109	2.0208	2.1443	2.2853	2.4462	2.6268	2.8434	3.0947	3.3922	3.7554	4.2003	4.7592	5.4804	6.4370	7.7389	9.4870
6	1.3806	1.4363	1.4948	1.5644	1.6399	1.7198	1.8074	1.9099	2.0192	2.1440	2.2846	2.4455	2.6268	2.8425	3.0939	3.3916	3.7547	4.1995	4.7583	5.4800	6.4351	7.7468	9.4859
7	1.3796	1.4352	1.4938	1.5639	1.6392	1.7190	1.8069	1.9092	2.0184	2.1435	2.2838	2.4448	2.6266	2.8417	3.0931	3.3907	3.7541	4.1990	4.7575	5.4790	6.4341	7.7347	9.4847
8	1.3786	1.4343	1.4931	1.5632	1.6384	1.7183	1.8062	1.9084	2.0177	2.1428	2.2832	2.4441	2.6259	2.8411	3.0925	3.3900	3.7535	4.1981	4.7570	5.4785	6.4356	7.7338	9.4835
9	1.3774	1.4331	1.4920	1.5625	1.6378	1.7178	1.8053	1.9076	2.0171	2.1420	2.2826	2.4434	2.6252	2.8405	3.0919	3.3897	3.7528	4.1976	4.7564	5.4781	6.4346	7.7339	9.4824
10	1.3766	1.4325	1.4917	1.5615	1.6369	1.7172	1.8044	1.9067	2.0166	2.1411	2.2821	2.4426	2.6245	2.8401	3.0915	3.3892	3.7522	4.1968	4.7556	5.4775	6.4348	7.7330	9.4812
11	1.3757	1.4317	1.4910	1.5608	1.6361	1.7164	1.8037	1.9060	2.0159	2.1404	2.2814	2.4419	2.6238	2.8394	3.0906	3.3885	3.7514	4.1964	4.7549	5.4770	6.4333	7.7319	9.4801
12	1.3748	1.4308	1.4902	1.5600	1.6352	1.7155	1.8032	1.9052	2.0150	2.1398	2.2806	2.4412	2.6233	2.8385	3.0899	3.3877	3.7508	4.1956	4.7547	5.4759	6.4329	7.7322	9.4797
13	1.3740	1.4302	1.4899	1.5590	1.6343	1.7148	1.8023	1.9044	2.0144	2.1390	2.2800	2.4405	2.6226	2.8379	3.0893	3.3872	3.7502	4.1950	4.7540	5.4755	6.4325	7.7317	9.4784
14	1.3731	1.4294	1.4892	1.5582	1.6334	1.7140	1.8015	1.9036	2.0137	2.1382	2.2793	2.4397	2.6219	2.8373	3.0887	3.3866	3.7495	4.1943	4.7531	5.4754	6.4315	7.7309	9.4766
15	1.3722	1.4284	1.4884	1.5573	1.6326	1.7132	1.8007	1.9027	2.0129	2.1374	2.2785	2.4390	2.6213	2.8367	3.0880	3.3860	3.7488	4.1938	4.7524	5.4746	6.4309	7.7305	9.4776
16	1.3713	1.4277	1.4877	1.5565	1.6317	1.7124	1.7999	1.9019	2.0122	2.1366	2.2778	2.4382	2.6207	2.8360	3.0874	3.3855	3.7482	4.1930	4.7518	5.4737	6.4303	7.7300	9.4749
17	1.3704	1.4268	1.4870	1.5556	1.6309	1.7117	1.7990	1.9011	2.0115	2.1358	2.2771	2.4374	2.6201	2.8354	3.0868	3.3849	3.7477	4.1923	4.7511	5.4731	6.4220	7.7289	9.4639
18	1.3696	1.4260	1.4863	1.5547	1.6300	1.7109	1.7982	1.9002	2.0107	2.1350	2.2763	2.4367	2.6195	2.8347	3.0861	3.3843	3.7468	4.1917	4.7506	5.4726	6.4289	7.7288	9.4755
19	1.3687	1.4252	1.4855	1.5539	1.6292	1.7101	1.7975	1.8994	2.0099	2.1342	2.2756	2.4359	2.6188	2.8340	3.0854	3.3836	3.7462	4.1910	4.7499	5.4723	6.4283	7.7282	9.4676
20	1.3679	1.4245	1.4849	1.5531	1.6283	1.7093	1.7967	1.8986	2.0092	2.1334	2.2748	2.4351	2.6181	2.8333	3.0847	3.3830	3.7455	4.1904	4.7491	5.4713	6.4276	7.7272	9.4744

Analytical results 6000x2000mm

Volume of deformation - analytical results - 6000x2000mm plate

Thickness [mm] \ Radius [mm]	25000	24000	23000	22000	21000	20000	19000	18000	17000	16000	15000	14000	13000	12000	11000	10000	9000	8000	7000	6000	5000	4000	3000
4	1.3690	1.4257	1.4873	1.5543	1.6277	1.7082	1.7971	1.8956	2.0055	2.1287	2.2680	2.4264	2.6083	2.8191	3.0663	3.3598	3.7134	4.1467	4.6881	5.3786	6.2769	7.4505	8.8664
5	1.3686	1.4252	1.4868	1.5538	1.6272	1.7077	1.7966	1.8952	2.0050	2.1283	2.2675	2.4260	2.6079	2.8188	3.0659	3.3594	3.7131	4.1464	4.6878	5.3784	6.2766	7.4499	8.8649
6	1.3681	1.4247	1.4863	1.5534	1.6267	1.7073	1.7961	1.8947	2.0046	2.1279	2.2671	2.4256	2.6075	2.8184	3.0656	3.3591	3.7128	4.1461	4.6875	5.3781	6.2762	7.4493	8.8633
7	1.3676	1.4243	1.4858	1.5529	1.6262	1.7068	1.7957	1.8942	2.0041	2.1274	2.2667	2.4252	2.6071	2.8180	3.0652	3.3588	3.7124	4.1458	4.6872	5.3778	6.2759	7.4488	8.8618
8	1.3671	1.4238	1.4853	1.5524	1.6257	1.7063	1.7952	1.8938	2.0037	2.1270	2.2662	2.4247	2.6067	2.8176	3.0649	3.3584	3.7121	4.1456	4.6870	5.3775	6.2755	7.4482	8.8603
9	1.3666	1.4233	1.4848	1.5519	1.6253	1.7058	1.7947	1.8933	2.0032	2.1265	2.2658	2.4243	2.6063	2.8172	3.0645	3.3581	3.7118	4.1453	4.6867	5.3772	6.2752	7.4476	8.8588
10	1.3661	1.4228	1.4843	1.5514	1.6248	1.7054	1.7943	1.8929	2.0028	2.1261	2.2654	2.4239	2.6059	2.8169	3.0642	3.3578	3.7115	4.1450	4.6864	5.3769	6.2748	7.4470	8.8572
11	1.3656	1.4223	1.4839	1.5509	1.6243	1.7049	1.7938	1.8924	2.0023	2.1257	2.2650	2.4235	2.6055	2.8165	3.0638	3.3574	3.7112	4.1447	4.6861	5.3767	6.2745	7.4465	8.8557
12	1.3651	1.4218	1.4834	1.5505	1.6238	1.7044	1.7933	1.8919	2.0019	2.1252	2.2645	2.4231	2.6051	2.8161	3.0634	3.3571	3.7109	4.1444	4.6858	5.3764	6.2742	7.4459	8.8542
13	1.3646	1.4213	1.4829	1.5500	1.6234	1.7040	1.7929	1.8915	2.0014	2.1248	2.2641	2.4227	2.6047	2.8157	3.0631	3.3568	3.7106	4.1441	4.6856	5.3761	6.2738	7.4453	8.8527
14	1.3641	1.4208	1.4824	1.5495	1.6229	1.7035	1.7924	1.8910	2.0010	2.1243	2.2637	2.4223	2.6043	2.8153	3.0627	3.3564	3.7103	4.1438	4.6853	5.3758	6.2735	7.4447	8.8512
15	1.3637	1.4204	1.4819	1.5490	1.6224	1.7030	1.7919	1.8906	2.0005	2.1239	2.2633	2.4219	2.6039	2.8150	3.0624	3.3561	3.7099	4.1435	4.6850	5.3755	6.2731	7.4442	8.8497
16	1.3632	1.4199	1.4814	1.5485	1.6219	1.7025	1.7915	1.8901	2.0001	2.1235	2.2628	2.4214	2.6035	2.8146	3.0620	3.3557	3.7096	4.1432	4.6847	5.3753	6.2728	7.4436	8.8481
17	1.3627	1.4194	1.4810	1.5481	1.6215	1.7021	1.7910	1.8897	1.9996	2.1230	2.2624	2.4210	2.6031	2.8142	3.0617	3.3554	3.7093	4.1429	4.6845	5.3750	6.2725	7.4430	8.8466
18	1.3622	1.4189	1.4805	1.5476	1.6210	1.7016	1.7906	1.8892	1.9992	2.1226	2.2620	2.4206	2.6027	2.8138	3.0613	3.3551	3.7090	4.1426	4.6842	5.3747	6.2721	7.4424	8.8451
19	1.3617	1.4184	1.4800	1.5471	1.6205	1.7011	1.7901	1.8888	1.9988	2.1222	2.2616	2.4202	2.6023	2.8135	3.0609	3.3547	3.7087	4.1424	4.6839	5.3744	6.2718	7.4419	8.8436
20	1.3612	1.4179	1.4795	1.5466	1.6200	1.7007	1.7896	1.8883	1.9983	2.1217	2.2611	2.4198	2.6019	2.8131	3.0606	3.3544	3.7084	4.1421	4.6836	5.3741	6.2714	7.4413	8.8421

Validation 6000x2000mm

	Absolute deviation	Minimum deviation	Maximum deviation	Standard deviation
6000x2000mm	0.83%	0.36%	6.55%	0.55%

Volume of deformation - validation analytical results - 6000x2000mm plate

Thickness [mm] \ Radius [mm]	25000	24000	23000	22000	21000	20000	19000	18000	17000	16000	15000	14000	13000	12000	11000	10000	9000	8000	7000	6000	5000	4000	3000
4	0.91%	0.71%	0.64%	0.85%	0.88%	0.72%	0.72%	0.78%	0.60%	0.83%	0.69%	0.84%	0.84%	0.82%	0.88%	1.01%	1.12%	1.28%	1.51%	1.87%	2.50%	3.74%	6.55%
5	0.95%	0.84%	0.60%	0.73%	0.86%	0.79%	0.60%	0.82%	0.78%	0.75%	0.78%	0.83%	0.72%	0.87%	0.93%	0.97%	1.13%	1.28%	1.50%	1.86%	2.49%	3.73%	
6	0.91%	0.80%	0.57%	0.71%	0.80%	0.73%	0.62%	0.79%	0.73%	0.75%	0.77%	0.81%	0.73%	0.85%	0.91%	0.96%	1.12%	1.27%	1.49%	1.86%	2.47%	3.84%	
7	0.87%	0.76%	0.54%	0.70%	0.79%	0.71%	0.62%	0.78%	0.71%	0.75%	0.75%	0.80%	0.74%	0.83%	0.90%	0.94%	1.11%	1.27%	1.48%	1.85%	2.46%		
8	0.84%	0.73%	0.52%	0.69%	0.77%	0.70%	0.61%	0.77%	0.69%	0.74%	0.74%	0.79%	0.73%	0.83%	0.89%	0.93%	1.10%	1.25%	1.47%	1.84%			
9	0.78%	0.68%	0.48%	0.68%	0.76%	0.69%	0.59%	0.75%	0.69%	0.72%	0.74%	0.78%	0.72%	0.82%	0.88%	0.93%	1.09%	1.25%	1.47%	1.84%			
10	0.76%	0.68%	0.50%	0.65%	0.74%	0.69%	0.56%	0.73%	0.69%	0.70%	0.73%	0.76%	0.71%	0.82%	0.88%	0.93%	1.08%	1.24%	1.45%				
11	0.73%	0.65%	0.48%	0.63%	0.72%	0.67%	0.55%	0.71%	0.67%	0.69%	0.72%	0.76%	0.70%	0.81%	0.87%	0.92%	1.07%	1.23%	1.45%				
12	0.70%	0.63%	0.46%	0.61%	0.70%	0.65%	0.54%	0.70%	0.65%	0.68%	0.71%	0.74%	0.69%	0.79%	0.85%	0.90%	1.06%	1.22%					
13	0.68%	0.62%	0.47%	0.58%	0.67%	0.63%	0.52%	0.68%	0.64%	0.66%	0.70%	0.73%	0.68%	0.78%	0.85%	0.90%	1.06%						
14	0.65%	0.60%	0.45%	0.56%	0.65%	0.61%	0.50%	0.66%	0.63%	0.65%	0.68%	0.71%	0.67%	0.77%	0.84%	0.89%	1.05%						
15	0.62%	0.56%	0.43%	0.53%	0.62%	0.60%	0.49%	0.64%	0.62%	0.63%	0.67%	0.70%	0.66%	0.77%	0.83%	0.88%							
16	0.59%	0.54%	0.42%	0.51%	0.60%	0.58%	0.47%	0.62%	0.60%	0.62%	0.66%	0.69%	0.66%	0.76%	0.82%								
17	0.56%	0.52%	0.41%	0.48%	0.58%	0.56%	0.45%	0.60%	0.59%	0.60%	0.64%	0.67%	0.65%	0.75%	0.81%								
18	0.54%	0.50%	0.39%	0.46%	0.56%	0.54%	0.43%	0.58%	0.57%	0.58%	0.63%	0.66%	0.64%	0.74%									
19	0.51%	0.48%	0.37%	0.44%	0.53%	0.52%	0.41%	0.56%	0.56%	0.56%	0.62%	0.64%	0.63%										
20	0.49%	0.46%	0.36%	0.42%	0.51%	0.50%	0.39%	0.54%	0.54%	0.55%	0.60%	0.63%	0.62%										

Numerical results 6000x3000mm

Volume of deformation - numerical results - 6000x3000mm plate																						
Radius [mm]		25000	24000	23000	22000	21000	20000	19000	18000	17000	16000	15000	14000	13000	12000	11000	10000	9000	8000	7000	6000	5000	4000	3000
Thickness [mm]	4	2.0721	2.1534	2.2449	2.3509	2.4620	2.5796	2.7155	2.8672	3.0278	3.2181	3.4237	3.6702	3.9447	4.2635	4.6400	5.0907	5.6322	6.2998	7.1385	8.2203	9.6559	11.5854	14.2191
	5	2.0720	2.1551	2.2424	2.3477	2.4614	2.5812	2.7110	2.8659	3.0302	3.2161	3.4268	3.6688	3.9407	4.2637	4.6409	5.0873	5.6322	6.2991	7.1374	8.2193	9.6548	11.5993	14.2204
	6	2.0704	2.1535	2.2410	2.3463	2.4593	2.5786	2.7108	2.8644	3.0277	3.2140	3.4259	3.6675	3.9397	4.2627	4.6399	5.0860	5.6310	6.2985	7.1358	8.2190	9.6537	11.5825	14.2216
	7	2.0677	2.1506	2.2396	2.3461	2.4585	2.5776	2.7099	2.8629	3.0263	3.2147	3.4246	3.6664	3.9393	4.2613	4.6383	5.0852	5.6304	6.2974	7.1345	8.2169	9.6526	11.5832	14.2228
	8	2.0665	2.1494	2.2384	2.3448	2.4572	2.5764	2.7088	2.8618	3.0251	3.2135	3.4235	3.6654	3.9384	4.2602	4.6374	5.0844	5.6293	6.2959	7.1345	8.2166	9.6522	11.5445	14.2239
	9	2.0652	2.1484	2.2370	2.3432	2.4558	2.5754	2.7075	2.8605	3.0242	3.2123	3.4225	3.6641	3.9373	4.2592	4.6363	5.0832	5.6281	6.2951	7.1337	8.2154	9.6509	11.5979	14.2254
	10	2.0644	2.1480	2.2365	2.3414	2.4543	2.5743	2.7059	2.8592	3.0235	3.2108	3.4218	3.6628	3.9356	4.2588	4.6355	5.0823	5.6269	6.2941	7.1323	8.2140	9.6502	11.5968	14.2266
	11	2.0629	2.1466	2.2353	2.3402	2.4530	2.5731	2.7049	2.8579	3.0222	3.2097	3.4205	3.6617	3.9346	4.2575	4.6345	5.0812	5.6259	6.2926	7.1307	8.2140	9.6472	11.5981	14.2278
	12	2.0614	2.1451	2.2339	2.3391	2.4516	2.5717	2.7039	2.8567	3.0209	3.2086	3.4192	3.6606	3.9338	4.2558	4.6331	5.0800	5.6248	6.2920	7.1303	8.2070	9.6461	11.5953	14.2291
	13	2.0599	2.1437	2.2326	2.3378	2.4504	2.5706	2.7026	2.8554	3.0198	3.2073	3.4182	3.6593	3.9326	4.2548	4.6322	5.0788	5.6233	6.2910	7.1282	8.2105	9.6453	11.5860	14.2303
	14	2.0585	2.1424	2.2316	2.3364	2.4490	2.5694	2.7013	2.8541	3.0187	3.2060	3.4170	3.6583	3.9315	4.2538	4.6308	5.0777	5.6223	6.2893	7.1271	8.2094	9.6431	11.5956	14.2073
	15	2.0571	2.1411	2.2305	2.3351	2.4477	2.5682	2.7000	2.8528	3.0176	3.2047	3.4157	3.6569	3.9303	4.2528	4.6297	5.0765	5.6211	6.2882	7.1263	8.2093	9.6440	11.5892	14.2305
	16	2.0557	2.1399	2.2294	2.3337	2.4464	2.5670	2.6987	2.8515	3.0164	3.2034	3.4146	3.6556	3.9292	4.2517	4.6291	5.0756	5.6200	6.2871	7.1252	8.2084	9.6433	11.5930	14.2285
	17	2.0544	2.1386	2.2283	2.3323	2.4450	2.5658	2.6974	2.8501	3.0152	3.2022	3.4135	3.6544	3.9279	4.2506	4.6276	5.0745	5.6189	6.2859	7.1240	8.2076	9.6436	11.5911	14.2111
	18	2.0530	2.1373	2.2272	2.3310	2.4437	2.5645	2.6961	2.8488	3.0140	3.2010	3.4123	3.6532	3.9267	4.2495	4.6265	5.0736	5.6177	6.2848	7.1229	8.2052	9.6395	11.5914	14.2056
	19	2.0516	2.1360	2.2259	2.3296	2.4423	2.5632	2.6949	2.8475	3.0128	3.1997	3.4111	3.6520	3.9256	4.2484	4.6254	5.0724	5.6165	6.2837	7.1218	8.2043	9.6413	11.5852	14.1995
	20	2.0502	2.1346	2.2247	2.3283	2.4410	2.5619	2.6936	2.8462	3.0116	3.1984	3.4099	3.6507	3.9244	4.2472	4.6243	5.0713	5.6154	6.2825	7.1206	8.2029	9.6371	11.5845	14.1880

Analytical results 6000x3000mm

Volume of deformation - analytical results - 6000x3000mm plate																						
Radius [mm]		25000	24000	23000	22000	21000	20000	19000	18000	17000	16000	15000	14000	13000	12000	11000	10000	9000	8000	7000	6000	5000	4000	3000
Thickness [mm]	4	2.0539	2.1388	2.2309	2.3314	2.4412	2.5619	2.6951	2.8428	3.0075	3.1923	3.4010	3.6386	3.9113	4.2276	4.5983	5.0384	5.5688	6.2188	7.0308	8.0667	9.4138	11.1734	13.2939
	5	2.0535	2.1384	2.2305	2.3310	2.4409	2.5616	2.6948	2.8425	3.0072	3.1920	3.4007	3.6383	3.9111	4.2273	4.5981	5.0383	5.5687	6.2187	7.0307	8.0664	9.4135	11.1728	13.2924
	6	2.0531	2.1380	2.2302	2.3306	2.4405	2.5613	2.6945	2.8422	3.0069	3.1917	3.4005	3.6381	3.9109	4.2271	4.5979	5.0381	5.5685	6.2185	7.0305	8.0662	9.4132	11.1722	13.2910
	7	2.0526	2.1375	2.2298	2.3302	2.4402	2.5609	2.6941	2.8419	3.0066	3.1915	3.4002	3.6379	3.9107	4.2269	4.5977	5.0379	5.5683	6.2183	7.0303	8.0659	9.4128	11.1716	13.2895
	8	2.0522	2.1371	2.2294	2.3299	2.4398	2.5606	2.6938	2.8416	3.0063	3.1912	3.4000	3.6376	3.9104	4.2267	4.5975	5.0377	5.5681	6.2181	7.0301	8.0657	9.4125	11.1710	13.2881
	9	2.0518	2.1367	2.2290	2.3295	2.4395	2.5602	2.6935	2.8413	3.0061	3.1909	3.3997	3.6374	3.9102	4.2265	4.5973	5.0375	5.5680	6.2180	7.0299	8.0655	9.4121	11.1704	13.2866
	10	2.0514	2.1363	2.2286	2.3291	2.4391	2.5599	2.6932	2.8410	3.0058	3.1907	3.3995	3.6371	3.9100	4.2263	4.5971	5.0374	5.5678	6.2178	7.0297	8.0652	9.4118	11.1698	13.2852
	11	2.0509	2.1359	2.2282	2.3288	2.4387	2.5596	2.6929	2.8407	3.0055	3.1904	3.3992	3.6369	3.9098	4.2261	4.5969	5.0372	5.5676	6.2176	7.0295	8.0650	9.4115	11.1692	13.2838
	12	2.0505	2.1355	2.2278	2.3284	2.4384	2.5592	2.6925	2.8404	3.0052	3.1901	3.3990	3.6367	3.9096	4.2259	4.5967	5.0370	5.5674	6.2174	7.0293	8.0648	9.4111	11.1686	13.2823
	13	2.0501	2.1351	2.2274	2.3280	2.4380	2.5589	2.6922	2.8401	3.0049	3.1898	3.3987	3.6364	3.9093	4.2257	4.5965	5.0368	5.5673	6.2173	7.0291	8.0645	9.4108	11.1680	13.2809
	14	2.0497	2.1347	2.2270	2.3276	2.4377	2.5585	2.6919	2.8398	3.0046	3.1896	3.3985	3.6362	3.9091	4.2255	4.5963	5.0366	5.5671	6.2171	7.0289	8.0643	9.4104	11.1674	13.2794
	15	2.0492	2.1343	2.2266	2.3273	2.4373	2.5582	2.6916	2.8395	3.0043	3.1893	3.3982	3.6360	3.9089	4.2253	4.5962	5.0365	5.5669	6.2169	7.0287	8.0641	9.4101	11.1668	13.2780
	16	2.0488	2.1339	2.2262	2.3269	2.4370	2.5579	2.6913	2.8392	3.0041	3.1890	3.3980	3.6357	3.9087	4.2251	4.5960	5.0363	5.5667	6.2167	7.0285	8.0638	9.4098	11.1662	13.2765
	17	2.0484	2.1335	2.2259	2.3265	2.4366	2.5575	2.6909	2.8388	3.0038	3.1888	3.3977	3.6355	3.9085	4.2249	4.5958	5.0361	5.5666	6.2165	7.0283	8.0636	9.4094	11.1656	13.2751
	18	2.0480	2.1331	2.2255	2.3261	2.4363	2.5572	2.6906	2.8385	3.0035	3.1885	3.3975	3.6353	3.9082	4.2247	4.5956	5.0359	5.5664	6.2164	7.0281	8.0634	9.4091	11.1650	13.2737
	19	2.0475	2.1327	2.2251	2.3258	2.4359	2.5568	2.6903	2.8382	3.0032	3.1882	3.3972	3.6350	3.9080	4.2245	4.5954	5.0357	5.5662	6.2162	7.0280	8.0631	9.4087	11.1644	13.2722
	20	2.0471	2.1322	2.2247	2.3254	2.4355	2.5565	2.6900	2.8379	3.0029	3.1880	3.3969	3.6348	3.9078	4.2243	4.5952	5.0355	5.5660	6.2160	7.0278	8.0629	9.4084	11.1638	13.2708

Validation 6000x3000mm

	Absolute deviation	Minimum deviation	Maximum deviation	Standard deviation
6000x3000mm	0.72%	0.00%	6.51%	0.59%

Volume of deformation - validation analytical results - 6000x3000mm plate																						
Radius [mm]		25000	24000	23000	22000	21000	20000	19000	18000	17000	16000	15000	14000	13000	12000	11000	10000	9000	8000	7000	6000	5000	4000	3000
Thickness [mm]	4	0.88%	0.68%	0.62%	0.83%	0.84%	0.68%	0.75%	0.85%	0.67%	0.80%	0.66%	0.86%	0.85%	0.84%	0.90%	1.03%	1.13%	1.29%	1.51%	1.87%	2.51%	3.56%	6.51%
	5	0.89%	0.78%	0.53%	0.71%	0.83%	0.76%	0.60%	0.81%	0.76%	0.75%	0.76%	0.83%	0.75%	0.85%	0.92%	0.96%	1.13%	1.28%	1.50%	1.86%	2.50%	3.68%	
	6	0.84%	0.72%	0.48%	0.67%	0.76%	0.67%	0.60%	0.77%	0.69%	0.69%	0.74%	0.80%	0.73%	0.83%	0.90%	0.94%	1.11%	1.27%	1.48%	1.86%	2.49%	3.54%	
	7	0.73%	0.61%	0.44%	0.68%	0.74%	0.65%	0.58%	0.74%	0.65%	0.72%	0.71%	0.78%	0.73%	0.81%	0.88%	0.93%	1.10%	1.26%	1.46%	1.84%	2.48%		
	8	0.69%	0.57%	0.40%	0.63%	0.71%	0.61%	0.55%	0.71%	0.62%	0.69%	0.69%	0.76%	0.71%	0.79%	0.86%	0.92%	1.09%	1.23%	1.46%	1.84%			
	9	0.65%	0.54%	0.36%	0.59%	0.66%	0.59%	0.52%	0.67%	0.60%	0.67%	0.67%	0.73%	0.69%	0.77%	0.84%	0.90%	1.07%	1.23%	1.45%	1.83%			
	10	0.63%	0.54%	0.36%	0.52%	0.62%	0.56%	0.47%	0.64%	0.58%	0.63%	0.65%	0.70%	0.65%	0.76%	0.83%	0.88%	1.05%	1.21%	1.44%				
	11	0.58%	0.50%	0.32%	0.49%	0.58%	0.53%	0.44%	0.60%	0.55%	0.60%	0.62%	0.68%	0.63%	0.74%	0.81%	0.87%	1.04%	1.19%	1.42%				
	12	0.53%	0.45%	0.27%	0.46%	0.54%	0.49%	0.42%	0.57%	0.52%	0.58%	0.59%	0.65%	0.62%	0.70%	0.79%	0.85%	1.02%	1.18%					
	13	0.48%	0.40%	0.23%	0.42%	0.50%	0.46%	0.38%	0.54%	0.49%	0.55%	0.57%	0.63%	0.59%	0.68%	0.77%	0.83%	1.00%						
	14	0.43%	0.36%	0.21%	0.38%	0.46%	0.42%	0.35%	0.50%	0.47%	0.51%	0.54%	0.60%	0.57%	0.66%	0.74%	0.81%	0.98%						
	15	0.38%	0.32%	0.17%	0.34%	0.42%	0.39%	0.31%	0.47%	0.44%	0.48%	0.51%	0.57%	0.55%	0.65%	0.73%	0.79%							
	16	0.34%	0.28%	0.14%	0.29%	0.39%	0.36%	0.28%	0.43%	0.41%	0.45%	0.49%	0.54%	0.52%	0.63%	0.72%								
	17	0.29%	0.24%	0.11%	0.25%	0.34%	0.32%	0.24%	0.40%	0.38%	0.42%	0.46%	0.52%	0.49%	0.61%	0.69%								
	18	0.24%	0.20%	0.08%	0.21%	0.30%	0.28%	0.21%	0.36%	0.35%	0.39%	0.44%	0.49%	0.47%	0.58%									
	19	0.20%	0.15%	0.04%	0.17%	0.26%	0.25%	0.17%	0.33%	0.32%	0.36%	0.41%	0.47%	0.45%										
	20	0.15%	0.11%	0.00%	0.12%	0.22%	0.21%	0.13%	0.29%	0.29%	0.33%	0.38%	0.44%	0.42%										

Appendix C. Cavity pressure

In this appendix the results of the volumes of deformation of curved plates subjected to pressure loads are presented. Methods to calculate the results are discussed in Chapter 5. The results are presented for a 1x1m, 2x2m, 3x3m, 4x3m, 5x3m and 6x3m plate, which covers the range of plates up to the size of jumbo glass plates, bent along their longest edge. The thicknesses considered for each plate size are 8mm, 10mm and 12mm. The radius of curvature ranges from flat to 8m, which is within realistic curvatures based on a maximum cold-bending stress along the edge of the plate of σ'_{max} <63.5 N/mm^2. Furthermore, results of two case studies, as discussed in Chapter 6.4, are presented. First, the results are presented by means of P-V tables and corresponding diagrams. Thereafter, resulting load sharing pressures and effective isochoric pressures of symmetric and asymmetric IGU's are presented.

C.1. P-V tables and diagrams

Overview deviations

Overview deviations P-V diagrams		
	Relative deviation	Absolute deviation
1000x1000	-21.02%	21.02%
2000x2000	-23.56%	24.22%
3000x3000	-42.05%	42.05%
4000x3000	-45.25%	46.44%
5000x3000	-50.58%	51.15%
6000x3000	-62.20%	63.17%
Average	**-40.78%**	**41.34%**

Overview deviations per plate

1000x1000mm, relative deviations			
	t=8mm	t=10mm	t=12mm
R=8000mm	-29.99%	-33.46%	-32.31%
R=12000mm	-28.30%	-24.13%	-19.67%
R=16000mm	-21.30%	-16.09%	-12.26%
R=20000mm	-15.45%	-11.08%	-8.17%
		Average	**-21.02%**

1000x1000mm, absolute deviations			
	t=8mm	t=10mm	t=12mm
R=8000mm	29.99%	33.46%	32.31%
R=12000mm	28.30%	24.13%	19.67%
R=16000mm	21.30%	16.09%	12.26%
R=20000mm	15.45%	11.08%	8.17%
		Average	**21.02%**

2000x2000mm, relative deviations			
	t=8mm	t=10mm	t=12mm
R=8000mm	-44.03%	-40.48%	-39.31%
R=12000mm	-16.95%	-18.13%	-21.36%
R=16000mm	-7.56%	-13.59%	-20.24%
R=20000mm	-17.23%	-18.83%	-25.01%
		Average	**-23.56%**

2000x2000mm, absolute deviations			
	t=8mm	t=10mm	t=12mm
R=8000mm	44.03%	40.48%	39.31%
R=12000mm	16.95%	18.13%	21.36%
R=16000mm	8.85%	13.59%	20.24%
R=20000mm	23.83%	18.89%	25.01%
		Average	**24.22%**

3000x3000mm, relative deviations			
	t=8mm	t=10mm	t=12mm
R=8000mm	-80.49%	-75.55%	-72.74%
R=12000mm	-56.19%	-48.80%	-44.17%
R=16000mm	-33.80%	-26.80%	-23.90%
R=20000mm	-17.48%	-12.55%	-12.21%
		Average	**-42.05%**

3000x3000mm, absolute deviations			
	t=8mm	t=10mm	t=12mm
R=8000mm	80.49%	75.55%	72.74%
R=12000mm	56.19%	48.80%	44.17%
R=16000mm	33.80%	26.80%	23.90%
R=20000mm	17.48%	12.55%	12.21%
		Average	**42.05%**

4000x3000mm, relative deviations			
	t=8mm	t=10mm	t=12mm
R=8000mm	-83.92%	-80.42%	-76.91%
R=12000mm	-65.46%	-3.35%	-48.05%
R=16000mm	-44.10%	-28.80%	-17.01%
R=20000mm	-22.77%	-3.41%	-68.84%
		Average	**-45.25%**

4000x3000mm, absolute deviations			
	t=8mm	t=10mm	t=12mm
R=8000mm	83.92%	80.42%	76.91%
R=12000mm	65.46%	3.35%	48.05%
R=16000mm	44.10%	28.80%	17.01%
R=20000mm	26.22%	11.95%	71.05%
		Average	**46.44%**

5000x3000mm, relative deviations			
	t=8mm	t=10mm	t=12mm
R=8000mm	-82.51%	-79.47%	-76.83%
R=12000mm	-66.44%	-58.91%	-52.97%
R=16000mm	-50.57%	-37.08%	-26.28%
R=20000mm	-33.41%	-16.24%	-26.28%
		Average	**-50.58%**

5000x3000mm, absolute deviations			
	t=8mm	t=10mm	t=12mm
R=8000mm	82.51%	79.47%	76.83%
R=12000mm	66.44%	58.91%	52.97%
R=16000mm	50.57%	37.08%	26.28%
R=20000mm	35.69%	20.75%	26.28%
		Average	**51.15%**

6000x3000mm, relative deviations			
	t=8mm	t=10mm	t=12mm
R=8000mm	-82.66%	-94.55%	-76.98%
R=12000mm	-65.51%	-89.31%	-53.17%
R=16000mm	-49.74%	-54.06%	-26.35%
R=20000mm	-82.12%	-72.35%	0.45%
		Average	**-62.20%**

6000x3000mm, absolute deviations			
	t=8mm	t=10mm	t=12mm
R=8000mm	82.66%	94.55%	76.98%
R=12000mm	65.51%	89.31%	53.17%
R=16000mm	49.74%	54.06%	26.35%
R=20000mm	82.12%	72.35%	11.26%
		Average	**63.17%**

3600x1800mm, relative deviations			
	t=8mm	t=10mm	t=12mm
R=11500mm	-80.74%	-77.55%	-74.78%
		Average	**-77.69%**

3600x1800mm, absolute deviations			
	t=8mm	t=10mm	t=12mm
R=28000mm	80.74%	77.55%	74.78%
		Average	**77.69%**

5500x2500mm, relative deviations			
	t=14mm	t=16mm	t=18mm
R=11500mm	-63.21%	-61.49%	-60.56%
		Average	**-61.75%**

5500x2500mm, absolute deviations			
	t=14mm	t=16mm	t=18mm
R=28000mm	63.21%	61.49%	60.56%
		Average	**61.75%**

1000x1000mm, P-V Tables

Volume of deformation 1000x1000x8_R=8000				
	Numerical	Analytical		
P [kN/m2]	[mm3]	[mm3]	Rel. dev.	Abs. Dev
-1.0	-276664.4	-206665.3	-25.30%	25.30%
-0.9	-250453.9	-185998.8	-25.74%	25.74%
-0.8	-223959.0	-165332.2	-26.18%	26.18%
-0.7	-197167.0	-144665.7	-26.63%	26.63%
-0.6	-170065.0	-123999.2	-27.09%	27.09%
-0.5	-142639.5	-103332.6	-27.56%	27.56%
-0.4	-114722.7	-82666.1	-27.94%	27.94%
-0.3	-86605.7	-61999.6	-28.41%	28.41%
-0.2	-58122.9	-41333.1	-28.89%	28.89%
-0.1	-29455.4	-20666.5	-29.84%	29.84%
0.0	-	-	-	-
0.1	29455.4	20666.5	-29.84%	29.84%
0.2	59769.3	41333.1	-30.85%	30.85%
0.3	90311.3	61999.6	-31.35%	31.35%
0.4	121434.0	82666.1	-31.93%	31.93%
0.5	152915.9	103332.6	-32.43%	32.43%
0.6	184891.8	123999.2	-32.93%	32.93%
0.7	217379.2	144665.7	-33.45%	33.45%
0.8	250395.6	165332.2	-33.97%	33.97%
0.9	283958.6	185998.8	-34.50%	34.50%
1.0	318086.2	206665.3	-35.03%	35.03%
		Average	**-29.99%**	**29.99%**

Volume of deformation 1000x1000x10_R=8000				
	Numerical	Analytical		
P [kN/m2]	[mm3]	[mm3]	Rel. dev.	Abs. Dev
-1.0	-196551.8	-135718.0	-30.95%	30.95%
-0.9	-177537.4	-122146.2	-31.20%	31.20%
-0.8	-158391.5	-108574.4	-31.45%	31.45%
-0.7	-139111.2	-95002.6	-31.71%	31.71%
-0.6	-119693.5	-81430.8	-31.97%	31.97%
-0.5	-100135.5	-67859.0	-32.23%	32.23%
-0.4	-80434.3	-54287.2	-32.51%	32.51%
-0.3	-60453.0	-40715.4	-32.65%	32.65%
-0.2	-40754.1	-27143.6	-33.40%	33.40%
-0.1	-20376.5	-13571.8	-33.40%	33.40%
0.0	-	-	-	-
0.1	20378.6	13571.8	-33.40%	33.40%
0.2	40756.2	27143.6	-33.40%	33.40%
0.3	61877.5	40715.4	-34.20%	34.20%
0.4	82832.9	54287.2	-34.46%	34.46%
0.5	103958.2	67859.0	-34.72%	34.72%
0.6	125256.2	81430.8	-34.99%	34.99%
0.7	146730.0	95002.6	-35.25%	35.25%
0.8	168382.3	108574.4	-35.52%	35.52%
0.9	190216.0	122146.2	-35.79%	35.79%
1.0	212233.9	135718.0	-36.05%	36.05%
		Average	**-33.46%**	**33.46%**

Volume of deformation 1000x1000x12_R=8000				
	Numerical	Analytical		
P [kN/m2]	[mm3]	[mm3]	Rel. dev.	Abs. Dev
-1.0	-134637.0	-92898.7	-31.00%	31.00%
-0.9	-121401.6	-83608.8	-31.13%	31.13%
-0.8	-108116.6	-74318.9	-31.26%	31.26%
-0.7	-94781.6	-65029.1	-31.39%	31.39%
-0.6	-81396.3	-55739.2	-31.52%	31.52%
-0.5	-67960.0	-46449.3	-31.65%	31.65%
-0.4	-54472.4	-37159.5	-31.78%	31.78%
-0.3	-41157.3	-27869.6	-32.29%	32.29%
-0.2	-27438.2	-18579.7	-32.29%	32.29%
-0.1	-13719.1	-9289.9	-32.28%	32.28%
0.0	-	-	-	-
0.1	13719.2	9289.9	-32.29%	32.29%
0.2	27438.3	18579.7	-32.29%	32.29%
0.3	41157.4	27869.6	-32.29%	32.29%
0.4	55328.4	37159.5	-32.84%	32.84%
0.5	69297.4	46449.3	-32.97%	32.97%
0.6	83321.9	55739.2	-33.10%	33.10%
0.7	97402.3	65029.1	-33.24%	33.24%
0.8	111539.0	74318.9	-33.37%	33.37%
0.9	125732.3	83608.8	-33.50%	33.50%
1.0	139982.8	92898.7	-33.64%	33.64%
		Average	**-32.31%**	**32.31%**

Volume of deformation 1000x1000x8_R=12000				
	Numerical	Analytical		
P [kN/m2]	[mm3]	[mm3]	Rel. dev.	Abs. Dev
-1.0	-422488.7	-332005.9	-21.42%	21.42%
-0.9	-383481.8	-298805.3	-22.08%	22.08%
-0.8	-343832.4	-265604.7	-22.75%	22.75%
-0.7	-303718.3	-232404.1	-23.48%	23.48%
-0.6	-262564.4	-199203.5	-24.13%	24.13%
-0.5	-220742.7	-166003.0	-24.80%	24.80%
-0.4	-178164.6	-132802.4	-25.46%	25.46%
-0.3	-134879.5	-99601.8	-26.16%	26.16%
-0.2	-90702.6	-66401.2	-26.79%	26.79%
-0.1	-45787.6	-33200.6	-27.49%	27.49%
0.0	-	-	-	-
0.1	46697.5	33200.6	-28.90%	28.90%
0.2	94339.7	66401.2	-29.61%	29.61%
0.3	142958.7	99601.8	-30.33%	30.33%
0.4	192582.6	132802.4	-31.04%	31.04%
0.5	243235.3	166003.0	-31.75%	31.75%
0.6	294935.5	199203.5	-32.46%	32.46%
0.7	347696.5	232404.1	-33.16%	33.16%
0.8	402372.1	265604.7	-33.99%	33.99%
0.9	457805.7	298805.3	-34.73%	34.73%
1.0	514528.6	332005.9	-35.47%	35.47%
		Average	**-28.30%**	**28.30%**

Volume of deformation 1000x1000x10_R=12000				
	Numerical	Analytical		
P [kN/m2]	[mm3]	[mm3]	Rel. dev.	Abs. Dev
-1.0	-251137.8	-197208.7	-21.47%	21.47%
-0.9	-226811.9	-177487.8	-21.75%	21.75%
-0.8	-202322.2	-157766.9	-22.02%	22.02%
-0.7	-177610.1	-138046.1	-22.28%	22.28%
-0.6	-152782.7	-118325.2	-22.55%	22.55%
-0.5	-127783.0	-98604.3	-22.83%	22.83%
-0.4	-102496.9	-78883.5	-23.04%	23.04%
-0.3	-77143.1	-59162.6	-23.31%	23.31%
-0.2	-51610.0	-39441.7	-23.58%	23.58%
-0.1	-25983.2	-19720.9	-24.10%	24.10%
0.0	-	-	-	-
0.1	25988.3	19720.9	-24.12%	24.12%
0.2	52355.0	39441.7	-24.66%	24.66%
0.3	78812.4	59162.6	-24.93%	24.93%
0.4	105458.8	78883.5	-25.20%	25.20%
0.5	132295.1	98604.3	-25.47%	25.47%
0.6	159321.8	118325.2	-25.73%	25.73%
0.7	186539.4	138046.1	-26.00%	26.00%
0.8	213948.0	157766.9	-26.26%	26.26%
0.9	241547.5	177487.8	-26.52%	26.52%
1.0	269337.5	197208.7	-26.78%	26.78%
		Average	**-24.13%**	**24.13%**

Volume of deformation 1000x1000x12_R=12000				
	Numerical	Analytical		
P [kN/m2]	[mm3]	[mm3]	Rel. dev.	Abs. Dev
-1.0	-153493.5	-125032.0	-18.54%	18.54%
-0.9	-138357.7	-112528.8	-18.67%	18.67%
-0.8	-123177.6	-100025.6	-18.80%	18.80%
-0.7	-107953.1	-87522.4	-18.93%	18.93%
-0.6	-92684.0	-75019.2	-19.06%	19.06%
-0.5	-77370.3	-62516.0	-19.20%	19.20%
-0.4	-61888.5	-50012.8	-19.19%	19.19%
-0.3	-46483.8	-37509.6	-19.31%	19.31%
-0.2	-31118.8	-25006.4	-19.64%	19.64%
-0.1	-15559.3	-12503.2	-19.64%	19.64%
0.0	-	-	-	-
0.1	15559.7	12503.2	-19.64%	19.64%
0.2	31119.2	25006.4	-19.64%	19.64%
0.3	46889.7	37509.6	-20.00%	20.00%
0.4	62609.7	50012.8	-20.12%	20.12%
0.5	78374.7	62516.0	-20.23%	20.23%
0.6	94184.8	75019.2	-20.35%	20.35%
0.7	110039.8	87522.4	-20.46%	20.46%
0.8	125939.7	100025.6	-20.58%	20.58%
0.9	141884.4	112528.8	-20.69%	20.69%
1.0	157873.7	125032.0	-20.80%	20.80%
		Average	**-19.67%**	**19.67%**

Volume of deformation 1000x1000x8_R=16000				
	Numerical	Analytical		
P [kN/m2]	[mm3]	[mm3]	Rel. dev.	Abs. Dev
-1.0	-475154.3	-404676.0	-14.83%	14.83%
-0.9	-431002.7	-364208.4	-15.50%	15.50%
-0.8	-386157.3	-323740.8	-16.16%	16.16%
-0.7	-340599.8	-283273.2	-16.83%	16.83%
-0.6	-294424.0	-242805.6	-17.53%	17.53%
-0.5	-247278.2	-202338.0	-18.17%	18.17%
-0.4	-199411.7	-161870.4	-18.83%	18.83%
-0.3	-150792.0	-121402.8	-19.49%	19.49%
-0.2	-101345.2	-80935.2	-20.14%	20.14%
-0.1	-51044.6	-40467.6	-20.72%	20.72%
0.0	-	-	-	-
0.1	51889.8	40467.6	-22.01%	22.01%
0.2	104632.3	80935.2	-22.65%	22.65%
0.3	158231.0	121402.8	-23.27%	23.27%
0.4	212681.6	161870.4	-23.89%	23.89%
0.5	267972.0	202338.0	-24.49%	24.49%
0.6	324082.4	242805.6	-25.08%	25.08%
0.7	380991.7	283273.2	-25.65%	25.65%
0.8	439439.0	323740.8	-26.33%	26.33%
0.9	498303.6	364208.4	-26.91%	26.91%
1.0	557986.2	404676.0	-27.48%	27.48%
		Average	**-21.30%**	**21.30%**

Volume of deformation 1000x1000x10_R=16000				
	Numerical	Analytical		
P [kN/m2]	[mm3]	[mm3]	Rel. dev.	Abs. Dev
-1.0	-264158.9	-227645.4	-13.82%	13.82%
-0.9	-238406.3	-204880.8	-14.06%	14.06%
-0.8	-212512.0	-182116.3	-14.30%	14.30%
-0.7	-186474.9	-159351.8	-14.55%	14.55%
-0.6	-160293.9	-136587.2	-14.79%	14.79%
-0.5	-133921.3	-113822.7	-15.01%	15.01%
-0.4	-107448.9	-91058.1	-15.25%	15.25%
-0.3	-80830.6	-68293.6	-15.51%	15.51%
-0.2	-54066.2	-45529.1	-15.79%	15.79%
-0.1	-27129.2	-22764.5	-16.09%	16.09%
0.0	-	-	-	-
0.1	27129.2	22764.5	-16.09%	16.09%
0.2	54554.3	45529.1	-16.54%	16.54%
0.3	82048.3	68293.6	-16.76%	16.76%
0.4	109685.4	91058.1	-16.98%	16.98%
0.5	137464.3	113822.7	-17.20%	17.20%
0.6	165383.6	136587.2	-17.41%	17.41%
0.7	193441.5	159351.8	-17.62%	17.62%
0.8	221635.8	182116.3	-17.83%	17.83%
0.9	249971.2	204880.8	-18.04%	18.04%
1.0	278431.7	227645.4	-18.24%	18.24%
		Average	**-16.09%**	**16.09%**

Volume of deformation 1000x1000x12_R=16000				
	Numerical	Analytical		
P [kN/m2]	[mm3]	[mm3]	Rel. dev.	Abs. Dev
-1.0	-156933.4	-139214.9	-11.29%	11.29%
-0.9	-141395.9	-125293.4	-11.39%	11.39%
-0.8	-125823.4	-111371.9	-11.49%	11.49%
-0.7	-110216.2	-97450.4	-11.58%	11.58%
-0.6	-94574.3	-83528.9	-11.68%	11.68%
-0.5	-78897.7	-69607.5	-11.78%	11.78%
-0.4	-63186.7	-55686.0	-11.87%	11.87%
-0.3	-47441.2	-41764.5	-11.97%	11.97%
-0.2	-31661.5	-27843.0	-12.06%	12.06%
-0.1	-15863.1	-13921.5	-12.24%	12.24%
0.0	-	-	-	-
0.1	15863.1	13921.5	-12.24%	12.24%
0.2	31796.6	27843.0	-12.43%	12.43%
0.3	47745.0	41764.5	-12.53%	12.53%
0.4	63726.7	55686.0	-12.62%	12.62%
0.5	79850.7	69607.5	-12.83%	12.83%
0.6	95899.3	83528.9	-12.90%	12.90%
0.7	111980.4	97450.4	-12.98%	12.98%
0.8	128093.6	111371.9	-13.05%	13.05%
0.9	144238.7	125293.4	-13.13%	13.13%
1.0	160415.4	139214.9	-13.22%	13.22%
		Average	**-12.26%**	**12.26%**

Volume of deformation 1000x1000x8_R=20000				
P [kN/m2]	Numerical [mm3]	Analytical [mm3]	Rel. dev.	Abs. Dev
-1.0	-494936.6	-446715.6	-9.74%	9.74%
-0.9	-448524.8	-402044.1	-10.36%	10.36%
-0.8	-401452.9	-357372.5	-10.98%	10.98%
-0.7	-353711.4	-312700.9	-11.59%	11.59%
-0.6	-305291.8	-268029.4	-12.21%	12.21%
-0.5	-256196.3	-223357.8	-12.82%	12.82%
-0.4	-206342.4	-178686.2	-13.40%	13.40%
-0.3	-155819.5	-134014.7	-13.99%	13.99%
-0.2	-104575.9	-89343.1	-14.57%	14.57%
-0.1	-52600.8	-44671.6	-15.07%	15.07%
0.0	-	-	-	-
0.1	53293.9	44671.6	-16.18%	16.18%
0.2	107272.0	89343.1	-16.71%	16.71%
0.3	161918.8	134014.7	-17.23%	17.23%
0.4	217217.6	178686.2	-17.74%	17.74%
0.5	273145.8	223357.8	-18.23%	18.23%
0.6	329639.5	268029.4	-18.69%	18.69%
0.7	387024.2	312700.9	-19.20%	19.20%
0.8	444822.5	357372.5	-19.66%	19.66%
0.9	503005.2	402044.1	-20.07%	20.07%
1.0	561808.5	446715.6	-20.49%	20.49%
		Average	**-15.45%**	**15.45%**

Volume of deformation 1000x1000x10_R=20000				
P [kN/m2]	Numerical [mm3]	Analytical [mm3]	Rel. dev.	Abs. Dev
-1.0	-268343.9	-243804.6	-9.14%	9.14%
-0.9	-242065.1	-219424.2	-9.35%	9.35%
-0.8	-215665.2	-195043.7	-9.56%	9.56%
-0.7	-189144.0	-170663.2	-9.77%	9.77%
-0.6	-162501.6	-146282.8	-9.98%	9.98%
-0.5	-135700.2	-121902.3	-10.17%	10.17%
-0.4	-108814.8	-97521.8	-10.38%	10.38%
-0.3	-81809.4	-73141.4	-10.60%	10.60%
-0.2	-54684.8	-48760.9	-10.83%	10.83%
-0.1	-27442.1	-24380.5	-11.16%	11.16%
0.0	-	-	-	-
0.1	27477.7	24380.5	-11.27%	11.27%
0.2	55069.4	48760.9	-11.46%	11.46%
0.3	82773.4	73141.4	-11.64%	11.64%
0.4	110587.5	97521.8	-11.81%	11.81%
0.5	138514.9	121902.3	-11.99%	11.99%
0.6	166542.8	146282.8	-12.17%	12.17%
0.7	194673.8	170663.2	-12.33%	12.33%
0.8	222922.1	195043.7	-12.51%	12.51%
0.9	251251.1	219424.2	-12.67%	12.67%
1.0	279674.4	243804.6	-12.83%	12.83%
		Average	**-11.08%**	**11.08%**

Volume of deformation 1000x1000x12_R=20000				
P [kN/m2]	Numerical [mm3]	Analytical [mm3]	Rel. dev.	Abs. Dev
-1.0	-158035.3	-146338.9	-7.40%	7.40%
-0.9	-142324.0	-131705.0	-7.46%	7.46%
-0.8	-126622.0	-117071.1	-7.54%	7.54%
-0.7	-110891.6	-102437.3	-7.62%	7.62%
-0.6	-95133.0	-87803.4	-7.70%	7.70%
-0.5	-79346.3	-73169.5	-7.78%	7.78%
-0.4	-63531.8	-58535.6	-7.86%	7.86%
-0.3	-47689.7	-43901.7	-7.94%	7.94%
-0.2	-31820.2	-29267.8	-8.02%	8.02%
-0.1	-15935.9	-14633.9	-8.17%	8.17%
0.0	-	-	-	-
0.1	15935.9	14633.9	-8.17%	8.17%
0.2	31926.7	29267.8	-8.33%	8.33%
0.3	47929.2	43901.7	-8.40%	8.40%
0.4	63957.5	58535.6	-8.48%	8.48%
0.5	80011.3	73169.5	-8.55%	8.55%
0.6	96095.3	87803.4	-8.63%	8.63%
0.7	112199.0	102437.3	-8.70%	8.70%
0.8	128327.3	117071.1	-8.77%	8.77%
0.9	144479.6	131705.0	-8.84%	8.84%
1.0	160655.6	146338.9	-8.91%	8.91%
		Average	**-8.17%**	**8.17%**

1000x1000x8mm, P-V Diagram

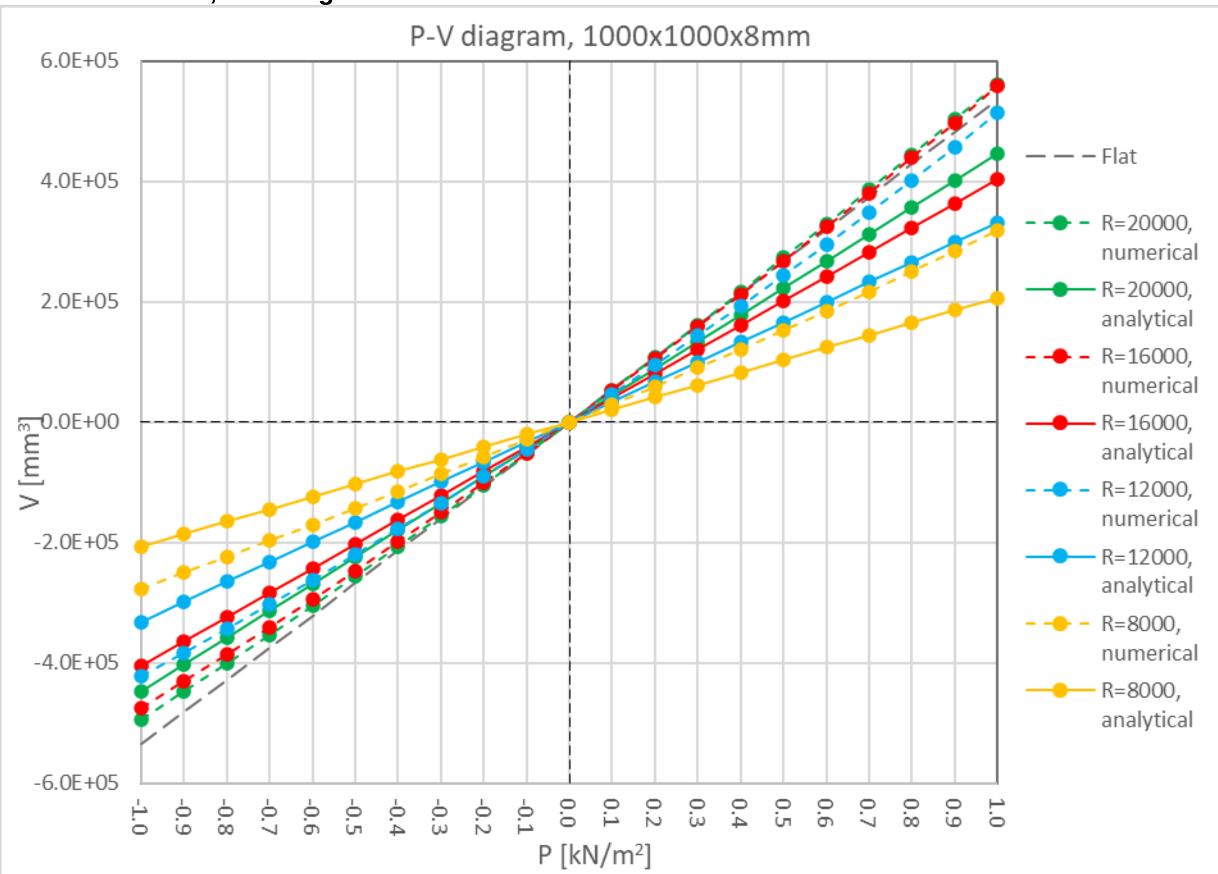

1000x1000x10mm, P-V Diagram

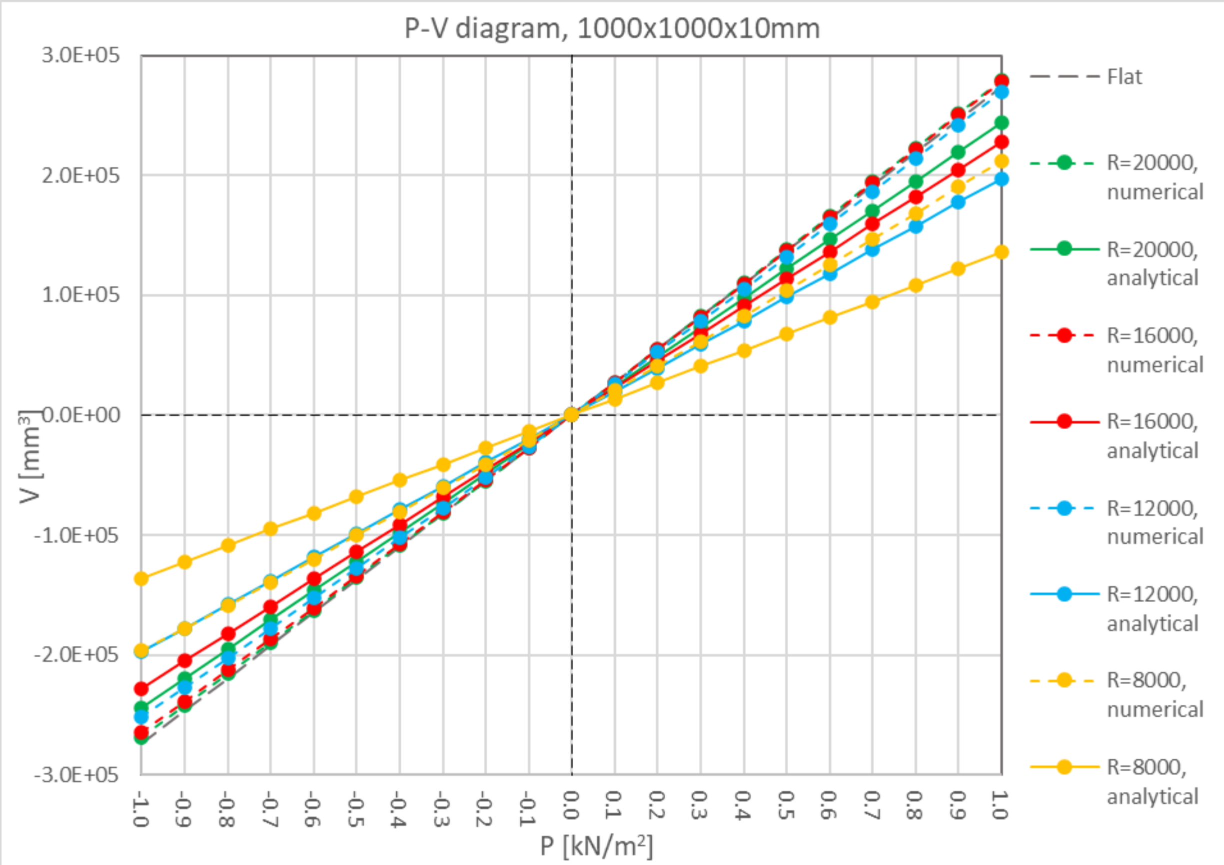

1000x1000x12mm, P-V Diagram

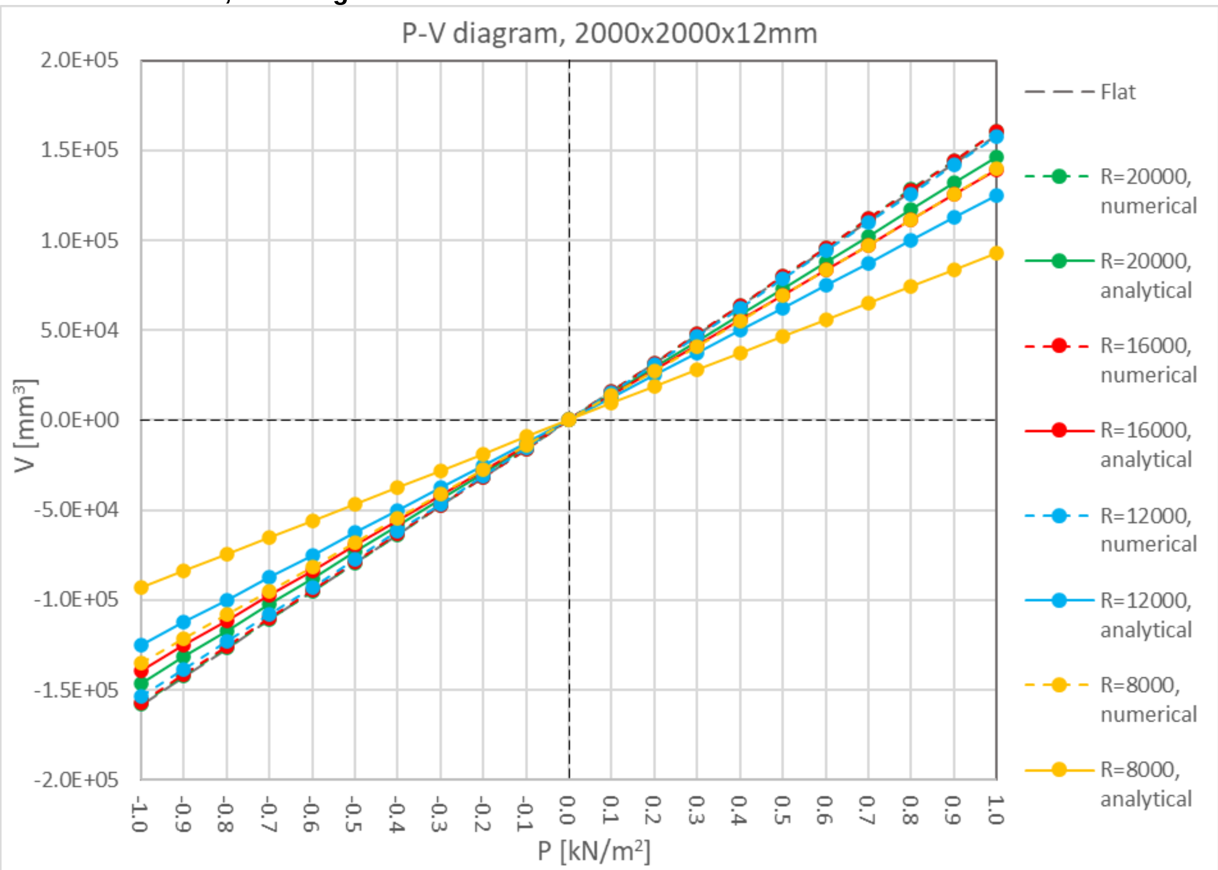

2000x2000mm, P-V Tables

Volume of deformation 2000x2000x8_R=8000				
P [kN/m2]	Numerical [mm3]	Analytical [mm3]	Rel. dev.	Abs. Dev
-1.0	-1532344.0	-884548.8	-42.27%	42.27%
-0.9	-1383036.4	-796093.9	-42.44%	42.44%
-0.8	-1232934.4	-707639.0	-42.61%	42.61%
-0.7	-1082109.1	-619184.1	-42.78%	42.78%
-0.6	-930241.5	-530729.3	-42.95%	42.95%
-0.5	-777524.1	-442274.4	-43.12%	43.12%
-0.4	-623827.7	-353819.5	-43.28%	43.28%
-0.3	-469313.2	-265364.6	-43.46%	43.46%
-0.2	-313855.2	-176909.8	-43.63%	43.63%
-0.1	-157431.0	-88454.9	-43.81%	43.81%
0.0	-	-	-	-
0.1	158458.8	88454.9	-44.18%	44.18%
0.2	317961.6	176909.8	-44.36%	44.36%
0.3	478556.7	265364.6	-44.55%	44.55%
0.4	640263.4	353819.5	-44.74%	44.74%
0.5	803143.0	442274.4	-44.93%	44.93%
0.6	967102.7	530729.3	-45.12%	45.12%
0.7	1132259.2	619184.1	-45.31%	45.31%
0.8	1298626.0	707639.0	-45.51%	45.51%
0.9	1466218.5	796093.9	-45.70%	45.70%
1.0	1635068.8	884548.8	-45.90%	45.90%
		Average	**-44.03%**	**44.03%**

Volume of deformation 2000x2000x10_R=8000				
P [kN/m2]	Numerical [mm3]	Analytical [mm3]	Rel. dev.	Abs. Dev
-1.0	-1120854.8	-678086.0	-39.50%	39.50%
-0.9	-1010333.4	-610277.4	-39.60%	39.60%
-0.8	-899441.4	-542468.8	-39.69%	39.69%
-0.7	-788248.4	-474660.2	-39.78%	39.78%
-0.6	-676705.3	-406851.6	-39.88%	39.88%
-0.5	-564829.6	-339043.0	-39.97%	39.97%
-0.4	-452578.8	-271234.4	-40.07%	40.07%
-0.3	-339970.2	-203425.8	-40.16%	40.16%
-0.2	-227007.4	-135617.2	-40.26%	40.26%
-0.1	-113847.5	-67808.6	-40.44%	40.44%
0.0	-	-	-	-
0.1	113938.3	67808.6	-40.49%	40.49%
0.2	228670.8	135617.2	-40.69%	40.69%
0.3	343516.5	203425.8	-40.78%	40.78%
0.4	458766.1	271234.4	-40.88%	40.88%
0.5	574396.0	339043.0	-40.97%	40.97%
0.6	690427.6	406851.6	-41.07%	41.07%
0.7	806866.8	474660.2	-41.17%	41.17%
0.8	923724.6	542468.8	-41.27%	41.27%
0.9	1040960.2	610277.4	-41.37%	41.37%
1.0	1158632.6	678086.0	-41.48%	41.48%
		Average	**-40.48%**	**40.48%**

Volume of deformation 2000x2000x12_R=8000				
P [kN/m2]	Numerical [mm3]	Analytical [mm3]	Rel. dev.	Abs. Dev
-1.0	-885367.3	-543529.7	-38.61%	38.61%
-0.9	-797726.1	-489176.7	-38.68%	38.68%
-0.8	-709886.3	-434823.8	-38.75%	38.75%
-0.7	-621854.4	-380470.8	-38.82%	38.82%
-0.6	-533627.9	-326117.8	-38.89%	38.89%
-0.5	-445199.9	-271764.9	-38.96%	38.96%
-0.4	-356571.7	-217411.9	-39.03%	39.03%
-0.3	-267739.5	-163058.9	-39.10%	39.10%
-0.2	-179082.9	-108705.9	-39.30%	39.30%
-0.1	-89525.2	-54353.0	-39.29%	39.29%
0.0	-	-	-	-
0.1	89541.7	54353.0	-39.30%	39.30%
0.2	179070.8	108705.9	-39.29%	39.29%
0.3	269673.6	163058.9	-39.53%	39.53%
0.4	359959.8	217411.9	-39.60%	39.60%
0.5	450458.6	271764.9	-39.67%	39.67%
0.6	541181.3	326117.8	-39.74%	39.74%
0.7	632106.8	380470.8	-39.81%	39.81%
0.8	723289.2	434823.8	-39.88%	39.88%
0.9	814657.9	489176.7	-39.95%	39.95%
1.0	906249.0	543529.7	-40.02%	40.02%
		Average	**-39.31%**	**39.31%**

Volume of deformation 2000x2000x8_R=12000				
P [kN/m2]	Numerical [mm3]	Analytical [mm3]	Rel. dev.	Abs. Dev
-1.0	-2865685.6	-2515129.9	-12.23%	12.23%
-0.9	-2592053.8	-2263616.9	-12.67%	12.67%
-0.8	-2315816.3	-2012103.9	-13.11%	13.11%
-0.7	-2036832.4	-1760590.9	-13.56%	13.56%
-0.6	-1755011.7	-1509077.9	-14.01%	14.01%
-0.5	-1470287.2	-1257564.9	-14.47%	14.47%
-0.4	-1182642.3	-1006052.0	-14.93%	14.93%
-0.3	-891848.4	-754539.0	-15.40%	15.40%
-0.2	-597871.7	-503026.0	-15.86%	15.86%
-0.1	-300651.0	-251513.0	-16.34%	16.34%
0.0	-	-	-	-
0.1	304256.3	251513.0	-17.34%	17.34%
0.2	612113.4	503026.0	-17.82%	17.82%
0.3	923763.3	754539.0	-18.32%	18.32%
0.4	1239432.6	1006052.0	-18.83%	18.83%
0.5	1559085.1	1257564.9	-19.34%	19.34%
0.6	1882963.7	1509077.9	-19.86%	19.86%
0.7	2211087.1	1760590.9	-20.37%	20.37%
0.8	2545660.3	2012103.9	-20.96%	20.96%
0.9	2883990.5	2263616.9	-21.51%	21.51%
1.0	3227525.2	2515129.9	-22.07%	22.07%
		Average	**-16.95%**	**16.95%**

Volume of deformation 2000x2000x10_R=12000				
P [kN/m2]	Numerical [mm3]	Analytical [mm3]	Rel. dev.	Abs. Dev
-1.0	-2218312.0	-1897417.0	-14.47%	14.47%
-0.9	-2004551.8	-1707675.3	-14.81%	14.81%
-0.8	-1789472.4	-1517933.6	-15.17%	15.17%
-0.7	-1572198.0	-1328191.9	-15.52%	15.52%
-0.6	-1353215.3	-1138450.2	-15.87%	15.87%
-0.5	-1132482.3	-948708.5	-16.23%	16.23%
-0.4	-909876.7	-758966.8	-16.59%	16.59%
-0.3	-685426.4	-569225.1	-16.95%	16.95%
-0.2	-458990.2	-379483.4	-17.32%	17.32%
-0.1	-230552.3	-189741.7	-17.70%	17.70%
0.0	-	-	-	-
0.1	232620.2	189741.7	-18.43%	18.43%
0.2	467425.7	379483.4	-18.81%	18.81%
0.3	704499.3	569225.1	-19.20%	19.20%
0.4	943883.5	758966.8	-19.59%	19.59%
0.5	1185726.0	948708.5	-19.99%	19.99%
0.6	1429956.1	1138450.2	-20.39%	20.39%
0.7	1676714.5	1328191.9	-20.79%	20.79%
0.8	1926059.7	1517933.6	-21.19%	21.19%
0.9	2178120.3	1707675.3	-21.60%	21.60%
1.0	2432847.0	1897417.0	-22.01%	22.01%
		Average	**-18.13%**	**18.13%**

Volume of deformation 2000x2000x12_R=12000				
P [kN/m2]	Numerical [mm3]	Analytical [mm3]	Rel. dev.	Abs. Dev
-1.0	-1825354.4	-1492106.0	-18.26%	18.26%
-0.9	-1648672.5	-1342895.4	-18.55%	18.55%
-0.8	-1470817.8	-1193684.8	-18.84%	18.84%
-0.7	-1291717.6	-1044474.2	-19.14%	19.14%
-0.6	-1111344.2	-895263.6	-19.44%	19.44%
-0.5	-929595.8	-746053.0	-19.74%	19.74%
-0.4	-746551.9	-596842.4	-20.05%	20.05%
-0.3	-562119.9	-447631.8	-20.37%	20.37%
-0.2	-376181.2	-298421.2	-20.67%	20.67%
-0.1	-189556.9	-149210.6	-21.28%	21.28%
0.0	-	-	-	-
0.1	189560.6	149210.6	-21.29%	21.29%
0.2	382316.3	298421.2	-21.94%	21.94%
0.3	575882.5	447631.8	-22.27%	22.27%
0.4	771115.5	596842.4	-22.60%	22.60%
0.5	968066.4	746053.0	-22.93%	22.93%
0.6	1166843.8	895263.6	-23.27%	23.27%
0.7	1367345.5	1044474.2	-23.61%	23.61%
0.8	1569685.5	1193684.8	-23.95%	23.95%
0.9	1773911.4	1342895.4	-24.30%	24.30%
1.0	1980140.9	1492106.0	-24.65%	24.65%
		Average	**-21.36%**	**21.36%**

Volume of deformation 2000x2000x8_R=16000				
P [kN/m2]	Numerical [mm3]	Analytical [mm3]	Rel. dev.	Abs. Dev
-1.0	-4550895.0	-4763940.8	4.68%	4.68%
-0.9	-4136352.8	-4287546.7	3.66%	3.66%
-0.8	-3714321.5	-3811152.7	2.61%	2.61%
-0.7	-3284306.8	-3334758.6	1.54%	1.54%
-0.6	-2845827.7	-2858364.5	0.44%	0.44%
-0.5	-2398241.3	-2381970.4	-0.68%	0.68%
-0.4	-1940902.3	-1905576.3	-1.82%	1.82%
-0.3	-1473579.6	-1429182.2	-3.01%	3.01%
-0.2	-994587.9	-952788.2	-4.20%	4.20%
-0.1	-503747.9	-476394.1	-5.43%	5.43%
0.0	-	-	-	-
0.1	517886.9	476394.1	-8.01%	8.01%
0.2	1051216.5	952788.2	-9.36%	9.36%
0.3	1601412.7	1429182.2	-10.75%	10.75%
0.4	2169777.3	1905576.3	-12.18%	12.18%
0.5	2762589.1	2381970.4	-13.78%	13.78%
0.6	3377927.8	2858364.5	-15.38%	15.38%
0.7	4021051.7	3334758.6	-17.07%	17.07%
0.8	4696646.1	3811152.7	-18.85%	18.85%
0.9	5410901.6	4287546.7	-20.76%	20.76%
1.0	6172908.2	4763940.8	-22.83%	22.83%
		Average	**-7.56%**	**8.85%**

Volume of deformation 2000x2000x10_R=16000				
P [kN/m2]	Numerical [mm3]	Analytical [mm3]	Rel. dev.	Abs. Dev
-1.0	-3633427.1	-3498820.1	-3.70%	3.70%
-0.9	-3299202.8	-3148938.1	-4.55%	4.55%
-0.8	-2959441.2	-2799056.1	-5.42%	5.42%
-0.7	-2613819.1	-2449174.1	-6.30%	6.30%
-0.6	-2262149.7	-2099292.1	-7.20%	7.20%
-0.5	-1903897.9	-1749410.1	-8.11%	8.11%
-0.4	-1539267.3	-1399528.0	-9.08%	9.08%
-0.3	-1166525.2	-1049646.0	-10.02%	10.02%
-0.2	-786127.8	-699764.0	-10.99%	10.99%
-0.1	-397542.9	-349882.0	-11.99%	11.99%
0.0	-	-	-	-
0.1	407241.3	349882.0	-14.08%	14.08%
0.2	824888.5	699764.0	-15.17%	15.17%
0.3	1253747.5	1049646.0	-16.28%	16.28%
0.4	1694686.7	1399528.0	-17.42%	17.42%
0.5	2148556.9	1749410.1	-18.58%	18.58%
0.6	2620432.1	2099292.1	-19.89%	19.89%
0.7	3107139.3	2449174.1	-21.18%	21.18%
0.8	3612594.0	2799056.1	-22.52%	22.52%
0.9	4139331.1	3148938.1	-23.93%	23.93%
1.0	4690480.5	3498820.1	-25.41%	25.41%
		Average	**-13.59%**	**13.59%**

Volume of deformation 2000x2000x12_R=16000				
P [kN/m2]	Numerical [mm3]	Analytical [mm3]	Rel. dev.	Abs. Dev
-1.0	-3039251.1	-2665857.2	-12.29%	12.29%
-0.9	-2757467.1	-2399271.5	-12.99%	12.99%
-0.8	-2471323.1	-2132685.7	-13.70%	13.70%
-0.7	-2180700.5	-1866100.0	-14.43%	14.43%
-0.6	-1886448.8	-1599514.3	-15.21%	15.21%
-0.5	-1585754.2	-1332928.6	-15.94%	15.94%
-0.4	-1280059.2	-1066342.9	-16.70%	16.70%
-0.3	-968927.1	-799757.2	-17.46%	17.46%
-0.2	-652124.7	-533171.4	-18.24%	18.24%
-0.1	-329268.1	-266585.7	-19.04%	19.04%
0.0	-	-	-	-
0.1	336463.9	266585.7	-20.77%	20.77%
0.2	680123.5	533171.4	-21.61%	21.61%
0.3	1031721.0	799757.2	-22.48%	22.48%
0.4	1391595.0	1066342.9	-23.37%	23.37%
0.5	1760408.0	1332928.6	-24.28%	24.28%
0.6	2138583.4	1599514.3	-25.21%	25.21%
0.7	2526736.3	1866100.0	-26.15%	26.15%
0.8	2931964.8	2132685.7	-27.26%	27.26%
0.9	3346522.0	2399271.5	-28.31%	28.31%
1.0	3775194.1	2665857.2	-29.38%	29.38%
		Average	**-20.24%**	**20.24%**

Volume of deformation 2000x2000x8_R=20000				
P [kN/m2]	Numerical [mm3]	Analytical [mm3]	Rel. dev.	Abs. Dev
-1.0	-6367246.7	-7327928.6	15.09%	15.09%
-0.9	-5822890.8	-6595135.7	13.26%	13.26%
-0.8	-5263319.9	-5862342.9	11.38%	11.38%
-0.7	-4687355.5	-5129550.0	9.43%	9.43%
-0.6	-4092854.4	-4396757.2	7.43%	7.43%
-0.5	-3478279.7	-3663964.3	5.34%	5.34%
-0.4	-2841167.0	-2931171.4	3.17%	3.17%
-0.3	-2178560.7	-2198378.6	0.91%	0.91%
-0.2	-1488003.8	-1465585.7	-1.51%	1.51%
-0.1	-762973.3	-732792.9	-3.96%	3.96%
0.0	-	-	-	-
0.1	808884.6	732792.9	-9.41%	9.41%
0.2	1672799.4	1465585.7	-12.39%	12.39%
0.3	2610022.7	2198378.6	-15.77%	15.77%
0.4	3639264.0	2931171.4	-19.46%	19.46%
0.5	4799236.4	3663964.3	-23.66%	23.66%
0.6	6167542.1	4396757.2	-28.71%	28.71%
0.7	7937826.2	5129550.0	-35.38%	35.38%
0.8	48096721.4	5862342.9	-87.81%	87.81%
0.9	49963702.1	6595135.7	-86.80%	86.80%
1.0	51678823.1	7327928.6	-85.82%	85.82%
		Average	**-17.23%**	**23.83%**

Volume of deformation 2000x2000x10_R=20000				
P [kN/m2]	Numerical [mm3]	Analytical [mm3]	Rel. dev.	Abs. Dev
-1.0	-5168331.3	-5203915.7	0.69%	0.69%
-0.9	-4720367.6	-4683524.1	-0.78%	0.78%
-0.8	-4260694.9	-4163132.5	-2.29%	2.29%
-0.7	-3788026.1	-3642741.0	-3.84%	3.84%
-0.6	-3301520.1	-3122349.4	-5.43%	5.43%
-0.5	-2799913.8	-2601957.8	-7.07%	7.07%
-0.4	-2281661.7	-2081566.3	-8.77%	8.77%
-0.3	-1746333.6	-1561174.7	-10.60%	10.60%
-0.2	-1187867.1	-1040783.1	-12.38%	12.38%
-0.1	-606990.3	-520391.6	-14.27%	14.27%
0.0	-	-	-	-
0.1	637383.5	520391.6	-18.36%	18.36%
0.2	1309743.8	1040783.1	-20.54%	20.54%
0.3	2022380.5	1561174.7	-22.81%	22.81%
0.4	2791239.7	2081566.3	-25.43%	25.43%
0.5	3621001.7	2601957.8	-28.14%	28.14%
0.6	4532982.2	3122349.4	-31.12%	31.12%
0.7	5558315.9	3642741.0	-34.46%	34.46%
0.8	6749174.7	4163132.5	-38.32%	38.32%
0.9	8219724.0	4683524.1	-43.02%	43.02%
1.0	10323681.2	5203915.7	-49.59%	49.59%
		Average	**-18.83%**	**18.89%**

Volume of deformation 2000x2000x12_R=20000				
P [kN/m2]	Numerical [mm3]	Analytical [mm3]	Rel. dev.	Abs. Dev
-1.0	-4312368.0	-3826631.6	-11.26%	11.26%
-0.9	-3931380.6	-3443968.4	-12.40%	12.40%
-0.8	-3541416.7	-3061305.3	-13.56%	13.56%
-0.7	-3141812.2	-2678642.1	-14.74%	14.74%
-0.6	-2731899.4	-2295979.0	-15.96%	15.96%
-0.5	-2310701.6	-1913315.8	-17.20%	17.20%
-0.4	-1879229.8	-1530652.6	-18.55%	18.55%
-0.3	-1431763.4	-1147989.5	-19.82%	19.82%
-0.2	-970494.4	-765326.3	-21.14%	21.14%
-0.1	-493864.6	-382663.2	-22.52%	22.52%
0.0	-	-	-	-
0.1	513190.0	382663.2	-25.43%	25.43%
0.2	1047949.3	765326.3	-26.97%	26.97%
0.3	1606371.1	1147989.5	-28.54%	28.54%
0.4	2191015.3	1530652.6	-30.14%	30.14%
0.5	2813404.0	1913315.8	-31.99%	31.99%
0.6	3469720.5	2295979.0	-33.83%	33.83%
0.7	4170305.4	2678642.1	-35.77%	35.77%
0.8	4923992.9	3061305.3	-37.83%	37.83%
0.9	5744943.3	3443968.4	-40.05%	40.05%
1.0	6650055.5	3826631.6	-42.46%	42.46%
		Average	**-25.01%**	**25.01%**

2000x2000x8mm, P-V Diagram

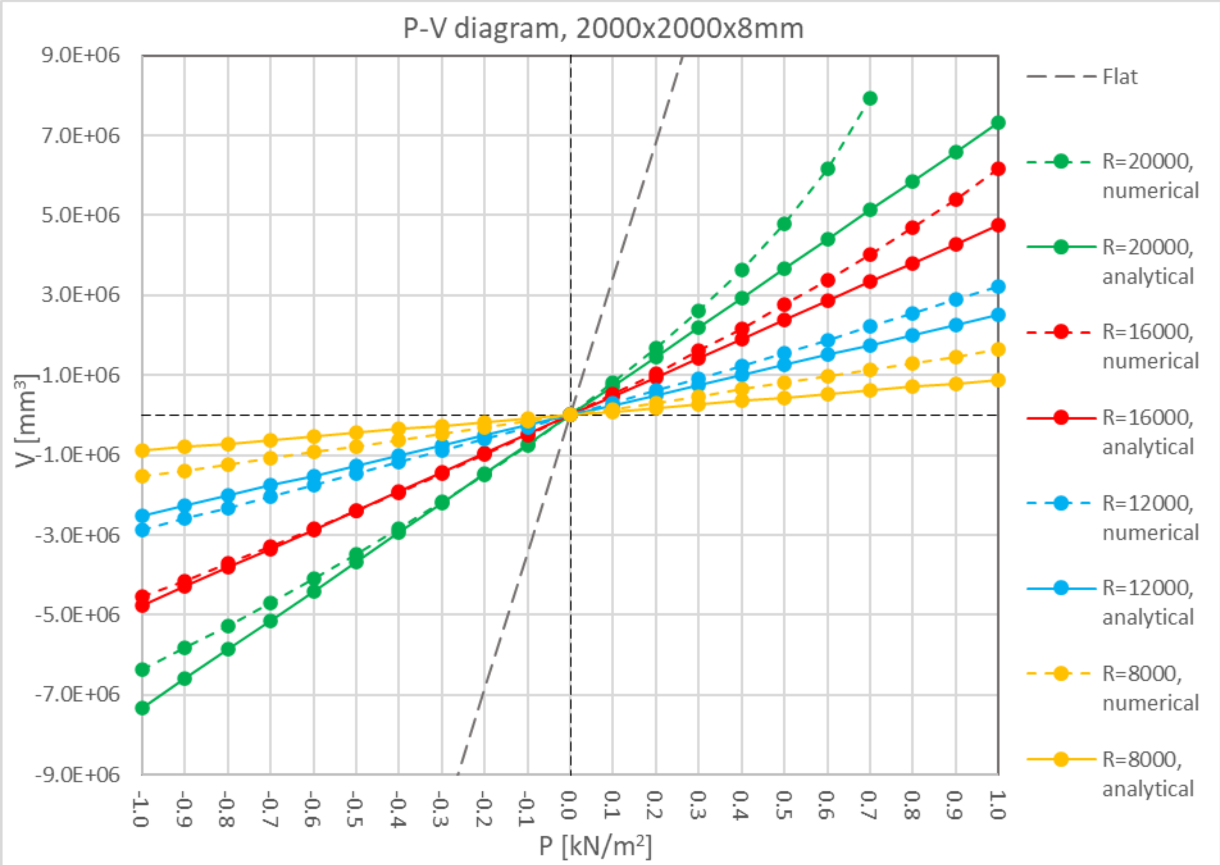

2000x2000x10mm, P-V Diagram

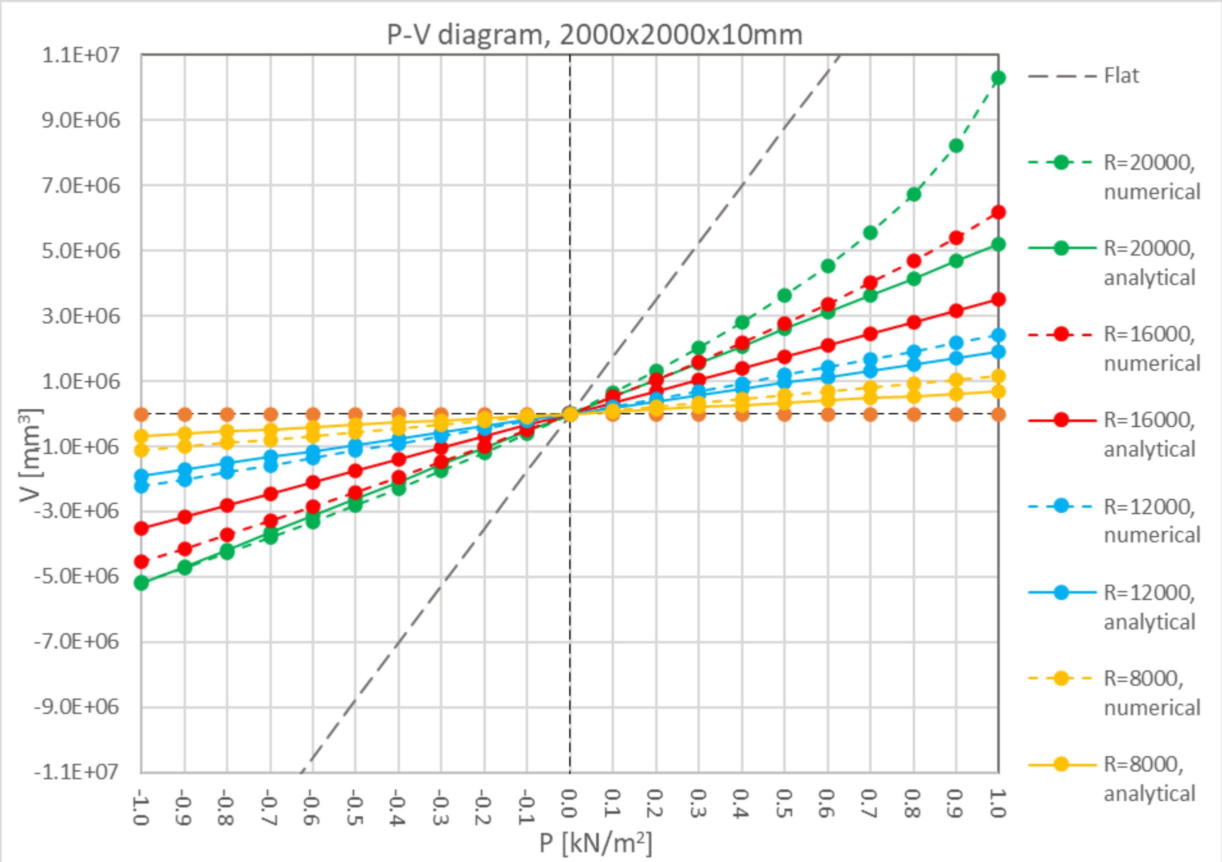

2000x2000x12mm, P-V Diagram

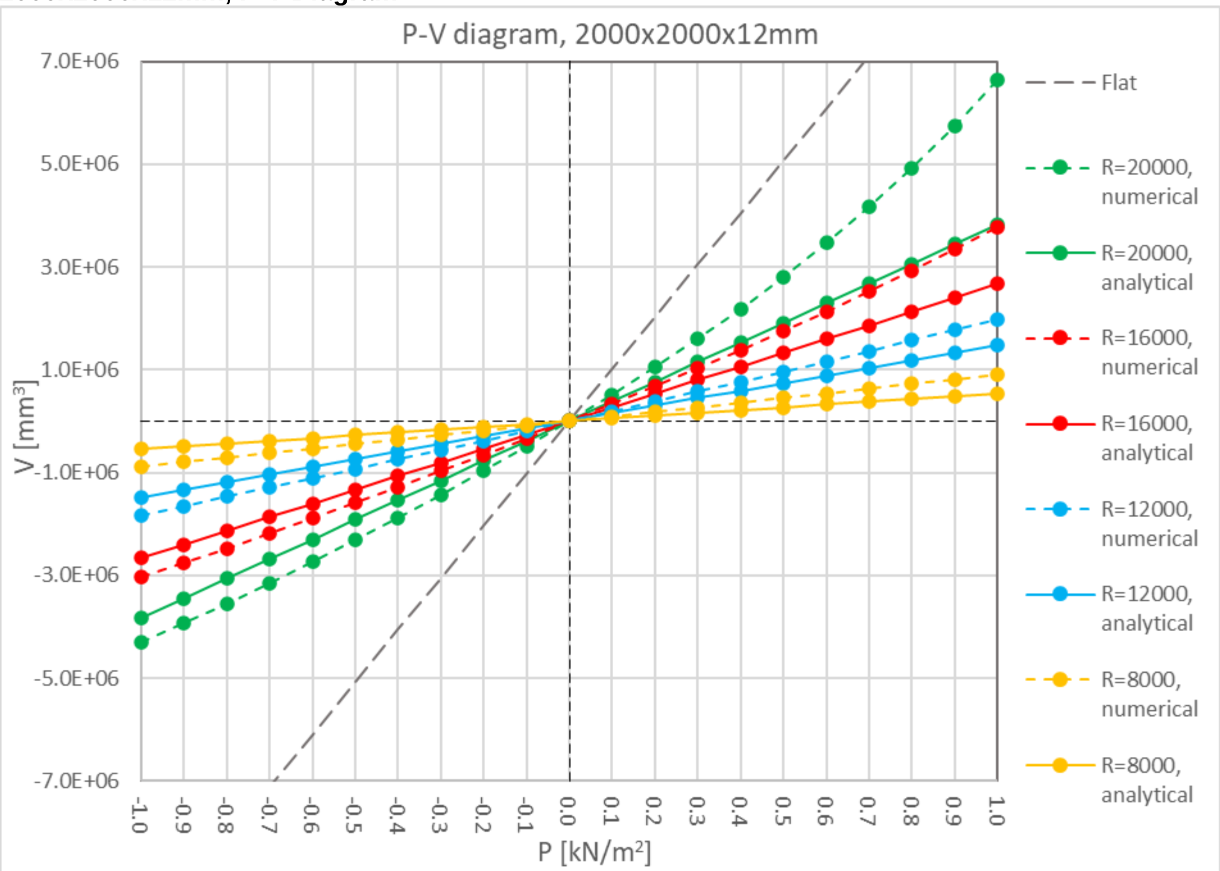

3000x3000mm, P-V Tables

Volume of deformation 3000x3000x8_R=8000				
P [kN/m2]	Numerical [mm3]	Analytical [mm3]	Rel. dev.	Abs. Dev
-1.0	-6346241.0	-1410766.8	-77.77%	77.77%
-0.9	-5772871.5	-1269690.1	-78.01%	78.01%
-0.8	-5188237.0	-1128613.4	-78.25%	78.25%
-0.7	-4591639.5	-987536.7	-78.49%	78.49%
-0.6	-3982114.2	-846460.1	-78.74%	78.74%
-0.5	-3358908.4	-705383.4	-79.00%	79.00%
-0.4	-2721041.5	-564306.7	-79.26%	79.26%
-0.3	-2067407.3	-423230.0	-79.53%	79.53%
-0.2	-1397218.9	-282153.4	-79.81%	79.81%
-0.1	-708265.4	-141076.7	-80.08%	80.08%
0.0	-	-	-	-
0.1	729192.0	141076.7	-80.65%	80.65%
0.2	1481001.7	282153.4	-80.95%	80.95%
0.3	2256298.8	423230.0	-81.24%	81.24%
0.4	3061902.8	564306.7	-81.57%	81.57%
0.5	3894830.6	705383.4	-81.89%	81.89%
0.6	4759491.2	846460.1	-82.22%	82.22%
0.7	5659180.3	987536.7	-82.55%	82.55%
0.8	6596912.1	1128613.4	-82.89%	82.89%
0.9	7576565.9	1269690.1	-83.24%	83.24%
1.0	8602506.3	1410766.8	-83.60%	83.60%
		Average	**-80.49%**	**80.49%**

Volume of deformation 3000x3000x10_R=8000				
P [kN/m2]	Numerical [mm3]	Analytical [mm3]	Rel. dev.	Abs. Dev
-1.0	-4236037.7	-1105532.4	-73.90%	73.90%
-0.9	-3829998.9	-994979.2	-74.02%	74.02%
-0.8	-3419821.6	-884425.9	-74.14%	74.14%
-0.7	-3005324.9	-773872.7	-74.25%	74.25%
-0.6	-2586413.3	-663319.4	-74.35%	74.35%
-0.5	-2163460.4	-552766.2	-74.45%	74.45%
-0.4	-1734825.5	-442213.0	-74.51%	74.51%
-0.3	-1301406.8	-331659.7	-74.52%	74.52%
-0.2	-862894.1	-221106.5	-74.38%	74.38%
-0.1	-419168.5	-110553.2	-73.63%	73.63%
0.0	-	-	-	-
0.1	485089.8	110553.2	-77.21%	77.21%
0.2	946197.5	221106.5	-76.63%	76.63%
0.3	1413329.5	331659.7	-76.53%	76.53%
0.4	1886804.7	442213.0	-76.56%	76.56%
0.5	2366718.8	552766.2	-76.64%	76.64%
0.6	2853343.7	663319.4	-76.75%	76.75%
0.7	3349840.3	773872.7	-76.90%	76.90%
0.8	3852226.5	884425.9	-77.04%	77.04%
0.9	4362585.3	994979.2	-77.19%	77.19%
1.0	4881182.1	1105532.4	-77.35%	77.35%
		Average	**-75.55%**	**75.55%**

Volume of deformation 3000x3000x12_R=8000				
P [kN/m2]	Numerical [mm3]	Analytical [mm3]	Rel. dev.	Abs. Dev
-1.0	-3078884.6	-901537.3	-70.72%	70.72%
-0.9	-2779416.2	-811383.5	-70.81%	70.81%
-0.8	-2477509.8	-721229.8	-70.89%	70.89%
-0.7	-2173928.4	-631076.1	-70.97%	70.97%
-0.6	-1868748.7	-540922.4	-71.05%	71.05%
-0.5	-1561827.7	-450768.6	-71.14%	71.14%
-0.4	-1253176.7	-360614.9	-71.22%	71.22%
-0.3	-942703.2	-270461.2	-71.31%	71.31%
-0.2	-630338.5	-180307.5	-71.40%	71.40%
-0.1	-316146.9	-90153.7	-71.48%	71.48%
0.0	-	-	-	-
0.1	318111.5	90153.7	-71.66%	71.66%
0.2	638245.2	180307.5	-71.75%	71.75%
0.3	960453.4	270461.2	-71.84%	71.84%
0.4	*7157584.4*	360614.9	-94.96%	94.96%
0.5	1611214.1	450768.6	-72.02%	72.02%
0.6	1939880.9	540922.4	-72.12%	72.12%
0.7	2270739.3	631076.1	-72.21%	72.21%
0.8	2603863.9	721229.8	-72.30%	72.30%
0.9	2939259.1	811383.5	-72.39%	72.39%
1.0	3276994.7	901537.3	-72.49%	72.49%
		Average	**-72.74%**	**72.74%**

Volume of deformation 3000x3000x8_R=12000				
P [kN/m2]	Numerical [mm3]	Analytical [mm3]	Rel. dev.	Abs. Dev
-1.0	-9488511.6	-4766160.1	-49.77%	49.77%
-0.9	-8623944.8	-4289544.1	-50.26%	50.26%
-0.8	-7744875.2	-3812928.1	-50.77%	50.77%
-0.7	-6850067.1	-3336312.1	-51.30%	51.30%
-0.6	-5938187.1	-2859696.1	-51.84%	51.84%
-0.5	-5007442.2	-2383080.1	-52.41%	52.41%
-0.4	-4056215.9	-1906464.0	-53.00%	53.00%
-0.3	-3082385.2	-1429848.0	-53.61%	53.61%
-0.2	-2083552.8	-953232.0	-54.25%	54.25%
-0.1	-1057168.6	-476616.0	-54.92%	54.92%
0.0	-	-	-	-
0.1	1091209.1	476616.0	-56.32%	56.32%
0.2	2220028.9	953232.0	-57.06%	57.06%
0.3	3393557.2	1429848.0	-57.87%	57.87%
0.4	4614859.4	1906464.0	-58.69%	58.69%
0.5	5891271.2	2383080.1	-59.55%	59.55%
0.6	7230643.7	2859696.1	-60.45%	60.45%
0.7	8641543.3	3336312.1	-61.39%	61.39%
0.8	10134737.9	3812928.1	-62.38%	62.38%
0.9	11722528.0	4289544.1	-63.41%	63.41%
1.0	13419402.8	4766160.1	-64.48%	64.48%
		Average	**-56.19%**	**56.19%**

Volume of deformation 3000x3000x10_R=12000				
P [kN/m2]	Numerical [mm3]	Analytical [mm3]	Rel. dev.	Abs. Dev
-1.0	-6794381.7	-3693781.9	-45.63%	45.63%
-0.9	-6146079.1	-3324403.7	-45.91%	45.91%
-0.8	-5491694.6	-2955025.5	-46.19%	46.19%
-0.7	-4830965.6	-2585647.3	-46.48%	46.48%
-0.6	-4163545.5	-2216269.1	-46.77%	46.77%
-0.5	-3489129.8	-1846890.9	-47.07%	47.07%
-0.4	-2807400.5	-1477512.7	-47.37%	47.37%
-0.3	-2118187.3	-1108134.6	-47.68%	47.68%
-0.2	-1420642.4	-738756.4	-48.00%	48.00%
-0.1	-714770.4	-369378.2	-48.32%	48.32%
0.0	-	-	-	-
0.1	724143.1	369378.2	-48.99%	48.99%
0.2	1458142.0	738756.4	-49.34%	49.34%
0.3	2202467.0	1108134.6	-49.69%	49.69%
0.4	2957563.0	1477512.7	-50.04%	50.04%
0.5	3723775.4	1846890.9	-50.40%	50.40%
0.6	4505348.0	2216269.1	-50.81%	50.81%
0.7	5298290.9	2585647.3	-51.20%	51.20%
0.8	6105225.9	2955025.5	-51.60%	51.60%
0.9	6927214.2	3324403.7	-52.01%	52.01%
1.0	7765056.8	3693781.9	-52.43%	52.43%
		Average	**-48.80%**	**48.80%**

Volume of deformation 3000x3000x12_R=12000				
P [kN/m2]	Numerical [mm3]	Analytical [mm3]	Rel. dev.	Abs. Dev
-1.0	-5183223.4	-2985352.1	-42.40%	42.40%
-0.9	-4678237.9	-2686816.9	-42.57%	42.57%
-0.8	-4170510.5	-2388281.7	-42.73%	42.73%
-0.7	-3659887.9	-2089746.4	-42.90%	42.90%
-0.6	-3146648.6	-1791211.2	-43.08%	43.08%
-0.5	-2630016.6	-1492676.0	-43.24%	43.24%
-0.4	-2110396.8	-1194140.8	-43.42%	43.42%
-0.3	-1587695.8	-895605.6	-43.59%	43.59%
-0.2	-1061798.3	-597070.4	-43.77%	43.77%
-0.1	-532559.0	-298535.2	-43.94%	43.94%
0.0	-	-	-	-
0.1	536094.3	298535.2	-44.31%	44.31%
0.2	1075746.8	597070.4	-44.50%	44.50%
0.3	1619121.9	895605.6	-44.69%	44.69%
0.4	2166257.2	1194140.8	-44.88%	44.88%
0.5	2717195.2	1492676.0	-45.07%	45.07%
0.6	3272067.9	1791211.2	-45.26%	45.26%
0.7	3830960.9	2089746.4	-45.45%	45.45%
0.8	4394011.4	2388281.7	-45.65%	45.65%
0.9	4961181.1	2686816.9	-45.84%	45.84%
1.0	5532573.1	2985352.1	-46.04%	46.04%
		Average	**-44.17%**	**44.17%**

Volume of deformation 3000x3000x8_R=16000				
P [kN/m2]	Numerical [mm3]	Analytical [mm3]	Rel. dev.	Abs. Dev
-1.0	-13586934.2	-10325604.8	-24.00%	24.00%
-0.9	-12341904.7	-9293044.3	-24.70%	24.70%
-0.8	-11077435.6	-8260483.8	-25.43%	25.43%
-0.7	-9791861.8	-7227923.4	-26.18%	26.18%
-0.6	-8483376.9	-6195362.9	-26.97%	26.97%
-0.5	-7149866.3	-5162802.4	-27.79%	27.79%
-0.4	-5788682.5	-4130241.9	-28.65%	28.65%
-0.3	-4397010.5	-3097681.4	-29.55%	29.55%
-0.2	-2971232.2	-2065121.0	-30.50%	30.50%
-0.1	-1507234.0	-1032560.5	-31.49%	31.49%
0.0	-	-	-	-
0.1	1556227.0	1032560.5	-33.65%	33.65%
0.2	3167540.5	2065121.0	-34.80%	34.80%
0.3	4847182.1	3097681.4	-36.09%	36.09%
0.4	6601496.7	4130241.9	-37.43%	37.43%
0.5	8445962.6	5162802.4	-38.87%	38.87%
0.6	10397231.9	6195362.9	-40.41%	40.41%
0.7	12476447.1	7227923.4	-42.07%	42.07%
0.8	14709817.7	8260483.8	-43.84%	43.84%
0.9	17129924.3	9293044.3	-45.75%	45.75%
1.0	19776129.9	10325604.8	-47.79%	47.79%
		Average	**-33.80%**	**33.80%**

Volume of deformation 3000x3000x10_R=16000				
P [kN/m2]	Numerical [mm3]	Analytical [mm3]	Rel. dev.	Abs. Dev
-1.0	-10140928.4	-7936497.7	-21.74%	21.74%
-0.9	-9178351.5	-7142848.0	-22.18%	22.18%
-0.8	-8205713.3	-6349198.2	-22.62%	22.62%
-0.7	-7222563.2	-5555548.4	-23.08%	23.08%
-0.6	-6228451.9	-4761898.6	-23.55%	23.55%
-0.5	-5222828.0	-3968248.9	-24.02%	24.02%
-0.4	-4205014.7	-3174599.1	-24.50%	24.50%
-0.3	-3174838.2	-2380949.3	-25.01%	25.01%
-0.2	-2130726.6	-1587299.5	-25.50%	25.50%
-0.1	-1072752.6	-793649.8	-26.02%	26.02%
0.0	-	-	-	-
0.1	1088493.0	793649.8	-27.09%	27.09%
0.2	2193528.9	1587299.5	-27.64%	27.64%
0.3	3316040.0	2380949.3	-28.20%	28.20%
0.4	4456756.2	3174599.1	-28.77%	28.77%
0.5	5620319.6	3968248.9	-29.39%	29.39%
0.6	6803931.7	4761898.6	-30.01%	30.01%
0.7	8010815.5	5555548.4	-30.65%	30.65%
0.8	9242833.1	6349198.2	-31.31%	31.31%
0.9	10501847.7	7142848.0	-31.98%	31.98%
1.0	11790185.2	7936497.7	-32.69%	32.69%
		Average	**-26.80%**	**26.80%**

Volume of deformation 3000x3000x12_R=16000				
P [kN/m2]	Numerical [mm3]	Analytical [mm3]	Rel. dev.	Abs. Dev
-1.0	-8020504.0	-6371315.3	-20.56%	20.56%
-0.9	-7246963.3	-5734183.8	-20.87%	20.87%
-0.8	-6467503.9	-5097052.3	-21.19%	21.19%
-0.7	-5681960.9	-4459920.7	-21.51%	21.51%
-0.6	-4890192.2	-3822789.2	-21.83%	21.83%
-0.5	-4092508.4	-3185657.7	-22.16%	22.16%
-0.4	-3287674.0	-2548526.1	-22.48%	22.48%
-0.3	-2476222.8	-1911394.6	-22.81%	22.81%
-0.2	-1657979.5	-1274263.1	-23.14%	23.14%
-0.1	-832597.5	-637131.5	-23.48%	23.48%
0.0	-	-	-	-
0.1	840328.1	637131.5	-24.18%	24.18%
0.2	1688296.7	1274263.1	-24.52%	24.52%
0.3	2544352.4	1911394.6	-24.88%	24.88%
0.4	3408577.6	2548526.1	-25.23%	25.23%
0.5	4281234.5	3185657.7	-25.59%	25.59%
0.6	5162586.9	3822789.2	-25.95%	25.95%
0.7	6052724.4	4459920.7	-26.32%	26.32%
0.8	6951871.3	5097052.3	-26.68%	26.68%
0.9	7865778.7	5734183.8	-27.10%	27.10%
1.0	8786659.4	6371315.3	-27.49%	27.49%
		Average	**-23.90%**	**23.90%**

Volume of deformation 3000x3000x8_R=20000				
P [kN/m2]	Numerical [mm3]	Analytical [mm3]	Rel. dev.	Abs. Dev
-1.0	-18488209.0	-17837963.9	-3.52%	3.52%
-0.9	-16815184.9	-16054167.5	-4.53%	4.53%
-0.8	-15111448.3	-14270371.1	-5.57%	5.57%
-0.7	-13374701.7	-12486574.7	-6.64%	6.64%
-0.6	-11602306.5	-10702778.3	-7.75%	7.75%
-0.5	-9791257.4	-8918982.0	-8.91%	8.91%
-0.4	-7937726.4	-7135185.6	-10.11%	10.11%
-0.3	-6037640.8	-5351389.2	-11.37%	11.37%
-0.2	-4085830.8	-3567592.8	-12.68%	12.68%
-0.1	-2075868.5	-1783796.4	-14.07%	14.07%
0.0	-	-	-	-
0.1	2150773.8	1783796.4	-17.06%	17.06%
0.2	4386355.0	3567592.8	-18.67%	18.67%
0.3	6730303.6	5351389.2	-20.49%	20.49%
0.4	9194583.6	7135185.6	-22.40%	22.40%
0.5	11809163.6	8918982.0	-24.47%	24.47%
0.6	14610091.2	10702778.3	-26.74%	26.74%
0.7	17646049.9	12486574.7	-29.24%	29.24%
0.8	20983128.9	14270371.1	-31.99%	31.99%
0.9	24708496.3	16054167.5	-35.03%	35.03%
1.0	28931257.6	17837963.9	-38.34%	38.34%
		Average	**-17.48%**	**17.48%**

Volume of deformation 3000x3000x10_R=20000				
P [kN/m2]	Numerical [mm3]	Analytical [mm3]	Rel. dev.	Abs. Dev
-1.0	-14185181.0	-13608025.7	-4.07%	4.07%
-0.9	-12865353.6	-12247223.1	-4.80%	4.80%
-0.8	-11526575.1	-10886420.5	-5.55%	5.55%
-0.7	-10167916.2	-9525618.0	-6.32%	6.32%
-0.6	-8788310.5	-8164815.4	-7.09%	7.09%
-0.5	-7386686.3	-6804012.8	-7.89%	7.89%
-0.4	-5961810.8	-5443210.3	-8.70%	8.70%
-0.3	-4512128.4	-4082407.7	-9.52%	9.52%
-0.2	-3036554.3	-2721605.1	-10.37%	10.37%
-0.1	-1532937.7	-1360802.6	-11.23%	11.23%
0.0	-	-	-	-
0.1	1564436.1	1360802.6	-13.02%	13.02%
0.2	3162370.1	2721605.1	-13.94%	13.94%
0.3	4795799.8	4082407.7	-14.88%	14.88%
0.4	6470662.7	5443210.3	-15.88%	15.88%
0.5	8186665.2	6804012.8	-16.89%	16.89%
0.6	9948960.2	8164815.4	-17.93%	17.93%
0.7	11761639.0	9525618.0	-19.01%	19.01%
0.8	13629853.6	10886420.5	-20.13%	20.13%
0.9	15559760.3	12247223.1	-21.29%	21.29%
1.0	17557950.9	13608025.7	-22.50%	22.50%
		Average	**-12.55%**	**12.55%**

Volume of deformation 3000x3000x12_R=20000				
P [kN/m2]	Numerical [mm3]	Analytical [mm3]	Rel. dev.	Abs. Dev
-1.0	-11483598.9	-10838776.9	-5.62%	5.62%
-0.9	-10401060.0	-9754899.2	-6.21%	6.21%
-0.8	-9305458.3	-8671021.5	-6.82%	6.82%
-0.7	-8196298.6	-7587143.8	-7.43%	7.43%
-0.6	-7072900.9	-6503266.1	-8.05%	8.05%
-0.5	-5934708.3	-5419388.4	-8.68%	8.68%
-0.4	-4781926.0	-4335510.7	-9.34%	9.34%
-0.3	-3612016.0	-3251633.1	-9.98%	9.98%
-0.2	-2425677.7	-2167755.4	-10.63%	10.63%
-0.1	-1221990.8	-1083877.7	-11.30%	11.30%
0.0	-	-	-	-
0.1	1241138.4	1083877.7	-12.67%	12.67%
0.2	2502513.4	2167755.4	-13.38%	13.38%
0.3	3784948.8	3251633.1	-14.09%	14.09%
0.4	5089551.5	4335510.7	-14.82%	14.82%
0.5	6417076.5	5419388.4	-15.55%	15.55%
0.6	7768550.6	6503266.1	-16.29%	16.29%
0.7	9154449.7	7587143.8	-17.12%	17.12%
0.8	10563871.3	8671021.5	-17.92%	17.92%
0.9	12003795.8	9754899.2	-18.73%	18.73%
1.0	13476466.3	10838776.9	-19.57%	19.57%
		Average	**-12.21%**	**12.21%**

3000x3000x8mm, P-V Diagram

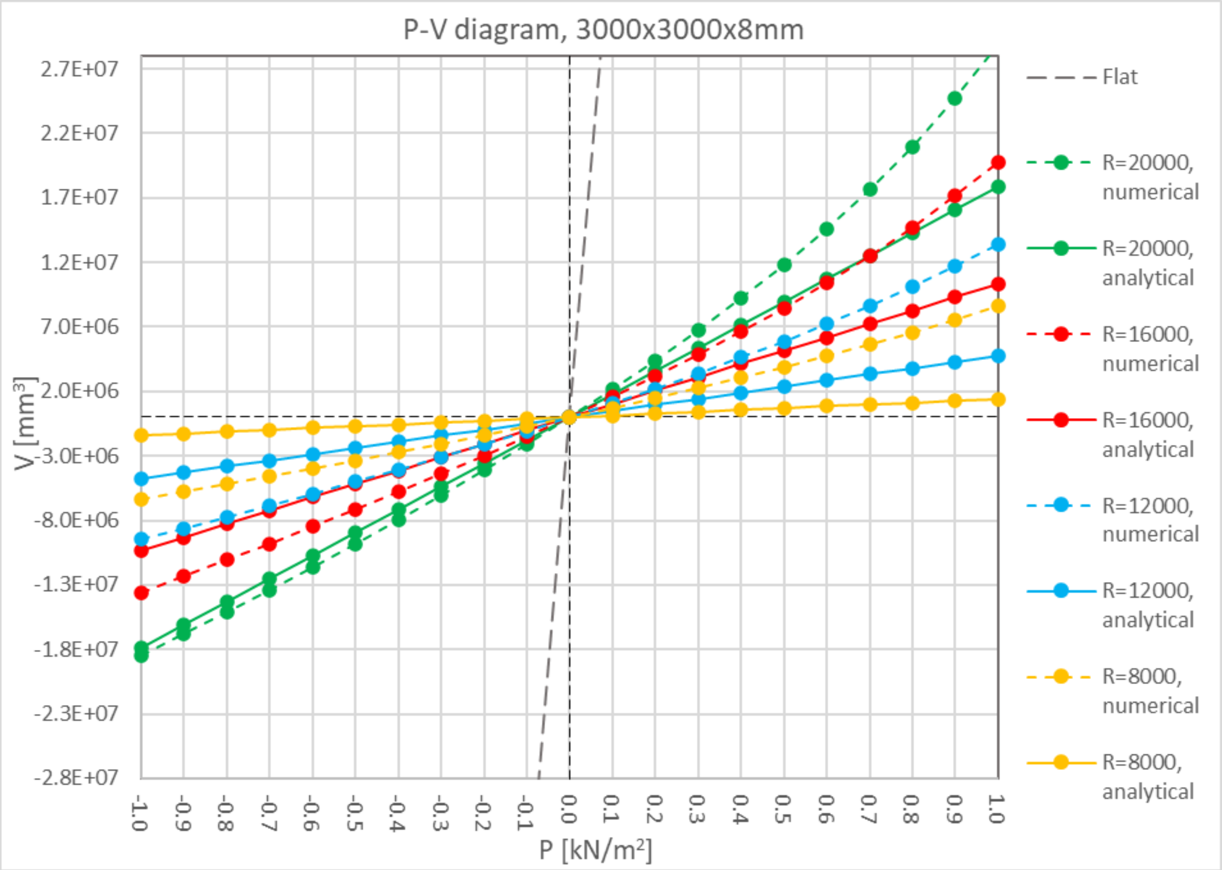

3000x3000x10mm, P-V Diagram

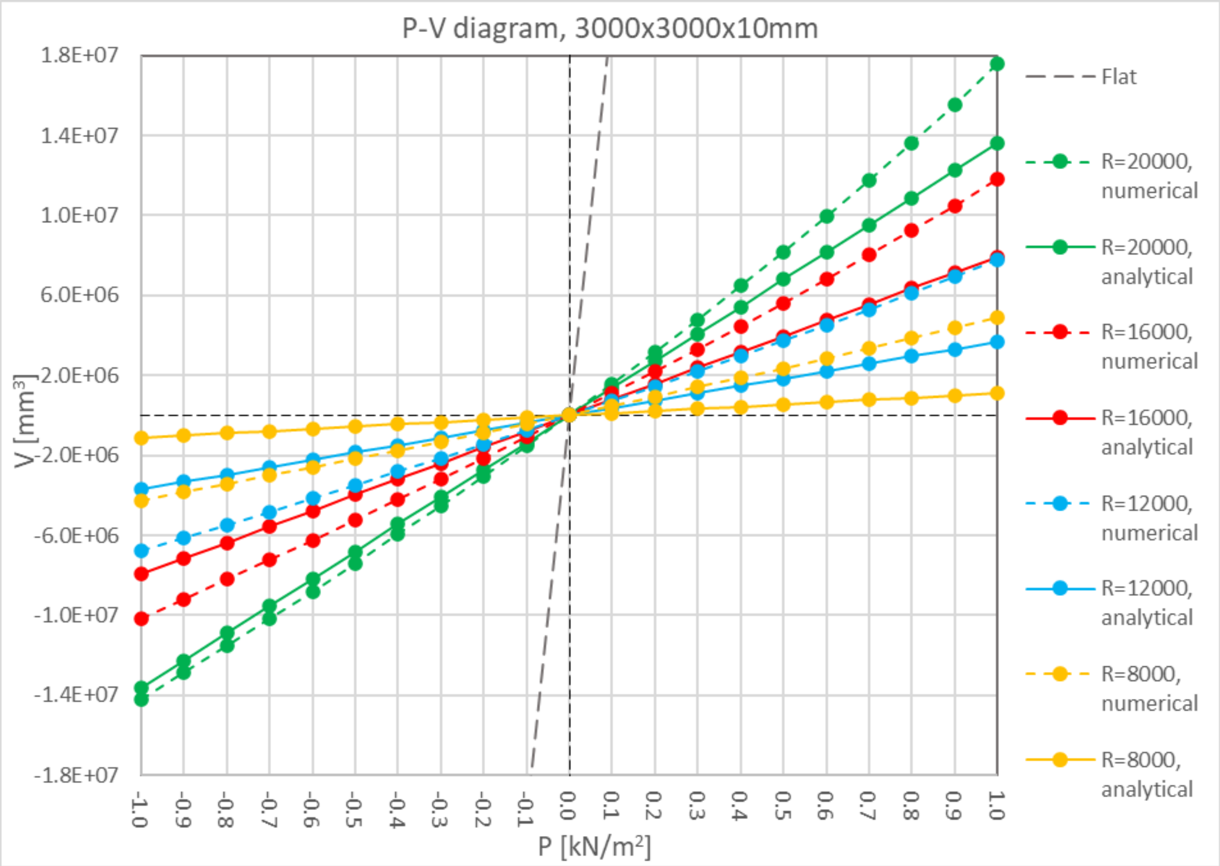

3000x3000x12mm, P-V Diagram

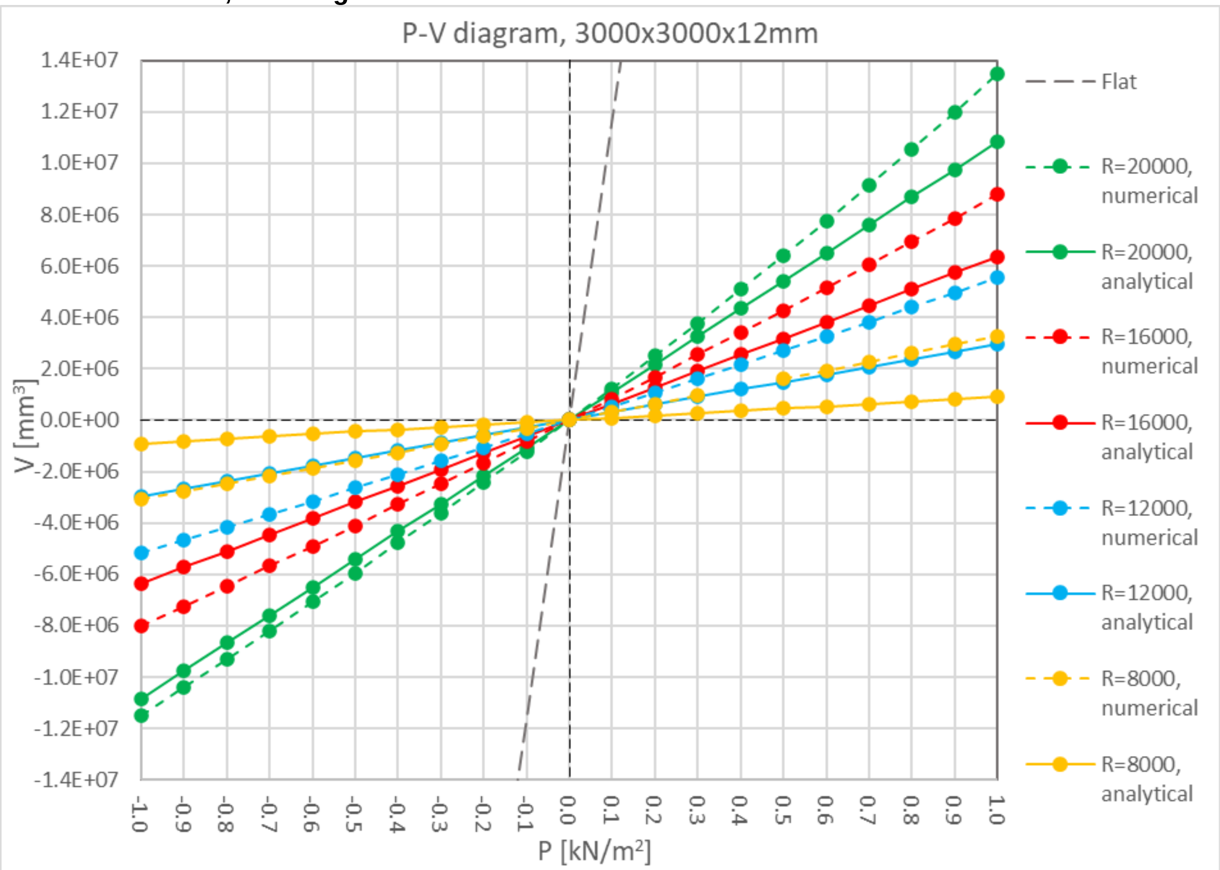

4000x3000mm, P-V Tables

Volume of deformation 4000x3000x8_R=8000				
P [kN/m2]	Numerical [mm3]	Analytical [mm3]	Rel. dev.	Abs. Dev
-1.0	-9640030.1	-1879886.0	-80.50%	80.50%
-0.9	-8804887.2	-1691897.4	-80.78%	80.78%
-0.8	-7947074.9	-1503908.8	-81.08%	81.08%
-0.7	-7064837.0	-1315920.2	-81.37%	81.37%
-0.6	-6156237.5	-1127931.6	-81.68%	81.68%
-0.5	-5219033.7	-939943.0	-81.99%	81.99%
-0.4	-4250531.9	-751954.4	-82.31%	82.31%
-0.3	-3247962.5	-563965.8	-82.64%	82.64%
-0.2	-2207906.3	-375977.2	-82.97%	82.97%
-0.1	-1126550.5	-187988.6	-83.31%	83.31%
0.0	-	-	-	-
0.1	1179326.9	187988.6	-84.06%	84.06%
0.2	2414073.9	375977.2	-84.43%	84.43%
0.3	3717292.0	563965.8	-84.83%	84.83%
0.4	5093647.7	751954.4	-85.24%	85.24%
0.5	6556812.0	939943.0	-85.66%	85.66%
0.6	8121423.0	1127931.6	-86.11%	86.11%
0.7	9806887.5	1315920.2	-86.58%	86.58%
0.8	11638862.1	1503908.8	-87.08%	87.08%
0.9	13653051.2	1691897.4	-87.61%	87.61%
1.0	15900225.5	1879886.0	-88.18%	88.18%
		Average	**-83.92%**	**83.92%**

Volume of deformation 4000x3000x10_R=8000				
P [kN/m2]	Numerical [mm3]	Analytical [mm3]	Rel. dev.	Abs. Dev
-1.0	-6763761.9	-1479681.9	-78.12%	78.12%
-0.9	-6145602.9	-1331713.7	-78.33%	78.33%
-0.8	-5516259.2	-1183745.5	-78.54%	78.54%
-0.7	-4875172.6	-1035777.3	-78.75%	78.75%
-0.6	-4221722.6	-887809.1	-78.97%	78.97%
-0.5	-3555235.5	-739840.9	-79.19%	79.19%
-0.4	-2874992.0	-591872.7	-79.41%	79.41%
-0.3	-2180791.6	-443904.6	-79.64%	79.64%
-0.2	-1470179.1	-295936.4	-79.87%	79.87%
-0.1	-743660.9	-147968.2	-80.10%	80.10%
0.0	-	-	-	-
0.1	762040.5	147968.2	-80.58%	80.58%
0.2	1543478.9	295936.4	-80.83%	80.83%
0.3	2345298.6	443904.6	-81.07%	81.07%
0.4	3168426.8	591872.7	-81.32%	81.32%
0.5	4019717.5	739840.9	-81.59%	81.59%
0.6	4894219.6	887809.1	-81.86%	81.86%
0.7	5796588.9	1035777.3	-82.13%	82.13%
0.8	6728903.0	1183745.5	-82.41%	82.41%
0.9	7693807.1	1331713.7	-82.69%	82.69%
1.0	8694586.9	1479681.9	-82.98%	82.98%
		Average	**-80.42%**	**80.42%**

Volume of deformation 4000x3000x12_R=8000				
P [kN/m2]	Numerical [mm3]	Analytical [mm3]	Rel. dev.	Abs. Dev
-1.0	-4906355.8	-1211952.4	-75.30%	75.30%
-0.9	-4442499.9	-1090757.2	-75.45%	75.45%
-0.8	-3973179.0	-969561.9	-75.60%	75.60%
-0.7	-3498159.7	-848366.7	-75.75%	75.75%
-0.6	-3017324.3	-727171.5	-75.90%	75.90%
-0.5	-2531041.9	-605976.2	-76.06%	76.06%
-0.4	-2037578.9	-484781.0	-76.21%	76.21%
-0.3	-1537836.4	-363585.7	-76.36%	76.36%
-0.2	-1031448.9	-242390.5	-76.50%	76.50%
-0.1	-518227.9	-121195.2	-76.61%	76.61%
0.0	-	-	-	-
0.1	529988.3	121195.2	-77.13%	77.13%
0.2	1065585.6	242390.5	-77.25%	77.25%
0.3	1609105.1	363585.7	-77.40%	77.40%
0.4	2160796.2	484781.0	-77.56%	77.56%
0.5	2721005.9	605976.2	-77.73%	77.73%
0.6	3289780.4	727171.5	-77.90%	77.90%
0.7	3870499.7	848366.7	-78.08%	78.08%
0.8	4459341.6	969561.9	-78.26%	78.26%
0.9	5058394.2	1090757.2	-78.44%	78.44%
1.0	5668083.7	1211952.4	-78.62%	78.62%
		Average	**-76.91%**	**76.91%**

Volume of deformation 4000x3000x8_R=12000				
P [kN/m2]	Numerical [mm3]	Analytical [mm3]	Rel. dev.	Abs. Dev
-1.0	-13780680.4	-6427058.0	-53.36%	53.36%
-0.9	-12642469.9	-5784352.2	-54.25%	54.25%
-0.8	-11467246.6	-5141646.4	-55.16%	55.16%
-0.7	-10250850.4	-4498940.6	-56.11%	56.11%
-0.6	-8988120.7	-3856234.8	-57.10%	57.10%
-0.5	-7673131.7	-3213529.0	-58.12%	58.12%
-0.4	-6298784.4	-2570823.2	-59.19%	59.19%
-0.3	-4856503.2	-1928117.4	-60.30%	60.30%
-0.2	-3335606.1	-1285411.6	-61.46%	61.46%
-0.1	-1723342.4	-642705.8	-62.71%	62.71%
0.0	-	-	-	-
0.1	1847854.7	642705.8	-65.22%	65.22%
0.2	3856488.4	1285411.6	-66.67%	66.67%
0.3	6060092.0	1928117.4	-68.18%	68.18%
0.4	8512677.5	2570823.2	-69.80%	69.80%
0.5	11290905.6	3213529.0	-71.54%	71.54%
0.6	14512106.1	3856234.8	-73.43%	73.43%
0.7	18364003.7	4498940.6	-75.50%	75.50%
0.8	23160310.8	5141646.4	-77.80%	77.80%
0.9	29410495.7	5784352.2	-80.33%	80.33%
1.0	37669743.3	6427058.0	-82.94%	82.94%
		Average	**-65.46%**	**65.46%**

Volume of deformation 4000x3000x10_R=12000				
P [kN/m2]	Numerical [mm3]	Analytical [mm3]	Rel. dev.	Abs. Dev
-1.0	-5098684.2	-5015140.1	-1.64%	1.64%
-0.9	-4587636.6	-4513626.1	-1.61%	1.61%
-0.8	-4078091.6	-4012112.1	-1.62%	1.62%
-0.7	-3569914.2	-3510598.1	-1.66%	1.66%
-0.6	-3061849.3	-3009084.1	-1.72%	1.72%
-0.5	-2554120.3	-2507570.1	-1.82%	1.82%
-0.4	-2048980.5	-2006056.0	-2.09%	2.09%
-0.3	-1537774.0	-1504542.0	-2.16%	2.16%
-0.2	-1026530.8	-1003028.0	-2.29%	2.29%
-0.1	-514370.4	-501514.0	-2.50%	2.50%
0.0	-	-	-	-
0.1	516986.1	501514.0	-2.99%	2.99%
0.2	1036324.3	1003028.0	-3.21%	3.21%
0.3	1557381.7	1504542.0	-3.39%	3.39%
0.4	2090859.6	2006056.0	-4.06%	4.06%
0.5	2624774.7	2507570.1	-4.47%	4.47%
0.6	3164972.7	3009084.1	-4.93%	4.93%
0.7	3711329.7	3510598.1	-5.41%	5.41%
0.8	4264623.0	4012112.1	-5.92%	5.92%
0.9	4825846.8	4513626.1	-6.47%	6.47%
1.0	5395627.8	5015140.1	-7.05%	7.05%
		Average	**-3.35%**	**3.35%**

Volume of deformation 4000x3000x12_R=12000				
P [kN/m2]	Numerical [mm3]	Analytical [mm3]	Rel. dev.	Abs. Dev
-1.0	-7205712.7	-4079111.4	-43.39%	43.39%
-0.9	-6533348.3	-3671200.2	-43.81%	43.81%
-0.8	-5851631.0	-3263289.1	-44.23%	44.23%
-0.7	-5160101.7	-2855378.0	-44.66%	44.66%
-0.6	-4458264.9	-2447466.8	-45.10%	45.10%
-0.5	-3745581.6	-2039555.7	-45.55%	45.55%
-0.4	-3021585.1	-1631644.5	-46.00%	46.00%
-0.3	-2285990.7	-1223733.4	-46.47%	46.47%
-0.2	-1537378.9	-815822.3	-46.93%	46.93%
-0.1	-775706.2	-407911.1	-47.41%	47.41%
0.0	-	-	-	-
0.1	789992.7	407911.1	-48.37%	48.37%
0.2	1595630.5	815822.3	-48.87%	48.87%
0.3	2417446.2	1223733.4	-49.38%	49.38%
0.4	3256186.6	1631644.5	-49.89%	49.89%
0.5	4112445.5	2039555.7	-50.41%	50.41%
0.6	4992717.6	2447466.8	-50.98%	50.98%
0.7	5890923.0	2855378.0	-51.53%	51.53%
0.8	6811297.0	3263289.1	-52.09%	52.09%
0.9	7755177.0	3671200.2	-52.66%	52.66%
1.0	8724126.1	4079111.4	-53.24%	53.24%
		Average	**-48.05%**	**48.05%**

Volume of deformation 4000x3000x8_R=16000				
P [kN/m2]	Numerical [mm3]	Analytical [mm3]	Rel. dev.	Abs. Dev
-1.0	-17744079.0	-14084498.0	-20.62%	20.62%
-0.9	-16280037.8	-12676048.2	-22.14%	22.14%
-0.8	-14772649.3	-11267598.4	-23.73%	23.73%
-0.7	-13216365.1	-9859148.6	-25.40%	25.40%
-0.6	-11603492.7	-8450698.8	-27.17%	27.17%
-0.5	-9924682.0	-7042249.0	-29.04%	29.04%
-0.4	-8168256.3	-5633799.2	-31.03%	31.03%
-0.3	-6319707.6	-4225349.4	-33.14%	33.14%
-0.2	-4359687.3	-2816899.6	-35.39%	35.39%
-0.1	-2263701.3	-1408449.8	-37.78%	37.78%
0.0	-	-	-	-
0.1	2480122.3	1408449.8	-43.21%	43.21%
0.2	5240584.4	2816899.6	-46.25%	46.25%
0.3	8373706.7	4225349.4	-49.54%	49.54%
0.4	12024913.9	5633799.2	-53.15%	53.15%
0.5	16422073.5	7042249.0	-57.12%	57.12%
0.6	21923383.4	8450698.8	-61.45%	61.45%
0.7	29012843.3	9859148.6	-66.02%	66.02%
0.8	37941114.1	11267598.4	-70.30%	70.30%
0.9	48055966.1	12676048.2	-73.62%	73.62%
1.0	58306798.4	14084498.0	-75.84%	75.84%
		Average	**-44.10%**	**44.10%**

Volume of deformation 4000x3000x10_R=16000				
P [kN/m2]	Numerical [mm3]	Analytical [mm3]	Rel. dev.	Abs. Dev
-1.0	-12914177.4	-10918226.5	-15.46%	15.46%
-0.9	-11764880.7	-9826403.8	-16.48%	16.48%
-0.8	-10591718.9	-8734581.2	-17.53%	17.53%
-0.7	-9392477.0	-7642758.5	-18.63%	18.63%
-0.6	-8164721.8	-6550935.9	-19.77%	19.77%
-0.5	-6905257.6	-5459113.2	-20.94%	20.94%
-0.4	-5611017.5	-4367290.6	-22.17%	22.17%
-0.3	-4278128.1	-3275467.9	-23.44%	23.44%
-0.2	-2902068.9	-2183645.3	-24.76%	24.76%
-0.1	-1477821.8	-1091822.6	-26.12%	26.12%
0.0	-	-	-	-
0.1	1540160.6	1091822.6	-29.11%	29.11%
0.2	3147893.3	2183645.3	-30.63%	30.63%
0.3	4837720.9	3275467.9	-32.29%	32.29%
0.4	6617243.4	4367290.6	-34.00%	34.00%
0.5	8501894.2	5459113.2	-35.79%	35.79%
0.6	10509546.4	6550935.9	-37.67%	37.67%
0.7	12660337.6	7642758.5	-39.63%	39.63%
0.8	14980053.5	8734581.2	-41.69%	41.69%
0.9	17499496.1	9826403.8	-43.85%	43.85%
1.0	20256665.4	10918226.5	-46.10%	46.10%
		Average	**-28.80%**	**28.80%**

Volume of deformation 4000x3000x12_R=16000				
P [kN/m2]	Numerical [mm3]	Analytical [mm3]	Rel. dev.	Abs. Dev
-1.0	-9720448.8	-8831631.2	-9.14%	9.14%
-0.9	-8812984.4	-7948468.1	-9.81%	9.81%
-0.8	-7893419.0	-7065305.0	-10.49%	10.49%
-0.7	-6961022.0	-6182141.9	-11.19%	11.19%
-0.6	-6015030.3	-5298978.7	-11.90%	11.90%
-0.5	-5054551.8	-4415815.6	-12.64%	12.64%
-0.4	-4078661.2	-3532652.5	-13.39%	13.39%
-0.3	-3086912.1	-2649489.4	-14.17%	14.17%
-0.2	-2076739.3	-1766326.2	-14.95%	14.95%
-0.1	-1048271.7	-883163.1	-15.75%	15.75%
0.0	-	-	-	-
0.1	1069673.4	883163.1	-17.44%	17.44%
0.2	2162097.6	1766326.2	-18.30%	18.30%
0.3	3278727.1	2649489.4	-19.19%	19.19%
0.4	4420922.3	3532652.5	-20.09%	20.09%
0.5	5595557.9	4415815.6	-21.08%	21.08%
0.6	6798798.8	5298978.7	-22.06%	22.06%
0.7	8035417.2	6182141.9	-23.06%	23.06%
0.8	9308375.1	7065305.0	-24.10%	24.10%
0.9	10620558.8	7948468.1	-25.16%	25.16%
1.0	11975913.8	8831631.2	-26.26%	26.26%
		Average	**-17.01%**	**17.01%**

Volume of deformation 4000x3000x8_R=20000				
P [kN/m2]	Numerical [mm3]	Analytical [mm3]	Rel. dev.	Abs. Dev
-1.0	-22176362.1	-24622436.0	11.03%	11.03%
-0.9	-20310659.3	-22160192.4	9.11%	9.11%
-0.8	-18400310.8	-19697948.8	7.05%	7.05%
-0.7	-16436698.5	-17235705.2	4.86%	4.86%
-0.6	-14412058.7	-14773461.6	2.51%	2.51%
-0.5	-12314682.8	-12311218.0	-0.03%	0.03%
-0.4	-10129699.8	-9848974.4	-2.77%	2.77%
-0.3	-7837572.6	-7386730.8	-5.75%	5.75%
-0.2	-5411983.7	-4924487.2	-9.01%	9.01%
-0.1	-2816608.0	-2462243.6	-12.58%	12.58%
0.0	-	-	-	-
0.1	3109844.5	2462243.6	-20.82%	20.82%
0.2	6633370.3	4924487.2	-25.76%	25.76%
0.3	10740171.7	7386730.8	-31.22%	31.22%
0.4	15716612.1	9848974.4	-37.33%	37.33%
0.5	22008943.8	12311218.0	-44.06%	44.06%
0.6	30151993.4	14773461.6	-51.00%	51.00%
0.7	40215341.8	17235705.2	-57.14%	57.14%
0.8	51289470.0	19697948.8	-61.59%	61.59%
0.9	62390266.6	22160192.4	-64.48%	64.48%
1.0	73113211.7	24622436.0	-66.32%	66.32%
		Average	-22.77%	26.22%

Volume of deformation 4000x3000x10_R=20000				
P [kN/m2]	Numerical [mm3]	Analytical [mm3]	Rel. dev.	Abs. Dev
-1.0	-16471810.1	-18968472.1	15.16%	15.16%
-0.9	-14993504.2	-17071624.9	13.86%	13.86%
-0.8	-13487892.7	-15174777.7	12.51%	12.51%
-0.7	-11952163.4	-13277930.5	11.09%	11.09%
-0.6	-10383069.4	-11381083.3	9.61%	9.61%
-0.5	-8776897.4	-9484236.1	8.06%	8.06%
-0.4	-7128999.7	-7587388.9	6.43%	6.43%
-0.3	-5434147.1	-5690541.6	4.72%	4.72%
-0.2	-3686030.0	-3793694.4	2.92%	2.92%
-0.1	-1877152.1	-1896847.2	1.05%	1.05%
0.0	-	-	-	-
0.1	1961125.9	1896847.2	-3.28%	3.28%
0.2	4012558.0	3793694.4	-5.45%	5.45%
0.3	6179289.4	5690541.6	-7.91%	7.91%
0.4	8474542.0	7587388.9	-10.47%	10.47%
0.5	10926201.4	9484236.1	-13.20%	13.20%
0.6	13565749.1	11381083.3	-16.10%	16.10%
0.7	16432267.2	13277930.5	-19.20%	19.20%
0.8	19573803.8	15174777.7	-22.47%	22.47%
0.9	23047614.2	17071624.9	-25.93%	25.93%
1.0	26917710.6	18968472.1	-29.53%	29.53%
		Average	-3.41%	11.95%

Volume of deformation 4000x3000x12_R=20000				
P [kN/m2]	Numerical [mm3]	Analytical [mm3]	Rel. dev.	Abs. Dev
-1.0	-44557236.9	-15250255.4	-65.77%	65.77%
-0.9	-44438689.6	-13725229.9	-69.11%	69.11%
-0.8	-44318669.2	-12200204.3	-72.47%	72.47%
-0.7	-44197754.5	-10675178.8	-75.85%	75.85%
-0.6	-44073831.2	-9150153.3	-79.24%	79.24%
-0.5	-43950560.5	-7625127.7	-82.65%	82.65%
-0.4	-43821860.9	-6100102.2	-86.08%	86.08%
-0.3	-5585088.2	-4575076.6	-18.08%	18.08%
-0.2	-2911129.2	-3050051.1	4.77%	4.77%
-0.1	-1300288.3	-1525025.5	17.28%	17.28%
0.0	-	-	-	-
0.1	11580963.7	1525025.5	-86.83%	86.83%
0.2	22127152.7	3050051.1	-86.22%	86.22%
0.3	32049808.1	4575076.6	-85.73%	85.73%
0.4	41506242.4	6100102.2	-85.30%	85.30%
0.5	50618491.1	7625127.7	-84.94%	84.94%
0.6	59483626.1	9150153.3	-84.62%	84.62%
0.7	68153845.3	10675178.8	-84.34%	84.34%
0.8	76705369.5	12200204.3	-84.09%	84.09%
0.9	85179872.0	13725229.9	-83.89%	83.89%
1.0	93622876.9	15250255.4	-83.71%	83.71%
		Average	-68.84%	71.05%

4000x3000x8mm, P-V Diagram

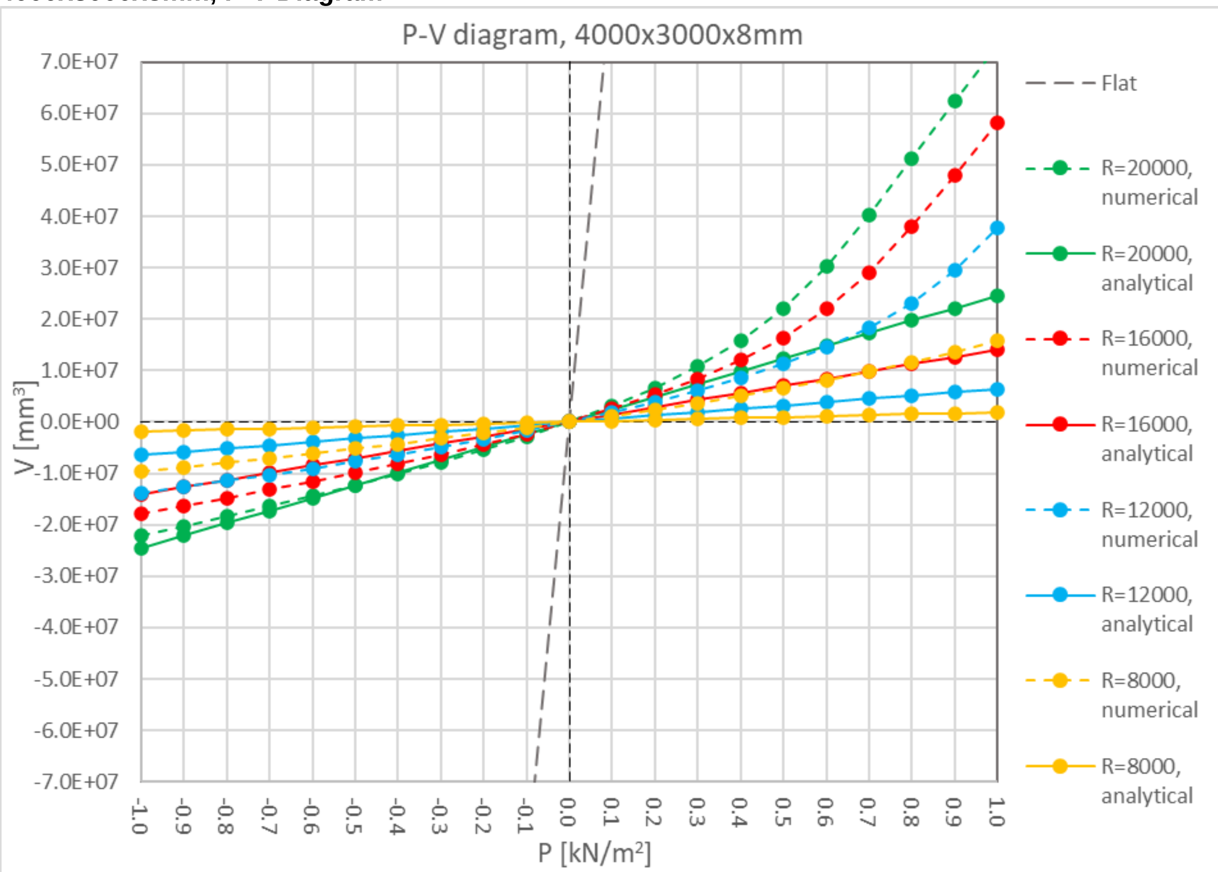

4000x3000x10mm, P-V Diagram

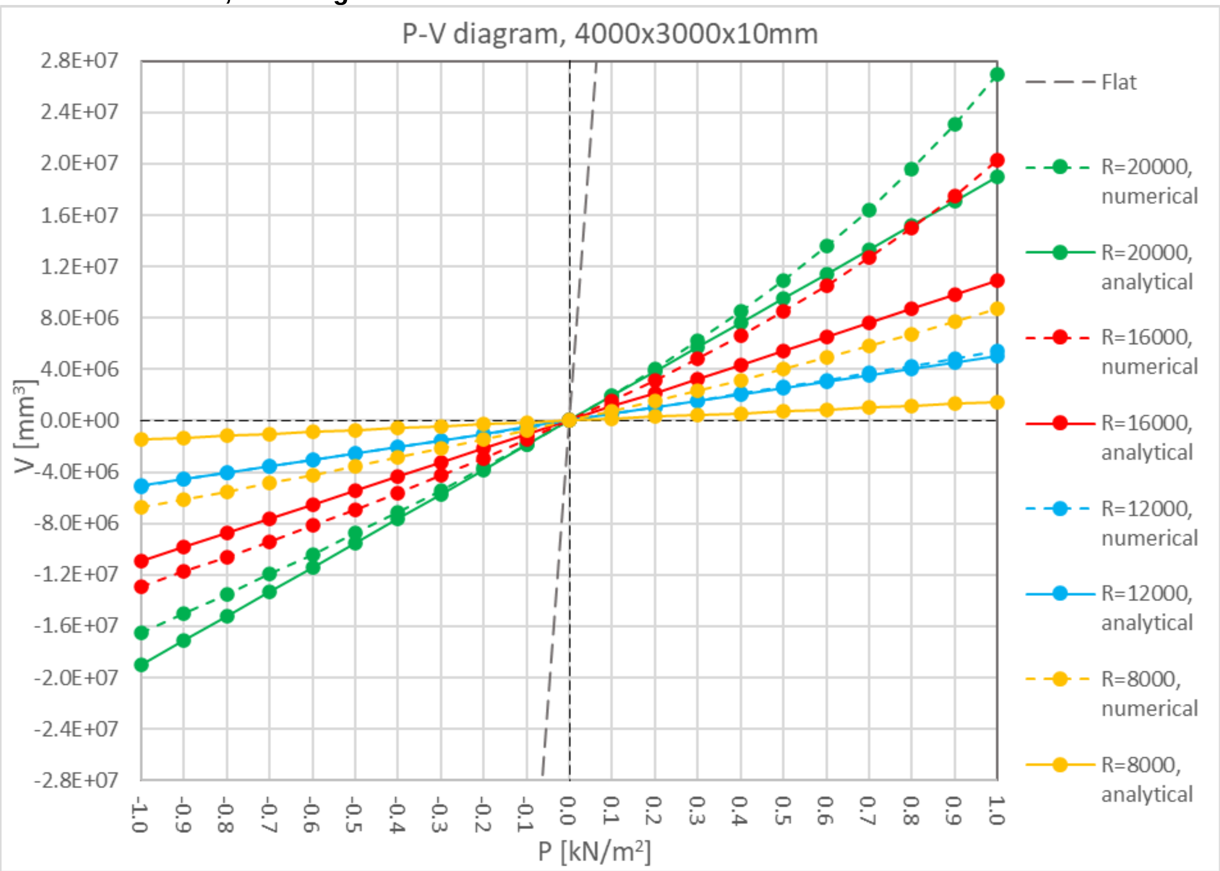

4000x3000x12mm, P-V Diagram

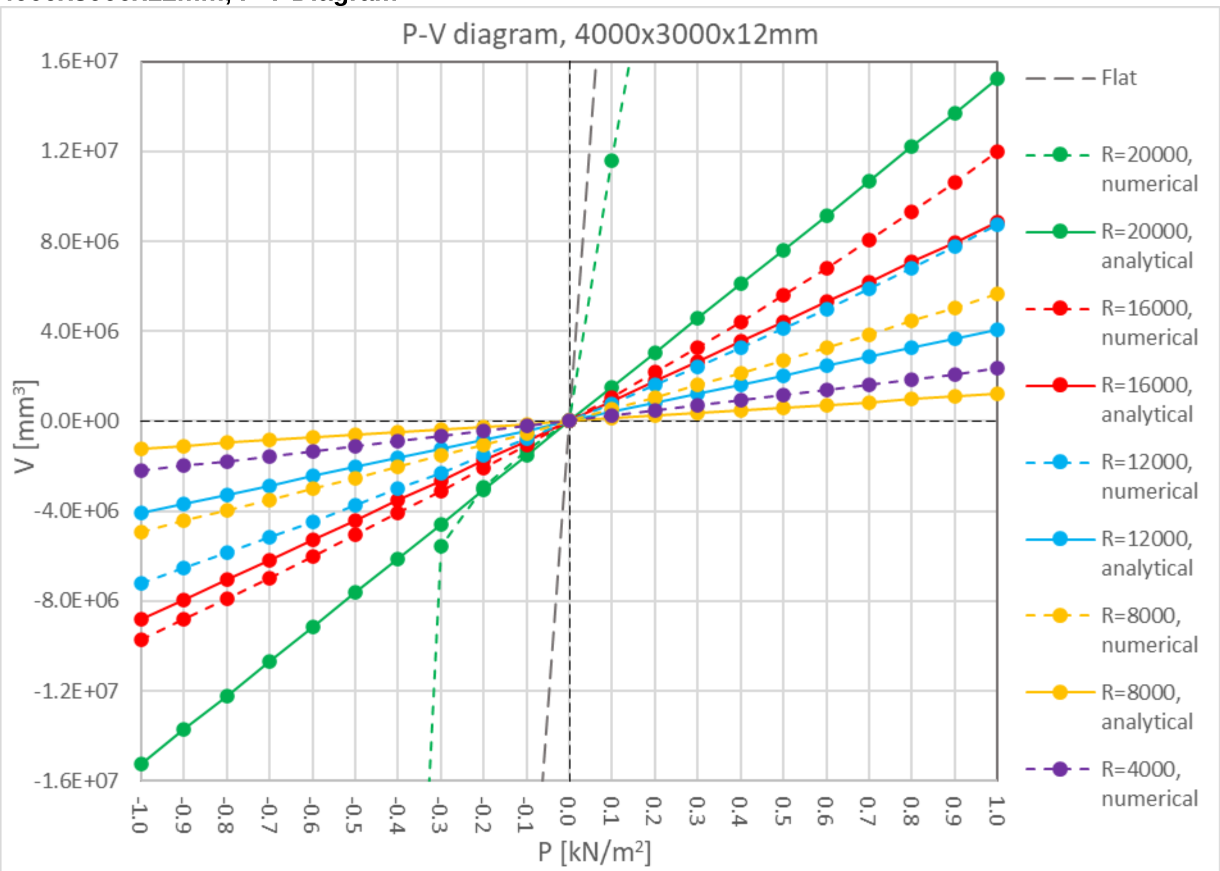

5000x3000mm, P-V Tables

Volume of deformation 5000x3000x8_R=8000				
	Numerical	Analytical		
P [kN/m2]	[mm3]	[mm3]	Rel. dev.	Abs. Dev
-1.0	-11214488.3	-2331834.4	-79.21%	79.21%
-0.9	-10224648.2	-2098651.0	-79.47%	79.47%
-0.8	-9211509.4	-1865467.5	-79.75%	79.75%
-0.7	-8173119.8	-1632284.1	-80.03%	80.03%
-0.6	-7107845.7	-1399100.7	-80.32%	80.32%
-0.5	-6013555.9	-1165917.2	-80.61%	80.61%
-0.4	-4887220.0	-932733.8	-80.91%	80.91%
-0.3	-3726175.0	-699550.3	-81.23%	81.23%
-0.2	-2526954.4	-466366.9	-81.54%	81.54%
-0.1	-1285577.4	-233183.4	-81.86%	81.86%
0.0	-	-	-	-
0.1	1343095.3	233183.4	-82.64%	82.64%
0.2	2740800.1	466366.9	-82.98%	82.98%
0.3	4208382.2	699550.3	-83.38%	83.38%
0.4	5750478.7	932733.8	-83.78%	83.78%
0.5	7380731.2	1165917.2	-84.20%	84.20%
0.6	9114137.5	1399100.7	-84.65%	84.65%
0.7	10970629.7	1632284.1	-85.12%	85.12%
0.8	12974704.7	1865467.5	-85.62%	85.62%
0.9	15161652.2	2098651.0	-86.16%	86.16%
1.0	17579211.5	2331834.4	-86.74%	86.74%
		Average	**-82.51%**	**82.51%**

Volume of deformation 5000x3000x10_R=8000				
	Numerical	Analytical		
P [kN/m2]	[mm3]	[mm3]	Rel. dev.	Abs. Dev
-1.0	-8110173.9	-1840246.8	-77.31%	77.31%
-0.9	-7361642.0	-1656222.1	-77.50%	77.50%
-0.8	-6601140.5	-1472197.4	-77.70%	77.70%
-0.7	-5827802.9	-1288172.7	-77.90%	77.90%
-0.6	-5041246.3	-1104148.1	-78.10%	78.10%
-0.5	-4240726.9	-920123.4	-78.30%	78.30%
-0.4	-3425428.5	-736098.7	-78.51%	78.51%
-0.3	-2594610.6	-552074.0	-78.72%	78.72%
-0.2	-1747243.0	-368049.4	-78.94%	78.94%
-0.1	-882577.2	-184024.7	-79.15%	79.15%
0.0	-	-	-	-
0.1	903395.2	184024.7	-79.63%	79.63%
0.2	1826964.9	368049.4	-79.85%	79.85%
0.3	2772388.2	552074.0	-80.09%	80.09%
0.4	3743294.0	736098.7	-80.34%	80.34%
0.5	4738996.7	920123.4	-80.58%	80.58%
0.6	5762522.4	1104148.1	-80.84%	80.84%
0.7	6815590.9	1288172.7	-81.10%	81.10%
0.8	7901172.0	1472197.4	-81.37%	81.37%
0.9	9022238.3	1656222.1	-81.64%	81.64%
1.0	10181785.5	1840246.8	-81.93%	81.93%
		Average	**-79.47%**	**79.47%**

Volume of deformation 5000x3000x12_R=8000				
	Numerical	Analytical		
P [kN/m2]	[mm3]	[mm3]	Rel. dev.	Abs. Dev
-1.0	-6125120.3	-1511258.7	-75.33%	75.33%
-0.9	-5546102.8	-1360132.9	-75.48%	75.48%
-0.8	-4960521.6	-1209007.0	-75.63%	75.63%
-0.7	-4368157.1	-1057881.1	-75.78%	75.78%
-0.6	-3768819.3	-906755.2	-75.94%	75.94%
-0.5	-3162149.4	-755629.4	-76.10%	76.10%
-0.4	-2548444.6	-604503.5	-76.28%	76.28%
-0.3	-1926473.7	-453377.6	-76.47%	76.47%
-0.2	-1296580.6	-302251.7	-76.69%	76.69%
-0.1	-658346.9	-151125.9	-77.04%	77.04%
0.0	-	-	-	-
0.1	644065.6	151125.9	-76.54%	76.54%
0.2	1309007.5	302251.7	-76.91%	76.91%
0.3	1983712.7	453377.6	-77.14%	77.14%
0.4	2667809.0	604503.5	-77.34%	77.34%
0.5	3362501.1	755629.4	-77.53%	77.53%
0.6	4067519.4	906755.2	-77.71%	77.71%
0.7	4787068.9	1057881.1	-77.90%	77.90%
0.8	5516771.5	1209007.0	-78.08%	78.08%
0.9	6258487.6	1360132.9	-78.27%	78.27%
1.0	7012883.8	1511258.7	-78.45%	78.45%
		Average	**-76.83%**	**76.83%**

Volume of deformation 5000x3000x8_R=12000				
	Numerical	Analytical		
P [kN/m2]	[mm3]	[mm3]	Rel. dev.	Abs. Dev
-1.0	-17386736.0	-8014612.2	-53.90%	53.90%
-0.9	-15939715.8	-7213151.0	-54.75%	54.75%
-0.8	-14447804.1	-6411689.8	-55.62%	55.62%
-0.7	-12904252.1	-5610228.6	-56.52%	56.52%
-0.6	-11303793.6	-4808767.3	-57.46%	57.46%
-0.5	-9640441.2	-4007306.1	-58.43%	58.43%
-0.4	-7904812.2	-3205844.9	-59.44%	59.44%
-0.3	-6088074.0	-2404383.7	-60.51%	60.51%
-0.2	-4176703.7	-1602922.4	-61.62%	61.62%
-0.1	-2155340.0	-801461.2	-62.82%	62.82%
0.0	-	-	-	-
0.1	2308492.7	801461.2	-65.28%	65.28%
0.2	4815449.7	1602922.4	-66.71%	66.71%
0.3	7569413.7	2404383.7	-68.24%	68.24%
0.4	10650486.6	3205844.9	-69.90%	69.90%
0.5	14184636.9	4007306.1	-71.75%	71.75%
0.6	18394769.4	4808767.3	-73.86%	73.86%
0.7	23735769.2	5610228.6	-76.36%	76.36%
0.8	31400135.6	6411689.8	-79.58%	79.58%
0.9	46773203.1	7213151.0	-84.58%	84.58%
1.0	94530850.5	8014612.2	-91.52%	91.52%
		Average	**-66.44%**	**66.44%**

Volume of deformation 5000x3000x10_R=12000				
	Numerical	Analytical		
P [kN/m2]	[mm3]	[mm3]	Rel. dev.	Abs. Dev
-1.0	-12833294.8	-6276270.1	-51.09%	51.09%
-0.9	-11703131.2	-5648643.1	-51.73%	51.73%
-0.8	-10546142.2	-5021016.1	-52.39%	52.39%
-0.7	-9359965.6	-4393389.1	-53.06%	53.06%
-0.6	-8142450.6	-3765762.1	-53.75%	53.75%
-0.5	-6890848.9	-3138135.1	-54.46%	54.46%
-0.4	-5602182.3	-2510508.0	-55.19%	55.19%
-0.3	-4273165.7	-1882881.0	-55.94%	55.94%
-0.2	-2899503.4	-1255254.0	-56.71%	56.71%
-0.1	-1476730.9	-627627.0	-57.50%	57.50%
0.0	-	-	-	-
0.1	1537470.9	627627.0	-59.18%	59.18%
0.2	3141388.0	1255254.0	-60.04%	60.04%
0.3	4823825.9	1882881.0	-60.97%	60.97%
0.4	6592557.6	2510508.0	-61.92%	61.92%
0.5	8461156.9	3138135.1	-62.91%	62.91%
0.6	10447306.6	3765762.1	-63.95%	63.95%
0.7	12570337.5	4393389.1	-65.05%	65.05%
0.8	14859614.5	5021016.1	-66.21%	66.21%
0.9	17354160.4	5648643.1	-67.45%	67.45%
1.0	20104607.7	6276270.1	-68.78%	68.78%
		Average	**-58.91%**	**58.91%**

Volume of deformation 5000x3000x12_R=12000				
	Numerical	Analytical		
P [kN/m2]	[mm3]	[mm3]	Rel. dev.	Abs. Dev
-1.0	-9749461.8	-5122699.9	-47.46%	47.46%
-0.9	-8856427.1	-4610429.9	-47.94%	47.94%
-0.8	-7947922.4	-4098160.0	-48.44%	48.44%
-0.7	-7022985.0	-3585890.0	-48.94%	48.94%
-0.6	-6080807.3	-3073620.0	-49.45%	49.45%
-0.5	-5120381.5	-2561350.0	-49.98%	49.98%
-0.4	-4140358.8	-2049080.0	-50.51%	50.51%
-0.3	-3139654.8	-1536810.0	-51.05%	51.05%
-0.2	-2117156.3	-1024540.0	-51.61%	51.61%
-0.1	-1070793.8	-512270.0	-52.16%	52.16%
0.0	-	-	-	-
0.1	1097292.2	512270.0	-53.32%	53.32%
0.2	2223243.2	1024540.0	-53.92%	53.92%
0.3	3378949.0	1536810.0	-54.52%	54.52%
0.4	4569262.9	2049080.0	-55.16%	55.16%
0.5	5794637.0	2561350.0	-55.80%	55.80%
0.6	7058378.3	3073620.0	-56.45%	56.45%
0.7	8364553.4	3585890.0	-57.13%	57.13%
0.8	9716299.8	4098160.0	-57.82%	57.82%
0.9	11119553.0	4610429.9	-58.54%	58.54%
1.0	12578527.8	5122699.9	-59.27%	59.27%
		Average	**-52.97%**	**52.97%**

Volume of deformation 5000x3000x8_R=16000				
	Numerical	Analytical		
P [kN/m2]	[mm3]	[mm3]	Rel. dev.	Abs. Dev
-1.0	-22901210.9	-17650517.5	-22.93%	22.93%
-0.9	-21066708.6	-15885465.7	-24.59%	24.59%
-0.8	-19171081.1	-14120414.0	-26.35%	26.35%
-0.7	-17201643.2	-12355362.2	-28.17%	28.17%
-0.6	-15150317.4	-10590310.5	-30.10%	30.10%
-0.5	-13002131.3	-8825258.7	-32.12%	32.12%
-0.4	-10741112.9	-7060207.0	-34.27%	34.27%
-0.3	-8344853.1	-5295155.2	-36.55%	36.55%
-0.2	-5785210.9	-3530103.5	-38.98%	38.98%
-0.1	-3022699.3	-1765051.7	-41.61%	41.61%
0.0	-	-	-	-
0.1	3363828.8	1765051.7	-47.53%	47.53%
0.2	7202171.4	3530103.5	-50.99%	50.99%
0.3	11744021.6	5295155.2	-54.91%	54.91%
0.4	17465236.9	7060207.0	-59.58%	59.58%
0.5	25577256.7	8825258.7	-65.50%	65.50%
0.6	41033354.7	10590310.5	-74.19%	74.19%
0.7	74661970.3	12355362.2	-83.45%	83.45%
0.8	100227481.7	14120414.0	-85.91%	85.91%
0.9	119126986.1	15885465.7	-86.67%	86.67%
1.0	135070750.6	17650517.5	-86.93%	86.93%
		Average	**-50.57%**	**50.57%**

Volume of deformation 5000x3000x10_R=16000				
	Numerical	Analytical		
P [kN/m2]	[mm3]	[mm3]	Rel. dev.	Abs. Dev
-1.0	-17127095.3	-13750133.6	-19.72%	19.72%
-0.9	-15663984.3	-12375120.2	-21.00%	21.00%
-0.8	-14160433.8	-11000106.9	-22.32%	22.32%
-0.7	-12612587.0	-9625093.5	-23.69%	23.69%
-0.6	-11015804.8	-8250080.2	-25.11%	25.11%
-0.5	-9364015.1	-6875066.8	-26.58%	26.58%
-0.4	-7650890.1	-5500053.4	-28.11%	28.11%
-0.3	-5868505.9	-4125040.1	-29.71%	29.71%
-0.2	-4007596.9	-2750026.7	-31.38%	31.38%
-0.1	-2056137.5	-1375013.4	-33.13%	33.13%
0.0	-	-	-	-
0.1	2178170.5	1375013.4	-36.87%	36.87%
0.2	4501063.3	2750026.7	-38.90%	38.90%
0.3	6996976.0	4125040.1	-41.05%	41.05%
0.4	9706174.9	5500053.4	-43.33%	43.33%
0.5	12683430.6	6875066.8	-45.79%	45.79%
0.6	16005578.4	8250080.2	-48.45%	48.45%
0.7	19789564.4	9625093.5	-51.36%	51.36%
0.8	24218285.6	11000106.9	-54.58%	54.58%
0.9	29605343.8	12375120.2	-58.20%	58.20%
1.0	36510593.2	13750133.6	-62.34%	62.34%
		Average	**-37.08%**	**37.08%**

Volume of deformation 5000x3000x12_R=16000				
	Numerical	Analytical		
P [kN/m2]	[mm3]	[mm3]	Rel. dev.	Abs. Dev
-1.0	-13107135.4	-11175664.4	-14.74%	14.74%
-0.9	-11930075.0	-10058098.0	-15.69%	15.69%
-0.8	-10729281.4	-8940531.6	-16.67%	16.67%
-0.7	-9502577.4	-7822965.1	-17.68%	17.68%
-0.6	-8248303.7	-6705398.7	-18.71%	18.71%
-0.5	-6964390.0	-5587832.2	-19.77%	19.77%
-0.4	-5648080.3	-4470265.8	-20.85%	20.85%
-0.3	-4296927.2	-3352699.3	-21.97%	21.97%
-0.2	-2907729.4	-2235132.9	-23.13%	23.13%
-0.1	-1476093.3	-1117566.4	-24.29%	24.29%
0.0	-	-	-	-
0.1	1526141.4	1117566.4	-26.77%	26.77%
0.2	3106705.8	2235132.9	-28.05%	28.05%
0.3	4749338.7	3352699.3	-29.41%	29.41%
0.4	6459657.9	4470265.8	-30.80%	30.80%
0.5	8245686.3	5587832.2	-32.23%	32.23%
0.6	10117807.7	6705398.7	-33.73%	33.73%
0.7	12087831.3	7822965.1	-35.28%	35.28%
0.8	14168770.0	8940531.6	-36.90%	36.90%
0.9	16378027.7	10058098.0	-38.59%	38.59%
1.0	18737190.4	11175664.4	-40.36%	40.36%
		Average	**-26.28%**	**26.28%**

Volume of deformation 5000x3000x8_R=20000				
P [kN/m2]	Numerical [mm3]	Analytical [mm3]	Rel. dev.	Abs. Dev
-1.0	-28363709.5	-31083454.7	9.59%	9.59%
-0.9	-26121371.6	-27975109.2	7.10%	7.10%
-0.8	-23806056.1	-24866763.8	4.46%	4.46%
-0.7	-21405355.1	-21758418.3	1.65%	1.65%
-0.6	-18904556.9	-18650072.8	-1.35%	1.35%
-0.5	-16282870.6	-15541727.4	-4.55%	4.55%
-0.4	-13514730.0	-12433381.9	-8.00%	8.00%
-0.3	-10565098.3	-9325036.4	-11.74%	11.74%
-0.2	-7384094.9	-6216690.9	-15.81%	15.81%
-0.1	-3899915.0	-3108345.5	-20.30%	20.30%
0.0	-	-	-	-
0.1	4502880.8	3108345.5	-30.97%	30.97%
0.2	9952672.7	6216690.9	-37.54%	37.54%
0.3	17111992.3	9325036.4	-45.51%	45.51%
0.4	28170891.5	12433381.9	-55.86%	55.86%
0.5	50185318.8	15541727.4	-69.03%	69.03%
0.6	77530282.1	18650072.8	-75.94%	75.94%
0.7	98810914.9	21758418.3	-77.98%	77.98%
0.8	116627652.5	24866763.8	-78.68%	78.68%
0.9	132564804.1	27975109.2	-78.90%	78.90%
1.0	147366263.7	31083454.7	-78.91%	78.91%
		Average	**-33.41%**	**35.69%**

Volume of deformation 5000x3000x10_R=20000				
P [kN/m2]	Numerical [mm3]	Analytical [mm3]	Rel. dev.	Abs. Dev
-1.0	-21404000.4	-24096824.1	12.58%	12.58%
-0.9	-19594871.3	-21687141.7	10.68%	10.68%
-0.8	-17736258.7	-19277459.3	8.69%	8.69%
-0.7	-15822025.3	-16867776.9	6.61%	6.61%
-0.6	-13845035.0	-14458094.5	4.43%	4.43%
-0.5	-11796655.9	-12048412.1	2.13%	2.13%
-0.4	-9665984.8	-9638729.6	-0.28%	0.28%
-0.3	-7439978.7	-7229047.2	-2.84%	2.84%
-0.2	-5101819.3	-4819364.8	-5.54%	5.54%
-0.1	-2630699.9	-2409682.4	-8.40%	8.40%
0.0	-	-	-	-
0.1	2830434.9	2409682.4	-14.87%	14.87%
0.2	5903712.6	4819364.8	-18.37%	18.37%
0.3	9288109.1	7229047.2	-22.17%	22.17%
0.4	13083127.6	9638729.6	-26.33%	26.33%
0.5	17435715.4	12048412.1	-30.90%	30.90%
0.6	22581750.7	14458094.5	-35.97%	35.97%
0.7	28901337.7	16867776.9	-41.64%	41.64%
0.8	37001670.7	19277459.3	-47.90%	47.90%
0.9	47602816.0	21687141.7	-54.44%	54.44%
1.0	60568528.6	24096824.1	-60.22%	60.22%
		Average	**-16.24%**	**20.75%**

Volume of deformation 5000x3000x12_R=20000				
P [kN/m2]	Numerical [mm3]	Analytical [mm3]	Rel. dev.	Abs. Dev
-1.0	-13107135.4	-11175664.4	-14.74%	14.74%
-0.9	-11930075.0	-10058098.0	-15.69%	15.69%
-0.8	-10729281.4	-8940531.6	-16.67%	16.67%
-0.7	-9502577.4	-7822965.1	-17.68%	17.68%
-0.6	-8248303.7	-6705398.7	-18.71%	18.71%
-0.5	-6964390.0	-5587832.2	-19.77%	19.77%
-0.4	-5648080.3	-4470265.8	-20.85%	20.85%
-0.3	-4296927.2	-3352699.3	-21.97%	21.97%
-0.2	-2907729.4	-2235132.9	-23.13%	23.13%
-0.1	-1476093.3	-1117566.4	-24.29%	24.29%
0.0	-	-	-	-
0.1	1526141.4	1117566.4	-26.77%	26.77%
0.2	3106705.8	2235132.9	-28.05%	28.05%
0.3	4749338.7	3352699.3	-29.41%	29.41%
0.4	6459657.9	4470265.8	-30.80%	30.80%
0.5	8245686.3	5587832.2	-32.23%	32.23%
0.6	10117807.7	6705398.7	-33.73%	33.73%
0.7	12087831.3	7822965.1	-35.28%	35.28%
0.8	14168770.0	8940531.6	-36.90%	36.90%
0.9	16378027.7	10058098.0	-38.59%	38.59%
1.0	18737190.4	11175664.4	-40.36%	40.36%
		Average	**-26.28%**	**26.28%**

5000x3000x8mm, P-V Diagram

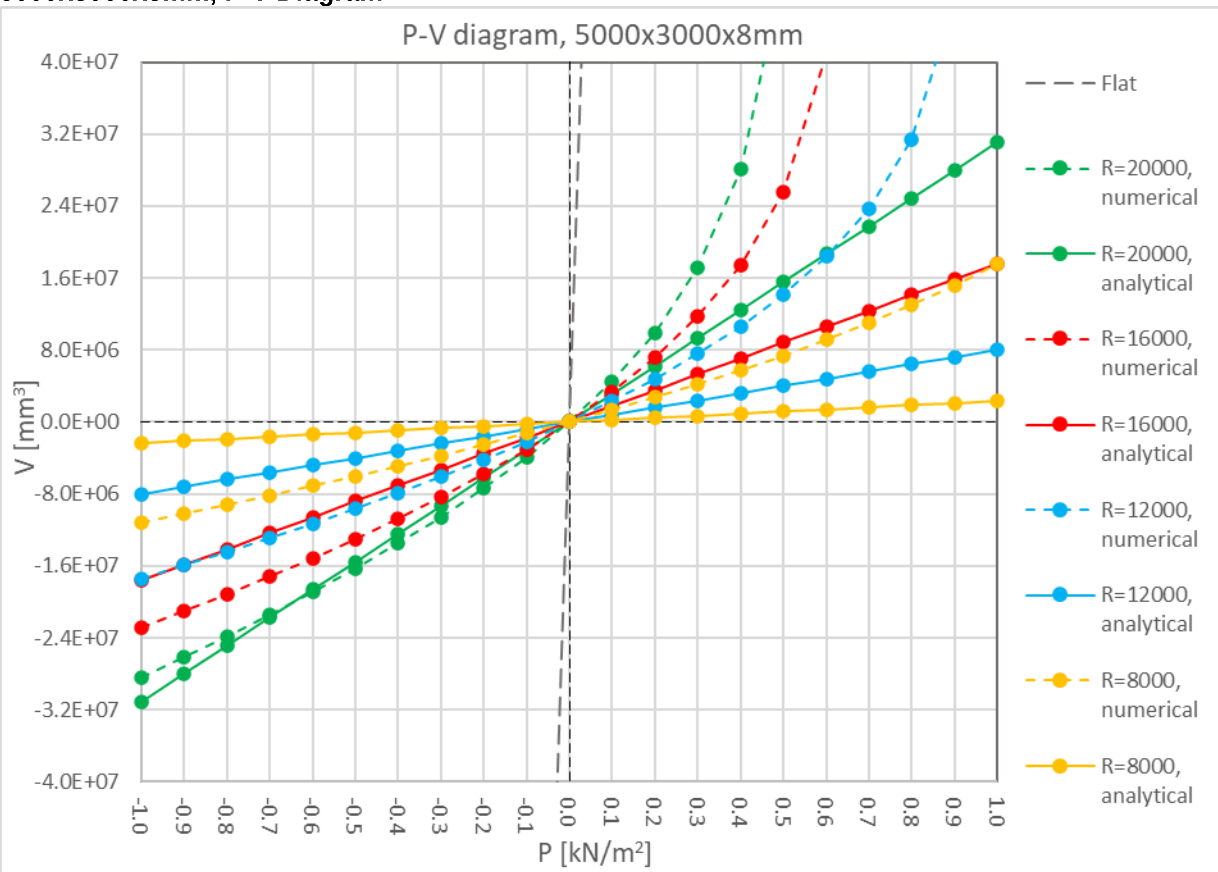

5000x3000x10mm, P-V Diagram

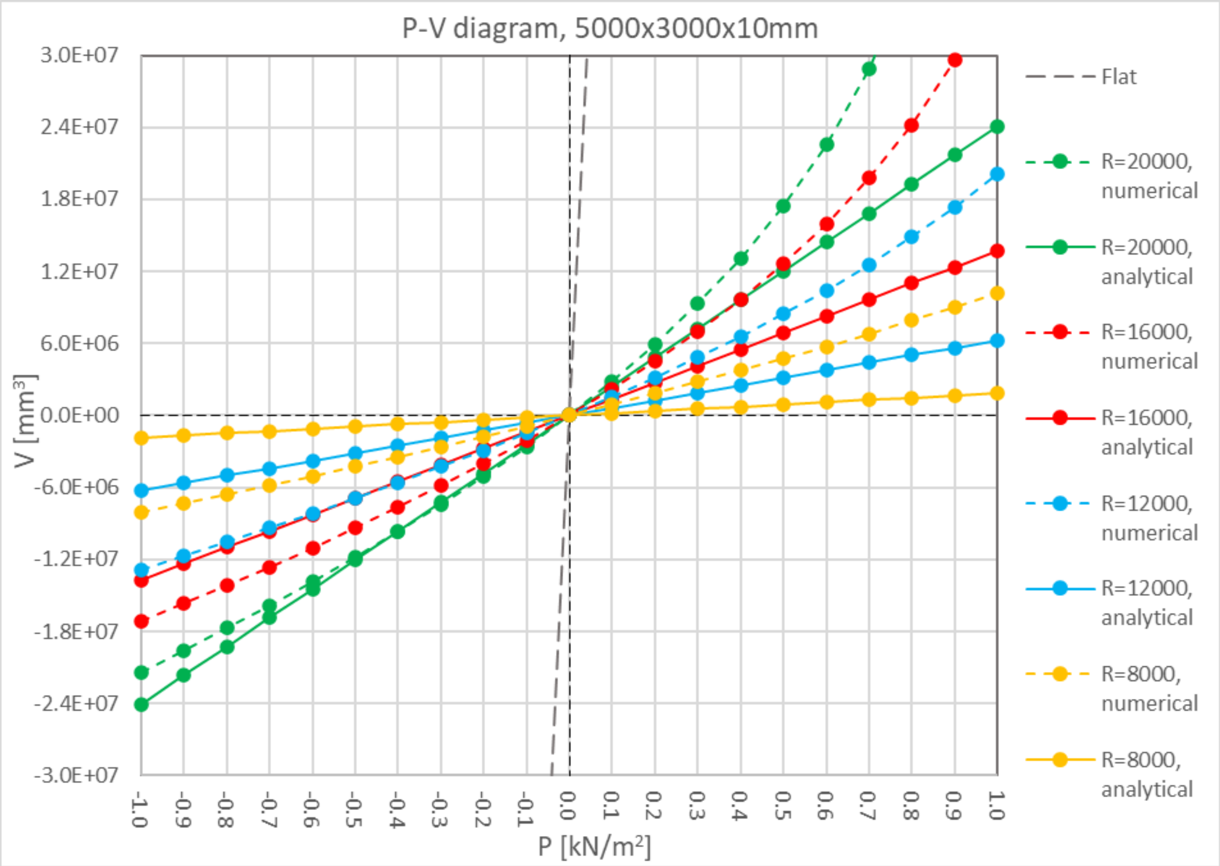

5000x3000x12mm, P-V Diagram

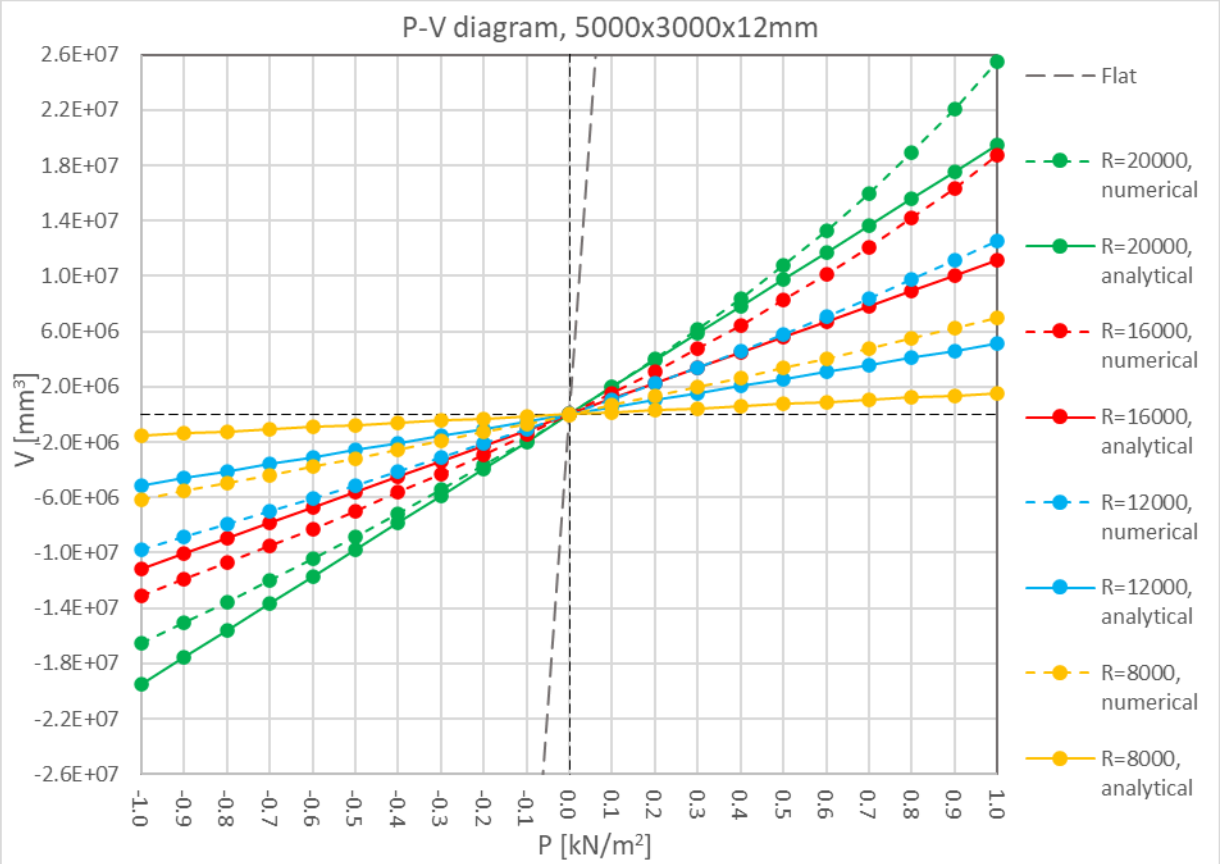

6000x3000mm, P-V Tables

Volume of deformation 6000x3000x8_R=8000				
	Numerical	Analytical		
P [kN/m2]	[mm3]	[mm3]	Rel. dev.	Abs. Dev
-1.0	-12992406.2	-2768659.2	-78.69%	78.69%
-0.9	-11863288.0	-2491793.2	-79.00%	79.00%
-0.8	-10705132.4	-2214927.3	-79.31%	79.31%
-0.7	-9516097.2	-1938061.4	-79.63%	79.63%
-0.6	-8292773.8	-1661195.5	-79.97%	79.97%
-0.5	-7031944.7	-1384329.6	-80.31%	80.31%
-0.4	-5729694.4	-1107463.7	-80.67%	80.67%
-0.3	-4381344.0	-830597.7	-81.04%	81.04%
-0.2	-2981572.7	-553731.8	-81.43%	81.43%
-0.1	-1523786.6	-276865.9	-81.83%	81.83%
0.0	-	-	-	-
0.1	1599064.2	276865.9	-82.69%	82.69%
0.2	3285143.5	553731.8	-83.14%	83.14%
0.3	5072708.0	830597.7	-83.63%	83.63%
0.4	6981080.3	1107463.7	-84.14%	84.14%
0.5	9033608.1	1384329.6	-84.68%	84.68%
0.6	11263737.5	1661195.5	-85.25%	85.25%
0.7	13714581.9	1938061.4	-85.87%	85.87%
0.8	16451456.5	2214927.3	-86.54%	86.54%
0.9	19567472.8	2491793.2	-87.27%	87.27%
1.0	23211892.9	2768659.2	-88.07%	88.07%
		Average	**-82.66%**	**82.66%**

Volume of deformation 6000x3000x10_R=8000				
	Numerical	Analytical		
P [kN/m2]	[mm3]	[mm3]	Rel. dev.	Abs. Dev
-1.0	-38992015.2	-2189276.4	-94.39%	94.39%
-0.9	-35190359.2	-1970348.7	-94.40%	94.40%
-0.8	-31376585.2	-1751421.1	-94.42%	94.42%
-0.7	-27526918.2	-1532493.5	-94.43%	94.43%
-0.6	-23654248.4	-1313565.8	-94.45%	94.45%
-0.5	-19664177.9	-1094638.2	-94.43%	94.43%
-0.4	-15814850.9	-875710.6	-94.46%	94.46%
-0.3	-11895745.3	-656782.9	-94.48%	94.48%
-0.2	-7956922.9	-437855.3	-94.50%	94.50%
-0.1	-3993488.6	-218927.6	-94.52%	94.52%
0.0	-	-	-	-
0.1	4013814.9	218927.6	-94.55%	94.55%
0.2	8049551.9	437855.3	-94.56%	94.56%
0.3	12103075.1	656782.9	-94.57%	94.57%
0.4	16307175.4	875710.6	-94.63%	94.63%
0.5	20461404.4	1094638.2	-94.65%	94.65%
0.6	24630232.0	1313565.8	-94.67%	94.67%
0.7	28836693.3	1532493.5	-94.69%	94.69%
0.8	33115471.4	1751421.1	-94.71%	94.71%
0.9	37401764.8	1970348.7	-94.73%	94.73%
1.0	41726387.8	2189276.4	-94.75%	94.75%
		Average	**-94.55%**	**94.55%**

Volume of deformation 6000x3000x12_R=8000				
	Numerical	Analytical		
P [kN/m2]	[mm3]	[mm3]	Rel. dev.	Abs. Dev
-1.0	-7350144.4	-1801479.2	-75.49%	75.49%
-0.9	-6655323.4	-1621331.3	-75.64%	75.64%
-0.8	-5952625.9	-1441183.4	-75.79%	75.79%
-0.7	-5241788.5	-1261035.4	-75.94%	75.94%
-0.6	-4522583.2	-1080887.5	-76.10%	76.10%
-0.5	-3794579.3	-900739.6	-76.26%	76.26%
-0.4	-3058133.5	-720591.7	-76.44%	76.44%
-0.3	-2311768.4	-540443.8	-76.62%	76.62%
-0.2	-1555896.7	-360295.8	-76.84%	76.84%
-0.1	-790016.3	-180147.9	-77.20%	77.20%
0.0	-	-	-	-
0.1	772878.7	180147.9	-76.69%	76.69%
0.2	1570809.0	360295.8	-77.06%	77.06%
0.3	2380455.3	540443.8	-77.30%	77.30%
0.4	3201370.9	720591.7	-77.49%	77.49%
0.5	4035001.3	900739.6	-77.68%	77.68%
0.6	4881023.2	1080887.5	-77.86%	77.86%
0.7	5744482.7	1261035.4	-78.05%	78.05%
0.8	6620125.8	1441183.4	-78.23%	78.23%
0.9	7510185.2	1621331.3	-78.41%	78.41%
1.0	8415460.6	1801479.2	-78.59%	78.59%
		Average	**-76.98%**	**76.98%**

Volume of deformation 6000x3000x8_R=12000				
	Numerical	Analytical		
P [kN/m2]	[mm3]	[mm3]	Rel. dev.	Abs. Dev
-1.0	-20142227.1	-9536049.9	-52.66%	52.66%
-0.9	-18447204.4	-8582444.9	-53.48%	53.48%
-0.8	-16703716.6	-7628840.0	-54.33%	54.33%
-0.7	-14906153.5	-6675235.0	-55.22%	55.22%
-0.6	-13047684.6	-5721630.0	-56.15%	56.15%
-0.5	-11119995.7	-4768025.0	-57.12%	57.12%
-0.4	-9114061.8	-3814420.0	-58.15%	58.15%
-0.3	-7016624.5	-2860815.0	-59.23%	59.23%
-0.2	-4812802.9	-1907210.0	-60.37%	60.37%
-0.1	-2483470.8	-953605.0	-61.60%	61.60%
0.0	-	-	-	-
0.1	2670532.8	953605.0	-64.29%	64.29%
0.2	5581769.4	1907210.0	-65.83%	65.83%
0.3	8804436.3	2860815.0	-67.51%	67.51%
0.4	12453001.2	3814420.0	-69.37%	69.37%
0.5	16715745.5	4768025.0	-71.48%	71.48%
0.6	21933211.8	5721630.0	-73.91%	73.91%
0.7	28797212.8	6675235.0	-76.82%	76.82%
0.8	38876233.4	7628840.0	-80.38%	80.38%
0.9	55105284.5	8582444.9	-84.43%	84.43%
1.0	78213195.5	9536049.9	-87.81%	87.81%
		Average	**-65.51%**	**65.51%**

Volume of deformation 6000x3000x10_R=12000				
	Numerical	Analytical		
P [kN/m2]	[mm3]	[mm3]	Rel. dev.	Abs. Dev
-1.0	-66539972.0	-7484462.1	-88.75%	88.75%
-0.9	-60123559.6	-6736015.9	-88.80%	88.80%
-0.8	-53679882.9	-5987569.7	-88.85%	88.85%
-0.7	-47171191.1	-5239123.4	-88.89%	88.89%
-0.6	-40621851.5	-4490677.2	-88.95%	88.95%
-0.5	-34036549.8	-3742231.0	-89.01%	89.01%
-0.4	-27335404.3	-2993784.8	-89.05%	89.05%
-0.3	-20599135.5	-2245338.6	-89.10%	89.10%
-0.2	-13804795.7	-1496892.4	-89.16%	89.16%
-0.1	-6945683.9	-748446.2	-89.22%	89.22%
0.0	-	-	-	-
0.1	7013580.2	748446.2	-89.33%	89.33%
0.2	14078992.0	1496892.4	-89.37%	89.37%
0.3	21306891.1	2245338.6	-89.46%	89.46%
0.4	28602319.7	2993784.8	-89.53%	89.53%
0.5	35980583.2	3742231.0	-89.60%	89.60%
0.6	43510530.9	4490677.2	-89.68%	89.68%
0.7	51126582.3	5239123.4	-89.75%	89.75%
0.8	58889277.2	5987569.7	-89.83%	89.83%
0.9	66765645.4	6736015.9	-89.91%	89.91%
1.0	74832070.9	7484462.1	-90.00%	90.00%
		Average	**-89.31%**	**89.31%**

Volume of deformation 6000x3000x12_R=12000				
	Numerical	Analytical		
P [kN/m2]	[mm3]	[mm3]	Rel. dev.	Abs. Dev
-1.0	-11699354.2	-6121929.5	-47.67%	47.67%
-0.9	-10627712.5	-5509736.5	-48.16%	48.16%
-0.8	-9537506.9	-4897543.6	-48.65%	48.65%
-0.7	-8427582.0	-4285350.6	-49.15%	49.15%
-0.6	-7296968.8	-3673157.7	-49.66%	49.66%
-0.5	-6144457.8	-3060964.7	-50.18%	50.18%
-0.4	-4968430.5	-2448771.8	-50.71%	50.71%
-0.3	-3767585.7	-1836578.8	-51.25%	51.25%
-0.2	-2540587.6	-1224385.9	-51.81%	51.81%
-0.1	-1284952.6	-612192.9	-52.36%	52.36%
0.0	-	-	-	-
0.1	1316750.7	612192.9	-53.51%	53.51%
0.2	2667891.9	1224385.9	-54.11%	54.11%
0.3	4054738.8	1836578.8	-54.71%	54.71%
0.4	5483115.5	2448771.8	-55.34%	55.34%
0.5	6953564.4	3060964.7	-55.98%	55.98%
0.6	8470053.9	3673157.7	-56.63%	56.63%
0.7	10037464.1	4285350.6	-57.31%	57.31%
0.8	11659559.7	4897543.6	-58.00%	58.00%
0.9	13343463.6	5509736.5	-58.71%	58.71%
1.0	15094233.3	6121929.5	-59.44%	59.44%
		Average	**-53.17%**	**53.17%**

Volume of deformation 6000x3000x8_R=16000				
	Numerical	Analytical		
P [kN/m2]	[mm3]	[mm3]	Rel. dev.	Abs. Dev
-1.0	-26977651.8	-21042120.7	-22.00%	22.00%
-0.9	-24769137.7	-18937908.6	-23.54%	23.54%
-0.8	-22492076.1	-16833696.5	-25.16%	25.16%
-0.7	-20135604.7	-14729484.5	-26.85%	26.85%
-0.6	-17689488.3	-12625272.4	-28.63%	28.63%
-0.5	-15140202.4	-10521060.3	-30.51%	30.51%
-0.4	-12470773.6	-8416848.3	-32.51%	32.51%
-0.3	-9658099.7	-6312636.2	-34.64%	34.64%
-0.2	-6672939.3	-4208424.1	-36.93%	36.93%
-0.1	-3475569.8	-2104212.1	-39.46%	39.46%
0.0	-	-	-	-
0.1	3834082.1	2104212.1	-45.12%	45.12%
0.2	8181622.2	4208424.1	-48.56%	48.56%
0.3	13289633.3	6312636.2	-52.50%	52.50%
0.4	19679046.9	8416848.3	-57.23%	57.23%
0.5	28647410.5	10521060.3	-63.27%	63.27%
0.6	44701427.8	12625272.4	-71.76%	71.76%
0.7	85095475.5	14729484.5	-82.69%	82.69%
0.8	179680498.3	16833696.5	-90.63%	90.63%
0.9	219334747.0	18937908.6	-91.37%	91.37%
1.0	246010390.5	21042120.7	-91.45%	91.45%
		Average	**-49.74%**	**49.74%**

Volume of deformation 6000x3000x10_R=16000				
	Numerical	Analytical		
P [kN/m2]	[mm3]	[mm3]	Rel. dev.	Abs. Dev
-1.0	-25947616.3	-16438512.8	-36.65%	36.65%
-0.9	-23758097.8	-14794661.5	-37.73%	37.73%
-0.8	-21507532.2	-13150810.2	-38.85%	38.85%
-0.7	-19188390.3	-11506959.0	-40.03%	40.03%
-0.6	-16791833.0	-9863107.7	-41.26%	41.26%
-0.5	-14307905.9	-8219256.4	-42.55%	42.55%
-0.4	-11723838.5	-6575405.1	-43.91%	43.91%
-0.3	-9024028.2	-4931553.8	-45.35%	45.35%
-0.2	-6188518.3	-3287702.6	-46.87%	46.87%
-0.1	-3192158.8	-1643851.3	-48.50%	48.50%
0.0	-	-	-	-
0.1	3431777.6	1643851.3	-52.10%	52.10%
0.2	7168815.4	3287702.6	-54.14%	54.14%
0.3	11302355.5	4931553.8	-56.37%	56.37%
0.4	15981008.4	6575405.1	-58.85%	58.85%
0.5	21451728.1	8219256.4	-61.68%	61.68%
0.6	28181201.6	9863107.7	-65.00%	65.00%
0.7	37211014.3	11506959.0	-69.08%	69.08%
0.8	51528929.2	13150810.2	-74.48%	74.48%
0.9	80592060.1	14794661.5	-81.64%	81.64%
1.0	118618903.5	16438512.8	-86.14%	86.14%
		Average	**-54.06%**	**54.06%**

Volume of deformation 6000x3000x12_R=16000				
	Numerical	Analytical		
P [kN/m2]	[mm3]	[mm3]	Rel. dev.	Abs. Dev
-1.0	-15728562.5	-13398881.0	-14.81%	14.81%
-0.9	-14316090.0	-12058992.9	-15.77%	15.77%
-0.8	-12875137.7	-10719104.8	-16.75%	16.75%
-0.7	-11403092.9	-9379216.7	-17.75%	17.75%
-0.6	-9897964.4	-8039328.6	-18.78%	18.78%
-0.5	-8357267.9	-6699440.5	-19.84%	19.84%
-0.4	-6777696.4	-5359552.4	-20.92%	20.92%
-0.3	-5156312.7	-4019664.3	-22.04%	22.04%
-0.2	-3489275.3	-2679776.2	-23.20%	23.20%
-0.1	-1771312.0	-1339888.1	-24.36%	24.36%
0.0	-	-	-	-
0.1	1831369.7	1339888.1	-26.84%	26.84%
0.2	3728046.9	2679776.2	-28.12%	28.12%
0.3	5699206.4	4019664.3	-29.47%	29.47%
0.4	7751589.5	5359552.4	-30.86%	30.86%
0.5	9894823.6	6699440.5	-32.29%	32.29%
0.6	12141369.3	8039328.6	-33.79%	33.79%
0.7	14505397.6	9379216.7	-35.34%	35.34%
0.8	17002524.0	10719104.8	-36.96%	36.96%
0.9	19653633.2	12058992.9	-38.64%	38.64%
1.0	22484628.5	13398881.0	-40.41%	40.41%
		Average	**-26.35%**	**26.35%**

Volume of deformation 6000x3000x8_R=20000				
P [kN/m2]	Numerical [mm3]	Analytical [mm3]	Rel. dev.	Abs. Dev
-1.0	-193192871.1	-37227901.9	-80.73%	80.73%
-0.9	-172957124.6	-33505111.7	-80.63%	80.63%
-0.8	-153254982.4	-29782321.5	-80.57%	80.57%
-0.7	-133933008.0	-26059531.3	-80.54%	80.54%
-0.6	-114880222.6	-22336741.1	-80.56%	80.56%
-0.5	-95957970.7	-18613950.9	-80.60%	80.60%
-0.4	-77072027.7	-14891160.7	-80.68%	80.68%
-0.3	-58133616.9	-11168370.6	-80.79%	80.79%
-0.2	-39058942.7	-7445580.4	-80.94%	80.94%
-0.1	-19757043.1	-3722790.2	-81.16%	81.16%
0.0	-	-	-	-
0.1	20179256.0	3722790.2	-81.55%	81.55%
0.2	41129063.8	7445580.4	-81.90%	81.90%
0.3	62854593.6	11168370.6	-82.23%	82.23%
0.4	85652165.7	14891160.7	-82.61%	82.61%
0.5	109791083.4	18613950.9	-83.05%	83.05%
0.6	135709755.4	22336741.1	-83.54%	83.54%
0.7	163834769.2	26059531.3	-84.09%	84.09%
0.8	194965414.1	29782321.5	-84.72%	84.72%
0.9	229844824.1	33505111.7	-85.42%	85.42%
1.0	269428197.2	37227901.9	-86.18%	86.18%
		Average	**-82.12%**	**82.12%**

Volume of deformation 6000x3000x10_R=20000				
P [kN/m2]	Numerical [mm3]	Analytical [mm3]	Rel. dev.	Abs. Dev
-1.0	-100257270.3	-28970556.6	-71.10%	71.10%
-0.9	-90432142.8	-26073500.9	-71.17%	71.17%
-0.8	-80589351.7	-23176445.3	-71.24%	71.24%
-0.7	-70724620.6	-20279389.6	-71.33%	71.33%
-0.6	-60817117.4	-17382333.9	-71.42%	71.42%
-0.5	-50857884.4	-14485278.3	-71.52%	71.52%
-0.4	-40845113.8	-11588222.6	-71.63%	71.63%
-0.3	-30788816.7	-8691167.0	-71.77%	71.77%
-0.2	-20596421.5	-5794111.3	-71.87%	71.87%
-0.1	-10346565.3	-2897055.7	-72.00%	72.00%
0.0	-	-	-	-
0.1	10466538.3	2897055.7	-72.32%	72.32%
0.2	21016894.8	5794111.3	-72.43%	72.43%
0.3	31797655.6	8691167.0	-72.67%	72.67%
0.4	42670178.2	11588222.6	-72.84%	72.84%
0.5	53751440.7	14485278.3	-73.05%	73.05%
0.6	64991437.7	17382333.9	-73.25%	73.25%
0.7	76442128.1	20279389.6	-73.47%	73.47%
0.8	88128030.7	23176445.3	-73.70%	73.70%
0.9	100075904.0	26073500.9	-73.95%	73.95%
1.0	112301365.5	28970556.6	-74.20%	74.20%
		Average	**-72.35%**	**72.35%**

Volume of deformation 6000x3000x12_R=20000				
P [kN/m2]	Numerical [mm3]	Analytical [mm3]	Rel. dev.	Abs. Dev
-1.0	-19824095.4	-23520705.0	18.65%	18.65%
-0.9	-18055362.0	-21168634.5	17.24%	17.24%
-0.8	-16249526.0	-18816564.0	15.80%	15.80%
-0.7	-14404989.0	-16464493.5	14.30%	14.30%
-0.6	-12517024.9	-14112423.0	12.75%	12.75%
-0.5	-10581713.7	-11760352.5	11.14%	11.14%
-0.4	-8594302.9	-9408282.0	9.47%	9.47%
-0.3	-6549515.1	-7056211.5	7.74%	7.74%
-0.2	-4440226.4	-4704141.0	5.94%	5.94%
-0.1	-2259646.4	-2352070.5	4.09%	4.09%
0.0	-	-	-	-
0.1	2351665.9	2352070.5	0.02%	0.02%
0.2	4801803.7	4704141.0	-2.03%	2.03%
0.3	7370836.7	7056211.5	-4.27%	4.27%
0.4	10071297.4	9408282.0	-6.58%	6.58%
0.5	12925132.6	11760352.5	-9.01%	9.01%
0.6	15958556.9	14112423.0	-11.57%	11.57%
0.7	19201817.2	16464493.5	-14.26%	14.26%
0.8	22694991.5	18816564.0	-17.09%	17.09%
0.9	26486726.8	21168634.5	-20.08%	20.08%
1.0	30638907.1	23520705.0	-23.23%	23.23%
		Average	**0.45%**	**11.26%**

6000x3000x8mm, P-V Diagram

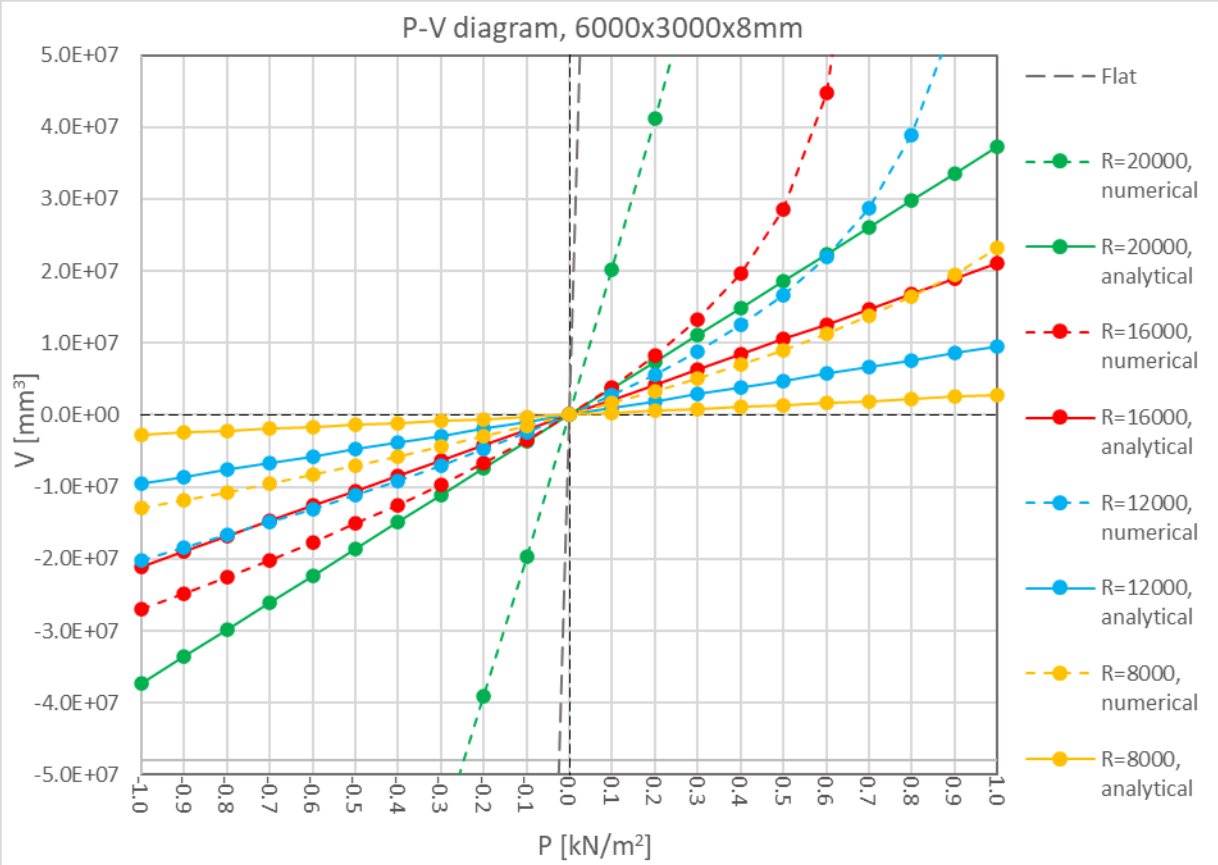

6000x3000x10mm, P-V Diagram

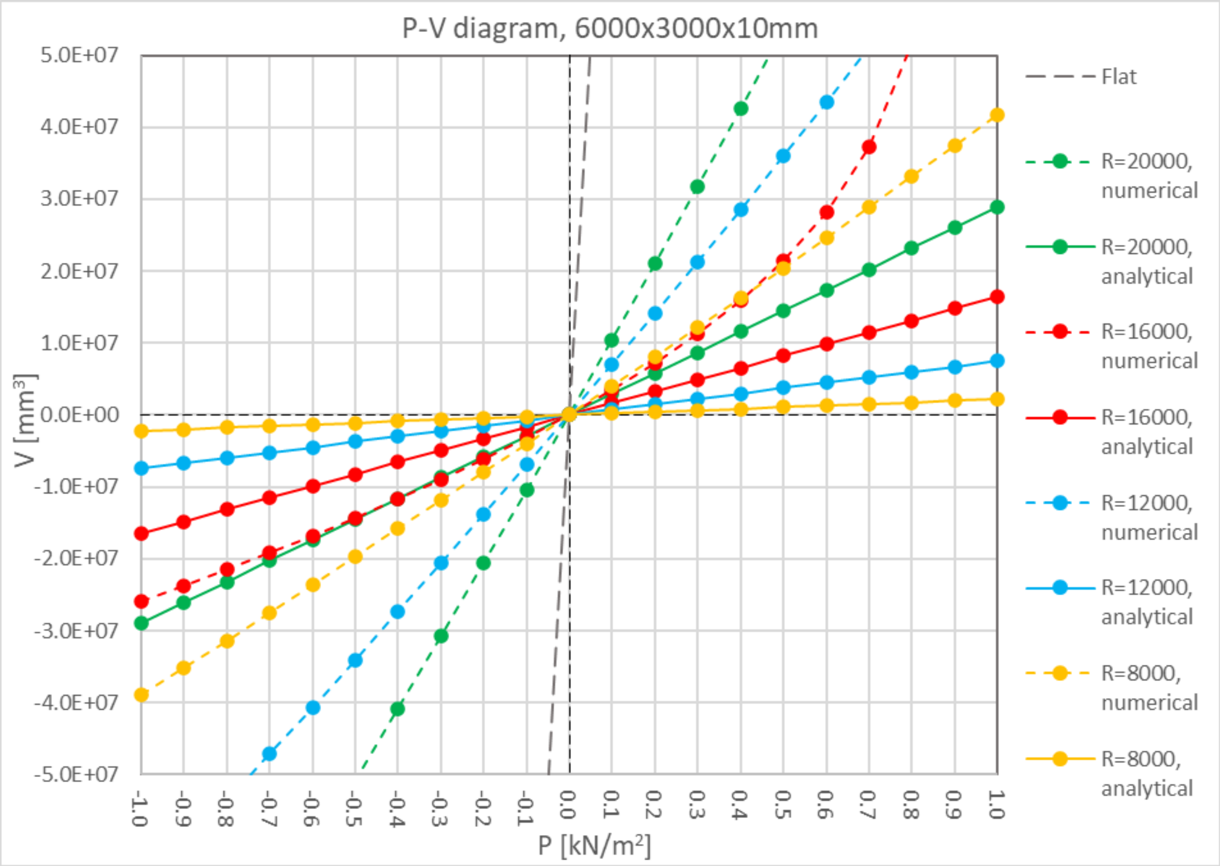

6000x3000x12mm, P-V Diagram

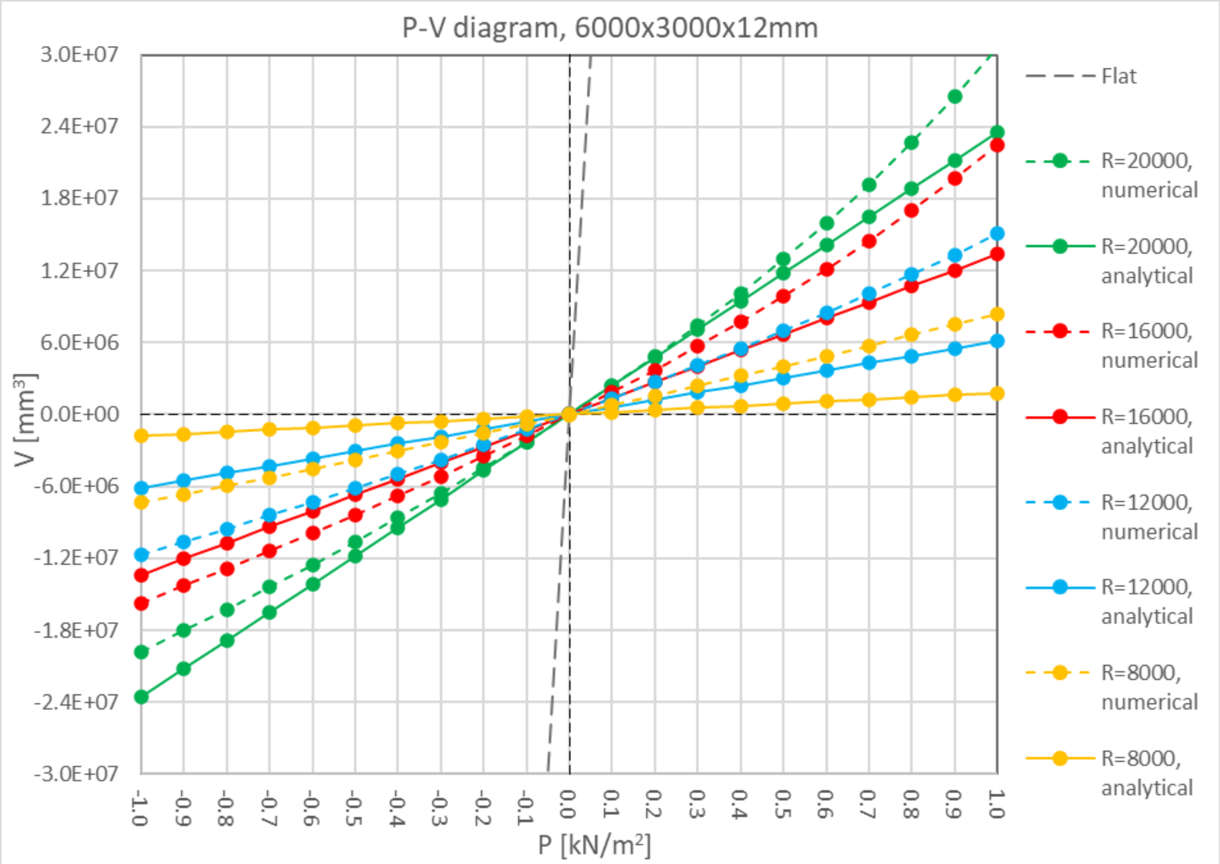

Case studies, P-V Tables

Volume of deformation 3600x1800x8_R=11500				
P [kN/m2]	Numerical [mm3]	Analytical [mm3]	Rel. dev.	Abs. Dev
-1.0	-18334902.7	-4054321.7	-77.89%	77.89%
-0.9	-16677274.6	-3648889.5	-78.12%	78.12%
-0.8	-14988193.4	-3243457.4	-78.36%	78.36%
-0.7	-13265256.8	-2838025.2	-78.61%	78.61%
-0.6	-11505774.0	-2432593.0	-78.86%	78.86%
-0.5	-9706961.1	-2027160.8	-79.12%	79.12%
-0.4	-7865740.9	-1621728.7	-79.38%	79.38%
-0.3	-5978287.0	-1216296.5	-79.65%	79.65%
-0.2	-4041136.7	-810864.3	-79.93%	79.93%
-0.1	-2048375.3	-405432.2	-80.21%	80.21%
0.0	-	-	-	-
0.1	2121349.2	405432.2	-80.89%	80.89%
0.2	4311043.6	810864.3	-81.19%	81.19%
0.3	6578682.3	1216296.5	-81.51%	81.51%
0.4	8942810.0	1621728.7	-81.87%	81.87%
0.5	11403914.8	2027160.8	-82.22%	82.22%
0.6	13978709.9	2432593.0	-82.60%	82.60%
0.7	16682944.3	2838025.2	-82.99%	82.99%
0.8	19536498.1	3243457.4	-83.40%	83.40%
0.9	22562159.9	3648889.5	-83.83%	83.83%
1.0	25789996.2	4054321.7	-84.28%	84.28%
		Average	**-80.74%**	**80.74%**

Volume of deformation 3600x1800x10_R=11500				
P [kN/m2]	Numerical [mm3]	Analytical [mm3]	Rel. dev.	Abs. Dev
-1.0	-12890653.3	-3117656.5	-75.81%	75.81%
-0.9	-11671531.5	-2805890.8	-75.96%	75.96%
-0.8	-10438050.9	-2494125.2	-76.11%	76.11%
-0.7	-9189660.4	-2182359.5	-76.25%	76.25%
-0.6	-7925441.6	-1870593.9	-76.40%	76.40%
-0.5	-6644814.0	-1558828.2	-76.54%	76.54%
-0.4	-5347706.6	-1247062.6	-76.68%	76.68%
-0.3	-4031405.5	-935296.9	-76.80%	76.80%
-0.2	-2696665.7	-623531.3	-76.88%	76.88%
-0.1	-1342222.0	-311765.6	-76.77%	76.77%
0.0	-	-	-	-
0.1	1429865.6	311765.6	-78.20%	78.20%
0.2	2849522.6	623531.3	-78.12%	78.12%
0.3	4293274.6	935296.9	-78.21%	78.21%
0.4	5762357.0	1247062.6	-78.36%	78.36%
0.5	7257478.4	1558828.2	-78.52%	78.52%
0.6	8779859.0	1870593.9	-78.69%	78.69%
0.7	10339968.5	2182359.5	-78.89%	78.89%
0.8	11927136.2	2494125.2	-79.09%	79.09%
0.9	13548536.6	2805890.8	-79.29%	79.29%
1.0	15206043.0	3117656.5	-79.50%	79.50%
		Average	**-77.55%**	**77.55%**

Volume of deformation 3600x1800x12_R=11500				
P [kN/m2]	Numerical [mm3]	Analytical [mm3]	Rel. dev.	Abs. Dev
-1.0	-9513665.4	-2497031.1	-73.75%	73.75%
-0.9	-8593869.2	-2247328.0	-73.85%	73.85%
-0.8	-7667509.3	-1997624.9	-73.95%	73.95%
-0.7	-6735262.2	-1747921.8	-74.05%	74.05%
-0.6	-5795073.2	-1498218.7	-74.15%	74.15%
-0.5	-4847967.3	-1248515.6	-74.25%	74.25%
-0.4	-3893567.4	-998812.4	-74.35%	74.35%
-0.3	-2931950.8	-749109.3	-74.45%	74.45%
-0.2	-1962744.5	-499406.2	-74.56%	74.56%
-0.1	-985406.9	-249703.1	-74.66%	74.66%
0.0	-	-	-	-
0.1	993223.8	249703.1	-74.86%	74.86%
0.2	1995280.1	499406.2	-74.97%	74.97%
0.3	3006488.7	749109.3	-75.08%	75.08%
0.4	4026411.1	998812.4	-75.19%	75.19%
0.5	5055704.4	1248515.6	-75.30%	75.30%
0.6	6094556.1	1498218.7	-75.42%	75.42%
0.7	7143018.4	1747921.8	-75.53%	75.53%
0.8	8201706.4	1997624.9	-75.64%	75.64%
0.9	9270570.5	2247328.0	-75.76%	75.76%
1.0	10350018.6	2497031.1	-75.87%	75.87%
		Average	**-74.78%**	**74.78%**

Volume of deformation 5500x2500x8_R=28000				
P [kN/m2]	Numerical [mm3]	Analytical [mm3]	Rel. dev.	Abs. Dev
-1.0	-73933566.5	-29984024.1	-59.44%	59.44%
-0.9	-67038903.5	-26985621.7	-59.75%	59.75%
-0.8	-60053297.3	-23987219.3	-60.06%	60.06%
-0.7	-52970735.4	-20988816.9	-60.38%	60.38%
-0.6	-45784145.0	-17990414.5	-60.71%	60.71%
-0.5	-38486087.6	-14992012.1	-61.05%	61.05%
-0.4	-31068278.8	-11993609.6	-61.40%	61.40%
-0.3	-23521269.1	-8995207.2	-61.76%	61.76%
-0.2	-15835733.8	-5996804.8	-62.13%	62.13%
-0.1	-7997220.4	-2998402.4	-62.51%	62.51%
0.0	-	-	-	-
0.1	8183158.2	2998402.4	-63.36%	63.36%
0.2	16555824.0	5996804.8	-63.78%	63.78%
0.3	25137105.3	8995207.2	-64.22%	64.22%
0.4	33964985.3	11993609.6	-64.69%	64.69%
0.5	43043586.4	14992012.1	-65.17%	65.17%
0.6	52407165.9	17990414.5	-65.67%	65.67%
0.7	62086065.0	20988816.9	-66.19%	66.19%
0.8	72115486.3	23987219.3	-66.74%	66.74%
0.9	82537782.0	26985621.7	-67.31%	67.31%
1.0	93395457.8	29984024.1	-67.90%	67.90%
		Average	**-63.21%**	**63.21%**

Volume of deformation 5500x2500x10_R=28000				
P [kN/m2]	Numerical [mm3]	Analytical [mm3]	Rel. dev.	Abs. Dev
-1.0	-60214868.7	-24610559.1	-59.13%	59.13%
-0.9	-54467220.0	-22149503.2	-59.33%	59.33%
-0.8	-48666148.6	-19688447.3	-59.54%	59.54%
-0.7	-42809141.6	-17227391.4	-59.76%	59.76%
-0.6	-36893642.0	-14766335.5	-59.98%	59.98%
-0.5	-30916776.5	-12305279.6	-60.20%	60.20%
-0.4	-24875473.1	-9844223.6	-60.43%	60.43%
-0.3	-18767626.3	-7383167.7	-60.66%	60.66%
-0.2	-12587180.8	-4922111.8	-60.90%	60.90%
-0.1	-6332645.2	-2461055.9	-61.14%	61.14%
0.0	-	-	-	-
0.1	6415394.1	2461055.9	-61.64%	61.64%
0.2	12917815.1	4922111.8	-61.90%	61.90%
0.3	19511910.9	7383167.7	-62.16%	62.16%
0.4	26201850.8	9844223.6	-62.43%	62.43%
0.5	32992128.0	12305279.6	-62.70%	62.70%
0.6	39908382.5	14766335.5	-63.00%	63.00%
0.7	46931214.5	17227391.4	-63.29%	63.29%
0.8	54077682.2	19688447.3	-63.59%	63.59%
0.9	61356128.9	22149503.2	-63.90%	63.90%
1.0	68775227.8	24610559.1	-64.22%	64.22%
		Average	**-61.49%**	**61.49%**

Volume of deformation 5500x2500x12_R=28000				
P [kN/m2]	Numerical [mm3]	Analytical [mm3]	Rel. dev.	Abs. Dev
-1.0	-49985803.4	-20470754.1	-59.05%	59.05%
-0.9	-45143914.8	-18423678.6	-59.19%	59.19%
-0.8	-40270552.1	-16376603.2	-59.33%	59.33%
-0.7	-35364635.7	-14329527.8	-59.48%	59.48%
-0.6	-30425195.4	-12282452.4	-59.63%	59.63%
-0.5	-25453027.0	-10235377.0	-59.79%	59.79%
-0.4	-20442479.6	-8188301.6	-59.94%	59.94%
-0.3	-15395697.5	-6141226.2	-60.11%	60.11%
-0.2	-10311408.5	-4094150.8	-60.29%	60.29%
-0.1	-5188219.7	-2047075.4	-60.54%	60.54%
0.0	-	-	-	-
0.1	5180717.2	2047075.4	-60.49%	60.49%
0.2	10429357.1	4094150.8	-60.74%	60.74%
0.3	15722556.6	6141226.2	-60.94%	60.94%
0.4	21061856.0	8188301.6	-61.12%	61.12%
0.5	26448380.3	10235377.0	-61.30%	61.30%
0.6	31883798.8	12282452.4	-61.48%	61.48%
0.7	37369114.1	14329527.8	-61.65%	61.65%
0.8	42905751.2	16376603.2	-61.83%	61.83%
0.9	48520212.5	18423678.6	-62.03%	62.03%
1.0	54177077.4	20470754.1	-62.22%	62.22%
		Average	**-60.56%**	**60.56%**

3600x1800mm, R = 11500mm, P-V Diagram (Case study Van Gogh)

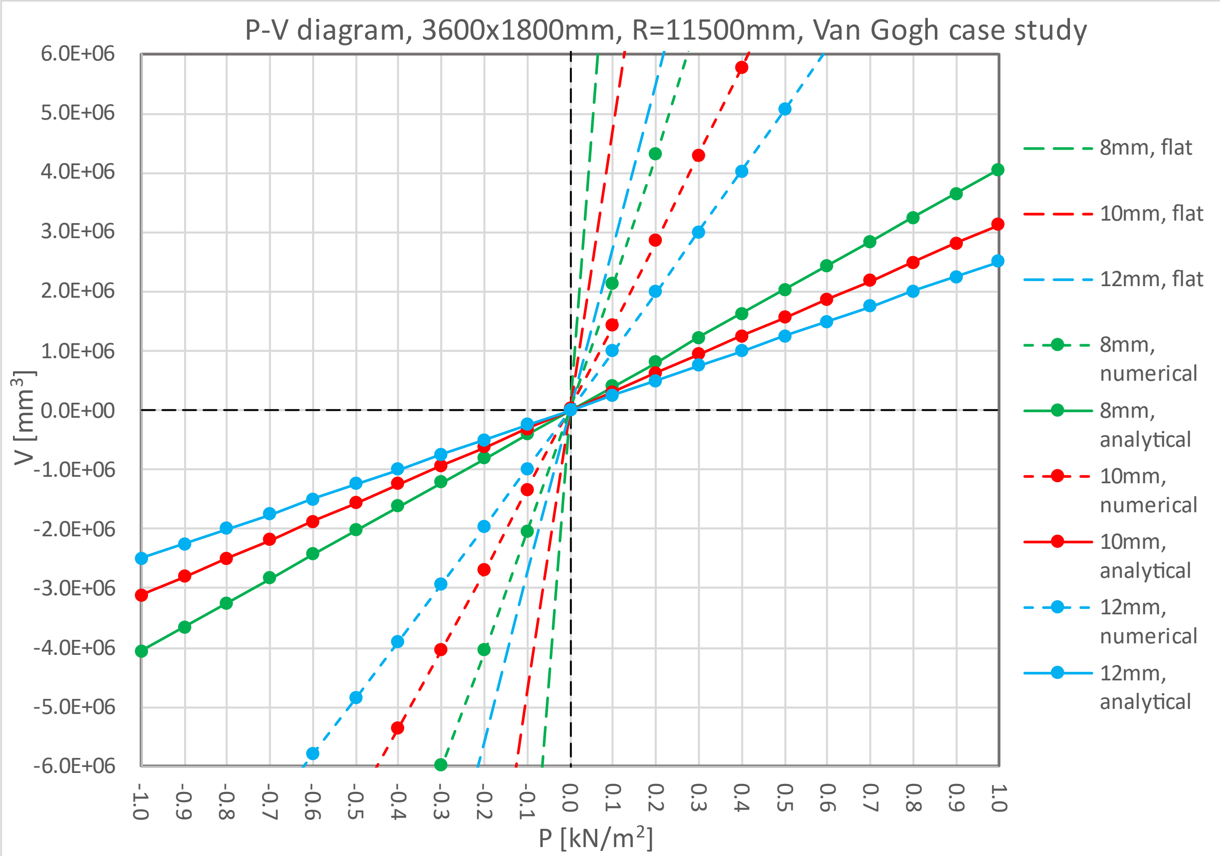

5500x2500mm, R=28000mm, P-V Diagram (Case study Melle)

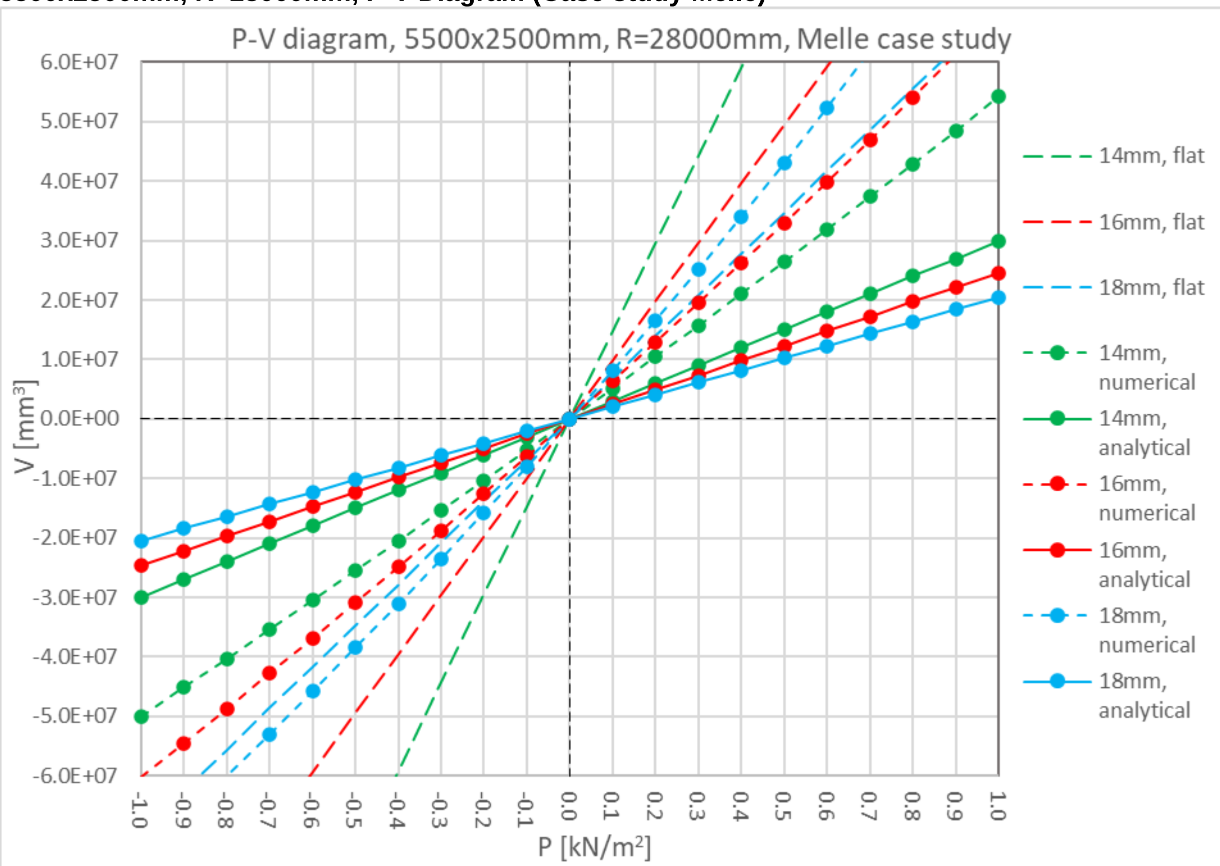

C.2. Cavity pressure symmetric IGU's

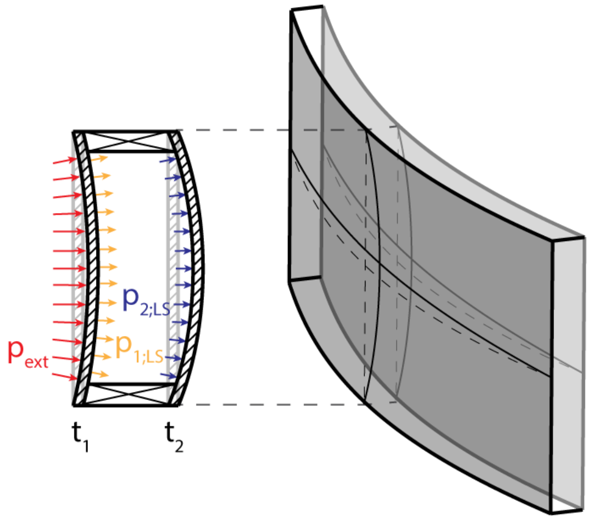

Overview deviations load sharing symmetric IGU's, per plate size

Overview deviations load sharing symmetric IGU's, per configuration				
	8-16-8	10-16-10	12-16-12	Average
1000x1000	2.45%	2.73%	2.57%	**2.58%**
2000x2000	1.83%	2.29%	2.61%	**2.24%**
3000x3000	4.96%	4.73%	5.13%	**4.94%**
4000x3000	5.52%	6.16%	5.54%	**5.74%**
5000x3000	5.20%	5.71%	5.60%	**5.50%**
6000x3000	5.39%	7.33%	7.85%	**6.86%**
Average	**4.22%**	**4.83%**	**4.88%**	**4.64%**

Overview deviations load sharing symmetric IGU's, per design radius

Overview deviations load sharing symmetric IGU's, per design radius							
	1000x1000	2000x2000	3000x3000	4000x3000	5000x3000	6000x3000	Average
20000	1.20%	1.25%	0.80%	1.18%	0.82%	1.07%	**1.05%**
16000	1.78%	1.08%	1.45%	1.60%	2.15%	2.40%	**1.74%**
12000	2.82%	1.42%	3.95%	5.78%	4.85%	6.57%	**4.23%**
8000	4.53%	5.21%	13.56%	14.39%	14.19%	17.38%	**11.55%**
Average	**2.58%**	**2.24%**	**4.94%**	**5.74%**	**5.50%**	**6.86%**	**4.64%**

Deviation case study symmetric Van Gogh

Deviation case study symmetric Van Gogh			
	8-15-8	10-15-10	12-15-12
3600x1800, R=11500	0.94%	**0.28%**	1.45%

Deviation case study symmetric Melle

Deviation case study symmetric Melle			
	14-15-14	16-15-16	18-15-18
5500x2500, R=28000	0.84%	**1.43%**	1.92%

1000x1000x8-16-8

1000x1000x8-16-8					
Radius [mm]	p1;LS, numerical [kN/m2]	p2;LS, numerical [kN/m2]	p1;LS, analytical [kN/m2]	p2;LS, analytical [kN/m2]	Deviation p2;LS
24000	*0.564*	*0.436*	*0.564*	*0.436*	
20000	0.562	0.438	0.575	0.425	1.31%
16000	0.562	0.438	0.581	0.419	1.88%
12000	0.568	0.432	0.596	0.404	2.81%
8000	0.603	0.400	0.638	0.362	3.79%
				Average	**2.45%**

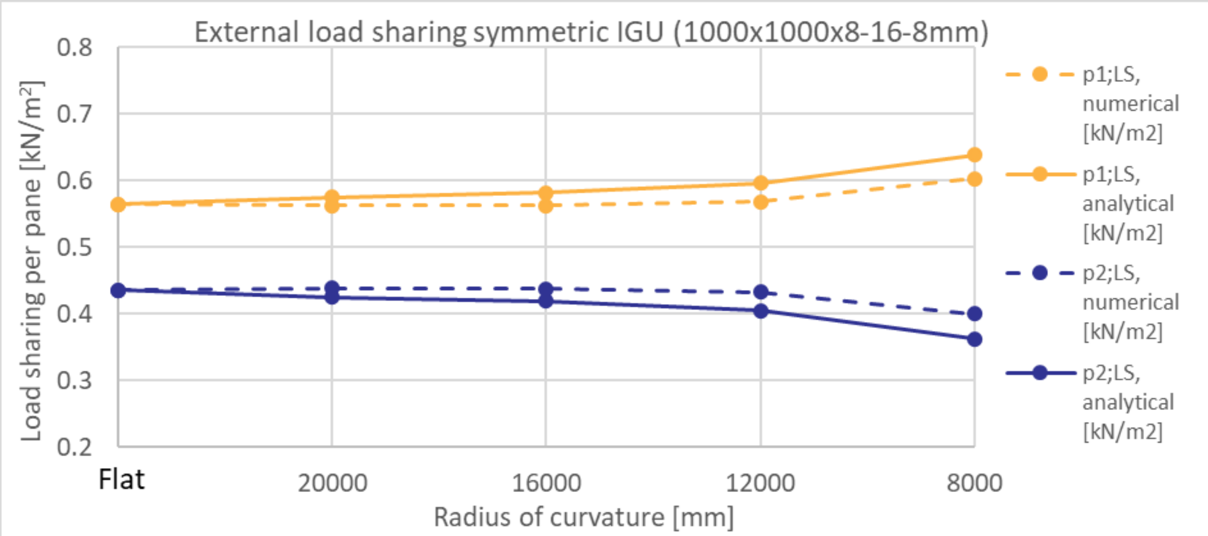

1000x1000x10-16-10

1000x1000x10-16-10					
Radius [mm]	p1;LS, numerical [kN/m2]	p2;LS, numerical [kN/m2]	p1;LS, analytical [kN/m2]	p2;LS, analytical [kN/m2]	Deviation p2;LS
24000	*0.612*	*0.388*	*0.612*	*0.388*	
20000	0.610	0.391	0.622	0.378	1.25%
16000	0.610	0.390	0.628	0.372	1.86%
12000	0.613	0.387	0.643	0.357	2.99%
8000	0.635	0.365	0.684	0.316	4.82%
				Average	**2.73%**

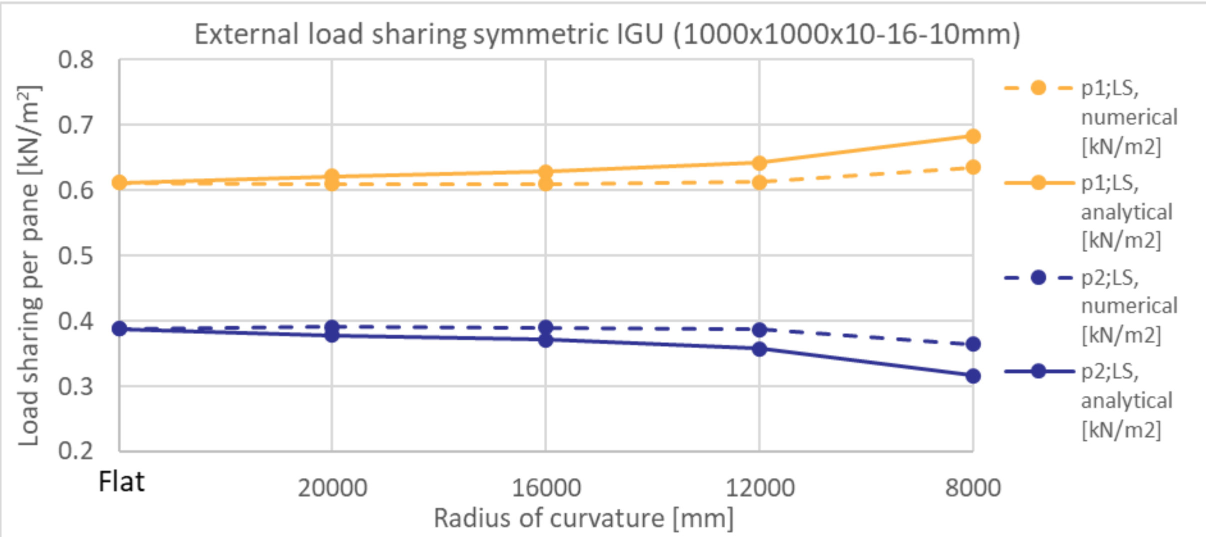

1000x1000x12-16-12

1000x1000x12-16-12					
Radius [mm]	p1;LS, numerical [kN/m2]	p2;LS, numerical [kN/m2]	p1;LS, analytical [kN/m2]	p2;LS, analytical [kN/m2]	Deviation p2;LS
24000	*0.666*	*0.334*	*0.666*	*0.334*	
20000	0.665	0.336	0.675	0.325	1.04%
16000	0.665	0.336	0.681	0.319	1.61%
12000	0.666	0.334	0.693	0.307	2.67%
8000	0.680	0.320	0.729	0.271	4.98%
				Average	**2.57%**

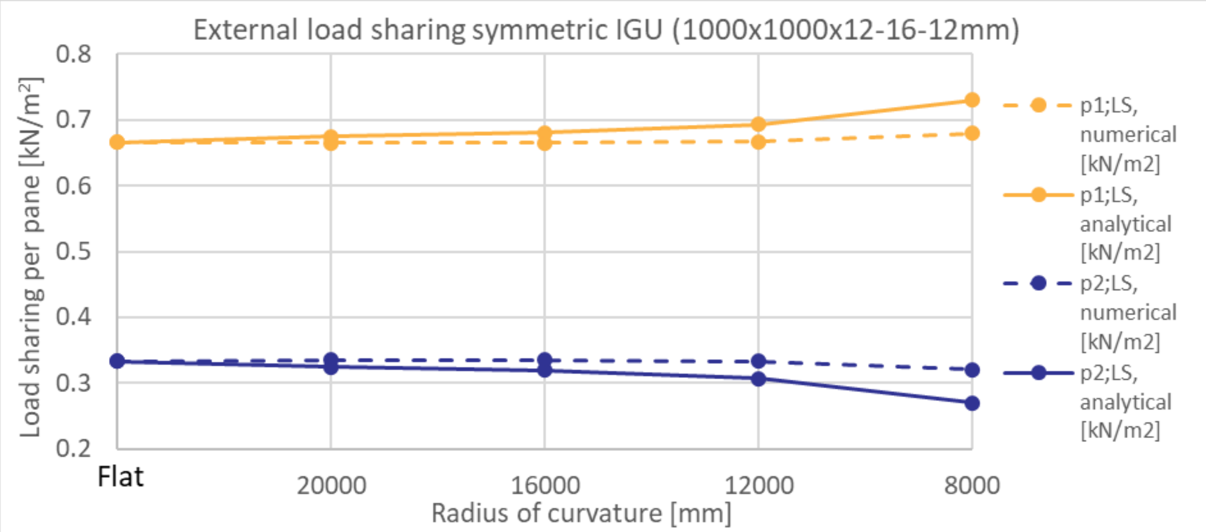

2000x2000x8-16-8

2000x2000x8-16-8					
Radius [mm]	p1;LS, numerical [kN/m2]	p2;LS, numerical [kN/m2]	p1;LS, analytical [kN/m2]	p2;LS, analytical [kN/m2]	Deviation p2;LS
24000	*0.505*	*0.495*	*0.505*	*0.495*	
20000	0.517	0.483	0.521	0.479	0.39%
16000	0.523	0.477	0.531	0.469	0.82%
12000	0.545	0.456	0.556	0.444	1.11%
8000	0.581	0.419	0.631	0.369	5.00%
				Average	**1.83%**

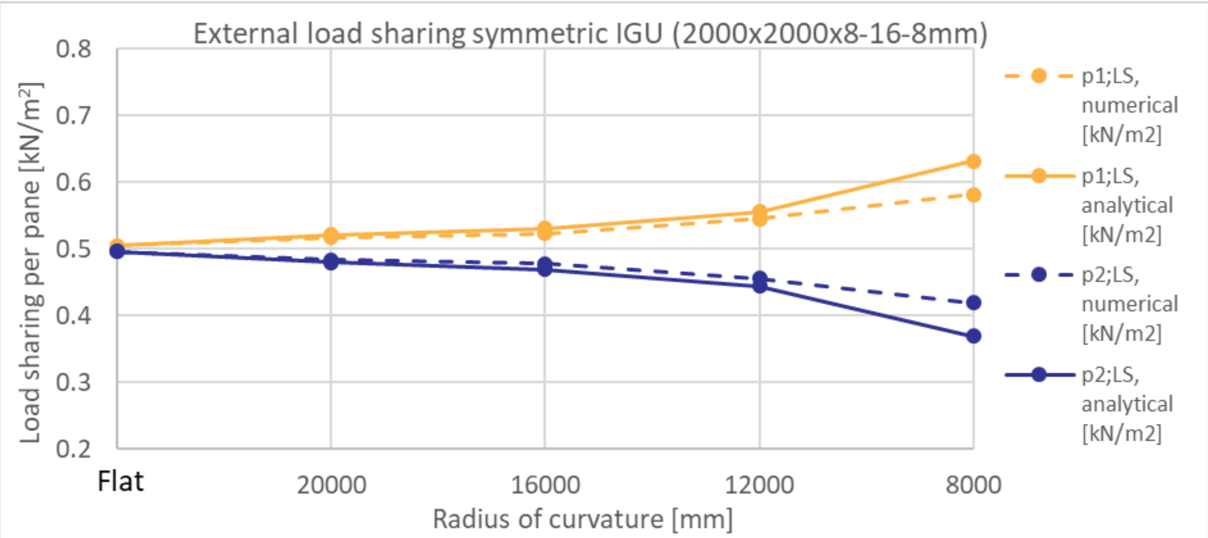

2000x2000x10-16-10

2000x2000x10-16-10					
Radius [mm]	p1;LS, numerical [kN/m2]	p2;LS, numerical [kN/m2]	p1;LS, analytical [kN/m2]	p2;LS, analytical [kN/m2]	Deviation p2;LS
24000	*0.509*	*0.491*	*0.509*	*0.491*	
20000	0.512	0.488	0.528	0.472	1.62%
16000	0.531	0.469	0.541	0.459	1.01%
12000	0.558	0.442	0.571	0.429	1.35%
8000	0.607	0.393	0.659	0.341	5.19%
				Average	**2.29%**

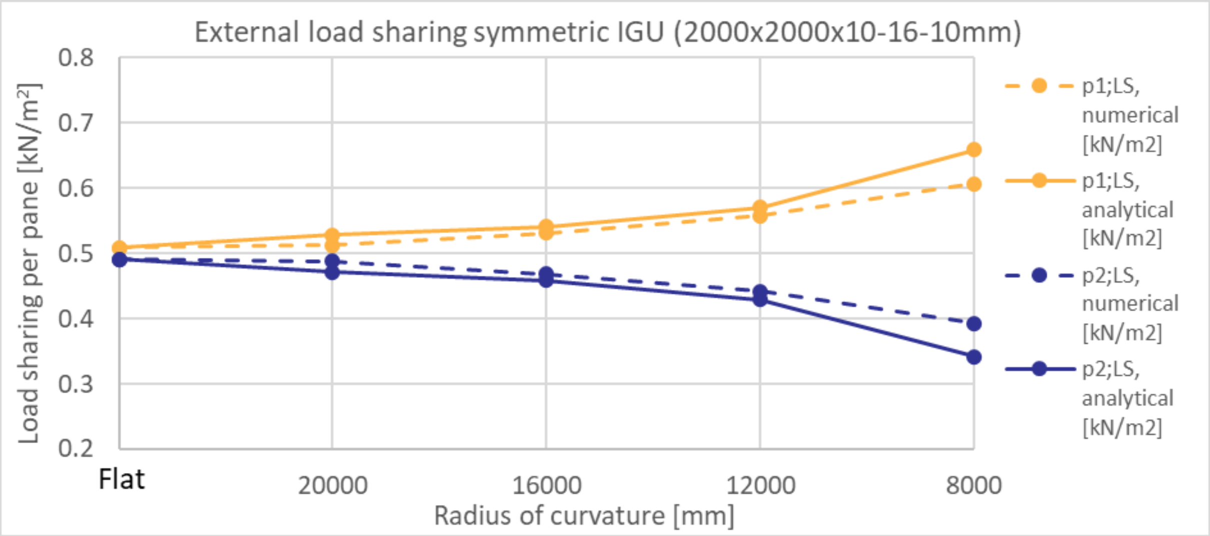

2000x2000x12-16-12

2000x2000x12-16-12					
Radius [mm]	p1;LS, numerical [kN/m2]	p2;LS, numerical [kN/m2]	p1;LS, analytical [kN/m2]	p2;LS, analytical [kN/m2]	Deviation p2;LS
24000	*0.515*	*0.485*	*0.515*	*0.485*	
20000	0.520	0.480	0.538	0.462	1.76%
16000	0.539	0.462	0.553	0.447	1.43%
12000	0.569	0.431	0.587	0.413	1.80%
8000	0.629	0.371	0.683	0.317	5.45%
				Average	**2.61%**

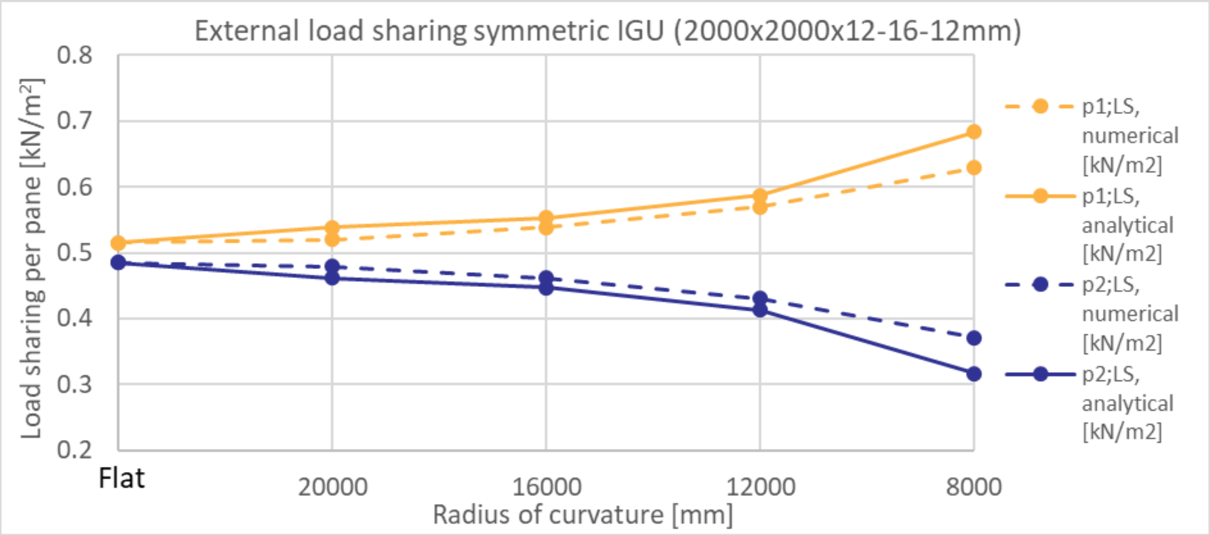

3000x3000x8-16-8

3000x3000x8-16-8					
Radius [mm]	p1;LS, numerical [kN/m2]	p2;LS, numerical [kN/m2]	p1;LS, analytical [kN/m2]	p2;LS, analytical [kN/m2]	Deviation p2;LS
24000	*0.501*	*0.499*	*0.501*	*0.499*	
20000	0.508	0.492	0.519	0.481	1.10%
16000	0.515	0.485	0.532	0.468	1.74%
12000	0.524	0.476	0.565	0.435	4.10%
8000	0.538	0.462	0.667	0.333	12.91%
				Average	**4.96%**

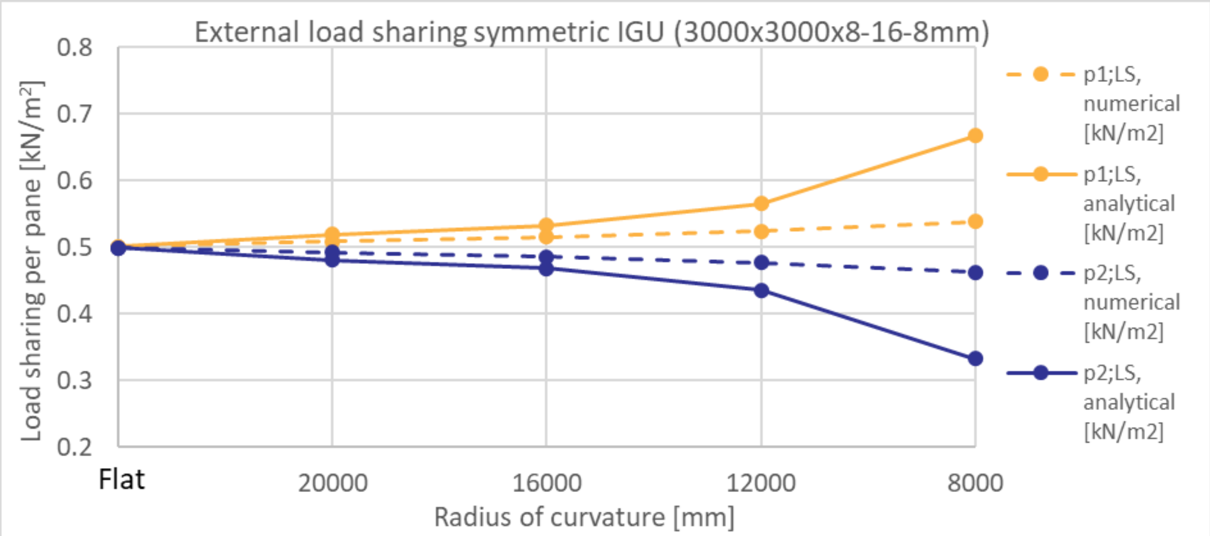

3000x3000x10-16-10

3000x3000x10-16-10					
Radius [mm]	p1;LS, numerical [kN/m2]	p2;LS, numerical [kN/m2]	p1;LS, analytical [kN/m2]	p2;LS, analytical [kN/m2]	Deviation p2;LS
24000	*0.502*	*0.498*	*0.502*	*0.498*	
20000	0.518	0.482	0.525	0.475	0.67%
16000	0.528	0.472	0.541	0.459	1.33%
12000	0.542	0.458	0.580	0.420	3.85%
8000	0.564	0.436	0.695	0.305	13.09%
				Average	**4.73%**

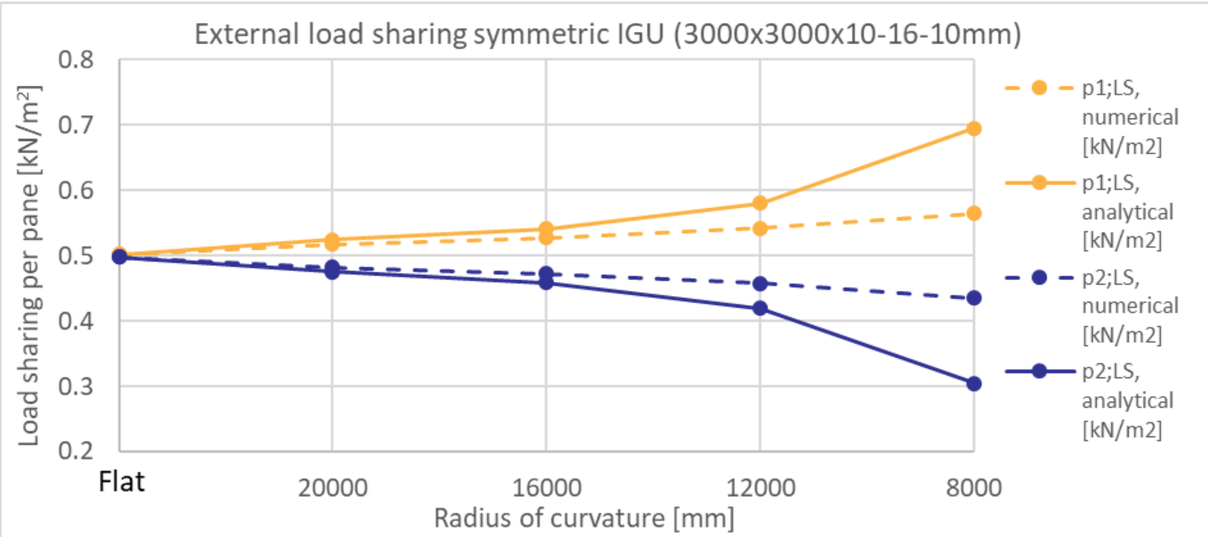

3000x3000x12-16-12

3000x3000x12-16-12					
Radius [mm]	p1;LS, numerical [kN/m2]	p2;LS, numerical [kN/m2]	p1;LS, analytical [kN/m2]	p2;LS, analytical [kN/m2]	Deviation p2;LS
24000	*0.503*	*0.497*	*0.503*	*0.497*	
20000	0.524	0.476	0.531	0.469	0.64%
16000	0.537	0.463	0.550	0.450	1.29%
12000	0.557	0.443	0.596	0.404	3.89%
8000	0.573	0.427	0.720	0.280	14.69%
				Average	**5.13%**

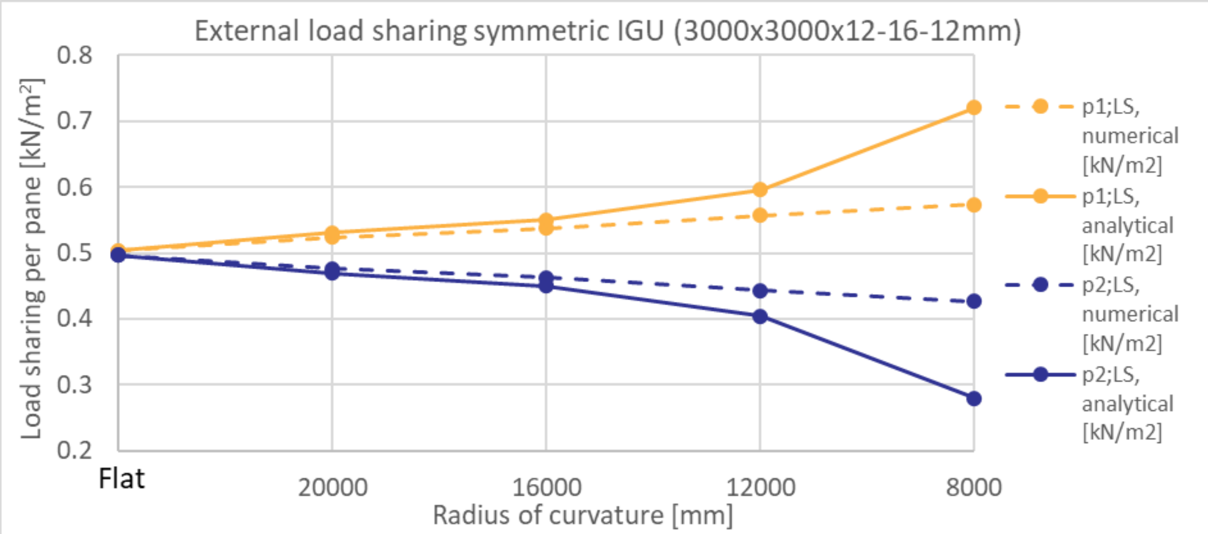

4000x3000x8-16-8

4000x3000x8-16-8					
Radius [mm]	p1;LS, numerical [kN/m2]	p2;LS, numerical [kN/m2]	p1;LS, analytical [kN/m2]	p2;LS, analytical [kN/m2]	Deviation p2;LS
24000	*0.501*	*0.499*	*0.501*	*0.499*	
20000	0.512	0.488	0.518	0.482	0.67%
16000	0.515	0.485	0.531	0.469	1.62%
12000	0.506	0.494	0.564	0.436	5.76%
8000	0.527	0.473	0.667	0.333	14.01%
				Average	**5.52%**

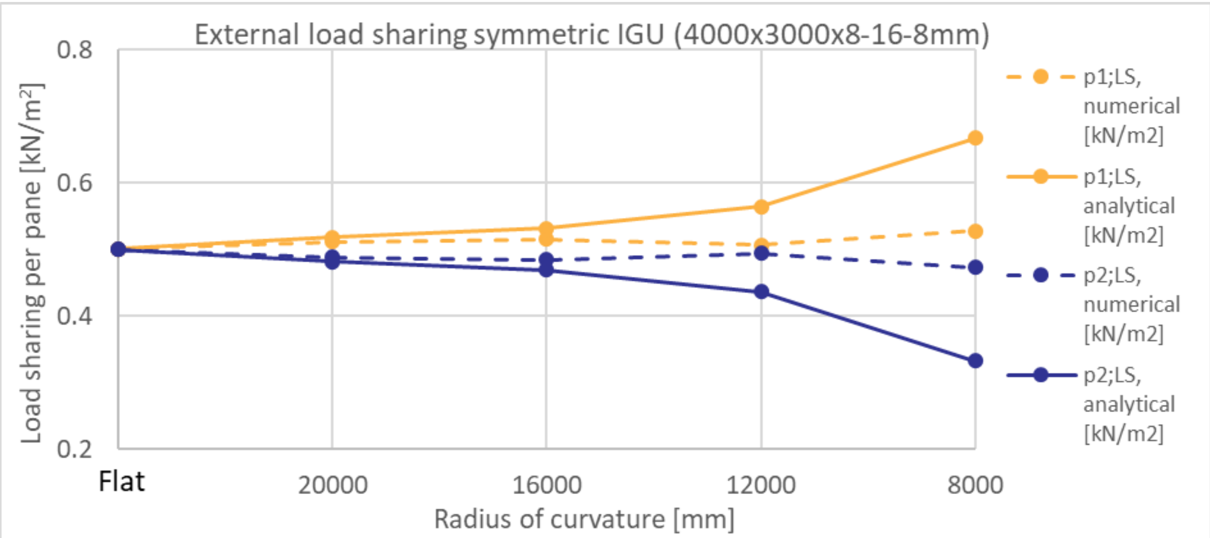

4000x3000x10-16-10

4000x3000x10-16-10					
Radius [mm]	p1;LS, numerical [kN/m2]	p2;LS, numerical [kN/m2]	p1;LS, analytical [kN/m2]	p2;LS, analytical [kN/m2]	Deviation p2;LS
24000	*0.501*	*0.499*	*0.501*	*0.499*	
20000	0.514	0.486	0.524	0.476	1.01%
16000	0.520	0.480	0.540	0.460	1.97%
12000	0.508	0.492	0.579	0.421	7.14%
8000	0.550	0.451	0.695	0.305	14.53%
				Average	**6.16%**

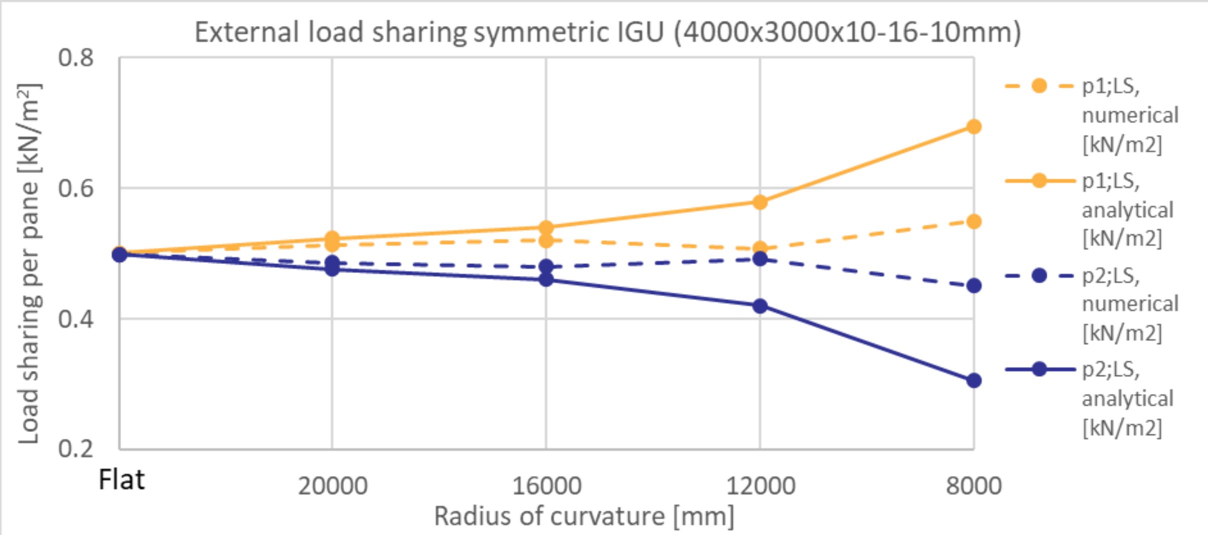

4000x3000x12-16-12

4000x3000x12-16-12					
Radius [mm]	p1;LS, numerical [kN/m2]	p2;LS, numerical [kN/m2]	p1;LS, analytical [kN/m2]	p2;LS, analytical [kN/m2]	Deviation p2;LS
24000	*0.502*	*0.498*	*0.502*	*0.498*	
20000	0.511	0.489	0.529	0.471	1.85%
16000	0.536	0.464	0.548	0.452	1.20%
12000	0.549	0.451	0.594	0.406	4.45%
8000	0.573	0.427	0.719	0.281	14.64%
				Average	**5.54%**

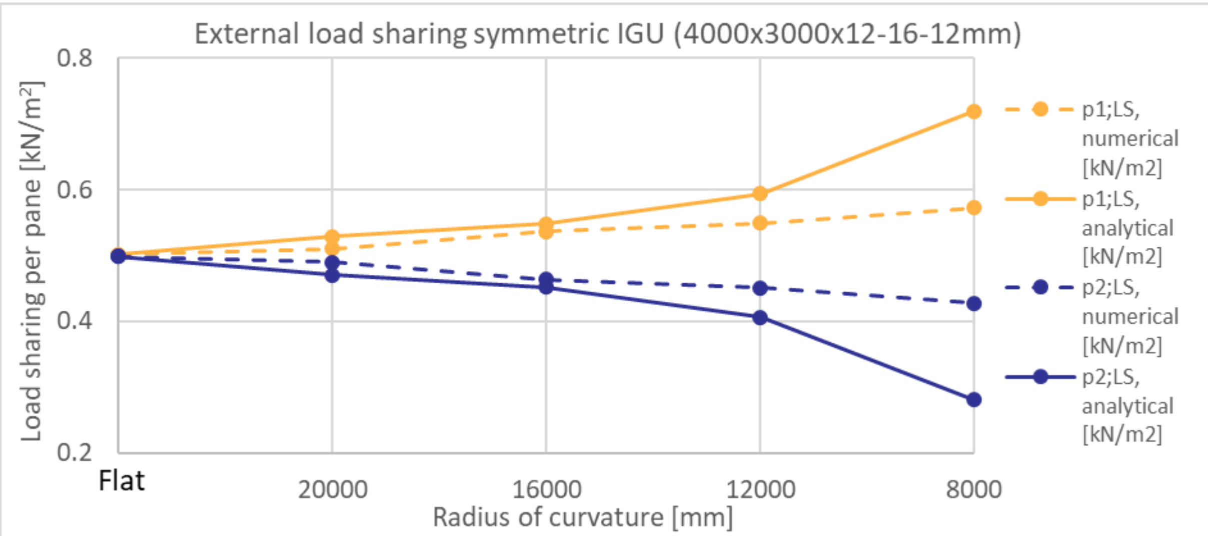

5000x3000x8-16-8

5000x3000x8-16-8					
Radius [mm]	p1;LS, numerical [kN/m2]	p2;LS, numerical [kN/m2]	p1;LS, analytical [kN/m2]	p2;LS, analytical [kN/m2]	Deviation p2;LS
24000	*0.500*	*0.500*	*0.500*	*0.500*	
20000	0.508	0.492	0.518	0.482	1.01%
16000	0.513	0.487	0.531	0.469	1.81%
12000	0.521	0.479	0.564	0.436	4.29%
8000	0.531	0.469	0.668	0.332	13.67%
				Average	**5.20%**

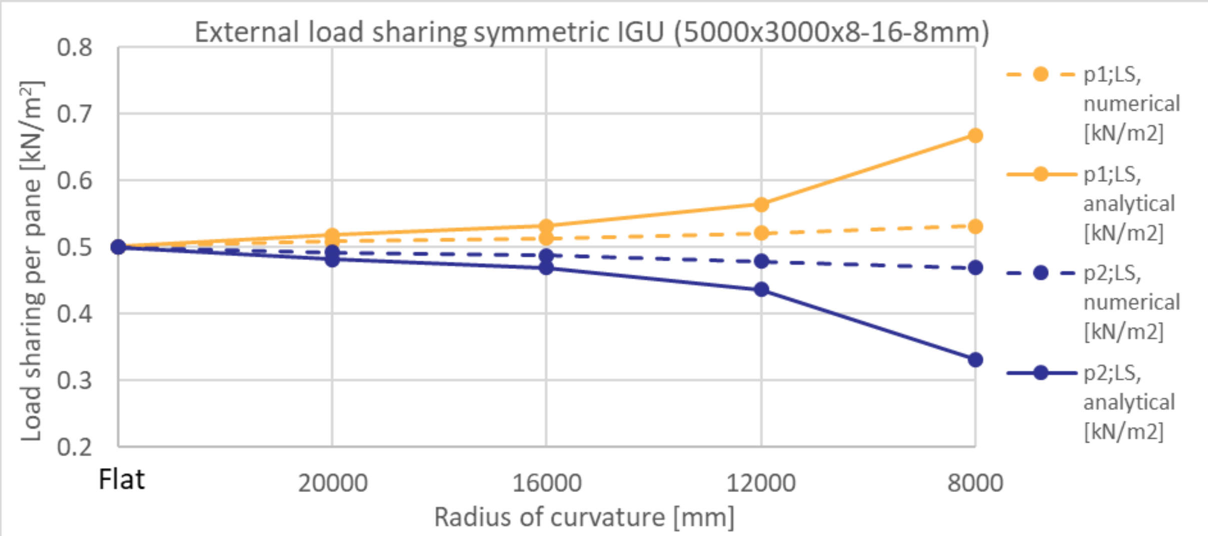

5000x3000x10-16-10

5000x3000x10-16-10					
Radius [mm]	p1;LS, numerical [kN/m2]	p2;LS, numerical [kN/m2]	p1;LS, analytical [kN/m2]	p2;LS, analytical [kN/m2]	Deviation p2;LS
24000	*0.501*	*0.499*	*0.501*	*0.499*	
20000	0.517	0.483	0.523	0.477	0.59%
16000	0.512	0.488	0.539	0.461	2.74%
12000	0.527	0.473	0.579	0.421	5.23%
8000	0.553	0.447	0.695	0.305	14.26%
				Average	**5.71%**

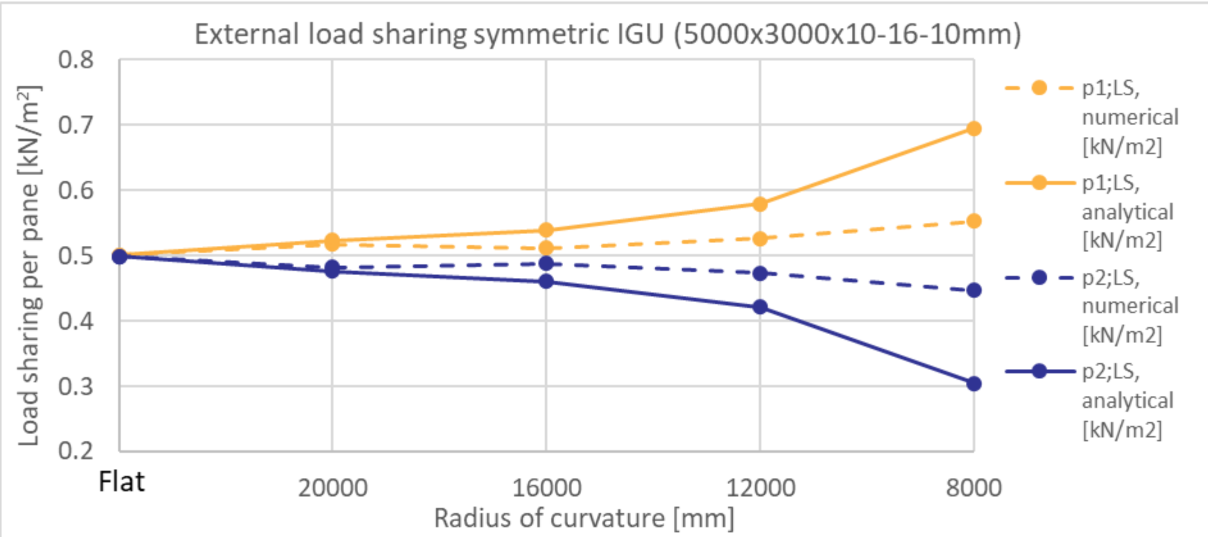

5000x3000x12-16-12

5000x3000x12-16-12					
Radius [mm]	p1;LS, numerical [kN/m2]	p2;LS, numerical [kN/m2]	p1;LS, analytical [kN/m2]	p2;LS, analytical [kN/m2]	Deviation p2;LS
24000	*0.501*	*0.499*	*0.501*	*0.499*	
20000	0.520	0.480	0.529	0.471	0.85%
16000	0.529	0.471	0.548	0.452	1.89%
12000	0.543	0.457	0.594	0.406	5.04%
8000	0.573	0.427	0.719	0.281	14.62%
				Average	**5.60%**

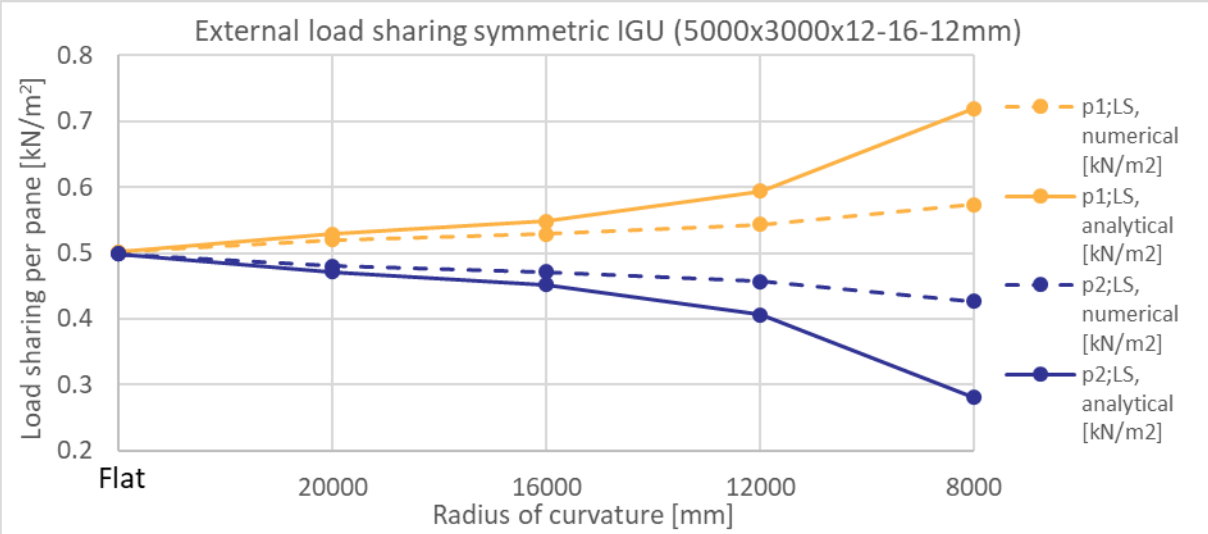

6000x3000x8-16-8

6000x3000x8-16-8					
Radius [mm]	p1;LS, numerical [kN/m2]	p2;LS, numerical [kN/m2]	p1;LS, analytical [kN/m2]	p2;LS, analytical [kN/m2]	Deviation p2;LS
24000	*0.500*	*0.500*	*50.04%*	*49.96%*	
20000	0.503	0.497	0.518	0.482	1.50%
16000	0.514	0.486	0.531	0.469	1.75%
12000	0.522	0.478	0.565	0.435	4.28%
8000	0.529	0.471	0.669	0.331	14.03%
				Average	**5.39%**

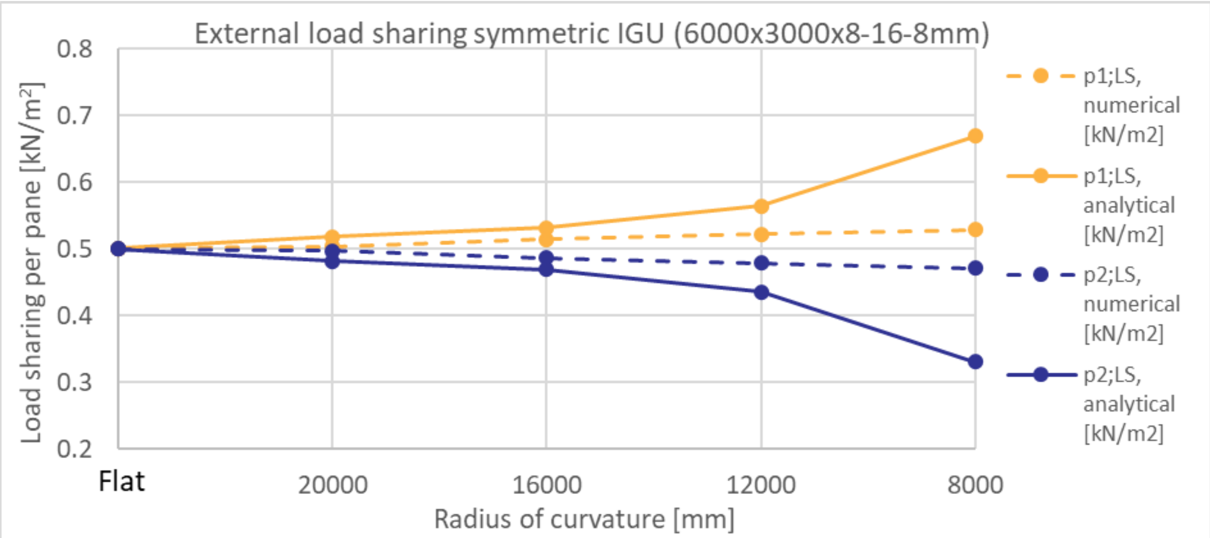

6000x3000x10-16-10

6000x3000x10-16-10					
Radius [mm]	p1;LS, numerical [kN/m2]	p2;LS, numerical [kN/m2]	p1;LS, analytical [kN/m2]	p2;LS, analytical [kN/m2]	Deviation p2;LS
24000	*0.501*	*0.499*	*0.501*	*0.499*	
20000	0.517	0.483	0.523	0.477	0.62%
16000	0.505	0.495	0.540	0.460	3.50%
12000	0.508	0.492	0.580	0.420	7.14%
8000	0.516	0.484	0.696	0.304	18.07%
				Average	**7.33%**

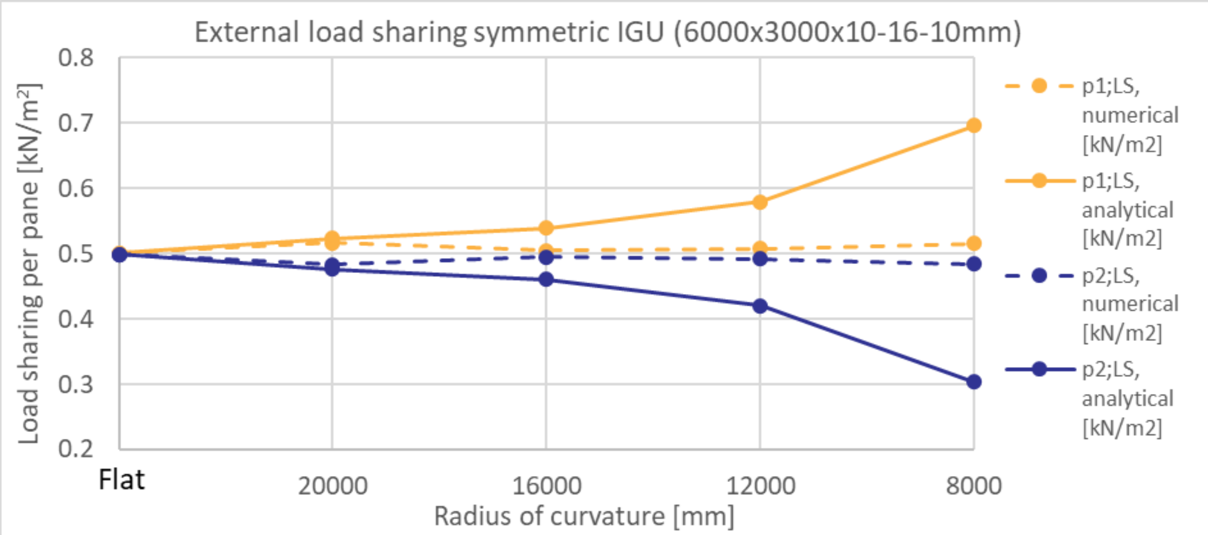

6000x3000x12-16-12

6000x3000x12-16-12					
Radius [mm]	p1;LS, numerical [kN/m2]	p2;LS, numerical [kN/m2]	p1;LS, analytical [kN/m2]	p2;LS, analytical [kN/m2]	Deviation p2;LS
24000	*0.501*	*0.499*	*0.501*	*0.499*	
20000	0.517	0.483	0.528	0.472	1.11%
16000	0.528	0.472	0.548	0.452	1.96%
12000	0.511	0.489	0.594	0.406	8.28%
8000	0.520	0.480	0.720	0.280	20.05%
				Average	**7.85%**

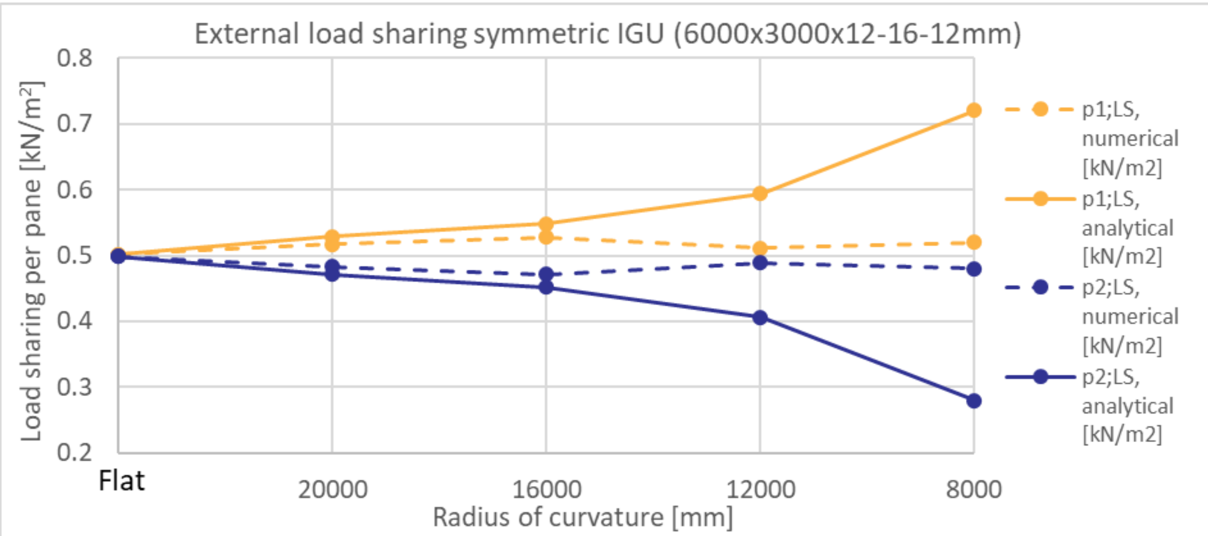

Case study Van Gogh

3600x1800x8-15-8					
Radius [mm]	p1;LS, numerical [kN/m2]	p2;LS, numerical [kN/m2]	p1;LS, analytical [kN/m2]	p2;LS, analytical [kN/m2]	Deviation p2;LS
Flat	*0.503*	*0.497*	*0.503*	*0.497*	
11500	0.543	0.457	0.553	0.447	0.94%

3600x1800x10-15-10					
Radius [mm]	p1;LS, numerical [kN/m2]	p2;LS, numerical [kN/m2]	p1;LS, analytical [kN/m2]	p2;LS, analytical [kN/m2]	Deviation p2;LS
Flat	*0.505*	*0.495*	*0.505*	*0.495*	
11500	0.569	0.431	0.566	0.434	0.28%

3600x1800x12-15-12					
Radius [mm]	p1;LS, numerical [kN/m2]	p2;LS, numerical [kN/m2]	p1;LS, analytical [kN/m2]	p2;LS, analytical [kN/m2]	Deviation p2;LS
Flat	*0.508*	*0.492*	*0.508*	*0.492*	
11500	0.595	0.405	0.580	0.420	1.45%

Case study Melle

5500x2500x14-15-14					
Radius [mm]	p1;LS, numerical [kN/m2]	p2;LS, numerical [kN/m2]	p1;LS, analytical [kN/m2]	p2;LS, analytical [kN/m2]	Deviation p2;LS
Flat	*0.503*	*0.497*	*0.503*	*0.497*	
28000	0.525	0.475	0.516	0.484	0.84%

5500x2500x16-15-16					
Radius [mm]	p1;LS, numerical [kN/m2]	p2;LS, numerical [kN/m2]	p1;LS, analytical [kN/m2]	p2;LS, analytical [kN/m2]	Deviation p2;LS
Flat	*0.505*	*0.495*	*0.503*	*0.497*	
28000	0.534	0.466	0.520	0.480	1.43%

5500x2500x18-15-18					
Radius [mm]	p1;LS, numerical [kN/m2]	p2;LS, numerical [kN/m2]	p1;LS, analytical [kN/m2]	p2;LS, analytical [kN/m2]	Deviation p2;LS
Flat	*0.507*	*0.493*	*0.507*	*0.493*	
28000	0.543	0.457	0.524	0.476	1.92%

C.3. Cavity pressure asymmetric IGU's

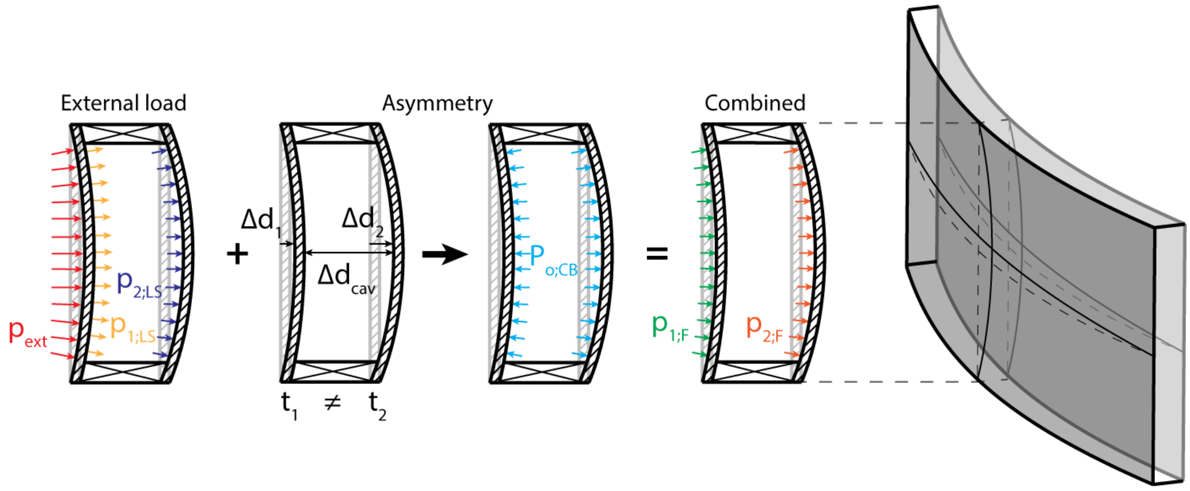

Overview deviations load sharing asymmetric IGU's, per plate size

Overview deviations load sharing asymmetric IGU's, per configuration							
	8-16-10	8-16-12	10-16-8	10-16-12	12-16-8	12-16-10	Average
1000x1000	4.00%	4.95%	1.35%	3.99%	1.17%	1.46%	**2.82%**
2000x2000	2.82%	3.49%	2.47%	2.31%	3.71%	3.08%	**2.98%**
3000x3000	8.52%	6.87%	2.32%	4.19%	2.10%	2.50%	**4.42%**
4000x3000	12.70%	19.45%	11.22%	24.49%	11.45%	18.62%	**16.32%**
5000x3000	10.31%	13.52%	4.06%	9.59%	5.30%	4.28%	**7.84%**
6000x3000	15.63%	13.01%	26.16%	16.97%	22.82%	11.72%	**17.72%**
Average	**9.00%**	**10.22%**	**7.93%**	**10.26%**	**7.76%**	**6.94%**	**8.68%**

Overview deviations isochoric pressure asymmetric IGU's, per configuration							
	8-16-10	8-16-12	10-16-8	10-16-12	12-16-8	12-16-10	Average
1000x1000	0.41%	5.92%	1.19%	10.23%	9.94%	11.13%	**6.47%**
2000x2000	9.91%	17.68%	10.61%	8.75%	20.96%	9.75%	**12.94%**
3000x3000	12.78%	25.97%	13.11%	13.11%	27.12%	13.56%	**17.61%**
4000x3000	2.28%	3.02%	2.28%	2.84%	3.63%	2.84%	**2.81%**
5000x3000	3.15%	8.79%	3.15%	6.56%	8.27%	6.48%	**6.07%**
6000x3000	1.17%	3.14%	1.17%	2.25%	3.14%	2.25%	**2.19%**
Average	**4.95%**	**10.75%**	**5.25%**	**7.29%**	**12.18%**	**7.67%**	**8.01%**

Overview deviations combined pressure asymmetric IGU's, per configuration							
	8-16-10	8-16-12	10-16-8	10-16-12	12-16-8	12-16-10	Average
1000x1000	3.63%	10.87%	0.33%	14.22%	9.60%	9.67%	**8.05%**
2000x2000	11.87%	19.87%	8.97%	10.15%	18.53%	7.23%	**12.77%**
3000x3000	21.31%	27.37%	12.11%	17.31%	27.86%	11.06%	**19.50%**
4000x3000	11.93%	19.50%	9.08%	24.96%	10.28%	19.09%	**15.81%**
5000x3000	7.17%	4.73%	5.91%	3.04%	8.59%	8.75%	**6.36%**
6000x3000	14.76%	12.20%	25.28%	17.44%	20.41%	9.98%	**16.68%**
Average	**11.78%**	**15.76%**	**10.28%**	**14.52%**	**15.88%**	**10.96%**	**13.20%**

Overview deviations load sharing asymmetric IGU's, per design radius

Overview deviations load sharing asymmetric IGU's, per design radius							
	1000x1000	2000x2000	3000x3000	4000x3000	5000x3000	6000x3000	Average
20000	1.59%	3.00%	1.11%	23.76%	5.77%	17.36%	**8.76%**
16000	2.17%	2.30%	2.42%	6.02%	5.30%	17.75%	**6.00%**
12000	3.06%	1.39%	4.84%	21.03%	6.09%	16.24%	**8.78%**
8000	4.46%	5.24%	9.30%	14.47%	14.22%	19.52%	**11.20%**
Average	**2.82%**	**2.98%**	**4.42%**	**16.32%**	**7.84%**	**17.72%**	**8.68%**

Overview deviations isochoric pressure asymmetric IGU's, per design radius							
	1000x1000	2000x2000	3000x3000	4000x3000	5000x3000	6000x3000	Average
20000	1.80%	1.34%	1.81%	3.11%	2.00%	1.25%	**1.89%**
16000	3.53%	4.34%	4.46%	0.70%	2.99%	2.25%	**3.05%**
12000	6.47%	12.55%	13.25%	5.12%	4.65%	0.63%	**7.11%**
8000	14.07%	33.53%	50.91%	2.32%	14.63%	4.62%	**20.01%**
Average	**6.47%**	**12.94%**	**17.61%**	**2.81%**	**6.07%**	**2.19%**	**8.01%**

Overview deviations combined pressure asymmetric IGU's, per design radius							
	1000x1000	2000x2000	3000x3000	4000x3000	5000x3000	6000x3000	Average
20000	3.27%	1.66%	2.83%	20.64%	3.77%	16.60%	**8.13%**
16000	5.49%	2.05%	6.88%	5.76%	2.79%	16.05%	**6.50%**
12000	8.87%	11.91%	17.59%	22.42%	4.91%	16.19%	**13.65%**
8000	14.57%	35.46%	50.71%	14.40%	13.98%	17.87%	**24.50%**
Average	**8.05%**	**12.77%**	**19.50%**	**15.81%**	**6.36%**	**16.68%**	**13.20%**

Deviation case study asymmetric Van Gogh

Deviation case study load sharing asymmetric Van Gogh							
	8-15-10	8-15-12	10-15-8	10-15-12	12-15-8	12-15-10	Average
3600x1800, R=11500	3.78%	5.51%	2.97%	1.99%	5.33%	3.27%	3.81%

Deviation case study isochoric pressure asymmetric Van Gogh							
	8-15-10	8-15-12	10-15-8	10-15-12	12-15-8	12-15-10	Average
3600x1800, R=11500	3.13%	8.47%	2.53%	6.93%	6.87%	6.23%	5.69%

Deviation case study combined pressure asymmetric Van Gogh							
	8-15-10	8-15-12	10-15-8	10-15-12	12-15-8	12-15-10	Average
3600x1800, R=11500	0.65%	2.95%	0.44%	4.94%	1.53%	2.96%	2.24%

Deviation case study asymmetric Melle

Deviation case study load sharing asymmetric Melle							
	14-15-16	14-15-18	16-15-14	16-15-18	18-15-14	18-15-16	Average
5500x2500, R=28000	0.23%	0.20%	2.53%	1.30%	2.87%	2.28%	1.57%

Deviation case study isochoric pressure asymmetric Melle							
	14-15-16	14-15-18	16-15-14	16-15-18	18-15-14	18-15-16	Average
5500x2500, R=28000	4.52%	10.08%	4.52%	5.85%	9.78%	5.85%	6.77%

Deviation case study combined pressure asymmetric Melle							
	14-15-16	14-15-18	16-15-14	16-15-18	18-15-14	18-15-16	Average
5500x2500, R=28000	4.75%	9.88%	2.00%	7.16%	6.91%	3.57%	5.71%

1000x1000x8-16-10

1000x1000x8-16-10, pressures in kN/m2														
	p1;LS, numerical	p2;LS, numerical	p2;CB, numerical	p1;F, numerical	p2;F, numerical	p1;LS, analytical	p2;LS, analytical	p2;CB, analytical	p1;F, analytical	p2;F, analytical		deviation p2;LS	deviation P'CB	deviation p2;F
24000	*0.447*	*0.553*	*0.000*	*0.447*	*0.553*	*0.447*	*0.553*	*0.000*	*0.447*	*0.553*		-	-	-
20000	0.445	0.556	-0.047	0.492	0.509	0.473	0.527	-0.047	0.520	0.480		2.92%	0.02%	2.90%
16000	0.448	0.552	-0.093	0.541	0.459	0.487	0.513	-0.094	0.581	0.419		3.90%	0.07%	3.97%
12000	0.467	0.533	-0.225	0.692	0.308	0.516	0.484	-0.219	0.735	0.265		4.91%	0.59%	4.32%
8000	0.543	0.456	-0.716	1.259	-0.260	0.586	0.414	-0.707	1.293	-0.293		4.26%	0.94%	3.31%
											Avg.	**4.00%**	**0.41%**	**3.63%**

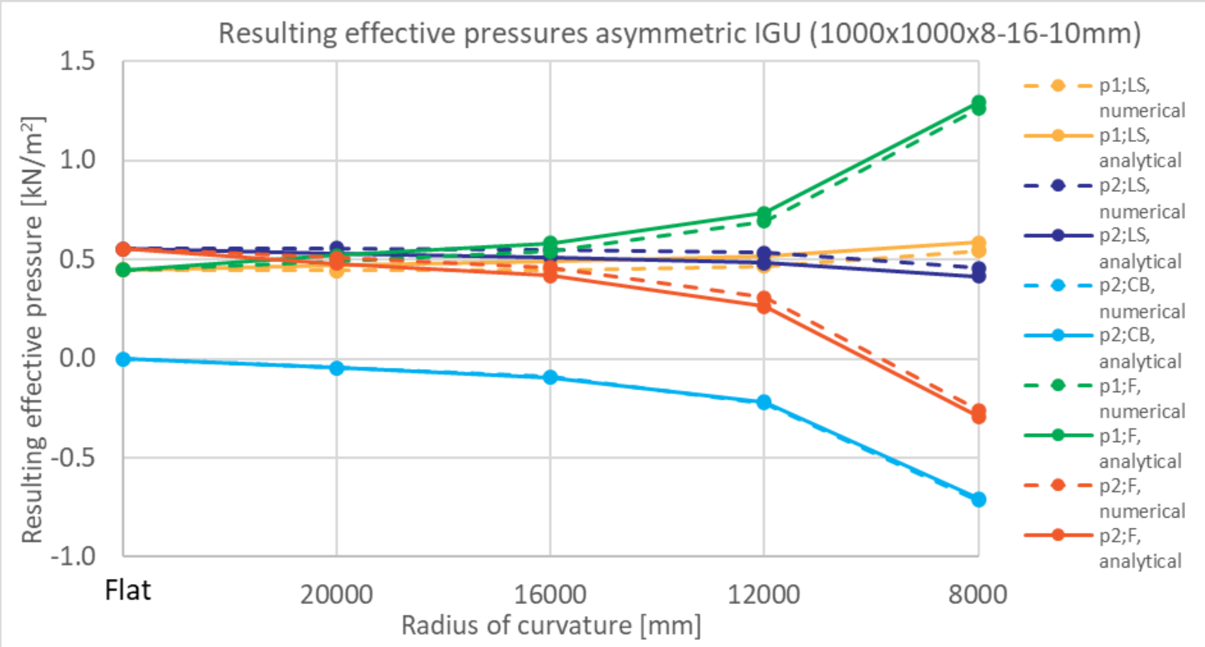

1000x1000x8-16-12

1000x1000x8-16-12, pressures in kN/m2														
	p1;LS, numerical	p2;LS, numerical	p2;CB, numerical	p1;F, numerical	p2;F, numerical	p1;LS, analytical	p2;LS, analytical	p2;CB, analytical	p1;F, analytical	p2;F, analytical		deviation p2;LS	deviation P'CB	deviation p2;F
24000	*0.372*	*0.628*	*0.000*	*0.372*	*0.628*	*0.372*	*0.628*	*0.000*	*0.372*	*0.628*		-	-	-
20000	0.370	0.630	-0.085	0.455	0.545	0.404	0.596	-0.107	0.511	0.489		3.41%	2.20%	5.61%
16000	0.375	0.625	-0.169	0.544	0.456	0.423	0.577	-0.212	0.635	0.365		4.76%	4.33%	9.10%
12000	0.397	0.603	-0.422	0.819	0.181	0.459	0.541	-0.489	0.949	0.051		6.25%	6.74%	12.99%
8000	0.493	0.506	-1.439	1.932	-0.933	0.548	0.452	-1.543	2.091	-1.091		5.38%	10.40%	15.77%
											Avg.	**4.95%**	**5.92%**	**10.87%**

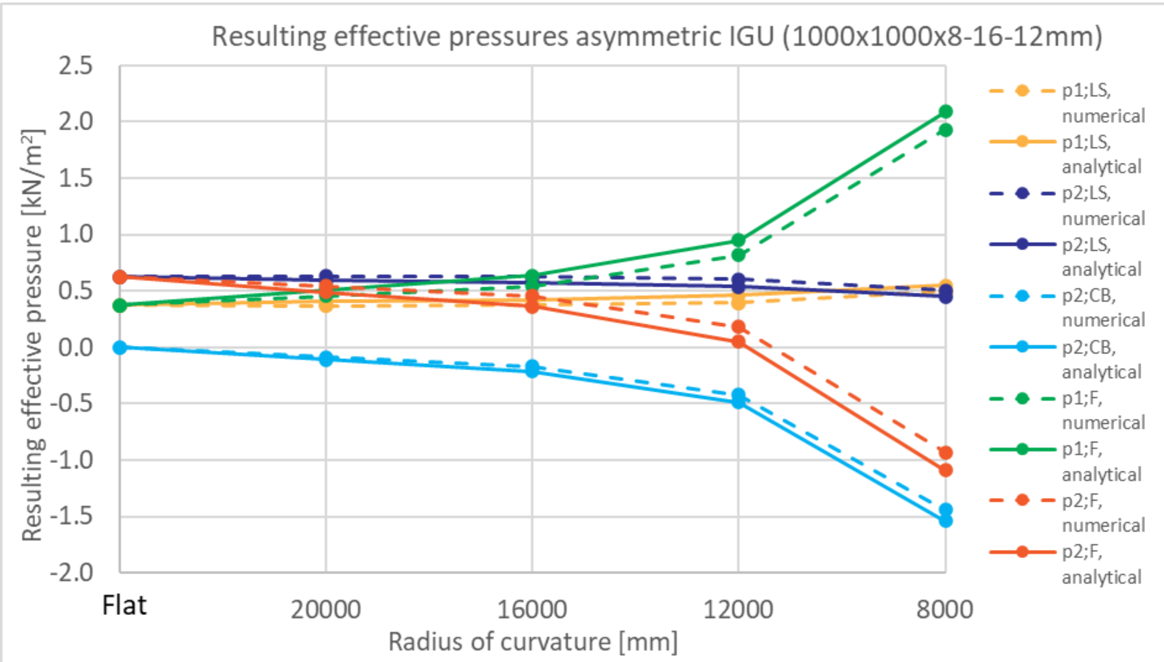

1000x1000x10-16-8

1000x1000x10-16-8, pressures in kN/m2															
	p1;LS, numerical	p2;LS, numerical	p2;CB, numerical	p1;F, numerical	p2;F, numerical		p1;LS, analytical	p2;LS, analytical	p2;CB, analytical	p1;F, analytical	p2;F, analytical		deviation p2;LS	deviation P'CB	deviation p2;F
24000	*0.717*	*0.283*	*0.000*	*0.717*	*0.283*		*0.717*	*0.283*	*0.000*	*0.717*	*0.283*		-	-	-
20000	0.713	0.286	0.047	0.666	0.333		0.712	0.288	0.047	0.666	0.334		0.16%	0.02%	0.14%
16000	0.711	0.289	0.093	0.618	0.382		0.712	0.288	0.094	0.618	0.382		0.05%	0.07%	0.03%
12000	0.703	0.298	0.217	0.486	0.515		0.713	0.287	0.219	0.494	0.506		1.05%	0.21%	0.84%
8000	0.687	0.313	0.662	0.025	0.975		0.728	0.272	0.707	0.022	0.978		4.14%	4.46%	0.32%
												Avg.	**1.35%**	**1.19%**	**0.33%**

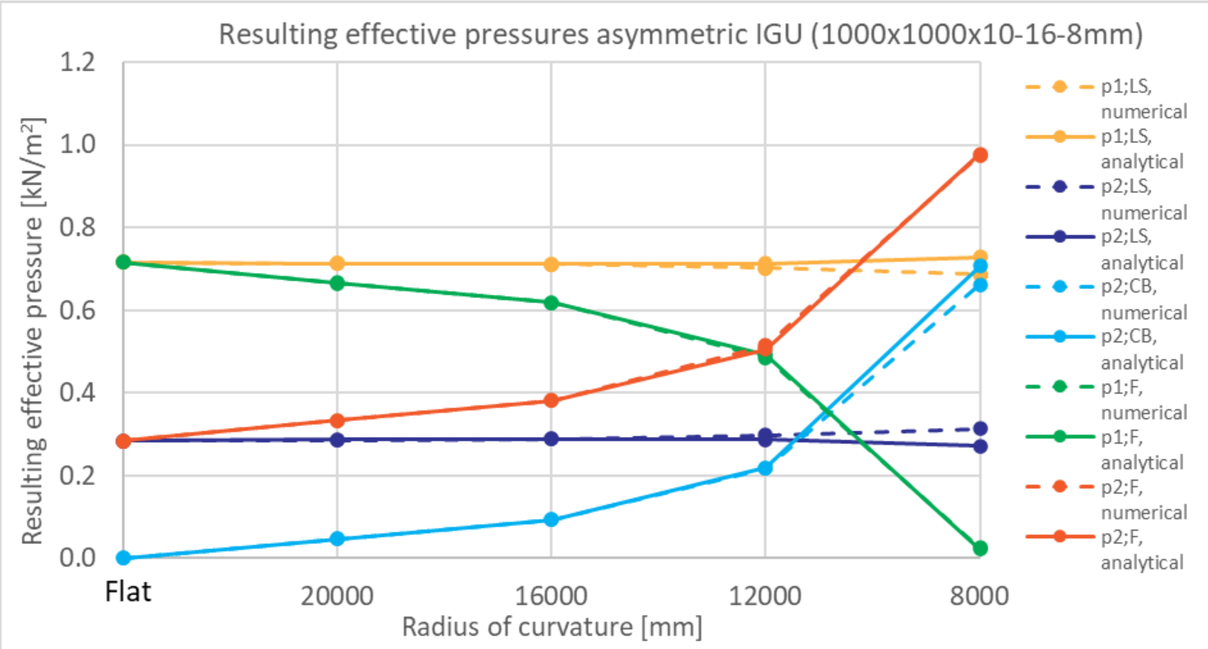

1000x1000x10-16-12

1000x1000x10-16-12, pressures in kN/m2															
	p1;LS, numerical	p2;LS, numerical	p2;CB, numerical	p1;F, numerical	p2;F, numerical		p1;LS, analytical	p2;LS, analytical	p2;CB, analytical	p1;F, analytical	p2;F, analytical		deviation p2;LS	deviation P'CB	deviation p2;F
24000	*0.536*	*0.464*	*0.000*	*0.536*	*0.464*		*0.536*	*0.464*	*0.000*	*0.536*	*0.464*		-	-	-
20000	0.534	0.466	-0.048	0.582	0.418		0.555	0.445	-0.080	0.634	0.366		2.10%	3.18%	5.28%
16000	0.535	0.465	-0.093	0.628	0.372		0.566	0.434	-0.153	0.719	0.281		3.04%	6.02%	9.06%
12000	0.543	0.458	-0.225	0.768	0.233		0.589	0.411	-0.334	0.923	0.077		4.65%	10.93%	15.58%
8000	0.588	0.413	-0.756	1.344	-0.343		0.648	0.352	-0.964	1.612	-0.612		6.17%	20.77%	26.94%
												Avg.	**3.99%**	**10.23%**	**14.22%**

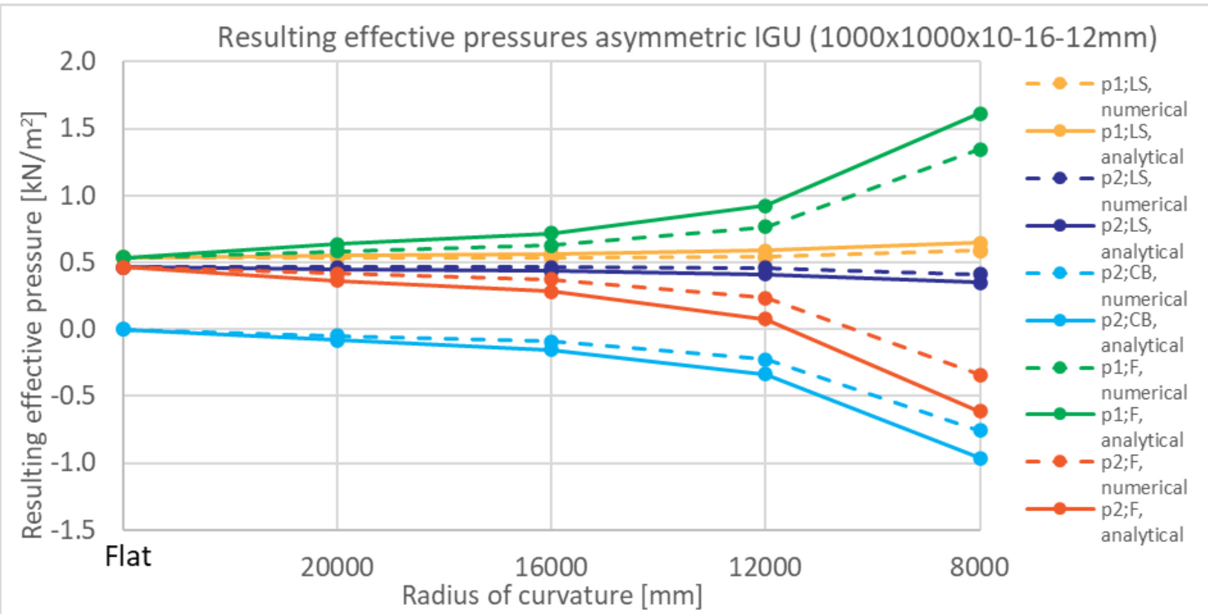

1000x1000x12-16-8

1000x1000x12-16-8, pressures in kN/m2															
	p1;LS, numerical	p2;LS, numerical	p2;CB, numerical	p1;F, numerical	p2;F, numerical		p1;LS, analytical	p2;LS, analytical	p2;CB, analytical	p1;F, analytical	p2;F, analytical		deviation p2;LS	deviation P'CB	deviation p2;F
24000	*0.814*	*0.186*	*0.000*	*0.814*	*0.186*		*0.814*	*0.186*	*0.000*	*0.814*	*0.186*		-	-	-
20000	0.812	0.189	0.085	0.727	0.274		0.805	0.195	0.107	0.698	0.302		0.62%	2.20%	2.83%
16000	0.809	0.191	0.166	0.643	0.357		0.802	0.198	0.212	0.589	0.411		0.71%	4.63%	5.34%
12000	0.800	0.200	0.398	0.402	0.598		0.797	0.203	0.489	0.307	0.693		0.32%	9.14%	9.46%
8000	0.766	0.234	1.305	-0.539	1.539		0.797	0.203	1.543	-0.746	1.746		3.04%	23.80%	20.76%
												Avg.	**1.17%**	**9.94%**	**9.60%**

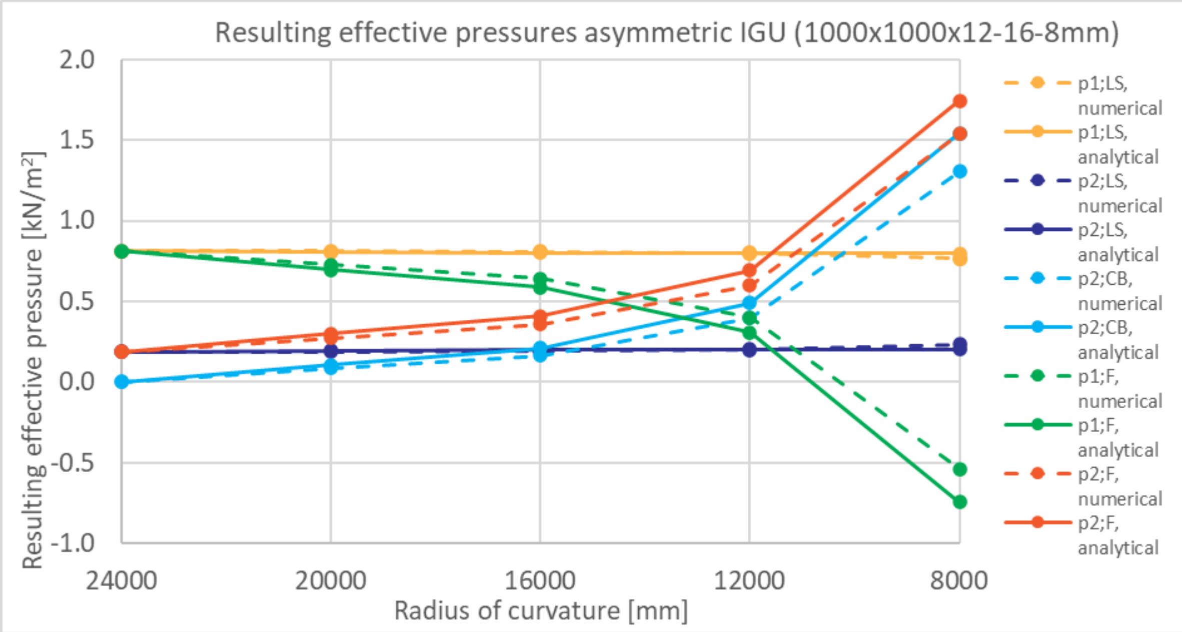

1000x1000x12-16-10

1000x1000x12-16-10, pressures in kN/m2															
	p1;LS, numerical	p2;LS, numerical	p2;CB, numerical	p1;F, numerical	p2;F, numerical		p1;LS, analytical	p2;LS, analytical	p2;CB, analytical	p1;F, analytical	p2;F, analytical		deviation p2;LS	deviation P'CB	deviation p2;F
24000	*0.731*	*0.269*	*0.000*	*0.731*	*0.269*		*0.731*	*0.269*	*0.000*	*0.731*	*0.269*		-	-	-
20000	0.730	0.270	0.048	0.682	0.318		0.733	0.267	0.080	0.653	0.347		0.31%	3.18%	2.87%
16000	0.729	0.271	0.093	0.636	0.364		0.735	0.265	0.153	0.581	0.419		0.56%	6.02%	5.46%
12000	0.727	0.273	0.222	0.505	0.495		0.739	0.261	0.334	0.405	0.595		1.21%	11.23%	10.02%
8000	0.722	0.278	0.723	-0.001	1.001		0.759	0.241	0.964	-0.204	1.204		3.75%	24.07%	20.32%
												Avg.	**1.46%**	**11.13%**	**9.67%**

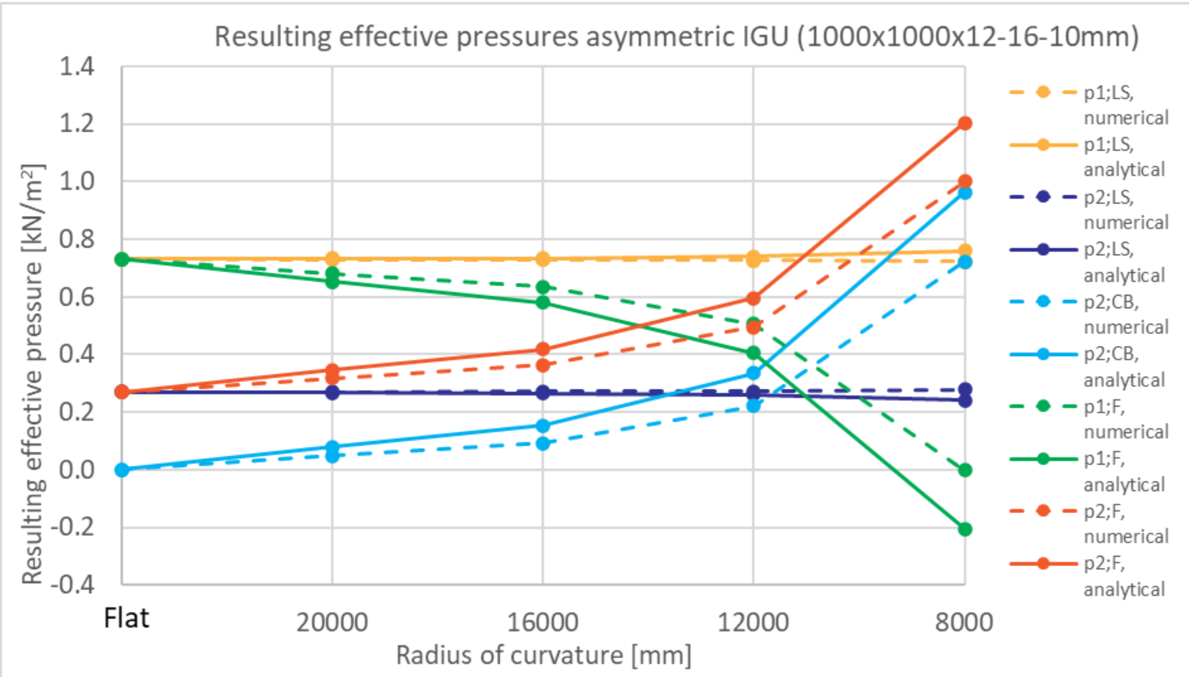

2000x2000x8-16-10

2000x2000x8-16-10, pressures in kN/m2														
	p1;LS, numerical	p2;LS, numerical	p2;CB, numerical	p1;F, numerical	p2;F, numerical		p1;LS, analytical	p2;LS, analytical	p2;CB, analytical	p1;F, analytical	p2;F, analytical		deviation p2;LS	deviation P'CB	deviation p2;F
24000	*0.347*	*0.653*	*0.000*	*0.347*	*0.653*		*0.347*	*0.653*	*0.000*	*0.347*	*0.653*		-	-	-
20000	0.464	0.536	-0.119	0.583	0.417		0.443	0.557	-0.125	0.568	0.432		2.09%	0.55%	1.54%
16000	0.476	0.524	-0.164	0.640	0.360		0.464	0.536	-0.197	0.662	0.338		1.16%	3.34%	2.18%
12000	0.492	0.508	-0.241	0.733	0.267		0.501	0.499	-0.341	0.842	0.158		0.89%	9.96%	10.85%
8000	0.525	0.475	-0.377	0.902	0.098		0.596	0.404	-0.635	1.231	-0.231		7.14%	25.77%	32.91%
												Avg.	**2.82%**	**9.91%**	**11.87%**

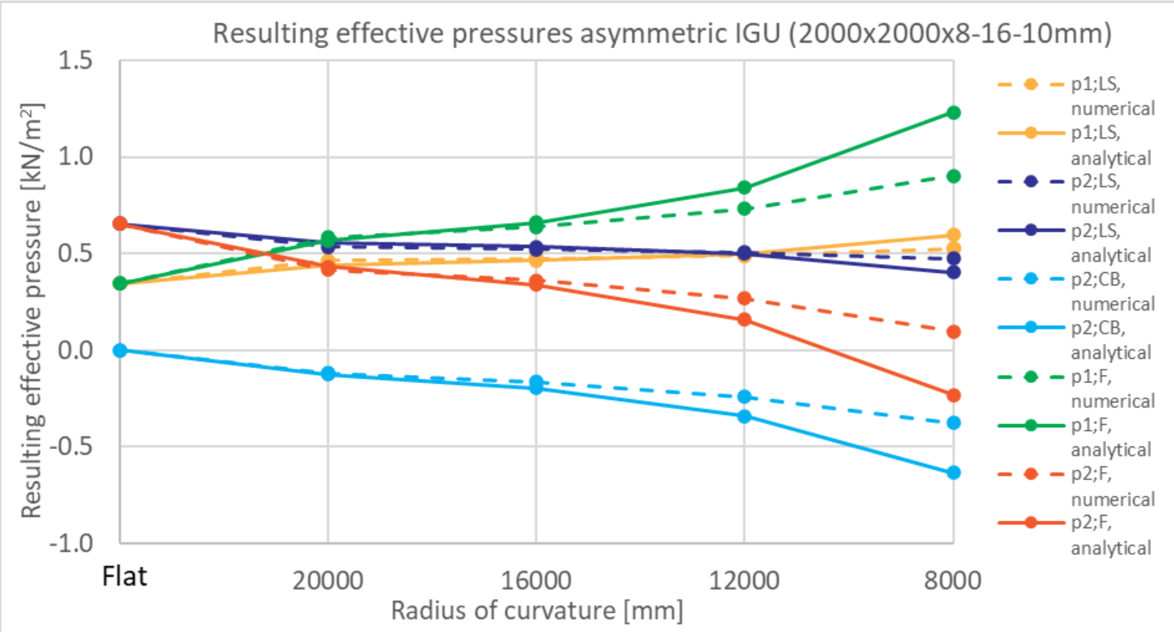

2000x2000x8-16-12

2000x2000x8-16-12, pressures in kN/m2														
	p1;LS, numerical	p2;LS, numerical	p2;CB, numerical	p1;F, numerical	p2;F, numerical		p1;LS, analytical	p2;LS, analytical	p2;CB, analytical	p1;F, analytical	p2;F, analytical		deviation p2;LS	deviation P'CB	deviation p2;F
24000	*0.239*	*0.761*	*0.000*	*0.239*	*0.761*		*0.239*	*0.761*	*0.000*	*0.239*	*0.761*		-	-	-
20000	0.407	0.592	-0.267	0.674	0.325		0.378	0.622	-0.268	0.646	0.354		2.97%	0.14%	2.83%
16000	0.433	0.566	-0.377	0.810	0.189		0.409	0.591	-0.424	0.833	0.167		2.48%	4.74%	2.26%
12000	0.453	0.547	-0.562	1.015	-0.015		0.457	0.543	-0.733	1.191	-0.191		0.43%	17.12%	17.55%
8000	0.488	0.511	-0.888	1.376	-0.377		0.570	0.430	-1.375	1.945	-0.945		8.09%	48.74%	56.83%
												Avg.	**3.49%**	**17.68%**	**19.87%**

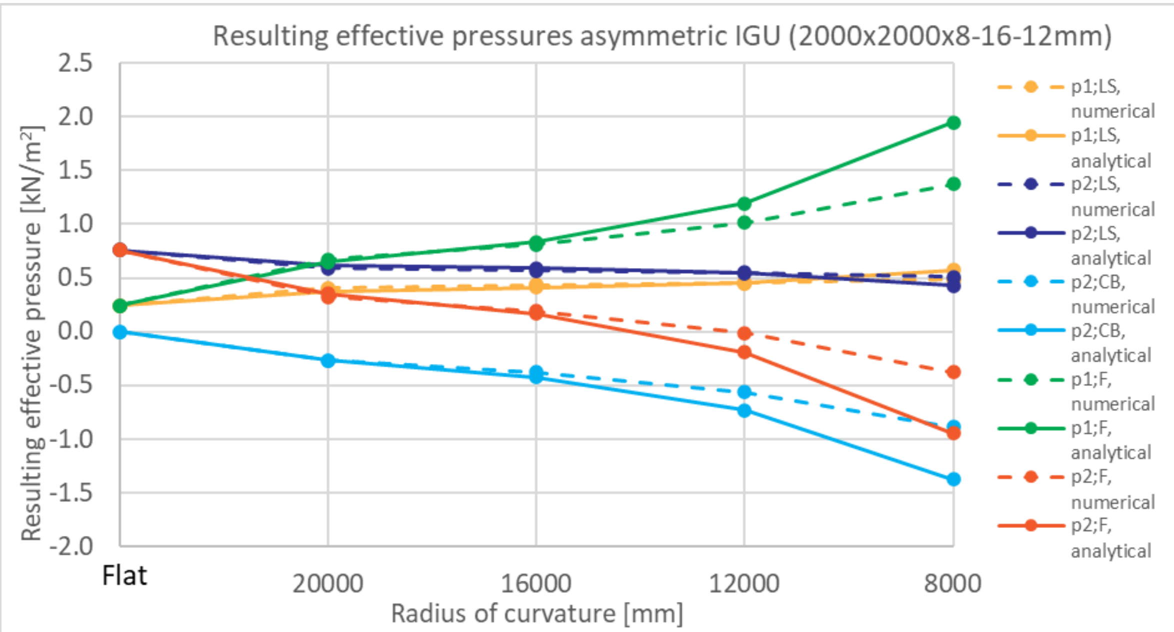

2000x2000x10-16-8

2000x2000x10-16-8, pressures in kN/m2															
	p1;LS, numerical	p2;LS, numerical	p2;CB, numerical	p1;F, numerical	p2;F, numerical		p1;LS, analytical	p2;LS, analytical	p2;CB, analytical	p1;F, analytical	p2;F, analytical		deviation p2;LS	deviation P'CB	deviation p2;F
24000	*0.665*	*0.335*	*0.000*	*0.665*	*0.335*		*0.665*	*0.335*	*0.000*	*0.665*	*0.335*		-	-	-
20000	0.573	0.427	0.110	0.463	0.537		0.605	0.395	0.125	0.480	0.520		3.12%	1.45%	1.67%
16000	0.584	0.415	0.158	0.426	0.573		0.607	0.393	0.197	0.409	0.591		2.13%	3.94%	1.81%
12000	0.609	0.391	0.235	0.374	0.626		0.624	0.376	0.341	0.283	0.717		1.51%	10.56%	9.05%
8000	0.659	0.341	0.370	0.289	0.711		0.691	0.309	0.635	0.056	0.944		3.13%	26.47%	23.34%
												Avg.	**2.47%**	**10.61%**	**8.97%**

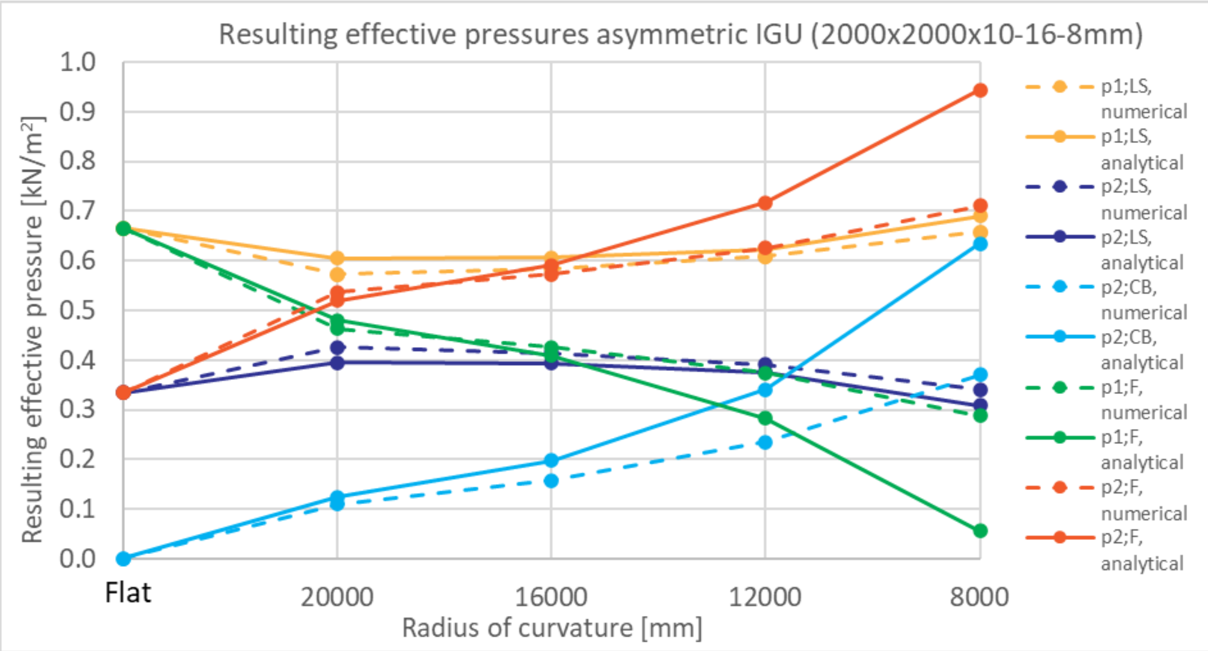

2000x2000x10-16-12

2000x2000x10-16-12, pressures in kN/m2															
	p1;LS, numerical	p2;LS, numerical	p2;CB, numerical	p1;F, numerical	p2;F, numerical		p1;LS, analytical	p2;LS, analytical	p2;CB, analytical	p1;F, analytical	p2;F, analytical		deviation p2;LS	deviation P'CB	deviation p2;F
24000	*0.381*	*0.619*	*0.000*	*0.381*	*0.619*		*0.381*	*0.619*	*0.000*	*0.381*	*0.619*		-	-	-
20000	0.473	0.527	-0.150	0.623	0.377		0.461	0.539	-0.159	0.620	0.380		1.15%	0.87%	0.27%
16000	0.495	0.506	-0.222	0.717	0.284		0.485	0.515	-0.247	0.732	0.268		0.96%	2.50%	1.54%
12000	0.519	0.481	-0.341	0.860	0.140		0.528	0.472	-0.423	0.951	0.049		0.90%	8.24%	9.14%
8000	0.571	0.429	-0.562	1.133	-0.133		0.634	0.366	-0.796	1.430	-0.430		6.26%	23.39%	29.65%
												Avg.	**2.31%**	**8.75%**	**10.15%**

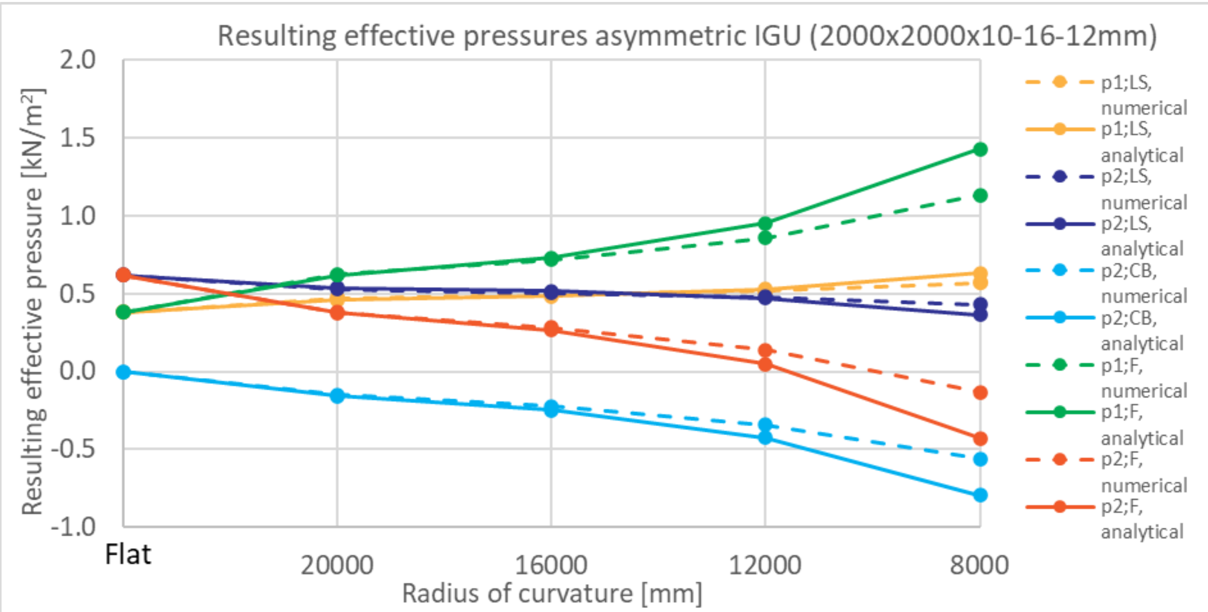

2000x2000x12-16-8

2000x2000x12-16-8, pressures in kN/m2														
	p1;LS, numerical	p2;LS, numerical	p2;CB, numerical	p1;F, numerical	p2;F, numerical	p1;LS, analytical	p2;LS, analytical	p2;CB, analytical	p1;F, analytical	p2;F, analytical		deviation p2;LS	deviation P'CB	deviation p2;F
24000	*0.775*	*0.225*	*0.000*	*0.775*	*0.225*	*0.775*	*0.225*	*0.000*	*0.775*	*0.225*		-	-	-
20000	0.618	0.383	0.236	0.382	0.619	0.675	0.325	0.268	0.407	0.593		5.81%	3.24%	2.57%
16000	0.627	0.374	0.346	0.281	0.720	0.669	0.331	0.424	0.245	0.755		4.34%	7.84%	3.50%
12000	0.656	0.344	0.531	0.125	0.875	0.678	0.322	0.733	-0.055	1.055		2.20%	20.22%	18.02%
8000	0.711	0.289	0.850	-0.140	1.139	0.736	0.264	1.375	-0.639	1.639		2.50%	52.54%	50.04%
											Avg.	**3.71%**	**20.96%**	**18.53%**

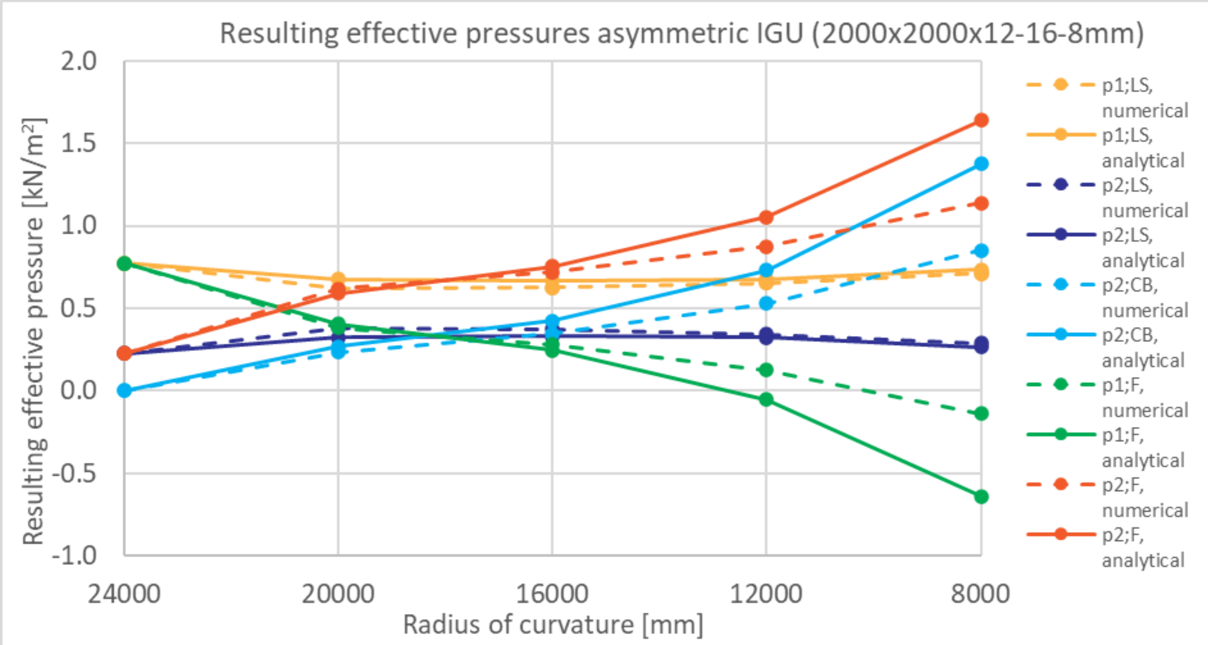

2000x2000x12-16-10

2000x2000x12-16-10, pressures in kN/m2														
	p1;LS, numerical	p2;LS, numerical	p2;CB, numerical	p1;F, numerical	p2;F, numerical	p1;LS, analytical	p2;LS, analytical	p2;CB, analytical	p1;F, analytical	p2;F, analytical		deviation p2;LS	deviation P'CB	deviation p2;F
24000	*0.642*	*0.358*	*0.000*	*0.642*	*0.358*	*0.642*	*0.358*	*0.000*	*0.642*	*0.358*		-	-	-
20000	0.575	0.425	0.141	0.434	0.566	0.604	0.396	0.159	0.445	0.555		2.89%	1.77%	1.11%
16000	0.580	0.420	0.210	0.370	0.630	0.608	0.392	0.247	0.361	0.639		2.71%	3.70%	0.99%
12000	0.605	0.395	0.331	0.274	0.726	0.629	0.371	0.423	0.205	0.795		2.40%	9.24%	6.83%
8000	0.663	0.337	0.553	0.110	0.890	0.706	0.294	0.796	-0.089	1.089		4.31%	24.29%	19.98%
											Avg.	**3.08%**	**9.75%**	**7.23%**

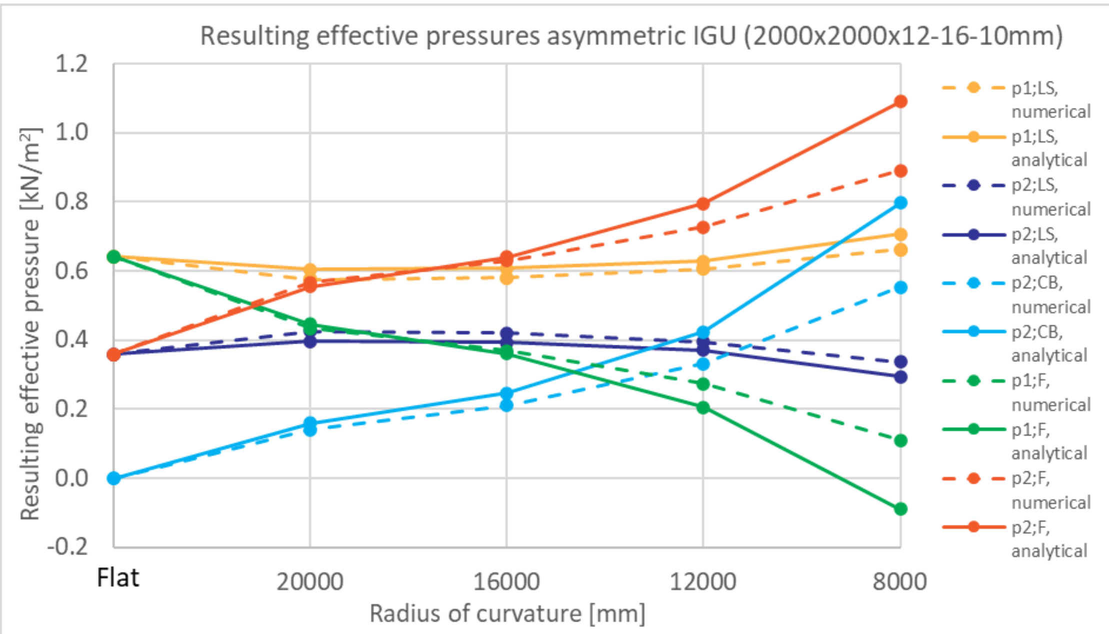

3000x3000x8-16-10

3000x3000x8-16-10, pressures in kN/m2															
	p1;LS, numerical	p2;LS, numerical	p2;CB, numerical	p1;F, numerical	p2;F, numerical		p1;LS, analytical	p2;LS, analytical	p2;CB, analytical	p1;F, analytical	p2;F, analytical		deviation p2;LS	deviation P'CB	deviation p2;F
24000	*0.340*	*0.660*	*0.000*	*0.340*	*0.660*		*0.340*	*0.660*	*0.000*	*0.340*	*0.660*		-	-	-
20000	0.437	0.564	-0.067	0.504	0.497		0.457	0.543	-0.084	0.541	0.459		2.12%	1.71%	3.83%
16000	0.434	0.566	-0.083	0.517	0.483		0.475	0.525	-0.121	0.597	0.403		4.08%	3.83%	7.91%
12000	0.434	0.566	-0.104	0.538	0.462		0.517	0.483	-0.207	0.725	0.275		8.29%	10.32%	18.61%
8000	0.445	0.555	-0.134	0.579	0.421		0.641	0.359	-0.487	1.128	-0.128		19.60%	35.27%	54.87%
												Avg.	**8.52%**	**12.78%**	**21.31%**

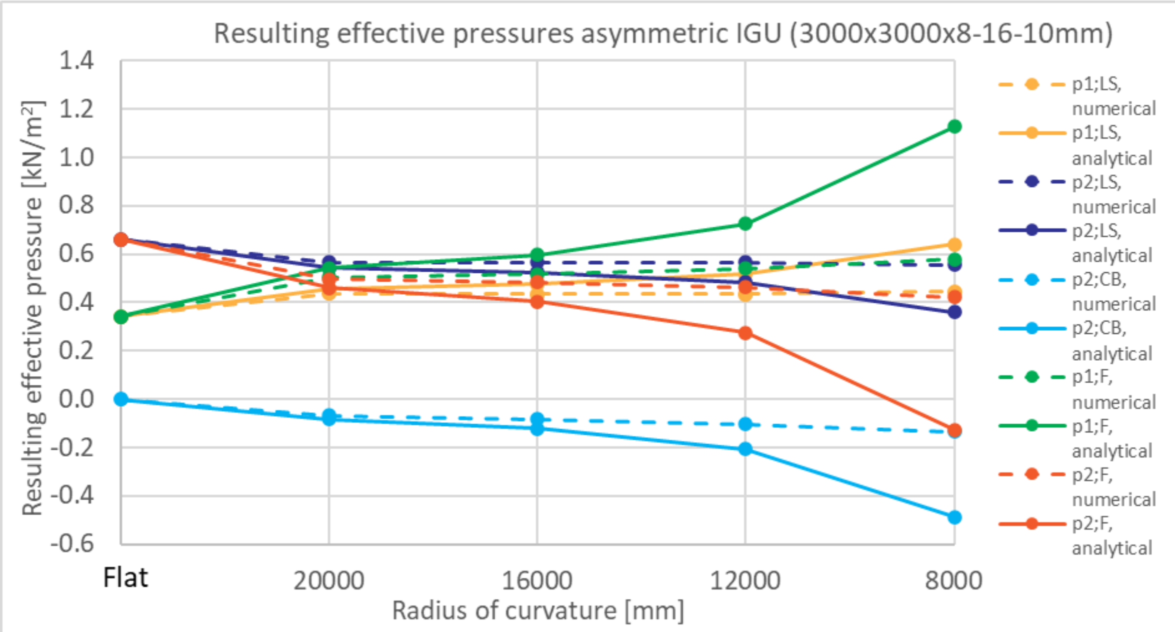

3000x3000x8-16-12

3000x3000x8-16-12, pressures in kN/m2															
	p1;LS, numerical	p2;LS, numerical	p2;CB, numerical	p1;F, numerical	p2;F, numerical		p1;LS, analytical	p2;LS, analytical	p2;CB, analytical	p1;F, analytical	p2;F, analytical		deviation p2;LS	deviation P'CB	deviation p2;F
24000	*0.231*	*0.769*	*0.000*	*0.231*	*0.769*		*0.231*	*0.769*	*0.000*	*0.231*	*0.769*		-	-	-
20000	0.390	0.609	-0.156	0.546	0.453		0.407	0.593	-0.182	0.589	0.411		1.66%	2.60%	4.26%
16000	0.383	0.617	-0.197	0.580	0.420		0.430	0.570	-0.263	0.693	0.307		4.70%	6.60%	11.31%
12000	0.378	0.622	-0.254	0.632	0.368		0.480	0.520	-0.450	0.930	0.070		10.19%	19.60%	29.79%
8000	0.731	0.269	-0.306	1.037	-0.037		0.622	0.378	-1.057	1.678	-0.678		10.93%	75.08%	64.15%
												Avg.	**6.87%**	**25.97%**	**27.37%**

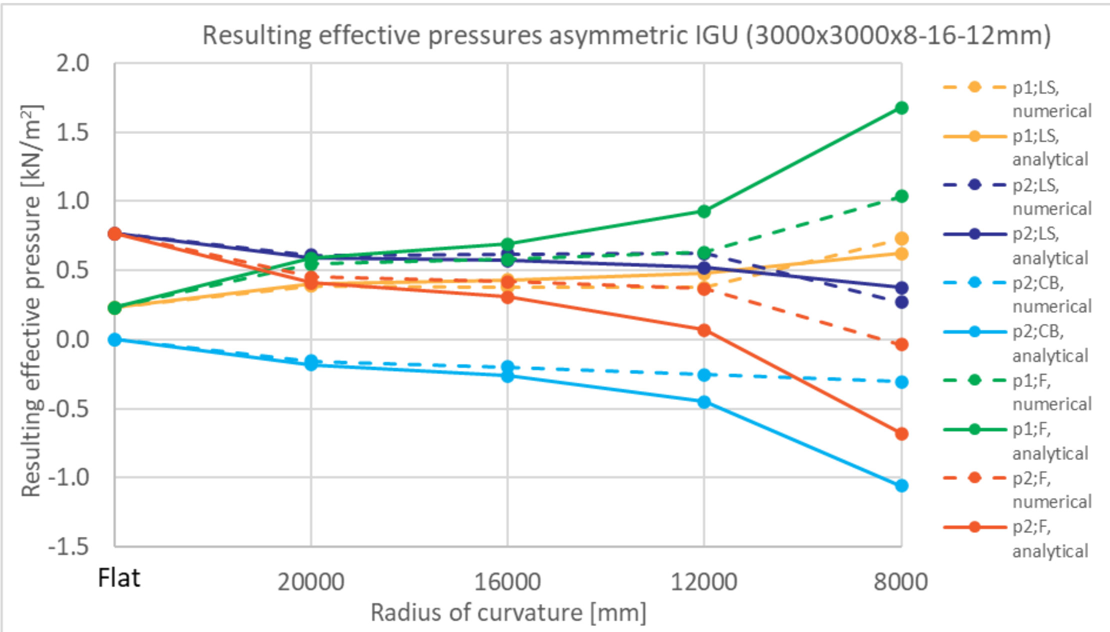

3000x3000x10-16-8

3000x3000x10-16-8, pressures in kN/m2															
	p1;LS, numerical	p2;LS, numerical	p2;CB, numerical	p1;F, numerical	p2;F, numerical		p1;LS, analytical	p2;LS, analytical	p2;CB, analytical	p1;F, analytical	p2;F, analytical		deviation p2;LS	deviation P'CB	deviation p2;F
24000	*0.662*	*0.338*	*0.000*	*0.662*	*0.338*		*0.662*	*0.338*	*0.000*	*0.662*	*0.338*		-	-	-
20000	0.599	0.402	0.067	0.532	0.469		0.586	0.414	0.084	0.502	0.498		1.25%	1.71%	2.96%
16000	0.608	0.392	0.083	0.525	0.475		0.597	0.403	0.121	0.475	0.525		1.11%	3.83%	4.94%
12000	0.629	0.371	0.101	0.528	0.472		0.626	0.374	0.207	0.419	0.581		0.29%	10.62%	10.91%
8000	0.653	0.347	0.124	0.529	0.471		0.719	0.281	0.487	0.232	0.768		6.62%	36.27%	29.65%
												Avg.	**2.32%**	**13.11%**	**12.11%**

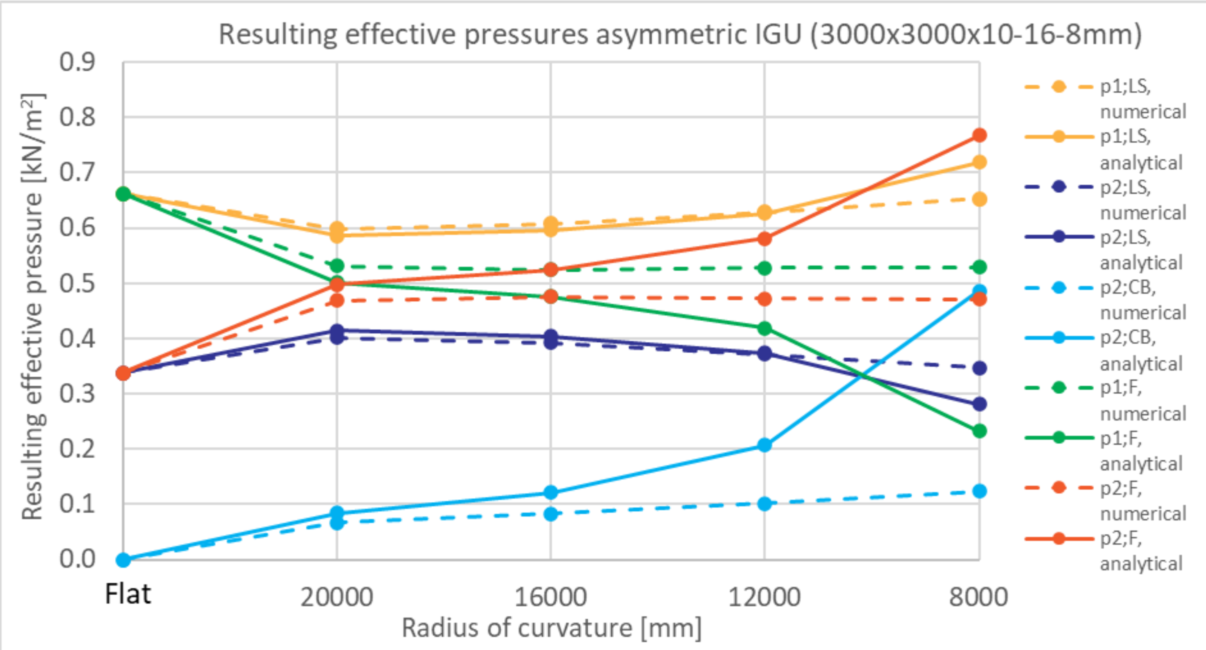

3000x3000x10-16-12

3000x3000x10-16-12, pressures in kN/m2															
	p1;LS, numerical	p2;LS, numerical	p2;CB, numerical	p1;F, numerical	p2;F, numerical		p1;LS, analytical	p2;LS, analytical	p2;CB, analytical	p1;F, analytical	p2;F, analytical		deviation p2;LS	deviation P'CB	deviation p2;F
24000	*0.369*	*0.631*	*0.000*	*0.369*	*0.631*		*0.369*	*0.631*	*0.000*	*0.369*	*0.631*		-	-	-
20000	0.468	0.531	-0.097	0.565	0.434		0.474	0.526	-0.105	0.579	0.421		0.50%	0.83%	1.33%
16000	0.473	0.528	-0.127	0.600	0.401		0.495	0.505	-0.152	0.647	0.353		2.33%	2.51%	4.84%
12000	0.481	0.519	-0.171	0.652	0.348		0.544	0.456	-0.260	0.803	0.197		6.23%	8.88%	15.11%
8000	1.593	0.400	-0.205	1.798	0.195		0.677	0.323	-0.607	1.284	-0.284		7.71%	40.23%	47.94%
												Avg.	**4.19%**	**13.11%**	**17.31%**

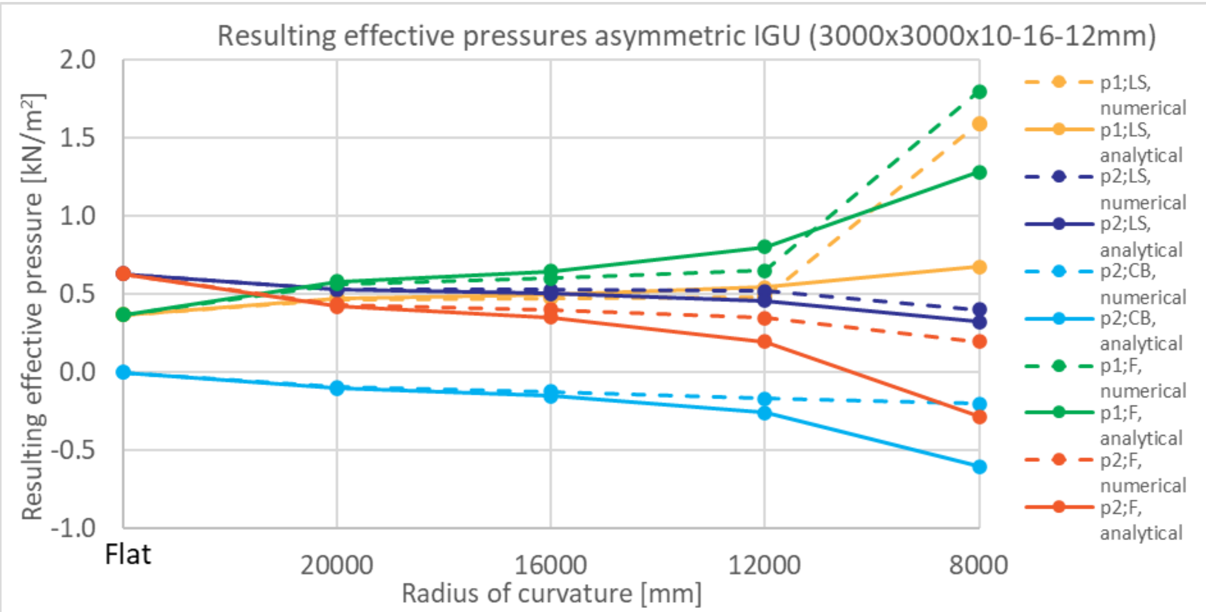

3000x3000x12-16-8

3000x3000x12-16-8, pressures in kN/m2														
	p1;LS, numerical	p2;LS, numerical	p2;CB, numerical	p1;F, numerical	p2;F, numerical	p1;LS, analytical	p2;LS, analytical	p2;CB, analytical	p1;F, analytical	p2;F, analytical		deviation p2;LS	deviation P'CB	deviation p2;F
24000	*0.772*	*0.228*	*0.000*	*0.772*	*0.228*	*0.772*	*0.228*	*0.000*	*0.772*	*0.228*		-	-	-
20000	0.648	0.352	0.150	0.498	0.502	0.640	0.360	0.182	0.458	0.542		0.86%	3.20%	4.06%
16000	0.672	0.329	0.190	0.482	0.519	0.648	0.352	0.263	0.385	0.615		2.29%	7.30%	9.59%
12000	0.701	0.300	0.240	0.461	0.540	0.674	0.326	0.450	0.224	0.776		2.54%	21.00%	23.54%
8000	0.731	0.269	0.287	0.444	0.556	0.758	0.242	1.057	-0.298	1.298		2.71%	76.98%	74.27%
											Avg.	**2.10%**	**27.12%**	**27.86%**

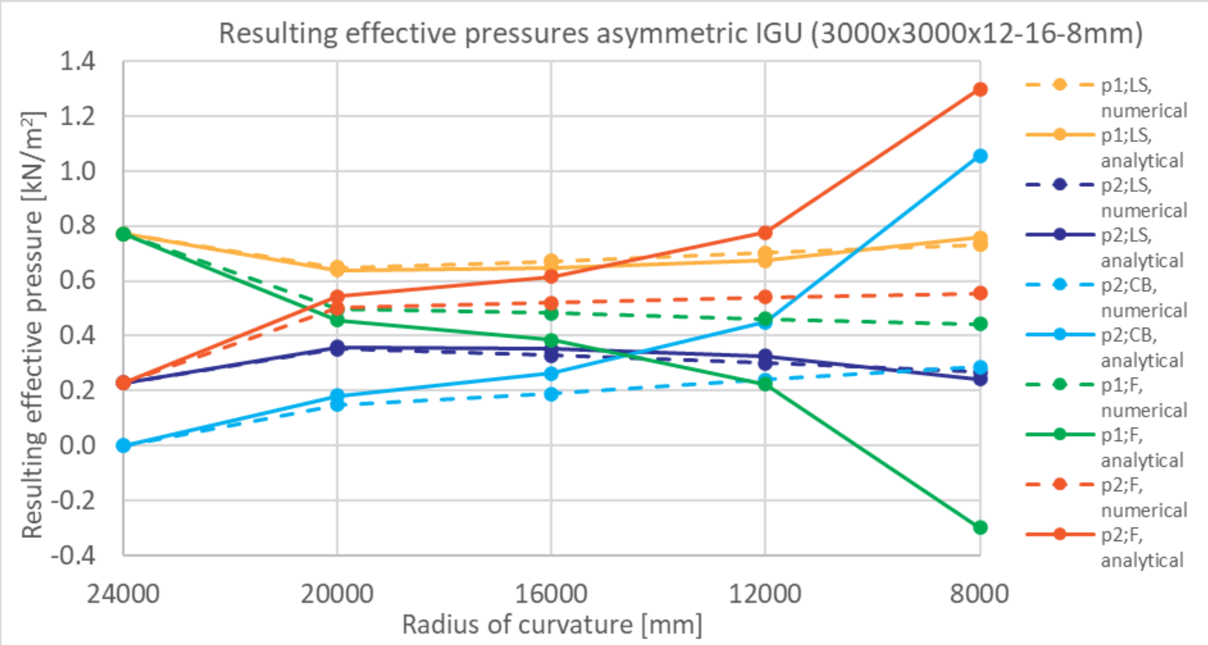

3000x3000x12-16-10

3000x3000x12-16-10, pressures in kN/m2														
	p1;LS, numerical	p2;LS, numerical	p2;CB, numerical	p1;F, numerical	p2;F, numerical	p1;LS, analytical	p2;LS, analytical	p2;CB, analytical	p1;F, analytical	p2;F, analytical		deviation p2;LS	deviation P'CB	deviation p2;F
24000	*0.635*	*0.365*	*0.000*	*0.635*	*0.365*	*0.635*	*0.365*	*0.000*	*0.635*	*0.365*		-	-	-
20000	0.578	0.422	0.097	0.481	0.519	0.581	0.419	0.105	0.476	0.524		0.28%	0.83%	0.55%
16000	0.595	0.406	0.125	0.470	0.531	0.595	0.405	0.152	0.443	0.557		0.03%	2.71%	2.68%
12000	0.616	0.384	0.169	0.447	0.553	0.631	0.369	0.260	0.371	0.629		1.48%	9.08%	7.59%
8000	0.654	0.345	0.191	0.463	0.536	0.737	0.263	0.607	0.129	0.871		8.20%	41.63%	33.42%
											Avg.	**2.50%**	**13.56%**	**11.06%**

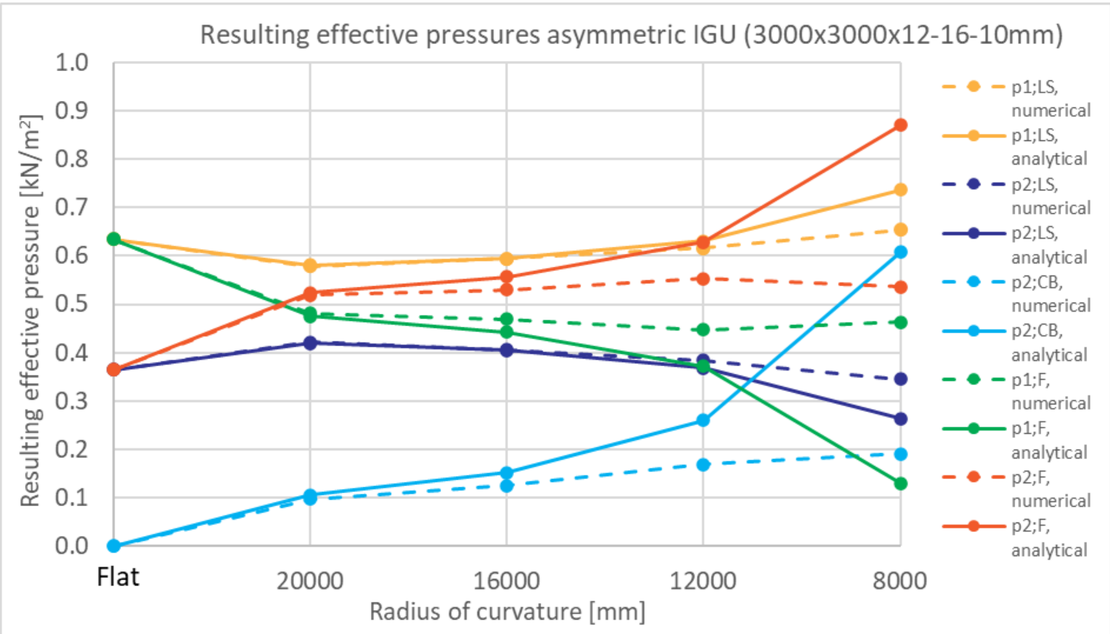

4000x3000x8-16-10

4000x3000x8-16-10, pressures in kN/m2															
	p1;LS, numerical	p2;LS, numerical	p2;CB, numerical	p1;F, numerical	p2;F, numerical		p1;LS, analytical	p2;LS, analytical	p2;CB, analytical	p1;F, analytical	p2;F, analytical		deviation p2;LS	deviation P'CB	deviation p2;F
24000	*0.340*	*0.660*	*0.000*	*0.340*	*0.660*		*0.340*	*0.660*	*0.000*	*0.340*	*0.660*		-	-	-
20000	0.411	0.600	-0.042	0.453	0.558		0.459	0.541	-0.037	0.496	0.504		5.86%	0.50%	5.35%
16000	0.404	0.597	-0.049	0.453	0.548		0.476	0.524	-0.052	0.528	0.472		7.31%	0.29%	7.60%
12000	0.690	0.310	-0.023	0.713	0.287		0.518	0.482	-0.079	0.597	0.403		17.20%	5.60%	11.60%
8000	0.438	0.563	-0.077	0.515	0.486		0.642	0.358	-0.104	0.746	0.254		20.43%	2.72%	23.15%
												Avg.	**12.70%**	**2.28%**	**11.93%**

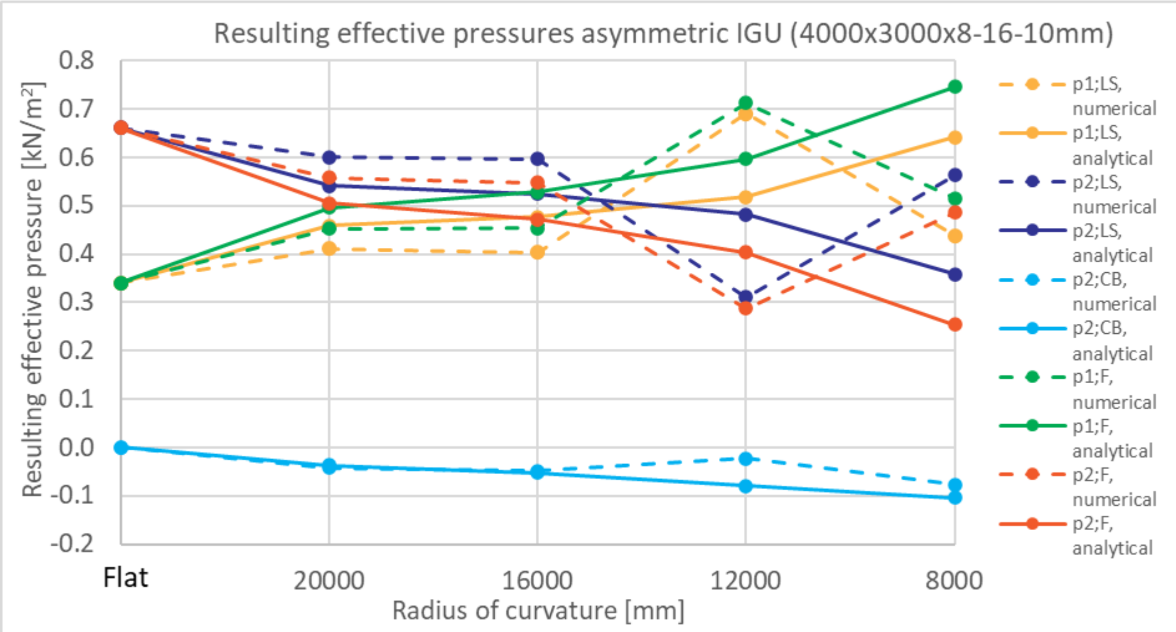

4000x3000x8-16-12

4000x3000x8-16-12, pressures in kN/m2															
	p1;LS, numerical	p2;LS, numerical	p2;CB, numerical	p1;F, numerical	p2;F, numerical		p1;LS, analytical	p2;LS, analytical	p2;CB, analytical	p1;F, analytical	p2;F, analytical		deviation p2;LS	deviation P'CB	deviation p2;F
24000	*0.230*	*0.770*	*0.000*	*0.230*	*0.770*		*0.230*	*0.770*	*0.000*	*0.230*	*0.770*		-	-	-
20000	0.685	0.316	-0.025	0.710	0.291		0.410	0.590	-0.081	0.491	0.509		27.33%	5.56%	21.77%
16000	0.321	0.678	-0.117	0.438	0.561		0.432	0.568	-0.113	0.545	0.455		11.02%	0.39%	10.63%
12000	0.335	0.664	-0.146	0.481	0.518		0.481	0.519	-0.172	0.653	0.347		14.54%	2.60%	17.14%
8000	0.373	0.627	-0.191	0.564	0.436		0.622	0.378	-0.226	0.849	0.151		24.91%	3.54%	28.45%
												Avg.	**19.45%**	**3.02%**	**19.50%**

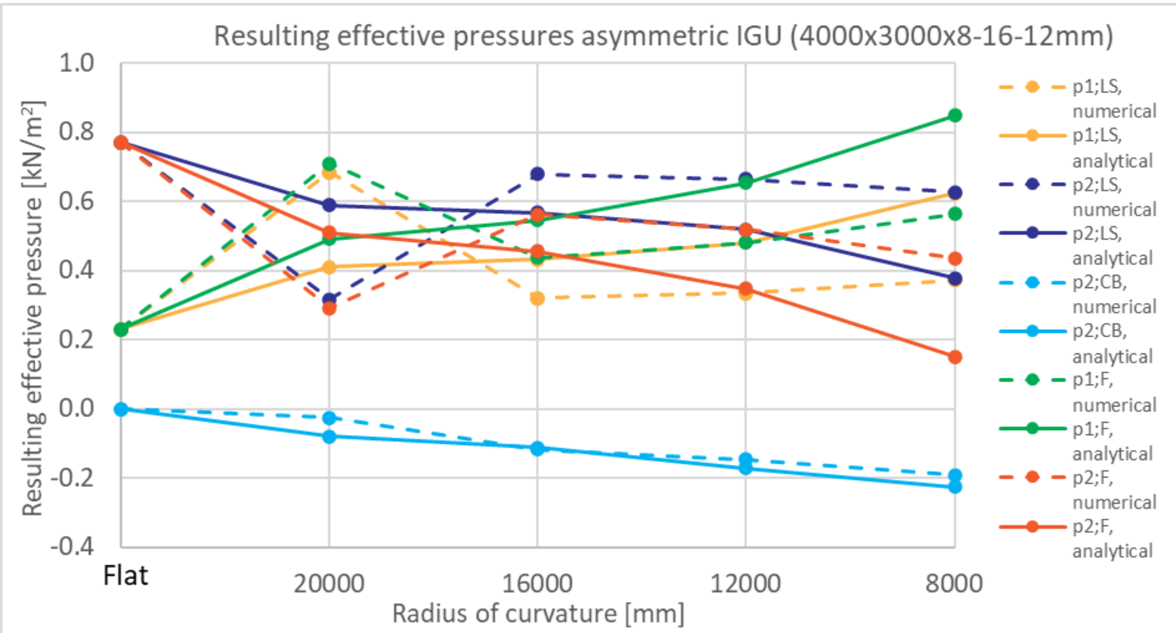

4000x3000x10-16-8

4000x3000x10-16-8, pressures in kN/m2															
	p1;LS, numerical	p2;LS, numerical	p2;CB, numerical	p1;F, numerical	p2;F, numerical		p1;LS, analytical	p2;LS, analytical	p2;CB, analytical	p1;F, analytical	p2;F, analytical		deviation p2;LS	deviation P'CB	deviation p2;F
24000	*0.662*	*0.338*	*0.000*	*0.662*	*0.338*		*0.662*	*0.338*	*0.000*	*0.662*	*0.338*		-	-	-
20000	0.625	0.375	0.042	0.583	0.417		0.583	0.417	0.037	0.546	0.454		4.21%	0.50%	3.71%
16000	0.630	0.370	0.049	0.581	0.419		0.594	0.406	0.052	0.542	0.458		3.57%	0.29%	3.87%
12000	0.334	0.666	0.023	0.311	0.689		0.624	0.376	0.079	0.545	0.455		28.94%	5.60%	23.33%
8000	0.636	0.363	0.077	0.559	0.440		0.718	0.282	0.104	0.614	0.386		8.14%	2.72%	5.42%
												Avg.	**11.22%**	**2.28%**	**9.08%**

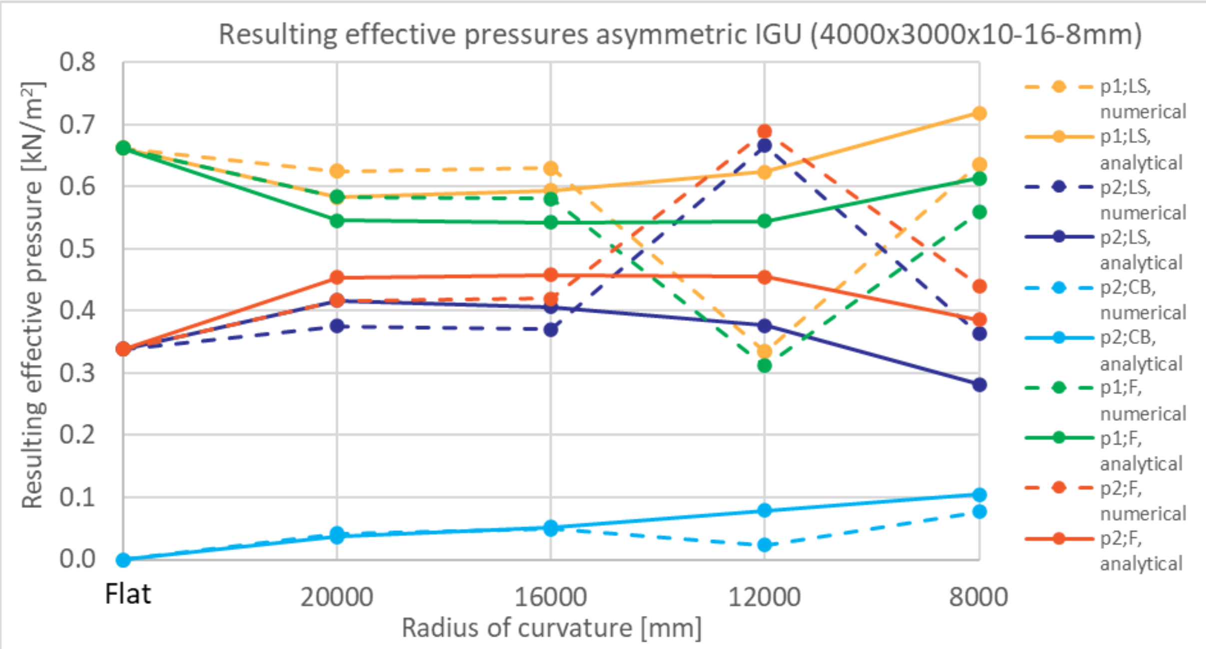

4000x3000x10-16-12

4000x3000x10-16-12, pressures in kN/m2															
	p1;LS, numerical	p2;LS, numerical	p2;CB, numerical	p1;F, numerical	p2;F, numerical		p1;LS, analytical	p2;LS, analytical	p2;CB, analytical	p1;F, analytical	p2;F, analytical		deviation p2;LS	deviation P'CB	deviation p2;F
24000	*0.368*	*0.632*	*0.000*	*0.368*	*0.632*		*0.368*	*0.632*	*0.000*	*0.368*	*0.632*		-	-	-
20000	0.829	0.172	-0.014	0.843	0.158		0.475	0.525	-0.047	0.521	0.479		35.31%	3.28%	32.03%
16000	0.442	0.559	-0.078	0.520	0.481		0.495	0.505	-0.065	0.561	0.439		5.40%	1.25%	4.14%
12000	0.167	0.833	-0.033	0.200	0.800		0.543	0.457	-0.099	0.642	0.358		37.61%	6.62%	44.23%
8000	0.481	0.520	-0.132	0.613	0.388		0.677	0.323	-0.130	0.807	0.193		19.65%	0.20%	19.45%
												Avg.	**24.49%**	**2.84%**	**24.96%**

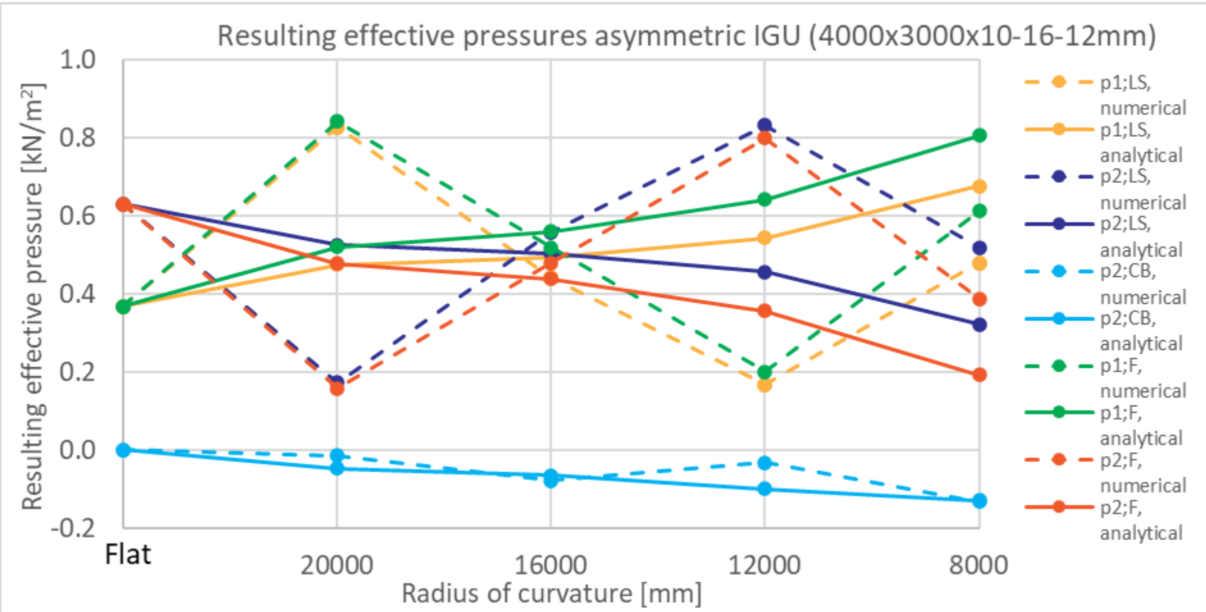

4000x3000x12-16-8

4000x3000x12-16-8, pressures in kN/m2														
	p1;LS, numerical	p2;LS, numerical	p2;CB, numerical	p1;F, numerical	p2;F, numerical	p1;LS, analytical	p2;LS, analytical	p2;CB, analytical	p1;F, analytical	p2;F, analytical		deviation p2;LS	deviation P'CB	deviation p2;F
24000	*0.772*	*0.228*	*0.000*	*0.772*	*0.228*	*0.772*	*0.228*	*0.000*	*0.772*	*0.228*		-	-	-
20000	0.328	0.672	0.025	0.303	0.697	0.635	0.365	0.081	0.554	0.446		30.67%	5.56%	25.11%
16000	0.709	0.290	0.106	0.603	0.396	0.644	0.356	0.113	0.531	0.469		6.63%	0.71%	7.34%
12000	0.715	0.284	0.135	0.580	0.419	0.671	0.329	0.172	0.499	0.501		4.47%	3.70%	8.17%
8000	0.716	0.284	0.181	0.535	0.465	0.757	0.243	0.226	0.530	0.470		4.03%	4.54%	0.51%
											Avg.	**11.45%**	**3.63%**	**10.28%**

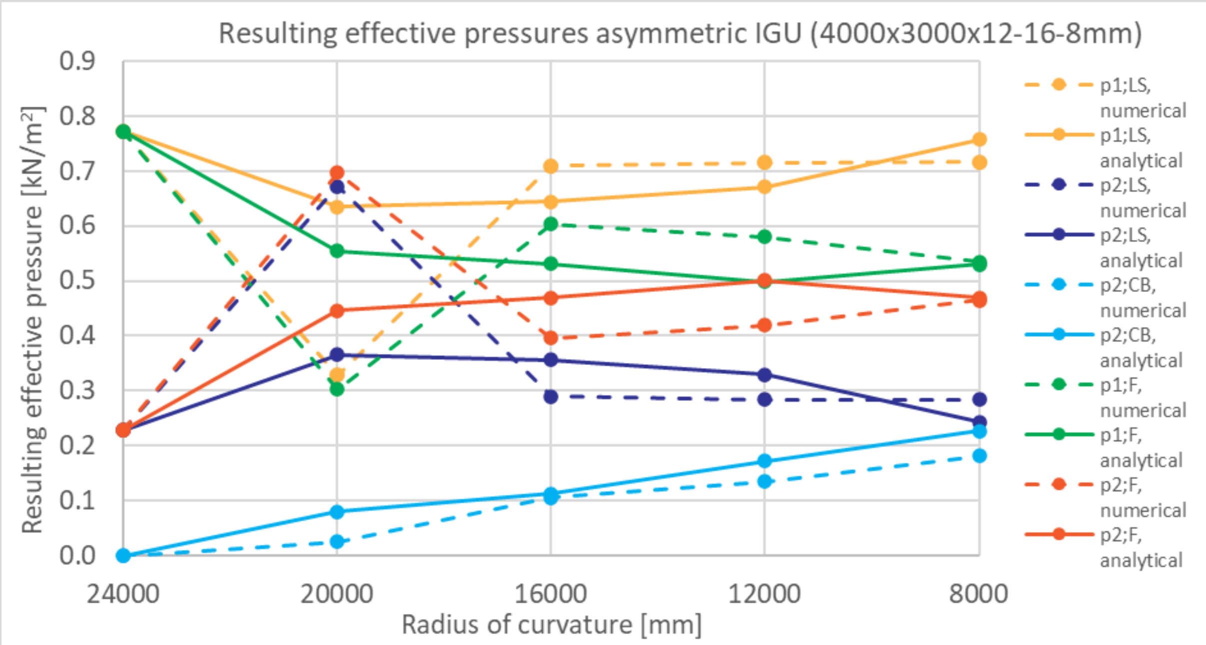

4000x3000x12-16-10

4000x3000x12-16-10, pressures in kN/m2														
	p1;LS, numerical	p2;LS, numerical	p2;CB, numerical	p1;F, numerical	p2;F, numerical	p1;LS, analytical	p2;LS, analytical	p2;CB, analytical	p1;F, analytical	p2;F, analytical		deviation p2;LS	deviation P'CB	deviation p2;F
24000	*0.634*	*0.366*	*0.000*	*0.634*	*0.366*	*0.634*	*0.366*	*0.000*	*0.634*	*0.366*		-	-	-
20000	0.185	0.814	0.014	0.171	0.828	0.578	0.422	0.047	0.531	0.469		39.17%	3.28%	35.89%
16000	0.614	0.386	0.078	0.536	0.464	0.592	0.408	0.065	0.526	0.474		2.23%	1.25%	0.98%
12000	0.863	0.137	0.033	0.830	0.170	0.629	0.371	0.099	0.529	0.471		23.43%	6.62%	30.06%
8000	0.639	0.361	0.128	0.511	0.489	0.735	0.265	0.130	0.605	0.395		9.64%	0.20%	9.44%
											Avg.	**18.62%**	**2.84%**	**19.09%**

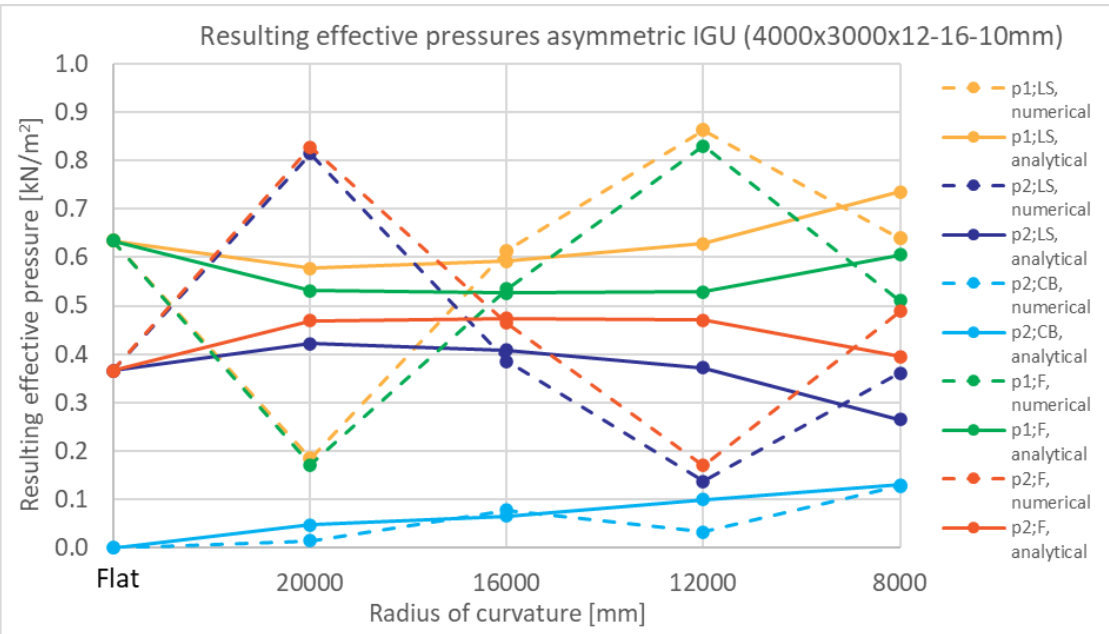

5000x3000x8-16-10

5000x3000x8-16-10, pressures in kN/m2															
	p1;LS, numerical	p2;LS, numerical	p2;CB, numerical	p1;F, numerical	p2;F, numerical		p1;LS, analytical	p2;LS, analytical	p2;CB, analytical	p1;F, analytical	p2;F, analytical		deviation p2;LS	deviation P'CB	deviation p2;F
24000	*0.339*	*0.661*	*0.000*	*0.339*	*0.661*		*0.339*	*0.661*	*0.000*	*0.339*	*0.661*		-	-	-
20000	0.421	0.600	-0.029	0.450	0.571		0.460	0.540	-0.019	0.479	0.521		5.98%	1.01%	4.97%
16000	0.415	0.586	-0.040	0.455	0.546		0.477	0.523	-0.024	0.501	0.499		6.30%	1.62%	4.68%
12000	0.420	0.580	-0.050	0.470	0.530		0.519	0.481	-0.028	0.546	0.454		9.83%	2.24%	7.59%
8000	0.451	0.548	-0.075	0.526	0.473		0.643	0.357	0.002	0.641	0.359		19.14%	7.72%	11.42%
												Avg.	**10.31%**	**3.15%**	**7.17%**

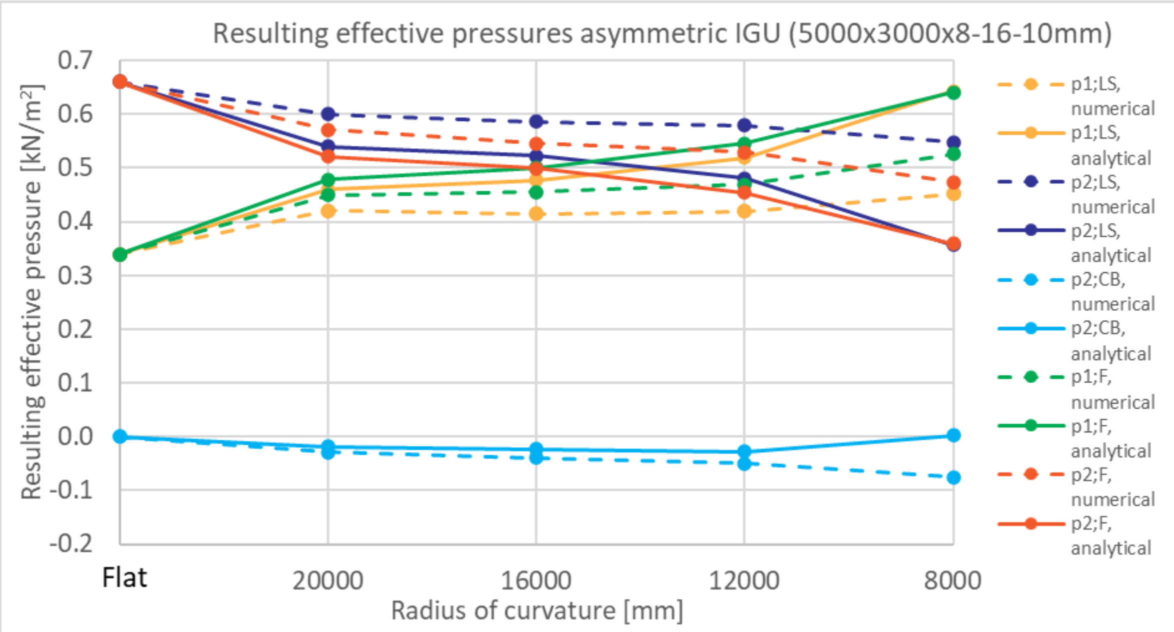

5000x3000x8-16-12

5000x3000x8-16-12, pressures in kN/m2															
	p1;LS, numerical	p2;LS, numerical	p2;CB, numerical	p1;F, numerical	p2;F, numerical		p1;LS, analytical	p2;LS, analytical	p2;CB, analytical	p1;F, analytical	p2;F, analytical		deviation p2;LS	deviation P'CB	deviation p2;F
24000	*0.230*	*0.770*	*0.000*	*0.230*	*0.770*		*0.230*	*0.770*	*0.000*	*0.230*	*0.770*		-	-	-
20000	0.330	0.670	-0.069	0.399	0.601		0.413	0.587	-0.041	0.454	0.546		8.30%	2.78%	5.52%
16000	0.329	0.670	-0.093	0.422	0.577		0.434	0.566	-0.052	0.486	0.514		10.42%	4.13%	6.30%
12000	0.358	0.641	-0.129	0.487	0.512		0.483	0.517	-0.060	0.543	0.457		12.33%	6.89%	5.44%
8000	0.395	0.606	-0.209	0.604	0.397		0.624	0.376	0.005	0.619	0.381		23.03%	21.38%	1.65%
												Avg.	**13.52%**	**8.79%**	**4.73%**

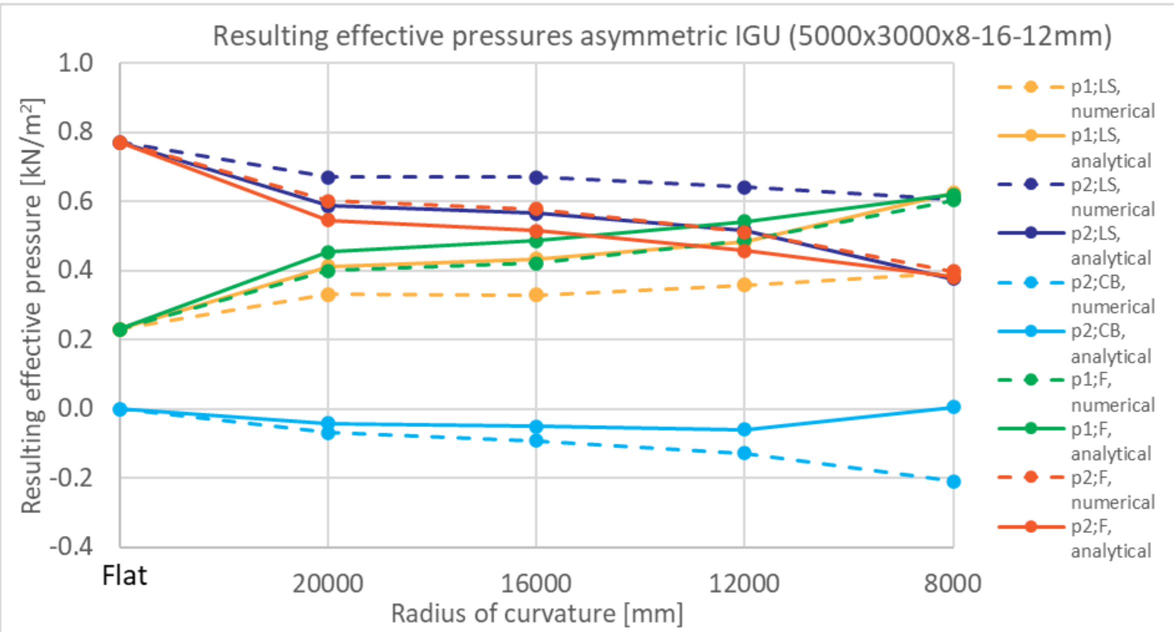

5000x3000x10-16-8

5000x3000x10-16-8, pressures in kN/m2														
	p1;LS, numerical	p2;LS, numerical	p2;CB, numerical	p1;F, numerical	p2;F, numerical	p1;LS, analytical	p2;LS, analytical	p2;CB, analytical	p1;F, analytical	p2;F, analytical		deviation p2;LS	deviation P'CB	deviation p2;F
24000	*0.662*	*0.338*	*0.000*	*0.662*	*0.338*	*0.662*	*0.338*	*0.000*	*0.662*	*0.338*		-	-	-
20000	0.630	0.370	0.029	0.601	0.399	0.581	0.419	0.019	0.562	0.438		4.89%	1.01%	3.88%
16000	0.609	0.391	0.040	0.569	0.431	0.593	0.407	0.024	0.569	0.431		1.59%	1.62%	0.03%
12000	0.613	0.387	0.050	0.563	0.437	0.623	0.377	0.028	0.595	0.405		0.98%	2.24%	3.21%
8000	0.631	0.370	0.075	0.556	0.445	0.718	0.282	-0.002	0.721	0.279		8.79%	7.72%	16.51%
											Avg.	**4.06%**	**3.15%**	**5.91%**

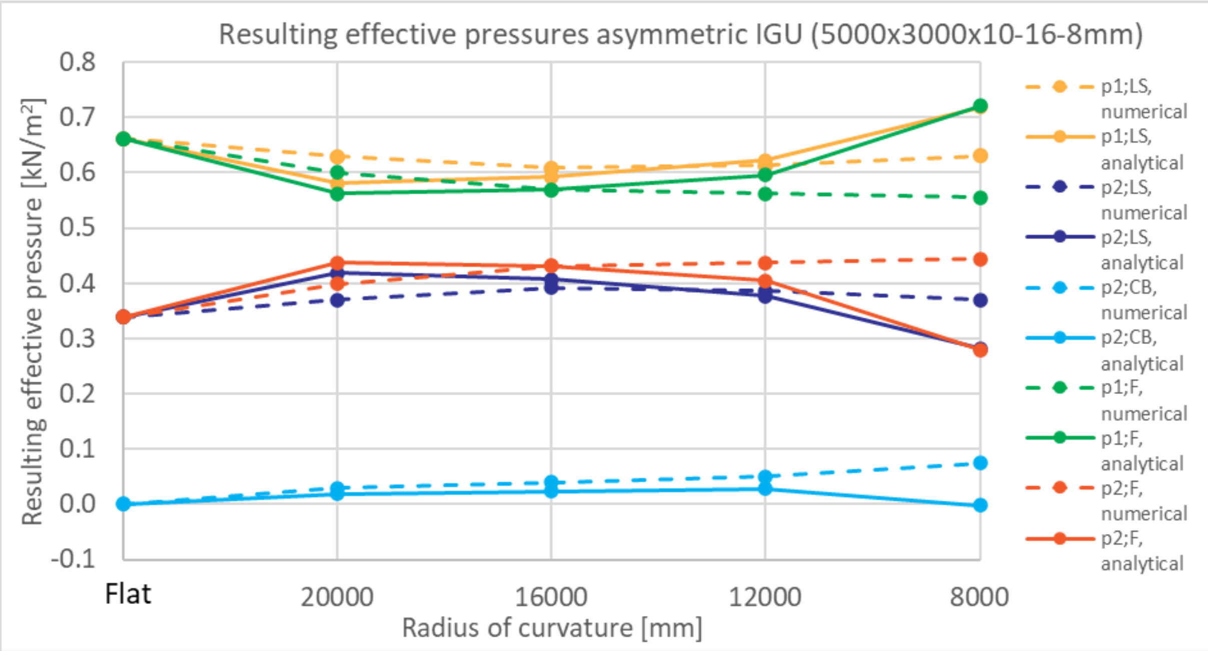

5000x3000x10-16-12

5000x3000x10-16-12, pressures in kN/m2														
	p1;LS, numerical	p2;LS, numerical	p2;CB, numerical	p1;F, numerical	p2;F, numerical	p1;LS, analytical	p2;LS, analytical	p2;CB, analytical	p1;F, analytical	p2;F, analytical		deviation p2;LS	deviation P'CB	deviation p2;F
24000	*0.368*	*0.632*	*0.000*	*0.368*	*0.632*	*0.368*	*0.632*	*0.000*	*0.368*	*0.632*		-	-	-
20000	0.422	0.578	-0.046	0.468	0.532	0.475	0.525	-0.024	0.499	0.501		5.36%	2.21%	3.15%
16000	0.437	0.563	-0.062	0.499	0.501	0.496	0.504	-0.030	0.526	0.474		5.85%	3.21%	2.64%
12000	0.459	0.542	-0.088	0.547	0.454	0.544	0.456	-0.035	0.578	0.422		8.60%	5.34%	3.26%
8000	0.493	0.508	-0.152	0.645	0.356	0.678	0.322	0.003	0.675	0.325		18.57%	15.48%	3.09%
											Avg.	**9.59%**	**6.56%**	**3.04%**

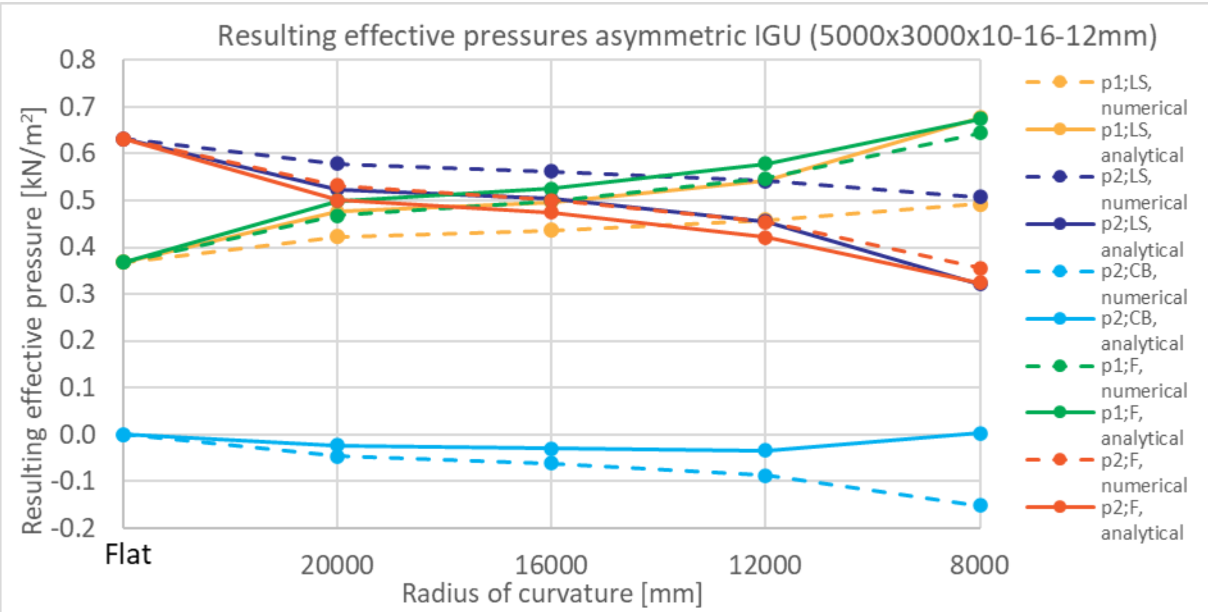

5000x3000x12-16-8

5000x3000x12-16-8, pressures in kN/m2														
	p1;LS, numerical	p2;LS, numerical	p2;CB, numerical	p1;F, numerical	p2;F, numerical	p1;LS, analytical	p2;LS, analytical	p2;CB, analytical	p1;F, analytical	p2;F, analytical		deviation p2;LS	deviation P'CB	deviation p2;F
24000	*0.772*	*0.228*	*0.000*	*0.772*	*0.228*	*0.772*	*0.228*	*0.000*	*0.772*	*0.228*		-	-	-
20000	0.702	0.298	0.069	0.633	0.367	0.632	0.368	0.041	0.591	0.409		6.98%	2.78%	4.20%
16000	0.721	0.300	0.093	0.628	0.393	0.642	0.358	0.052	0.590	0.410		5.83%	4.13%	1.71%
12000	0.704	0.300	0.119	0.585	0.419	0.669	0.331	0.060	0.609	0.391		3.05%	5.89%	2.84%
8000	0.704	0.297	0.198	0.506	0.495	0.756	0.244	-0.005	0.761	0.239		5.34%	20.28%	25.62%
											Avg.	**5.30%**	**8.27%**	**8.59%**

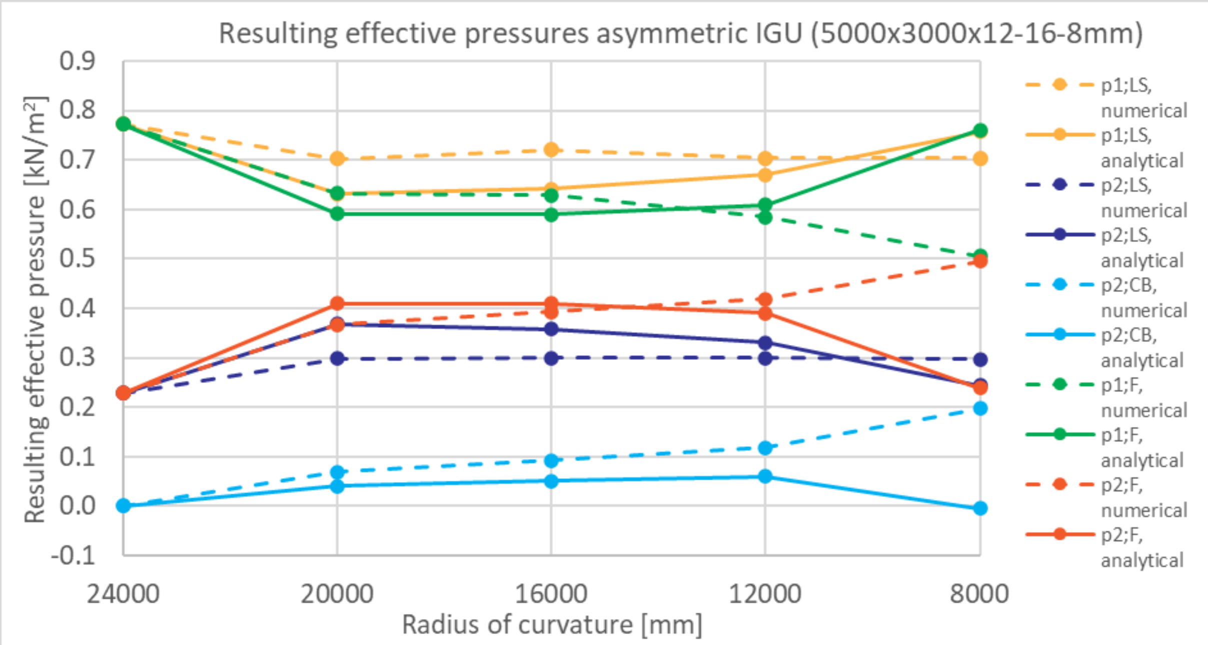

5000x3000x12-16-10

5000x3000x12-16-10, pressures in kN/m2														
	p1;LS, numerical	p2;LS, numerical	p2;CB, numerical	p1;F, numerical	p2;F, numerical	p1;LS, analytical	p2;LS, analytical	p2;CB, analytical	p1;F, analytical	p2;F, analytical		deviation p2;LS	deviation P'CB	deviation p2;F
24000	*0.634*	*0.366*	*0.000*	*0.634*	*0.366*	*0.634*	*0.366*	*0.000*	*0.634*	*0.366*		-	-	-
20000	0.608	0.393	0.046	0.562	0.439	0.576	0.424	0.024	0.552	0.448		3.12%	2.21%	0.91%
16000	0.610	0.391	0.062	0.548	0.453	0.590	0.410	0.030	0.561	0.439		1.82%	3.21%	1.39%
12000	0.611	0.390	0.088	0.523	0.478	0.628	0.372	0.035	0.593	0.407		1.75%	5.34%	7.09%
8000	0.631	0.369	0.149	0.482	0.518	0.736	0.264	-0.003	0.738	0.262		10.43%	15.18%	25.61%
											Avg.	**4.28%**	**6.48%**	**8.75%**

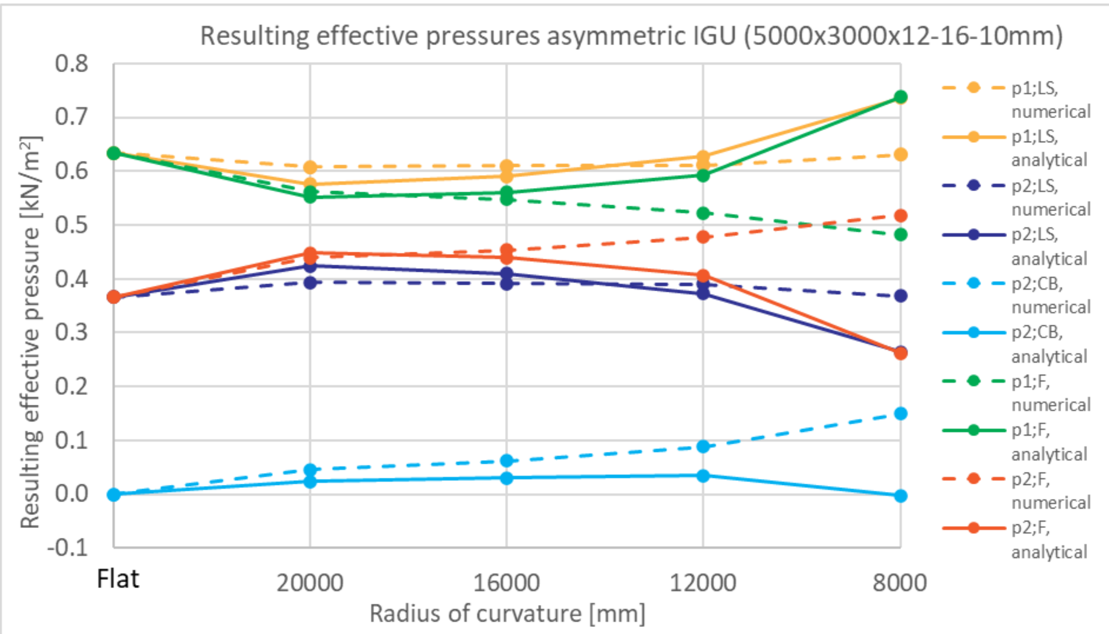

6000x3000x8-16-10

6000x3000x8-16-10, pressures in kN/m2														
	p1;LS, numerical	p2;LS, numerical	p2;CB, numerical	p1;F, numerical	p2;F, numerical	p1;LS, analytical	p2;LS, analytical	p2;CB, analytical	p1;F, analytical	p2;F, analytical		deviation p2;LS	deviation P'CB	deviation p2;F
24000	*0.339*	*0.661*	*0.000*	*0.339*	*0.661*	*0.339*	*0.661*	*0.000*	*0.339*	*0.661*		-	-	-
20000	0.214	0.786	-0.009	0.223	0.777	0.461	0.539	-0.010	0.471	0.529		24.66%	0.11%	24.77%
16000	0.655	0.345	-0.019	0.674	0.326	0.478	0.522	-0.014	0.492	0.508		17.71%	0.49%	18.21%
12000	0.669	0.331	-0.015	0.684	0.316	0.520	0.480	-0.023	0.543	0.457		14.92%	0.81%	14.11%
8000	0.697	0.303	-0.032	0.729	0.271	0.645	0.355	-0.065	0.709	0.291		5.23%	3.28%	1.95%
											Avg.	**15.63%**	**1.17%**	**14.76%**

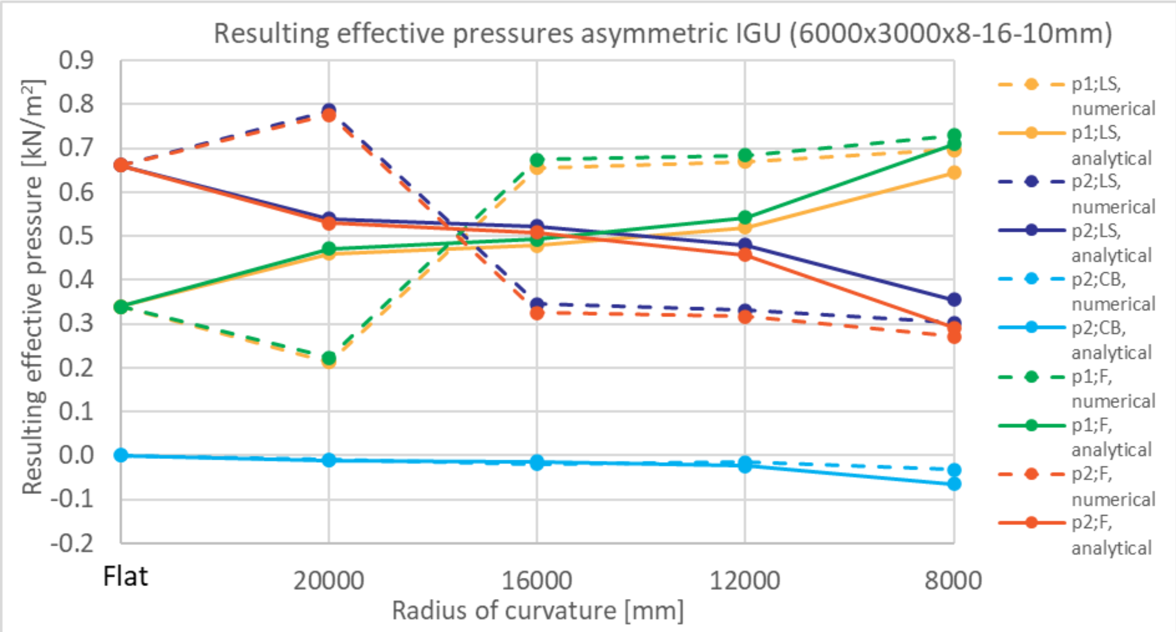

6000x3000x8-16-12

6000x3000x8-16-12, pressures in kN/m2														
	p1;LS, numerical	p2;LS, numerical	p2;CB, numerical	p1;F, numerical	p2;F, numerical	p1;LS, analytical	p2;LS, analytical	p2;CB, analytical	p1;F, analytical	p2;F, analytical		deviation p2;LS	deviation P'CB	deviation p2;F
24000	*0.229*	*0.771*	*0.000*	*0.229*	*0.771*	*0.229*	*0.771*	*0.000*	*0.229*	*0.771*		-	-	-
20000	0.143	0.856	-0.021	0.164	0.835	0.414	0.586	-0.022	0.436	0.564		27.06%	0.10%	27.16%
16000	0.346	0.655	-0.093	0.439	0.562	0.435	0.565	-0.031	0.466	0.534		9.01%	6.24%	2.77%
12000	0.627	0.373	-0.057	0.684	0.316	0.484	0.516	-0.050	0.534	0.466		14.32%	0.67%	14.99%
8000	0.643	0.357	-0.085	0.728	0.272	0.626	0.374	-0.141	0.766	0.234		1.66%	5.55%	3.89%
											Avg.	**13.01%**	**3.14%**	**12.20%**

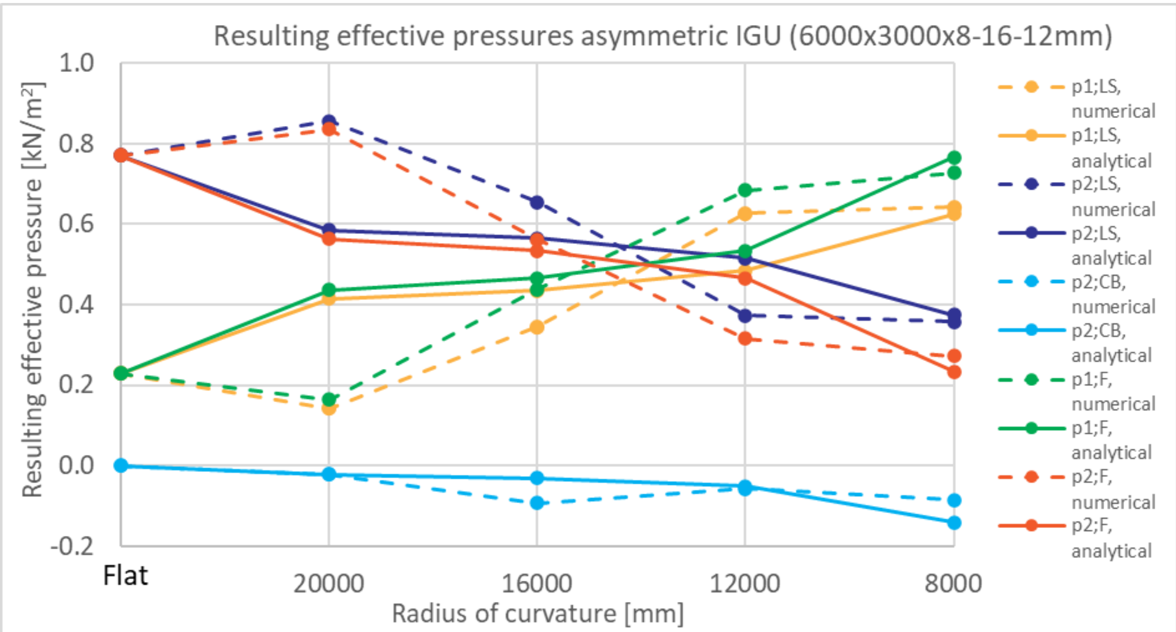

6000x3000x10-16-8

6000x3000x10-16-8, pressures in kN/m2															
	p1;LS, numerical	p2;LS, numerical	p2;CB, numerical	p1;F, numerical	p2;F, numerical		p1;LS, analytical	p2;LS, analytical	p2;CB, analytical	p1;F, analytical	p2;F, analytical		deviation p2;LS	deviation P'CB	deviation p2;F
24000	*0.662*	*0.338*	*0.000*	*0.662*	*0.338*		*0.662*	*0.338*	*0.000*	*0.662*	*0.338*		-	-	-
20000	0.797	0.203	0.009	0.788	0.212		0.580	0.420	0.010	0.570	0.430		21.66%	0.11%	21.77%
16000	0.435	0.600	0.019	0.416	0.619		0.592	0.408	0.014	0.578	0.422		19.22%	0.49%	19.71%
12000	0.357	0.644	0.015	0.342	0.659		0.623	0.377	0.023	0.600	0.400		26.68%	0.81%	25.87%
8000	0.349	0.652	0.032	0.317	0.684		0.719	0.281	0.065	0.654	0.346		37.07%	3.28%	33.79%
												Avg.	**26.16%**	**1.17%**	**25.28%**

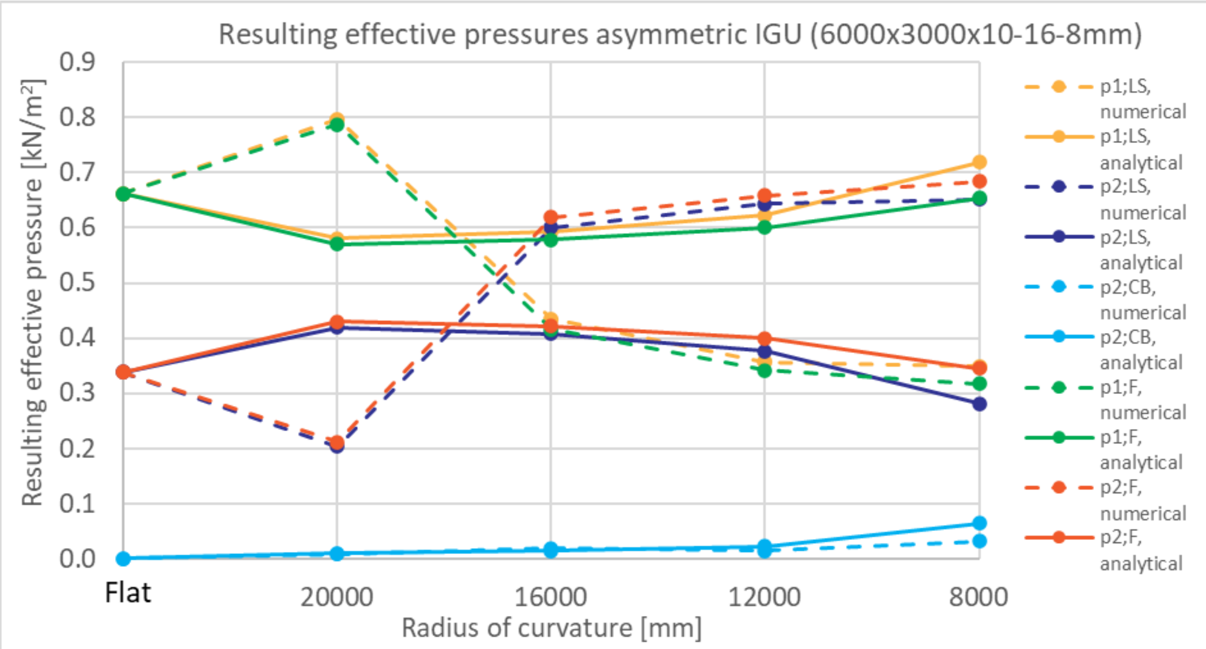

6000x3000x10-16-12

6000x3000x10-16-12, pressures in kN/m2															
	p1;LS, numerical	p2;LS, numerical	p2;CB, numerical	p1;F, numerical	p2;F, numerical		p1;LS, analytical	p2;LS, analytical	p2;CB, analytical	p1;F, analytical	p2;F, analytical		deviation p2;LS	deviation P'CB	deviation p2;F
24000	*0.368*	*0.632*	*0.000*	*0.368*	*0.632*		*0.368*	*0.632*	*0.000*	*0.368*	*0.632*		-	-	-
20000	0.432	0.568	-0.048	0.480	0.520		0.476	0.524	-0.013	0.489	0.511		4.43%	3.53%	0.90%
16000	0.190	0.811	-0.018	0.208	0.793		0.497	0.503	-0.018	0.514	0.486		30.77%	0.03%	30.73%
12000	0.442	0.558	-0.025	0.467	0.533		0.545	0.455	-0.029	0.574	0.426		10.24%	0.39%	10.64%
8000	0.456	0.545	-0.030	0.486	0.515		0.679	0.321	-0.080	0.760	0.240		22.45%	5.04%	27.49%
												Avg.	**16.97%**	**2.25%**	**17.44%**

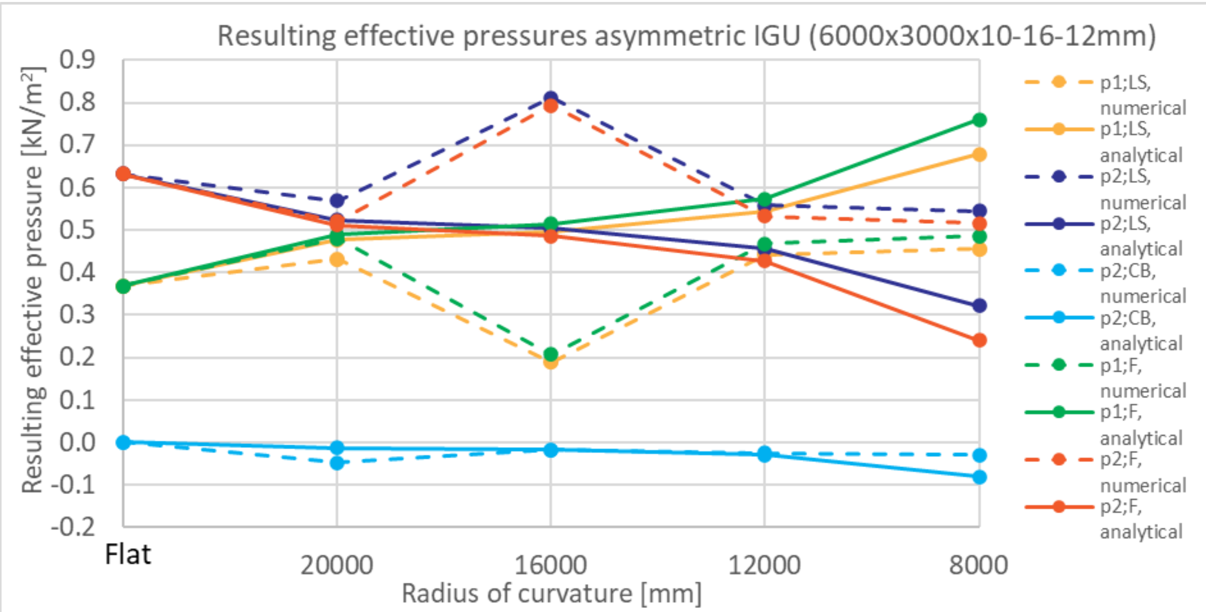

6000x3000x12-16-8

	6000x3000x12-16-8, pressures in kN/m2														
	p1;LS, numerical	p2;LS, numerical	p2;CB, numerical	p1;F, numerical	p2;F, numerical		p1;LS, analytical	p2;LS, analytical	p2;CB, analytical	p1;F, analytical	p2;F, analytical		deviation p2;LS	deviation P'CB	deviation p2;F
24000	*0.772*	*0.228*	*0.000*	*0.772*	*0.228*		*0.772*	*0.228*	*0.000*	*0.772*	*0.228*		-	-	-
20000	0.869	0.131	0.021	0.848	0.152		0.630	0.370	0.022	0.608	0.392		23.85%	0.10%	23.95%
16000	0.697	0.304	0.093	0.604	0.397		0.641	0.359	0.031	0.610	0.390		5.56%	6.24%	0.68%
12000	0.404	0.596	0.057	0.347	0.653		0.669	0.331	0.050	0.619	0.381		26.50%	0.67%	27.17%
8000	0.403	0.597	0.085	0.318	0.682		0.757	0.243	0.141	0.616	0.384		35.36%	5.55%	29.81%
												Avg.	**22.82%**	**3.14%**	**20.41%**

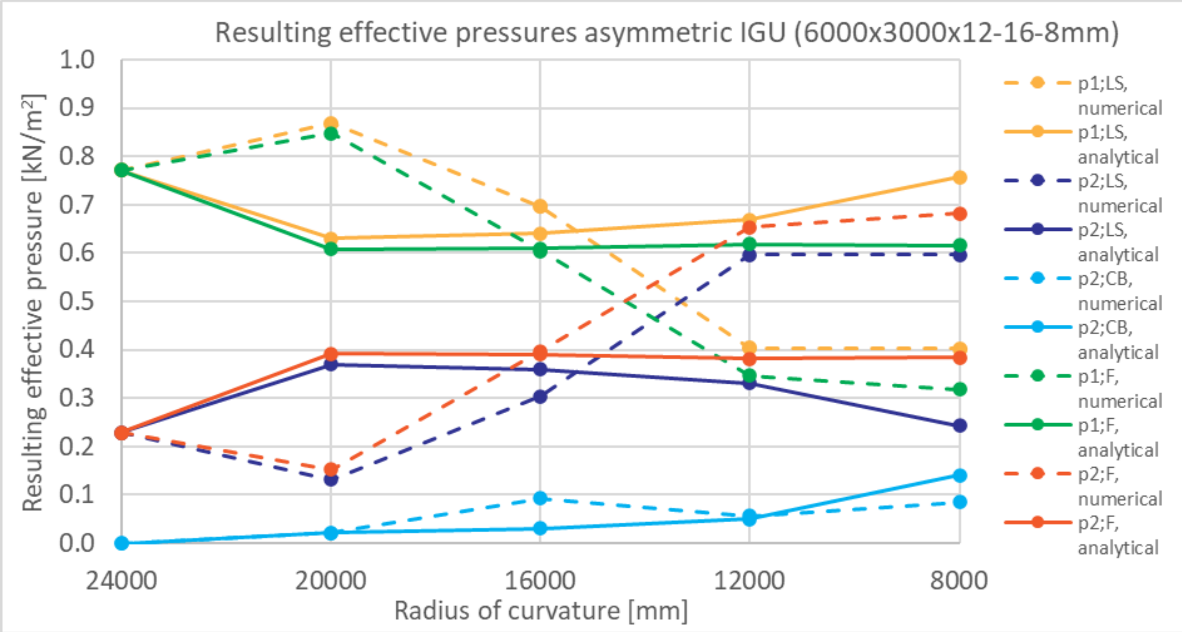

6000x3000x12-16-10

	6000x3000x12-16-10, pressures in kN/m2														
	p1;LS, numerical	p2;LS, numerical	p2;CB, numerical	p1;F, numerical	p2;F, numerical		p1;LS, analytical	p2;LS, analytical	p2;CB, analytical	p1;F, analytical	p2;F, analytical		deviation p2;LS	deviation P'CB	deviation p2;F
24000	*0.634*	*0.366*	*0.000*	*0.634*	*0.366*		*0.634*	*0.366*	*0.000*	*0.634*	*0.366*		-	-	-
20000	0.600	0.400	0.048	0.552	0.448		0.575	0.425	0.013	0.562	0.438		2.50%	3.53%	1.03%
16000	0.833	0.168	0.018	0.815	0.186		0.590	0.410	0.018	0.572	0.428		24.25%	0.03%	24.22%
12000	0.580	0.420	0.025	0.555	0.445		0.628	0.372	0.029	0.599	0.401		4.79%	0.39%	4.40%
8000	0.582	0.417	0.030	0.552	0.447		0.736	0.264	0.080	0.656	0.344		15.33%	5.04%	10.28%
												Avg.	**11.72%**	**2.25%**	**9.98%**

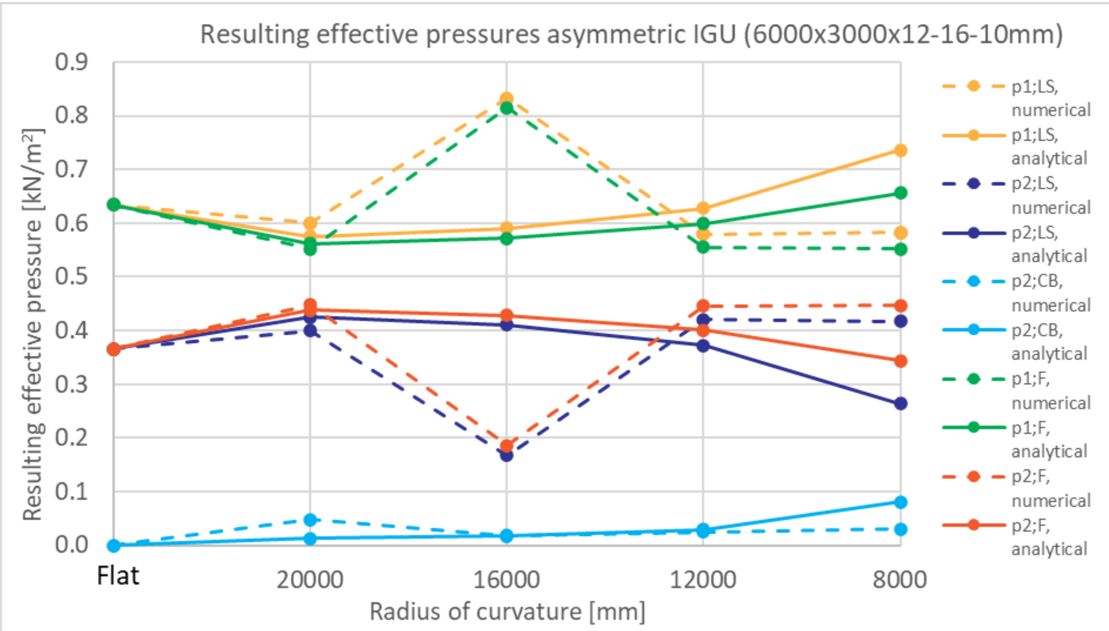

Case study Van Gogh

3600x1800x8-15-10, pressures in kN/m2															
	p1, external, numerical	p2, external, numerical	dP, numerical	p1, final, numerical	p2, final, numerical		p1, external, analytical	p2, external, analytical	dP, analytical	p1, final, analytical	p2, final, analytical		deviation p2, external	deviation dP	deviation p2, final
Flat	*0.343*	*0.657*	*0.000*	*0.343*	*0.657*		*0.343*	*0.343*	*0.000*	*0.343*	*0.657*		-	-	-
11500	0.463	0.537	-0.130	0.594	0.406		0.501	0.499	-0.076	0.577	0.423		3.78%	5.40%	1.67%

3600x1800x8-15-12, pressures in kN/m2															
	p1, external, numerical	p2, external, numerical	dP, numerical	p1, final, numerical	p2, final, numerical		p1, external, analytical	p2, external, analytical	dP, analytical	p1, final, analytical	p2, final, analytical		deviation p2, external	deviation dP	deviation p2, final
Flat	*0.235*	*0.765*	*0.000*	*0.235*	*0.765*		*0.235*	*0.235*	*0.000*	*0.235*	*0.765*		-	-	-
11500	0.404	0.595	-0.349	0.753	0.246		0.460	0.540	-0.183	0.643	0.357		5.51%	16.57%	11.08%

3600x1800x10-15-8, pressures in kN/m2															
	p1, external, numerical	p2, external, numerical	dP, numerical	p1, final, numerical	p2, final, numerical		p1, external, analytical	p2, external, analytical	dP, analytical	p1, final, analytical	p2, final, analytical		deviation p2, external	deviation dP	deviation p2, final
Flat	*0.664*	*0.336*	*0.000*	*0.664*	*0.336*		*0.664*	*0.664*	*0.000*	*0.664*	*0.336*		-	-	-
11500	0.646	0.354	0.091	0.555	0.445		0.616	0.384	0.060	0.556	0.444		2.97%	3.07%	0.06%

3600x1800x10-15-12, pressures in kN/m2															
	p1, external, numerical	p2, external, numerical	dP, numerical	p1, final, numerical	p2, final, numerical		p1, external, analytical	p2, external, analytical	dP, analytical	p1, final, analytical	p2, final, analytical		deviation p2, external	deviation dP	deviation p2, final
Flat	*0.374*	*0.626*	*0.000*	*0.374*	*0.626*		*0.374*	*0.374*	*0.000*	*0.374*	*0.626*		-	-	-
11500	0.506	0.495	-0.177	0.683	0.318		0.525	0.475	-0.092	0.617	0.383		1.99%	8.54%	6.54%

3600x1800x12-15-8, pressures in kN/m2															
	p1, external, numerical	p2, external, numerical	dP, numerical	p1, final, numerical	p2, final, numerical		p1, external, analytical	p2, external, analytical	dP, analytical	p1, final, analytical	p2, final, analytical		deviation p2, external	deviation dP	deviation p2, final
Flat	*0.773*	*0.227*	*0.000*	*0.773*	*0.227*		*0.773*	*0.773*	*0.000*	*0.773*	*0.227*		-	-	-
11500	0.721	0.279	0.179	0.541	0.459		0.667	0.333	0.120	0.547	0.453		5.33%	5.86%	0.58%

3600x1800x12-15-10, pressures in kN/m2															
	p1, external, numerical	p2, external, numerical	dP, numerical	p1, final, numerical	p2, final, numerical		p1, external, analytical	p2, external, analytical	dP, analytical	p1, final, analytical	p2, final, analytical		deviation p2, external	deviation dP	deviation p2, final
Flat	*0.638*	*0.362*	*0.000*	*0.638*	*0.362*		*0.638*	*0.638*	*0.000*	*0.638*	*0.362*		-	-	-
11500	0.653	0.347	0.130	0.523	0.477		0.620	0.380	0.076	0.544	0.456		3.27%	5.42%	2.12%

Case study Melle

5500x2500x14-15-16, pressures in kN/m2															
	p1, external, numerical	p2, external, numerical	dP, numerical	p1, final, numerical	p2, final, numerical		p1, external, analytical	p2, external, analytical	dP, analytical	p1, final, analytical	p2, final, analytical		deviation p2, external	deviation dP	deviation p2, final
Flat	*0.406*	*0.594*	*0.000*	*0.406*	*0.594*		*0.406*	*0.406*	*0.000*	*0.406*	*0.594*		-	-	-
28000	0.473	0.527	-0.071	0.544	0.456		0.470	0.530	-0.022	0.493	0.507		0.23%	4.86%	5.13%

5500x2500x14-15-18, pressures in kN/m2															
	p1, external, numerical	p2, external, numerical	dP, numerical	p1, final, numerical	p2, final, numerical		p1, external, analytical	p2, external, analytical	dP, analytical	p1, final, analytical	p2, final, analytical		deviation p2, external	deviation dP	deviation p2, final
Flat	*0.326*	*0.674*	*0.000*	*0.326*	*0.674*		*0.326*	*0.326*	*0.000*	*0.326*	*0.674*		-	-	-
28000	0.426	0.573	-0.173	0.599	0.400		0.429	0.571	-0.053	0.482	0.518		0.20%	11.96%	11.79%

5500x2500x16-15-14, pressures in kN/m2															
	p1, external, numerical	p2, external, numerical	dP, numerical	p1, final, numerical	p2, final, numerical		p1, external, analytical	p2, external, analytical	dP, analytical	p1, final, analytical	p2, final, analytical		deviation p2, external	deviation dP	deviation p2, final
Flat	*0.602*	*0.398*	*0.000*	*0.602*	*0.398*		*0.602*	*0.602*	*0.000*	*0.602*	*0.398*		-	-	-
28000	0.590	0.409	0.058	0.532	0.467		0.565	0.435	0.019	0.547	0.453		2.53%	3.95%	1.37%

5500x2500x16-15-18, pressures in kN/m2															
	p1, external, numerical	p2, external, numerical	dP, numerical	p1, final, numerical	p2, final, numerical		p1, external, analytical	p2, external, analytical	dP, analytical	p1, final, analytical	p2, final, analytical		deviation p2, external	deviation dP	deviation p2, final
Flat	*0.420*	*0.580*	*0.000*	*0.420*	*0.580*		*0.420*	*0.420*	*0.000*	*0.420*	*0.580*		-	-	-
11500	0.490	0.509	-0.086	0.576	0.423		0.478	0.522	-0.027	0.504	0.496		1.30%	5.93%	7.28%

5500x2500x18-15-14, pressures in kN/m2															
	p1, external, numerical	p2, external, numerical	dP, numerical	p1, final, numerical	p2, final, numerical		p1, external, analytical	p2, external, analytical	dP, analytical	p1, final, analytical	p2, final, analytical		deviation p2, external	deviation dP	deviation p2, final
Flat	*0.683*	*0.317*	*0.000*	*0.683*	*0.317*		*0.683*	*0.683*	*0.000*	*0.683*	*0.317*		-	-	-
28000	0.639	0.361	0.113	0.526	0.474		0.610	0.390	0.037	0.573	0.427		2.87%	7.60%	4.71%

5500x2500x18-15-16, pressures in kN/m2															
	p1, external, numerical	p2, external, numerical	dP, numerical	p1, final, numerical	p2, final, numerical		p1, external, analytical	p2, external, analytical	dP, analytical	p1, final, analytical	p2, final, analytical		deviation p2, external	deviation dP	deviation p2, final
Flat	*0.592*	*0.408*	*0.000*	*0.592*	*0.408*		*0.592*	*0.592*	*0.000*	*0.592*	*0.408*		-	-	-
28000	0.589	0.412	0.072	0.517	0.484		0.565	0.435	0.022	0.543	0.457		2.28%	4.97%	2.68%